C O M M U N I C A T I O N S

FACULTY OF SCIENCES
UNIVERSITY OF ANKARA

DE LA FACULTE DES SCIENCES
DE L'UNIVERSITE D'ANKARA

Series A1: Mathematics and Statistics

VOLUME: 72 **Number: 2** **YEAR: 2023**

Faculty of Sciences, Ankara University
06100 Beşevler, Ankara-Turkey

ISSN 1303-5991 e-ISSN 2618-6470

C O M M U N I C A T I O N S

FACULTY OF SCIENCES
UNIVERSITY OF ANKARA

DE LA FACULTE DES SCIENCES
DE L'UNIVERSITE D'ANKARA

Series A1: Mathematics and Statistics

Volume: 72 **Number: 2** **Year: 2023**

Correspondence Address:
COMMUNICATIONS EDITORIAL OFFICE
Ankara University, Faculty of Sciences,
06100 Tandoğan, ANKARA – TURKEY
Tel: (90) 312-2126720 Fax: (90) 312-2235000
e-mail: commun@science.ankara.edu.tr
http://communications.science.ankara.edu.tr/index.php?series=A1

Print:
Ankara University Press
İncitaş Sokak No:10 06510 Beşevler
ANKARA – TURKEY
Tel: (90) 312-2136655

C O M M U N I C A T I O N S

FACULTY OF SCIENCES
UNIVERSITY OF ANKARA

DE LA FACULTE DES SCIENCES
DE L'UNIVERSITE D'ANKARA

Series A1: Mathematics and Statistics

VOLUME: 72 **Number: 2** **YEAR: 2023**

Faculty of Sciences, Ankara University
06100 Beşevler, Ankara-Turkey

ISSN 1303-5991 e-ISSN 2618-6470

C O M M U N I C A T I O N S

FACULTY OF SCIENCES
UNIVERSITY OF ANKARA

DE LA FACULTE DES SCIENCES DE
L'UNIVERSITE D'ANKARA

Series A1: Mathematics and Statistics

Volume: 72 **Number: 2** **Year: 2023**

Research Articles

http://communications.science.ankara.edu.tr

Commun.Fac.Sci.Univ.Ank.Ser. A1 Math. Stat.
Volume 72, Number 2, Pages 286–306 (2023)
DOI:10.31801/cfsuasmas.1097797
ISSN 1303-5991 E-ISSN 2618-6470

COMMUNICATIONS SERIES A1

Research Article; Received: April 3, 2022; Accepted: November 24, 2022

ANALYSIS OF A PRODUCTION INVENTORY SYSTEM WITH MAP ARRIVALS, PHASE-TYPE SERVICES AND VACATION TO PRODUCTION FACILITY

Serife OZKAR
Department of International Trade and Logistics, Balikesir University, Balikesir, TÜRKİYE

Abstract. In this paper, we discuss a production inventory system with service times. Customers arrive in the system according to a Markovian arrival process. The service times follow a phase-type distribution. We assume that there is an infinite waiting space for customers. Arriving customers demand only one unit of item from the inventory. The production facility produces items according to an (s, S)-policy. Once the inventory level becomes the maximum level S, the production facility goes on a vacation of random duration. When the production facility returns from the vacation, if the inventory level depletes to the fixed level s, it is immediately switched on and starts production until the inventory level becomes S. Otherwise, if the inventory level is greater than s on return from the vacation, it takes another vacation. The vacation times are exponentially distributed. The production inventory system in the steady-state is analyzed by using the matrix-geometric method. A numerical study is performed on the system performance measures. Besides, an optimization study is discussed for the inventory policy.

1. Introduction

In classical inventory systems, demanded items are directly delivered from stock and the amount of time required to service is negligible. Demand occurred during stockout periods either result in lost sales or is satisfied only after the arrival of the replenishments. In contrast, in most real-life situations, a positive amount of time is needed for procedures such as preparation, packing, and loading of items in the inventory. Inventory systems have positive service times are denominated queueing-inventory systems. A detailed survey of the literature for queueing-inventory systems can be found in [7] and [4].

2020 *Mathematics Subject Classification.* 60K25, 90B05, 90B22.
Keywords. Production inventory system, vacation, phase-type distribution, Markovian arrival process, matrix geometric method.
serife.ozkar@balikesir.edu.tr, 0000-0003-3475-5666.

In classical queueing systems (the absence of vacation), the server will be idle whenever there is no customer to service. On the other hand, the vacation of a server facilitates improved utilization of server idle time. That is, in this vacation period, the server can be utilized for some other ancillary work that will improve the productivity of an organization. The queueing systems with vacation have been extensively studied. We refer to [17] and [5] for more details on this topic.

Considering the server vacation, the queueing-inventory systems have been studied very little in the literature. The literature can be divided into two main groups: (i) *in the queueing-inventory systems*, the server goes on vacation when there is no customer in the system and/or there is no item in the inventory and (ii) *in the production inventory systems with a service facility*, the server goes on vacation when there is no customer in the system and/or there is no item in the inventory or the production goes on vacation when the inventory level becomes S.

Queueing-inventory systems where the server goes on vacation when there is no customer in the system and/or there is no item in the inventory. [11] is the first study considering a vacation to server in the inventory systems with positive service times. In this study, at a service completion epoch if no customer is in the system and/or no item in the inventory, the server goes on vacation. When, on return from this vacation, if the system is again found to have either no customer waiting or no item on stock or both, the server goes on another vacation. A perishable queueing-inventory system with early and delayed vacations of the server was studied in [10]. The server is in the operational state only if the level of inventory in the system and the number of the claims in the queue are positive. If at least one of the values is zero, the server takes a vacation. When the inventory level is zero, the server enters an early vacation. If during this period the inventory replenishes, and the any claim in the queue, the server starts service; otherwise it goes to a delayed vacation. [2] investigated a retrial queueing-inventory system with two heterogeneous servers in which the first server is unreliable server and the second server permits for vacation. The second server leaves for a vacation when the server finds either the inventory level is zero and/or the number of customers in the queue is zero. At completion of the vacation, there is at least two commodities and at least two customers in the queue, then the second server starts the service immediately. Otherwise, the server takes another vacation. [16] discussed a finite source queueing-inventory system with two heterogeneous servers. Both servers can take a vacation whenever the inventory level reaches zero and/or the customer level reaches zero. At the end of a vacation period, the service starts if there is a positive inventory and at least one customer in the system. Otherwise, the server takes another vacation.

Queueing-inventory systems where the server goes on vacation when there is no item in the inventory. An inventory system with retrial demands and server vacation was studied by [15]. The server takes a vacation whenever the inventory level becomes zero. When the returns from vacation, if the inventory level is zero, the server starts another vacation. Otherwise, it is ready to serve any arriving demands. [14] extended the paper in [15] by adding a new feature, called idle time for server, in addition to vacation. At the time of the stockout, the server idles for random time, so that if the replenishment is received during the idle time, the server is immediately available to service. At the end of idle time, if the replenishment is not received, the server takes a vacation. On return from any vacation, if the stock is already replenished, the server becomes available, otherwise, it's idle time starts which may be followed by another vacation. [13] discussed a finite-source inventory system with postponed demands and modified M vacation policy. As distinct from the vacation policy introduced in [14] the server can take at most M inactive periods repeatedly until replenishment takes place. [20] considered a queueing-inventory system with ROS policy and server vacations. Once completion of the serving, if the server finds the inventory is empty, the server leaves for a vacation. At the end of the vacation, if the server finds that the inventory is not empty, the server is available to serve, otherwise, the server takes another vacation.

Queueing-inventory systems where the server goes on vacation when there is no customer in the system. [3] studied a perishable queueing-inventory system with delayed vacation and negative customers. If the server finds queue is empty at service completion epoch, the server goes on a delay time. If the delay time is completed before the arrival of a customer, the server takes a vacation. At the end of the vacation period, service commences if there is a customer in the queue. Otherwise, the server starts another vacation. A perishable queueing-inventory system with server vacation was discussed by [6]. Upon service completion, server takes a vacation if there are no customers in the queue and it starts service at the end of the vacation if the number of customers in the system exceeds some threshold; otherwise, it takes another vacation. Up to this point all papers mentioned are related to the server's vacation. In these papers, the server stops servicing because of no items in the inventory and/or no customer in the system. [9] studied a queueing-inventory system with working vacations. The server takes a vacation only in the absence of customers in the system at a service completion epoch. The server continues to provide service at a lower rate than in normal mode of service during working vacations. After a service completion during the working vacation period, if there are customers in the system, the server comes back to the normal mode. Otherwise, if there are no customers in the system, the server continues the vacation.

Production queueing-inventory systems where the server goes on vacation when there is no customer in the system and/or there is no item in the inventory. [8] studied a production inventory system with service time and server vacation. The items for the inventory are produced according to an (s, S) policy. Production starts whenever the inventory level falls to s and continues until the inventory level reaches S. If the server finds either the inventory level is zero and/or the number of customers in the system is zero, the server takes a vacation. At the completion of the vacation period if there is no customers or no inventory or both, the server goes on another vacation.

Production queueing-inventory systems where the production goes on vacation when the inventory level becomes S. [19] considered a production-inventory system with service time, perishable item and production interruptions. The production is interrupted for a vacation once the inventory level becomes S. On return from a vacation, if the inventory level depletes to s, the production is switched on. It starts production and is kept in the on mode until the inventory level becomes S. A production inventory system with service time and production vacations was also studied by [18]. Customers arrive in the system according to a Poisson process. The service times of the customers follow an exponential distribution. A production facility produces items according to an (s, S) policy and the production time for each item is exponentially distributed. The production takes a vacation whose length has exponential distribution once the inventory level becomes S. At the end of the vacation if the inventory level depletes to s, the production is immediately switched on and it starts production until the inventory level becomes S.

In this paper we extend the model studied in [18] by considering a Markovian arrival process for governing the arrival of the customers and phase type distributions for service times. The paper is structured as follows. The assumptions and description of the model are elaborated in Section 2. The steady state solution of the model including the stability condition and some performance measures of the system are discussed in Section 3. In Section 4, the total expected cost function is structured and presented sensitivity analysis with numerical examples. Finally, some concluding remarks are given in Section 5.

2. Model Description

We analyze a production queueing-inventory system with production vacations as demonstrated in Figure 1. Customers arrive in the system according to a Markovian

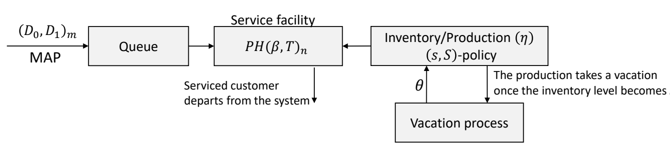

FIGURE 1. A production inventory system with production vacations.

arrival process (MAP) with representation $(\boldsymbol{D}_0, \boldsymbol{D}_1)$ of order m. The underlying Markov chain of the MAP is governed by the matrix $\boldsymbol{D}$ $(= \boldsymbol{D}_0 + \boldsymbol{D}_1)$. Such that, the matrix $\boldsymbol{D}_0$ denotes the transition rates without arrival while the matrix $\boldsymbol{D}_1$ denotes the transition rates with arrival. So, the arrival rate is given by $\lambda = \boldsymbol{\delta} \boldsymbol{D}_1 \boldsymbol{e}$ where $\boldsymbol{\delta}$ is the stationary probability vector of the generator matrix $\boldsymbol{D}$ and it is satisfied

$$\boldsymbol{\delta} \boldsymbol{D} = \boldsymbol{0}, \ \boldsymbol{\delta} \boldsymbol{e} = 1. \tag{1}$$

For detailed information about MAPs, we refer to the study in [1].

When the inventory level is positive, an arriving customer finding the server idle gets into service immediately. Otherwise, the customer enters into a waiting space (queue) with infinite size to be served under the first-come first-served ($FCFS$) discipline. On the other hand, when the inventory is empty, no customer is allowed to join the queue. That is, all arriving customers are lost during the stochout case.

Each arriving customer demands a single item from the inventory. A served customer leaves immediately the system and the on-hand inventory is decreased by one at service completion epoch. The service time follows a phase-type distribution with representation $(\boldsymbol{\beta}, \boldsymbol{T})$ of order n where $\boldsymbol{\beta}$ is the initial probability vector, $\boldsymbol{\beta e} = 1$, $\boldsymbol{T}$ is an infinitesimal generator matrix holding the transition rates among the n transient states; $\boldsymbol{T}^0$ is a column vector contains the absorption rates into state 0 from the transient states. It is clear that $\boldsymbol{Te} + \boldsymbol{T}^0 = \mathbf{0}$. The phase-type distribution has the service rate $\mu = 1/[\boldsymbol{\beta}(-\boldsymbol{T})^{-1}\boldsymbol{e}]$. The properties in detail of phase-type distributions are given in [12].

The production inventory system studied has a single production facility that produces one type of item. The production time is exponentially distributed with parameter η. The inventory level in the system is governed by the (s, S)-policy. Once the inventory level becomes the maximum level S, the production facility takes a vacation whose duration follows an exponential distribution with parameter θ. When the production facility returns from the vacation, if the inventory level depletes to the fixed level s, it is immediately switched on and starts production until the inventory level becomes S. Otherwise, if the inventory level is greater than s on return from the vacation, it takes another vacation.

3. The Steady-State Analysis

The steady-state analysis of the production inventory system described is performed in this section. Let $N(t), I(t), K(t)$, $J_1(t)$ and $J_2(t)$ denote, respectively, the number of customers in the system, the inventory level, the state of the production process, the phase of the service and the phase of the arrival, at time t. The state of the production process is given by

$$K(t) = \begin{cases} 0 & \text{, if the production is taking a vacation,} \\ 1 & \text{, if the production is in ON mode.} \end{cases}$$

The process $\{(N(t), I(t), K(t), J_1(t), J_2(t)) : t \geq 0\}$ is a continuous-time Markov chain and the state space is given by

$$\Omega = \{i_0\} \cup \{i_1, i \geq 1\},$$

where

$$i_0 = \{(0, j, k, j_2) : 0 \leq j \leq S-1, k = 0, 1, 1 \leq j_2 \leq m\} \cup \\ \{(0, S, 0, j_2) : 1 \leq j_2 \leq m\}$$

and

$$i_1 = \{(i, j, k, j_1, j_2) : 0 \leq j \leq S-1, k = 0, 1, 1 \leq j_1 \leq n, 1 \leq j_2 \leq m\} \cup \\ \{(i, S, 0, j_1, j_2) : 1 \leq j_1 \leq n, 1 \leq j_2 \leq m\}.$$

The level $(0, j, 0, j_2)$ of dimension m corresponds to the case when the system is idle, the inventory level j, $0 \le j \le S$, the production process is on vacation and the arrival process is in one of m phases. The level $(0, j, 1, j_2)$ of dimension m corresponds to the case when the system is idle, the inventory level j, $0 \le j \le S-1$, the production process is in ON mode and the arrival process is in one of m phases.

The level $(i, j, 0, j_1, j_2)$of dimension mn corresponds to the case when there is i customers in the system, the inventory level j, $0 \le j \le S$, the production process is on vacation, the service process is in one of n phases and the arrival process is in one of m phases. The level $(i, j, 1, j_1, j_2)$ of dimension mn corresponds to the case when there is i customers in the system, the inventory level j, $0 \le j \le S-1$, the production process is in ON mode, the service process is in one of n phases and the arrival process is in one of m phases.

The infinitesimal generator matrix of the quasi-birth-and-death (QBD) process has a block-tridiagonal matrix structure and is given by

$$\boldsymbol{Q} = \begin{pmatrix} \boldsymbol{A}_0 & \boldsymbol{C}_0 & & & \\ \boldsymbol{B}_0 & \boldsymbol{A} & \boldsymbol{C} & & \\ & \boldsymbol{B} & \boldsymbol{A} & \boldsymbol{C} & \\ & & \ddots & \ddots & \ddots \end{pmatrix}. \tag{2}$$

At this point, we need to set up some notation for use in sequel. $\boldsymbol{e}$ is a unit column vector; $\boldsymbol{e}_i$ is a column vector with 1 in the i^{th} position and 0 elsewhere; $\boldsymbol{e}(j)$ is a unit column vector is of dimension j and $\boldsymbol{I}_k$ is an identity matrix of order k. The symbols $\otimes$ and $\oplus$ represent the Kronecker product and the Kronecker sum, respectively. If $\boldsymbol{A}$ is a matrix of order $m \times n$ and if $\boldsymbol{B}$ is a matrix of order $p \times q$, then the Kronecker product of the two matrices is given by $\boldsymbol{A} \otimes \boldsymbol{B}$, a matrix of order $mp \times nq$; the Kronecker sum of two square matrices, say, $\boldsymbol{G}$ of order g and $\boldsymbol{H}$ of h, is given by $\boldsymbol{G} \oplus \boldsymbol{H} = \boldsymbol{G} \otimes \boldsymbol{I}_h + \boldsymbol{I}_g \otimes \boldsymbol{H}$, a square matrix of order gh. Finally, for the dimensions of the matrices we define $d_1 = (2S+1)m$ and $d_2 = (2S+1)mn$.

The matrices $\boldsymbol{A}_0$ and $\boldsymbol{A}$ in the main diagonal of the matrix $\boldsymbol{Q}$ have dimensions $(d_1 \times d_1)$ and $(d_2 \times d_2)$, respectively.

$$\boldsymbol{A}_0 = \begin{pmatrix} \hat{\boldsymbol{A}}_1 & \hat{\boldsymbol{A}}_4 & & & & & & & & \\ & \hat{\boldsymbol{A}}_2 & \hat{\boldsymbol{A}}_4 & & & & & & & \\ & & \ddots & \ddots & & & & & & \\ & & & \hat{\boldsymbol{A}}_2 & \hat{\boldsymbol{A}}_4 & & & & & \\ & & & & \hat{\boldsymbol{A}}_3 & \hat{\boldsymbol{A}}_4 & & & & \\ & & & & & \ddots & \ddots & & & \\ & & & & & & \hat{\boldsymbol{A}}_3 & \hat{\boldsymbol{A}}_4 & & \\ & & & & & & & \hat{\boldsymbol{A}}_3 & \hat{\boldsymbol{A}}_5 & \\ & & & & & & & & \boldsymbol{D}_0 & \end{pmatrix},$$

with

$$\hat{\boldsymbol{A}}_1 = \begin{pmatrix} -\theta \boldsymbol{I}_m & \theta \boldsymbol{I}_m \\ \boldsymbol{0} & -\eta \boldsymbol{I}_m \end{pmatrix}, \ \hat{\boldsymbol{A}}_2 = \begin{pmatrix} \boldsymbol{D}_0 - \theta \boldsymbol{I}_m & \theta \boldsymbol{I}_m \\ \boldsymbol{0} & \boldsymbol{D}_0 - \eta \boldsymbol{I}_m \end{pmatrix},$$

$$\hat{\boldsymbol{A}}_3 = \begin{pmatrix} \boldsymbol{D}_0 & \boldsymbol{0} \\ \boldsymbol{0} & \boldsymbol{D}_0 - \eta \boldsymbol{I}_m \end{pmatrix}, \ \hat{\boldsymbol{A}}_4 = \begin{pmatrix} \boldsymbol{0} & \boldsymbol{0} \\ \boldsymbol{0} & \eta \boldsymbol{I}_m \end{pmatrix}, \ \hat{\boldsymbol{A}}_5 = \begin{pmatrix} \boldsymbol{0} \\ \eta \boldsymbol{I}_m \end{pmatrix}.$$

$$\boldsymbol{A} = \begin{pmatrix} \tilde{\boldsymbol{A}}_1 & \tilde{\boldsymbol{A}}_4 & & & & & & & \\ & \tilde{\boldsymbol{A}}_2 & \tilde{\boldsymbol{A}}_4 & & & & & & \\ & & \ddots & \ddots & & & & & \\ & & & \tilde{\boldsymbol{A}}_2 & \tilde{\boldsymbol{A}}_4 & & & & \\ & & & & \tilde{\boldsymbol{A}}_3 & \tilde{\boldsymbol{A}}_4 & & & \\ & & & & & \ddots & \ddots & & \\ & & & & & & \tilde{\boldsymbol{A}}_3 & \tilde{\boldsymbol{A}}_4 & \\ & & & & & & & \tilde{\boldsymbol{A}}_3 & \tilde{\boldsymbol{A}}_5 \\ & & & & & & & & \boldsymbol{T} \oplus \boldsymbol{D}_0 \end{pmatrix},$$

with

$$\tilde{\boldsymbol{A}}_1 = \begin{pmatrix} -\theta \boldsymbol{I}_{mn} & \theta \boldsymbol{I}_{mn} \\ \boldsymbol{0} & -\eta \boldsymbol{I}_{mn} \end{pmatrix}, \ \tilde{\boldsymbol{A}}_2 = \begin{pmatrix} \boldsymbol{T} \oplus \boldsymbol{D}_0 - \theta \boldsymbol{I}_{mn} & \theta \boldsymbol{I}_{mn} \\ \boldsymbol{0} & \boldsymbol{T} \oplus \boldsymbol{D}_0 - \eta \boldsymbol{I}_{mn} \end{pmatrix},$$

$$\tilde{\boldsymbol{A}}_3 = \begin{pmatrix} \boldsymbol{T} \oplus \boldsymbol{D}_0 & \boldsymbol{0} \\ \boldsymbol{0} & \boldsymbol{T} \oplus \boldsymbol{D}_0 - \eta \boldsymbol{I}_{mn} \end{pmatrix}, \ \tilde{\boldsymbol{A}}_4 = \begin{pmatrix} \boldsymbol{0} & \boldsymbol{0} \\ \boldsymbol{0} & \eta \boldsymbol{I}_{mn} \end{pmatrix}, \ \tilde{\boldsymbol{A}}_5 = \begin{pmatrix} \boldsymbol{0} \\ \eta \boldsymbol{I}_{mn} \end{pmatrix}.$$

The matrices $\boldsymbol{B}_0$ and $\boldsymbol{B}$ in the lower diagonal of the matrix $\boldsymbol{Q}$ have dimensions $(d_2 \times d_1)$ and $(d_2 \times d_2)$, respectively.

$$\boldsymbol{B}_0 = \begin{pmatrix} \boldsymbol{0} & & & & \\ \hat{\boldsymbol{B}}_1 & \boldsymbol{0} & & & \\ & \ddots & \ddots & & \\ & & \hat{\boldsymbol{B}}_1 & \boldsymbol{0} & \\ & & & \hat{\boldsymbol{B}}_2 & \boldsymbol{0} \end{pmatrix} \text{ with}$$

$$\hat{\boldsymbol{B}}_1 = \begin{pmatrix} \boldsymbol{T}^0 \otimes \boldsymbol{I}_m & \boldsymbol{0} \\ \boldsymbol{0} & \boldsymbol{T}^0 \otimes \boldsymbol{I}_m \end{pmatrix}, \ \hat{\boldsymbol{B}}_2 = \begin{pmatrix} \boldsymbol{T}^0 \otimes \boldsymbol{I}_m & \boldsymbol{0} \end{pmatrix}.$$

$$\boldsymbol{B} = \begin{pmatrix} \boldsymbol{0} & & & & \\ \tilde{\boldsymbol{B}}_1 & \boldsymbol{0} & & & \\ & \ddots & \ddots & & \\ & & \tilde{\boldsymbol{B}}_1 & \boldsymbol{0} & \\ & & & \tilde{\boldsymbol{B}}_2 & \boldsymbol{0} \end{pmatrix} \text{ with}$$

$$\tilde{\boldsymbol{B}}_1 = \begin{pmatrix} \boldsymbol{T}^0\boldsymbol{\beta} \otimes \boldsymbol{I}_m & \boldsymbol{0} \\ \boldsymbol{0} & \boldsymbol{T}^0\boldsymbol{\beta} \otimes \boldsymbol{I}_m \end{pmatrix}, \; \tilde{\boldsymbol{B}}_2 = \begin{pmatrix} \boldsymbol{T}^0\boldsymbol{\beta} \otimes \boldsymbol{I}_m & \boldsymbol{0} \end{pmatrix}.$$

The matrices $\boldsymbol{C}_0$ and $\boldsymbol{C}$ in the upper diagonal of the matrix $\boldsymbol{Q}$ have dimensions $(d_1 \times d_2)$ and $(d_2 \times d_2)$, respectively.

$$\boldsymbol{C}_0 = \begin{pmatrix} \boldsymbol{0} & & & & \\ & \hat{\boldsymbol{C}}_1 & & & \\ & & \ddots & & \\ & & & \hat{\boldsymbol{C}}_1 & \\ & & & & \hat{\boldsymbol{C}}_2 \end{pmatrix} \text{ with}$$

$$\hat{\boldsymbol{C}}_1 = \begin{pmatrix} \boldsymbol{\beta} \otimes \boldsymbol{D}_1 & \boldsymbol{0} \\ \boldsymbol{0} & \boldsymbol{\beta} \otimes \boldsymbol{D}_1 \end{pmatrix}, \; \hat{\boldsymbol{C}}_2 = \begin{pmatrix} \boldsymbol{\beta} \otimes \boldsymbol{D}_1 \end{pmatrix}.$$

$$\boldsymbol{C} = \begin{pmatrix} \boldsymbol{0} & & & & \\ & \tilde{\boldsymbol{C}}_1 & & & \\ & & \ddots & & \\ & & & \tilde{\boldsymbol{C}}_1 & \\ & & & & \tilde{\boldsymbol{C}}_2 \end{pmatrix} \text{ with}$$

$$\tilde{\boldsymbol{C}}_1 = \begin{pmatrix} \boldsymbol{I}_n \otimes \boldsymbol{D}_1 & \boldsymbol{0} \\ \boldsymbol{0} & \boldsymbol{I}_n \otimes \boldsymbol{D}_1 \end{pmatrix}, \; \tilde{\boldsymbol{C}}_2 = \begin{pmatrix} \boldsymbol{I}_n \otimes \boldsymbol{D}_1 \end{pmatrix}.$$

3.1. **The stability condition.** Let $\boldsymbol{\pi} = (\boldsymbol{\pi}_{0,0}, \boldsymbol{\pi}_{0,1}, \boldsymbol{\pi}_{1,0}, \boldsymbol{\pi}_{1,1}, \cdots, \boldsymbol{\pi}_{s,0}, \boldsymbol{\pi}_{s,1}, \cdots, \boldsymbol{\pi}_{S-1,0}, \boldsymbol{\pi}_{S-1,1}, \boldsymbol{\pi}_{S,0})$ denote the steady-state probability vector of the generator matrix $\boldsymbol{F} = \boldsymbol{A} + \boldsymbol{B} + \boldsymbol{C}$. The probability vector satisfies

$$\boldsymbol{\pi}\boldsymbol{F} = \boldsymbol{0}, \; \boldsymbol{\pi}\boldsymbol{e} = 1. \tag{3}$$

The steady-state equations in (3) can be rewritten as following.

$$\begin{aligned}
-\boldsymbol{\pi}_{0,0}\theta\boldsymbol{I} + \boldsymbol{\pi}_{1,0}(\boldsymbol{T}^0\boldsymbol{\beta} \otimes \boldsymbol{I}_m) &= \boldsymbol{0}, & \\
\boldsymbol{\pi}_{i,0}[(\boldsymbol{I}_n \otimes \boldsymbol{D}_1) + (\boldsymbol{T} \oplus \boldsymbol{D}_0) - \theta\boldsymbol{I}] + \boldsymbol{\pi}_{i+1,0}(\boldsymbol{T}^0\boldsymbol{\beta} \otimes \boldsymbol{I}_m) &= \boldsymbol{0}, & 1 \le i \le s, \\
\boldsymbol{\pi}_{i,0}[(\boldsymbol{I}_n \otimes \boldsymbol{D}_1) + (\boldsymbol{T} \oplus \boldsymbol{D}_0)] + \boldsymbol{\pi}_{i+1,0}(\boldsymbol{T}^0\boldsymbol{\beta} \otimes \boldsymbol{I}_m) &= \boldsymbol{0}, & s+1 \le i \le S-1, \\
\boldsymbol{\pi}_{S-1,1}\eta\boldsymbol{I} + \boldsymbol{\pi}_{S,0}[(\boldsymbol{I}_n \otimes \boldsymbol{D}_1) + (\boldsymbol{T} \oplus \boldsymbol{D}_0)] &= \boldsymbol{0}, & \\
\\
\boldsymbol{\pi}_{0,0}\theta\boldsymbol{I} - \boldsymbol{\pi}_{0,1}\eta\boldsymbol{I} + \boldsymbol{\pi}_{1,1}(\boldsymbol{T}^0\boldsymbol{\beta} \otimes \boldsymbol{I}_m) &= \boldsymbol{0}, & \\
\boldsymbol{\pi}_{i-1,1}\eta\boldsymbol{I} + \boldsymbol{\pi}_{i,0}\theta\boldsymbol{I} + \boldsymbol{\pi}_{i,1}[(\boldsymbol{I}_n \otimes \boldsymbol{D}_1) + (\boldsymbol{T} \oplus \boldsymbol{D}_0) - \eta\boldsymbol{I}] & & \\
+\boldsymbol{\pi}_{i+1,1}(\boldsymbol{T}^0\boldsymbol{\beta} \otimes \boldsymbol{I}_m) &= \boldsymbol{0}, & 1 \le i \le s, \\
\boldsymbol{\pi}_{i-1,1}\eta\boldsymbol{I} + \boldsymbol{\pi}_{i,1}[(\boldsymbol{I}_n \otimes \boldsymbol{D}_1) + (\boldsymbol{T} \oplus \boldsymbol{D}_0) - \eta\boldsymbol{I}] & & \\
+\boldsymbol{\pi}_{i+1,1}(\boldsymbol{T}^0\boldsymbol{\beta} \otimes \boldsymbol{I}_m) &= \boldsymbol{0}, & s+1 \le i \le S-2, \\
\boldsymbol{\pi}_{S-2,1}\eta\boldsymbol{I} + \boldsymbol{\pi}_{S-1,1}[(\boldsymbol{I}_n \otimes \boldsymbol{D}_1) + (\boldsymbol{T} \oplus \boldsymbol{D}_0) - \eta\boldsymbol{I}] &= \boldsymbol{0}, &
\end{aligned} \tag{4}$$

with the normalizing condition

$$\sum_{i=0}^{S-1}(\boldsymbol{\pi}_{i,0}+\boldsymbol{\pi}_{i,1})\boldsymbol{e}+\boldsymbol{\pi}_{S,0}\boldsymbol{e}=1. \tag{5}$$

The production inventory model with service facility under study is stable *if and only if* $\boldsymbol{\pi}\boldsymbol{C}\boldsymbol{e}<\boldsymbol{\pi}\boldsymbol{B}\boldsymbol{e}$ (see, e.g., [12]). The stability condition is given as

$$\Big[\sum_{i=1}^{S-1}(\boldsymbol{\pi}_{i,0}+\boldsymbol{\pi}_{i,1})+\boldsymbol{\pi}_{S,0}\Big](\boldsymbol{I}_n\otimes\boldsymbol{D}_1)\boldsymbol{e}\ <\ \Big[\sum_{i=1}^{S-1}(\boldsymbol{\pi}_{i,0}+\boldsymbol{\pi}_{i,1})+\boldsymbol{\pi}_{S,0}\Big](\boldsymbol{T}^0\boldsymbol{\beta}\otimes\boldsymbol{I}_m)\boldsymbol{e}. \tag{6}$$

Now adding the equations given in (4) we obtain

$$\Big[\sum_{i=1}^{S-1}(\boldsymbol{\pi}_{i,0}+\boldsymbol{\pi}_{i,1})+\boldsymbol{\pi}_{S,0}\Big][(\boldsymbol{T}+\boldsymbol{T}^0\boldsymbol{\beta})\oplus\boldsymbol{D}]=\boldsymbol{0}. \tag{7}$$

Post-multiplying the equation in (7) by $(\boldsymbol{e}_n\otimes\boldsymbol{I}_m)$ and using the arrival rate $\lambda=\boldsymbol{\delta}\boldsymbol{D}_1\boldsymbol{e}$ we get

$$\Big[\sum_{i=1}^{S-1}(\boldsymbol{\pi}_{i,0}+\boldsymbol{\pi}_{i,1})+\boldsymbol{\pi}_{S,0}\Big](\boldsymbol{e}_n\otimes\boldsymbol{I}_m)\boldsymbol{D}_1\boldsymbol{e}_m=\lambda\Big[\sum_{i=1}^{S-1}(\boldsymbol{\pi}_{i,0}+\boldsymbol{\pi}_{i,1})+\boldsymbol{\pi}_{S,0}\Big]\boldsymbol{e}. \tag{8}$$

Then we obtain the left-side of the equation given in (6) by using the normalizing condition in (5) and the equation in (8) given as

$$\Big[\sum_{i=1}^{S-1}(\boldsymbol{\pi}_{i,0}+\boldsymbol{\pi}_{i,1})+\boldsymbol{\pi}_{S,0}\Big](\boldsymbol{I}_n\otimes\boldsymbol{D}_1)\boldsymbol{e}=\lambda[1-(\boldsymbol{\pi}_{0,0}+\boldsymbol{\pi}_{0,1})\boldsymbol{e}]. \tag{9}$$

Post-multiplying the equation in (7) by $(\boldsymbol{I}_n\otimes\boldsymbol{e}_m)$ and using the service rate $\mu=1/[\boldsymbol{\beta}(-\boldsymbol{T})^{-1}\boldsymbol{e}]$ we get

$$\Big[\sum_{i=1}^{S-1}(\boldsymbol{\pi}_{i,0}+\boldsymbol{\pi}_{i,1})+\boldsymbol{\pi}_{S,0}\Big](\boldsymbol{T}^0\boldsymbol{\beta}\otimes\boldsymbol{e}_m)\boldsymbol{e}_n=\mu\Big[\sum_{i=1}^{S-1}(\boldsymbol{\pi}_{i,0}+\boldsymbol{\pi}_{i,1})+\boldsymbol{\pi}_{S,0}\Big]\boldsymbol{e}. \tag{10}$$

The right-side of the equation given in (6) is obtained by using the normalizing condition in (5) and the equation in (10) given as

$$\Big[\sum_{i=1}^{S-1}(\boldsymbol{\pi}_{i,0}+\boldsymbol{\pi}_{i,1})+\boldsymbol{\pi}_{S,0}\Big](\boldsymbol{T}^0\boldsymbol{\beta}\otimes\boldsymbol{I}_m)\boldsymbol{e}=\mu[1-(\boldsymbol{\pi}_{0,0}+\boldsymbol{\pi}_{0,1})\boldsymbol{e}]. \tag{11}$$

Finally the stability condition given in (6) is given by

$$\lambda[1-(\boldsymbol{\pi}_{0,0}+\boldsymbol{\pi}_{0,1})\boldsymbol{e}]\ <\ \mu[1-(\boldsymbol{\pi}_{0,0}+\boldsymbol{\pi}_{0,1})\boldsymbol{e}].$$

It is clear that $(\boldsymbol{\pi}_{0,0}+\boldsymbol{\pi}_{0,1})\boldsymbol{e}\neq 1$, so we establish the following theorem.

Theorem 1. *The production inventory system with service facility under study is stable if and only if the following condition is satisfied.*

$$\lambda \ < \ \mu \tag{12}$$

where λ and μ are the arrival rate and the service rate, respectively.

3.2. **The steady-state probability vector.** Let $\boldsymbol{x} = (\boldsymbol{x}(0), \boldsymbol{x}(1), \boldsymbol{x}(2), \cdots)$ denote the steady-state probability vector of the generator matrix $\boldsymbol{Q}$ given in (2). The probability vector satisfies

$$\boldsymbol{xQ} = \boldsymbol{0}, \ \boldsymbol{xe} = 1. \tag{13}$$

The vector $\boldsymbol{x}(0)$ of dimension $(2S+1)m$ is further partitioned into vectors of dimension m as $\boldsymbol{x}(0) = [\boldsymbol{x}(0,0,0), \boldsymbol{x}(0,0,1), \cdots, \boldsymbol{x}(0,S-1,0), \boldsymbol{x}(0,S-1,1), \boldsymbol{x}(0,S,0)]$. The vector $\boldsymbol{x}(0,j,0)$, $0 \le j \le S$, gives the probability that the system is idle, the inventory level is j, the production process is on vacation and the arrival process is in one of m phases. The vector $\boldsymbol{x}(0,j,1)$, $0 \le j \le S-1$, gives the probability that the system is idle, the inventory level is j, the production process is in ON mode and the arrival process is in one of m phases.

The vector $\boldsymbol{x}(i)$, $i \ge 1$, of dimension $(2S+1)mn$ is further partitioned into vectors of dimension mn as $\boldsymbol{x}(i) = [\boldsymbol{x}(i,0,0), \boldsymbol{x}(i,0,1), \cdots, \boldsymbol{x}(i,S-1,0), \boldsymbol{x}(i,S-1,1), \boldsymbol{x}(i,S,0)]$. The vector $\boldsymbol{x}(i,j,0)$, $0 \le j \le S$, gives the probability that the number of customers in the system is i, the inventory level is j, the production process is on vacation and the service process and the arrival process are in various phases. The vector $\boldsymbol{x}(i,j,1)$, $0 \le j \le S-1$, gives the probability that the number of customers in the system is i, the inventory level is j, the production process is in ON mode and the service process and the arrival process are in various phases.

Under the stability condition given in (12) the steady-state probability vector $\boldsymbol{x}$ is obtained (see [12]) as

$$\boldsymbol{x}(i) = \boldsymbol{x}(1)\boldsymbol{R}^{i-1}, \ i > 1, \tag{14}$$

where the matrix $\boldsymbol{R}$ is the minimal nonnegative solution to the following matrix quadratic equation

$$\boldsymbol{R}^2\boldsymbol{B} + \boldsymbol{RA} + \boldsymbol{C} = \boldsymbol{0}, \tag{15}$$

and the vectors, $\boldsymbol{x}(0)$ and $\boldsymbol{x}(1)$ are obtained by solving

$$\begin{aligned} \boldsymbol{x}(0)\boldsymbol{A}_0 + \boldsymbol{x}(1)\boldsymbol{B}_0 = \boldsymbol{0}, \\ \boldsymbol{x}(0)\boldsymbol{C}_0 + \boldsymbol{x}(1)[\boldsymbol{A} + \boldsymbol{RB}] = \boldsymbol{0}, \end{aligned} \tag{16}$$

subject to the normalizing condition

$$\boldsymbol{x}(0)\boldsymbol{e} + \boldsymbol{x}(1)(\boldsymbol{I} - \boldsymbol{R})^{-1}\boldsymbol{e} = 1. \tag{17}$$

3.3. **The performance measures.** Some performance measures of the production inventory system under study are listed in this section.

1. *The probability that there is no customer in the system*

$$P_{idle} = \boldsymbol{x}(0)\boldsymbol{e}.$$

2. *The mean number of customers in the system*

$$E_N = \sum_{i=1}^{\infty} i\ \boldsymbol{x}(i)\boldsymbol{e} = \boldsymbol{x}(1)(\boldsymbol{I} - \boldsymbol{R})^{-2}\boldsymbol{e}.$$

3. *The mean production rate*

$$E_{PR} = \eta\Big[\sum_{j=0}^{S-1} \boldsymbol{x}(0,j,1)\boldsymbol{e} + \sum_{i=1}^{\infty}\sum_{j=0}^{S-1} \boldsymbol{x}(i,j,1)\boldsymbol{e}\Big].$$

4. *The mean loss rate of customers*

$$E_{LR} = \lambda\Big[[\boldsymbol{x}(0,0,0) + \boldsymbol{x}(0,0,1)]\boldsymbol{e} + \sum_{i=1}^{\infty}[\boldsymbol{x}(i,0,0) + \boldsymbol{x}(i,0,1)]\boldsymbol{e}\Big].$$

5. *The mean number of items in the inventory when the production is switched ON*

$$EI_R = \sum_{j=0}^{S-1} j\ x(0,j,1)\boldsymbol{e} + \sum_{i=1}^{\infty}\sum_{j=0}^{S-1} j\ x(i,j,1)\boldsymbol{e}$$

6. *The mean number of items in the inventory when the production is switched OFF for a vacation*

$$EI_V = \sum_{j=0}^{S} j\ x(0,j,0)\boldsymbol{e} + \sum_{i=1}^{\infty}\sum_{j=0}^{S} j\ x(i,j,0)\boldsymbol{e}$$

7. *The mean number of items in the inventory*

$$EI = EI_R + EI_V$$

4. Numerical Study

In this section, we perform the numerical examples similar to ones given in [18] to see the effects of various parameters on the system performance measures and to discuss the optimum inventory policies under various scenarios by using a constructed cost function. In other words, the examples in [18] were performed by considering an exponential distribution for both of the inter-arrival times and the service times. We expand the examples for different phase-type distributions. So, we consider the same values used in [18] for the parameters in the all examples.

For the arrival process, we consider the following five sets of values for $\boldsymbol{D}_0$ and $\boldsymbol{D}_1$. The five arrival processes have the same mean of 1 but each one of them is qualitatively different. The values of the standard deviation of the inter-arrival times of the arrival processes with respect to ERLA are, respectively, 1, 1.41421, 3.17451, 1.99336, and 1.99336. The MAP processes are normalized to have a specific arrival rate λ as given in [1]. The arrival processes labeled MNCA and MPCA have negative and positive correlation for two successive inter-arrival times with values -0.4889 and 0.4889, respectively, whereas the first three arrival processes have zero correlation for two successive inter-arrival times.

Erlang distribution (**ERLA**):

$$\boldsymbol{D}_0 = \begin{pmatrix} -2 & 2 \\ 0 & -2 \end{pmatrix}, \ \boldsymbol{D}_1 = \begin{pmatrix} 0 & 0 \\ 2 & 0 \end{pmatrix}.$$

Exponential distribution (**EXPA**):

$$\boldsymbol{D}_0 = \begin{pmatrix} -1 \end{pmatrix}, \ \boldsymbol{D}_1 = \begin{pmatrix} 1 \end{pmatrix}.$$

Hyperexponential distribution (**HEXA**):

$$\boldsymbol{D}_0 = \begin{pmatrix} -1.9 & 0 \\ 0 & -0.19 \end{pmatrix}, \ \boldsymbol{D}_1 = \begin{pmatrix} 1.71 & 0.19 \\ 0.171 & 0.019 \end{pmatrix}.$$

MAP with negative correlation (**MNCA**):

$$\boldsymbol{D}_0 = \begin{pmatrix} -1.00222 & 1.00222 & 0 \\ 0 & -1.00222 & 0 \\ 0 & 0 & -225.75 \end{pmatrix}, \ \boldsymbol{D}_1 = \begin{pmatrix} 0 & 0 & 0 \\ 0.01002 & 0 & 0.9922 \\ 223.4925 & 0 & 2.2575 \end{pmatrix}.$$

MAP with positive correlation (**MPCA**):

$$\boldsymbol{D}_0 = \begin{pmatrix} -1.00222 & 1.00222 & 0 \\ 0 & -1.00222 & 0 \\ 0 & 0 & -225.75 \end{pmatrix}, \ \boldsymbol{D}_1 = \begin{pmatrix} 0 & 0 & 0 \\ 0.9922 & 0 & 0.01002 \\ 2.2575 & 0 & 223.4925 \end{pmatrix}.$$

For the service times, we consider three phase-type distributions with parameter $(\boldsymbol{\beta}, \boldsymbol{T})$. The three phase-type distributions have the same mean of 1 but each one of them is qualitatively different. The values of the standard deviation of the distributions are, respectively, 0.70711, 1, and 2.24472. The distributions are normalized at a specific value for the service rate μ.

Erlang distribution (**ERLS**):

$$\boldsymbol{\beta} = \begin{pmatrix} 1, & 0 \end{pmatrix}, \ \boldsymbol{T} = \begin{pmatrix} -2 & 2 \\ 0 & -2 \end{pmatrix}.$$

Exponential distribution (**EXPS**):

$$\boldsymbol{\beta} = \begin{pmatrix} 1 \end{pmatrix}, \ \boldsymbol{T} = \begin{pmatrix} -1 \end{pmatrix}.$$

Hyperexponential distribution (**HEXS**):

$$\boldsymbol{\beta} = \begin{pmatrix} 0.9, & 0.1 \end{pmatrix}, \quad \boldsymbol{T} = \begin{pmatrix} -1.9 & 0 \\ 0 & -0.19 \end{pmatrix}.$$

4.1. **The effect of the parameters on the performance measures.** The purpose of all examples in this section is to examine how some of the performance measures are effected by the increasing values of parameters. We assume that the inventory policy is $(s, S) = (5, 45)$ and the service rate is $\mu = 4$ for all examples.

Example 1: The effect of the arrival rate λ on the performance measures such as E_{PR} and E_{LR}, is represented in Table 1. Also, the effect on the performance measures consist of EI, EI_V and EI_R is illustrated in Figure 2. For the purposes we fixed $\eta = 2.5$ and $\theta = 1.5$.

TABLE 1. The performance measures for the increasing values of λ

		E_{PR}			E_{LR}		
λ		ERLS	EXPS	HEXS	ERLS	EXPS	HEXS
1.5	ERLA	1.4980	1.4979	1.4957	0.0020	0.0021	0.0043
	EXPA	1.4960	**1.4958**	1.4932	0.0040	**0.0042**	0.0068
	HEXA	1.4807	1.4802	1.4759	0.0193	0.0198	0.0241
	MNCA	1.4959	1.4957	1.4930	0.0041	0.0043	0.0070
	MPCA	1.3472	1.3467	1.3424	0.1527	0.1533	0.1575
2.3	ERLA	2.2691	2.2682	2.2544	0.0309	0.0318	0.0456
	EXPA	2.2549	**2.2539**	2.2388	0.0451	**0.0461**	0.0612
	HEXA	2.1552	2.1539	2.1379	0.1448	0.1461	0.1621
	MNCA	2.2546	2.2535	2.2381	0.0454	0.0465	0.0619
	MPCA	1.9021	1.9013	1.8939	0.3977	0.3985	0.4058
3.1	ERLA	2.5000	2.5000	2.4950	0.6000	0.6000	0.6050
	EXPA	2.4998	**2.4998**	2.4936	0.6002	**0.6002**	0.6064
	HEXA	2.4644	2.4636	2.4490	0.6356	0.6364	0.6510
	MNCA	2.4998	2.4997	2.4935	0.6002	0.6003	0.6065
	MPCA	2.2945	2.2938	2.2856	0.8055	0.8062	0.8144

From Table 1 we notice the following observations.

- When the arrival rate λ is increased, the mean production rate E_{PR} and the mean loss rate of customers E_{LR} increase.
- The increase the variability in the inter-arrival times causes the values of E_{PR} to decrease. Moreover, at the values of E_{PR} are looked, we should note that the MAP process with positive correlation labeled MPCA is significantly separated from the other MAP processes, especially for the systems where the traffic intensity is low (the cases of $\lambda = 1.5$ and $\lambda = 2.3$).

- The values of E_{LR} increase as the variability in the inter-arrival times increases. The values of E_{LR} are dramatically more at the processes named HEXA and MPCA.
- Compared to MAP process, the distribution of the service times has less effect on the values of E_{PR} and E_{LR}. The increase the variability in the service times induces a decrement on E_{PR} and an increment on E_{LR}.

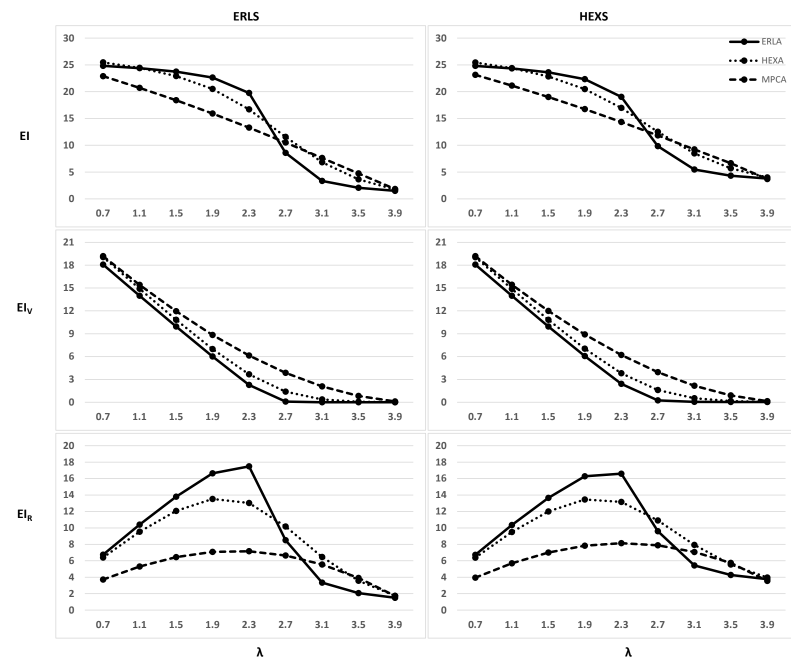

FIGURE 2. The effect of the arrival rate on the inventory level

When the arrival rate λ is increased, the mean number of items in the inventory EI decreases. The effect of variability in the arrival process on EI changes differently depending on the arrival rate. That is, as the variability increases the values of EI decrease for the low arrival rates while increases for the high arrival rates. The behaviour of EI $(= EI_V + EI_R)$ is detailed consideringly its components in Figure 2. When the arrival rate λ is increased, the values of EI_V decrease for all arrival and service scenarios. On the other hand, the values of EI_R firstly increase and then decrease after a certain point. That is, while the values of λ increases, the values of EI_R have a concave structure. The variability in the arrival process affects the concave structure, for example, ERLA with low variability has a faster decline compared to other arrival processes. The decrease in the values of EI_R occurs when the arrival rate λ is greater than the production rate η (=2.5). We note that in the case of HEXA where the variability is high, the break starts earlier.

Example 2: The effect of the production rate η on the performance measures such as E_{PR} and E_{LR} is represented in Table 2. Also, the effect on the performance measures consist of EI, EI_V and EI_R is illustrated in Figure 3. For this example we fixed $\lambda = 1.5$ and $\theta = 1.5$.

TABLE 2. The performance measures for the increasing values of η

		E_{PR}			E_{LR}		
η		ERLS	EXPS	HEXS	ERLS	EXPS	HEXS
	ERLA	1.3938	1.3937	1.3928	0.1062	0.1063	0.1072
	EXPA	1.3862	**1.3862**	1.3849	0.1138	**0.1138**	0.1151
1.4	HEXA	1.3136	1.3135	1.3121	0.1864	0.1865	0.1879
	MNCA	1.3860	1.3859	1.3846	0.1140	0.1141	0.1154
	MPCA	1.0994	1.0993	1.0985	0.4006	0.4007	0.4015
	ERLA	1.4779	1.4778	1.4758	0.0221	0.0222	0.0242
	EXPA	1.4673	**1.4671**	1.4649	0.0327	**0.0329**	0.0351
1.6	HEXA	1.3928	1.3926	1.3901	0.1072	0.1074	0.1099
	MNCA	1.4671	1.4669	1.4645	0.0329	0.0331	0.0355
	MPCA	1.1615	1.1614	1.1602	0.3385	0.3386	0.3398
	ERLA	1.4903	1.4902	1.4881	0.0097	0.0098	0.0119
	EXPA	1.4841	**1.4839**	1.4816	0.0159	**0.0161**	0.0184
1.8	HEXA	1.4339	1.4336	1.4305	0.0661	0.0664	0.0695
	MNCA	1.4840	1.4837	1.4813	0.0160	0.0163	0.0187
	MPCA	1.2139	1.2137	1.2122	0.2860	0.2862	0.2878

From Table 2 we notice the following observations.

- As is to be expected when the production rate η is increased, the mean production rate E_{PR} increases and the mean loss rate of customers E_{LR} decreases due to there is more items in the inventory.
- The increase the variability in the inter-arrival times causes the values of E_{PR} to decrease. On the cases of HEXA and MPCA the decrement is significantly different compared the other MAP processes.
- The values of E_{LR} increase as the variability in the inter-arrival times increases. It is dramatically more on MPCA.
- We do not see that the variability of the service distribution has a significant effect on the values of E_{PR} and E_{LR}. Even so, it can be said that the HEXS with high variability is distinguished from the others.

When the production rate η is increased, the mean number of items in the inventory EI increase. It is clear in Figure 3. The variability in the arrival process causes differently effects on EI depending on the production rate. In other words, as the variability increases the value of EI increases for the low production rate and decreases for the high production rate. The results for its components EI_V and EI_R are also illustrated in Figure 3. When the production rate η is increased, the values of EI_V increase for all scenarios. As the values of η increases, the values of EI_R have a concave structure except the arrival process labeled MPCA. We can say that the variability in the arrival process affects the concave structure. That is, ERLA with low variability has a faster increment compared to HEXA with high variability.

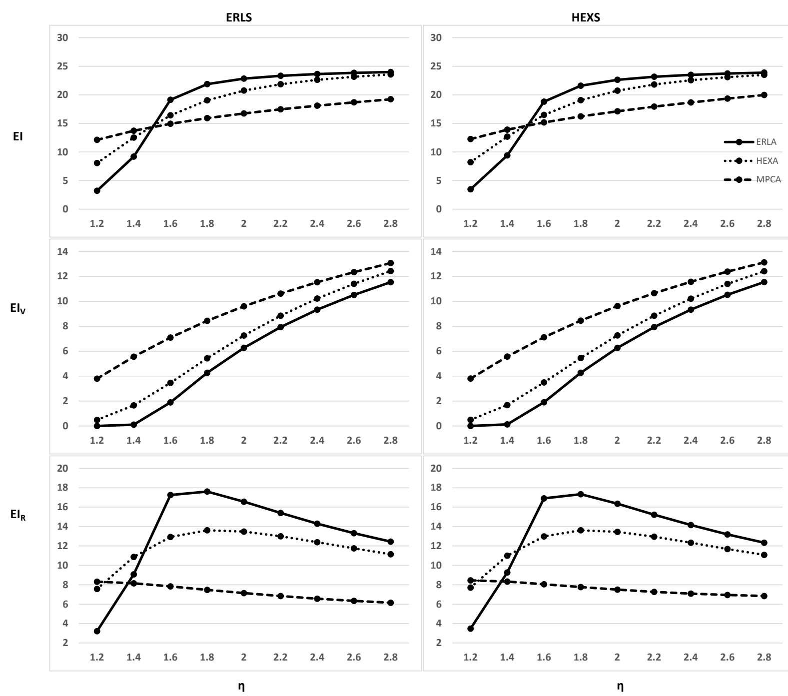

FIGURE 3. The effect of the production rate on the inventory level

Example 3: The effect of the vacation rate θ on the performance measures such as E_{PR} and E_{LR}, is represented in Table 3. We fixed $\lambda = 1.5$ and $\eta = 2.5$ for this example.

Looking at the values in Table 3, it is seen that similar comments in Table 2 will be made here as well. When the vacation rate θ is increased, the values of E_{PR} increase and the values of E_{LR} decrease. The increase the variability in arrival processes causes the values of E_{PR} to decrease and the values of E_{LR} to increase. These changes are significantly different on the cases of HEXA and MPCA. When the variability of the service distribution is observed, it is seen that the HEXS with high variability is distinguished from the others. When the vacation rate θ is increased, EI increase. As the variability in the arrival process increases the values of EI and its components EI_V and EI_R increase. So, the concave structure in the values of EI_R does not exist as the vacation rate θ increases.

TABLE 3. The performance measures for the increasing values of θ

		E_{PR}			E_{LR}		
θ		ERLS	EXPS	HEXS	ERLS	EXPS	HEXS
	ERLA	1.4893	1.4890	1.4861	0.0107	0.0110	0.0139
	EXPA	1.4862	**1.4859**	1.4826	0.0138	**0.0141**	0.0174
0.6	HEXA	1.4676	1.4671	1.4625	0.0324	0.0329	0.0375
	MNCA	1.4863	1.4858	1.4824	0.0137	0.0142	0.0176
	MPCA	1.3424	1.3418	1.3374	0.1576	0.1582	0.1626
	ERLA	1.4951	1.4949	1.4923	0.0049	0.0051	0.0077
	EXPA	1.4924	**1.4922**	1.4893	0.0076	**0.0078**	0.0107
0.9	HEXA	1.4753	1.4747	1.4703	0.0247	0.0253	0.0297
	MNCA	1.4924	1.4921	1.4890	0.0076	0.0079	0.0110
	MPCA	1.3453	1.3447	1.3404	0.1547	0.1553	0.1596
	ERLA	1.4971	1.4969	1.4946	0.0029	0.0031	0.0054
	EXPA	1.4948	**1.4946**	1.4919	0.0052	**0.0054**	0.0081
1.2	HEXA	1.4787	1.4782	1.4739	0.0213	0.0218	0.0261
	MNCA	1.4948	1.4945	1.4917	0.0052	0.0055	0.0083
	MPCA	1.3465	1.3460	1.3417	0.1535	0.1540	0.1583

4.2. **Optimization.** In this section we construct a objective function, ETC, giving the expected total cost per unit of time, and then discuss an optimization problem under various scenarios.

In the cost function, c_{lost}, c_s, c_p and c_h denote, respectively, cost incured due to the loss of customers, cost per unit of time of servicing per customer, cost per unit time of producing per inventory and cost per unit of time of holding per inventory.

$$ETC = c_{lost}E_{LR} + c_sEN + c_pE_{PR} + c_hEI$$

Towards finding the optimum values for the inventory policy and the total cost, we fixed the unit values of the costs by $c_{lost} = 200$, $c_h = 1$, $c_p = 10$ and $c_s = 2$. Also, we consider the other parameters as follows. The optimum values are given for various λ and fixed $\mu = 2.5$, $\theta = 0.8$ and $\eta = 2.5$ in Table 4; for various η and fixed $\lambda = 1.5$, $\theta = 0.8$ and $\mu = 2.5$ in Table 5; for various θ and fixed $\lambda = 2$, $\mu = 2.5$ and $\eta = 2.5$ in Table 6; and for various μ and fixed $\lambda = 1$, $\theta = 0.8$ and $\eta = 2.5$ in Table 7. We should remark that the above ETC function and considered the values for the costs and parameters are the same ones given in [18].

The optimum values of the inventory policy, (s^*, S^*), and the optimum total cost increase as the arrival rate λ increases in Table 4. On the other hand, Table 5 and

Table 6 show that both the values of the optimum policy and the optimum cost decreases as the production rate η increases and as the vacation rate θ increases, respectively. As μ increases, the optimum inventory policy remains almost the same except to the arrival process labeled MPCA in Table 7. The process requests more item on hand inventory with the increasing service rate. Also, Table 7 represents that the increase the service rate μ causes the decrement on the optimum total cost for all scenarios.

It can be seen in Tables 4-7 that the variability in the arrival process and the service process both have a significant effect on the optimum values. As the variability in the arrival process or the variability in the service process increase, both the optimum inventory policy increases and the optimum total cost increases.

Table 4. The optimum policy for the increasing values of λ

		ERLS		EXPS		HEXS	
	λ	(s^*, S^*)	Cost	(s^*, S^*)	Cost	(s^*, S^*)	Cost
ERLA	1	(7,8)	18.4140	(7,8)	18.6544	(8,9)	21.3692
	1.3	(9,10)	23.4965	(9,10)	23.9754	(11,12)	29.0665
	1.6	(11,12)	28.8253	(11,12)	29.7873	(15,16)	38.9059
EXPA	1	(7,8)	19.2833	**(7,8)**	**19.6339**	(9,10)	22.2820
	1.3	(9,10)	24.5579	**(10,11)**	**25.1954**	(12,13)	30.1895
	1.6	(11,12)	30.3250	**(12,13)**	**31.4095**	(16,17)	40.4592
HEXA	1	(9,10)	21.7124	(9,10)	22.2780	(10,11)	25.7178
	1.3	(11,12)	28.5094	(12,13)	29.6037	(14,15)	35.6625
	1.6	(14,15)	37.1754	(15,16)	38.9603	(19,20)	49.2598
MNCA	1	(8,9)	19.6845	(8,9)	19.9280	(8,9)	22.5474
	1.3	(9,10)	24.9916	(10,11)	25.5240	(12,13)	30.4506
	1.6	(11,12)	30.7686	(12,13)	31.7932	(16,17)	40.7547
MPCA	1	(9,14)	93.2177	(10,15)	95.2172	(14,19)	104.7880
	1.3	(12,17)	140.8718	(13,18)	143.5009	(20,24)	156.8172
	1.6	(15,20)	216.2425	(17,22)	219.6613	(26,30)	237.9998

5. Conclusions

In this study, we considered a production inventory system with MAP arrivals and phase-type service times. The production facility in the system is governed by (s, S)-policy and can be taken a vacation. We obtained the stability condition in closed form and then analyzed the production inventory system in the steady-state by using the matrix-geometric method. Some numerical examples were performed to see the effect of the parameters on the system performance measures and to define the optimum inventory policy. In all the examples, we observed that the variability in the inter-arrival times and the variability in the service times affect

TABLE 5. The optimum policy for the increasing values of η

		ERLS		EXPS		HEXS	
	η	(s^*, S^*)	Cost	(s^*, S^*)	Cost	(s^*, S^*)	Cost
ERLA	2.2	(10,12)	27.3130	(11,12)	28.0789	(15,16)	36.1313
	2.8	(10,11)	26.9440	(10,11)	27.6879	(13,14)	34.7214
	3.4	(9,11)	27.0759	(10,11)	27.7608	(12,13)	34.0837
EXPA	2.2	(11,12)	28.9516	**(11,12)**	**29.8165**	(16,17)	37.7226
	2.8	(10,11)	28.1052	**(11,12)**	**29.0030**	(13,14)	35.9469
	3.4	(10,11)	28.1014	**(10,11)**	**28.9231**	(12,13)	35.1845
HEXA	2.2	(15,16)	36.3293	(16,17)	37.7399	(19,20)	46.5107
	2.8	(12,13)	32.9618	(12,13)	34.4631	(16,17)	42.6655
	3.4	(11,12)	32.4254	(12,13)	33.7934	(14,15)	41.0429
MNCA	2.2	(12,13)	29.3807	(12,13)	30.2023	(16,17)	38.0177
	2.8	(10,11)	28.4921	(11,12)	29.3866	(13,14)	36.2475
	3.4	(10,11)	28.4689	(10,11)	29.2740	(12,13)	35.4591
MPCA	2.2	(15,19)	201.1493	(16,22)	203.5517	(26,31)	218.4687
	2.8	(13,16)	180.9230	(14,18)	183.7347	(21,24)	198.6872
	3.4	(11,14)	178.3297	(12,15)	180.2573	(18,20)	191.2252

TABLE 6. The optimum policy for the increasing values of θ

		ERLS		EXPS		HEXS	
	θ	(s^*, S^*)	Cost	(s^*, S^*)	Cost	(s^*, S^*)	Cost
ERLA	0.6	(16,17)	39.2035	(17,18)	41.6564	(25,26)	62.2963
	1	(13,14)	37.3256	(15,16)	39.9393	(22,23)	61.2640
	1.4	(12,13)	36.7212	(14,15)	39.3947	(21,22)	60.9467
EXPA	0.6	(17,18)	41.9681	**(18,19)**	**44.5635**	(25,26)	65.1413
	1	(14,15)	40.3000	**(15,16)**	**43.0441**	(23,24)	64.1669
	1.4	(13,14)	39.7809	**(14,15)**	**42.5706**	(22,23)	63.8602
HEXA	0.6	(19,20)	57.7754	(21,22)	61.2931	(29,30)	83.5578
	1	(17,18)	56.6264	(19,20)	60.2413	(27,28)	82.7774
	1.4	(16,17)	56.2707	(18,19)	59.9048	(26,27)	82.5154
MNCA	0.6	(17,18)	42.4377	(18,19)	44.9924	(25,26)	65.4902
	1	(14,15)	40.7755	(16,17)	43.4808	(23,24)	64.5153
	1.4	(13,14)	40.2577	(15,16)	43.0026	(22,23)	64.2096
MPCA	0.6	(20,26)	446.6197	(23,29)	451.8148	(37,41)	482.5901
	1	(20,24)	446.1006	(22,27)	451.3087	(36,39)	482.0961
	1.4	(19,23)	445.9109	(22,26)	451.1244	(35,38)	481.9004

the values of the performance measures and the optimum inventory policy. These observations are very important in the modelling of real systems. The production

TABLE 7. The optimum policy for the increasing values of μ

		ERLS		EXPS		HEXS	
	μ	(s^*, S^*)	Cost	(s^*, S^*)	Cost	(s^*, S^*)	Cost
ERLA	1.9	(7,8)	18.9509	(7,8)	19.4664	(8,9)	24.0530
	2.2	(7,8)	18.6219	(7,8)	18.9634	(8,9)	22.4089
	2.5	(7,8)	18.4140	(7,8)	18.6544	(8,9)	21.3692
EXPA	1.9	(7,8)	19.8580	**(7,8)**	**20.5228**	(9,10)	24.9252
	2.2	(7,8)	19.4955	**(7,8)**	**19.9673**	(9,10)	23.2919
	2.5	(7,8)	19.2833	**(7,8)**	**19.6339**	(9,10)	22.2820
HEXA	1.9	(8,9)	22.9172	(9,10)	23.9924	(10,11)	29.3001
	2.2	(8,9)	22.1004	(9,10)	22.8603	(10,11)	27.0563
	2.5	(9,10)	21.7124	(9,10)	22.2780	(10,11)	25.7178
MNCA	1.9	(7,8)	20.2947	(8,9)	20.8661	(9,10)	25.2099
	2.2	(7,9)	19.9420	(8,9)	20.2841	(9,10)	23.5695
	2.5	(8,9)	19.6845	(8,9)	19.9280	(9,10)	22.5532
MPCA	1.9	(9,12)	132.4985	(10,13)	134.3205	(14,17)	143.5750
	2.2	(9,13)	106.7248	(10,14)	108.7262	(15,18)	118.3877
	2.5	(9,14)	93.2177	(10,15)	95.2172	(14,19)	104.7880

inventory model considered in this paper can be studied further in a number of ways. Some specific ones are as follows. First, one can generalize this to include $BMAP$ arrivals and/or batch services. Secondly, the production times and/or the vacation times can be considered as a phase-type distribution. Thirdly, it would be interesting to study the present model considering a hidden Markov model where allows us to talk about both observed events and hidden events that we think of as causal factors.

Declaration of Competing Interests The author declares that she has no competing interest.

REFERENCES

[1] Chakravarthy, S. R., Markovian arrival processes, *Wiley Encyclopedia of Operations Research and Management Science*, (2010). https://doi.org/10.1002/9780470400531.eorms0499

[2] Jeganathan, K., Abdul Reiyas, M., Padmasekaran, S., Lakshmanan, K., Two heterogeneous servers queueing-inventory system with multiple vacations and server interruptions, *Adv. Model. Optim.*, 20(1) (2018), 113–133.

[3] Jeganathan, K., Padmasekaran, S., Kingsly, S. J., A perishable inventory-queueing model with delayed vacation, negative and impatient customers, *Math. Model. Geom.*, 4(3) (2016), 11–30. https://doi.org/10.26456/MMG/2016-432

[4] Karthikeyan, K., Sudhesh, R., Recent review article on queueing inventory systems, *Research Journal of Pharmacy and Technology*, 9(11) (2016), 1451–1461. https://doi.org/10.5958/0974-360X.2016.00421.2

[5] Ke, J. C., Wu, C.H., Zhang, Z. G. Recent developments in vacation queueing models, *Int. J. Oper. Res.*, 7(4) (2010), 3–8.

[6] Koroliuk, V. S., Melikov, A. Z., Ponomarenko, L. A., Rustamov, A. M., Models of perishable queueing-inventory systems with server vacations, *Cybern. Syst. Anal.*, 54(1) (2018), 31–44. https://doi.org/10.1007/s10559-018-0005-4

[7] Krishnamoorthy, A., Lakshmy, B., Manikandan, R., A survey on inventory models with positive service time, *OPSEARCH*, 48(2) (2011), 153–169. https://doi.org/10.1007/s12597-010-0032-z

[8] Krishnamoorthy, A., Narayanan, V. C., Production inventory with service time and vacation to the server, *IMA J. Manag. Math.*, 22(2011), 33–45.

[9] Manikandan, R., Nair, S. S., An $M/M/1$ queueing-inventory system with working vacations, vacation interruptions and lost sales, *Autom Remote Control*, 81(4) (2020), 746–759. https://doi.org/10.1134/S0005117920040141

[10] Melikov, A. Z., Rustamov, A. M., Ponomarenko, L. A, Approximate analysis of a queueing-inventory system with early and delayed server vacations, *Autom Remote Control*, 78(11) (2017), 1991–2003. https://doi.org/10.1134/S0005117917110054

[11] Narayanan, V. C., Deepak, T. G., Krishnamoorthy, A., Krishnakumar, B., On an (s, S) inventory policy with service time, vacation to server and correlated lead time, *Quality Technology & Quantitative Management*, 5(2) (2008), 129–143. https://doi.org/10.1080/16843703.2008.11673392

[12] Neuts, M. F. Matrix-Geometric Solutions in Stochastic Models: An Algorithmic Approach, The Johns Hopkins University Press, Baltimore, MD. [1994 version is Dover Edition], 1981.

[13] Padmavathi, I., Lawrence, A. S., Sivakumar, B., A finite-source inventory system with postponed demands and modified M vacation policy, *OPSEARCH*, 53(1) (2016), 41–62. https://doi.org/10.1007/s12597-015-0224-7

[14] Padmavathi, I., Sivakumar, B., Arivarignan, G., A retrial inventory system with single and modified multiple vacation for server, *Ann. Oper. Res.*, 233 (2015), 335–364. https://doi.org/10.1007/s10479-013-1417-1

[15] Sivakumar, B., An inventory system with retrial demands and multiple server vacation, *Quality Technology & Quantitative Management*, 8(2) (2011), 125–146. https://doi.org/10.1080/16843703.2011.11673252

[16] Suganya, C., Lawrence, A. S., Sivakumar, B., A finite-source inventory system with service facility, multiple vacations of two heterogeneous servers, *Int. J. Inf. Manag. Sci.*, 29 (2018), 257–277.

[17] Tian, N., Zhang, Z. G., Vacation Queueing Models: Theory and Applications, Springer-Verlang, New York, 2006.

[18] Yue, D., Qin, Y., A production inventory system with service time and production vacations, *J. Syst. Sci. Syst. Eng.*, 28 (2019), 168–180. https://doi.org/10.1007/s11518-018-5402-8

[19] Yue, D., Wang, S., Zhang, Y., A production-inventory system with a service facility and production interruptions for perishable items, In: Quan-Lin Li, Jinting Wang and Hai-Bo Yu (ed) Stochastic Models in Reliability, Network Security and System Safety, Communications in Computer and Information Science 1102, Springer Nature Singapore, (2019), 410–428.

[20] Zhang, Y., Yue, D., Yue, W., A queueing-inventory system with random order size policy and server vacations, *Ann. Oper. Res.*, (2020). https://doi.org/10.1007/s10479-020-03859-3

http://communications.science.ankara.edu.tr

Commun.Fac.Sci.Univ.Ank.Ser. A1 Math. Stat.
Volume 72, Number 2, Pages 307–330 (2023)
DOI:10.31801/cfsuasmas.1083750
ISSN 1303-5991 E-ISSN 2618-6470

Research Article; Received: March 6, 2022; Accepted: November 25, 2022

A NONLINEAR TRANSFORMATION BETWEEN SPACE CURVES DEFINED BY CURVATURE-TORSION RELATIONS IN 3-DIMENSIONAL EUCLIDEAN SPACE

Emre ÖZTÜRK

Data Analysis Department, Turkish Court of Accounts, Ankara, TÜRKİYE

Abstract. In this paper, we define a nonlinear transformation between space curves which preserves the ratio of τ/κ of the given curve in $3-$dimensional Euclidean space $\mathbb{E}^3$. We investigate invariant and associated curves of this transformation by the help of curvature and torsion functions of the base curve. Moreover, we define a new curve (family) so-called *quasi-slant helix,* and we obtain some characterizations in terms of the curvatures of this curve. Finally, we examine some curves in the kinematics, and give the pictures of some special curves and their images with respect to the transformation.

1. Introduction

In differential geometry, the curvature function $\kappa(s)$which describes the measure of the deviation from the line, and the torsion function $\tau(s)$ which describes the measure of the deviation from the plane, are known as the *natural* or *intrinsic* equations of a curve. It is a well-known fact that these functions are unique for all space curves (fundamental theorem of space curves) [21]. A lot of special curves have been characterized in terms of the curvature functions in Euclidean space, see [3,5–9,11–16,19–22]. Perhaps the most well-known of these is the helix curve. A curve of constant slope or helix is defined by the property that its tangent vector field makes a constant angle with a fixed direction. The fixed direction is called the axis of the helical curve. A classical result stated by M.A. Lancret in 1802 and first proved by B. de Saint Venant in 1845 is: "A necessary and sufficient condition in order to a curve be a helix is that the ratio of curvature to torsion be constant" [21].

Slant helices, which were previously studied by some mathematicians but were firstly characterized by Izumiya and Takeuchi [9] in 2004, can be considered as a generalization of the helix curve. Similar to tangent vectors of the helices, the

2020 *Mathematics Subject Classification.* 14H45, 53A04, 97G50.
Keywords. Mannheim curve, constant pitch curve, nonlinear transformation, slant helix.
emreozturk1471@gmail.com; 0000-0001-6638-3233.

normal vector field of the slant helices makes a constant angle with a fixed direction. The intrinsic equations and tangent vector field of slant helices expressed by Menninger, see [13]. In [6], slant helices with nonzero geodesic curvature of normal indicatrix ($\sigma(s) \neq 0$) are called as *proper slant helix* and the intrinsic equations of these curves calculated in the light of [11]. Moreover, in [22], the authors defined the alternative frame to these curves, and obtained the characterization of some special slant helices with the help of the same frame.

The intrinsic equations of some pair of curves that have been widely studied in the past, such as Bertrand and Mannheim curve pairs, continue to be studied by using different frames in different spaces, see [2,8,12,15,16].

In kinematics, a curve called as "osculating helix" associate to each space curve in Euclidean space. Osculating helix can be expressed with the help of two functions so-called *radius* (r) and *pitch function* (p). These functions are given by

$$r(s) = \kappa(s)/(\kappa^2(s) + \tau^2(s)),$$

and

$$p(s) = \tau(s)/(\kappa^2(s) + \tau^2(s)).$$

see [2]. Notice that, these functions can be defined for any space curve, and the radius function of Mannheim curve is constant. In contrast to Mannheim curves, the curves whose curvatures are given by $\tau(s)/\left(\kappa^2(s) + \tau^2(s)\right) = \mu$, $\mu \in \mathbb{R}$, are not encountered in the literature frequently. These curves called as *constant pitch curve* in [2] . Selig and Carricato [20] expressed that any Frenet-Serret motion is persistent on a space curve in Euclidean space if and only if the pitch function of the curve is constant. In addition, they stated the curvature functions of constant pitch curve in trigonometric and rational form. For Frenet-Serret motion on the slant helix, see [10].

In this study, we define a nonlinear transformation between space curves with the help of radius and pitch functions (Definition 2). We give the algebraic structure of this transformation by Theorem 2. Moreover, we show that the only slant helix which remains invariant under this transformation is a constant precession curve (Theorem 3). In Section 4.2, we investigate evolute of the image curve of this transformation, and we define a *new curve* (family) by Definition 3. In the last section, we illustrate some of curves and their images, under the mentioned transformation.

2. Preliminaries

Let $\mathbb{E}^3$ be the 3$-$dimensional Euclidean space equipped with the inner product $\boldsymbol{u} \cdot \boldsymbol{v} = u_1v_1 + u_2v_2 + u_3v_3$, where $\boldsymbol{u} = (u_1, u_2, u_3)$ and $\boldsymbol{v} = (v_1, v_2, v_3) \in \mathbb{R}^3$. The norm of $\boldsymbol{u}$ is given by $|\boldsymbol{u}| = \sqrt{\boldsymbol{u} \cdot \boldsymbol{u}}$ and the vector product is given by

$$\boldsymbol{u} \times \boldsymbol{v} = \mathbf{det} \begin{pmatrix} \boldsymbol{e}_1 & \boldsymbol{e}_2 & \boldsymbol{e}_3 \\ u_1 & u_2 & u_3 \\ v_1 & v_2 & v_3 \end{pmatrix},$$

where $\{\boldsymbol{e}_1, \boldsymbol{e}_2, \boldsymbol{e}_3\}$ is the standard basis of $\mathbb{E}^3$.

Let $\alpha : I \to \mathbb{E}^3$ be a differentiable curve parameterized by an arbitrary parameter t and $\alpha'(t) \times \alpha''(t) \neq 0$, where $\alpha'(t) = (d\alpha/dt)(t)$ and I is an open interval. At each point of the curve, there exists a moving frame $\{\boldsymbol{t}(t), \boldsymbol{n}(t), \boldsymbol{b}(t)\}$ associated to the curve which is defined by

$$\boldsymbol{t}(t) = \frac{\alpha'(t)}{|\alpha'(t)|}, \qquad \boldsymbol{n}(t) = \boldsymbol{b}(t) \times \boldsymbol{t}(t), \qquad \boldsymbol{b}(t) = \frac{\alpha'(t) \times \alpha''(t)}{|\alpha'(t) \times \alpha''(t)|},$$

where $\boldsymbol{t}$ is the tangent vector, $\boldsymbol{n}$ is the principal normal vector and $\boldsymbol{b}$ is the binormal vector of the curve α. The Frenet-Serret formula of this curve is given by

$$\begin{pmatrix} \boldsymbol{t}'(t) \\ \boldsymbol{n}'(t) \\ \boldsymbol{b}'(t) \end{pmatrix} = \begin{pmatrix} 0 & |\alpha'(t)|\,\kappa(t) & 0 \\ -|\alpha'(t)|\,\kappa(t) & 0 & |\alpha'(t)|\,\tau(t) \\ 0 & -|\alpha'(t)|\,\tau(t) & 0 \end{pmatrix} \begin{pmatrix} \boldsymbol{t}(t) \\ \boldsymbol{n}(t) \\ \boldsymbol{b}(t) \end{pmatrix},$$

where

$$\kappa(t) = \frac{|\alpha'(t) \times \alpha''(t)|}{|\alpha'(t)|^3}, \qquad \tau(t) = \frac{(\alpha'(t) \times \alpha''(t)) \cdot \alpha'''(t)}{|\alpha'(t) \times \alpha''(t)|^2}.$$

Moreover, we say that α is non-degenerate, or α satisfies the non-degenerate condition if $\alpha'(t) \times \alpha''(t) \neq 0$ for all $t \in I$. If α is a unit speed curve, that is, $|\alpha'(s)| = 1$ for all s, then the tangent vector, the principal normal vector, and the binormal vector are given by

$$\boldsymbol{t}(s) = \alpha'(s), \qquad \boldsymbol{n}(s) = \frac{\alpha''(s)}{|\alpha''(s)|}, \qquad \boldsymbol{b}(s) = \boldsymbol{t}(s) \times \boldsymbol{n}(s).$$

Then $\{\boldsymbol{t}(s), \boldsymbol{n}(s), \boldsymbol{b}(s)\}$ is a moving frame of $\alpha(s)$ and we have the Frenet-Serret formula:

$$\begin{pmatrix} \boldsymbol{t}'(s) \\ \boldsymbol{n}'(s) \\ \boldsymbol{b}'(s) \end{pmatrix} = \begin{pmatrix} 0 & \kappa(s) & 0 \\ -\kappa(s) & 0 & \tau(s) \\ 0 & -\tau(s) & 0 \end{pmatrix} \begin{pmatrix} \boldsymbol{t}(s) \\ \boldsymbol{n}(s) \\ \boldsymbol{b}(s) \end{pmatrix},$$

where

$$\kappa(s) = |\alpha''(s)|, \qquad \tau(s) = \frac{\det(\alpha'(s), \alpha''(s), \alpha'''(s))}{\kappa^2(s)}.$$

Let $\alpha : I \to \mathbb{E}^3$ be a regular curve (i.e., $\alpha'(s) \neq 0$). The vector $\boldsymbol{w}(s) = \tau(s)\boldsymbol{t}(s) + \kappa(s)\boldsymbol{b}(s)$ is called the *Darboux vector* of α. The normalization of the Darboux vector is defined by

$$\widetilde{\boldsymbol{w}} = \frac{\tau(s)\boldsymbol{t}(s) + \kappa(s)\boldsymbol{b}(s)}{\sqrt{\tau^2(s) + \kappa^2(s)}},$$

which is called the *Darboux indicatrix* of α.

A regular curve $\alpha : I \to \mathbb{E}^3$ with $\kappa(s) \neq 0$ is called a *Mannheim curve* if its principal normal lines are binormal lines of another curve $\widehat{\alpha}$ at corresponding points. In this case, $\widehat{\alpha}$ is called a *Mannheim mate* of α. For a space curve α, it is a Mannheim curve if and only if there exists nonzero constant λ such that

$\kappa(s) = \lambda\left(\kappa^2(s) + \tau^2(s)\right)$ for any $s \in I$. It is clear that circular helices are Mannheim curves, see [23].

The concept of the slant helix is firstly introduced by Izumiya and Takeuchi [9]. They characterized the slant helices by following proposition:

Proposition 1. *Let γ be a unit speed curve with $\kappa(s) \neq 0$. Then γ is a slant helix if and only if*

$$\sigma(s) = \left(\frac{\kappa^2}{\left(\kappa^2 + \tau^2\right)^{3/2}}\left(\frac{\tau}{\kappa}\right)'\right)(s)$$

is a constant function where, σ is geodesic curvature of the normal indicatrix of the curve.

Moreover, in recent years, some mathematicians characterized the slant helices in terms of curvatures of the curve, see [1, 6, 13]. In [6], the proper slant helices characterized by following:

Theorem 1. *A unit–speed Frenet curve $\alpha(s) : I \to \mathbb{E}^3$ with Frenet–Serret apparatus $\{\kappa, \tau, \boldsymbol{t}, \boldsymbol{n}, \boldsymbol{b}\}$ is a proper slant helix if and only if $(\tau/\kappa)(s) = f(s)/\sqrt{1 - f^2(s)}$, where $f(s) = c\int \kappa ds$ with nonzero constant c.*

Also, the following result given in [6]:

Corollary 1. *A unit speed Frenet curve $\alpha(s) : I \to \mathbb{E}^3$ with curvature $\kappa = 1$ is a Salkowski curve if and only if its torsion is of the form*

$$\tau(s) = \frac{cs}{\sqrt{1 - c^2 s^2}},$$

where c is a nonzero constant.

Now we make a brief introduction to the concepts that related to the kinematics, in the light of [2] and [20].

2.1. **Osculating helix.**

Definition 1. *For any given regular arc-length parameterized space curve α with non-vanishing curvature and torsion; there exits a circular helix $\overline{\alpha}$ such that accompanying corresponding to each points of $\alpha(s_0)$ with the same curvature and torsion at that point, i.e. $\overline{\kappa}(s_0) = \kappa(s_0)$ and $\overline{\tau}(s_0) = \tau(s_0)$. The circular helix $\overline{\alpha}$ is called the osculating helix to the curve α and has the same Frenet frame as α at $\alpha(s_0)$.*

Notice that, the order of contact of $\overline{\alpha}$ and α at any point is at least two, see [21]. Moreover, the axis of the osculating helix intersects the principal normal $\boldsymbol{n}(s_0)$ of α orthogonally, at a distance of $r(s_0)$ from the corresponding point $\alpha(s_0)$. Therefore, the axis of the osculating helix of $\overline{\alpha}(s_0)$ corresponding to the point $\alpha(s_0)$ is given by

$$\boldsymbol{a}(s_0) = \alpha(s_0) + r(s_0)\,\boldsymbol{n}(s_0), \tag{1}$$

where r is the radius of the osculating helix at $\alpha(s_0)$. Here

$$r(s) = \kappa(s) / \left(\kappa^2(s) + \tau^2(s)\right),$$

where $\kappa(s)$ and $\tau(s)$ are the curvature, and the torsion function of α, respectively. The axis $\boldsymbol{a}$ is can be called as axial curve. We note that this axis corresponds to the base curve of fixed axode of any Frenet-Serret motion along α, see [20].

It can be observed from Eq. (1) that r is constant and $\boldsymbol{a}$ is the Mannheim mate of α when α is a Mannheim curve. Furthermore, the following proposition can be given:

Proposition 2. *The tangent vector field of* $\boldsymbol{a}$ *is parallel to the Darboux vector at the corresponding point of the curve* α *if and only if* α *is a Mannheim curve.*

Proof. Let the tangent vector field of $\boldsymbol{a}$ be parallel to the Darboux vector of α, i.e. $\boldsymbol{a}'(s) = \lambda(\tau\,\boldsymbol{t} + \kappa\boldsymbol{b})(s)$, where λ is constant and $\boldsymbol{a}'(s) = (d\boldsymbol{a}/ds)(s)$. From Eq. (1) we have

$$\boldsymbol{a}'(s) = (1 - r(s)\kappa(s))\,\boldsymbol{t}(s) + r'(s)\boldsymbol{n}(s) + r(s)\,\tau(s)\,\boldsymbol{b}(s).$$

Therefore,

$$\lambda(\tau\,\boldsymbol{t} + \kappa\boldsymbol{b})(s) = (1 - r(s)\,\kappa(s))\,\boldsymbol{t}(s) + r'(s)\,\boldsymbol{n}(s) + r(s)\,\tau(s)\,\boldsymbol{b}(s). \qquad (2)$$

From Eq. (2) we obtain $r'(s) = 0$ and $\frac{\tau(s)}{1 - r(s)\kappa(s)} = \frac{\kappa(s)}{r(s)\tau(s)}$. Hence,

$$r(s) = \kappa(s) / \left(\kappa^2(s) + \tau^2(s)\right)$$

is constant and α is a Mannheim curve. Conversely, if α is a Mannheim curve, then r is constant, and $\boldsymbol{a}'(s) = (1 - r\kappa(s))\,\boldsymbol{t}(s) + r\tau(s)\,\boldsymbol{b}(s)$. Since

$$r = \kappa(s) / \left(\kappa^2(s) + \tau^2(s)\right),$$

we obtain,

$$\frac{1 - r\kappa(s)}{r\tau(s)} = \frac{1 - \frac{\kappa^2(s)}{\kappa^2(s) + \tau^2(s)}}{\frac{\kappa(s)\tau(s)}{\kappa^2(s) + \tau^2(s)}} = \frac{\tau(s)}{\kappa(s)},$$

which requires the tangent vector field of $\boldsymbol{a}$ parallel to the Darboux vector of α. □

Any circular helix is determined by its pitch function $p(s)$ and the radius function $r(s)$ of the cylinder on which it lies where, $p(s) = \tau(s) / \left(\kappa^2(s) + \tau^2(s)\right)$ and $r(s) = \kappa(s) / \left(\kappa^2(s) + \tau^2(s)\right)$. Osculating helix is also determined by the functions $p(s)$ and $r(s)$. By the help of this idea, the pitch and radius functions of any space curve can be defined. Notice that, for circular helix, both radius and pitch function are constant, and Mannheim curves have constant radius function. The pitch function confront in the kinematics, in particular, in persistent rigid body motions. It is well-known that, Frenet-Serret motions are persistent along space curve $\alpha(s) : I \to \mathbb{E}^n$ if and only if the pitch function of the curve is constant for all $s \in I$, see [20].

Remark 1. *The pitch function of space curves corresponds to the distribution parameter of the ruled surfaces whose rulings are the normal vector of the base curve.*

Curves with constant pitch function are called as *constant pitch curve* in [2]. Constant pitch curves can be seen as one dimensional realisations of persistent sub-manifolds. The curvature and torsion functions of this curve can be given by

$$\kappa(\theta) = \frac{1}{2p}\cos\theta; \qquad \tau(\theta) = \frac{1}{2p}(1+\sin\theta),$$

where θ is the parameter and $p = \tau(\theta) / \left(\kappa^2(\theta) + \tau^2(\theta)\right)$ is constant. The curvature and torsion functions can also be parameterized by the rational functions,

$$\kappa(s) = \frac{1-s^2}{2p(1+s^2)}; \qquad \tau(s) = \frac{(1+s)^2}{2p(1+s^2)}.$$

see [20].

2.2. **Fixed axode.** In [20], the fixed axode of a Frenet-Serret motion is given by

$$\boldsymbol{a}(s,\lambda) = \alpha(s) + \frac{\kappa(s)}{\kappa^2(s)+\tau^2(s)}\boldsymbol{n}(s) + \lambda\boldsymbol{w}(s), \tag{3}$$

where $\boldsymbol{w}$ is the Darboux vector and $\boldsymbol{n}$ is the principal normal of α. It is obvious that $\boldsymbol{a}$ is a ruled surface with base curve $\alpha(s) + \left(\kappa(s)/\left(\kappa^2(s)+\tau^2(s)\right)\right)\boldsymbol{n}(s)$ and rulings $\boldsymbol{w}(s)$. As stated in [20], $\boldsymbol{a}(s,\lambda)$ is not developable in general. On the other hand, we give the elementary proof of the following proposition:

Proposition 3. *Assume that γ is a unit speed curve and $\overline{\boldsymbol{w}}$ is the unit Darboux vector of γ. The ruled surface*

$$\overline{\boldsymbol{a}}(s,\lambda) = \gamma(s) + \frac{\kappa(s)}{\kappa^2(s)+\tau^2(s)}\boldsymbol{n}(s) + \lambda\overline{\boldsymbol{w}}(s)$$

is developable if and only if γ is a Mannheim curve.

Proof. Let $\overline{\boldsymbol{a}}$ be a developable surface. Any ruled surface in Euclidean space is developable if the distribution parameter of this surface vanishes. Moreover, the distribution parameter of ruled surface $\overline{\boldsymbol{a}}(s,\lambda)$ is given by

$$P = \frac{\det\left(\Delta'(s), \overline{\boldsymbol{w}}(s), \overline{\boldsymbol{w}}'(s)\right)}{\overline{\boldsymbol{w}}'(s)\cdot\overline{\boldsymbol{w}}'(s)},$$

where $\Delta(s) = \gamma(s) + r(s)\boldsymbol{n}(s)$ with $r(s) = \kappa(s)/\left(\kappa^2(s)+\tau^2(s)\right)$. Since γ is a unit speed curve and $\overline{\boldsymbol{w}}(s) = \frac{1}{\sqrt{\kappa^2(s)+\tau^2(s)}}\left(\tau(s)\boldsymbol{t}(s) + \kappa(s)\boldsymbol{b}(s)\right)$, we have $\Delta'(s) = (1 - r(s)\kappa(s))\boldsymbol{t}(s) + r'(s)\boldsymbol{n}(s) + r(s)\tau(s)\boldsymbol{b}(s)$ and

$$\overline{\boldsymbol{w}}'(s) = \left(\frac{\tau(s)}{\sqrt{\kappa^2(s)+\tau^2(s)}}\right)'\boldsymbol{t}(s) + \left(\frac{\kappa(s)}{\sqrt{\kappa^2(s)+\tau^2(s)}}\right)'\boldsymbol{b}(s).$$

By straightforward calculations we obtain

$$\Delta'(s) \times \overline{\boldsymbol{w}}(s) = \frac{1}{\sqrt{\kappa^2(s)+\tau^2(s)}} \left\{ r'(s)\kappa(s)\boldsymbol{t}(s) + \left[r(s)\left(\kappa^2(s)+\tau^2(s)\right) - \kappa(s) \right] \boldsymbol{n}(s) - r'(s)\tau(s)\boldsymbol{b}(s) \right\}.$$

Therefore we have

$$(\Delta'(s) \times \overline{\boldsymbol{w}}(s)) \cdot \overline{\boldsymbol{w}}'(s) = \frac{r'(s)}{\sqrt{\kappa^2(s)+\tau^2(s)}} \left(\kappa(s) \left(\frac{\tau(s)}{\sqrt{\kappa^2(s)+\tau^2(s)}} \right)' - \tau(s) \left(\frac{\kappa(s)}{\sqrt{\kappa^2(s)+\tau^2(s)}} \right)' \right).$$

Since $\det(\Delta'(s), \overline{\boldsymbol{w}}(s), \overline{\boldsymbol{w}}'(s)) = (\Delta'(s) \times \overline{\boldsymbol{w}}(s)) \cdot \overline{\boldsymbol{w}}'(s)$, the distribution parameter of $\overline{\boldsymbol{a}}$ is as follows:

$$P = \frac{(\Delta'(s) \times \overline{\boldsymbol{w}}(s)) \cdot \overline{\boldsymbol{w}}'(s)}{\overline{\boldsymbol{w}}'(s) \cdot \overline{\boldsymbol{w}}'(s)} = \frac{\frac{r'(s)}{\sqrt{\kappa^2(s)+\tau^2(s)}} \left(\kappa(s) \left(\frac{\tau(s)}{\sqrt{\kappa^2(s)+\tau^2(s)}} \right)' - \tau(s) \left(\frac{\kappa(s)}{\sqrt{\kappa^2(s)+\tau^2(s)}} \right)' \right)}{\left\{ \left(\frac{\kappa(s)}{\sqrt{\kappa^2(s)+\tau^2(s)}} \right)' \right\}^2 + \left\{ \left(\frac{\tau(s)}{\sqrt{\kappa^2(s)+\tau^2(s)}} \right)' \right\}^2}. \tag{4}$$

From Eq. (4), only $r'(s) = 0$ gives the solution. Hence, $r = \kappa(s)/(\kappa^2(s) + \tau^2(s))$ is constant and γ is a Mannheim curve. Conversely, $r = \kappa(s)/\left(\kappa^2(s) + \tau^2(s)\right)$ is constant when γ is a Mannheim curve. Since $\Delta'(s) = (1 - r\kappa(s))\boldsymbol{t}(s) + r\tau(s)\boldsymbol{b}(s)$ and $\overline{\boldsymbol{w}}(s) = \frac{1}{\sqrt{\kappa^2(s)+\tau^2(s)}}(\tau(s)\boldsymbol{t}(s) + \kappa(s)\boldsymbol{b}(s))$,

$$\begin{aligned} \Delta'(s) \times \overline{\boldsymbol{w}}(s) &= [(1 - r\kappa(s))\boldsymbol{t}(s) + r\tau(s)\boldsymbol{b}(s)] \times \frac{1}{\sqrt{\kappa^2(s)+\tau^2(s)}}(\tau(s)\boldsymbol{t}(s) + \kappa(s)\boldsymbol{b}(s)) \\ &= \frac{1}{\sqrt{\kappa^2(s)+\tau^2(s)}}\left[(1 - r\kappa(s))\kappa(s)(-\boldsymbol{n}(s)) + r\tau^2(s)\boldsymbol{n}(s)\right] \end{aligned}$$

which requires $\Delta'(s) \times \overline{\boldsymbol{w}}(s) = 0$ and $P = 0$. Therefore, $\overline{\boldsymbol{a}}$ is developable. □

3. Geometric Properties of Transformation

3.1. **Fundamentals.** In the light of the ideas at previous section, we introduce a nonlinear transformation between space curves which preserves ratio of curvature and torsion of a given curve.

Definition 2. *Let α and $\overline{\alpha} : I \to \mathbb{E}^3$ be non-degenerate curves with curvature pair (κ, τ) and $(\overline{\kappa}, \overline{\tau})$, respectively. The map $\mathfrak{s} : \alpha \to \overline{\alpha}$, $(\kappa, \tau) \to (\overline{\kappa}, \overline{\tau})$ is called as slope preserving transformation ($\mathcal{SPT}$) such that the curvatures of $\overline{\alpha}$ are given by*

$$\overline{\kappa}(s) = \frac{\kappa(s)}{\kappa^2(s) + \tau^2(s)}; \quad \overline{\tau}(s) = \frac{\tau(s)}{\kappa^2(s) + \tau^2(s)},$$

where s is the arc-length parameter of α. Here α and $\overline{\alpha}$ are called as base curve and image curve of $\mathfrak{s}$, respectively and $(\alpha, \overline{\alpha})$ is called as $\mathcal{SPT}$ pair.

Definition of $\mathcal{SPT}$ requires $\overline{\tau}/\overline{\kappa} = \tau/\kappa$, and this explains why we called the transformation of $\mathfrak{s}$ as $\mathcal{SPT}$. Notice that, the curvature and torsion of the image curve correspond to the radius and pitch functions of the osculating helix of the base curve, respectively. It is easy to see that $\mathfrak{s}$ fixes $\left(\kappa(s)/\sqrt{\kappa^2(s)+\tau^2(s)}, \tau(s)/\sqrt{\kappa^2(s)+\tau^2(s)}\right)$. Also, the *Darboux* vectors of the $\mathcal{SPT}$ *pair* satisfy $|\boldsymbol{w}(s)|\,|\overline{\boldsymbol{w}}(s)| = 1$ i.e.,

$$\left(\kappa^2(s)+\tau^2(s)\right)\left(\overline{\kappa}^2(s)+\overline{\tau}^2(s)\right) = 1.$$

Remark 2. *The image curve has constant curvature (resp. constant torsion) when the base curve is Mannheim curve (resp. constant pitch curve).*

Remark 3. *It is also possible to define $\mathcal{SPT}$ between planar curves. Since $\tau = 0$ for planar curves, $\mathfrak{s}(\kappa(s), 0) = (1/\kappa(s), 0)$, where $\kappa(s) \neq 0$ for all $s \in I$. Therefore, $\mathcal{SPT}$ maps curvature κ to the radius of curvature of planar curves. On the other hand, because of the curvatures vanish, $\mathcal{SPT}$ is not defined for the lines. Hence, $\mathfrak{s}$ is not linear but some curves and some of geometric properties remain invariant under $\mathcal{SPT}$ as we show in the next.*

Now, we obtain a relation between the osculating helix of the image curve and the curvatures of the base curve.

Let $\mathfrak{s} : \alpha \to \overline{\alpha}$ be an $\mathcal{SPT}$, and $(\kappa_\alpha, \tau_\alpha)$ and $(\kappa_{\overline{\alpha}}, \tau_{\overline{\alpha}})$ be the curvature pairs of α and $\overline{\alpha}$ respectively. Let γ be an osculating helix of the image curve $\overline{\alpha}$. In this case, the *pitch function* $p_\gamma^{\overline{\alpha}}$ and *radius function* $r_\gamma^{\overline{\alpha}}$ of γ are given by

$$p_\gamma^{\overline{\alpha}} = \frac{\tau_{\overline{\alpha}}}{\kappa_{\overline{\alpha}}^2 + \tau_{\overline{\alpha}}{}^2} = \frac{\frac{\tau_\alpha}{\kappa_\alpha^2+\tau_\alpha^2}}{\left(\frac{\kappa_\alpha}{\kappa_\alpha^2+\tau_\alpha^2}\right)^2 + \left(\frac{\tau_\alpha}{\kappa_\alpha^2+\tau_\alpha^2}\right)^2} = \tau_\alpha,$$

and

$$r_\gamma^{\overline{\alpha}} = \frac{\kappa_{\overline{\alpha}}}{\kappa_{\overline{\alpha}}^2 + \tau_{\overline{\alpha}}{}^2} = \frac{\frac{\kappa_\alpha}{\kappa_\alpha^2+\tau_\alpha^2}}{\left(\frac{\kappa_\alpha}{\kappa_\alpha^2+\tau_\alpha^2}\right)^2 + \left(\frac{\tau_\alpha}{\kappa_\alpha^2+\tau_\alpha^2}\right)^2} = \kappa_\alpha.$$

Hence, the radius function of osculating helix of the image curve is constant if and only if either the base curve has constant curvature or the image curve is Mannheim curve. On the other hand, the pitch function of osculating helix of the image curve is constant if and only if either the base curve has constant torsion or the image curve is constant pitch curve. Also, the radius function or the pitch function of osculating helix of the *base curve* remain invariant under $\mathcal{SPT}$ if and only if $|\boldsymbol{w}(s)| = 1$, where $\boldsymbol{w}$ is the Darboux vector of the base curve.

The following theorem characterizes the algebraic structure of $\mathcal{SPT}$ with respect to composition of functions.

Theorem 2. *Let α and $\overline{\alpha} : I \to \mathbb{E}^3$ be non-degenerate curves, and $\mathfrak{s} : \alpha \to \overline{\alpha}$ be an $\mathcal{SPT}$. Then the followings are hold:*

(1) $\mathfrak{s}$ is $1-1$ and $\mathfrak{s}^{-1}$ is an $\mathcal{SPT}$.

(2) $\mathfrak{s}(\lambda\kappa(s), \lambda\tau(s)) = \dfrac{1}{\lambda}\mathfrak{s}(\kappa(s), \tau(s))$, where λ is nonzero constant.

(3) $\mathcal{S} = \langle\mathfrak{s}\rangle$ is a cyclic group of order 2 with respect to composition of functions.

Proof. Let $(\alpha, \overline{\alpha})$ and $(\beta, \overline{\beta})$ be an $\mathcal{SPT}$ *pair,* and $\kappa_{\overline{\alpha}} = \kappa_{\overline{\beta}}$, $\tau_{\overline{\alpha}} = \tau_{\overline{\beta}}$. Since $\mathcal{SPT}$ preserves ratio of curvatures of the base curve, we have $\tau_\beta/\tau_\alpha = \kappa_\beta/\kappa_\alpha$. The assumption and the identity of $|\boldsymbol{w}(s)|\,|\overline{\boldsymbol{w}}(s)| = 1$ requires

$$\frac{\kappa_{\overline{\alpha}}^2 + \tau_{\overline{\alpha}}^2}{\kappa_{\overline{\beta}}^2 + \tau_{\overline{\beta}}^2} = \frac{\tau_{\overline{\alpha}}/\tau_\alpha}{\tau_{\overline{\beta}}/\tau_\beta} = \frac{\tau_\beta}{\tau_\alpha} = \frac{\kappa_\beta}{\kappa_\alpha} = 1.$$

Hence, we have $\kappa_\alpha = \kappa_\beta$, $\tau_\alpha = \tau_\beta$ and $\mathfrak{s}$ is $1-1$. Moreover, for all non-degenerate image curves, up to fundamental theorem of the local theory of the curves, there exists only one base curve. Therefore, $\mathfrak{s}$ is surjective. Now fix $\mathfrak{s}^{-1} = \mathfrak{s}^\star$ and $\mathfrak{s}^\star(\kappa, \tau) = (\kappa^\star, \tau^\star)$. Since $\mathfrak{s} \circ \mathfrak{s}^\star = I$, we have $(\mathfrak{s} \circ \mathfrak{s}^\star)(\kappa, \tau) = \mathfrak{s}(\kappa^\star, \tau^\star) = (\kappa, \tau)$, where "$\circ$" represents the composition of functions. Since

$$\mathfrak{s}(\kappa^\star, \tau^\star) = \left(\frac{\kappa^\star}{(\kappa^\star)^2 + (\tau^\star)^2}, \frac{\tau^\star}{(\kappa^\star)^2 + (\tau^\star)^2}\right),$$

we obtain

$$\kappa = \frac{\kappa^\star}{(\kappa^\star)^2 + (\tau^\star)^2}\ ;\ \tau = \frac{\tau^\star}{(\kappa^\star)^2 + (\tau^\star)^2}. \tag{5}$$

It follows from Eq. (5) that, $|\boldsymbol{w}|\,|\boldsymbol{w}^\star| = 1$. So, we have $\kappa^\star = \kappa/\left(\kappa^2 + \tau^2\right)$ and $\tau^\star = \tau/\left(\kappa^2 + \tau^2\right)$. Hence, $\mathfrak{s}^\star(\kappa, \tau) = (\kappa^\star, \tau^\star) = \left(\kappa/\left(\kappa^2 + \tau^2\right), \tau/\left(\kappa^2 + \tau^2\right)\right)$ which proves that $\mathfrak{s}^\star = \mathfrak{s}^{-1}$ is also $\mathcal{SPT}$. The rest of the proof is obvious. □

Remark 4. *In Theorem 2, we observe that*

$$s^2\ (\kappa, \tau) = s(s(\kappa, \tau)) = s\left(\frac{\kappa}{\kappa^2 + \tau^2}, \frac{\tau}{\kappa^2 + \tau^2}\right) = (\kappa, \tau)$$

which requires $s^2 = I$.

3.2. **Invariants of $\mathcal{SPT}$.** Let us recall the definition of $\mathcal{SPT}$, $\mathfrak{s} : (\kappa, \tau) \to (\overline{\kappa}, \overline{\tau})$. The identity of $\overline{\tau}/\overline{\kappa} = \tau/\kappa$ requires that the base curve remain invariant under the $\mathcal{SPT}$ when the base curve characterized by ratio of curvature and torsion, and arc-length parameters of the curves are common. Such as, helices and rectifying curves transform to helices and rectifying curves under the $\mathcal{SPT}$, respectively. Furthermore, the base curve remains invariant when the curvatures of the curve satisfy $\kappa^2(s) + \tau^2(s) = 1$. For example, the curve with curvature $\kappa(s) = \sin\varphi(s)$ and torsion $\tau(s) = \cos\varphi(s)$ remains invariant under the $\mathcal{SPT}$. Besides, constant precession curve has the curvatures of $\kappa(s) = w\sin(\mu s)$ and $\tau(s) = w\cos(\mu s)$, where $w > 0$ and μ are constant. Under the $\mathcal{SPT}$, these curvatures transform to $\overline{\kappa} = (1/w)\sin(\mu s)$ and $\overline{\tau} = (1/w)\cos(\mu s)$ which requires the image curve is also constant precession curve. Hence, constant precession curve remains invariant under the $\mathcal{SPT}$.

Let $(\alpha, \overline{\alpha})$ be an $\mathcal{SPT}$ pair. Respectively the curvature and the torsion of the tangent indicatrix of α is given by $\kappa_{\boldsymbol{\alpha}}^{\boldsymbol{t}}(s) = \sqrt{1+f^2(s)}$ and $\tau_{\boldsymbol{\alpha}}^{\boldsymbol{t}}(s) = \sigma(s)\sqrt{1+f^2(s)}$, where $f(s) = (\tau/\kappa)(s)$ and $\sigma(s)$ is the geodesic curvature of the normal indicatrix of α. Since $\mathcal{SPT}$ preserves the ratio of τ/κ, we obtain $\kappa_{\overline{\alpha}}^{\overline{\boldsymbol{t}}}(s) = \kappa_{\alpha}^{\boldsymbol{t}}(s)$. Therefore, curvature of the tangent indicatrix remains invariant under the $\mathcal{SPT}$. On the other hand, $\tau_{\boldsymbol{\alpha}}^{\boldsymbol{t}}(s) = \sigma(s)\sqrt{1+f^2(s)} = f'(s)/\left(\kappa(s)\left(1+f^2(s)\right)\right)$. Therefore, torsion of the tangent indicatrix of the curve remains invariant under $\mathcal{SPT}$ if and only if $\kappa(s) = \overline{\kappa}(s)$ or $|\boldsymbol{w}(s)| = 1$.

It is well known that the curvatures of slant helices can be given by $\kappa(s) = (1/m)\varphi'(s)\cos\varphi(s)$ and $\tau(s) = (1/m)\varphi'(s)\sin\varphi(s)$, where φ is a differentiable function of s and $m = \cot\theta \neq 0$ is a constant, see [13]. Depends on intrinsic equations of slant helices, we give the following theorem:

Theorem 3. *The proper slant helices remain invariant under the $\mathcal{SPT}$ if and only if φ is a linear function of arc-length parameter of the curve.*

Proof. Let the $\mathcal{SPT}$ leaves the slant helices invariant, that is, both base curve and image curve be a *proper* slant helix. The curvatures of the base curve are given by $\kappa(s) = (1/m)\varphi'(s)\cos\varphi(s)$, and $\tau(s) = (1/m)\varphi'(s)\sin\varphi(s)$, where m is nonzero constant. By definition of $\mathcal{SPT}$ we obtain $(\overline{\tau}/\overline{\kappa})(s) = (\tau/\kappa)(s) = \tan\varphi(s)$ and $\overline{\kappa}(s) = m\cos\varphi(s)/\varphi'(s)$. The geodesic curvature of the normal indicatrix of $\overline{\alpha}$ as follows:

$$\overline{\sigma} = \left(\frac{1}{\overline{\kappa}\left(1+\left(\frac{\overline{\tau}}{\overline{\kappa}}\right)^2\right)^{3/2}}\left(\frac{\overline{\tau}}{\overline{\kappa}}\right)'\right)(s) = \frac{\varphi'(s)}{m}.$$

Since $\overline{\sigma}$ is constant, φ is a linear function of s. Conversely, if φ is a linear function of s, it is enough to prove that $\overline{\alpha}$ is a slant helix when α is a slant helix and $\mathfrak{s} : \alpha \to \overline{\alpha}$ is an $\mathcal{SPT}$. From the assumption, we find $\varphi' = c$, and $\kappa(s) = a\cos\varphi(s)$, $\tau(s) = a\sin\varphi(s)$, where both c and $a = c/m$ are constant. It follows from $\overline{\kappa}(s) = \kappa(s)/\left(\kappa^2(s)+\tau^2(s)\right) = \cos\varphi(s)/a$ and $(\overline{\tau}/\overline{\kappa})(s) = (\tau/\kappa)(s) = \tan\varphi(s)$ that

$$\overline{\sigma}(s) = \left(\frac{1}{\overline{\kappa}\left(1+\left(\frac{\overline{\tau}}{\overline{\kappa}}\right)^2\right)^{3/2}}\left(\frac{\overline{\tau}}{\overline{\kappa}}\right)'\right)(s) = a,$$

which is constant. Hence, under the $\mathcal{SPT}$*,* the image curve is also slant helix and this completes the proof. □

Corollary 2. *The proper slant helix α remains invariant under the $\mathcal{SPT}$ if and only if α is a constant precession curve.*

3.3. **Bertrand and Mannheim curves.** Let $\alpha : I \to \mathbb{E}^3$ be a parameterized regular curve (not necessarily by arc length) with $\kappa(t) \neq 0$, $\tau(t) \neq 0$, $t \in I$. The curve α is called a *Bertrand curve* if there exits a curve $\alpha^* : I \to \mathbb{E}^3$ such that the normal lines of α and α^* at $t \in I$ are equal. In this case, α^* called a *Bertrand mate* of α, and we can write

$$\alpha^*(t) = \alpha(t) + \lambda \boldsymbol{n}(t). \tag{6}$$

Notice that λ is constant in Eq. (6). Moreover, α is a Bertrand curve if and only if there exits a linear relation $A\kappa(t) + B\tau(t) = 1$, $t \in I$,where A, B are nonzero constants and κ and τ are the curvature and torsion of α, respectively [5]. On the other hand, if $\alpha : I \to \mathbb{E}^3$ is a non-degenerate curve with the arc-length parameter, then $B\kappa(s) - A\tau(s) \neq 0$ for all $s \in I$. Furthermore, the curvature κ^* and the torsion τ^* of α^* are given by

$$\kappa^*(s) = \frac{|B\kappa(s) - A\tau(s)|}{(A^2 + B^2)\,|\tau(s)|}; \quad \tau^*(s) = \frac{1}{(A^2 + B^2)\,\tau(s)}. \tag{7}$$

see [8].

Let $\alpha : I \to \mathbb{E}^3$ be a unit speed Bertrand curve, α^* be a Bertrand mate of α, and $\mathfrak{s} : \alpha \to \alpha^*$ be an $\mathcal{SPT}$ *in Euclidean space* $\mathbb{E}^3$. It follows from $\tau^*(s) = \tau(s) / \left(\kappa^2(s) + \tau^2(s)\right)$, $A\kappa(s) + B\tau(s) = 1$ and Eq. (7) that,

$$\frac{\kappa}{\tau} = \pm\sqrt{A^2 + B^2 - 1}. \tag{8}$$

Here we assume that $A^2 + B^2 > 1$. Otherwise, we can't find the curvatures of the curve. From Eq. (8) and $A\kappa(s) + B\tau(s) = 1$, we obtain both the curvature κ and the torsion τ are constant. Therefore, both α and α^* are circular helix. Consequently, if α and α^* are Bertrand curves under $\mathcal{SPT}$*, then both* α and α^* are circular helix. In fact, there is no non-degenerate Bertrand curves with respect to $\mathcal{SPT}$. Assume that $(\alpha, \widehat{\alpha})$ is a Mannheim pair under the $\mathcal{SPT}$ i.e., α is a Mannheim curve and $\widehat{\alpha}$ is Mannheim mate of α when $\mathfrak{s} : \alpha \to \widehat{\alpha}$ is an $\mathcal{SPT}$, in Euclidean space $\mathbb{E}^3$. It is well-known that if Mannheim curve is a generalized helix, then Mannheim mate is a straight line, see [12]. From the definition of Mannheim curve and $\mathcal{SPT}$, the curvature of the image curve is obtained as $\widehat{\kappa}(s) = \kappa(s) / \left(\kappa^2(s) + \tau^2(s)\right) = \lambda$ which is constant. It follows from $\widehat{\tau}(s) = \tau(s) / \left(\kappa^2(s) + \tau^2(s)\right) = \left(\kappa^2(s) + \tau^2(s)\right) / \tau(s)$ that, the torsion of the image curve $\widehat{\tau} = \pm 1$ is also constant, i.e., Mannheim mate is circular helix. In this case, curvatures of Mannheim curve satisfy $\tau(s) = \pm(\kappa^2(s) + \tau^2(s))$. Furthermore, $\lambda = \kappa(s) / \left(\kappa^2(s) + \tau^2(s)\right)$ is constant. Hence, curvatures of the base curve satisfy $\tau/\kappa = \pm 1/\lambda$ which is constant. The last equality requires that the base curve (Mannheim curve) is generalized helix which is contradiction. Consequently, there is no suitable Mannheim pair with respect to $\mathcal{SPT}$ in Euclidean space $\mathbb{E}^3$. Therefore, we will consider only Mannheim curve (with its curvature and torsion), not the Mannheim pairs, under the $\mathcal{SPT}$ in the next.

4. Associated Curves of $\mathcal{SPT}$

4.1. **Slant helices.**

Proposition 4. *Let* $\mathfrak{s} : \alpha \to \overline{\alpha}$ *be an* $\mathcal{SPT}$ *in Euclidean space* $\mathbb{E}^3$*, and the normal vector of* $\overline{\alpha}$ *makes constant angle with a fixed line. Then* α *is a Mannheim curve with non-constant slope if and only if* $\overline{\alpha}$ *is a Salkowski curve.*

Proof. Let α be a Mannheim curve with non-constant slope. Since α is a Mannheim curve, $\overline{\kappa}(s) = \kappa(s) / \left(\kappa^2(s) + \tau^2(s)\right) = \lambda$ is constant. Because of $(\tau/\kappa)'(s) \neq 0$,

$$\overline{\tau}(s) = \frac{\tau(s)}{\kappa^2(s) + \tau^2(s)} = \frac{\lambda\tau(s)}{\kappa(s)}$$

is non-constant. From the assumption, and up to rigid movements or up to the antipodal map, $\overline{\alpha}$ is a Salkowski curve. Conversely, if $\overline{\alpha}$ is a Salkowski curve, then $\overline{\kappa}(s) = \kappa(s) / \left(\kappa^2(s) + \tau^2(s)\right)$ is constant and $\overline{\tau}(s)$ is non-constant. This completes the proof. □

Corollary 3. *Let* $\mathfrak{s} : \alpha \to \overline{\alpha}$ *be an* $\mathcal{SPT}$ *in Euclidean space* $\mathbb{E}^3$*, and the normal vector of* $\overline{\alpha}$ *makes constant angle with a fixed line. Then* α *is a constant pitch curve with non-constant slope if and only if* $\overline{\alpha}$ *is an anti-Salkowski curve.*

Theorem 4. *Let* $\mathfrak{s} : \alpha \to \overline{\alpha}$ *be an* $\mathcal{SPT}$ *in Euclidean space* $\mathbb{E}^3$*. If* α *is a Salkowski curve, then the followings are hold:*

(1) $\overline{\alpha}$ is a Mannheim curve.

(2) The curvatures of Mannheim mate of $\overline{\alpha}$ satisfy

$$\widetilde{\kappa}(s)\,\widetilde{\tau}(s) \mp c\left(1 + \widetilde{\tau}^2(s)\right) = 0,$$

where $\widetilde{\kappa}$ and $\widetilde{\tau}$ are the curvature and torsion of the Mannheim mate $\widetilde{\alpha}$ respectively, and c is a nonzero constant.

Proof. Let α be a Salkowski curve and $\overline{\alpha}$ be an image curve with respect to $\mathcal{SPT}$. Since the base curve is Salkowski curve, the curvature of α is constant but its torsion is non-constant. Without loss of generality, we can assume $\kappa \equiv 1$. From Corollary 1, the torsion of the base curve is given by $\tau(s) = cs/\sqrt{1 - c^2 s^2}$, where c is a nonzero constant. Since $\overline{\alpha}$ is an image curve with respect to $\mathcal{SPT}$, the curvatures of this curve satisfy

$$\frac{\overline{\kappa}(s)}{\overline{\kappa}^2(s) + \overline{\tau}^2(s)} = \frac{\frac{\kappa(s)}{\kappa^2(s)+\tau^2(s)}}{\left(\frac{\kappa(s)}{\kappa^2(s)+\tau^2(s)}\right)^2 + \left(\frac{\tau(s)}{\kappa^2(s)+\tau^2(s)}\right)^2} = \kappa = 1.$$

Hence, $\overline{\alpha}$ is a Mannheim curve. Respectively, the curvature and torsion of $\overline{\alpha}$ are given by

$$\overline{\kappa}(s) = \frac{\kappa(s)}{\kappa^2(s) + \tau^2(s)} = \frac{1}{1 + \frac{c^2 s^2}{1 - c^2 s^2}} = 1 - c^2 s^2,$$

and

$$\overline{\tau}(s)=\frac{\tau(s)}{\kappa^2(s)+\tau^2(s)}=\frac{\frac{cs}{\sqrt{1-c^2s^2}}}{1+\frac{c^2s^2}{1-c^2s^2}}=cs\sqrt{1-c^2s^2}.$$

Suppose that $\widetilde{\alpha}$ is a Mannheim mate of $\overline{\alpha}$. By straightforward calculations, we find the curvature and the torsion of $\widetilde{\alpha}$ as follow:

$$\widetilde{\kappa}(s)=\frac{\overline{\kappa}(s)\left(\overline{\kappa}(s)\overline{\tau}'(s)-\overline{\kappa}'(s)\overline{\tau}(s)\right)}{|\lambda\overline{\tau}(s)|\left(\overline{\kappa}^2(s)+\overline{\tau}^2(s)\right)^{3/2}}=\mp\frac{1}{s\sqrt{1-c^2s^2}},\tag{9}$$

and

$$\widetilde{\tau}(s)=\frac{\overline{\kappa}^2(s)+\overline{\tau}^2(s)}{\overline{\tau}(s)}=\frac{\sqrt{1-c^2s^2}}{cs}.\tag{10}$$

From Eqs. (9) and (10) we obtain,

$$\frac{\widetilde{\kappa}(s)\widetilde{\tau}(s)}{1+\widetilde{\tau}^2(s)}=\mp c,$$

which completes the proof. □

Proposition 5. *Let $\gamma(s):I\to\mathbb{E}^3$ be a unit-speed Frenet curve with constant torsion $\tau\equiv 1$ and non-constant curvature $\kappa(s)$. If normal vectors of γ make a constant angle with a fixed line, then γ is an anti-Salkowski curve with curvature*

$$\kappa(s)=\frac{|\varphi(s)|}{\sqrt{1-\varphi^2(s)}},$$

where φ is a linear function of arc-lenght parameter of γ.

Proof. Let γ be a curve with constant torsion $\tau\equiv 1$ and non-constant curvature κ. If normal vectors of γ make a constant angle with a fixed line, then γ is an anti-Salkowski curve, see [14]. By Theorem 1 we have

$$\kappa(s)=\frac{\sqrt{1-f^2(s)}}{f(s)},\tag{11}$$

where $f(s)=c\int\kappa ds$ and c is a nonzero constant. Eq. (11) leads to the differential equation

$$f'(s)f(s)-c\sqrt{1-f^2(s)}=0,$$

which has solution

$$f(s)=\mp\sqrt{1-(cs+k)^2},\tag{12}$$

where $k\in\mathbb{R}$. It follows from Eqs. (11) and (12) that, $\kappa(s)=|\varphi(s)|/\sqrt{1-\varphi^2(s)}$, where $\varphi(s)=cs+k$. □

Corollary 4. *Let $\mathfrak{s}:\gamma\to\overline{\gamma}$ be an $\mathcal{SPT}$ in Euclidean space $\mathbb{E}^3$. If γ is an anti-Salkowski curve, then the followings are hold:*

(1) $\overline{\gamma}$ is a constant pitch curve.

(2) The curvatures of $\overline{\gamma}$ are given by

$$\overline{\kappa}(s) = |\varphi(s)| \sqrt{1-\varphi^2(s)}; \qquad \overline{\tau}(s) = 1-\varphi^2(s),$$

where φ is a linear function of arc-lenght parameter of γ.

Now we give the curvatures of a curve that is both a Mannheim curve and a slant helix (shortly Mannheim slant helix) in the following:

Proposition 6. *Let $(\alpha, \widehat{\alpha})$ be a Mannheim pair. If α is a slant helix, then the curvatures of the Mannheim pair as follows:*

$$\kappa(s) = \frac{1}{\lambda} \sec h^2 \varphi(s); \qquad \tau(s) = \frac{1}{\lambda} \sec h\varphi(s) \tanh \varphi(s),$$

and

$$\widehat{\kappa}(s) = \csc h\varphi(s); \qquad \widehat{\tau}(s) = \frac{1}{\lambda} \csc h\varphi(s),$$

where φ is a linear function of arc-lenght parameter of α and λ is nonzero constant.

Proof. Let α be a Mannheim slant helix. The equations $\kappa(s) = \lambda\left(\kappa^2(s) + \tau^2(s)\right)$ and $\sigma(s) = \left(\frac{\kappa^2}{(\kappa^2+\tau^2)^{3/2}}\left(\frac{\tau}{\kappa}\right)'\right)(s)$ leads to the differential equation

$$\sigma(s) = \pm\frac{\lambda}{2}\frac{\kappa'(s)}{\kappa(s)\sqrt{1-\lambda\kappa(s)}}.$$

Since $\sigma = c$ is constant, it follows:

$$\pm\frac{\lambda}{2}\kappa'(s) - c\kappa(s)\sqrt{1-\lambda\kappa(s)} = 0,$$

which has solution $\kappa(s) = \sec h^2\varphi(s)/\lambda$, where $\varphi(s) = \frac{c}{\lambda}s \pm \frac{c_1}{2}$ with $c_1 \in \mathbb{R}$. On the other hand, by Theorem 1 we obtain

$$f(s) = c\int \kappa ds = \tanh\varphi(s) + c_2,$$

where $c_2 \in \mathbb{R}$. Without loss of generality, we can assume that $c_2 = 0$. Hence, we find the torsion of α as

$$\tau(s) = \frac{\kappa(s) f(s)}{\sqrt{1-f^2(s)}} = \frac{1}{\lambda}\sec h\varphi(s)\tanh\varphi(s).$$

Finally, the curvatures of $\widehat{\alpha}$ as follow:

$$\widehat{\kappa}(s) = \frac{\kappa(s)(\kappa(s)\tau'(s) - \kappa'(s)\tau(s))}{|\lambda\tau(s)|\left(\kappa^2(s)+\tau^2(s)\right)^{3/2}} = \frac{1}{\sinh\varphi(s)},$$

and

$$\widehat{\tau}(s) = \frac{\kappa^2(s)+\tau^2(s)}{\tau(s)} = \frac{1}{\lambda\sinh\varphi(s)}.$$

Furthermore, $\widehat{\tau}/\widehat{\kappa} = 1/\lambda$ i.e., $\widehat{\alpha}$ is a generalized helix. The proof is complete. $\square$

Corollary 5. *Let $\mathfrak{s}:\alpha\to\overline{\alpha}$ be an $\mathcal{SPT}$ in Euclidean space $\mathbb{E}^3$. If the base curve is a Mannheim slant helix, then curvature of the normal indicatrix of the image curve is equal to the curvature of the base curve, i.e. $\overline{\sigma}=\kappa$.*

Proof. Let α be a Mannheim slant helix. Since $\kappa(s)=\sec h^2\varphi(s)/\lambda$, $\tau(s)=\sec h\varphi(s)\tanh\varphi(s)/\lambda$, and $\tau/\kappa=\overline{\tau}/\overline{\kappa}$, we obtain

$$\overline{\sigma}(s)=\left(\frac{1}{\overline{\kappa}\left(1+\left(\frac{\tau}{\kappa}\right)^2\right)^{3/2}}\left(\frac{\tau}{\kappa}\right)'\right)(s)=\frac{1}{\overline{\kappa}(s)}\sec h^2\varphi(s).$$

Besides, $\overline{\kappa}(s)=\kappa(s)/\left(\kappa^2(s)+\tau^2(s)\right)=\lambda$. Thus, $\overline{\sigma}(s)=\sec h^2\varphi(s)/\lambda=\kappa(s)$ which is intended. □

Opposite of the Corollary 5 is not true in general, but we have the following result:

Corollary 6. *The ratio of curvatures of the Mannheim slant helix α satisfy $(\tau/\kappa)(s)=\sinh(s+c)$, $c\in\mathbb{R}$ when $\mathfrak{s}:\alpha\to\overline{\alpha}$ is an $\mathcal{SPT}$ and $\overline{\sigma}=\kappa$.*

Proof. Assume that $\mathfrak{s}:\alpha\to\overline{\alpha}$ is an $\mathcal{SPT}$ and $\overline{\sigma}=\kappa$. Then we obtain

$$\frac{\kappa^2(s)}{\kappa^2(s)+\tau^2(s)}=\left(\frac{1}{\left(1+\left(\frac{\tau}{\kappa}\right)^2\right)^{3/2}}\left(\frac{\tau}{\kappa}\right)'\right)(s). \tag{13}$$

By substituting $f(s)=(\tau/\kappa)(s)$ in Eq. (13), it follows:

$$f'(s)-\sqrt{1+f^2(s)}=0,$$

which has solution $f(s)=\sinh(s+c)$, where $c\in\mathbb{R}$. This completes the proof. □

Remark 5. *If α is both a constant pitch curve and a slant helix (shortly constant slant pitch curve), then α has reversed curvatures with respect to Proposition 6, i.e. the curvature and the torsion of α as follows,*

$$\kappa(s)=\frac{1}{\lambda}\sec h\varphi(s)\tanh\varphi(s);\qquad \tau(s)=\frac{1}{\lambda}\sec h^2\varphi(s),$$

where φ is a linear function of arc-length parameter of α. Furthermore, $\overline{\kappa}(s)=\lambda\sinh\varphi(s)$ and $\overline{\tau}$ is constant when the base curve is a constant slant pitch curve.

In the light of Proposition 6, one can consider both Mannheim curve and rectifying curve or namely Mannheim rectifying curve. The curvatures of this curve satisfy both $\kappa(s)/\left(\kappa^2(s)+\tau^2(s)\right)=\lambda$ and $(\tau/\kappa)(s)=\varphi(s)$, where λ is nonzero constant and φ is a linear function of arc-length parameter of the curve. Therefore, we obtain the curvatures of Mannheim rectifying curve as

$$\kappa(s)=\frac{1}{\lambda\left(1+\varphi^2(s)\right)};\qquad \tau(s)=\frac{\varphi(s)}{\lambda\left(1+\varphi^2(s)\right)}.$$

If α is a Mannheim rectifying curve and $\mathfrak{s}:\alpha\rightarrow\overline{\alpha}$ is an $\mathcal{SPT}$, then we find the curvatures of $\overline{\alpha}$ as $\overline{\kappa}=\lambda$ and $\overline{\tau}(s)=\lambda\varphi(s)$. Thus, $\mathcal{SPT}$ maps Mannheim rectifying curve to the rectifying curve, but not to the Mannheim curve.

Remark 6. *We can suggest that $\kappa(s)=\varepsilon\sec h^2\phi(s)$ and $\tau(s)=\varepsilon\sec h\phi(s)\tanh\phi(s)$ for curvatures of Mannheim rectifying curve, where $\varepsilon\in\mathbb{R}$, $\phi(s)=\arcsin h\varphi(s)$ and φ is linear function of arc-length parameter of the curve. These curvatures are similar to the curvatures of the Mannheim slant helix apart from ϕ being non-linear.*

4.2. **Evolute of the image curve and quasi-slant helix.** Let α and $\overline{\alpha}:I\rightarrow\mathbb{E}^3$ be non-degenerate curves. If the tangent vectors of the curves satisfy $\boldsymbol{t}(s)\cdot\overline{\boldsymbol{t}}(s)=0$ for all $s\in I$, then $\overline{\alpha}$ is called as involute of α, and its parametric equation given by

$$\overline{\alpha}(s)=\alpha(s)+(-s+c)\,\boldsymbol{t}(s),$$

where $c\in\mathbb{R}$. In this case, α is called as evolute of $\overline{\alpha}$. The curvatures of $\overline{\alpha}$ can be given by curvatures of α as follows:

$$\overline{\kappa}(s)=\frac{\sqrt{\kappa^2(s)+\tau^2(s)}}{|(-s+c)|\,\kappa(s)};\quad \overline{\tau}(s)=\frac{\kappa(s)\,\tau'(s)-\kappa'(s)\,\tau(s)}{(-s+c)\,\kappa(s)\,(\kappa^2(s)+\tau^2(s))}$$

see [7].

Proposition 7. *Let α and $\overline{\alpha}:I\rightarrow\mathbb{E}^3$ be different non-degenerate curves and $\mathfrak{s}:\alpha\rightarrow\overline{\alpha}$ be an $\mathcal{SPT}$. There is no slant helix as a base curve of $\mathcal{SPT}$ when the image curve is involute of α.*

Proof. Let α be a slant helix and $\overline{\alpha}$ be an involute curve of α. Respectively the curvature and the torsion of the image curve are as follow:

$$\overline{\kappa}(s)=\frac{\sqrt{\kappa^2(s)+\tau^2(s)}}{|(-s+c)|\,\kappa(s)}=\frac{\kappa(s)}{\kappa^2(s)+\tau^2(s)},\tag{14}$$

and

$$\overline{\tau}(s)=\frac{\kappa(s)\,\tau'(s)-\kappa'(s)\,\tau(s)}{(-s+c)\,\kappa(s)\,(\kappa^2(s)+\tau^2(s))}=\frac{\tau(s)}{\kappa^2(s)+\tau^2(s)}.\tag{15}$$

From Eqs. (14) and (15), it follows:

$$\left(\frac{\overline{\tau}}{\overline{\kappa}}\right)(s)=\left(\frac{\tau}{\kappa}\right)(s)=\pm\sigma(s).$$

Since α is a slant helix, $\sigma=\pm\tau/\kappa$ is constant. On the other hand, from Eq. (15) we obtain

$$-s+c=\left(\frac{\tau}{\kappa}\right)'(s)\left(\frac{\kappa}{\tau}\right)(s)=0,$$

which is a contradiction. Therefore, there is no slant helix as a base curve when the image curve is involute curve. □

In accordance with Proposition 7, the following question occurs:

"*Which base curves are the evolute of the image curve with respect to $\mathcal{SPT}$?*"

To answer this question, we define a *new curve* (family) as follows:

Definition 3. *Let $\alpha : I \to \mathbb{E}^3$ be a C^3 space curve with non-constant slope. If the curvatures of α satisfy*

$$\left(\frac{\tau}{\kappa}\right)(s) = \frac{\kappa^2(s)}{\left(\kappa^2(s)+\tau^2(s)\right)^{3/2}}\left(\frac{\tau}{\kappa}\right)'(s), \tag{16}$$

then α is called as quasi-slant helix.

In fact, the definition of quasi-slant helix determines family of curve in Euclidean space. Therefore, one can find different quasi slant helices whose have different intrinsic equations. The following example clarify this case:

Example 1. *Let $\mathcal{Q}$ be the family of quasi-slant helices, and $\alpha : I \to \mathbb{E}^3$ be a C^3 space curve with non-constant slope. The curvatures of $\kappa_\alpha(s) = \cos^2 s/\sin s$ and $\tau_\alpha(s) = \cos s$ satisfy Eq. (16). Therefore $\alpha \in \mathcal{Q}$. Furthermore, the curvatures of α satisfy the following algebraic equation:*

$$\mathcal{P}_\alpha(\kappa_\alpha, \tau_\alpha) = \tau_\alpha^4 + \kappa_\alpha^2\tau_\alpha^2 - \kappa_\alpha^2 = 0.$$

Here we can call $\mathcal{P}_\alpha$ as a curvature polynomial of α. Moreover, the curve $\gamma : I \to \mathbb{E}^3$ with curvatures $\kappa_\gamma(s) = \sec h^2 s \csc hs$ and $\tau_\gamma(s) = \sec h^2 s$ is also quasi-slant helix i.e., $\gamma \in \mathcal{Q}$. This curve has the same slope with Mannheim slant helix (Proposition 6) when $\lambda = 1$ and $\varphi(s) = s$. Furthermore, the curvature polynomial of γ can be given by

$$\mathcal{P}_\gamma(\kappa_\gamma, \tau_\gamma) = \tau_\gamma^3 + \kappa_\gamma^2\tau_\gamma - \kappa_\gamma^2 = 0.$$

One of the rational parameterization of the curvatures of quasi-slant helices can be given by

$$\kappa_\beta(s) = \frac{1}{s^2(s^2-1)} \;;\; \tau_\beta(s) = \frac{1}{s^2\sqrt{s^2-1}},$$

where β is a quasi-slant helix. Hence, the curvature polynomial of β is as follows:

$$\mathcal{P}_\beta(\kappa_\beta, \tau_\beta) = \tau_\beta^4 + \kappa_\beta^2\tau_\beta^2 - \kappa_\beta^3 = 0.$$

The example above obviously shows that we can find different quasi-slant helices whose have different intrinsic equations.

Proposition 8. *Let $\mathfrak{s} : \alpha \to \overline{\alpha}$ be an $\mathcal{SPT}$ in Euclidean space $\mathbb{E}^3$. $\overline{\alpha}$ is an involute of the base curve if and only if α is a quasi-slant helix with curvatures*

$$\kappa(s) = \frac{-s+c}{(1+\xi^2(s))^{3/2}}; \quad \tau(s) = \frac{(-s+c)\xi(s)}{(1+\xi^2(s))^{3/2}},$$

where $\xi(s) = c_1 e^{cs-s^2/2}$ and c, c_1 are constant.

Proof. Let $\overline{\alpha}$ be an involute of α. The curvatures of $\overline{\alpha}$ are given by

$$\overline{\kappa}(s) = \frac{\sqrt{\kappa^2(s)+\tau^2(s)}}{|-s+c|\,\kappa(s)} \;;\; \overline{\tau}(s) = \frac{\kappa(s)\tau'(s)-\kappa'(s)\tau(s)}{(-s+c)\,\kappa(s)\left(\kappa^2(s)+\tau^2(s)\right)}, \tag{17}$$

where c is a constant. By the parameter change, we can assume that $-s+c>0$. From Eq. (17) we obtain

$$\left(\frac{\overline{\tau}}{\overline{\kappa}}\right)(s)=\left(\frac{\tau}{\kappa}\right)(s)=\frac{\kappa(s)\,\tau'(s)-\kappa'(s)\,\tau(s)}{\left(\kappa^2(s)+\tau^2(s)\right)^{3/2}}, \tag{18}$$

which proves that α is a quasi-slant helix. Since $\overline{\kappa}(s)=\kappa(s)/(\kappa^2(s)+\tau^2(s))$, we find

$$(-s+c)\,\kappa^2(s)=\left(\kappa^2(s)+\tau^2(s)\right)^{3/2}. \tag{19}$$

Eq. (18) and $\xi(s)=(\tau/\kappa)(s)$ leads to the differential equation

$$\xi'(s)-(-s+c)\xi(s)=0,$$

which has solution

$$\xi(s)=(\tau/\kappa)(s)=c_1e^{cs-s^2/2}, \tag{20}$$

where $c_1\in\mathbb{R}$. From Eqs. (19) and (20) we obtain the curvatures of α. Conversely, by straightforward calculations we obtain

$$\overline{\kappa}(s)=\kappa(s)/\left(\kappa^2(s)+\tau^2(s)\right)=\frac{\sqrt{1+\xi^2(s)}}{(-s+c)},$$

where $-s+c>0$ and $\xi(s)=(\tau/\kappa)(s)$. Besides,

$$\overline{\tau}(s)=\tau(s)/\left(\kappa^2(s)+\tau^2(s)\right)=\frac{\sqrt{\kappa^2(s)+\tau^2(s)}}{(-s+c)\,\kappa(s)}\frac{\tau(s)}{\kappa(s)}. \tag{21}$$

By substituting $(\tau/\kappa)(s)=\sigma(s)$ in (21) we find

$$\overline{\tau}(s)=\frac{\tau'(s)\kappa(s)-\tau(s)\kappa'(s)}{(-s+c)\,\kappa(s)\,(\kappa^2(s)+\tau^2(s))},$$

which completes the proof. □

Corollary 7. *Let $\mathfrak{s}:\alpha\to\overline{\alpha}$ be an $\mathcal{SPT}$ in Euclidean space $\mathbb{E}^3$. $\mathfrak{s}$ preserves quasi-slant helices if and only if $\overline{\sigma}=\sigma$.*

Remark 7. *The curvatures of slant helices satisfy $f'(s)/\left(1+f^2(s)\right)^{3/2}=\lambda\kappa(s)$, where $f(s)=(\tau/\kappa)(s)$ with $\lambda\in\mathbb{R}$. Slightly different, curvatures of quasi-slant helices satisfy $f'(s)/\left(1+f^2(s)\right)^{3/2}=f(s)\,\kappa(s)$.*

4.3. **Curves in kinematics.** It is a well-known fact that the Frenet-Serret motion based on a curve is persistent if and only if $\tau(s)/\left(\kappa^2(s)+\tau^2(s)\right)$ is a constant, where $\kappa(s)$ and $\tau(s)$ are the curvature and torsion functions of the curve, see [4,20]. Moreover, if $\tau(s)/\left(\kappa^2(s)+\tau^2(s)\right)=p$, $p\neq 0$ then we say that the curve generates a $p-$persistent Frenet-Serret motion.

Remark 8. *Let $\mathfrak{s}:\alpha\to\overline{\alpha}$ be an $\mathcal{SPT}$ in Euclidean space $\mathbb{E}^3$. It is easy to see that the Frenet-Serret motion is persistent on the base curve (resp. image curve) of $\mathcal{SPT}$ if and only if torsion of the image curve (resp. base curve) is constant.*

In the following, we give the requirement that the Frenet-Serret motion is persistent on the quasi-slant helices.

Lemma 1. *Assume that α is a quasi-slant helix in Euclidean space $\mathbb{E}^3$. The Frenet-Serret motion is persistent on α if and only if $\sigma(s)\rho(s)/\left(1+\sigma^2(s)\right)$ is constant, where $\rho(s)=1/\kappa(s)$ is the radius of the curvature of α.*

Proof. Let α be a quasi-slant helix with curvature $\kappa(s)$ and torsion $\tau(s)$. The pitch function $\tau(s)/\left(\kappa^2(s)+\tau^2(s)\right)$ is constant when the Frenet-Serret motion is persistent on α. Since α is a quasi-slant helix, $\tau(s)=\sigma(s)\kappa(s)$. Therefore,

$$\frac{\tau(s)}{\kappa^2(s)+\tau^2(s)}=\frac{\sigma(s)\kappa(s)}{\kappa^2(s)+\sigma^2(s)\kappa^2(s)}=\frac{\sigma(s)\rho(s)}{1+\sigma^2(s)},$$

which is constant. Conversely, we obtain

$$\sigma(s)\rho(s)/\left(1+\sigma^2(s)\right)=\tau(s)/\left(\kappa^2(s)+\tau^2(s)\right)=\lambda$$

where λ is a nonzero constant. The proof is complete. □

Corollary 8. *Assume that α is a quasi-slant helix and $\mathfrak{s}:\alpha\to\overline{\alpha}$ is an $\mathcal{SPT}$ in Euclidean space $\mathbb{E}^3$. The Frenet-Serret motion is persistent on α if and only if*

$$\frac{\overline{\sigma}(s)}{\overline{\kappa}(s)\left(\overline{\sigma}^2(s)+\frac{1}{|\overline{w}(s)|^2}\right)}$$

is constant.

Proof. Since $\overline{\sigma}(s)=\frac{1}{\overline{\kappa}(s)\left(1+\left(\frac{\overline{\tau}(s)}{\overline{\kappa}(s)}\right)^2\right)^{3/2}}\left(\frac{\overline{\tau}}{\overline{\kappa}}\right)'(s)$ and $\overline{\tau}/\overline{\kappa}=\tau/\kappa$, it is written $\overline{\sigma}(s)=\frac{1}{\overline{\kappa}(s)\left(1+\left(\frac{\tau(s)}{\kappa(s)}\right)^2\right)^{3/2}}\left(\frac{\tau}{\kappa}\right)'(s)=\frac{\sigma(s)\kappa(s)}{\overline{\kappa}(s)}$ or $\sigma(s)=\frac{\overline{\sigma}(s)\overline{\kappa}(s)}{\kappa(s)}$. From Lemma 1 we get the intended. □

Theorem 5. *Let $\mathfrak{s}:\alpha\to\overline{\alpha}$ be an $\mathcal{SPT}$ and $\overline{\alpha}$ be a slant helix in Euclidean space $\mathbb{E}^3$. If α generates $p-$persistent Frenet-Serret motion $(p\neq 0)$, then the geodesic curvature of the normal indicatrix of $\overline{\alpha}$ satisfies the following:*

$$\frac{1}{2}|p|\leq|\overline{\sigma}(s)|.$$

Proof. Assume that α generates the $p-$persistent Frenet-Serret motion in $\mathbb{E}^3$. The curvatures of this curve are given by

$$\kappa(\theta)=\frac{1}{2p}\cos\theta;\qquad\tau(\theta)=\frac{1}{2p}(1+\sin\theta),$$

where θ is a parameter. Thereby, the curvatures of $\overline{\alpha}$ as follow:

$$\overline{\kappa}(s)=\frac{\kappa(s)}{\kappa^2(s)+\tau^2(s)}=\frac{p\cos\theta}{1+\sin\theta};\qquad\overline{\tau}(s)=\frac{\tau(s)}{\kappa^2(s)+\tau^2(s)}=p.$$

Since $\overline{\alpha}$ is slant helix, it follows:

$$\overline{\sigma} = \frac{1}{\overline{\kappa}(s)\left(1+\left(\frac{\overline{\tau}(s)}{\overline{\kappa}(s)}\right)^2\right)}\left(\frac{\overline{\tau}(s)}{\overline{\kappa}(s)}\right)' = \frac{p}{\sqrt{2}}\frac{\sqrt{1-\sin\theta}}{\cos\theta}.$$

Hence $\sqrt{1-\sin\theta}/\cos\theta = \lambda$, where λ is nonzero constant. This leads to $\lambda^2 = 1/(1+\sin\theta) \Rightarrow \sin\theta = 1/\lambda^2 - 1$. By definition of *sinus function* we obtain $1/\sqrt{2} \leq |\lambda|$. From $\lambda = \sqrt{2}\overline{\sigma}/p$, we have the intended. □

Let $\mathfrak{s} : \alpha \to \overline{\alpha}$ be an $\mathcal{SPT}$ in Euclidean space $\mathbb{E}^3$. Let us recall the fixed axode along any space curve α, $\boldsymbol{a}(s,\lambda) = \alpha(s) + \frac{\kappa(s)}{\kappa^2(s)+\tau^2(s)}\boldsymbol{n}(s) + \lambda\boldsymbol{w}(s)$. Since $\overline{\kappa}(s) = \kappa(s)/\left(\kappa^2(s)+\tau^2(s)\right)$ and $\overline{\tau}(s) = \tau(s)/\left(\kappa^2(s)+\tau^2(s)\right)$, the fixed axode along $\overline{\alpha}$ is given by

$$\overline{\boldsymbol{a}}(s,\lambda) = \overline{\alpha}(s) + \kappa(s)\overline{\boldsymbol{n}}(s) + \overline{\lambda}\overline{\boldsymbol{w}}(s).$$

where $\overline{\boldsymbol{n}}$ is the principal normal, $\overline{\boldsymbol{w}}$ is the Darboux vector of $\overline{\alpha}$. Thus, we can conclude the following:

Theorem 6. *Let $\mathfrak{s} : \alpha \to \overline{\alpha}$ be an $\mathcal{SPT}$ in Euclidean space $\mathbb{E}^3$, and both base curve and image curve be a unit speed curve with the same arc-length parameter s. In this case, $\mathfrak{s}$ preserves the distribution parameter of fixed axode of α if and only if $\overline{\kappa}(s) = \kappa(s) + c$, where c is a constant.*

Proof. Assume that $\mathfrak{s}$ preserves the distribution parameter of fixed axode of α. Let P and $\overline{P}$ be the distribution parameters of fixed axodes of α and $\overline{\alpha}$, respectively. The distribution parameters of fixed axodes are given by

$$P = \frac{\det\left(\Delta'(s), \boldsymbol{w}(s), \boldsymbol{w}'(s)\right)}{\boldsymbol{w}'(s)\cdot\boldsymbol{w}'(s)} \; ; \; \overline{P} = \frac{\det\left(\overline{\Delta}'(s), \overline{\boldsymbol{w}}(s), \overline{\boldsymbol{w}}'(s)\right)}{\overline{\boldsymbol{w}}'(s)\cdot\overline{\boldsymbol{w}}'(s)},$$

where $\Delta(s) = \alpha(s) + \frac{\kappa(s)}{\kappa^2(s)+\tau^2(s)}\boldsymbol{n}(s)$ and $\overline{\Delta}(s) = \overline{\alpha}(s) + \kappa\overline{\boldsymbol{n}}(s)$. By straightforward calculations we obtain $\Delta'(s) = (1-\kappa(s)\overline{\kappa}(s))\boldsymbol{t}(s) + \overline{\kappa}'(s)\boldsymbol{n}(s) + \overline{\kappa}(s)\tau(s)\boldsymbol{b}(s)$ and $\boldsymbol{w}'(s) = \tau'(s)\boldsymbol{t}(s) + \kappa'(s)\boldsymbol{b}(s)$. It can be seen that

$$\Delta'(s) \times \boldsymbol{w}(s) = \overline{\kappa}'(s)\left(\kappa(s)\boldsymbol{t}(s) - \tau(s)\boldsymbol{b}(s)\right)$$

and $(\Delta'(s) \times \boldsymbol{w}(s)) \cdot \boldsymbol{w}'(s) = \overline{\kappa}'(s)\left(\kappa(s)\tau'(s) - \tau(s)\kappa'(s)\right)$. Hence, the distribution parameter of fixed axode of α is as follows:

$$P = \frac{\overline{\kappa}'(s)\left(\kappa(s)\tau'(s) - \tau(s)\kappa'(s)\right)}{\left(\kappa'(s)\right)^2 + \left(\tau'(s)\right)^2}. \tag{22}$$

Similarly, we find the distribution parameter of fixed axode of $\overline{\alpha}$ as

$$\overline{P} = \frac{\kappa'(s)\left(\kappa(s)\tau'(s) - \tau(s)\kappa'(s)\right)}{\left(\kappa'(s)\right)^2 + \left(\tau'(s)\right)^2}. \tag{23}$$

From Eqs. (22) and (23), $\overline{\kappa}'(s) = \kappa'(s)$ or $\overline{\kappa}(s) = \kappa(s) + c$, where c is constant. Conversely, $\overline{\kappa}(s) = \kappa(s) + c$ requires $\overline{\kappa}'(s) = \kappa'(s)$. It is easily obtain that $P = \overline{P}$ which completes the proof. □

5. Examples

In this section, some curves and their images under $\mathcal{SPT}$ are illustrated by *Mathematica* software. First, we recall the following informations and give an example of Mannheim slant helix. The intrinsic equations of slant helices are presented by Menninger in [13] as follows:

$$\kappa(s) = c\beta'(s)\cos\beta(s); \quad \tau(s) = c\beta'(s)\sin\beta(s),$$

where c is constant and β is differentiable function of arc-length parameter of the curve. Furthermore, the tangent vectors of slant helices are characterized by

$$T(s) = \frac{1}{2}\begin{pmatrix} \xi_1\cos\xi_2\Pi(s) + \xi_2\cos\xi_1\Pi(s) \\ \xi_1\sin\xi_2\Pi(s) + \xi_2\sin\xi_1\Pi(s) \\ 2\frac{n}{m}\sin n\Pi(s) \end{pmatrix}, \tag{24}$$

where $\Pi(s) = \beta(s)/n$, $\xi_1 = 1 - n$, $\xi_2 = 1 + n$, with $n = \cos\theta$ and $m = \cot\theta$.

In the following example, parametric equation of Mannheim slant helix, its picture, and its image curve under $\mathcal{SPT}$ are obtained in accordance with [13].

Example 2. *Substituting $\lambda = 1$ and $\varphi(s) = s$ in Proposition 6 gives $\kappa(s) = 1/\cosh^2 s$ and $\tau(s) = \sec hs\tanh s$. This leads to the differential equation*

$$c\beta'(s)\cos\beta(s) = \frac{1}{\cosh^2 s},$$

which has solution

$$\beta(s) = \arcsin\left(\frac{ck + \tanh s}{c}\right), \tag{25}$$

where $k \in \mathbb{R}$. To simplify Eq. (25), we can take $k = 0$ and $c = 1$. It follows from Eq. (24) that

$$T(s) = \begin{pmatrix} \sec h^3 s, \\ \frac{3}{2}\tanh s - \tanh^3 s, \\ \frac{\sqrt{3}}{2}\tanh s \end{pmatrix},$$

where $\theta = \pi/3$, $n = 1/2$, $m = 1/\sqrt{3}$, $\xi_1 = 1/2$, $\xi_2 = 3/2$, $\beta(s) = \arcsin(\tanh s)$, $\Pi(s) = \beta(s)/n = 2\arcsin(\tanh s)$. Thus, we obtain the parametric equation and picture of the Mannheim slant helix (Figure 1 (a)) as follows:

$$\alpha(s) = \begin{pmatrix} \arctan\left(\tanh\frac{s}{2}\right) + \frac{1}{2}\tanh s\sec hs, \\ \frac{1}{2}\log(\cosh s) - \frac{1}{2}\sec h^2 s, \\ \frac{\sqrt{3}}{2}\log(\cosh s) \end{pmatrix}.$$

Curvatures of the image curve $\overline{\alpha}$ with respect to $\mathfrak{s} : \alpha \to \overline{\alpha}$ can be given by

$$\overline{\kappa}(s) = 1; \quad \overline{\tau}(s) = \sinh s.$$

Picture of the image curve $\overline{\alpha}$ illustrated by Figure 1 (b).

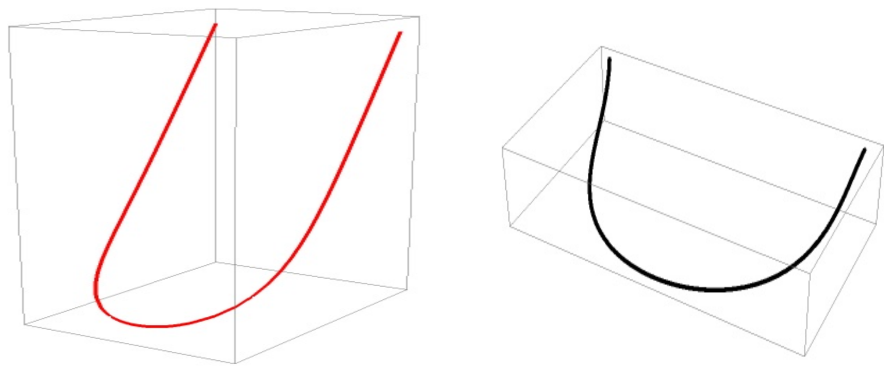

(a) Mannheim slant helix (b) Image of Mannheim slant helix

FIGURE 1. Mannheim slant helix and image curve

Example 3. *Let us recall the trigonometric parameterization of curvatures of the constant pitch curves, $\kappa(\theta) = \cos\theta/2p$ and $\tau(\theta) = (1+\sin\theta)/2p$. By substituting $p = 1$ we obtain $\kappa(\theta) = \cos\theta/2$ and $\tau(\theta) = (1+\sin\theta)/2$. We give the picture of the curve with curvature $\kappa(\theta)$ and torsion $\tau(\theta)$ by Figure 2 (a).*

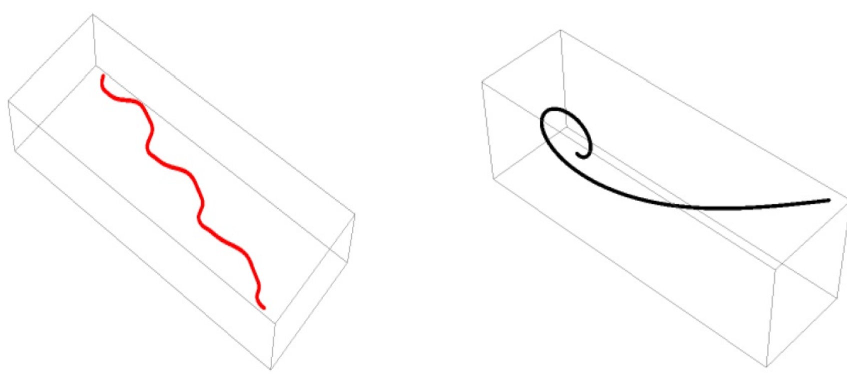

(a) Constant pitch curve (b) Image of constant pitch curve

FIGURE 2. Constant pitch curve and image curve

Moreover, curvatures of the image curve of constant pitch curve under $\mathcal{SPT}$ can be given by

$$\overline{\kappa}(\theta) = \frac{\cos\theta}{1+\sin\theta}; \quad \overline{\tau}(\theta) = 1.$$

The picture of this curve illustrated by Figure 2 (b).

Example 4. *One of trigonometric reparameterization of curvatures of the quasi-slant helix can be given by*

$$\kappa(s) = \frac{\cos^2\left(\frac{2s-1}{2}\right)}{\sin\left(\frac{2s-1}{2}\right)}; \quad \tau(s) = \cos\left(\frac{2s-1}{2}\right).$$

The picture of this curve illustrated by Figure 3 (a), where $1/3 \leq s < 1/2$.

$$\overline{\kappa}\,(s) = \sin\left(\frac{2s-1}{2}\right); \quad \overline{\tau}\,(s) = \frac{\sin^2\left(\frac{2s-1}{2}\right)}{\cos\left(\frac{2s-1}{2}\right)}.$$

The picture of this curve illustrated by Figure 3 (b), where $1 \leq s \leq 2$.

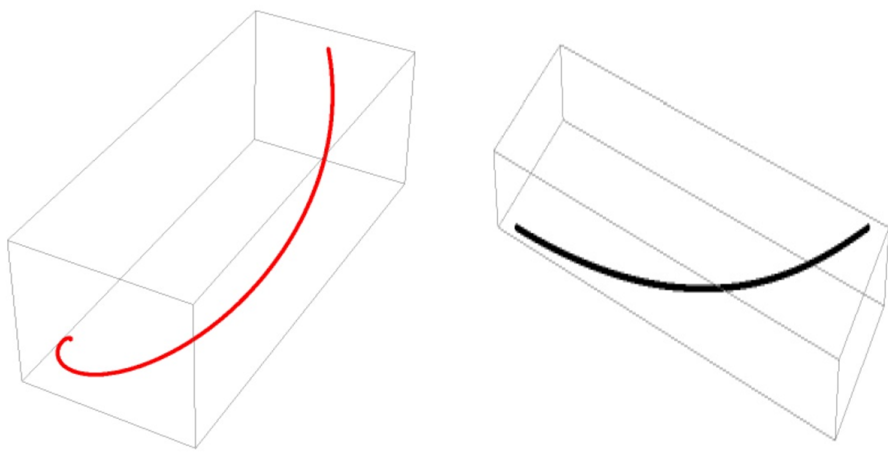

(a) Quasi-slant helix (b) Image of quasi-slant helix

Figure 3. Quasi-slant helix and image curve

Declaration of Competing Interests There is no competing interests to declare among the authors.

References

[1] Ali, A.T, Position vectors of slant helices in Euclidean 3-space, *Journal of the Egyptian Mathematical Society,* 20 (2012), 1-6. doi: 10.1016/j.joems.2011.12.005

[2] Bhat, V. S., Haribaskar, R., A pair of kinematically related space curves, *International Journal of Geometric Methods in Modern Physics,* 15(1850180) (2018), 17 pp. doi: 10.1142/S0219887818501803

[3] Blum, R., A remarkable class of Mannheim curves, *Canad. Math. Bull.,* 9 (1966), 223–228. https://doi.org/10.4153/CMB-1966-030-9

[4] Bottema, O., Roth, B., Theoretical Kinematics, New York, Dover Publications, 1990.

[5] Do Carmo, M. P., Differential Geometry of Curves and Surfaces, Translated from the Portuguese, Englewood Cliffs, NJ, USA, Prentice-Hall, Inc., 1976.

[6] Deshmukh, S., Alghanemi, A., Farouki, R. T., Space curves defined by curvature-torsion relations and associated helices, *Filomat Journal*, 33 (2019), 4951–4966. doi: 10.2298/FIL1915951D

[7] Eisenhart, L. P., An Introduction to Differential Geometry with Use of the Tensor Calculus, Princeton, Princeton University Press, 1947.

[8] Honda, S., Takahashi, M., Bertrand and Mannheim curves of framed curves in the 3-dimensional Euclidean space, *Turkish Journal of Mathematics*, 44 (2020), 883–899. doi: 10.3906/mat-1905-63

[9] Izumiya, S., Takeuchi, N., New special curves and developable surfaces, *Turkish Journal of Mathematics*, 28 (2004), 153–163.

[10] Kahveci, D., Yaylı, Y., Persistent rigid-body motions on slant helices, *International Journal of Geometric Methods in Modern Physics,* 16(1950193) (2019), 15 pp. doi: 10.1142/S0219887819501937

[11] Kim, D. S., Chung, H. S., Cho, K. H., Space curves satisfying $\tau/\kappa = as + b$, *Honam Math. J.,* 1 (1993), 5–9.

[12] Liu, H., Wang, F., Mannheim partner curves in 3-space, *Journal of Geometry,* 88 (2008), 120–126. doi: 10.1007/s00022-007-1949-0

[13] Menninger, A., Characterization of the slant helix as successor curve of the general helix, *International Electronic Journal of Geometry,* 7 (2014), 84–91. doi: 10.36890/iejg.593986

[14] Monterde, J., Salkowski curves revisited: A family of curves with constant curvature and non-constant torsion, *Computer Aided Geometric Design,* 26 (2009), 271–278. doi: 10.1016/j.cagd.2008.10.002

[15] Orbay, K., Kasap, E., On Mannheim partner curves in $\mathbb{E}^3$, *International Journal of Physical Sciences,* 4 (2009), 261–264.

[16] Öztürk, E., Mannheim curves in 3−dimensional Euclidean space, *International Scientific and Vocational Journal,* 4 (2020), 86–89. doi: 10.47897/bilmes.818723

[17] Öztürk, E., Geometric elements of constant precession curve, *Hagia Sophia Journal of Geometry,* 2 (2020), 48-55.

[18] Öztürk, E., Yaylı, Y., W−curves in Lorentz-Minkowski space, *Mathematical Sciences and Applications e-Notes*, 5 (2017), 76-88. doi: 10.36753/mathenot.421740

[19] Salkowski, E., Zur Transformation von Raumkurven, *Mathematische Annalen*, 66 (1909), 517–557.

[20] Selig, J. M., Carricato, M., Persistent rigid-body motions and Study's "Ribaucor" problem, *Journal of Geometry,* 108 (2017), 149–169. doi: 10.1007/s00022-016-0331-5

[21] Struik, D. J., Lectures on Classical Differential Geometry, Reprint of the Second Edition, New York, NY, USA: Dover Publications, Inc., 1988.

[22] Uzunoğlu, B., Gök, İ., Yaylı, Y., A new approach on curves of constant precession, *Applied Mathematics and Computation,* 275 (2016), 317–323. doi: 10.1016/j.amc.2015.11.083

[23] Wang, Y., Chang, Y., Mannheim curves and spherical curves, *International Journal of Geometric Methods in Modern Physics*, 17(2050101) (2020), 15 pp. doi: 10.1142/S0219887820501017

http://communications.science.ankara.edu.tr

Commun.Fac.Sci.Univ.Ank.Ser. A1 Math. Stat.
Volume 72, Number 2, Pages 331–339 (2023)
DOI:10.31801/cfsuasmas.1062426
ISSN 1303-5991 E-ISSN 2618-6470

Research Article; Received: January 24, 2022; Accepted: November 27, 2022

TIMELIKE ROTATIONAL HYPERSURFACES WITH TIMELIKE AXIS IN MINKOWSKI FOUR-SPACE

Erhan GÜLER

Department of Mathematics, Faculty of Sciences, Bartın University
Kutlubey Campus, 74100 Bartın, TÜRKİYE

Abstract. We introduce the timelike rotational hypersurfaces $\mathbf{x}$ with timelike axis in Minkowski 4-space $\mathbb{E}_1^4$. We obtain the equations for the curvatures of the hypersurface. Moreover, we present a theorem for the rotational hypersurfaces with timelike axis supplying $\Delta \mathbf{x} = \mathcal{T}\mathbf{x}$, where $\mathcal{T}$ is a 4×4 real matrix.

1. Introduction

Geometers have been focused on the geometry of the surfaces and hypersurfaces in space forms for years. Some of the works on the topic are indicated in alphabetical order:

Arslan et al. [1] studied the generalized rotation surfaces in Euclidean four space $\mathbb{E}^4$; Arslan, et al. [2] worked the Weyl pseudosymmetric hypersurfaces; Arslan and Milousheva [3] focused the meridian surfaces of elliptic or hyperbolic type in Minkowski 4-space $\mathbb{E}_1^4$; Arvanitoyeorgos et al. [4] introduced the Lorentz hypersurfaces satisfying $\Delta H = \alpha H$ in $\mathbb{E}_1^4$; Beneki et al. [5] served the helicoidal surfaces in Minkowski 3-space; Chen [6] worked the total mean curvature and the finite type submanifolds; Cheng and Wan [7] presented the complete hypersurfaces in $\mathbb{R}^4$ with CMC; Cheng and Yau [8] studied the hypersurfaces with constant scalar curvature; Dillen et al. [9] stated the rotation hypersurfaces in $\mathbb{S}^n \times \mathbb{R}$ and $\mathbb{H}^n \times \mathbb{R}$; Do Carmo and Dajczer [10] derived the rotation hypersurfaces in spaces of constant curvature; Dursun [11] considered the hypersurfaces with pointwise 1-type Gauss map.

On the other hand, Dursun and Turgay [12] worked the space-like surfaces in $\mathbb{E}_1^4$ with pointwise 1-type Gauss map; Ferrandez et al. [13] focused some class of conformally at Euclidean hypersurfaces; Ganchev and Milousheva [14] considered the general rotational surfaces in $\mathbb{E}_1^4$; Güler [15] introduced the helical hypersurfaces in

2020 *Mathematics Subject Classification.* 53A35, 53C42.
Keywords. Rotational hypersurface, timelike axis, Laplace–Beltrami operator, curvature, Minkowski 4-space.
eguler@bartin.edu.tr; 0000-0003-3264-6239.

$\mathbb{E}_1^4$; Güler [16] obtained the fundamental form IV with the curvatures of the hypersphere; Güler [17] worked the rotational hypersurfaces satisfying $\Delta^I R = AR$ in $\mathbb{E}^4$; Güler et al. [18] examined the Gauss map and the third Laplace−Beltrami operator of the rotational hypersurface in 4-space; Güler et al. [19] studied Laplace−Beltrami operator of a helicoidal hypersurface in four-space; Güler and Turgay [20] focused the Cheng−Yau operator and Gauss map of the rotational hypersurfaces in 4-space.

Hasanis and Vlachos [21] worked hypersurfaces in $\mathbb{E}^4$ with harmonic mean curvature vector field; Kim and Turgay [22] served the surfaces with L_1-pointwise 1-type Gauss map in $\mathbb{E}^4$; Lawson [23] introduced the minimal submanifolds; Magid et al. [24] focused the affine umbilical surfaces in $\mathbb{R}^4$; Moore [25] revealed the surfaces of rotation in $\mathbb{E}^4$; Moore [26] also indicated the rotation surfaces of constant curvature in $\mathbb{E}^4$; O'Neill [27] presented the semi-Riemannian geometry.

Takahashi [28] served that minimal surfaces and spheres are the only surfaces in $\mathbb{E}^3$ satisfying the condition $\Delta r = \lambda r$, $\lambda \in \mathbb{R}$; Turgay and Upadhyay [29] worked the biconservative hypersurfaces in 4-dimensional Riemannian space forms.

In this work, we consider the timelike rotational hypersurfaces $\mathbf{x}$ with timelike axis in Minkowski 4-space $\mathbb{E}_1^4$. We give the notions of $\mathbb{E}_1^4$ in Section 2. In Section 3, we present the definition of the timelike rotational hypersurfaces with timelike axis, and compute its curvatures. In addition, we give the timelike rotational hypersurfaces with timelike axis supplying $\Delta \mathbf{x} = \mathcal{T}\mathbf{x}$, where $\mathcal{T}$ is a 4×4 real matrix in Section 4. Finally, we serve the results and conclusion in the last section.

2. Preliminaries

In this section, we indicate the first and second fundamental forms, matrix of the shape operator $\mathbf{S}$, the curvatures $\mathfrak{C}_i$ of the hypersurface $\mathbf{x} = \mathbf{x}(u, v, w)$ in Minkowski 4-space $\mathbb{E}_1^4$. We identify a vector (a,b,c,d) with its transpose $(\text{a,b,c,d})^t$ in the rest of this paper.

Let $\mathbf{x}$ be an isometric immersion of a hypersurface from M_1^3 to $\mathbb{E}_1^4 = (\mathbb{R}^4, \cdot)$, where $\overrightarrow{x} \cdot \overrightarrow{y} = x_1 y_1 + x_2 y_2 + x_3 y_3 - x_4 y_4$ is a Lorentzian inner product of vectors $\overrightarrow{x} = (x_1, x_2, x_3, x_4)$, $\overrightarrow{y} = (y_1, y_2, y_3, y_4)$, and x_i are the pseudo-Euclidean coordinates of type $(3, 1)$. The vector product of $\overrightarrow{x} = (x_1, x_2, x_3, x_4)$, $\overrightarrow{y} = (y_1, y_2, y_3, y_4)$, $\overrightarrow{z} = (z_1, z_2, z_3, z_4)$ of $\mathbb{E}_1^4$ is defined by

$$\overrightarrow{x} \times \overrightarrow{y} \times \overrightarrow{z} = \det \begin{pmatrix} e_1 & e_2 & e_3 & -e_4 \\ x_1 & x_2 & x_3 & x_4 \\ y_1 & y_2 & y_3 & y_4 \\ z_1 & z_2 & z_3 & z_4 \end{pmatrix}.$$

A vector $\overrightarrow{x}$ is called timelike if $\overrightarrow{x} \cdot \overrightarrow{x} < 0$, and a hypersurface $\mathbf{x}$ is timelike if $\mathbf{x} \cdot \mathbf{x} < 0$. In $\mathbb{E}_1^4$, the hypersurface $\mathbf{x}$ has the following first and second fundamental form matrices, resp.,

$$I=\begin{pmatrix} E & F & A\\ F & G & B\\ A & B & C\end{pmatrix},\quad II=\begin{pmatrix} L & M & P\\ M & N & T\\ P & T & V\end{pmatrix},$$

and

$$\begin{aligned}\det I &= (EG-F^2)C-EB^2+2FAB-GA^2,\\ \det II &= \left(LN-M^2\right)V-LT^2+2MPT-NP^2,\end{aligned}$$

where

$$\begin{aligned}E &= \mathbf{x}_u\cdot\mathbf{x}_u, F=\mathbf{x}_u\cdot\mathbf{x}_v, G=\mathbf{x}_v\cdot\mathbf{x}_v, A=\mathbf{x}_u\cdot\mathbf{x}_w, B=\mathbf{x}_v\cdot\mathbf{x}_w, C=\mathbf{x}_w\cdot\mathbf{x}_w,\\ L &= \mathbf{x}_{uu}\cdot e, M=\mathbf{x}_{uv}\cdot e, N=\mathbf{x}_{vv}\cdot e, P=\mathbf{x}_{uw}\cdot e, T=\mathbf{x}_{vw}\cdot e, V=\mathbf{x}_{ww}\cdot e,\end{aligned}$$

and also e is the Gauss map of the hypersurface $\mathbf{x}$:

$$e=\frac{\mathbf{x}_u\times\mathbf{x}_v\times\mathbf{x}_w}{\|\mathbf{x}_u\times\mathbf{x}_v\times\mathbf{x}_w\|}. \tag{1}$$

The shape operator matrix $\mathbf{S}=I^{-1}\cdot II$ is defined by

$$\mathbf{S}=\frac{1}{\det I}\begin{pmatrix} s_{11} & s_{12} & s_{13}\\ s_{21} & s_{22} & s_{23}\\ s_{31} & s_{32} & s_{33}\end{pmatrix},$$

where

$$\begin{aligned}s_{11} &= ABM-CFM-AGP+BFP+CGL-B^2L,\\ s_{12} &= ABN-CFN-AGT+BFT+CGM-B^2M,\\ s_{13} &= ABT-CFT-AGV+BFV+CGP-B^2P,\\ s_{21} &= ABL-CFL+AFP-BPE+CME-A^2M,\\ s_{22} &= ABM-CFM+AFT-BTE+CNE-A^2N,\\ s_{23} &= ABP-CFP+AFV-BVE+CTE-A^2T,\\ s_{31} &= -AGL+BFL+AFM-BME+GPE-F^2P,\\ s_{32} &= -AGM+BFM+AFN-BNE+GTE-F^2T,\\ s_{33} &= -AGP+BFP+AFT-BTE+GVE-F^2V.\end{aligned}$$

Theorem 1. *The hypersurface $\mathbf{x}$ in $\mathbb{E}_1^4$ has the following curvature formulas, $\mathfrak{C}_0=1$ (by definition),*

$$\mathfrak{C}_1 = \frac{\left\{\begin{array}{c}(EN+GL-2FM)C+(EG-F^2)V-LB^2-NA^2\\ -2(APG-BPF-ATF+BTE-ABM)\end{array}\right\}}{3\left[(EG-F^2)C-EB^2+2FAB-GA^2\right]}, \tag{2}$$

$$\mathfrak{C}_2 = \frac{\left\{\begin{array}{c}(EN+GL-2FM)V+\left(LN-M^2\right)C-ET^2-GP^2\\ -2\left(APN-BPM-ATM+BTL-PTF\right)\end{array}\right\}}{3\left[(EG-F^2)C-EB^2+2FAB-GA^2\right]}, \tag{3}$$

$$\mathfrak{C}_3 = \frac{\left(LN - M^2\right)V - LT^2 + 2MPT - NP^2}{(EG - F^2)C - EB^2 + 2FAB - GA^2}. \quad (4)$$

See [16] for Euclidean details. Next, we define the rotational hypersurface in $\mathbb{E}_1^4$.

Definition 1. *Let $\gamma : I \subset \mathbb{R} \longrightarrow \Pi$ be a curve in a plane Π and ℓ be a straight line in Π in $\mathbb{E}_1^4$. A rotational hypersurface in $\mathbb{E}_1^4$ is defined as a hypersurface rotating a curve γ around a line ℓ (called the profile curve and the axis, respectively).*

Therefore, we introduce the rotational hypersurfaces with timelike axis in $\mathbb{E}_1^4$ in the following section.

3. Timelike Rotational Surfaces with Timelike Axis

We may suppose ℓ spanned by the timelike vector $(1,0,0,0)^t$. The orthogonal matrix is given by

$$\mathbf{A}(v,w) = \begin{pmatrix} \cos v \cos w & -\sin v & -\cos v \sin w & 0 \\ \sin v \cos w & \cos v & -\sin v \sin w & 0 \\ \sin w & 0 & \cos w & 0 \\ 0 & 0 & 0 & 1 \end{pmatrix}, \quad (5)$$

where $v, w \in \mathbb{R}$. The following holds: $\det \mathbf{A} = 1$, $\mathbf{A}.\ell = \ell$, $\mathbf{A}^t \varepsilon \mathbf{A} = \varepsilon$, where $\varepsilon = diag(1,1,1,-1)$. Supposing the axis of rotation is ℓ, there is a Lorentz transformation that the axis is ℓ transformed to the x_4-axis of $\mathbb{E}_1^4$. The parametrization of the timelike profile curve is given by $\gamma(u) = (u, 0, 0, \varphi(u))$. Here, we assume that the profile curve is timelike, i.e., $\gamma' \cdot \gamma' = 1 - \varphi'^2 < 0$, $\varphi(u) : \mathrm{I} \subset \mathbb{R} \longrightarrow \mathbb{R}$ is a differentiable function for all $u \in$I. So, the rotational hypersurface spanned by the vector $(0,0,0,1)$, is given by $\mathbf{x}(u,v,w) = \mathbf{A}(v,w)\gamma(u)^t$ in $\mathbb{E}_1^4$, where $u \in$I, $v, w \in \mathbb{R}$. If $w = 0$, we get the rotational surface with timelike axis as in three dimensional Minkowski space $\mathbb{E}_1^3$.

Next, we obtain the curvatures of the following rotational hypersurface with timelike axis

$$\mathbf{x}(u,v,w) = \begin{pmatrix} u \cos v \cos w \\ u \sin v \cos w \\ u \sin w \\ \varphi(u) \end{pmatrix}, \quad (6)$$

where $u \in \mathbb{R} - \{0\}$ and $0 \le v, w \le 2\pi$. Using the first differentials of (6), we get the first fundamental form matrix as follows

$$I = \begin{pmatrix} 1 - \varphi'^2 & 0 & 0 \\ 0 & u^2 \cos^2 w & 0 \\ 0 & 0 & u^2 \end{pmatrix},$$

where $\varphi = \varphi(u)$, $\varphi' = \frac{d\varphi}{du}$. We obtain $\det I = u^4(1 - \varphi'^2)\cos^2 w < 0$. So, the hypersurface is the timelike rotational hypersurface with timelike axis. Using the second differentials with respect to u, v, w, we have the second fundamental form matrix as follows

$$II = \begin{pmatrix} -\frac{\varphi''}{(\varphi'^2-1)^{1/2}} & 0 & 0 \\ 0 & -\frac{u\varphi' \cos^2 w}{(\varphi'^2-1)^{1/2}} & 0 \\ 0 & 0 & -\frac{u\varphi'}{(\varphi'^2-1)^{1/2}} \end{pmatrix},$$

and $\det II = -\frac{u^2\varphi'^2\varphi'' \cos^2 w}{(\varphi'^2-1)^{3/2}}$. Therefore, the shape operator matrix of the hypersurface is given by

$$\mathbf{S} = \begin{pmatrix} \frac{\varphi''}{(\varphi'^2-1)^{3/2}} & 0 & 0 \\ 0 & -\frac{\varphi'}{u(\varphi'^2-1)^{1/2}} & 0 \\ 0 & 0 & -\frac{\varphi'}{u(\varphi'^2-1)^{1/2}} \end{pmatrix}.$$

Finally, we calculate the curvatures of the timelike rotational hypersurface with timelike axis, and give the results of it in the following.

Corollary 1. *The timelike rotational hypersurface* (6) *with timelike axis has the following curvatures*

$$\begin{aligned} \mathfrak{C}_1 &= H = \frac{u\varphi'' - 2\left(\varphi'^2 - 1\right)\varphi'}{3u(\varphi'^2 - 1)^{3/2}}, \\ \mathfrak{C}_2 &= \frac{-2u\varphi'\varphi'' + \left(\varphi'^2 - 1\right)\varphi'^2}{3u^2(\varphi'^2 - 1)^2}, \\ \mathfrak{C}_3 &= K = \frac{\varphi'^2\varphi''}{u^2(\varphi'^2 - 1)^{5/2}}. \end{aligned}$$

Proof. By using the eqs. (2) , (3) , (4) for the timelike rotational hypersurface with timelike axis (6) , we get the curvatures.

Corollary 2. *When the timelike rotational hypersurface* (6) *with timelike axis has* $\mathfrak{C}_i = 0$, $i = 1, 2, 3$, *respectively, then it has the following general* φ *solutions, respectively,*

$$\begin{aligned} u\varphi'' - 2\varphi'^3 + 2\varphi' = 0 \quad &\Leftrightarrow \quad \varphi = \mp i^{1/2} e^{-c_1/2} F\left[i \operatorname{arg\,sinh}\left((ie^{c_1}u)^{1/2}\right), -1\right] + c_2 \\ &\qquad \text{or } \varphi = c_1, \\ 2u\varphi'\varphi'' - \varphi'^4 + \varphi'^2 = 0 \quad &\Leftrightarrow \quad \varphi = \mp 2e^{-2c_1}\left(1 + e^{2c_1}u\right)^{1/2} + c_2 \\ &\qquad \text{or } \varphi = c_1, \\ \varphi'^2\varphi'' = 0 \quad &\Leftrightarrow \quad \varphi = c_1 u + c_2 \text{ or } \varphi = c_1, \end{aligned}$$

where $F[\phi, m] = \int_0^\phi \left(1 - m\sin^2\theta\right)^{-1/2} d\theta$ *gives the elliptic integral of the first kind for* $-\pi/2 < \phi < \pi/2$, $i = (-1)^{1/2}$, $c_1, c_2 \in \mathbb{R}$.

4. Timelike Rotational Surfaces with Timelike Axis Satisfying $\Delta\mathbf{x} = \mathcal{T}\mathbf{x}$

Definition 2. *The Laplace−Beltrami operator of the hypersurface* $\mathbf{x}(u,v,w)\mid_{D\subset\mathbb{R}^4}$ *of class* C^3 *is given by*

$$\Delta\mathbf{x} = \frac{1}{(\det I)^{1/2}}\left\{\begin{array}{c} \frac{\partial}{\partial u}\left(\frac{(CG-B^2)\mathbf{x}_u+(AB-CF)\mathbf{x}_v+(BF-AG)\mathbf{x}_w}{(\det I)^{1/2}}\right) \\ +\frac{\partial}{\partial v}\left(\frac{(AB-CF)\mathbf{x}_u+(CE-A^2)\mathbf{x}_v+(AF-BG)\mathbf{x}_w}{(\det I)^{1/2}}\right) \\ +\frac{\partial}{\partial w}\left(\frac{(BF-AG)\mathbf{x}_u+(AF-BG)\mathbf{x}_v+(EG-F^2)\mathbf{x}_w}{(\det I)^{1/2}}\right) \end{array}\right\}. \tag{7}$$

By using above definition with the hypersurface (6), we have the following Laplace−Beltrami operator

$$\Delta\mathbf{x} = \frac{u\varphi'' - 2\varphi'^3 + 2\varphi'}{uW^2}\begin{pmatrix} \varphi'\cos v\cos w \\ \varphi'\sin v\cos w \\ \varphi'\sin w \\ 1 \end{pmatrix},$$

where $W = \varphi'^2 - 1$. The Gauss map of the rotational hypersurface (6) with timelike axis is given by

$$e = \frac{1}{W^{1/2}}\begin{pmatrix} \varphi'\cos v\cos w \\ \varphi'\sin v\cos w \\ \varphi'\sin w \\ 1 \end{pmatrix}.$$

Considering $3He = \mathcal{T}\mathbf{x}$, we obtain

$$\begin{pmatrix} (\Psi\varphi' - t_{11}u)\cos v\cos w - t_{12}u\cos w\sin v - t_{13}u\sin w \\ t_{21} - u\cos v\cos w + (\Psi\varphi' - t_{22}u)\sin v\cos w - t_{23}u\sin w \\ -t_{31}u\cos v\cos w - t_{32}u\sin v\cos w + (\Psi\varphi' - t_{33}u)\sin w \\ \Psi \end{pmatrix}$$
$$= \begin{pmatrix} t_{14}\varphi(u) \\ t_{24}\varphi(u) \\ t_{34}\varphi(u) \\ t_{41}u\cos v\cos w + t_{42}u\sin v\cos w + t_{43}u\sin w + t_{44}\varphi(u) \end{pmatrix},$$

where $\mathcal{T}$ is a 4×4 real matrix with the components t_{ij}, and also $\Psi(u) = 3HW^{-1/2}$. The equation $\Delta\mathbf{x} = \mathcal{T}\mathbf{x}$ with respect to the first quantity I, and $\Delta\mathbf{x} = 3He$ give rises to the following system

$$\begin{aligned} (\Psi\varphi' - t_{11}u)\cos v\cos w - t_{12}u\sin v\cos w - t_{13}u\sin w &= t_{14}\varphi(u), \\ -t_{21}u\cos v\cos w + (\Psi\varphi' - t_{22}u)\sin v\cos w - t_{23}u\sin w &= t_{24}\varphi(u), \\ -t_{31}u\cos v\cos w - t_{32}u\sin v\cos w + (\Psi\varphi' - t_{33}u)\sin w &= t_{34}\varphi(u), \\ -t_{41}u\cos v\cos w - t_{42}u\sin v\cos w - t_{43}u\sin w + \Psi &= t_{44}\varphi(u). \end{aligned}$$

Differentiating ODE's two times depends on v, we have

$$t_{14} = t_{24} = t_{34} = t_{44} = 0, \quad \Psi = 0. \tag{8}$$

From (8) , we see the following

$$\begin{aligned} t_{11} u \cos v + t_{12} u \sin v &= 0, \\ t_{21} u \cos v + t_{22} u \sin v &= 0, \\ t_{31} u \cos v + t_{32} u \sin v &= 0, \\ t_{41} u \cos v + t_{42} u \sin v &= 0. \end{aligned}$$

When we use these equality in the equation system, we get

$$t_{13} = t_{23} = t_{33} = t_{43} = 0. \tag{9}$$

Then, matrix $\mathcal{T}$ becomes zero matrix. So, if $\Delta \mathbf{x} = \mathcal{T}\mathbf{x}$, then $\mathcal{T} = 0$ and the hypersurface is a minimal.

Also, the cos and sin are the linearly independent functions of v, then we obtain $t_{ij} = 0$. Since $\Psi = 3HW^{-1/2}$, we find $H = 0$. Therefore, $\mathbf{x}$ is a timelike minimal hypersurface with timelike axis.

Hence, we serve the following theorem:

Theorem 2. *Let timelike $\mathbf{x} : M_1^3 \longrightarrow \mathbb{E}_1^4$ be an isometric immersion given by (6). $\Delta \mathbf{x} = \mathcal{T}\mathbf{x}$, where $\mathcal{T}$ is a 4×4 real matrix iff $\mathbf{x}$ is a timelike minimal hypersurface with timelike axis, i.e., $H = \mathfrak{C}_1 = 0$.*

5. Results and Conclusion

The concepts of rotational hypersurfaces are studied by many mathematician and geometers. It is shown that the timelike rotational hypersurface has three different curvatures in Minkowski 4-space. Moreover, the minimality condition of it by using the Laplace−Beltrami operator has presented. These concepts propose for the other space forms may be useful in the future.

Declaration of Competing Interests The author declares that he has no known competing financial interests or personal relationships that could have appeared to influence the work reported in this paper.

References

[1] Arslan, K., Bayram, B. K., Bulca, B., Öztürk, G., Generalized rotation surfaces in $\mathbb{E}^4$, *Results Math.*, 61(3) (2012), 315–327. https://doi.org/10.1007/s00025-011-0103-3

[2] Arslan, K., Deszcz, R., Yaprak, Ş., On Weyl pseudosymmetric hypersurfaces, *Colloq. Math.*, 72(2) (1997), 353–361.

[3] Arslan, K., Milousheva, V., Meridian surfaces of elliptic or hyperbolic type with pointwise 1-type Gauss map in Minkowski 4-space, *Taiwanese J. Math.*, 20(2) (2016), 311–332. https://doi.org/10.11650/tjm.19.2015.5722

[4] Arvanitoyeorgos, A. , Kaimakamis, G., Magid, M., Lorentz hypersurfaces in $\mathbb{E}_1^4$ satisfying $\Delta H = \alpha H$, *Illinois J. Math.*, 53(2) (2009), 581–590. https://doi.org/10.1215/ijm/1266934794

[5] Beneki, Chr. C., Kaimakamis, G., Papantoniou, B. J., Helicoidal surfaces in three-dimensional Minkowski space, *J. Math. Anal. Appl.*, 275 (2002), 586–614. https://doi.org/10.1016/S0022-247X(02)00269-X

[6] Chen, B. Y., Total Mean Curvature and Submanifolds of Finite Type, 2nd Ed., World Scientific, Singapore, 2014. https://doi.org/10.1142/9237

[7] Cheng, Q. M., Wan, Q. R., Complete hypersurfaces of $\mathbb{R}^4$ with constant mean curvature, *Monatsh. Math.*, 118 (1994), 171–204. https://doi.org/10.1007/BF01301688

[8] Cheng, S. Y., Yau, S. T., Hypersurfaces with constant scalar curvature, *Math. Ann.*, 225 (1977), 195–204. https://doi.org/10.1007/BF01425237

[9] Dillen, F., Fastenakels, J., Van der Veken, J., Rotation hypersurfaces of $\mathbb{S}^n \times \mathbb{R}$ and $\mathbb{H}^n \times \mathbb{R}$, *Note Mat.*, 29(1) (2009), 41–54. https://doi.org/10.1285/i15900932v29n1p41

[10] Do Carmo, M. P., Dajczer, M., Rotation hypersurfaces in spaces of constant curvature, *Trans. Am. Math. Soc.*, 277 (1983), 685–709. https://doi.org/10.1007/978-3-642-25588-517

[11] Dursun, U., Hypersurfaces with pointwise 1-type Gauss map, *Taiwanese J. Math.*, 11(5) (2007), 1407–1416. https://doi.org/10.11650/twjm/1500404873

[12] Dursun, U., Turgay, N. C., Space-like surfaces in Minkowski space $\mathbb{E}_1^4$ with pointwise 1-type Gauss map, *Ukr. Math. J.*, 71(1) (2019), 64–80. https://doi.org/10.1007/s11253-019-01625-8

[13] Ferrandez, A., Garay, O. J., Lucas, P., On a certain class of conformally flat Euclidean hypersurfaces, In Global Differential Geometry and Global Analysis, Lecture Notes in Mathematics, vol 1481. Springer, Heidelberg, Berlin, Germany, 1991, 48–54. https://doi.org/10.1007/BFb0083627

[14] Ganchev, G., Milousheva, V., General rotational surfaces in the 4-dimensional Minkowski space, *Turkish J. Math.*, 38 (2014), 883–895. https://doi.org/10.3906/mat-1312-10

[15] Güler, E., Helical hypersurfaces in Minkowski geometry $\mathbb{E}_1^4$, *Symmetry*, 12(8) (2020), 1–16. https://doi.org/10.3390/sym12081206

[16] Güler, E., Fundamental form IV and curvature formulas of the hypersphere, *Malaya J. Mat.*, 8(4) (2020), 2008–2011. https://doi.org/10.26637/MJM0804/0116

[17] Güler, E., Rotational hypersurfaces satisfying $\Delta^I R = AR$ in the four-dimensional Euclidean space, *J. Polytech.*, 24(2) (2021), 517–520. https://doi.org/10.2339/politeknik.670333

[18] Güler, E., Hacısalihoğlu, H. H., Kim, Y.H., The Gauss map and the third Laplace–Beltrami operator of the rotational hypersurface in 4-space, *Symmetry*, 10(9) (2018), 1–12. https://doi.org/10.3390/sym10090398

[19] Güler, E., Magid, M., Yaylı, Y., Laplace–Beltrami operator of a helicoidal hypersurface in four-space, *J. Geom. Symmetry Phys.*, 41 (2016), 77–95. https://doi.org/10.7546/jgsp-41-2016-77-95

[20] Güler, E., Turgay, N. C., Cheng–Yau operator and Gauss map of rotational hypersurfaces in 4-space, *Mediterr. J. Math.*, 16(3) (2019), 1–16. https://doi.org/10.1007/s00009-019-1333-y

[21] Hasanis, Th., Vlachos, Th., Hypersurfaces in $\mathbb{E}^4$ with harmonic mean curvature vector field, *Math. Nachr.*, 172 (1995), 145–169. https://doi.org/10.1002/mana.19951720112

[22] Kim, Y. H., Turgay, N. C., Surfaces in $\mathbb{E}^4$ with L_1-pointwise 1-type Gauss map, *Bull. Korean Math. Soc.*, 50(3) (2013), 935–949. http://dx.doi.org/10.4134/BKMS.2013.50.3.935

[23] Lawson, H. B., Lectures on Minimal Submanifolds, Vol. I., Second ed., Mathematics Lecture Series, 9. Publish or Perish, Wilmington, Del., 1980.

[24] Magid, M., Scharlach, C., Vrancken, L., Affine umbilical surfaces in $\mathbb{R}^4$, *Manuscripta Math.*, 88 (1995), 275–289. http://dx.doi.org/10.1007/BF02567823

[25] Moore, C., Surfaces of rotation in a space of four dimensions, *Ann. Math.*, 21 (1919), 81–93. https://doi.org/10.2307/2007223

[26] Moore, C., Rotation surfaces of constant curvature in space of four dimensions, *Bull. Amer. Math. Soc.*, 26 (1920), 454–460. https://doi.org/10.1090/S0002-9904-1920-03336-7

[27] O'Neill, B., Semi-Riemannian Geometry with Applications to Relativity, Academic Press, New York, 1983.

[28] Takahashi, T., Minimal immersions of Riemannian manifolds, *J. Math. Soc. Japan*, 18 (1966), 380–385. https://doi.org/10.2969/jmsj/01840380

[29] Turgay, N. C., Upadhyay, A., On biconservative hypersurfaces in 4-dimensional Riemannian space forms, *Math. Nachr.*, 292(4) (2019), 905–921. https://doi.org/10.1002/mana.201700328

http://communications.science.ankara.edu.tr

Commun.Fac.Sci.Univ.Ank.Ser. A1 Math. Stat.
Volume 72, Number 2, Pages 340–351 (2023)
DOI:10.31801/cfsuasmas.1181930
ISSN 1303-5991 E-ISSN 2618-6470

Research Article; Received: September 30, 2022; Accepted: December 20, 2022

A NEW PERSPECTIVE ON BICOMPLEX NUMBERS WITH LEONARDO NUMBER COMPONENTS

Murat TURAN[1], Sıddıka ÖZKALDI KARAKUŞ[2] and Semra KAYA NURKAN[3]

[1,2]Department of Mathematics, Faculty of Science, Bilecik Şeyh Edebali University, Bilecik, TÜRKİYE
[3]Department of Mathematics, Faculty of Arts and Sciences, Uşak University, Uşak, TÜRKİYE

Abstract. In the present paper, the bicomplex Leonardo numbers will be introduced with the use of Leonardo numbers and some important algebraic properties including recurrence relation, generating function, Catalan's and Cassini's identities, Binet's formula, sum formulas will also be obtained.

1. Introduction

It is an old and interesting problem to obtain a natural extension of complex numbers and many mathematicians have studied this by defining multicomplex numbers, and corresponding function theory. One of these extensions is quaternions which have been described by S.W. Hamilton [7], and the other one is bicomplex numbers which have been described by C. Segre [17] in order to formulate physical problems in a 4-dimensional space. There are some differences between these extensions in the perspective of commutativity and forming a division algebra. Namely, quaternions are non commutative and form a division algebra, while bicomplex numbers are commutative and do not form a division algebra.

In [15], Price has developed the bicomplex algebra and function theory. Indeed, bicomplex algebra is a 2-dimensional Clifford algebra, satisfy the commutative multiplication on $\mathbb{C}$ and also has important applications in image processing, geometry and theoretical physics (see [15, 16]).

It is well known that a complex number $x \in \mathbb{C}$ is represented as $x = x_1 + x_2 i$, such that $x_1, x_2 \in \mathbb{R}$, $i^2 = -1$ and a bicomplex numbers $x \in \mathbb{C}_2$ is written as

2020 *Mathematics Subject Classification.* 11B37, 11B39, 05A15.
Keywords. Fibonacci numbers, bicomplex numbers, Leonardo numbers.
[1] murat199869@gmail.com; 0000-0001-9684-7924
[2] siddika.karakus@bilecik.edu.tr; 0000-0002-2699-4109
[3] semra.kaya@usak.edu.tr-Corresponding author; 0000-0001-6473-4458.

$$x = x_1 + x_2 i + x_3 j + x_4 ij \tag{1}$$

by the basis $1, i, j, ij$ where $x_s \in \mathbb{R}$, $1 \leq s \leq 4$ and $i^2 = j^2 = -1$, $ij = ji$ with $(ij)^2 = 1$.

Notice that $ij \in \mathbb{C}_2$, but $ij \notin \mathbb{C}$. From equation (1), the space of the bicomplex numbers $\mathbb{C}_2$ can be seen of dimension 4 over $\mathbb{R}$, since the space of complex numbers $\mathbb{C}$ is of dimension 2 over $\mathbb{R}$.

For any two bicomplex numbers $z = z_1 + z_2 i + z_3 j + z_4 ij$ and $w = w_1 + w_2 i + w_3 j + w_4 ij$, addition, multiplication and scalar multiplication of an element in $\mathbb{C}_2$ by a real number c are given, respectively

$$z + w = (z_1 + w_1) + (z_2 + w_2)\, i + (z_3 + w_3)\, j + (z_4 + w_4)\, ij$$

$$\begin{aligned} z \cdot w &= (z_1 w_1 - z_2 w_2 - z_3 w_3 + z_4 w_4) + (z_1 w_2 + z_2 w_1 - z_3 w_4 - z_4 w_3)\, i \\ &+ (z_1 w_3 + z_3 w_1 - z_2 w_4 - z_4 w_2)\, j + (z_1 w_4 + z_4 w_1 + z_2 w_3 + z_3 w_2)\, ij \end{aligned} \tag{2}$$

$$cz = cz_1 + cz_2 i + cz_3 j + cz_4 ij.$$

Note that there is a big difference between $\mathbb{C}$ and $\mathbb{C}_2$: $\mathbb{C}$ form a field while $\mathbb{C}_2$ do not since it contains divisors of zero. Now we are ready to turn our main topic since we have given brief overview of bicomplex numbers. For more details, we refer the reader to [13, 15] which are dealing with bicomplex analysis.

One of the well known as below and most examined sequences is Fibonacci and also they are many notable sequences of integers. In the existing literature, one can find many papers on Fibonacci and Lucas numbers, (see [8, 9, 11]). Moreover, they have been examined on different number systems, for example, quaternions and hybrid numbers [2, 6, 10, 14, 22]. It is benefical to recall the definitions of Fibonacci and Lucas sequences: for $n \geq 0$,

$$F_{n+2} = F_{n+1} + F_n$$

$$L_{n+2} = L_{n+1} + L_n$$

where $F_0 = 0$, $F_1 = 1$, $L_0 = 2$ and $L_1 = 1$, respectively. The Binet's formulas for F_n and L_n are

$$F_n = \frac{\phi^n - \psi^n}{\phi - \psi} \tag{3}$$

$$L_n = \phi^n + \psi^n, \tag{4}$$

where ϕ and ψ are the roots of the characteristic equation $x^2 - x - 1 = 0$.

In the present paper, we deal with Leonardo sequence which has similar properties with Fibonacci sequence and denote the nth Leonardo numbers by L_{e_n}. Some properties of Leonardo numbers have been given by Catarino and Borges in [4] and it is noteworthy to recall that Leonardo sequence is given via this recurrence relation: for $n \geq 2$,

$$L_{e_n} = L_{e_{n-1}} + L_{e_{n-2}} + 1, \tag{5}$$

with the initial conditions $L_{e_0} = L_{e_1} = 1$. One can find many sequences of integers indexed in *The Online Encyclopedia of Integer Sequences*, being in this case $\{L_{e_n}\}$: $A001595$ in [19].

Also, the following relation holds for Leonardo numbers for $n \geq 2$,

$$L_{e_{n+1}} = 2L_{e_n} - L_{e_{n-2}}. \tag{6}$$

The Binet formula of the Leonardo numbers is

$$L_{e_n} = \frac{2\phi^{n+1} - 2\psi^{n+1} - \phi + \psi}{\phi - \psi} \tag{7}$$

where ϕ and ψ are roots of characteristic equation $x^3 - 2x^2 + 1 = 0$.

By Binet formula, the relationship between Leonardo and Fibonacci numbers is

$$L_{e_n} = 2F_{n+1} - 1 \tag{8}$$

where F_n is nth Fibonacci number.

In [4], Cassini's, Catalan's and d'Ocagne's identities have been obtained for Leonardo numbers by Catarino et /it al. Moreover they have presented the 2-dimensional recurrences relations and matrix representation of Leonardo numbers. In [18], Shannon have defined generalized Leonardo numbers which are considered Asveld's extension and Horadam's generalized sequence.

Now, we are ready to recall some identities involving Fibonacci, Lucas and Leonardo numbers as follows, for more details related to them, please refer [1, 4, 11, 22]:

$$F_n + L_n = 2F_{n+1} \tag{9}$$

$$F_{n+r}F_{n+s} - F_nF_{n+r+s} = (-1)^n F_rF_s \tag{10}$$

$$L_{e_{n+m}} + (-1)^m L_{e_{n-m}} = L_m(L_{e_n} + 1) - 1 - (-1)^m \tag{11}$$

$$L_{e_{n+m}} - (-1)^m L_{e_{n-m}} = L_{n+1}(L_{e_{m-1}} + 1) - 1 + (-1)^m \tag{12}$$

$$F_n^2 - F_{n+r}F_{n-r} = (-1)^{n-r} F_r^2 \tag{13}$$

$$L_{r+s} - (-1)^s L_{r-s} = 5F_rF_s \tag{14}$$

$$\sum_{k=1}^{n} (-1)^{k-1} F_{k+1} = (-1)^{n-1} F_n. \tag{15}$$

In the existing literature, there are also different generalizations of Fibonacci and Lucas numbers. One of these generalizations is the bicomplex Fibonacci and Lucas numbers and they have been defined by Nurkan et /it al. and some properties have been presented in [14]. They have defined the bicomplex version of Fibonacci and bicomplex Lucas numbers as follows:

$$BF_n = F_n + F_{n+1}i + F_{n+2}j + F_{n+3}ij \tag{16}$$

$$BL_n = L_n + L_{n+1}i + L_{n+2}j + L_{n+3}ij \tag{17}$$

where F_n and L_n are nth Fibonacci and Lucas sequences, respectively. Furthermore, Torunbalcı have defined the bicomplex Fibonacci quaternions in [21] by

$$\begin{aligned} BF_n &= F_n + iF_{n+1} + jF_{n+2} + ijF_{n+3}, \\ &= F_n + iF_{n+1} + (F_{n+2} + iF_{n+3})\, j \end{aligned}$$

where i, j and ij satisfy the conditions $i^2 = j^2 = -1$, $ij = ji$ with $(ij)^2 = 1$.

In [12] the authors have investigated Leonardo Pisano polynomials and hybrinomials with the use of the Leonardo Pisano numbers and hybrid numbers. They have also obtained the basic algebraic properties and some identities of these polynomials and hybrinomials.

With the motivation of these mentioned papers, here, we introduce the bicomplex numbers with Leonardo number components. We also aim to obtain generating function, Binet's formula, recurrence relation, summation formula, Catalan's, Cassini's and other identities.

For more details about Leonardo numbers, see [3–5, 12, 20].

2. Bicomplex Leonardo Numbers

In this section, by introducing the bicomplex Leonardo numbers, we study Binet's formula, summation formulas, Catalan's and Cassini's identities and generating function.

Definition 1. *For $n \geqslant 1$, the nth bicomplex Leonardo numbers are defined by*

$$\mathbb{BL}_{e_n} = L_{e_n} + L_{e_{n+1}} i + L_{e_{n+2}} j + L_{e_{n+3}} ij. \tag{18}$$

Throughout the paper, nth bicomplex Leonardo numbers is denoted by $\mathbb{BL}_{e_n}$.

From the recurrence relation (5) and the definition of bicomplex Leonardo numbers (18), for $n \geq 2$ we get

$$\begin{aligned} \mathbb{BL}_{e_n} &= (L_{e_{n-1}} + L_{e_{n-2}} + 1) + (L_{e_n} + L_{e_{n-1}} + 1)i \\ &\quad +(L_{e_{n+1}} + L_{e_n} + 1)j + (L_{e_{n+2}} + L_{e_{n+1}} + 1)ij, \\ &= \mathbb{BL}_{e_{n-1}} + \mathbb{BL}_{e_{n-2}} + C. \end{aligned}$$

For the sake of the shortness, we express $1 + i + j + ij$ by C along the paper. Also initial conditions are $\mathbb{BL}_{e_0} = 1 + i + 3j + 5ij$ and $\mathbb{BL}_{e_1} = 1 + 3i + 5j + 9ij$.

Another recurrence relation of bicomplex Leonardo numbers can also be given by

$$\mathbb{BL}_{e_{n+1}} = 2\mathbb{BL}_{e_n} - \mathbb{BL}_{e_{n-2}} \tag{19}$$

for $n \geqslant 2$. Using the definition of bicomplex Leonardo numbers (18) and the recurrence relation of Leonardo numbers (6), for $n \geqslant 2$ we get

$$\begin{aligned} \mathbb{BL}_{e_{n+1}} &= 2L_{e_n} - L_{e_{n-2}} + (2L_{e_{n+1}} - L_{e_{n-1}})i \\ &\quad +(2L_{e_{n+2}} - L_{e_n})j + (2L_{e_{n+3}} - L_{e_{n+1}})ij \\ &= 2\mathbb{BL}_{e_n} - \mathbb{BL}_{e_{n-2}} \end{aligned}$$

with the initial values $\mathbb{BL}_{e_0} = 1 + i + 3j + 5ij$ and $\mathbb{BL}_{e_1} = 1 + 3i + 5j + 9ij$.

Theorem 1. *The generation function for the bicomplex Leonardo numbers denoted by $g\mathbb{BL}_{e_n}(t)$ is*

$$g\mathbb{BL}_{e_n}(t) = \frac{\mathbb{BL}_{e_0} + t(-1 + i - j - ij) + t^2(1 - i - j - 3ij)}{1 - 2t + t^3}.$$

Proof. Let the formal power series expression of the generating function for $\{\mathbb{BL}_{e_n}\}_{n=0}^{\infty}$ be as

$$g\mathbb{BL}_{e_n}(t) = \sum_{n=0}^{\infty} \mathbb{BL}_{e_n} t^n. \tag{20}$$

That is

$$g\mathbb{BL}_{e_n}(t) = \mathbb{BL}_{e_0} + \mathbb{BL}_{e_1} t + \mathbb{BL}_{e_2} t^2 + ... + \mathbb{BL}_{e_k} t^k + ...$$

Then, we have

$$\begin{aligned}
\left(1 - 2t + t^3\right) g\mathbb{BL}_{e_n}(t) &= \left(1 - 2t + t^3\right) \begin{pmatrix} \mathbb{BL}_{e_0} + \mathbb{BL}_{e_1} t \\ +\mathbb{BL}_{e_2} t^2 + ... + \mathbb{BL}_{e_k} t^k + ... \end{pmatrix} \\
\left(1 - 2t + t^3\right) g\mathbb{BL}_{e_n}(t) &= \mathbb{BL}_{e_0} + \mathbb{BL}_{e_1} t + \mathbb{BL}_{e_2} t^2 + ... + \\
&\quad -2\mathbb{BL}_{e_0} t - 2\mathbb{BL}_{e_1} t^2 - 2\mathbb{BL}_{e_2} t^3 - ... \\
&\quad +\mathbb{BL}_{e_0} t^3 + \mathbb{BL}_{e_1} t^4 + \mathbb{BL}_{e_2} t^5 + ... \\
&= \mathbb{BL}_{e_0} + t\left(\mathbb{BL}_{e_1} - 2\mathbb{BL}_{e_0}\right) + t^2\left(\mathbb{BL}_{e_2} - 2\mathbb{BL}_{e_1}\right) \\
&\quad +t^3\left(\mathbb{BL}_{e_3} - 2\mathbb{BL}_{e_2} + \mathbb{BL}_{e_0}\right) + ... \\
&\quad +t^{k+1}\left(\mathbb{BL}_{e_{k+1}} - 2\mathbb{BL}_{e_k} + \mathbb{BL}_{e_{k-2}}\right) + ...
\end{aligned}$$

Since the recurrence relation of bicomplex numbers (19) and also by using initial conditions, we get

$$\begin{aligned}
g\mathbb{BL}_{e_n}(t)(1 - 2t + t^3) &= (1 + i + 3j + 5ij) \\
&\quad +t(-1 + i - j - ij) + t^2(1 - i - j - 3ij).
\end{aligned}$$

Therefore, we get the generating function for $\{\mathbb{BL}_{e_n}\}_{n=0}^{\infty}$ as

$$\sum_{n=0}^{\infty} \mathbb{BL}_{e_n} t^n = \frac{\mathbb{BL}_{e_0} + t(-1 + i - j - ij) + t^2(1 - i - j - 3ij)}{1 - 2t + t^3}.$$

□

Theorem 2. *For any integer $n \geqslant 0$, we have*

$$\mathbb{BL}_{e_n} = 2BF_{n+1} - C. \tag{21}$$

Here BF_n is nth bicomplex Fibonacci number.

Proof. Using the definition of bicomplex Leonardo numbers (18) and the recurrence relation between Leonardo and Fibonacci numbers (8) we get

$$\begin{aligned}
\mathbb{BL}_{e_n} &= L_{e_n} + L_{e_{n+1}}i + L_{e_{n+2}}j + L_{e_{n+3}}ij, \\
&= (2F_{n+1} - 1) + (2F_{n+2} - 1)i \\
&\quad +(2F_{n+3} - 1)j + (2F_{n+4} - 1)ij \\
&= 2(F_{n+1} + F_{n+2}i + F_{n+3}j + F_{n+4}ij) - C \\
&= 2BF_{n+1} - C.
\end{aligned}$$

□

Theorem 3. *For any integer $n \geqslant 0$, the Binet's formula for $\mathbb{BL}_{e_n}$ is as follows:*

$$\mathbb{BL}_{e_n} = 2\left(\frac{\underline{\Phi}\phi^{n+1} - \underline{\Psi}\psi^{n+1}}{\phi - \psi}\right) - C \tag{22}$$

where $\underline{\Phi} = 1 + \phi i + \phi^2 j + \phi^3 ij$ and $\underline{\Psi} = 1 + \psi i + \psi^2 j + \psi^3 ij$.

Proof. By using the definition of bicomplex Leonardo numbers (18) and the Binet's formula of Leonardo numbers (7), we get

$$\mathbb{BL}_{e_n} = 2\left(\begin{array}{c} \frac{\phi^{n+1}-\psi^{n+1}}{\phi-\psi} + \frac{\phi^{n+2}-\psi^{n+2}}{\phi-\psi}i \\ +\frac{\phi^{n+3}-\psi^{n+3}}{\phi-\psi}j + \frac{\phi^{n+4}-\psi^{n+4}}{\phi-\psi}ij \end{array}\right) - (1 + i + j + ij).$$

If the expressions $\underline{\Phi} = 1 + \phi i + \phi^2 j + \phi^3 ij$, $\underline{\Psi} = 1 + \psi i + \psi^2 j + \psi^3 ij$ are used in the last equation, we can easily obtained the result. □

Theorem 4. *The summation formulas for $\mathbb{BL}_{e_n}$ are as follows for $n \geq 0$,*

1) $\sum_{k=0}^{n} \mathbb{BL}_{e_k} = \mathbb{BL}_{e_{n+2}} - (n+2)C - (2i + 4j + 8ij)$,

2) $\sum_{k=0}^{n} \mathbb{BL}_{e_{2k}} = \mathbb{BL}_{e_{2n+1}} - nC - (2i + 2j + 4ij)$,

3) $\sum_{k=0}^{n} \mathbb{BL}_{e_{2k+1}} = \mathbb{BL}_{e_{2n+2}} - (n+2)C - (2j + 4ij)$.

Also for $n \geq 1$

4) $\sum_{r=0}^{n} (-1)^{r-1} \mathbb{BL}_{e_r} = \begin{cases} -\left(\mathbb{BL}_{e_{n-1}} + 2 + 2j + 2ij\right), & n \text{ is even} \\ \mathbb{BL}_{e_{n-1}} - 1 + i - j - ij, & n \text{ is odd.} \end{cases}$

Proof. With the use of the sums and products of terms of the Leonardo sequence proposition (3.1) in [4] and also the definition of bicomplex Leonardo numbers, the proof of (1), (2) and (3) follows easily.

In order to prove (4); we obtain

$$\sum_{r=0}^{n} (-1)^{r-1} \mathbb{BL}_{e_r} = \sum_{r=0}^{n} (-1)^{r-1} L_{e_r} + i\sum_{r=0}^{n} (-1)^{r-1} L_{e_{r+1}}$$

$$+j\sum_{r=0}^{n}(-1)^{r-1}L_{e_{r+2}}+ij\sum_{r=0}^{n}(-1)^{r-1}L_{e_{r+3}}$$

from the definition of $\mathbb{BL}_{e_n}$. Then by using (5), (8) and (15) we get

$$\sum_{r=0}^{n}(-1)^{r-1}\mathbb{BL}_{e_r}=\begin{cases}(-2BF_n-1+i-j-ij), & n \text{ is even}\\ (2BF_n-2-2j-2ij), & n \text{ is odd.}\end{cases}$$

where BF_n is nth bicomplex Fibonacci number. Taking into account (21) we complete the proof. □

Now the following interesting identities in accordance with the Binet's formula (22) for $\{L_{e_n}\}$ can be presented as follows:

Theorem 5. ***(Catalan's Identity)*** *For positive integers n and r with $n \geq r$, we have*

$$\begin{aligned}\mathbb{BL}_{e_n}^2-\mathbb{BL}_{e_{n-r}}\mathbb{BL}_{e_{n+r}} &= (\mathbb{BL}_{e_{n-r}}+\mathbb{BL}_{e_{n+r}}-2\mathbb{BL}_{e_n})C\\ &\quad +12(-1)^{n-r+1}(2j+ij)F_r^2.\end{aligned} \tag{23}$$

Proof. First, by using (22) to left hand side (LHS) then, we get

$$\begin{aligned}LHS &= \left(2\left(\frac{\underline{\Phi}\phi^{n+1}-\underline{\Psi}\psi^{n+1}}{\phi-\psi}\right)-C\right)\left(2\left(\frac{\underline{\Phi}\phi^{n+1}-\underline{\Psi}\psi^{n+1}}{\phi-\psi}\right)-C\right)\\ &- \left(2\left(\frac{\underline{\Phi}\phi^{n-r+1}-\underline{\Psi}\psi^{n-r+1}}{\phi-\psi}\right)-C\right)\left(2\left(\frac{\underline{\Phi}\phi^{n+r+1}-\underline{\Psi}\psi^{n+r+1}}{\phi-\psi}\right)-C\right).\end{aligned} \tag{24}$$

By considering ϕ, ψ, $\underline{\Phi}=1+\phi i+\phi^2 j+\phi^3 ij$ and $\underline{\Psi}=1+\psi i+\psi^2 j+\psi^3 ij$ then, we also have

$$\underline{\Phi}.\underline{\Psi}=6j+3ij. \tag{25}$$

By taking into account (13) and (25) in (LHS), one can get

$$\begin{aligned}LHS &= (\mathbb{BL}_{e_{n-r}}+\mathbb{BL}_{e_{n+r}}-2\mathbb{BL}_{e_n})C\\ &\quad +12(-1)^{n-r+1}(2j+ij)F_r^2\end{aligned}$$

which completes the proof. □

Remark that, if one takes in the case $r=1$ in (23) and using the relation (1.5), then Catalan's identity reduces to Cassini's identity for $\mathbb{BL}_{e_n}$.

Corollary 1. ***(Cassini's Identity)*** *For $n \geq 1$, we have*

$$\begin{aligned}\mathbb{BL}_{e_n}^2-\mathbb{BL}_{e_{n-1}}\mathbb{BL}_{e_{n+1}} &= (\mathbb{BL}_{e_{n-1}}-\mathbb{BL}_{e_{n-2}})C\\ &\quad +12(-1)^n(2j+ij).\end{aligned}$$

Theorem 6. *The following holds between the Fibonacci numbers and bicomplex Leonardo numbers*

$$\begin{aligned}\mathbb{BL}_{e_{k+m}}\mathbb{BL}_{e_{k+s}}-\mathbb{BL}_{e_k}\mathbb{BL}_{e_{k+m+s}} &= (\mathbb{BL}_{e_k}-\mathbb{BL}_{e_{k+m}}+\mathbb{BL}_{e_{k+m+s}}-\mathbb{BL}_{e_{k+s}})C \\ &\quad +12(-1)^{k+1}F_mF_s\left(2j+ij\right).\end{aligned}$$

Here k, m, and s be positive integers.

Proof. By using the Binet's formula (22) to left hand side (LHS), we get

$$\begin{aligned}LHS &= \left(\frac{2\underline{\Phi}\phi^{k+m+1}-2\underline{\Psi}\psi^{k+m+1}}{\phi-\psi}-C\right)\left(\frac{2\underline{\Phi}\phi^{k+s+1}-2\underline{\Psi}\psi^{k+s+1}}{\phi-\psi}-C\right) \\ &\quad -\left(\frac{2\underline{\Phi}\phi^{k+1}-2\underline{\Psi}\psi^{k+1}}{\phi-\psi}-C\right)\left(\frac{2\underline{\Phi}\phi^{k+m+s+1}-2\underline{\Psi}\psi^{k+m+s+1}}{\phi-\psi}-C\right) \\ &= (\mathbb{BL}_{e_k}-\mathbb{BL}_{e_{k+m}}+\mathbb{BL}_{e_{k+m+s}}-\mathbb{BL}_{e_{k+s}})C \\ &\quad +\frac{4\underline{\Phi}.\underline{\Psi}}{(\phi-\psi)^2}\left(\phi^{k+1}\psi^{k+1}\left(-\phi^m\psi^s-\phi^s\psi^m+\psi^{m+s}+\phi^{m+s}\right)\right).\end{aligned}$$

Then with the use of Vajda's identity for Fibonacci numbers (10) and (25), we have

$$\begin{aligned}LHS &= (\mathbb{BL}_{e_k}-\mathbb{BL}_{e_{k+m}}+\mathbb{BL}_{e_{k+m+s}}-\mathbb{BL}_{e_{k+s}})C \\ &\quad +12(-1)^{k+1}F_mF_s\left(2j+ij\right).\end{aligned}$$

□

Theorem 7. *The following identities between the Lucas, Leonardo, bicomplex Lucas and bicomplex Leonardo numbers are as follows:*

$$\mathbb{BL}_{e_{n+m}}+(-1)^m\mathbb{BL}_{e_{n-m}} = L_m\mathbb{BL}_{e_n}+(L_m-(-1)^m-1)C \quad (26)$$

$$\mathbb{BL}_{e_{n+m}}-(-1)^m\mathbb{BL}_{e_{n-m}} = (L_{e_{m-1}}+1)BL_{n+1}+((-1)^m-1)C. \quad (27)$$

Here n and m are positive integers, with $n \geq m$.

Proof. For the proof of (26), by using the definition of bicomplex Leonardo numbers to left hand side (LHS), we get

$$\begin{aligned}LHS &= (L_{e_{n+m}}+(-1)^mL_{e_{n-m}})+(L_{e_{n+m+1}}+(-1)^mL_{e_{n-m+1}})i \\ &\quad +(L_{e_{n+m+2}}+(-1)^mL_{e_{n-m+2}})j+(L_{e_{n+m+3}}+(-1)^mL_{e_{n-m+3}})ij.\end{aligned}$$

Taking into account (11), we obtain

$$LHS = L_m\mathbb{BL}_{e_n}+C(L_m-(-1)^m-1).$$

By taking into account (1.11) the proof of (27) can obtained in a similar manner. □

Theorem 8. *The following identity between the Fibonacci and bicomplex Leonardo numbers as follows:*

$$\mathbb{BL}_{e_{m+r}}\mathbb{BL}_{e_{m-r}}-\mathbb{BL}_{e_{m+s}}\mathbb{BL}_{e_{m-s}} = \left(\mathbb{BL}_{e_{m+s}}-\mathbb{BL}_{e_{m+r}}+\mathbb{BL}_{e_{m-s}}-\mathbb{BL}_{e_{m-r}}\right)C$$

$$+12\left(2j+ij\right)\left(\left(-1\right)^{m-s+1}F_s^2+\left(-1\right)^{m-r}F_r^2\right)$$

Here m, r and s are positive integers with $m \geq r$ and $m \geq s$.

Proof. By using (22) to left hand side (LHS), we have

$$\begin{aligned} LHS &= \left(2\frac{\underline{\Phi}\phi^{m+r+1}-\underline{\Psi}\psi^{m+r+1}}{\phi-\psi}-C\right)\left(2\frac{\underline{\Phi}\phi^{m-r+1}-\underline{\Psi}\psi^{m-r+1}}{\phi-\psi}-C\right) \\ &\quad -\left(2\frac{\underline{\Phi}\phi^{m+s+1}-\underline{\Psi}\psi^{m+s+1}}{\phi-\psi}-C\right)\left(2\frac{\underline{\Phi}\phi^{m-s+1}-\underline{\Psi}\psi^{m-s+1}}{\phi-\psi}-C\right) \\ &= (\mathbb{BL}_{e_{m+s}}-\mathbb{BL}_{e_{m+r}}+\mathbb{BL}_{e_{m-s}}-\mathbb{BL}_{e_{m-r}})C \\ &\quad -\frac{4\underline{\Phi}\underline{\Psi}}{(\phi-\psi)^2}\left(\phi^m\psi^m\left(-\phi^r\psi^{-r}-\phi^{-r}\psi^r+\phi^s\psi^{-s}+\phi^{-s}\psi^s\right)\right). \\ &= (\mathbb{BL}_{e_{m+s}}-\mathbb{BL}_{e_{m+r}}+\mathbb{BL}_{e_{m-s}}-\mathbb{BL}_{e_{m-r}})C \\ &\quad -4\underline{\Phi}.\underline{\Psi}\left[\frac{\phi^m\psi^m}{(\phi-\psi)^2}\left(\phi^s\psi^{-s}+\phi^{-s}\psi^s-2\right)-\frac{\phi^m\psi^m}{(\phi-\psi)^2}\left(\phi^r\psi^{-r}+\phi^{-r}\psi^r-2\right)\right] \end{aligned}$$

On the other hand, we can show that

$$\begin{aligned} F_m^2-F_{m+r}F_{m-r} &= \left(-1\right)^{m-r}F_r^2 \\ &= \frac{\phi^m\psi^m}{(\phi-\psi)^2}\left(\phi^r\psi^{-r}+\phi^{-r}\psi^r-2\right). \end{aligned}$$

Also by using above equation and (25) in (LHS), we get

$$\begin{aligned} LHS &= \left(\mathbb{BL}_{e_{m+s}}-\mathbb{BL}_{e_{m+r}}+\mathbb{BL}_{e_{m-s}}-\mathbb{BL}_{e_{m-r}}\right)C \\ &\quad +12\left(2j+ij\right)\left(\left(-1\right)^{m-s+1}F_s^2+\left(-1\right)^{m-r}F_r^2\right). \end{aligned}$$

□

Theorem 9. *The following identity between the Lucas and bicomplex Leonardo numbers is provided:*

$$\begin{aligned} \mathbb{BL}_{e_n}\mathbb{BL}_{e_m}-\mathbb{BL}_{e_s}\mathbb{BL}_{e_r} &= \left(\mathbb{BL}_{e_s}-\mathbb{BL}_{e_n}+\mathbb{BL}_{e_r}-\mathbb{BL}_{e_m}\right)C \\ &\quad +\frac{12}{5}\left(2j+ij\right)\left(\left(-1\right)^m L_{n-m}-\left(-1\right)^r L_{s-r}\right). \end{aligned}$$

Here n, m, s and r are positive integers with $n \geq m$, $s \geq r$ and $n+m=s+r$.

Proof. By using (22) to left hand side (LHS), we get

$$\begin{aligned} LHS &= \left(2\frac{\underline{\Phi}\phi^{n+1}-\underline{\Psi}\psi^{n+1}}{\phi-\psi}-C\right)\left(2\frac{\underline{\Phi}\phi^{m+1}-\underline{\Psi}\psi^{m+1}}{\phi-\psi}-C\right) \\ &\quad -\left(2\frac{\underline{\Phi}\phi^{s+1}-\underline{\Psi}\psi^{s+1}}{\phi-\psi}-C\right)\left(2\frac{\underline{\Phi}\phi^{r+1}-\underline{\Psi}\psi^{r+1}}{\phi-\psi}-C\right) \\ &= \left(\mathbb{BL}_{e_s}-\mathbb{BL}_{e_n}+\mathbb{BL}_{e_r}-\mathbb{BL}_{e_m}\right)C \end{aligned}$$

$$+\frac{4\underline{\Phi}.\underline{\Psi}}{(\phi-\psi)^2}\left(\phi^n\psi^m+\phi^m\psi^n-\phi^s\psi^r-\phi^r\psi^s\right).$$

From (14) and (25), we also obtain that

$$\begin{aligned} LHS &= \left(\mathbb{BL}_{e_s}-\mathbb{BL}_{e_n}+\mathbb{BL}_{e_r}-\mathbb{BL}_{e_m}\right)C \\ &\quad +\frac{12}{5}\left(2j+ij\right)\left((-1)^m L_{n-m}-(-1)^r L_{s-r}\right). \end{aligned}$$

This completes the proof. □

Theorem 10. *For r and s positive integers with $r\geq 1$, $s\geq 1$, then we have*

$$\begin{aligned} \mathbb{BL}_{e_{s+1}}\mathbb{BL}_{e_{r+1}}-\mathbb{BL}_{e_{s-1}}\mathbb{BL}_{e_{r-1}} &= 4\left[\begin{array}{c} -5F_{s+r+3}+5F_{s+r+7}+2i(F_{s+r+3}-F_{s+r+7}) \\ -2jF_{s+r+5}+4ijF_{s+r+5} \end{array}\right] \\ &\quad -(\mathbb{BL}_{e_s}+\mathbb{BL}_{e_r}+2C)C. \end{aligned}$$

Proof. By using (22) to left hand side (LHS), we get

$$\begin{aligned} LHS &= \left(2\frac{\underline{\Phi}\phi^{s+2}-\underline{\Psi}\psi^{s+2}}{\phi-\psi}-C\right)\left(2\frac{\underline{\Phi}\phi^{r+2}-\underline{\Psi}\psi^{r+2}}{\phi-\psi}-C\right) \\ &\quad -\left(2\frac{\underline{\Phi}\phi^{s}-\underline{\Psi}\psi^{s}}{\phi-\psi}-C\right)\left(2\frac{\underline{\Phi}\phi^{r}-\underline{\Psi}\psi^{r}}{\phi-\psi}-C\right) \\ &= -(\mathbb{BL}_{e_s}+\mathbb{BL}_{e_r}+2C)C \\ &\quad +\frac{4}{(\phi-\psi)^2}\left(\underline{\Phi}^2\phi^{s+r}\left(\phi^4-1\right)+\underline{\Psi}^2\psi^{s+r}\left(\psi^4-1\right)\right). \end{aligned}$$

Here, if we use the Binet formula for the Lucas numbers (4) and make the necessary calculations, we obtain

$$\begin{aligned} LHS &= -(\mathbb{BL}_{e_s}+\mathbb{BL}_{e_r}+2C)C \\ &\quad +\left(-2L_{s+r+5}+L_{s+r+1}+L_{s+r+9}\right)+i\left(4L_{s+r+5}-2L_{s+r+1}-L_{s+r+9}\right) \\ &\quad +j\left(-2L_{s+r+7}+2L_{s+r+3}\right)+k\left(4L_{s+r+7}-4L_{s+r+3}\right) \end{aligned}$$

Also by using the equation (14), we have

$$\begin{aligned} LHS &= -(\mathbb{BL}_{e_s}+\mathbb{BL}_{e_r}+2C)C \\ &\quad +4\left[\begin{array}{c} -5F_{s+r+3}+5F_{s+r+7}+2i(F_{s+r+3}-F_{s+r+7}) \\ -2jF_{s+r+5}+4ijF_{s+r+5} \end{array}\right]. \end{aligned}$$

This completes the proof. □

3. Conclusion

In the present paper, bicomplex Leonardo numbers with coefficients of basis of Leonardo numbers have been introduced. First of all the recurrence relation and generating function for these numbers have been obtained. Then summation formulas for these numbers have been provided. Furthermore, Catalan's and Cassini's identities and some interesting properties have been given.

Author Contribution Statements All authors contributed equally and significantly in writing this article. All authors read and approved the final manuscript.

Declaration of Competing Interests On behalf of all authors, the corresponding author states that there is no conflict of interest.

Acknowledgements The authors are thankful to the referees for making valuable suggestions leading to the better presentations of this paper.

References

[1] Alp, Y., Koçer, E. G., Some properties of Leonardo numbers, *Konuralp J. Math.*, 9(1) (2021), 183–189.
[2] Alp, Y., Koçer, E. G., Hybrid Leonardo numbers, *Chaos, Solitons and Fractals*, 150 (2021), 111–128. https://doi.org/10.1016/j.chaos.2021.111128
[3] Alves, F. R. V., Catarino, P. M. M. C., A forma matricial dos números de Leonardo,*Ciencia e natura*, 42 (2020), 1–6. https://doi.org/10.5902/2179460X41839
[4] Catarino, P., Borges, A., On Leonardo numbers, *Acta Mathematica Universitatis Comenianae*, 89(1) (2019), 75–86.
[5] Catarino, P., Borges, A., A note on incomplete Leonardo numbers, *Integers*, 20(7) (2020).
[6] Halıcı, S., On bicomplex Fibonacci numbers and their generalization, *In Models and Theories in Social Systems*, (2019), 509–524. https://doi.org/10.1007/978-3-030-00084-426
[7] Hamilton, W. R., Lectures on Quaternions, Hodges and Smith, Dublin, 1853.
[8] Hoggatt, V. E., Fibonacci and Lucas Numbers, A publication of the Fibonacci Association University of Santa Clara, Santa Clara, Houghton Mifflin Company, 1969.
[9] Horadam, A. F., Basic properties of a certain generalized sequence of numbers, *Fibonacci Quarterly* 3 (1965), 161–176.
[10] Kızılates C, Kone T. On higher order Fibonacci hyper complex numbers, *Chaos Solitons Fractals*, 148 (2021), 111044. https://doi.org/10.1016/j.chaos.2021.111044
[11] Koshy, T., Fibonacci and Lucas Numbers with Applications, John Wiley and Sons, Hoboken, NJ, USA, 2019.
[12] Kuruz, F., Dagdeviren, A., Catarino, P., On Leonardo Pisano hybrinomials, *Mathematics*, 9(22) (2021), 2923. https:/doi.org/10.3390/math9222923
[13] Luna-Elizarrarás, M. E., Shapiro, M., Struppa, D. C., Bicomplex numbers and their elementary functions, *Cubo* 14 (2012), 61–80.
[14] Nurkan, S. K., Guven, I. A., A Note on bicomplex Fibonacci and Lucas numbers, *International Journal of Pure and Applied Mathematics*, 120(3) (2018), 365–377. https:/doi.org/10.12732/ijpam.v120i3.7
[15] Price, G. B., An Introduction to Multicomplex Spaces and Functions, Monographs and Textbooks in Pure and Applied Mathematics, M. Dekker, New York, NY, USA, 1991.
[16] Rochon, D., Shapiro, M., On algebraic properties of bicomplex and hyperbolic numbers, *Anal. Univ. Oradea Fasc. Math.,* 11 (2004), 71–110.
[17] Segre, C., The real representation of complex elements and hyperalgebraic entities (Italian), *Math. Ann.*, 40 (1892), 413–467.
[18] Shannon, A. G., A note on generalized Leonardo numbers, *Notes Number Theory Discrete Math.*, 25(3) (2019), 97–101. https:/doi.org/10.7546/nntdm.2019.25.3.97-101.
[19] Sloane, N. J. A., The On-line Encyclopedia of Integers Sequences. 1964.

[20] Tan, E., Leung H. H., On Leonardo p-numbers, *Integers*, 23 (2023), 1-11. DOI: 10.5281/zenodo.7569221

[21] Torunbalcı, A., Bicomplex Fibonacci quaternions, *Chaos, Solitons and Fractals,* 106 (2018), 147–153. https://doi.org/10.1016/j.chaos.2017.11.026

[22] Vajda, S., Fibonacci and Lucas Numbers and The Golden Section, Ellis Horwood Limited Publ., England, 1989.

http://communications.science.ankara.edu.tr

Commun.Fac.Sci.Univ.Ank.Ser. A1 Math. Stat.
Volume 72, Number 2, Pages 352–362 (2023)
DOI:10.31801/cfsuasmas.1146782
ISSN 1303-5991 E-ISSN 2618-6470

COMMUNICATIONS SERIES A1

Research Article; Received: January 24, 2022; Accepted: November 27, 2022

UPPER BOUNDS FOR THE BLOW UP TIME FOR THE KIRCHHOFF-TYPE EQUATION

Yavuz DİNÇ[1], Erhan PİŞKİN[2] and Cemil TUNÇ[3]

[1]Department of Electronics Technical, Mardin Artuklu University, Mardin, TÜRKİYE
[2]Department of Mathematics, Dicle University, Diyarbakır, TÜRKİYE
[3]Department of Mathematics, Van Yuzuncu Yil University, Van, TÜRKİYE

Abstract. In this research, we take into account the Kirchhoff type equation with variable exponent. The Kirchhoff type equation is known as a kind of evolution equations,namely, PDEs, where t is an independent variable. This type problem can be extensively used in many mathematical models of various applied sciences such as flows of electrorheological fluids, thin liquid films, and so on. This research, we investigate the upper bound for blow up time under suitable conditions.

1. Introduction

In this work, we deal with the upper bounds of blow up time of solutions of the p-Kirchhoff type equation with variable exponent

$$\begin{cases} u_{tt} - M\left(\|\nabla u\|_p^p\right)\Delta_p u + |u_t|^{r(\cdot)-2} u_t = |u|^{q(\cdot)-2} u, & (x,t) \in \Omega \times (0,T), \\ u(x,0) = u_0(x), \ u_t(x,0) = u_1(x), & x \in \Omega, \\ u(x,t) = 0, & \partial\Omega \times (0,T), \end{cases} \tag{1}$$

where Ω is a bounded domain and this bounded has the smooth boundary $\partial\Omega$ in R^n $(n \geq 1)$. The term

$$\Delta_p u = \operatorname{div}\left(|\nabla u|^{p-2} \nabla u\right) \quad \text{with} \quad p \geq 2$$

is called and p-Laplacian and

$$M(s) = 1 + s.$$

2020 *Mathematics Subject Classification.* 35B44, 35L10, 46E35.
Keywords. Blow up, Kirchhoff-type equation, variable exponent.
[1] yavuzdinc@artuklu.edu.tr-Corresponding author; 0000-0003-0897-4101
[2] episkin@dicle.edu.tr; 0000-0001-6587-4479
[3] cemtunc@yahoo.com; 0000-0003-2909-8753.

The variable exponents $r(\cdot)$ and $q(\cdot)$ are taken as measurable functions on Ω satisfying

$$2 \le r^- \le r(x) \le r^+ < q^- \le q(x) \le q^+ \le q^*, \tag{2}$$

where

$$\begin{cases} r^- = ess\inf_{x\in\Omega} r(\cdot), & r^+ = ess\sup_{x\in\Omega} r(\cdot), \\ q^- = ess\inf_{x\in\Omega} q(\cdot), & q^+ = ess\sup_{x\in\Omega} q(\cdot), \end{cases}$$

and

$$q^* = \begin{cases} \infty, \text{ if } n = 1, 2, \\ \frac{2n}{n-2}, \text{ if } n \ge 3. \end{cases}$$

The problem (1) generalizes the model of Kirchhoff [8]. The Kirchhoff equation as an extension of the classical D'Alembert's wave equation for free vibrations of elastic strings. The equations with variable exponents can appear research fields such as image processing, nonlinear elasticity theory and electrorheological fluids [5,6,19].

In [14], the some problem (1) was studied. The authors proved the stability and the global existence of the solution with positive initial energy.

When $p \equiv 2$, (1) is reduced to following Kirchhoff equation

$$u_{tt} - M\left(\|\nabla u\|_2^2\right)\Delta u + u_t |u_t|^{r(\cdot)-2} = u|u|^{q(\cdot)-2}. \tag{3}$$

In [16], Pişkin studied Eq. (3) for the blow up of solutions.

When $M\left(\|\nabla u\|_2^2\right) \equiv 1$, (3) is reduced to following wave equation

$$u_{tt} - \Delta u + u_t |u_t|^{r(\cdot)-2} = u|u|^{q(\cdot)-2}. \tag{4}$$

In [13], Messaoudi et al. took into consideration equation Eq. (4). The authors discussed the local existence and the blow up of solutions.

Messaoudi and Talahmeh [12] considered the following quasilinear wave equation

$$u_{tt} - \operatorname{div}\left(|\nabla u|^{p(x)-2}\nabla u\right) + u_t |u_t|^{r(x)-2} = u|u|^{q(x)-2}. \tag{5}$$

They proved a finite-time blow-up for the solutions with negative initial energy and for certain solutions with positive energy. Later, Li et al. [10] proved the asymptotic stability of solutions (5). Recently, some other authors studied hyperbolic type equations with variable exponents (see [1,2,4,11,17,18,20,21]).

Motivated by the above studies, in this work, we consider the upper bounds of blow up time of the solution (1) under suitable conditions.

This work is outlined as the following: In the section 2, we give some results about the variable exponent Sobolev spaces ($W^{1,p(\cdot)}(\Omega)$) and Lebesgue spaces ($L^{p(\cdot)}(\Omega)$). In the last section, the upper bounds of blow up time will be proved.

2. Preliminaries

In this part, we give some results in relation to the variable exponent spaces ($L^{p(\cdot)}(\Omega)$ and $W^{1,p(\cdot)}(\Omega)$). For more details, see [6,7,9,15].

Let Ω is a bounded domain of R^n, $p:\Omega\to[1,\infty)$ be a measurable function. We define the variable exponent Lebesgue space by

$$L^{p(\cdot)}(\Omega)=\left\{u:\Omega\to R,\ u \text{ is measurable and } \rho_{p(.)}(\lambda u)\ <\infty,\ \text{ for some } \lambda>0\right\}$$

where

$$\rho_{p(.)}(u)=\int_{\Omega}|u|^{p(x)}\,dx.$$

The space $L^{p(\cdot)}(\Omega)$ endowed with the norm (Luxemburg norm)

$$\|u\|_{p(\cdot)}=\inf\left\{\lambda>0:\int_{\Omega}\left|\frac{u}{\lambda}\right|^{p(x)}dx\le 1\right\},$$

$L^{p(x)}(\Omega)$ is a Banach space.

Next we define the variable exponent Sobolev space $W^{1,p(x)}(\Omega)$ as follows

$$W^{1,p(\cdot)}(\Omega)=\left\{u\in L^{p(x)}(\Omega):\nabla u \text{ exists and } |\nabla u|\in L^{p(x)}(\Omega)\right\}.$$

It can be seen the Sobolev space with the variable exponent is a Banach space with respect to the norm

$$\|u\|_{1,p(x)}=\|u\|_{p(x)}+\|\nabla u\|_{p(x)}.$$

The space $W_0^{1,p(x)}(\Omega)$ is defined as the closure of $C_0^{\infty}(\Omega)$ in $W^{1,p(x)}(\Omega)$ with respect to the norm $\|u\|_{1,p(x)}$. For $u\in W_0^{1,p(x)}(\Omega)$, we define an equivalent norm

$$\|u\|_{1,p(x)}=\|\nabla u\|_{p(x)}.$$

The variable exponents $p(\cdot)$ and $q(\cdot)$ satisfy the log-Hölder continuity condition:

$$|p(x)-p(y)|\le-\frac{B}{\log|x-y|},\ \text{ for all } x,y\in\Omega \text{ and } |x-y|<\delta, \tag{6}$$

where $B>0$, $0<\delta<1$.

Lemma 1. *[6]. Suppose that (6) holds. Then*

$$\|u\|_{p(\cdot)}\le c\,\|\nabla u\|_{p(\cdot)},\ \textit{for all } u\in W_0^{1,p(\cdot)}(\Omega),$$

where $c=c\,(p^-,p^+,|\Omega|)>0$.

The above inequality is known as Poincare inequality.

Lemma 2. *[6]. Let $p(\cdot) \in C\left(\overline{\Omega}\right)$ and $q : \Omega \to [1, \infty)$ be a measurable function and satisfy*

$$\underset{x\in\overline{\Omega}}{essinf}(p^*(x) - q(x)) > 0.$$

Then the Sobolev embedding $W_0^{1,p(\cdot)}(\Omega) \hookrightarrow L^{q(\cdot)}(\Omega)$ is continuous and compact, here

$$p^*(x) = \begin{cases} \frac{np^-}{n-p^-}, & \text{if } p^- < n \\ \infty, & \text{if } p^- \geq n. \end{cases}$$

By combining arguments of [3, 13], we have the following local existence theorem.

Theorem 1. *Suppose that (2) and (6) hold, and let $(u_0, u_1) \in W_0^{1,p}(\Omega) \times L^2(\Omega)$, then there exists a unique solution $u(x,t)$ of the problem (1), which satisfies*

$$\begin{aligned} u &\in L^\infty\left([0,T); W_0^{1,p}(\Omega)\right), \\ u_t &\in L^\infty\left([0,T); L^2(\Omega)\right) \cap L^{r(\cdot)}(\Omega \times (0,T)). \end{aligned}$$

3. Upper bounds for blow up time

In this part, we will proved the the upper bounds of blow up of solutions for the problem (1). Firstly, we give the following lemma.

Lemma 3. *[13]. If $q : \Omega \to [1, \infty)$ is a measurable function and*

$$2 \leq q^- \leq q(\cdot) \leq q^+ < \frac{2n}{n-2}; \quad n \geq 3 \tag{7}$$

hold, then we have the following estimates:

i)

$$\rho_{q(.)}^{\frac{s}{q^-}}(u) \leq c\left(\|\nabla u\|^2 + \rho_{q(.)}(u)\right), \tag{8}$$

ii)

$$\|u\|_{q^-}^s \leq c\left(\|\nabla u\|^2 + \|u\|_{q^-}^{q^-}\right), \tag{9}$$

iii)

$$\rho_{q(.)}^{\frac{s}{q^-}}(u) \leq c\left(|F(t)| + \|u_t\|^2 + \rho_{q(.)}(u)\right), \tag{10}$$

iv)

$$\|u\|_{q^-}^s \leq c\left(|F(t)| + \|u_t\|^2 + \|u\|_{q^-}^{q^-}\right), \tag{11}$$

v)

$$c\|u\|_{q^-}^{q^-} \leq \rho_{q(.)}(u) \tag{12}$$

for any $u \in H_0^1(\Omega)$ and $2 \leq s \leq q$, where $c > 1$ a positive constant and $F(t) = -E(t)$.

Now, the main result of this work is given in the following theorem.

Theorem 2. *Let the assumptions of Theorem 1 hold true and suppose that*

$$E(0) < 0.$$

Then the solution of the problem (1) blows up in finite time.

Proof. Multiplying the equation in the problem (1) by u_t and integrating on Ω , we obtain

$$\int_\Omega u_t u_{tt} dx - \int_\Omega u_t M\left(\|\nabla u\|_p^p\right) \Delta_p u dx + \int_\Omega u_t |u_t|^{r(x)-2} u_t dx = \int_\Omega u_t |u|^{q(x)-2} u dx.$$

If each term is calculated separetely and if these found terms are written in their place, we get this equality.

$$\frac{d}{dt}\left[\frac{1}{2}\|u_t\|^2 + \frac{1}{p}\|\nabla u\|_p^p + \frac{1}{2p}\|\nabla u\|_p^{2p} - \int_\Omega \frac{1}{q(x)}|u|^{q(x)} dx\right] = -\int_\Omega |u_t|^{r(x)} dx,$$

$$E'(t) = -\|u_t\|_{r(x)}^{r(x)}, \tag{13}$$

where

$$E(t) = \frac{1}{2}\|u_t\|^2 + \frac{1}{p}\|\nabla u\|_p^p + \frac{1}{2p}\|\nabla u\|_p^{2p} - \int_\Omega \frac{1}{q(x)}|u|^{q(x)} dx. \tag{14}$$

Set

$$F(t) = -E(t),$$

then $E(0) < 0$ and (13) gives $F(t) \geq F(0) > 0$. Also, by the definition $F(t)$, we get

$$\begin{aligned} F(t) &= -\frac{1}{2}\|u_t\|^2 - \frac{1}{p}\|\nabla u\|_p^p - \frac{1}{2p}\|\nabla u\|_p^{2p} + \int_\Omega \frac{1}{q(x)}|u|^{q(x)} dx \\ &\leq \int_\Omega \frac{1}{q(x)}|u|^{q(x)} dx \\ &\leq \frac{1}{q^-}\rho_{q(.)}(u). \end{aligned} \tag{15}$$

Define

$$\Phi(t) = F^{1-\sigma}(t) + \varepsilon \int_\Omega u u_t dx, \tag{16}$$

where ε small to be chosen later and

$$0 < \sigma \leq \min\left\{\frac{q^- - r^+}{(r^+ - 1)q^-}, \frac{q^- - 2}{2q^-}\right\}. \tag{17}$$

Calculation the derivative of (16) and using the equation in the problem (1), we find

$$\Phi'(t) = (1-\sigma) F^{-\sigma}(t) F'(t) + \varepsilon \int_\Omega \left(u_t^2 + u u_{tt}\right) dx$$

$$= (1-\sigma) F^{-\sigma}(t) F'(t) + \varepsilon \|u_t\|^2 - \varepsilon \|\nabla u\|_p^p - \varepsilon \|\nabla u\|_p^{2p} + \varepsilon \int_\Omega |u|^{q(x)} dx - \varepsilon \int_\Omega u u_t |u_t|^{r(x)-2} dx. \tag{18}$$

Use the definition of the $F(t)$, it follows that

$$\begin{aligned} -\varepsilon q^-(1-\mu) F(t) &= \frac{\varepsilon q^-(1-\mu)}{2} \|u_t\|^2 + \frac{\varepsilon q^-(1-\mu)}{p} \|\nabla u\|_p^p \\ &+ \frac{\varepsilon q^-(1-\mu)}{2p} \|\nabla u\|_p^{2p} \\ &- \varepsilon q^-(1-\mu) \int_\Omega \frac{1}{q(x)} |u|^{q(x)} dx, \end{aligned} \tag{19}$$

where $0 < \mu < 1$.

Add and subtract (19) into (18), we obtain

$$\begin{aligned} \Phi'(t) \geq\ & (1-\sigma) F^{-\sigma}(t) F'(t) + \varepsilon q^-(1-\mu) F(t) \\ & + \varepsilon \left(\frac{q^-(1-\mu)}{2} + 1 \right) \|u_t\|^2 + \varepsilon \left(\frac{q^-(1-\mu)}{p} - 1 \right) \|\nabla u\|_p^p \\ & + \varepsilon \left(\frac{q^-(1-\mu)}{2} - 1 \right) \|\nabla u\|_p^{2p} + \varepsilon \mu \int_\Omega |u|^{q(x)} dx \\ & - \varepsilon \int_\Omega u u_t |u_t|^{r(x)-2} dx. \end{aligned} \tag{20}$$

Then, for μ small enough, we derive

$$\begin{aligned} \Phi'(t) \geq\ & \varepsilon \beta \left[F(t) + \|u_t\|^2 + \|\nabla u\|_p^p + \|\nabla u\|_p^{2p} + \rho_{q(.)}(u) \right] \\ & + (1-\sigma) F^{-\sigma}(t) F'(t) - \varepsilon \int_\Omega u u_t |u_t|^{r(x)-2} dx, \end{aligned} \tag{21}$$

where

$$\beta = \min \left\{ q^-(1-\mu),\ \varepsilon\mu,\ \frac{q^-(1-\mu)}{p} - 1, \frac{q^-(1-\mu)}{2} - 1,\ \frac{q^-(1-\mu)}{2} + 1 \right\} > 0$$

and

$$\rho_{q(\cdot)}(u) = \int_\Omega |u|^{q(\cdot)} dx.$$

By using Young inequality, the last term of (21) yields

$$XY \leq \frac{\delta^k X^k}{k} + \frac{\delta^{-l} Y^l}{l},$$

where $X, Y \geq 0,\ \delta > 0,\ k, l \in R^+$ such that $\frac{1}{k} + \frac{1}{l} = 1$. Hence, we have

$$\int_\Omega |u_t|^{r(x)-1} u dx \leq \int_\Omega \frac{1}{r(x)} \delta^{r(x)} |u|^{r(x)} dx + \int_\Omega \frac{r(x)-1}{r(x)} \delta^{-\frac{r(x)}{r(x)-1}} |u_t|^{r(x)} dx$$

$$\leq \frac{1}{r^-}\int_\Omega \delta^{r(x)}|u|^{r(x)}dx+\frac{r^+-1}{r^+}\int_\Omega \delta^{-\frac{r(x)}{r(x)-1}}|u_t|^{r(x)}dx, \quad (22)$$

where δ is constant depending on the time t and specified later. Using the inequality (22), we obtain from (21) that

$$\begin{aligned}\Phi'(t) \geq\ & \varepsilon\beta\left[F(t)+\|u_t\|^2+\|\nabla u\|_p^p+\|\nabla u\|_p^{2p}+\rho_{q(.)}(u)\right]\\ &+(1-\sigma)F^{-\sigma}(t)F'(t)-\varepsilon\frac{1}{r^-}\int_\Omega \delta^{r(x)}|u|^{r(x)}dx\\ &-\varepsilon\frac{r^+-1}{r^+}\int_\Omega \delta^{-\frac{r(x)}{r(x)-1}}|u_t|^{r(x)}dx. \quad (23)\end{aligned}$$

Therefore, by picking δ so that $\delta^{-\frac{r(x)}{r(x)-1}}=bF^{-\sigma}(t)$, where $b>0$ will be determined later, we have

$$\begin{aligned}\Phi'(t) \geq\ & \varepsilon\beta\left[F(t)+\|u_t\|^2+\|\nabla u\|_p^p+\|\nabla u\|_p^{2p}+\rho_{q(.)}(u)\right]\\ &+(1-\sigma)F^{-\sigma}(t)F'(t)-\varepsilon\frac{1}{r^-}\int_\Omega b^{1-r(x)}F^{\sigma(r(x)-1)}(t)|u|^{r(x)}dx\\ &-\varepsilon\frac{r^+-1}{r^+}\int_\Omega bF^{-\sigma}(t)|u_t|^{r(x)}dx\\ \geq\ & \varepsilon\beta\left[F(t)+\|u_t\|^2+\|\nabla u\|_p^p+\|\nabla u\|_p^{2p}+\rho_{q(.)}(u)\right]\\ &+(1-\sigma)F^{-\sigma}(t)F'(t)-\varepsilon\frac{b^{1-r^-}}{r^-}F^{\sigma\left(r^+-1\right)}(t)\int_\Omega |u|^{r(x)}dx\\ &-\varepsilon\left(\frac{r^+-1}{r^+}\right)bF^{-\sigma}(t)\int_\Omega |u_t|^{r(x)}dx\\ \geq\ & \varepsilon\beta\left[F(t)+\|u_t\|^2+\|\nabla u\|_p^p+\|\nabla u\|_p^{2p}+\rho_{q(.)}(u)\right]\\ &+\left[(1-\sigma)-\varepsilon\left(\frac{r^+-1}{r^+}\right)b\right]F^{-\sigma}(t)F'(t)\\ &-\varepsilon\frac{b^{1-r^-}}{r^-}F^{\sigma\left(r^+-1\right)}(t)\int_\Omega |u|^{r(x)}dx. \quad (24)\end{aligned}$$

By using (12) and (15), we get

$$F^{\sigma\left(r^+-1\right)}(t)\int_\Omega |u|^{r(x)}dx \leq F^{\sigma\left(r^+-1\right)}(t)\left[\int_{\Omega_-}|u|^{r^-}dx+\int_{\Omega_+}|u|^{r^+}dx\right]$$

$$\begin{aligned} &\leq F^{\sigma(r^+-1)}(t)\,c\left[\left(\int_{\Omega_-}|u|^{q^-}dx\right)^{\frac{r^-}{q^-}}+\left(\int_{\Omega_+}|u|^{q^-}dx\right)^{\frac{r^+}{q^-}}\right] \\ &= F^{\sigma(r^+-1)}(t)\,c\left[\|u\|_{q^-}^{r^-}+\|u\|_{q^-}^{r^+}\right] \\ &\leq c\left(\frac{1}{q^-}\rho_{q(.)}(u)\right)^{\sigma(r^+-1)}\left[\left(\rho_{q(.)}(u)\right)^{\frac{r^-}{q^-}}+\left(\rho_{q(.)}(u)\right)^{\frac{r^+}{q^-}}\right] \\ &= c_1\left[\left(\rho_{q(.)}(u)\right)^{\frac{r^-}{q^-}+\sigma(r^+-1)}+\left(\rho_{q(.)}(u)\right)^{\frac{r^+}{q^-}+\sigma(r^+-1)}\right] \quad (25) \end{aligned}$$

where $\Omega_- = \{x\in\Omega : |u|<1\}$ and $\Omega_+ = \{x\in\Omega : |u|\geq 1\}$.

We then use Lemma 3 and (17), for

$$s = r^- + \sigma q^-\left(r^+-1\right) \leq q^-$$

and

$$s = r^+ + \sigma q^-\left(r^+-1\right) \leq q^-,$$

to deduce, from (25),

$$F^{\sigma(r^+-1)}(t)\int_{\Omega}|u|^{r(x)}dx \leq c_1\left[\|\nabla u\|^2+\rho_{q(.)}(u)\right]. \quad (26)$$

Hence, substituting the inequality (26) into (24), we have

$$\begin{aligned} \Phi'(t) \geq\ &\varepsilon\left(\beta-\frac{b^{1-r^-}}{r^-}c_1\right)\left[F(t)+\|u_t\|^2+\|\nabla u\|_p^p+\|\nabla u\|_p^{2p}+\rho_{q(.)}(u)\right] \\ &+\left[(1-\sigma)-\varepsilon\left(\frac{r^+-1}{r^+}\right)b\right]F^{-\sigma}(t)\,F'(t). \quad (27) \end{aligned}$$

As for coming step, let b large enough so that $\gamma=\beta-\frac{b^{1-r^-}}{r^-}c_1>0$, and choose ε small enough such that $(1-\sigma)-\varepsilon\left(\frac{r^+-1}{r^+}\right)b\geq 0$ and

$$\Phi(t)\geq\Phi(0)=F^{1-\sigma}(0)+\varepsilon\int_{\Omega}u_0u_1dx>0,\ \forall t\geq 0. \quad (28)$$

Consequently, (27) yields

$$\begin{aligned} \Phi'(t) &\geq \varepsilon\gamma\left[F(t)+\|u_t\|^2+\|\nabla u\|_p^p+\|\nabla u\|_p^{2p}+\rho_{q(.)}(u)\right] \\ &\geq \varepsilon\gamma\left[F(t)+\|u_t\|^2+\|\nabla u\|_p^p+\|\nabla u\|_p^{2p}+\|u\|_{q^-}^{q^-}\right], \quad (29) \end{aligned}$$

due to (12). Therefore we get,

$$\Phi(t)\geq\Phi(0)>0,\ \text{for all } t\geq 0.$$

Using the Hölder inequality, we have

$$\begin{aligned}\left|\int_{\Omega} u u_t dx\right|^{\frac{1}{1-\sigma}} &\leq \|u\|^{\frac{1}{1-\sigma}} \|u_t\|^{\frac{1}{1-\sigma}} \\ &\leq C\left(\|u\|_{q^-}^{\frac{1}{1-\sigma}} \|u_t\|^{\frac{1}{1-\sigma}}\right).\end{aligned}$$

Thanks to Young inequality, we get

$$\left|\int_{\Omega} u u_t dx\right|^{\frac{1}{1-\sigma}} \leq C\left(\|u\|_{q^-}^{\frac{\alpha}{1-\sigma}} + \|u_t\|^{\frac{\theta}{1-\sigma}}\right), \tag{30}$$

for $\frac{1}{\alpha} + \frac{1}{\theta} = 1$. We take $\theta = 2(1-\sigma)$, to obtain $\frac{\alpha}{1-\sigma} = \frac{2}{1-2\sigma} \leq q^-$ by (17). Therefore, (30) becomes

$$\left|\int_{\Omega} u u_t dx\right|^{\frac{1}{1-\sigma}} \leq C\left(\|u_t\|^2 + \|u\|_{q^-}^{s}\right),$$

where $\frac{2}{1-2\sigma} \leq q^-$. By using (11), we get

$$\left|\int_{\Omega} u u_t dx\right|^{\frac{1}{1-\sigma}} \leq C\left(\|u_t\|^2 + \|u\|_{q^-}^{q^-} + F(t)\right).$$

Thus,

$$\begin{aligned}\Phi^{\frac{1}{1-\sigma}}(t) &= \left[F^{1-\sigma}(t) + \varepsilon\int_{\Omega} u u_t dx\right]^{\frac{1}{1-\sigma}} \\ &\leq 2^{\frac{\sigma}{1-\sigma}}\left(F(t) + \varepsilon^{\frac{1}{1-\sigma}}\left|\int_{\Omega} u u_t dx\right|^{\frac{1}{1-\sigma}}\right) \\ &\leq C\left(\|u_t\|^2 + \|u\|_{q^-}^{q^-} + F(t)\right) \\ &\leq C\left(F(t) + \|u_t\|^2 + \|\nabla u\|_p^p + \|\nabla u\|_p^{2p} + \|u\|_{q^-}^{q^-}\right)\end{aligned} \tag{31}$$

where

$$(a+b)^p \leq 2^{p-1}(a^p + b^p)$$

is used.

In summary, our aim here is to obtain an inequality between the derivative of the Φ function and its numerical power. By combining of (29) and (31), we get

$$\Phi'(t) \geq \mu\Phi^{\frac{1}{1-\sigma}}(t). \tag{32}$$

where $\mu > 0$.

Integrating the inequality (32) over $(0,t)$ yields

$$\Phi^{\frac{\sigma}{1-\sigma}}(t) \geq \frac{1}{\Psi^{-\frac{\sigma}{1-\sigma}}(0) - \frac{\mu\sigma t}{1-\sigma}}.$$

This shows that solution blows up in a finite time T^*, with

$$T^* \leq \frac{1-\sigma}{\mu\sigma\Phi^{\frac{\sigma}{1-\sigma}}(0)}.$$

Hence, we finish the proof.

Authors Contribution Statements All authors contributed equally to the writing of this paper. All authors read and approved the final manuscript.

Declaration of Competing Interests The authors declare that they have no competing interests.

Acknowledgement The authors thank the referees and editor for their valuable suggestions which made this paper much improved. In addition, this article was presented in summary at the 4th International Conference on Pure and Applied Mathematics (ICPAM - VAN 2022), Van-Turkey, 22-23 June 2022. □

References

[1] Abita, R., Existence and asymptotic behavior of solutions for degenerate nonlinear Kirchhoff strings with variable-exponent nonlinearities, *Acta Mathematica Vietnamica*, 46 (2021), 613-643. https://doi.org/10.1007/s40306-021-00420-7

[2] Alkhalifa, L., Dridi, H., Zennir, K., Blow-up of certain solutions to nonlinear wave equations in the Kirchhoff-type equation with variable exponents and positive initial energy, *Journal of Function Spaces*, (2021), 1-9. https://doi.org/10.1155/2021/5592918

[3] Antontsev, S. N., Ferreira, J., Pişkin, E., Cordeiro, S. M. S., Existence and non-existence of solutions for Timoshenko-type equations with variable exponents, *Nonlinear Analysis: Real World Applications,* 61 (2021) 1-13. https://doi.org/10.1016/j.nonrwa.2021.103341

[4] Antontsev, S. N., Ferreira, J., Pişkin, E., Existence and blow up of Petrovsky equation solutions with strong damping and variable exponents, *Electronic Journal of Differential Equations*, 2021 (2021) 1-18. https://digital.library.txstate.edu/handle/10877/14403

[5] Chen, Y., Levine, S., Rao, M., Variable exponent, linear growth functionals in image restoration, *SIAM Journal on Applied Mathematics*, 66 (2006) 1383-1406. https://doi.org/10.1137/050624522

[6] Diening, L., Hasto, P., Harjulehto, P., Ruzicka, M. M., Lebesgue and Sobolev Spaces with Variable Exponents, Springer-Verlag, 2011.

[7] Fan, X. L., Shen, J. S., Zhao, D., Sobolev embedding theorems for spaces $W^{k,p(x)}(\Omega)$, *J. Math. Anal. Appl.,* 263 (2001), 749-760. https://doi.org/10.1006/jmaa.2001.7618

[8] Kirchhoff, G., Mechanik, Teubner, 1883.

[9] Kovacik, O., Rakosnik, J., On spaces $L^{p(x)}(\Omega)$, and $W^{k,p(x)}(\Omega)$, *Czechoslovak Mathematical Journal*, 41 (1991), 592-618. http://dml.cz/dmlcz/102493

[10] Li, X., Guo, B., Liao, M., Asymptotic stability of solutions to quasilinear hyperbolic equations with variable sources, *Computers and Mathematics with Applications* 79 (2020), 1012-1022. https://doi.org/10.1016/j.camwa.2019.08.016

[11] Messaoudi, S.A., Bouhoufani, O., Hamchi, I., Alahyone, M., Existence and blow up in a system of wave equations with nonstandard nonlinearities, *Electronic Journal of Differential Equations,* 2021 (2021), 1-33. http://ejde.math.unt.edu/

[12] Messaoudi, S. A., Talahmeh, A. A., Blow up in solutions of a quasilinear wave equation with variable-exponent nonlinearities, *Math. Meth. Appl. Sci.*, 40 (2017), 6976-6986. https://doi.org/10.1002/mma.4505

[13] Messaoudi, S. A., Talahmeh, A. A., Al-Shail, J. H., Nonlinear damped wave equation: Existence and blow-up, *Comp. Math. Appl.*, 74 (2017), 3024-3041. https://doi.org/10.1016/j.camwa.2017.07.048

[14] Ouaoua, A., Khaldi, A., Maouni, M., Global existence and stability of solution for a p-Kirchhoff type hyperbolic equation with variable exponents, *Bol. Soc. Paran. Mat.*, 40 (2022), 1-12. http://dx.doi.org/10.5269/bspm.51464

[15] Pişkin, E., Sobolev Spaces, Seçkin Publishing, 2017 (in Turkish).

[16] Pişkin, E., Finite time blow up of solutions of the Kirchhoff-type equation with variable exponents, *Int. J. Nonlinear Anal. Appl.,* 11 (2020), 37- 45. http://dx.doi.org/10.22075/ijnaa.2019.16022.1841

[17] Pişkin, E., Finite time blow up of solutions for a strongly damped nonlinear Klein-Gordon equation with variable exponents, *Honam Mathematical J.*, 40(4) (2018), 771-783. https://doi.org/10.5831/HMJ.2018.40.4.771

[18] Pişkin, E., Yılmaz, N., Blow up of solutions for a system of strongly damped Petrovsky equations with variable exponents, *Acta Universitatis Apulensis*, 71 (2022), 87-99. doi: 10.17114/j.aua.2022.71.06

[19] Ruzicka, M., Electrorheological Fluids: Modeling and Mathematical Theory, Lecture Notes in Mathematics, Springer, 2000. http://hdl.handle.net/2433/63967

[20] Shahrouzi, M., Exponential growth of solutions for a variable-exponent fourth-order viscoelastic equation with nonlinear boundary feedback, *Ser. Math. Inform.*, 37 (2022), 507-520.

[21] Shahrouzi M., Ferreira J., Pişkin E., Stability result for a variable-exponent viscoelastic double-Kirchhoff type inverse source problem with nonlocal degenerate damping term, *Ricerche di Matematica*, https://doi.org/10.1007/s11587-022-00713-5 (in press).

http://communications.science.ankara.edu.tr

Commun.Fac.Sci.Univ.Ank.Ser. A1 Math. Stat.
Volume 72, Number 2, Pages 363–373 (2023)
DOI:10.31801/cfsuasmas.1067247
ISSN 1303-5991 E-ISSN 2618-6470

COMMUNICATIONS SERIES A1

Research Article; Received: February 2, 2022; Accepted: November 27, 2022

NOTES ON SOME PROPERTIES OF THE NATURAL RIEMANN EXTENSION

Filiz OCAK

Department of Mathematics, Karadeniz Technical University, Trabzon, TÜRKİYE

ABSTRACT. Let (M,∇) be an n-dimensional differentiable manifold with a torsion-free linear connection and T^*M its cotangent bundle. In this context we study some properties of the natural Riemann extension (M. Sekizawa (1987), O. Kowalski and M. Sekizawa (2011)) on the cotangent bundle T^*M. First, we give an alternative definition of the natural Riemann extension with respect to horizontal and vertical lifts. Secondly, we investigate metric connection for the natural Riemann extension. Finally, we present geodesics on the cotangent bundle T^*M endowed with the natural Riemann extension.

1. Introduction

Let (M,∇) be an n-dimensional C^{∞}-manifold with a torsion-free linear connection and $\pi : T^*M \to M$ be the natural projection from its cotangent bundle T^*M to M. For any local chart $\left(U, x^j\right),\ j = 1,...,n$ around $x \in M$ induces a local chart $\left(\pi^{-1}(U), x^j, x^{\bar{j}} = p_j\right),\ \bar{j} = n+1,...,2n$ around $(x,p) \in T^*M$, where $x^{\bar{j}} = p_j$ are the components of the covector p in each cotangent spaces $T^*_xM,\ x \in U$ endowed with the natural coframe $\left\{dx^j\right\},\ j = 1,...,n$. By $\Im^r_s(M)\,(\Im^r_s(T^*M))$ we take the module over $F(M)\,(F(T^*M))$ of C^{∞} tensor fields of type (r,s) on $M(T^*M)$.

In [18] Patterson and Walker defined a semi-Riemannian metric of signature (n,n) on the cotangent bundle T^*M of (M,∇), called the Riemann extension. The Riemann extension described by

$$^{R}\nabla\left(^{C}V, {}^{C}Z\right) = -\gamma\left(\nabla_V Z + \nabla_Z V\right),$$

where ^{C}V and ^{C}Z denote the complete lifts of the vector fields V and Z on M to T^*M and $\gamma\left(\nabla_V Z + \nabla_Z V\right) = p_h\left(V^j\nabla_j Z^h + Z^j\nabla_j V^h\right).$

2020 *Mathematics Subject Classification.* 53B20, 53C07, 53C22.

Keywords. Vertical and horizontal lift, adapted frame, geodesics, natural Riemann extension, cotangent bundle.

filiz.ocak@ktu.edu.tr; 0000-0003-4157-6404.

Since the tensor field ${}^{R}\nabla \in \Im_{2}^{0}(T^{*}M)$ is completely determined by its action upon the vector fields of type ${}^{H}\mathrm{V}$ and ${}^{V}\vartheta$, Aslanci *et al.*[3] give the following alternative definition for ${}^{R}\nabla$ by

$$\begin{aligned} {}^{R}\nabla\left({}^{H}V, {}^{H}Y\right) &= {}^{R}\nabla\left({}^{V}\vartheta, {}^{V}\omega\right) = 0, \\ {}^{R}\nabla\left({}^{V}\vartheta, {}^{H}Y\right) &= {}^{V}\left(\vartheta\left(Y\right)\right) = \vartheta\left(Y\right) \circ \pi \end{aligned}$$

for any $V, Y \in \Im_{0}^{1}(M)$ and $\vartheta, \omega \in \Im_{1}^{0}(M)$. The geometry of the Riemann extension and its generalization were intensively studied in many papers (see for example [2, 4, 8-11, 14, 15-17, 19, 21]).

The natural Riemann extension $\bar{g}$ as a generalization of the Riemann extension is given by Sekizawa in [20] (see also Kowalski and Sekizawa [12]) and defined by the three identities:

$$\begin{aligned} \bar{g}\left({}^{C}V, {}^{C}Z\right) &= -a^{V}\left(\nabla_{V}Z + \nabla_{Z}V\right) + b^{V}V^{V}Z, \\ \bar{g}\left({}^{C}V, {}^{V}\omega\right) &= a^{V}\left(\omega(V)\right), \\ \bar{g}\left({}^{V}\vartheta, {}^{V}\omega\right) &= 0 \end{aligned} \tag{1}$$

for any $V, Z \in \Im_{0}^{1}(M)$ and $\vartheta, \omega \in \Im_{1}^{0}(M)$, where ${}^{V}V = {}^{V}V_{(x,p)} = p(V_{x}) = \sum_{k=1}^{n} p_{k}V^{k}$ is a function and a, b are arbitrary constants. We may assume $a > 0$ without loss of generality. When $b \neq 0$ (resp. $b = 0$), $\bar{g}$ is called a proper (resp. a non-proper) natural Riemannian extension. As a particular situation, when $a = 1$ and $b = 0$, we get the Riemannian extension. For further references relation to the natural Riemann extension, see [5-7,13].

In this paper, we give an alternative definition of the natural Riemann extension with respect to horizontal lifts of vector fields and vertical lifts of covector fields. Also, we present the Levi-Civita connection and Christoffel symbols with respect to the adapted frame. In Sect. 4, we show that the horizontal lift ${}^{H}\nabla$ of the torsion-free connection ∇ to the cotangent bundle $T^{*}M$ is a metric connection with respect to the natural Riemann extension. In Theorem 3 , we find that the metric connection${}^{H}\nabla$ has a vanishing scalar curvature with respect to the natural Riemann extension. In Sect. 5, we investigate the geodesics on the cotangent bundle $T^{*}M$ with respect to the natural Riemann extension.

2. Preliminaries

Let $\vartheta = \vartheta_{k}dx^{k}$ and $V = V^{k}\frac{\partial}{\partial x^{k}}$ be the local statements in $U \subset M$ of a covector field (1-form) $\vartheta \in \Im_{1}^{0}(M)$ and a vector field $V \in \Im_{0}^{1}(M)$, respectively. The vertical lift ${}^{V}\vartheta$ of ϑ, the horizontal and complete lift ${}^{H}V$, ${}^{C}V$ of V are defined, respectively, by

$$\begin{aligned} {}^{V}\vartheta &= \sum_{k} \vartheta_{k}\partial_{\bar{k}}, \\ {}^{H}V &= V^{k}\partial_{k} + \sum_{k} p_{h}\Gamma_{kj}^{h}V^{j}\partial_{\bar{k}}, \end{aligned} \tag{2}$$

$$^{C}V = V^k \frac{\partial}{\partial x^k} - \sum_k p_h \partial_k V^h \frac{\partial}{\partial x^{\bar{k}}},$$

where $\frac{\partial}{\partial x^k} = \partial_k$, $\frac{\partial}{\partial x^{\bar{k}}} = \partial_{\bar{k}}$ and Γ^h_{kj} are the components of ∇ on M [21].

From (2), the complete lift ^{C}V of $V \in \Im^1_0(M)$ is expressed by

$$^{C}V = {}^{H}V - {}^{V}(p(\nabla V)), \tag{3}$$

where $p(\nabla V) = p_j \left(\nabla_h V^j\right) dx^h$.

In $U \subset M$, we write

$$V_{(t)} = \frac{\partial}{\partial x^t},\ \vartheta^{(t)} = dx^t,\ t = 1, 2, ..., n.$$

From (2) and the natural frame $\{\partial_k, \partial_{\bar{k}}\}$, we can see that these vector fields have, respectively, the local expressions

$$\begin{cases} {}^{V}\vartheta^{(t)} = \tilde{f}_{(\bar{t})} = \partial_{\bar{t}}, \\ {}^{H}V_{(t)} = \tilde{f}_{(t)} = \partial_t + \sum\limits_h p_a \Gamma^a_{ht} \partial_{\bar{h}}. \end{cases} \tag{4}$$

The set $\left\{{}^{H}V_{(t)}, {}^{V}\vartheta^{(t)}\right\} = \left\{\tilde{f}_{(t)}, \tilde{f}_{(\bar{t})}\right\} = \left\{\tilde{f}_{(\beta)}\right\}$ is called adapted frame to the connection ∇ in $\pi^{-1}(U) \subset T^*M$.

We now consider local 1-forms $\tilde{\omega}^\alpha$ in $\pi^{-1}(U)$ defined by

$$\tilde{\omega}^\alpha = \bar{A}^\alpha{}_B dx^B,$$

where

$$A^{-1} = \left(\bar{A}^\alpha{}_B\right) = \begin{pmatrix} \bar{A}^i{}_j & \bar{A}^i{}_{\bar{j}} \\ \bar{A}^{\bar{i}}{}_j & \bar{A}^{\bar{i}}{}_{\bar{j}} \end{pmatrix} = \begin{pmatrix} \delta^i_j & 0 \\ -p_a \Gamma^a_{ij} & \delta^j_i \end{pmatrix}. \tag{5}$$

The matrix (5) is the inverse of the matrix

$$A = \left(A_\beta{}^A\right) = \begin{pmatrix} A_j{}^i & A_{\bar{j}}{}^i \\ A_j{}^{\bar{i}} & A_{\bar{j}}{}^{\bar{i}} \end{pmatrix} = \begin{pmatrix} \delta^i_j & 0 \\ p_a \Gamma^a_{ij} & \delta^j_i \end{pmatrix} \tag{6}$$

of the transformation $\tilde{f}_\beta = A_\beta{}^A \partial_A$ (see [4]). In what follows, the set $\{\tilde{\omega}^\alpha\}$ is called the coframe dual of the adapted frame $\left\{\tilde{f}_{(\beta)}\right\}$, i.e. $\tilde{\omega}^\alpha\left(\tilde{f}_\beta\right) = \bar{A}^\alpha{}_B A_\beta{}^B = \delta^\alpha_\beta$.

The Lie bracket operations of the adapted frame $\left\{\tilde{f}_{(\beta)}\right\}$ on the cotangent bundle T^*M are given by

$$\begin{aligned} \left[\tilde{f}_{(t)}, \tilde{f}_{(l)}\right] &= p_a R_{tlk}{}^a \tilde{f}_{(\bar{k})}, \\ \left[\tilde{f}_{(\bar{t})}, \tilde{f}_{(\bar{l})}\right] &= 0, \\ \left[\tilde{f}_{(t)}, \tilde{f}_{(\bar{l})}\right] &= -\Gamma^l_{tk} \tilde{f}_{(\bar{k})}, \end{aligned} \tag{7}$$

where ${R_{tlk}}^a$ being local components of the curvature tensor R of ∇ on M.

Hence we have the undermentioned components for vector fields ${}^V\vartheta$, ${}^HV$ and ${}^CV$ on T^*M

$$ {}^V\vartheta = \begin{pmatrix} 0 \\ \vartheta_j \end{pmatrix}, \quad {}^HV = \begin{pmatrix} V^j \\ 0 \end{pmatrix} \text{ and } {}^CV = \begin{pmatrix} V^j \\ -p_h \nabla_j V^h \end{pmatrix} \tag{8} $$

in the adapted frame $\left\{ \tilde{f}_{(\beta)} \right\}$.

3. The Natural Riemann Extension

Using (1) and (3), the natural Riemann extension $\bar{g}$ is determined by its action on ${}^V\vartheta$, ${}^HV$. Then we find

$$ \begin{aligned} &\bar{g}\left({}^HV, {}^HZ\right) = b^V V^V Z = bp(V)p(Z), \\ &\bar{g}\left({}^HV, {}^V\omega\right) = a^V\left(\omega(V)\right) = \left(\omega(V)\right) \circ \pi, \\ &\bar{g}\left({}^V\vartheta, {}^V\omega\right) = 0 \end{aligned} \tag{9} $$

for any $V, Z \in \Im_0^1(M)$ and $\vartheta, \omega \in \Im_1^0(M)$, where $a > 0$, a, b are arbitrary constants and ${}^VV = {}^VV_{(x,p)} = p(V_x) = \sum_{k=1}^n p_k V^k = p(V)$ is a function. By virtue of (4) and (9), we obtain

$$ \begin{aligned} &\bar{g}\left({}^HV_{(j)}, {}^HZ_{(k)}\right) = \bar{g}\left(\tilde{f}_{(j)}, \tilde{f}_{(k)}\right) = \bar{g}_{jk} = bp_jp_k, \\ &\bar{g}\left({}^HV_{(j)}, {}^V\vartheta^{(k)}\right) = \bar{g}\left(\tilde{f}_{(j)}, \tilde{f}_{(\bar{k})}\right) = \bar{g}_{j\bar{k}} = adx^k\left(\frac{\partial}{\partial x^j}\right) = a\delta_j^k, \\ &\bar{g}\left({}^V\vartheta^{(j)}, {}^HV_{(k)}\right) = \bar{g}\left(\tilde{f}_{(\bar{j})}, \tilde{f}_{(k)}\right) = \bar{g}_{\bar{j}k} = adx^j\left(\frac{\partial}{\partial x^k}\right) = a\delta_k^j, \\ &\bar{g}\left({}^V\vartheta^{(j)}, {}^V\omega^{(k)}\right) = \bar{g}\left(\tilde{f}_{(\bar{j})}, \tilde{f}_{(\bar{k})}\right) = \bar{g}_{\bar{j}\bar{k}} = 0. \end{aligned} $$

As corollary, the natural Riemann extension $\bar{g} = (\bar{g})_{JK}$ has the following components with respect to the adapted frame $\left\{ \tilde{f}_{(\beta)} \right\}$:

$$ \bar{g} = \bar{g}_{JK} = \begin{pmatrix} \bar{g}_{jk} & \bar{g}_{j\bar{k}} \\ \bar{g}_{\bar{j}k} & \bar{g}_{\bar{j}\bar{k}} \end{pmatrix} = \begin{pmatrix} bp_jp_k & a\delta_j^k \\ a\delta_k^j & 0 \end{pmatrix}. \tag{10} $$

Using $\bar{g}_{JK}\tilde{g}^{KI} = \delta_J^I$, we obtain the inverse $\tilde{g}^{JK}$ of the matrix $\bar{g}_{JK}$ as follows

$$ \tilde{g} = \tilde{g}^{JK} = \begin{pmatrix} 0 & \frac{1}{a}\delta_k^j \\ \frac{1}{a}\delta_j^k & -\frac{b}{a^2}p_jp_k \end{pmatrix}. \tag{11} $$

The Levi-Civita connection $\bar{\nabla}$ of the natural Riemann extension $\bar{g}$ is given by the following formulas:

Theorem 1. *In adapted frame* $\left\{\tilde{f}_{(\beta)}\right\}$, *the Levi-Civita connection* $\bar{\nabla}$ *of the natural Riemann extension* $\bar{g}$ *on* T^*M *is given by the following equations:*

$$\begin{aligned} &i)\ \bar{\nabla}_{\tilde{f}_i}\tilde{f}_j = \left(\Gamma^l_{ij} - \frac{b}{2a}\left(\delta^l_i p_j + \delta^l_j p_i\right)\right)\tilde{f}_l + \left(\frac{b}{a}p_k p_l \Gamma^k_{ji} - p_k R_{jli}{}^k\right)\tilde{f}_{\bar{l}},\\ &ii)\ \bar{\nabla}_{\tilde{f}_i}\tilde{f}_{\bar{j}} = \left(\frac{b}{2a}\left(\delta^j_l p_i + \delta^j_i p_l\right) - \Gamma^j_{li}\right)\tilde{f}_{\bar{l}},\\ &iii)\ \bar{\nabla}_{\tilde{f}_{\bar{i}}}\tilde{f}_j = \frac{b}{2}\left(\delta^i_j p_l + \delta^i_l p_j\right)\tilde{f}_{\bar{l}},\\ &iv)\ \bar{\nabla}_{\tilde{f}_{\bar{i}}}\tilde{f}_{\bar{j}} = 0 \end{aligned} \tag{12}$$

where $R_{lji}{}^s$, Γ^l_{ij} *are respectively the components of the curvature tensor and coefficients of* ∇.

Proof. The Koszul formula is given by

$$\begin{aligned} 2\bar{g}\left(\bar{\nabla}_{\tilde{V}}\tilde{W},\tilde{Z}\right) &= \tilde{V}\left(\bar{g}\left(\tilde{W},\tilde{Z}\right)\right) + \tilde{W}\left(\bar{g}\left(\tilde{Z},\tilde{V}\right)\right) - \tilde{Z}\left(\bar{g}\left(\tilde{V},\tilde{W}\right)\right) - \bar{g}\left(\tilde{V},\left[\tilde{W},\tilde{Z}\right]\right)\\ &+ \bar{g}\left(\tilde{W},\left[\tilde{Z},\tilde{V}\right]\right) + \bar{g}\left(\tilde{Z},\left[\tilde{V},\tilde{W}\right]\right) \end{aligned}$$

for any $\tilde{V},\tilde{W},\tilde{Z}\in\Im^1_0(T^*M)$. In Koszul formula, we put $\tilde{V}=\tilde{f}_i,\tilde{f}_{\bar{i}},\tilde{W}=\tilde{f}_j,\tilde{f}_{\bar{j}},\ \tilde{Z}=\tilde{f}_k,\ \tilde{f}_{\bar{k}}$.
i) By using (4), (7) and (10), we have

$$\begin{aligned} 2\bar{g}\left(\bar{\nabla}_{\tilde{f}_i}\tilde{f}_j,\tilde{f}_t\right) &= \tilde{f}_i\left(\bar{g}\left(\tilde{f}_j,\tilde{f}_t\right)\right) + \tilde{f}_j\left(\bar{g}\left(\tilde{f}_t,\tilde{f}_i\right)\right) - \tilde{f}_t\left(\bar{g}\left(\tilde{f}_i,\tilde{f}_j\right)\right) - \bar{g}\left(\tilde{f}_i,\left[\tilde{f}_j,\tilde{f}_t\right]\right)\\ &+ \bar{g}\left(\tilde{f}_j,\left[\tilde{f}_t,\tilde{f}_i\right]\right) + \bar{g}\left(\tilde{f}_t,\left[\tilde{f}_i,\tilde{f}_j\right]\right)\\ &= \left(\partial_i + p_k\Gamma^k_{hi}\partial_{\bar{h}}\right)bp_jp_t + \left(\partial_j + p_k\Gamma^k_{hj}\partial_{\bar{h}}\right)bp_tp_i - \left(\partial_t + p_k\Gamma^k_{ht}\partial_{\bar{h}}\right)bp_ip_j\\ &- ap_kR_{jtl}{}^k\delta^l_i + ap_kR_{til}{}^k\delta^l_j + ap_kR_{ijl}{}^k\delta^l_t\\ &= bp_k\Gamma^k_{hi}\left(p_t\delta^h_j + p_j\delta^h_t\right) + bp_k\Gamma^k_{hj}\left(p_i\delta^h_t + p_t\delta^h_i\right) - bp_k\Gamma^k_{ht}\left(p_j\delta^h_i + p_i\delta^h_j\right)\\ &- ap_kR_{jti}{}^k + ap_kR_{tij}{}^k + ap_kR_{ijt}{}^k\\ &= 2bp_kp_t\Gamma^k_{ji} - 2ap_kR_{jti}{}^k\\ &= \left(2\frac{b}{a}p_kp_l\Gamma^k_{ji} - 2p_kR_{jli}{}^k\right)a\delta^l_t\\ &= 2\bar{g}\left(\left(\frac{b}{a}p_kp_l\Gamma^k_{ji} - p_kR_{jli}{}^k\right)\tilde{f}_{\bar{l}},\tilde{f}_t\right) \end{aligned}$$

and

$$\begin{aligned} 2\bar{g}\left(\bar{\nabla}_{\tilde{f}_i}\tilde{f}_j,\tilde{f}_{\bar{t}}\right) &= \tilde{f}_i\left(\bar{g}\left(\tilde{f}_j,\tilde{f}_{\bar{t}}\right)\right) + \tilde{f}_j\left(\bar{g}\left(\tilde{f}_{\bar{t}},\tilde{f}_i\right)\right) - \tilde{f}_{\bar{t}}\left(\bar{g}\left(\tilde{f}_i,\tilde{f}_j\right)\right) - \bar{g}\left(\tilde{f}_i,\left[\tilde{f}_j,\tilde{f}_{\bar{t}}\right]\right)\\ &\quad+\bar{g}\left(\tilde{f}_j,\left[\tilde{f}_{\bar{t}},\tilde{f}_i\right]\right) + \bar{g}\left(\tilde{f}_{\bar{t}},\left[\tilde{f}_i,\tilde{f}_j\right]\right)\\ &= -\partial_{\bar{t}}\left(bp_ip_j\right) + a\Gamma^t_{jk}\delta^k_i + a\Gamma^t_{ik}\delta^k_j \end{aligned}$$

$$= \quad 2a\Gamma^l_{ij}\delta^t_l - b\left(\delta^l_i p_j + \delta^l_j p_i\right)\delta^t_l$$
$$= \quad 2\bar{g}\left(\left(\Gamma^l_{ij} - \frac{b}{2a}\left(\delta^l_i p_j + \delta^l_j p_i\right)\right)\tilde{f}_l, \tilde{f}_{\bar{t}}\right).$$

For *ii), iii)* and *iv)* we get calculations similar to those above. □

Then we write $\bar{\nabla}_{\tilde{f}_\alpha}\tilde{f}_\beta = \bar{\Gamma}^\delta_{\alpha\beta}\tilde{f}_\delta$ in the adapted frame $\left\{\tilde{f}_{(\alpha)}\right\}$ of T^*M, where $\bar{\Gamma}^\delta_{\alpha\beta}$ is the coeffients of $\bar{\nabla}$. Using Theorem 1, we obtain

Corollary 1. *In adapted frame* $\left\{\tilde{f}_{(\beta)}\right\}$, *the components of the Christoffel symbols* $\bar{\Gamma}^\delta_{\alpha\beta}$ *of* $\bar{\nabla}$ *on* $(T^*M, \bar{g})$ *are found as follows*

$$\begin{aligned}
&\bar{\Gamma}^l_{ij} = \Gamma^l_{ij} - \frac{b}{2a}\left(\delta^l_i p_j + \delta^l_j p_i\right), && \bar{\Gamma}^{\bar{l}}_{ij} = \frac{b}{a}p_k p_l \Gamma^k_{ji} - p_k R_{jli}{}^k, \\
&\bar{\Gamma}^{\bar{l}}_{i\,\bar{j}} = \frac{b}{2a}\left(\delta^j_l p_i + \delta^j_i p_l\right) - \Gamma^j_{li}, && \bar{\Gamma}^{\bar{l}}_{\bar{i}\,j} = \frac{b}{2}\left(\delta^i_j p_l + \delta^i_l p_j\right), \\
&\bar{\Gamma}^{\bar{l}}_{\bar{i}\,\bar{j}} = \bar{\Gamma}^l_{\bar{i}\,\bar{j}} = \bar{\Gamma}^l_{\bar{i}\,j} = \bar{\Gamma}^l_{i\,\bar{j}} = 0.
\end{aligned} \tag{13}$$

Let $\tilde{V} = \tilde{V}^\alpha\tilde{f}_{(\alpha)} = \tilde{V}^i\tilde{f}_{(i)} + \tilde{V}^{\bar{i}}\tilde{f}_{(\bar{i})}$ be a vector field on T^*M. The covariant derivative of $\tilde{V}$ with respect to the Levi-Civita connection $\bar{\nabla}$ of the natural Riemann extension $\bar{g}$ is given by

$$\bar{\nabla}_\beta\tilde{V}^\alpha = \tilde{f}_{(\beta)}\tilde{V}^\alpha + \Gamma^\alpha_{\beta\gamma}\tilde{V}^\gamma.$$

Applying (4), (8) and (13), we find the following components for the covariant derivatives of the vector fields ${}^HV, {}^CV, {}^V\vartheta$ with respect to the Levi-Civita connection $\bar{\nabla}$ of the natural Riemann extension $\bar{g}$:

$$\begin{aligned}
&\bar{\nabla}_i{}^HV^j = \tilde{f}_{(i)}{}^HV^j + \bar{\Gamma}^j_{ik}{}^HV^k + \bar{\Gamma}^j_{i\bar{k}}{}^HV^{\bar{k}} = \nabla_i V^j - \frac{b}{2a}\left(p_i V^j + \delta^j_i p_k V^k\right), \\
&\bar{\nabla}_{\bar{i}}{}^HV^j = \tilde{f}_{(\bar{i})}{}^HV^j + \bar{\Gamma}^j_{\bar{i}k}{}^HV^k + \bar{\Gamma}^j_{\bar{i}\bar{k}}{}^HV^{\bar{k}} = 0, \\
&\bar{\nabla}_i{}^HV^{\bar{j}} = \tilde{f}_{(i)}{}^HV^{\bar{j}} + \bar{\Gamma}^{\bar{j}}_{ik}{}^HV^k + \bar{\Gamma}^{\bar{j}}_{i\bar{k}}{}^HV^{\bar{k}} = \frac{b}{a}p_t p_j \Gamma^t_{ki}V^k - p_t R_{kji}{}^t V^k, \\
&\bar{\nabla}_{\bar{i}}{}^HV^{\bar{j}} = \tilde{f}_{(\bar{i})}{}^HV^{\bar{j}} + \bar{\Gamma}^{\bar{j}}_{\bar{i}k}{}^HV^k + \bar{\Gamma}^{\bar{j}}_{\bar{i}\bar{k}}{}^HV^{\bar{k}} = \frac{b}{2}\left(p_j V^i + \delta^i_j p_k V^k\right). \\
&\bar{\nabla}_i{}^CV^j = \nabla_i V^j - \frac{b}{2a}\left(p_i V^j + \delta^j_i p_k V^k\right), \\
&\bar{\nabla}_{\bar{i}}{}^CV^j = 0, \\
&\bar{\nabla}_i{}^CV^{\bar{j}} = -p_t\nabla_i\nabla_j V^t + \frac{b}{a}p_t p_j \Gamma^t_{ki}V^k - \frac{b}{2a}p_t\left(p_i\nabla_j V^t + p_j\nabla_i V^t\right) - p_t R_{kji}{}^t V^k, \\
&\bar{\nabla}_{\bar{i}}{}^CV^{\bar{j}} = -\nabla_j V^i + \frac{b}{2}\left(p_j V^i + \delta^i_j p_k V^k\right). \\
&\bar{\nabla}_i{}^V\vartheta^j = 0, \\
&\bar{\nabla}_{\bar{i}}{}^V\vartheta^j = 0,
\end{aligned}$$

$$\bar{\nabla}_i{}^V\vartheta^{\bar{j}} = \nabla_i\vartheta_j + \frac{b}{2a}\left(p_i\vartheta_j + p_j\vartheta_i\right),$$
$$\bar{\nabla}_{\bar{i}}{}^V\vartheta^{\bar{j}} = 0.$$

Then, we get the following theorem:

Theorem 2. *The horizontal and complete lifts* ${}^HV, {}^CV \in \Im_0^1(T^*M)$ *of* $V \in \Im_0^1(M)$ *and the vertical lift* ${}^V\vartheta \in \Im_0^1(T^*M)$ *of* $\vartheta \in \Im_1^0(M)$ *are not parallel with respect to the Levi-Civita connection* $\bar{\nabla}$ *of the natural Riemann extension* $\bar{g}$.

4. The Metric Connection with Respect to the Natural Riemann Extension $\bar{g}$

The Levi-Civita connection $\bar{\nabla}$ of the natural Riemann extension $\bar{g}$ on the cotangent bundle T^*M is the unique connection which satisfies $\bar{\nabla}\bar{g} = 0$, and has no torsion. Further, there exists another connection which satisfies $\breve{\nabla}\bar{g} = 0$, and has non-trivial torsion tensor. This connection is called the metric connection of $\bar{g}$.

Now we consider the horizontal lift ${}^H\nabla$ of any connection ∇ on the cotangent bundle T^*M defined by

$$\begin{aligned} &{}^H\nabla_{{}^V\vartheta}{}^V\omega = 0\ , \qquad {}^H\nabla_{{}^V\vartheta}{}^HZ = 0, \\ &{}^H\nabla_{{}^HV}{}^V\omega = {}^V\left(\nabla_V\omega\right)\ , \qquad {}^H\nabla_{{}^HV}{}^HZ = {}^H\left(\nabla_VZ\right) \end{aligned} \tag{14}$$

for any $V, Z \in \Im_0^1(M)$ and $\vartheta, \omega \in \Im_1^0(M)$ [21].

Let ${}^H\Gamma_{\alpha\beta}^{\gamma}$ be coefficients of ${}^H\nabla$. Using the formula ${}^H\nabla_\alpha\tilde{f}_{(\beta)} = {}^H\Gamma_{\alpha\beta}^{\gamma}\tilde{f}_{(\gamma)}$, where ${}^H\nabla_\alpha = {}^H\nabla_{\tilde{f}_{(\alpha)}}$, we obtain

$$\begin{aligned} &{}^H\Gamma_{ij}^{k} = {}^H\Gamma_{ij}^{k}\ , \qquad {}^H\Gamma_{i\,\bar{j}}^{\bar{k}} = -{}^H\Gamma_{ik}^{j}, \\ &{}^H\Gamma_{\bar{i}\,\bar{j}}^{\bar{k}} = {}^H\Gamma_{i\,j}^{\bar{k}} = {}^H\Gamma_{\bar{i}\,\bar{j}}^{k} = {}^H\Gamma_{\bar{i}\,j}^{k} = {}^H\Gamma_{\bar{i}\,j}^{\bar{k}} = {}^H\Gamma_{i\,\bar{j}}^{k} = 0. \end{aligned} \tag{15}$$

The torsion tensor T of ${}^H\nabla$ is the skew–symmetric (1,2)-tensor field and satisfies the following:

$$T\left({}^V\vartheta, {}^V\omega\right) = 0, T\left({}^HV, {}^V\omega\right) = 0\ , T\left({}^HV, {}^HZ\right) = -\gamma R\left(V, Z\right),$$

where R denotes the curvature tensor of ∇ and $\gamma R\left(V,Z\right) = \sum_j p_h R_{klj}^h V^k Z^l \frac{\partial}{\partial x^{\bar{j}}}$ (see[21, p.287]).

From (9) and (14), we obtain

$$\begin{aligned} \left({}^H\nabla_{{}^V\vartheta}\bar{g}\right)\left({}^V\omega, {}^V\varepsilon\right) &= {}^H\nabla_{{}^V\vartheta}\bar{g}\left({}^V\omega, {}^V\varepsilon\right) - \bar{g}\left({}^H\nabla_{{}^V\vartheta}{}^V\omega, {}^V\varepsilon\right) - \bar{g}\left({}^V\omega, {}^H\nabla_{{}^V\vartheta}{}^V\varepsilon\right), \\ &= 0 \\ \left({}^H\nabla_{{}^HV}\bar{g}\right)\left({}^V\vartheta, {}^V\omega\right) &= {}^H\nabla_{{}^HV}\bar{g}\left({}^V\vartheta, {}^V\omega\right) - \bar{g}\left({}^H\nabla_{{}^HV}{}^V\vartheta, {}^V\omega\right) - \bar{g}\left({}^V\vartheta, {}^H\nabla_{{}^HV}{}^V\omega\right), \\ &= 0 \\ \left({}^H\nabla_{{}^V\vartheta}\bar{g}\right)\left({}^V\omega, {}^HZ\right) &= {}^H\nabla_{{}^V\vartheta}\bar{g}\left({}^V\omega, {}^HZ\right) - \bar{g}\left({}^H\nabla_{{}^V\vartheta}{}^V\omega, {}^HZ\right) - \bar{g}\left({}^V\vartheta, {}^H\nabla_{{}^V\omega}{}^HZ\right) \end{aligned}$$

$$= {}^{V}\vartheta\left(a\left({}^{V}\left(\omega\left(Z\right)\right)\right)\right) = 0,$$

$$\begin{aligned}
\left({}^{H}\nabla_{{}^{H}V}\bar{g}\right)\left({}^{V}\omega,{}^{H}Z\right) &= {}^{H}\nabla_{{}^{H}V}\bar{g}\left({}^{V}\omega,{}^{H}Z\right)-\bar{g}\left({}^{H}\nabla_{{}^{H}V}{}^{V}\omega,{}^{H}Z\right)-\bar{g}\left({}^{V}\omega,{}^{H}\nabla_{{}^{H}V}{}^{H}Z\right)\\
&= {}^{H}\nabla_{{}^{H}V}\left(a\left({}^{V}\left(\omega\left(Z\right)\right)\right)\right)-\bar{g}\left({}^{V}\left(\nabla_{V}\omega\right),{}^{H}Z\right)-\bar{g}\left({}^{V}\omega,{}^{H}\left(\nabla_{V}Z\right)\right)\\
&= \left({}^{H}\nabla_{{}^{H}V}a\right)\left({}^{V}\left(\omega\left(Z\right)\right)\right)+a\left({}^{V}\left(\nabla_{V}\left(\omega\left(Z\right)\right)\right)\right)-a\left({}^{V}\left(\left(\nabla_{V}\omega\right)\left(Z\right)\right)\right)\\
&+ a\left({}^{V}\left(\omega\left(\nabla_{V}Z\right)\right)\right)\\
&= a\left({}^{V}\left(\nabla_{V}\left(\omega\left(Z\right)\right)\right)\right)-a\left({}^{V}\left(\nabla_{V}\left(\omega\left(Z\right)\right)\right)\right)=0,
\end{aligned}$$

$$\begin{aligned}
\left({}^{H}\nabla_{{}^{V}\vartheta}\bar{g}\right)\left({}^{H}Z,{}^{V}\varepsilon\right) &= {}^{H}\nabla_{{}^{V}\vartheta}\bar{g}\left({}^{H}Z,{}^{V}\varepsilon\right)-\bar{g}\left({}^{H}\nabla_{{}^{V}\vartheta}{}^{H}Z,{}^{V}\varepsilon\right)-\bar{g}\left({}^{H}Z,{}^{H}\nabla_{{}^{V}\vartheta}{}^{V}\varepsilon\right),\\
&= 0,\\
\left({}^{H}\nabla_{{}^{H}V}\bar{g}\right)\left({}^{H}Z,{}^{V}\varepsilon\right) &= {}^{H}\nabla_{{}^{H}V}\bar{g}\left({}^{H}Z,{}^{V}\varepsilon\right)-\bar{g}\left({}^{H}\nabla_{{}^{H}V}{}^{H}Z,{}^{V}\varepsilon\right)-\bar{g}\left({}^{H}Z,{}^{H}\nabla_{{}^{H}V}{}^{V}\varepsilon\right)\\
&= {}^{H}\nabla_{{}^{H}V}\left(a^{V}\left(\varepsilon\left(Z\right)\right)\right)-\bar{g}\left({}^{H}\left(\nabla_{V}Z\right),{}^{V}\varepsilon\right)-\bar{g}\left({}^{H}Z,{}^{V}\left(\nabla_{V}\varepsilon\right)\right)\\
&= {}^{V}\left(\nabla_{V}\left(a\varepsilon\left(Z\right)\right)\right)-a^{V}\left(\varepsilon\left(\nabla_{V}Z\right)\right)-a^{V}\left(\left(\nabla_{V}\varepsilon\right)\left(Z\right)\right)=0,\\
\left({}^{H}\nabla_{{}^{V}\vartheta}\bar{g}\right)\left({}^{H}V,{}^{H}Z\right) &= {}^{H}\nabla_{{}^{V}\vartheta}\bar{g}\left({}^{H}V,{}^{H}Z\right)-\bar{g}\left({}^{H}\nabla_{{}^{V}\vartheta}{}^{H}V,{}^{H}Z\right)-\bar{g}\left({}^{H}V,{}^{H}\nabla_{{}^{V}\vartheta}{}^{H}Z\right),\\
&= 0,
\end{aligned}$$

$$\begin{aligned}
\left({}^{H}\nabla_{{}^{H}V}\bar{g}\right)\left({}^{H}Y,{}^{H}Z\right) &= {}^{H}\nabla_{{}^{H}V}\bar{g}\left({}^{H}Y,{}^{H}Z\right)-\bar{g}\left({}^{H}\nabla_{{}^{H}V}{}^{H}Y,{}^{H}Z\right)-\bar{g}\left({}^{H}Y,{}^{H}\nabla_{{}^{H}V}{}^{H}Z\right)\\
&= {}^{H}\nabla_{{}^{H}V}\left(bp\left(Y\right)p\left(X\right)\right)-{}^{V}\left(bp\left(\nabla_{V}Y\right)p\left(Z\right)\right)-{}^{V}\left(bp\left(Y\right)p\left(\nabla_{V}Z\right)\right)\\
&= {}^{V}\left(\nabla_{V}b\left(p\left(Y\right)\right)p\left(Z\right)\right)-{}^{V}\left(\nabla_{V}b\left(p\left(Y\right)\right)p\left(Z\right)\right)=0
\end{aligned}$$

for any $V,Y,Z\in\Im_{0}^{1}\left(M\right)$ and $\vartheta,\omega,\varepsilon\in\Im_{1}^{0}\left(M\right)$, i.e. the horizontal lift ${}^{H}\nabla$ of ∇ is a metric connection.

In [21], the Ricci tensor field ${}^{H}R_{\gamma\beta}$ of ${}^{H}\nabla$ is given by:

$$\begin{aligned}
&{}^{H}R_{kj}={}^{H}R_{\alpha kj}{}^{\alpha}={}^{H}R_{ikj}{}^{i}+{}^{H}R_{\bar{i}kj}{}^{\bar{i}}=R_{ikj}{}^{i}=R_{kj}\ ,\\
&{}^{H}R_{\bar{k}\bar{j}}={}^{H}R_{\bar{k}j}={}^{H}R_{k\bar{j}}=0,
\end{aligned}\tag{16}$$

where R_{kj} denotes the Ricci tensor field of ∇ on M.

Now using (11) and (16) the natural Riemann extension $\bar{g}$, the scalar curvature of ${}^{H}\nabla$ is generated by

$${}^{H}r=\bar{g}^{\gamma\beta H}R_{\gamma\beta}=\bar{g}^{jkH}R_{jk}+\bar{g}^{\bar{j}kH}R_{\bar{j}k}+\bar{g}^{j\bar{k}H}R_{j\bar{k}}+\bar{g}^{\bar{j}\bar{k}H}R_{\bar{j}\bar{k}}=0.$$

Thus we have

Theorem 3. *The cotangent bundle $T^{*}M$ with metric connection ${}^{H}\nabla$ has a vanishing scalar curvature with respect to the natural Riemann extension $\bar{g}$.*

5. Geodesics on the Cotangent Bundle with the Natural Riemann Extension

Let now we investigate the geodesics on the cotangent bundle with the natural Riemann extension. Let $C : x^h = x^h(t)$ be a curve in M and $\omega_h(t)$ be a covector field along C. Also, we take that $\tilde{C}$ be a curve on T^*M and locally given by

$$x^h = x^h(t), \ x^{\bar{h}} \overset{def}{=} p_h = \omega_h(t). \tag{17}$$

If the curve C satisfies at all the points the relation

$$\frac{\delta \omega_h}{dt} = \frac{d\omega_h}{dt} - \Gamma^i_{jh} \frac{dx^j}{dt} \omega_i = 0,$$

then the curve $\tilde{C}$ is said to be a horizontal lift of the curve C in M. Hence, the initial condition $\omega_h = \omega^0_h$ for $t = t_0$ is taken, there exists a unique horizontal lift given by (17).

If t is the arc length of a curve $x^A = x^A(t), A = (i, \bar{i})$ in T^*M, then the differential equations of the geodesic is given by

$$\frac{\delta^2 x^A}{dt^2} = \frac{d^2 x^A}{dt^2} + \bar{\Gamma}^A_{CB} \frac{dx^C}{dt} \frac{dx^B}{dt} = 0 \tag{18}$$

with respect to the induced coordinates $\left(x^i, x^{\bar{i}}\right) = \left(x^i, p_i\right)$ in T^*M, where $\bar{\Gamma}^A_{CB}$ are components of $\bar{\nabla}$ defined by (13).

Now, from (5), (6) and using the adapted frame $\left\{\tilde{f}_{(\beta)}\right\}$, we write the equation (18) as follow:

$$\theta^\alpha = \tilde{A}^\alpha{}_A dx^A,$$

i.e.

$$\theta^h = \tilde{A}^h{}_A dx^A = \delta^h_i dx^i = dx^h$$

for $\alpha = h$ and

$$\theta^{\bar{h}} = \tilde{A}^{\bar{h}}{}_A dx^A = -p_a \Gamma^a_{hj} dx^j + \delta^h_j dx^j = \delta p_h$$

for $\alpha = \bar{h}$. Also we put

$$\frac{\theta^h}{dt} = \tilde{A}^h{}_A \frac{dx^A}{dt} = \frac{dx^h}{dt},$$
$$\frac{\theta^{\bar{h}}}{dt} = \tilde{A}^{\bar{h}}{}_A \frac{dx^A}{dt} = \frac{\delta p_h}{dt}$$

along a curve $x^A = x^A(t)$ in T^*M. Hence,

$$\frac{d}{dt}\left(\frac{\theta^\alpha}{dt}\right) + \bar{\Gamma}^\alpha_{\gamma\beta} \frac{\theta^\gamma}{dt} \frac{\theta^\beta}{dt} = 0.$$

Using (18), we obtain

$$a)\ \frac{\delta^2 x^h}{dt^2}+\frac{b}{2a}\left(\delta_i^h p_j+\delta_j^h p_i\right)\frac{dx^i}{dt}\frac{dx^j}{dt}=0,$$

$$b)\ \frac{\delta^2 p_h}{dt^2}+p_s\left(\frac{b}{a}p_h\Gamma_{ji}^s-R_{jhi}{}^s\right)\frac{dx^i}{dt}\frac{dx^j}{dt}+\frac{b}{2}\left(\delta_j^i p_h+\delta_h^i p_j\right)\frac{\delta p_i}{dt}\frac{dx^j}{dt}$$
$$+\frac{b}{2a}\left(\delta_h^j p_i+\delta_i^j p_h\right)\frac{dx^i}{dt}\frac{\delta p_j}{dt}=0, \qquad (19)$$

where $\frac{\delta^2 p_h}{dt^2}=\frac{d}{dt}\left(\frac{\delta p_h}{dt}\right)-\Gamma_{jh}^s\frac{\delta p_s}{dt}\frac{dx^j}{dt}$.

Theorem 4. *Let $\tilde{C}$ be a curve expressed locally by $x^h=x^h(t)$, $p_h=\omega_h(t)$ with respect to the induced coordinate system $\left(x^i,x^{\bar{i}}\right)=\left(x^i,p_i\right)$ on T^*M. If the curve $\tilde{C}$ satisfies the equation (19), then it is a geodesic of the natural Riemann extension $\bar{g}$.*

Let us assume that the curve (19) lies on a fibre, namely $x^h=const$. Then we obtain

$$\frac{\delta^2 p_h}{dt^2}=0.$$

Then we find $p_h=k_h t+n_h$, where $k_h$and n_h are constant. With this selection, we have proved the following:

Theorem 5. *If geodesic $x^h=x^h(t)$, $p_h=p_h(t)$ lies on a fibre of T^*M endowed with the natural Riemann extension $\bar{g}$, then: $x^h=c^h$, $p_h=k_h t+n_h$ where c^h,k_h and n_h are constant.*

Let now $\tilde{C}:x^h=x^h(t),x^{\bar{h}}=p_h(t)=\omega_h(t)$ be a horizontal lift ($\frac{\delta p_h}{dt}=\frac{\delta\omega_h}{dt}=0$) of the geodesic $C:x^h=x^h(t)$ ($\frac{\delta^2 x^h}{dt^2}=0$) in M of ∇. Then by virtue of (19), we obtain

Theorem 6. *Let (M,∇) be an dimensional manifold with metric g and T^*M be its cotangent bundle with the natural Riemann extension $\bar{g}$. Then the horizontal lift of a geodesic on M need not be a geodesic on T^*M with respect to the connection $\bar{\nabla}$.*

Declaration of Competing Interests The author declares that they have no competing interests.

Acknowledgements The author thanks the referees for their valuable suggestions which made this paper much improved.

References

[1] Abbasi, M. T. K., Amri, N., Bejan, C. L., Conformal vector fields and Ricci soliton structures on natural Riemannian extensions, *Mediterr. J. Math.*, 18(55) (2021), 1-16. https://doi.org/10.1007/s00009-020-01690-5

[2] Aslanci, S., Cakan, R., On a cotangent bundle with deformed Riemannian extension, *Mediterr. J. Math.*, 11(4) (2014), 1251–1260. DOI 10.1007/s00009-013-0337-2

[3] Aslanci, S., Kazimova, S., Salimov, A. A, Some notes concerning Riemannian extensions, *Ukrainian Math. J.*, 62(5) (2010), 661–675.

[4] Bejan, C. L., Eken, Ş., A characterization of the Riemann extension in terms of harmonicity, *Czech. Math. J.*, 67(1) (2017), 197–206. DOI: 10.21136/CMJ.2017.0459-15

[5] Bejan, C. L., Kowalski, O., On some differential operators on natural Riemann extensions, *Ann. Glob. Anal. Geom.,* 48 (2015), 171-–180. DOI 10.1007/s10455-015-9463-3

[6] Bejan, C. L., Nakova, G., Amost para-Hermitian and almost paracontact metric structures induced by natural Riemann extensions, *Resulth Math.*, 74(15) (2019). https://doi.org/10.1007/s00025-018-0939-x

[7] Bejan, C. L., Meriç, Ş. E., Kılıç, E., Einstein metrics induced by natural Riemann extensions, *Adv. Appl. Clifford Algebras,* 27(3) (2017), 2333–2343. DOI 10.1007/s00006-017-0774-2

[8] Bilen, L., Gezer, A., On metric connections with torsion on the cotangent bundle with modified Riemannian extension, *J. Geom.* 109(6) (2018), 1–17. https://doi.org/10.1007/s00022-018-0411-9

[9] Calvino-Louzao, E., García-Río, E., Gilkey, P., Vázquez-Lorenzo, A., The geometry of modified Riemannian extensions, *Proc. R. Soc. Lond. Ser. A Math. Phys. Eng. Sci.*, 465 (2107) (2009), 2023—2040. https://www.jstor.org/stable/30245448

[10] Dryuma, V., The Riemannian extension in theory of differential equations and their application, *Mat. Fiz. Anal. Geom.*, 10(3) (2003), 307-–325.

[11] Gezer, A., Bilen, L., Cakmak, A., Properties of modified Riemannian extensions, *Zh. Mat. Fiz. Anal. Geom.,* 11(2) (2015), 159-–173. https://doi.org/10.15407/mag11.02.159

[12] Kowalski, O., Sekizawa, M., On natural Riemann extensions, *Publ. Math. Debr.,* 78(3–4) (2011), 709—721. DOI: 10.5486/PMD.2011.4992

[13] Kowalski, O., Sekizawa, M., Almost Osserman structures on natural Riemann extensions, *Differ. Geom. Appl.,* 31 (2013), 140—149. https://doi.org/10.1016/j.difgeo.2012.10.007

[14] Ocak, F., Notes about a new metric on the cotangent bundle, *Int. Electron. J. Geom.,* 12(2) (2019), 241–249.

[15] Ocak, F., Some properties of the Riemannian extensions, *Konuralp J. of Math.*, 7(2) (2019), 359–362.

[16] Ocak, F., Some notes on Riemannian extensions, *Balkan J. Geom. Appl.*, 24(1) (2019), 45–50.

[17] Ocak, F., Kazimova, S., On a new metric in the cotangent bundle, *Transactions of NAS of Azerbaijan Series of Physical-Technical and Mathematical Sciences,* 38(1) (2018), 128—138.

[18] Patterson, E. M., Walker, A. G., Riemannian extensions, *Quant. Jour. Math.*, 3 (1952), 19–28.

[19] Salimov, A., Cakan, R., On deformed Riemannian extensions associated with twin Norden metrics, *Chinese Annals of Math. Ser. B.,* 36 (2015), 345–354. DOI: 10.1007/s11401-015-0914-8

[20] Sekizawa, M., Natural transformations of affine connections on manifolds to metrics on cotangent bundles, *Proc. 14th Winter School. Srní, Czech, 1986, Suppl. Rend. Circ. Mat. Palermo, Ser.,* 14(2) (1987), 129—142.

[21] Yano, K., Ishihara, S., Tangent and Cotangent Bundles, Mercel Dekker, Inc., New York, 1973.

http://communications.science.ankara.edu.tr

Commun.Fac.Sci.Univ.Ank.Ser. A1 Math. Stat.
Volume 72, Number 2, Pages 374–385 (2023)
DOI:10.31801/cfsuasmas.1108176
ISSN 1303-5991 E-ISSN 2618-6470

COMMUNICATIONS SERIES A1

Research Article; Received: April 24, 2022; Accepted: November 29, 2022

CHROMATIC SCHULTZ POLYNOMIAL OF CERTAIN GRAPHS

Sudev NADUVATH

Department of Mathematics, CHRIST (Deemed to be University), Bangalore, INDIA

ABSTRACT. A topological index of a graph G is a real number which is preserved under isomorphism. Extensive studies on certain polynomials related to these topological indices have also been done recently. In a similar way, chromatic versions of certain topological indices and the related polynomials have also been discussed in the recent literature. In this paper, the chromatic versions of the Schultz polynomial and modified chromatic Schultz polynomial are introduced and determined this polynomial for certain fundamental graph classes.

1. Introduction

For all terms and definitions, not defined specifically in this paper, we refer to [10]. Further, for graph colouring, see [6,7]. Unless mentioned otherwise, all graphs considered here are undirected, simple, finite and connected.

A *proper vertex colouring* of a graph G is an assignment $\varphi : V(G) \to \mathcal{C}$ of the vertices of G, where $\mathcal{C} = \{c_1, c_2, c_3, \dots, c_\ell\}$ is a set of colours such that adjacent vertices of G have different colours. The cardinality of the minimum set of colours which allows a proper colouring of G is called the *chromatic number* of G and is denoted $\chi(G)$. The set of all vertices of G which have the colour c_i is called the *colour class* of that colour c_i in G. The cardinality of the colour class of a colour c_i is said to be the *strength* of that colour in G and is denoted by $\theta(c_i)$. We can also define a function $\zeta : V(G) \to \{1, 2, 3, \dots, \ell\}$ such that $\zeta(v_i) = s$ if and only if $\varphi(v_i) = c_s, c_s \in \mathcal{C}$.

A vertex colouring consisting of the colours having minimum subscripts may be called a *minimum parameter colouring* (see [8]). If we colour the vertices of G in such a way that c_1 is assigned to maximum possible number of vertices, then c_2 is assigned to maximum possible number of remaining uncoloured vertices and

---

2020 *Mathematics Subject Classification.* 05C15, 05C31.

Keywords. Chromatic Schultz polynomial, χ^--chromatic Schultz polynomial, χ^+-chromatic Schultz polynomial, modified chromatic Schultz polynomial.

sudevnk@gmail.com; 0000-0001-9692-4053.

proceed in this manner until all vertices are coloured, then such a colouring is called a χ^--*colouring* of G. In a similar manner, if c_ℓ is assigned to maximum possible number of vertices, then $c_{\ell-1}$ is assigned to maximum possible number of remaining uncoloured vertices and proceed in this manner until all vertices are coloured, then such a colouring is called a χ^+-*colouring* of G.

A *topological index* of a graph G is a real number which is preserved under isomorphism. The chromatic versions of certain topological indices have been introduced in [8]. The Schultz polynomials and modified Schultz polynomials of graphs are some of such widely studied polynomials (see [1,2,4]).

Some chromatic version of topological indices were introduced and studied in [8] and later the idea of chromatic topological polynomials was introduced in [9] In this paper, we discuss the chromatic versions of certain polynomials related to the topological indices of a graph G.

2. Chromatic Schultz Polynomial of Graphs

Note that throughout this study, we use the chromatic colourings of the graphs under consideration. Motivated by the studies on Schultz polynomial of graphs (see [1,2,4,5]), we can now introduce the chromatic version of the Schultz polynomial as follows:

Definition 1. Let G be a connected graph with chromatic number $\chi(G)$. Then, the *chromatic Schultz polynomial* of G, denoted by $\mathcal{S}_\chi(G,x)$, is defined as

$$\mathcal{S}_\chi(G,x) = \sum_{u,v\in V(G)} (\zeta(u)+\zeta(v))x^{d(u,v)}.$$

Definition 2. Let G be a connected graph with chromatic number φ^- and φ^+ be the minimal and maximal parameter colouring of G. Then,

(i) the χ^--*chromatic Schultz polynomial* of G, denoted by $\mathcal{S}_{\chi^-}(G,x)$, is defined as

$$\mathcal{S}_{\chi^-}(G,x) = \sum_{u,v\in V(G)} (\zeta_{\varphi^-}(u)+\zeta_{\varphi^-}(v))x^{d(u,v)};$$

and

(ii) the χ^+-*chromatic Schultz polynomial* of G, denoted by $\mathcal{S}_{\chi^+}(G,x)$, is defined as

$$\mathcal{S}_{\chi^+}(G,x) = \sum_{u,v\in V(G)} (\zeta_{\varphi^+}(u)+\zeta_{\varphi^+}(v))x^{d(u,v)}.$$

Now, we can determine the chromatic Schultz polynomials of certain fundamental graph classes.

2.1. Chromatic Schultz Polynomials of Paths.

In this section, we discuss the two types of chromatic Schultz polynomials of paths.

Theorem 1. *Let P_n be a path on n vertices. Then, we have*

$$\mathcal{S}_{\chi^-}(P_n,x)=\begin{cases}\sum\limits_{i=0}^{\frac{n-1}{2}}\left[(3n-6i-3)x+(3n-6i-1)\right]x^{2i}; & \text{if } n \text{ is odd;}\\ 3\cdot\sum\limits_{i=0}^{n}(n-i)x^i; & \text{if } n \text{ is even.}\end{cases}$$

Proof. Let $V=\{v_1,v_2,\dots,v_n\}$ be the vertex set of P_n, where the vertices are labelled consecutively. Note that $\chi(P_n)=2$. Let c_1,c_2 be the two colours we use for colouring P_n. We also note that te diameter of P_n is $n-1$. Hence, the power of the variable x varies from 0 to $n-1$ in the Schultz polynomial of P_n. Here, we need to consider the following two cases:

Case-1: Let n be odd. Then, with respect to a χ^--colouring, the vertices $v_1,v_3,v_5,\dots v_n$ get the colour c_1 and the vertices $v_2,v_4,v_6,\dots,v_{n-1}$ get the colour c_2. The possible colour pairs and their numbers in G in terms of the distances between them are listed in Table 1.

TABLE 1. A list of color pairs and the distance between them in an odd path.

Distance $d(u,v)$	Colour pairs	Number of pairs	Total number of pairs
0	(c_1,c_1)	$\frac{n+1}{2}$	n
	(c_2,c_2)	$\frac{n-1}{2}$	
1	(c_1,c_2)	$n-1$	$n-1$
2	(c_1,c_1)	$\frac{n-1}{2}$	$n-2$
	(c_2,c_2)	$\frac{n-3}{2}$	
3	(c_1,c_2)	$n-3$	$n-3$
4	(c_1,c_1)	$\frac{n-3}{2}$	$n-4$
	(c_2,c_2)	$\frac{n-5}{2}$	
5	(c_1,c_2)	$n-5$	$n-5$
6	(c_1,c_1)	$\frac{n-5}{2}$	$n-6$
	(c_2,c_2)	$\frac{n-7}{2}$	
$\vdots$	$\vdots$	$\vdots$	$\vdots$
$n-3$	(c_1,c_1)	2	3
	(c_2,c_2)	1	
$n-2$	(c_1,c_2)	2	2
$n-1$	(c_1,c_1)	1	1
	(c_2,c_2)	0	

In the above table, the possible distances between different pairs of vertices are written in the first column, the different colour pairs with respect to each distance is written in the second column and the number of corresponding colour pairs with respect to each distance is written in the third column. The total number of vertex pairs corresponding to each distance is written in the fourth column.

From Table-1, we note that for $0 \leq r \leq n$, the number of vertex pairs which are at a distance r is $n-r$ and in this case all colour pairs contain two colours, when r is odd. But, when r is even, all colour pairs contain the same colour - either (c_1, c_1) or (c_2, c_2). In this case, note that the number of (c_1, c_1)-colour pairs is $\frac{n-r+1}{2}$ and the number of (c_2, c_2)-colour pairs is $\frac{n-r-1}{2}$ so that total number of colour pairs is $n-r$. Hence,

$$\begin{aligned}
\mathcal{S}_{\chi^-}(P_n, x) &= \sum_{r \text{ odd}} (1+2)(n-r)x^r + \sum_{r \text{ even}} \left[\frac{n-r+1}{2} \cdot 2 + \frac{n-r-1}{2} \cdot 4\right] x^r \\
&= \sum_{r \text{ odd}} (3n-3r)x^r + \sum_{r \text{ even}} (3n-3r-1)x^r \\
&= \sum_{i=0}^{\frac{n-1}{2}} (3n-6i-3)x^{2i+1} + \sum_{i=0}^{\frac{n-1}{2}} (3n-6i-1)x^{2i} \\
&= \sum_{i=0}^{\frac{n-1}{2}} \left[(3n-6i-3)x + (3n-6i-1)\right] x^{2i}. \\
&\quad (\text{since } 3n-6i-3 = 0 \text{ at } i = \frac{n-1}{2}).
\end{aligned}$$

Case-2: Let n be even. Then, with respect to a χ^--colouring, the vertices $v_1, v_3, v_5, \ldots v_{n-1}$ get the colour c_1 and the vertices $v_2, v_4, v_6, \ldots v_n$ get the colour c_2. The possible colour pairs and their numbers in G in terms of the distances between them are listed in the following table.
From Table-2, we have

$$\begin{aligned}
\mathcal{S}_{\chi^-}(P_n, x) &= \sum_{r \text{ odd}} (1+2)(n-r)x^r + \sum_{r \text{ even}} \left[\frac{n-r}{2} \cdot 2 + \frac{n-r}{2} \cdot 4\right] x^r \\
&= \sum_{r \text{ odd}} (3n-3r)x^r + \sum_{r \text{ even}} (3n-3r)x^r \\
&= 3 \cdot \sum_{i=0}^{n-1} (n-i)x^i.
\end{aligned}$$

This completes the proof. □

Note that the χ^+-colouring of P_n can be obtained by interchanging the colours c_1 and c_2 in the χ^--colouring. Hence, as explained in the proof of above theorem, we have

TABLE 2. A list of color pairs and the distance between them in an even path.

Distance $d(u,v)$	Colour pairs	Number of pairs	Total number of pairs
0	(c_1, c_1)	$\frac{n}{2}$	n
	(c_2, c_2)	$\frac{n}{2}$	
1	(c_1, c_2)	$n-1$	$n-1$
2	(c_1, c_1)	$\frac{n-2}{2}$	$n-2$
	(c_2, c_2)	$\frac{n-2}{2}$	
3	(c_1, c_2)	$n-3$	$n-3$
4	(c_1, c_1)	$\frac{n-4}{2}$	$n-4$
	(c_2, c_2)	$\frac{n-4}{2}$	
5	(c_1, c_2)	$n-5$	$n-5$
6	(c_1, c_1)	$\frac{n-6}{2}$	$n-6$
	(c_2, c_2)	$\frac{n-6}{2}$	
$\vdots$	$\vdots$	$\vdots$	$\vdots$
$n-3$	(c_1, c_2)	3	3
$n-2$	(c_1, c_1)	1	2
	(c_2, c_2)	1	
$n-1$	(c_1, c_2)	1	1

Theorem 2. *Let P_n be a path on n vertices. Then, we have*

$$\mathcal{S}_{\chi^+}(P_n, x) = \begin{cases} \sum\limits_{i=0}^{\frac{n-1}{2}} \left[(3n-6i-3)x + (3n-6i+1)\right] x^{2i}; & \text{if } n \text{ is odd;} \\ 3 \cdot \sum\limits_{i=0}^{n-1} (n-i)x^i; & \text{if } n \text{ is even.} \end{cases}$$

2.2. **Chromatic Schultz Polynomial of Cycles.** In this section, we discuss the two types of chromatic Schultz polynomials of cycles.

Theorem 3. *Let C_n be a cycle on n vertices. Then, we have*

$$\mathcal{S}_{\chi^-}(C_n, x) = \begin{cases} \frac{3n(1-x^{\frac{n+2}{2}})}{1-x}; & \text{if } n \text{ is even;} \\ \frac{3(n+1)(1-x^{\frac{n+1}{2}})}{1-x}; & \text{if } n \text{ is odd.} \end{cases}$$

Proof. Let $V = \{v_1, v_2, \ldots, v_n\}$ be the vertex set of C_n, where the vertices are labelled consecutively from one end vertex to the other in a clockwise manner.

Note that if n is odd, then the diameter of C_n is $\frac{n-1}{2}$ and if n is even, the diameter of C_n is $\frac{n}{2}$. Hence, we have to consider the following two cases:

Case-1: Let n be even. Then, C_n is 2-colourable and we can label the vertices $v_1, v_3, v_5 \ldots, v_{n-1}$ by colour c_1 and the vertices $v_2, v_4, v_6 \ldots, v_n$ by colour c_2. Then, for $0 \leq i \leq \frac{n}{2}$, the possible colour pairs and their numbers can be obtained from the following table.

TABLE 3. A list of color pairs and the distance between them in an even cycle.

Distance $d(u,v)$	Colour pairs	Number of pairs	Total number of pairs
i, even	(c_1, c_1)	$\frac{n}{2}$	n
	(c_2, c_2)	$\frac{n}{2}$	
i, odd	(c_1, c_2)	n	n

Then, from Table 3, we have

$$\begin{aligned} \mathcal{S}_{\chi^-}(C_n, x) &= \sum_{i \text{ odd}} 3nx^i + \sum_{i \text{ even}} \left[\frac{n}{2} \cdot 2 + \frac{n}{2} \cdot 4\right] x^i \\ &= \sum_{i \text{ odd}} 3nx^i + \sum_{i \text{ even}} (n + 2n)x^i \\ &= \sum_{i=0}^{\frac{n}{2}} 3nx^i \\ &= \frac{3n(1 - x^{\frac{n+2}{2}})}{1 - x}. \end{aligned}$$

Case-2: Let n be odd. Then, $\chi(C_n) = 3$ and the vertices $v_1, v_3, v_5 \ldots, v_{n-1}$ by colour c_1 and the vertices $v_2, v_4, v_6 \ldots, v_{n-2}$ by colour c_2 and the vertex v_n gets colour c_3. Then, for $0 \leq i \leq \frac{n-1}{2}$, the possible colour pairs and their numbers can be obtained from Table 4.

When $i = 0$, we have

$$\sum_{v \in V} (\zeta(v) + \zeta(v))x^{d(v,v)} = \left[(2 + 4) \cdot \frac{n-1}{2} + 6 \cdot 1\right] x^0 = 3(n + 1)x^0$$

When $i > 0$ and is even, we have

$$\begin{aligned} \sum_{d(u,v)=i} (\zeta(u) + \zeta(v))x^{d(u,v)} &= \left[(2 + 4) \cdot \frac{n-r-1}{2} + 3(r - 1) + (4 + 5) \cdot 1\right] x^i \\ &= 3(n + 1)x^i \end{aligned}$$

TABLE 4. A list of color pairs and the distance between them in an odd cycle.

Distance $d(u,v)$	Colour pairs	Number of pairs	Total number of pairs
$i=0$	(c_1,c_1)	$\frac{n-1}{2}$	n
	(c_2,c_2)	$\frac{n-1}{2}$	
	(c_3,c_3)	1	
$i>0$ and even	(c_1,c_1)	$\frac{n-r-1}{2}$	n
	(c_1,c_2)	$r-1$	
	(c_2,c_2)	$\frac{n-r-1}{2}$	
	(c_1,c_3)	1	
	(c_2,c_3)	1	
$i>$, odd	(c_1,c_1)	$\frac{r-1}{2}$	n
	(c_1,c_2)	$n-r-1$	
	(c_2,c_2)	$\frac{r-1}{2}$	
	(c_1,c_3)	1	
	(c_2,c_3)	1	

Similarly, when $i>0$ and is odd, we have

$$\begin{aligned}\sum_{d(u,v)=i}(\zeta(u)+\zeta(v))x^{d(u,v)} &= \left[(2+4)\cdot\frac{r-1}{2}+3(n-r-1)+(4+5)\cdot 1\right]x^i \\ &= 3(n+1)x^i\end{aligned}$$

Therefore, $\mathcal{S}_{\chi^-}(C_n,x)=\sum\limits_{i=0}^{\frac{n+1}{2}}3(n+1)x^i=\frac{3(n+1)(1-x^{\frac{n+1}{2}})}{1-x}$, completing the proof. $\square$

Note that in the χ^--colouring of an even cycle C_n if we the colours c_1 and c_2, we get its χ^+-colouring. It can be observed that this change makes no change in the corresponding Schultz polynomial. But, for an odd cycle C_n, we have to interchange the colours c_1 and c_3 in its χ^--colouring and keep c_2 as it is to get a χ^+-colouring.

In view of this fact, the χ^+-chromatic Schultz polynomial of C_n is obtained in the following theorem.

Theorem 4. *Let C_n be a cycle on n vertices. Then, we have*

$$\mathcal{S}_{\chi^+}(C_n,x)=\begin{cases}\frac{3n(1-x^{\frac{n+2}{2}})}{1-x}; & \text{if } n \text{ is even;}\\ \frac{(5n-3)(1-x^{\frac{n+3}{2}})}{1-x}; & \text{if } n \text{ is odd.}\end{cases}$$

2.3. **Chromatic Schultz Polynomial of Complete Graphs.** Next, we consider the complete graph K_n. In K_n, we have $d(u,v)=1$ for any two $u,v \in V(G)$. Therefore, $\mathcal{S}_{\chi^-}(K_n,x)$ and $\mathcal{S}_{\chi^+}(K_n,x)$ are the same and are first degree polynomials. The following result provides the Schultz polynomial of a complete graph K_n.

Proposition 1. *For $n \geq 2$, $\mathcal{S}_{\chi^-}(K_n,x) = \mathcal{S}_{\chi^+}(K_n,x) = (n^2+n)+(2n^2-n-3)x$.*

Proof. In any proper vertex colouring, distinct vertices in K_n get distinct colours. Now, $\sum\limits_{v \in V} 2\zeta(v)x^0 = (2+4+6+\ldots+2n)x^0 = n(n+1)$. Also, we have

$$\begin{aligned}\sum_{d(u,v)=1} (\zeta(u)+\zeta(v))x^1 &= (3+4+5+\ldots+(2n-1))x = \left(\frac{2n-3}{2}(2n+2)\right)x\\ &= (2n-3)(n+1)x.\end{aligned}$$

Therefore, $\mathcal{S}_{\chi^-}(K_n,x) = (n^2+n)+(2n^2-n-3)x = \mathcal{S}_{\chi^+}(K_n,x)$. □

2.4. **Chromatic Schultz Polynomial of Complete Bipartite Graphs.** Next, let us consider the complete bipartite graphs $K_{a,b}$, where $a \geq b$.

Theorem 5. *For a complete bipartite $K_{a,b}, a \geq b, a+b=n$, we have $\mathcal{S}_{\chi^-}(K_n,x) = (2a+4b)+3abx+(a(a-1)+2b(b-1))x^2$ and $\mathcal{S}_{\chi^+}(K_n,x) = (4a+2b)+3abx+(2a(a-1)+b(b-1))x^2$.*

Proof. Note that $K_{a,b}$ is 2-colourable and its diameter is 2. Since $a \geq b$, with respect to all a vertices in the first partition get the colour c_1 and all b vertices in the second partition get colour c_2. Then, we have the following table. Then,

TABLE 5. A list of color pairs and the distance between them in a complete bipartite graph.

Distance $d(u,v)$	Colour pairs	Number of pairs	Total number of pairs
$i=0$	(c_1,c_1)	a	$a+b$
	(c_2,c_2)	b	
$i=1$	(c_1,c_2)	ab	ab
$i=2$	(c_1,c_1)	$\binom{a}{2}$	$\binom{a}{2}+\binom{b}{2}$
	(c_2,c_2)	$\binom{b}{2}$	

$$\begin{aligned}\mathcal{S}_{\chi^-}(K_{m,n},x) &= (2a+4b)+3abx+(2\cdot\binom{a}{2}+4\cdot\binom{b}{2})x^2\\ &= (2a+4b)+3abx+(a(a-1)+2b(b-1))x^2.\end{aligned}$$

In a similar way, by interchanging c_1 and c_2, we can prove that $\mathcal{S}_{\chi^+}(K_{m,n},x) = (4a+2b)+3abx+(2a(a-1)+b(b-1))x^2$. □

3. Modified Chromatic Schultz Polynomials

Definition 3. Let G be a connected graph with chromatic number $\chi(G)$. Then, the *modified chromatic Schultz polynomial* of G, denoted by $\mathcal{S}^*_\chi(G,x)$, is defined as

$$\mathcal{S}^*_\chi(G,x) = \sum_{u,v\in V(G)} (\zeta(u)\zeta(v))x^{d(u,v)}.$$

Definition 4. Let G be a connected graph with chromatic number φ^- and $varphi^+$ be the minimal and maximal parameter colouring of G. Then,

(i) the *modified χ^--chromatic Schultz polynomial* of G, denoted by $\mathcal{S}^*_{\chi^-}(G,x)$, is defined as

$$\mathcal{S}^*_{\chi^-}(G,x) = \sum_{u,v\in V(G)} (\zeta_{\varphi^-}(u)\cdot\zeta_{\varphi^-}(v))x^{d(u,v)};$$

and

(ii) the *χ^+-chromatic Schultz polynomial* of G, denoted by $\mathcal{S}^*_{\chi^+}(G,x)$, is defined as

$$\mathcal{S}^*_{\chi^+}(G,x) = \sum_{u,v\in V(G)} (\zeta_{\varphi^+}(u)\cdot\zeta_{\varphi^+}(v))x^{d(u,v)}.$$

The following theorems discuss the modified chromatic Schultz polynomials of paths.

Theorem 6. *Let P_n be a path on n vertices. Then, we have*

$$\mathcal{S}^*_{\chi^-}(P_n,x) = \begin{cases} \sum\limits_{i=0}^{\frac{n-1}{2}} \left[(2n-4i-2)x + (\frac{5n-10i-3}{2})\right] x^{2i}; & \text{if } n \text{ is odd;} \\ \sum\limits_{i=0}^{\frac{n-1}{2}} \left[(2n-4i-2)x + (\frac{5n-10i}{2})\right] x^{2i}; & \text{if } n \text{ is even.} \end{cases}$$

Proof. If n is odd, then from Table 1, we have

$$\begin{aligned} \mathcal{S}^*_{\chi^-}(P_n,x) &= \sum_{r \text{ odd}} 2(n-r)x^r + \sum_{r \text{ even}} \left[\frac{n-r+1}{2}\cdot 1 + \frac{n-r-1}{2}\cdot 4\right] x^r \\ &= \sum_{r \text{ odd}} (2n-2r)x^r + \sum_{r \text{ even}} \left(\frac{5n-5r-3}{2}\right) x^r \\ &= \sum_{i=0}^{\frac{n-1}{2}} (2n-4i-2)x^{2i+1} + \sum_{i=0}^{\frac{n-1}{2}} \left(\frac{5n-10i-3}{2}\right) x^{2i} \\ &= \sum_{i=0}^{\frac{n-1}{2}} \left[(2n-4i-2)x + \left(\frac{5n-10i-3}{2}\right)\right] x^{2i}. \end{aligned}$$

If n is even, then from Table 2, we have

$$\begin{aligned}
\mathcal{S}^*_{\chi^-}(P_n,x) &= \sum_{r\ \text{odd}} 2(n-r)x^r + \sum_{r\ \text{even}} \left[\frac{n-r}{2}\cdot 1 + \frac{n-r}{2}\cdot 4\right] x^r \\
&= \sum_{r\ \text{odd}} (2n-2r)x^r + \sum_{r\ \text{even}} \left(\frac{5n-5r}{2}\right) x^r \\
&= \sum_{i=0}^{\frac{n-1}{2}} (2n-4i-2)x^{2i+1} + \sum_{i=0}^{\frac{n-1}{2}} \left(\frac{5n-10i}{2}\right) x^{2i} \\
&= \sum_{i=0}^{\frac{n-1}{2}} \left[(2n-4i-2)x + \left(\frac{5n-10i}{2}\right)\right] x^{2i}.
\end{aligned}$$

This completes the proof. □

Similarly, by interchanging the colours c_1 and c_2, we have the following result.

Theorem 7. *Let P_n be a path on n vertices. Then,*

$$\mathcal{S}^*_{\chi^+}(P_n,x) = \begin{cases} \sum\limits_{i=0}^{\frac{n-1}{2}} \left[(2n-4i-2)x + (\frac{5n-10i+3}{2})\right] x^{2i}; & \text{if } n \text{ is odd;} \\ \sum\limits_{i=0}^{\frac{n-1}{2}} \left[(2n-4i-2)x + (\frac{5n-10i}{2})\right] x^{2i}; & \text{if } n \text{ is even.} \end{cases}$$

The following theorems discuss the modified chromatic Schultz polynomials of cycles.

Theorem 8. *Let C_n be a cycle on n vertices. Then, we have*

$$\mathcal{S}^*_{\chi^-}(C_n,x) = \begin{cases} \sum\limits_{i=0}^{\frac{n}{2}} \left(2nx + \frac{5n}{2}\right) x^{2i}; & \text{if } n \text{ is even;} \\ \frac{5n+17}{2} + \sum\limits_{i=1}^{\frac{n-1}{2}} \left[(2n+9i+10)x + \frac{5n-18i+13}{2}\right] x^{2i}; & \text{if } n \text{ is odd.} \end{cases}$$

Proof. If n is even and $r = d(u,v), u, v \in V(C_n)$, then from Table 3, we have

$$\begin{aligned}
\mathcal{S}^*_{\chi^-}(C_n,x) &= \sum_{r\ \text{odd}} 2nx^r + \sum_{r\ \text{even}} \left(\frac{n}{2}\cdot 1 + \frac{n}{2}\cdot 4\right) x^r \\
&= \sum_{r\ \text{odd}} 2nx^r + \sum_{r\ \text{even}} \frac{5n}{2} x^r \\
&= \sum_{i=0}^{\frac{n}{2}} 2nx^{2i+1} + \sum_{i=0}^{\frac{n}{2}} \frac{5n}{2} x^{2i} \\
&= \sum_{i=0}^{\frac{n}{2}} \left[2nx + \frac{5n}{2}\right] x^{2i}.
\end{aligned}$$

Let n be odd. Then, from Table 4,

$$\begin{aligned}
\mathcal{S}^*_{\chi^-}(C_n,x) &= \sum_{r=0}(\frac{n-1}{2}\cdot 1+\frac{n-1}{2}\cdot 4+9\cdot 1)+\\
&\quad \sum_{r>0 \text{ and odd}}\left(\frac{r-1}{2}(1+4)+2(n-r-1)+(3+6)\cdot 1\right)x^r+\\
&\quad \sum_{r>0 \text{ and even}}\left((1+4)\frac{n-r-1}{2}+2(r-1)+(3+6)\cdot 1\right)x^r\\
&= \frac{5n+17}{2}+\sum_{r \text{ odd}}\frac{4n+9r+11}{2}x^r+\sum_{r \text{ even}}\frac{5n-9r+13}{2}x^r\\
&= \frac{5n+17}{2}+\sum_{i=1}^{\frac{n-1}{2}}\frac{4n+18i+20}{2}x^{2i+1}+\sum_{i=1}^{\frac{n-1}{2}}\frac{5n-18i+13}{2}x^{2i}\\
&= \frac{5n+17}{2}+\sum_{i=1}^{\frac{n-1}{2}}\left[(2n+9i+10)x+\frac{5n-18i+13}{2}\right]x^{2i}.
\end{aligned}$$

This completes the proof. □

Similarly, interchanging c_1 and c_2 in even cycles and interchanging c_1 and c_3 in even cycles, we get

Theorem 9. *Let C_n be a cycle on n vertices. Then, we have*

$$\mathcal{S}^*_{\chi^+}(C_n,x)=\begin{cases}\frac{13n-11}{2}+\sum\limits_{i=1}^{\frac{n-1}{2}}\left[(6n+i-7)x+\frac{13n-2i-15}{2}\right]x^{2i}; & \text{if } n \text{ is odd;}\\ \sum\limits_{i=0}^{\frac{n}{2}}\left(2nx+\frac{5n}{2}\right)x^{2i}; & \text{if } n \text{ is even.}\end{cases}$$

The following result provides the modified Schultz polynomial of a complete bipartite graph $K_{a,b}$.

Theorem 10. *For a complete bipartite $K_{a,b}, a \geq b, a+b=n$, we have $\mathcal{S}^*_{\chi^-}(K_n,x)=(a+4b)+2abx+\left(\frac{a(a-1)}{2}+2b(b-1)\right)x^2$ and $\mathcal{S}_{\chi^+}(K_n,x)=(4a+b)+2abx+\left(2a(a-1)+\frac{b(b-1)}{2}\right)x^2$.*

Proof. The proof similar to that of Theorem 5. □

4. Conclusion

In this article, we have introduced a particular type of polynomial, called chromatic Schultz polynomial of graphs, as an analogue of the Schultz polynomial of graphs and determined this polynomial for certain fundamental graphs.

The study seems to be promising for further studies as the polynomial can be computed for many graph classes and classes of derived graphs. The chromatic Schultz polynomial can be determined for graph operations, graph products and graph powers. The study on Schultz polynomials with respect to different types of graph colourings also seem to be much promising. The concept can be extended to edge colourings and map colourings also.

These polynomials have so many applications in various fields like Mathematical Chemistry, Distribution Theory, Optimisation Techniques etc. In Chemistry, some interesting studies using the above-mentioned concepts are possible if $c(v_i)$ (or $\zeta(v_i)$) assumes the values such as energy, valency, bond strength etc. Similar studies are possible in various other fields. All these facts highlight the wide scope for further research in this area.

Declaration of Competing Interests The authors declare that they have no competing interest.

Acknowledgements The author of this article would like to dedicate this article to Dr Johan Kok, Visiting Professor, Christ University, Bangalore, who is a friend, collaborator and motivator, as a tribute to his untiring efforts in the field of Mathematics research. The author acknowledges the critical and constructive comments and suggestion by the anonymous referee, which improved the presentation and content of the article significantly.

References

[1] Abdullah, M. M., Ali, A. M., Schultz and modified Schultz polynomials for edge-identification chain and ring-for square graphs, *Baghdad Sci. J.*, 19(3) (2022), 560–568.

[2] Abdullah, M. M., Ali, A. M., Schultz and modified Schultz polynomials for edge-identification chain and ring for pentagon and hexagon graphs, *J. Phys: Conf. Ser.* , 1818(1) (2021), 012063.

[3] Brandstädt, A., Le, V. B., Spinrad, J. P., Graph Classes: A Survey, SIAM, Monographs on Discrete Mathematics and Applications, Philadelphia, 1999. http://dx.doi.org/10.1137/1.9780898719796

[4] Eliasi, M., Taeri, B., Schultz polynomials of composite graphs, *Appl. Anal. Discrete Math.*, 2 (2008), 285–296. doi:10.2298/AADM0802285E

[5] Eu, S. P., Yang, B. Y., Yeh, Y. N., Theoretical and computational developments generalized Wiener indices in hexagonal chains, *Int. J. Quantum Chem.*, 106(2) (2006), 426–435.

[6] Jensen, T. R., Toft, B., Graph Colouring Problems, John Wiley & Sons, New York, 1995.

[7] Kubale, M., Graph Colourings, American Math. Soc., Rhode Island, 2004.

[8] Kok, J., Sudev, N. K., Mary, U., On chromatic Zagreb indices of certain graphs, *Discrete Math. Algorithm. Appl.*, 9(1) (2017), 1–11. DOI:10.1142/S1793830917500148.

[9] Rose S., David, I., Naduvath, S., On chromatic D-polynomial of graphs, *Contemp. Stud. Discrete Math.*, 2(1) (2018), 31–43.

[10] West, D. B., Introduction to Graph Theory, Pearson Education, Delhi, 2001.

http://communications.science.ankara.edu.tr

Commun.Fac.Sci.Univ.Ank.Ser. A1 Math. Stat.
Volume 72, Number 2, Pages 386–396 (2023)
DOI:10.31801/cfsuasmas.1160606
ISSN 1303-5991 E-ISSN 2618-6470

Research Article; Received: August 11, 2022; Accepted: December 20, 2022

ADVANCED REFINEMENTS OF BEREZIN NUMBER INEQUALITIES

Mehmet GÜRDAL[1] and Hamdullah BAŞARAN[2]

[1,2]Depatment of Mathematics, Süleyman Demirel University, Isparta, TÜRKİYE

Abstract. For a bounded linear operator A on a functional Hilbert space $\mathcal{H}(\Omega)$, with normalized reproducing kernel $\widehat{k}_\eta := \frac{k_\eta}{\|k_\eta\|_{\mathcal{H}}}$, the Berezin symbol and Berezin number are defined respectively by $\widetilde{A}(\eta) := \left\langle A\widehat{k}_\eta, \widehat{k}_\eta \right\rangle_{\mathcal{H}}$ and $\operatorname{ber}(A) := \sup_{\eta\in\Omega} \left|\widetilde{A}(\eta)\right|$. A simple comparison of these properties produces the inequality $\operatorname{ber}(A) \leq \frac{1}{2}\left(\|A\|_{\operatorname{ber}} + \left\|A^2\right\|_{\operatorname{ber}}^{1/2}\right)$ (see [17]). In this paper, we prove further inequalities relating them, and also establish some inequalities for the Berezin number of operators on functional Hilbert spaces.

1. Introduction

In almost every field of engineering and research, mathematical inequalities are the most effective instrument for identifying and describing solutions to practical issues. The restrictions of the many types of operators covered in analysis courses, including mathematical and functional analysis, must be carefully considered while creating theory and applications. Numerous mathematicians and scientists have been affected by the Berezin transformation of an operator defined on the kernel generating the Hilbert space. Many scholar have investigated the Berezin radius inequality in-depth, and it is covered in (3) (see [12, 13]). Researchers are really motivated to make changes and additions to this difference [5, 7, 14, 27, 28]. The Berezin transform is used in this paper to create a number of inequalities, notably Kittaneh's inequalities (see, [21, 22]), for operators in the functional Hilbert space. A number of additional inequalities for the Berezin norm and the radius of the Berezin operators were also illustrated using the modifications discussed before.

2020 *Mathematics Subject Classification.* 47A30, 47A63.
Keywords. Berezin symbol, Berezin number, functional Hilbert space, positive operator.
[1] gurdalmehmet@sdu.edu.tr; 0000-0003-0866-1869
[2] 07hamdullahbasaran@gmail.com-Corresponding author; 0000-0002-9864-9515.

Related findings can be found in [23]. The foundational ideas required to move on with the research's findings will now be presented.

Assume that $\mathbb{L}(\mathcal{H})$ stands for the C^*-algebra of all bounded linear operators on a complex Hilbert space $\mathcal{H}$ with inner product $\langle .,. \rangle$. The numerical range $W(T)$ is the representation of the sphere of $\mathcal{H}$ under the corresponding quadratic form $x \to \langle Tx, x \rangle$ for a bounded linear operator T on a Hilbert space $\mathcal{H}$. In more specific terms, $W(T) = \{\langle Tx, x \rangle : x \in \mathcal{H}, \ \|x\| = 1\}$. Additionally, the numerical radius is specified as

$$w(T) = \sup_{\lambda \in W(T)} |\lambda| = \sup_{\|x\|=1} |\langle Tx, x \rangle| .$$

We recall that the usual operator norm of an operator T is defined to be

$$\|T\| = \sup \{\|Tx\| : x \in \mathcal{H}, \ \|x\| = 1\} .$$

Recall that if $A \in \mathbb{L}(\mathcal{H})$ and if f is a nonnegative increase on $[0, \infty]$, then $\|f(|A|)\| = f(\|A\|)$. Here $|A|$ represents positive operator $(A^*A)^{\frac{1}{2}}$.

Let Ω be a subset of a topological space X such that boundary $\partial\Omega$ is nonempty. Let $\mathcal{H} = \mathcal{H}(\Omega)$ be an infinite-dimensional Hilbert space of functions defined on Ω. We say that $\mathcal{H}$ is a functional Hilbert space (FHS) or reproducing kernel Hilbert space if the following two conditions are satisfied:

(i) for any $\eta \in \Omega$, the functionals $f \to f(\eta)$ are continuous on $\mathcal{H}$;

(ii) for any $\eta \in \Omega$, there exists $f_\eta \in \mathcal{H}$ such that $f_\eta(\eta)$:

According to the classical Riesz representation theorem, the assumption (i) implies that for any $\eta \in \Omega$ there exists $k_\eta \in \mathcal{H}$ such that

$$f(\eta) = \langle f, k_\eta \rangle , \ f \in \mathcal{H}.$$

The function k_η is called the reproducing kernel of $\mathcal{H}$ at point η. Note that by (ii), we surely have $k_\eta \neq 0$ and we denote $\widehat{k}_\eta$ as the normalized reproducing kernel, that is $\widehat{k}_\eta = \frac{k_\eta}{\|k_\eta\|}$.

The Berezin transform associates smooth functions with operators on Hilbert spaces of analytic functions.

Definition 1. *Let $\mathcal{H}$ be a FHS on a set Ω and let T be a bounded linear operator on $\mathcal{H}$.*
(i) For $\eta \in \Omega$, the Berezin transform of T at η (or Berezin symbol of T) is

$$\widetilde{T}(\eta) := \left\langle T\widehat{k}_\eta, \widehat{k}_\eta \right\rangle_{\mathcal{H}} .$$

(ii) The Berezin range of T (or Berezin set of T) is

$$\mathrm{Ber}(T) := \mathrm{Range}(\widetilde{T}) = \left\{ \widetilde{T}(\eta) : \eta \in \Omega \right\} .$$

(iii) The Berezin radius of T (or Berezin number of T) is

$$\mathrm{ber}(T) := \sup_{\eta \in \Omega} \left| \widetilde{T}(\eta) \right| .$$

We also define the following so-called Berezin norm of operators $T \in \mathcal{B}(\mathcal{H})$:

$$\|T\|_{\mathrm{Ber}} := \sup_{\eta \in \Omega} \left\| T\widehat{k}_\eta \right\|.$$

It is easy to see that actually $\|T\|_{\mathrm{Ber}}$ determines a new operator norm in $\mathbb{L}(\mathcal{H}(\Omega))$ (since the set of reproducing kernels $\{k_\eta : \eta \in \Omega\}$ span the space $\mathcal{H}(\Omega)$). It is also trivial that $\mathrm{ber}(T) \leq \|T\|_{\mathrm{Ber}} \leq \|T\|$ (for more facts about functional Hilbert spaces and Berezin symbol, see, Aronzajn [3], Berezin [9] and Chalendar et al. [11]).

The Berezin transform $\widetilde{T}$ is a bounded real-analytic function on Ω for each bounded operator T on $\mathcal{H}$. The Berezin transform $\widetilde{T}$ frequently reflects the characteristics of the operator T. Since F. Berezin first proposed the Berezin transform in [9], it has become an essential tool in operator theory due to the fact that the Berezin transforms of many significant operators include information about their fundamental characteristics. It is said that Karaev initially explicitly introduced the Berezin set and Berezin number in [19], also denoted as $\mathrm{Ber}(T)$ and $\mathrm{ber}(T)$, respectively.

In a FHS, the Berezin range of an operator T is a subset of the numerical range of T. Hence $\mathrm{ber}(T) \leq w(T)$. An operator's numeric range has a number of intriguing characteristics. For instance, it is common knowledge that an operator's numerical range's closure contains the operator's spectrum. We refer to [1, 2, 16, 24–26] for the fundamental attributes of the numerical radius.

For example, is it true, or under which additional conditions the following are true:

(i) $\mathrm{ber}(A) \geq \frac{1}{2}\|A\|$;

(ii)

$$\mathrm{ber}(A^n) \leq \mathrm{ber}(A)^n \tag{1}$$

for any integer $n \geq 1$; more generally, if A is not nilpotent, then

$$C_1 \mathrm{ber}(A)^n \leq \mathrm{ber}(A^n) \leq C_2 \mathrm{ber}(A)^n$$

for some constants $C_1, C_2 > 0$;

(iii) $\mathrm{ber}(AB) \leq \mathrm{ber}(A)\,\mathrm{ber}(B)$, where $A, B \in \mathcal{B}(\mathcal{H})$.

If $A = cI$ with $c \neq 0$, then obviously $\mathrm{ber}(A) = |c| > \dfrac{|c|}{2} = \dfrac{\|A\|}{2}$. However, it is known that in general the above inequality (i) is not satisfied (see Karaev [20]).

It is well-known that

$$\frac{1}{2}\|A\| \leq w(A) \leq \|A\| \tag{2}$$

and

$$\mathrm{ber}(A) \leq w(A) \leq \|A\| \tag{3}$$

for any $A \in \mathbb{L}(\mathcal{H})$. Additionally, Karaev introduced additional numerical properties of operators on the FHS in [19], including Berezin range and Berezin radius. See [4, 6, 13, 15, 20] for the fundamental characteristics and information on these novel concepts.

Huban et al. [18, Theorem 3.1] have showed the following result:

$$\operatorname{ber}(A) \leq \frac{1}{2}\left(\|A\|_{\operatorname{ber}} + \left\|A^2\right\|_{\operatorname{ber}}^{\frac{1}{2}}\right) \tag{4}$$

They also proved the following inequality as stronger than (4),

$$\operatorname{ber}(A) \leq \frac{1}{2}\left\||A| + |A^*|\right\|_{\operatorname{ber}}. \tag{5}$$

Another refinement has been established by same authors (see, [17, 18])

$$\operatorname{ber}^2(A) \leq \frac{1}{2}\left\||A|^2 + |A^*|^2\right\|_{\operatorname{ber}}. \tag{6}$$

Also, in the same paper, they showed that

$$\frac{1}{4}\left\||A|^2 + |A^*|^2\right\|_{\operatorname{ber}} \leq \operatorname{ber}^2(A). \tag{7}$$

In Section 2, we present an inequality that refines (4) and (6). Furthermore, we establish a refinement of the inequality (7).

In the paper, we need the following lemmas, which is important. The first lemma was introduced by Kittaneh in [22, Inequality 19].

Lemma 1. *If $A, B \in \mathbb{L}(\mathcal{H})$ is a positive operators, then we have*

$$\|A + B\| \leq \frac{1}{2}\left(\|A\| + \|B\|\sqrt{(\|A\| - \|B\|)^2 + 4\left\|A^{\frac{1}{2}}B^{\frac{1}{2}}\right\|^2}\right).$$

In particular

$$\left\||A|^2 + |A^*|^2\right\| \leq \left\|A^2\right\| + \left\|A^2\right\|$$

for any $A \in \mathbb{L}(\mathcal{H})$.

Second lemma is known in the literature as the generalized mixed Schwarz inequality (see, e.g., [21]).

Lemma 2. *Let $A, B \in \mathbb{L}(\mathcal{H})$ and let $x, y \in \mathcal{H}$ be any vector. If f, g are nonnegative continuous functions on $[0, \infty]$ satisfying $f(t).g(t) = t$, $(t \geq 0)$ then*

$$|\langle Ax, y\rangle| \leq \|f(|A|)x\| \, \|g(|A^*|)y\|.$$

In particular

$$|\langle Ax, y\rangle| \leq \sqrt{\left\langle |A|^{2(1-v)}x, x\right\rangle \left\langle |A|^{2v}y, y\right\rangle}, \ (0 \leq v \leq 1).$$

Lemma 3. *([10, Theorem IX.2.1])If $A, B \in \mathbb{L}(\mathcal{H})$ are positive operators, then we have*

$$\left\|A^t B^t\right\| \leq \|AB\|^t, \ (0 \leq t \leq 1).$$

2. Main Results

Using the same arguments as in [8, Theorem 1], we have the first result, a refinement of inequality (5).

Theorem 1. *Let $\mathcal{H}=\mathcal{H}(\Omega)$ be a FHS. If $A\in\mathbb{L}(\mathcal{H})$, then we have*

$$\operatorname{ber}(A)\leq\frac{1}{2}\min_{0\leq v\leq 1}\left\||A|^{2(1-v)}+|A^*|^{2v}\right\|_{\text{ber}}. \tag{8}$$

Proof. Let $\widehat{k}_\eta$ be an arbitrary. By utilizing Lemma 2 and the AM-GM inequality, we get

$$\begin{aligned}\left|\left\langle A\widehat{k}_\eta,\widehat{k}_\eta\right\rangle\right| &\leq\sqrt{\left\langle |A|^{2(1-v)}\widehat{k}_\eta,\widehat{k}_\eta\right\rangle\left\langle |A|^{2v}\widehat{k}_\eta,\widehat{k}_\eta\right\rangle}\\ &\leq\frac{1}{2}\left(\left\langle |A|^{2(1-v)}\widehat{k}_\eta,\widehat{k}_\eta\right\rangle+\left\langle |A|^{2v}\widehat{k}_\eta,\widehat{k}_\eta\right\rangle\right)\\ &\leq\frac{1}{2}\left\langle\left(|A|^{2(1-v)}+|A|^{2v}\right)\widehat{k}_\eta,\widehat{k}_\eta\right\rangle.\end{aligned}$$

Thus,

$$\left|\left\langle A\widehat{k}_\eta,\widehat{k}_\eta\right\rangle\right|\leq\frac{1}{2}\left\langle\left(|A|^{2(1-v)}+|A|^{2v}\right)\widehat{k}_\eta,\widehat{k}_\eta\right\rangle.$$

Now, taking the supremum over $\eta\in\Omega$ in the above inequality we reach

$$\operatorname{ber}(A)\leq\frac{1}{2}\left\||A|^{2(1-v)}+|A^*|^{2v}\right\|_{\text{ber}}. \tag{9}$$

Taking the minimum over all $v\in[0,1]$, we have

$$\operatorname{ber}(A)\leq\frac{1}{2}\min_{0\leq v\leq 1}\left\||A|^{2(1-v)}+|A^*|^{2v}\right\|_{\text{ber}}.$$

This completes the proof. □

The Theorem 1 accepts the following result.

Corollary 1. *If $A\in\mathbb{L}(\mathcal{H})$ and $0\leq v\leq 1$, then we have*

$$\operatorname{ber}(A)\leq\frac{1}{4}\left(\|A\|_{\text{ber}}^{2(1-v)}+\|A^*\|_{\text{ber}}^{2v}+\sqrt{\left(\|A\|_{\text{ber}}^{2(1-v)}-\|A\|_{\text{ber}}^{2v}\right)^2+4\left\||A|^{(1-v)}|A^*|^{v}\right\|_{\text{ber}}^2}\right).$$

Proof. Let $\widehat{k}_\eta$ be an arbitrary and $0\leq v\leq 1$. We get

$$\begin{aligned}&\left\||A|^{2(1-v)}+|A^*|^{2v}\right\|_{\text{ber}}\\ &\leq\frac{1}{2}\Bigg(\left\||A|^{2(1-v)}\right\|_{\text{ber}}+\left\||A^*|^{2v}\right\|_{\text{ber}}\\ &+\sqrt{\left(\left\||A|^{2(1-v)}\right\|_{\text{ber}}-\left\||A^*|^{2v}\right\|_{\text{ber}}\right)^2+4\left\||A|^{(1-v)}|A^*|^{v}\right\|_{\text{ber}}^2}\Bigg)\end{aligned}$$

(by Lemma 1)

$$= \frac{1}{2}\left(\|A\|_{\text{ber}}^{2(1-v)} + \|A^*\|_{\text{ber}}^{2v} + \sqrt{\left(\|A\|_{\text{ber}}^{2(1-v)} - \|A\|_{\text{ber}}^{2v} \right)^2 + 4 \left\| |A|^{(1-v)} |A^*|^{v} \right\|_{\text{ber}}^2} \right).$$

Thus, by (9),

$$\text{ber}(A) \le \tfrac{1}{4}\left(\|A\|_{\text{ber}}^{2(1-v)} + \||A^*|\|_{\text{ber}}^{2v} + \sqrt{\left(\|A\|_{\text{ber}}^{2(1-v)} - \|A\|_{\text{ber}}^{2v} \right)^2 + 4 \left\| |A|^{(1-v)} |A^*|^{v} \right\|_{\text{ber}}^2} \right).$$

□

Remark 1. *It follows from the Lemma 3 that*

$$\begin{aligned} \text{ber}(A) &\le \frac{1}{2}\left(\|A\|_{\text{ber}} + \left\| |A|^{\frac{1}{2}} |A^*|^{\frac{1}{2}} \right\|_{\text{ber}} \right) \le \frac{1}{2}\left(\|A\|_{\text{ber}} + \||A|\,|A^*|\|_{\text{ber}}^{\frac{1}{2}} \right) \\ &= \frac{1}{2}\left(\|A\|_{\text{ber}} + \left\|A^2\right\|_{\text{ber}}^{\frac{1}{2}} \right). \end{aligned} \tag{10}$$

Our second result interprets as follows. This result includes refinement of the inequality (6).

Theorem 2. *Let $\mathcal{H} = \mathcal{H}(\Omega)$ be a FHS. Assume that $A \in \mathbb{L}(\mathcal{H})$ and f, g are nonnegative continuous functions on $[0,\infty)$ satisfying $f(t)\,g(t) = t$, $(t \ge 0)$. Then we have*

$$\begin{aligned} \text{ber}^2(A) &\le \frac{1}{4}\left\| f^4(|A|) + g^4(|A^*|) \right\|_{\text{ber}} + \frac{1}{4}\left\| f^2(|A|)\,g^2(|A^*|) + g^2(|A^*|)\,f^2(|A|) \right\|_{\text{ber}} \\ &\le \frac{1}{4}\left\| f^4(|A|) + g^4(|A^*|) \right\|_{\text{ber}}. \end{aligned} \tag{11}$$

Proof. Let $\widehat{k}_\eta$ be a normalized reproducing kernel. Using the Lemma 2, AM-GM inequality and Cauchy-Schwarz inequality, we get

$$\begin{aligned} \left| \left\langle A\widehat{k}_\eta, \widehat{k}_\eta \right\rangle \right|^2 &\le \left\| f(|A|)\,\widehat{k}_\eta \right\| \left\| g(|A^*|)\,\widehat{k}_\eta \right\| \\ &\le \left\langle f^2(|A|)\,\widehat{k}_\eta, \widehat{k}_\eta \right\rangle \left\langle g^2(|A^*|)\,\widehat{k}_\eta, \widehat{k}_\eta \right\rangle \\ &\le \left(\frac{\left\langle f^2(|A|)\,\widehat{k}_\eta, \widehat{k}_\eta \right\rangle + \left\langle g^2(|A^*|)\,\widehat{k}_\eta, \widehat{k}_\eta \right\rangle}{2} \right)^2 \\ &\le \frac{1}{4}\left\langle \left(f^2(|A|) + g^2(|A^*|) \right) \widehat{k}_\eta, \widehat{k}_\eta \right\rangle^2 \\ &\le \frac{1}{4}\left\langle \left(f^2(|A|) + g^2(|A^*|) \right)^2 \widehat{k}_\eta, \widehat{k}_\eta \right\rangle \\ &= \frac{1}{4}\left\langle \left(f^4(|A|) + g^4(|A^*|) + f^2(|A|)\,g^2(|A^*|) + g^2(|A^*|)\,f^2(|A|) \right) \widehat{k}_\eta, \widehat{k}_\eta \right\rangle \\ &= \frac{1}{4}\left\langle \left(f^4(|A|) + g^4(|A^*|) \right) \widehat{k}_\eta, \widehat{k}_\eta \right\rangle \\ &+ \frac{1}{4}\left\langle \left(f^2(|A|)\,g^2(|A^*|) + g^2(|A^*|)\,f^2(|A|) \right) \widehat{k}_\eta, \widehat{k}_\eta \right\rangle. \end{aligned}$$

Hence,

$$\left|\left\langle A\widehat{k}_\eta,\widehat{k}_\eta\right\rangle\right|^2$$
$$\le \frac{1}{4}\left\langle \left(f^4(|A|)+g^4(|A^*|)\right)\widehat{k}_\eta,\widehat{k}_\eta\right\rangle+\frac{1}{4}\left\langle \left(f^2(|A|)\,g^2(|A^*|)+g^2(|A^*|)\,f^2(|A|)\right)\widehat{k}_\eta,\widehat{k}_\eta\right\rangle.$$

Now, we taking the supremum over $\eta\in\Omega$ in the above inequality we have

$$\operatorname{ber}^2(A)\le\frac{1}{4}\left\|f^4(|A|)+g^4(|A^*|)\right\|_{\mathrm{ber}}+\frac{1}{4}\left\|f^2(|A|)\,g^2(|A^*|)+g^2(|A^*|)\,f^2(|A|)\right\|_{\mathrm{ber}}. \tag{12}$$

Also, by [22, Corollary 1], we have

$$\begin{aligned}&\left\|f^2(|A|)\,g^2(|A^*|)+g^2(|A^*|)\,f^2(|A|)\right\|_{\mathrm{ber}}\\&=\frac{1}{2}\left\|\left(f^2(|A|)+g^2(|A^*|)\right)^2-\left(f^2(|A|)-g^2(|A^*|)\right)^2\right\|_{\mathrm{ber}}\\&\le\frac{1}{2}\left\|\left(f^2(|A|)+g^2(|A^*|)\right)^2+\left(f^2(|A|)-g^2(|A^*|)\right)^2\right\|_{\mathrm{ber}}\\&=\left\|f^4(|A|)+g^4(|A^*|)\right\|_{\mathrm{ber}}.\end{aligned} \tag{13}$$

When we combine the relations (12) and (13), we obtain (11). □

Corollary 2. *In the Theorem 2, if we accept* $f(t)=t^{1-v}$ *and* $g(t)=t^v$ *with* $0\le v\le 1$*, we obtain*

$$\begin{aligned}\operatorname{ber}^2(A)&\le\frac{1}{4}\left\||A|^{4(1-v)}+|A^*|^{4v}\right\|_{\mathrm{ber}}+\frac{1}{4}\left\||A|^{2(1-v)}|A^*|^{2v}+|A^*|^{2v}|A|^{2(1-v)}\right\|_{\mathrm{ber}}\\&\le\frac{1}{2}\left\||A|^{4(1-v)}+|A^*|^{4v}\right\|_{\mathrm{ber}}.\end{aligned}$$

In particular,

$$\operatorname{ber}^2(A)\le\frac{1}{4}\left\||A|^2+|A^*|^2\right\|_{\mathrm{ber}}+\frac{1}{4}\left\||A|\,|A^*|+|A^*|\,|A|\right\|_{\mathrm{ber}}\le\frac{1}{2}\left\||A|^2+|A^*|^2\right\|_{\mathrm{ber}}.$$

We obtain on both sides of

$$\operatorname{ber}^2(A)\le\frac{1}{4}\left(\left\||A|^2+|A^*|^2\right\|_{\mathrm{ber}}+\left\||A|\,|A^*|+|A^*|\,|A|\right\|_{\mathrm{ber}}\right) \tag{14}$$

for normal operator A.

The following consequence demonstrates that inequality (14) is likewise sharper than inequality (4).

Corollary 3. *If* $A\in\mathbb{L}(\mathcal{H})$*, then we have*

$$\operatorname{ber}(A)\le\frac{1}{2}\sqrt{\left\||A|^2+|A^*|^2\right\|_{\mathrm{ber}}+\left\||A|\,|A^*|+|A^*|\,|A|\right\|_{\mathrm{ber}}}\le\frac{1}{2}\left(\|A\|_{\mathrm{ber}}+\left\|A^2\right\|_{\mathrm{ber}}^{\frac{1}{2}}\right). \tag{15}$$

Proof. Since $\||A||A^*|\| = \|A^2\|$ and $|A| = |A^*|$ for any $A \in \mathbb{L}(\mathcal{H})$, it is clear that

$$\begin{aligned}\||A||A^*| + |A^*||A|\|_{\text{ber}} &\le \||A||A^*|\|_{\text{ber}} + \||A^*||A|\|_{\text{ber}} \\ &= \||A||A^*|\|_{\text{ber}} + \|(|A||A^*|)^*\|_{\text{ber}} \qquad (16) \\ &= 2\||A||A^*|\|_{\text{ber}} = 2\|A^2\|_{\text{ber}}.\end{aligned}$$

So, since $\|A\|^2 = \|A^2\|^{\frac{1}{2}}\|A^2\|^{\frac{1}{2}} \le \|A\|\|A^2\|^{\frac{1}{2}}$, we get

$$\begin{aligned}\text{ber}^2(A) &\le \frac{1}{4}\left(\left\||A|^2 + |A^*|^2\right\|_{\text{ber}} + \||A||A^*| + |A^*||A|\|_{\text{ber}}\right) \\ &\le \frac{1}{4}\left(\|A^2\|_{\text{ber}} + \|A\|_{\text{ber}}^2\right) + \frac{1}{4}\||A||A^*| + |A^*||A|\|_{\text{ber}} \quad \text{(by Lemma 1)} \\ &\le \frac{1}{4}\left(\|A^2\|_{\text{ber}} + \|A\|_{\text{ber}}^2\right) + \frac{1}{2}\|A^2\|_{\text{ber}} \\ &\quad \text{(by the inequality (16))} \\ &= \frac{1}{4}\left(\|A^2\|_{\text{ber}} + 3\|A\|_{\text{ber}}^2\right) \\ &\le \frac{1}{4}\left(\|A^2\|_{\text{ber}} + 2\|A\|_{\text{ber}}\|A^2\|_{\text{ber}}^{\frac{1}{2}} + \|A\|_{\text{ber}}^2\right) \\ &= \frac{1}{4}\left(\|A^2\|_{\text{ber}} + \|A^2\|_{\text{ber}}^{\frac{1}{2}}\right)^2.\end{aligned}$$

This gives the desired result. □

Remark 2. *According to the study in [17],*

$$\text{ber}^2(A) \le \frac{1}{4}\left\||A|^2 + |A^*|^2\right\|_{\text{ber}} + \frac{1}{2}\text{ber}(|A||A^*|). \qquad (17)$$

It is obvious that inequality (14) improves the inequality (17).

We need the following lemma (see, [23]).

Lemma 4. *If $A, B \in \mathbb{L}(\mathcal{H})$, then we have*

$$\begin{aligned}\|A+B\|_{\text{ber}} &\le \sqrt{\left\||A|^2 + |B|^2\right\|_{\text{ber}} + \|A^*B + B^*A\|_{\text{ber}}} \\ &\le \sqrt{\|A\|_{\text{ber}}^2 + \|B\|_{\text{ber}}^2 + 2\|A^*B\|_{\text{ber}}} \qquad (18) \\ &\le \|A\|_{\text{ber}} + \|B\|_{\text{ber}}.\end{aligned}$$

Our refinement of the inequality (7) is offered in the following theorem.

Theorem 3. *Let $\mathcal{H} = \mathcal{H}(\Omega)$ be a FHS. If $A \in \mathbb{L}(\mathcal{H})$, then*

$$\frac{1}{4}\left\||A|^2 + |A^*|^2\right\|_{\text{ber}} \le \frac{1}{2}\sqrt{2\text{ber}^4(A) + \frac{1}{8}\left\|(A+A^*)^2(A-A^*)^2\right\|_{\text{ber}}} \le \text{ber}^2(A). \qquad (19)$$

Proof. Let $\widehat{k}_\eta$ be a normalized reproducing kernel. Let $A = B+iC$ be the Cartesian decomposition of A. Then B and C are self-adjoint and

$$\left|\left\langle A\widehat{k}_\eta, \widehat{k}_\eta\right\rangle\right|^2 = \left\langle B\widehat{k}_\eta, \widehat{k}_\eta\right\rangle^2 + \left\langle C\widehat{k}_\eta, \widehat{k}_\eta\right\rangle^2.$$

Using a little calculation, we have

$$\|B\|_{\text{ber}} \leq \text{ber}(A) \text{ and } \|C\|_{\text{ber}} \leq \text{ber}(A). \tag{20}$$

Now, by using Lemma 4 and the submultiplicative property of usual operator norm, we get

$$\begin{aligned}
\frac{1}{4}\left\||A|^2 + |A^*|^2\right\|_{\text{ber}} &= \frac{1}{2}\left\|B^2 + C^2\right\|_{\text{ber}} \\
&\leq \frac{1}{2}\sqrt{\|B\|_{\text{ber}}^4 + \|C\|_{\text{ber}}^4 + 2\left\|B^2C^2\right\|_{\text{ber}}} \\
&\leq \frac{1}{2}\sqrt{2\text{ber}^4(A) + 2\left\|B^2C^2\right\|_{\text{ber}}} \\
&\quad \text{(by the inequality (20))} \\
&\leq \frac{1}{2}\sqrt{2\text{ber}^4(A) + 2\|B\|_{\text{ber}}^2\|C\|_{\text{ber}}^2} \\
&\leq \text{ber}^2(A).
\end{aligned}$$

Thus, from the above inequalities we get

$$\frac{1}{4}\left\||A|^2 + |A^*|^2\right\|_{\text{ber}} \leq \frac{1}{2}\sqrt{2\left(\text{ber}^4(A) + \left\|B^2C^2\right\|_{\text{ber}}\right)} \leq \text{ber}^2(A),$$

hence, we get (19) as required. □

Author Contribution Statements The authors contributed equally to this work. All authors read and approved the final copy of this paper.

Declaration of Competing Interests The authors declare that they have no known competing financial interest or personal relationships that could have appeared to influence the work reported in this paper.

Acknowledgement This work's abstract was given at the "4th International Conference on Pure and Applied Mathematics (ICPAM - VAN 2022)" on June 22–23, 2022 in Van, Turkey.

References

[1] Alomari, M. W., Refinements of some numerical radius inequalities for Hilbert space operators, *Linear Multilinear Algebra*, 69(7) (2021), 1208-1223. https://doi.org/10.1080/03081087.2019.1624682

[2] Alomari, M. W., Improvements of some numerical radius inequalities, *Azerb. J. Math.*, 12(1) (2022), 124-137.

[3] Aronzajn, N., Theory of reproducing kernels, *Trans. Amer. Math. Soc.*, 68 (1950), 337-404. https://doi.org/10.1090/S0002-9947-1950-0051437-7

[4] Bakherad, M., Some Berezin number inequalities for operator matrices, *Czechoslovak Math. J.*, 68(143:4) (2018), 997-1009. https://doi.org/10.21136/CMJ.2018.0048-17

[5] Bakherad, M., Garayev, M. T., Berezin number inequalities for operators, *Concr. Oper.*, 6(1) (2019), 33-43. http://doi.org/10.1515/conop-2019-0003

[6] Bakherad, M., Hajmohamadi, M., Lashkaripour R., Sahoo, S., Some extensions of Berezin number inequalities on operators, *Rocky Mountain J. Math.*, 51(6) (2021), 1941-1951. https://doi.org/10.1216/rmj.2021.51.1941

[7] Başaran, H., Gürdal, M., Berezin number inequalities via inequality, *Honam Math. J.,* 43(3) (2021)-523-537. https://doi.org/10.5831/HMJ.2021.43.3.523

[8] Başaran, H., Huban, M. B., Gürdal, M., Inequalities related to Berezin norm and Berezin number of operators, *Bull. Math. Anal. Appl.*, 14(2) (2022), 1-11. https://doi.org/10.54671/bmaa-2022-2-1

[9] Berezin, F. A., Covariant and contravariant symbols for operators, *Math. USSR-Izv.*, 6 (1972), 1117-1151. https://doi.org/10.1070/IM1972v006n05ABEH001913

[10] Bhatia, R., Matrix Analysis, New York, Springer-Verlag, 1997.

[11] Chalendar, I., Fricain, E., Gürdal, M., Karaev, M., Compactness and Berezin symbols, *Acta Sci. Math. (Szeged)*, 78(1-2) (2012), 315-329. https://doi.org/10.1007/BF03651352

[12] Garayev, M., Bouzeffour, F., Gürdal, M., Yangöz, C. M., Refinements of Kantorovich type, Schwarz and Berezin number inequalities, *Extracta Math.*, 35 (2020), 1-20. https://doi.org/10.17398/2605-5686.35.1.1

[13] Garayev, M. T., Guedri, H., Gürdal, M., Alsahli, G. M., On some problems for operators on the reproducing kernel Hilbert space, *Linear Multilinear Algebra*, 69(11) (2021), 2059-2077. https://doi.org/10.1080/03081087.2019.1659220

[14] Gürdal, M., Başaran, H., A-Berezin number of operators, *Proc. Inst. Math. Mech. Natl. Acad. Sci. Azerb.*, 48(1) (2022), 77-87. https://doi.org/10.30546/2409-4994.48.1.2022.77

[15] Hajmohamadi, M., Lashkaripour, R., Bakherad, M., Improvements of Berezin number inequalities, *Linear Multilinear Algebra*, 68(6) (2020), 1218-1229. https://doi.org/10.1080/03081087.2018.1538310

[16] Haydarbeygi, Z., Sababbeb, M., Moradi H. R., A convex treatment of numerical radius inequalities, *Czechoslovak Math. J.*, 72 (2022), 601–614. https://doi.org/10.21136/CMJ.2022.0068-21

[17] Huban, M. B., Başaran, H., Gürdal, M., New upper bounds related to the Berezin number inequalities, *J. Inequal. Spec. Funct.*, 12(3) (2021), 1-12.

[18] Huban, M. B., Başaran, H., Gürdal, M., Some new inequalities via Berezin numbers, *Turk. J. Math. Comput. Sci.*, 14(1) (2022), 129-137. https://doi.org/10.47000/tjmcs.1014841

[19] Karaev, M. T., Berezin symbol and invertibility of operators on the functional Hilbert spaces, *J. Funct. Anal.*, 238 (2006), 181-192. doi:10.1016/j.jfa.2006.04.030

[20] Karaev, M. T., Reproducing kernels and Berezin symbols techniques in various questions of operator theory, *Complex Anal. Oper. Theory*, 7 (2013), 983-1018. https://doi.org/10.1007/s11785-012-0232-z

[21] Kittaneh, F., Notes on some inequalities for Hilbert space operators, *Publ. Res. Ins. Math. Sci.*, 24 (1988), 283-293. https://doi.org/10.2977/prims/1195175202

[22] Kittaneh, F., Norm inequalities for sums and differences of positive operators, *Linear Algebra Appl.*, 383 (2004), 85-91. https://doi.org/10.1016/j.laa.2003.11.023

[23] Najafabadi, F. P., Moradi, H. R., Advanced refinements of numerical radius inequalities, *Int. J. Math. Model. Comput.*, 11(4) (2021), 1-10. https://doi.org/10.30495/IJM2C.2021.684828

[24] Omidvar, M. E., Moradi, H. R., Better bounds on the numerical radii of Hilbert space operators, *Linear Algebra Appl.*, 604 (2020) 265-277. https://doi.org/10.1016/j.laa.2020.06.021

[25] Omidvar, M. E., Moradi, H. R., Shebrawi, K., Sharpening some classical numerical radius inequalities, *Oper. Matrices.*, 12(2) (2018), 407-416. doi:10.7153/oam-2018-12-26
[26] Tafazoli, S., Moradi, H. R., Furuichi, S., Harikrishnan, P., Further inequalities for the numerical radius of Hilbert space operators, *J. Math. Inequal.*, 13(4) (2019), 955-967. doi:10.7153/jmi-2019-13-68
[27] Tapdigoglu, R., New Berezin symbol inequalities for operators on the reproducing kernel Hilbert space, *Oper. Matrices*, 15(3) (2021), 1445-1460. https://doi.org/10.7153/oam-2021-15-64
[28] Yamancı, U., Tunç, R., Gürdal, M., Berezin number, Grüss-type inequalities and their applications, *Bull. Malays. Math. Sci. Soc.*, 43(3) (2020), 2287-2296. https://doi.org/10.1007/s40840-019-00804-x

http://communications.science.ankara.edu.tr

Commun.Fac.Sci.Univ.Ank.Ser. A1 Math. Stat.
Volume 72, Number 2, Pages 397–406 (2023)
DOI:10.31801/cfsuasmas.1179189
ISSN 1303-5991 E-ISSN 2618-6470

Research Article; Received: September 23, 2022; Accepted: December 18, 2022

A NEW TRANSMUTATION: CONDITIONAL COPULA WITH EXPONENTIAL DISTRIBUTION

Hüseyin ÜNÖZKAN[1] and Mehmet YILMAZ[2]

[1]Halic University, Faculty of Engineering, Department of Industrial Engineering, İstanbul, TÜRKİYE
[2]Ankara University, Faculty of Science, Department of Statistics, Ankara, TÜRKİYE

Abstract. In these days, many different techniques are implemented for generating distributions. The core aim in generating distribution, is better modeling capability. With generating new distribution more reliable and appropriate models are available for data sets. In this paper, a new distribution is gained by evaluating the conditional diagonal section of the bivariate Farlie-Gumbel-Morgenstern distribution with exponential marginals. Specifications and characteristics of this new distribution are studied. The statistical assessment and some reliability analyzes are carried out. The success of the new distribution on statistical modeling is detected by using data sets in literature. It is concluded that this new distribution suggests a model that can be used effectively in many different lifetime data sets.

1. Introduction

The exponential distribution is one of the most popular statistical distributions. This valuable distribution has been used widely in modeling time data sets ([11], [4], [12]). Exponential distribution has also been used in modeling other kinds of data sets (see [12]).

Although this distribution is very capable of modeling very different kinds of lifetime data sets, in some data sets, the modeling success rate may be lower. In some studies-to fix this situation-researchers add more parameters for better modeling ([10], [2], [8].

Exponential distribution has some specialties that this distribution can be used efficiently in industrial engineering and stochastic processes. ([11], [4]). The most

2020 *Mathematics Subject Classification.* 62E10, 62E15.
Keywords. Farlie-Gumbel-Morgenstern distribution, copula, reliability analysis, generating distribution, exponential distribution.

[1] huseyinunozkan@halic.edu.tr-Corresponding author; 0000-0001-9659-287X
[2] mehmetyilmaz@ankara.edu.tr; 0000-0002-9762-6688.

important and most known specialty of Exponential distribution is memoryless specialty. Exponential distribution also has a constant hazard rate.

In this study, main aim is generating an efficient statistical distribution which is more appropriate in some data sets than exponential distribution and other lifetime distributions.

We use Farlie-Gumbel-Morgenstern distribution and each marginal distribution in that copula function is Exponential distribution. A very similar technique was used in a study to gain a new distribution ([14]). In this study a different condition is carried out for achieving a new distribution. In this article, Exponential distribution gains better capability.

In this study, a new distribution for analyzing many different kinds of time data sets was suggested. This new distribution gains good results in modeling customer waiting times, time intervals in earthquakes and broken times in mechanic instruments. In our presentation at first new distribution is derived. And then the properties of new distribution are shown, and important characteristics are introduced. Section 4 illustrates the application of the new distribution on three data sets. There is the comparison of new distribution with most known lifetime distributions via data sets in the literature.

2. Material and Method

Theorem 1. ***(Sklar's Theorem):*** *Let F be a joint cumulative distribution function and H and G are continuous marginals, then there is a unique copula function C in R for every x and y ([13]).*

$$F(x,y) = C\left(H(x), G(y)\right).$$

Farlie-Gumbel-Morgenstern (FGM) copula with marginals has a formula as follows ([9])

$$C\left(u,v\right) = uv + \lambda uv\left(1-u\right)\left(1-v\right).$$

Two dimensional FGM with marginals $H\left(x\right)$ and $G\left(y\right)$ is as follows.

$$F\left(x,y\right) = H\left(x\right)G\left(y\right)\left[1+\lambda \bar{H}\left(x\right)\bar{G}\left(y\right)\right],$$

where $\bar{H}$ and $\bar{G}$ are the respective survival functions and $\lambda \in [-1,1]$ represents association parameter.

First, we assume that H and G are the same. Next, we will deal with the probability that the first component will fail in this range, when it is known that the second component fails in the range $(0,t]$. Then the conditional distribution function is as below.

$$\begin{aligned} Pr\left(X \leq t | Y \leq t\right) &= \frac{H\left(t\right) G\left(t\right) \left[1 + \lambda \bar{H}\left(t\right) \bar{G}\left(t\right)\right]}{G\left(t\right)} \\ &= H\left(t\right) \left[1 + \lambda \bar{H}\left(t\right) \bar{G}\left(t\right)\right] \\ &= H\left(t\right) \left[1 + \lambda \bar{H}^2\left(t\right)\right] \\ &= \left(1 + \lambda\right) H\left(t\right) - \lambda H\left(t\right) \left(1 - \bar{H}^2\left(t\right)\right). \end{aligned}$$

Thus, we obtain a univariate distribution. Let a random variable T distributed as above and F stand for this new distribution. Now, we explore what the association parameter means in this univariate case:
By taking $1 + \lambda = 2\delta$, where $\delta \in [0, 1]$, we have

$$\begin{aligned} F(t) &= \left(1 + \lambda\right) H\left(t\right) - \lambda H\left(t\right) \left(1 - \bar{H}^2\left(t\right)\right) \\ &= 2\delta H\left(t\right) + (1 - 2\delta) H\left(t\right) \left(1 - \bar{H}^2\left(t\right)\right) \\ &= \delta\left[2H\left(t\right) - 2H^2(t) + H^3(t)\right] + (1 - \delta) H\left(t\right) \left(1 - \bar{H}^2\left(t\right)\right). \end{aligned}$$

The expression in square brackets is actually a convex combination of two distribution functions as follows:

$$\frac{2}{3}\left(3H\left(t\right) - 3H^2(t) + H^3(t)\right) + \frac{1}{3}H^3(t),$$

where components respectively represent the distributions of $min\{T_1, T_2, T_3\}$ and $max\{T_1, T_2, T_3\}$, when T_1, T_2 and T_3 are independently distributed as H. Accordingly, $H\left(t\right)\left(1 - \bar{H}^2(t)\right)$ represents a distribution of $max\{T_1, min\{T_2, T_3\}\}$. Thus, F is a distribution function representing the convex combination of two distribution functions, while λ represents a transformed combination parameter.
Hence, probability density function (pdf) of this distribution is as below.

$$f\left(t\right) = h\left(t\right)\left(1 + \lambda \overline{H}\left(t\right)\left(1 - 3H\left(t\right)\right)\right),$$

where $h\left(t\right)$ is a pdf of base distribution. In prospect of $H\left(t\right) = 1 - e^{-\theta t}$, we have

$$F\left(t\right) = \left(1 - e^{-\theta t}\right)\left(1 + \lambda e^{-2\theta t}\right), \tag{1}$$

and pdf of this distribution is as below.

$$f\left(t\right) = \theta e^{-\theta t}\left(1 + \lambda\left(e^{-2\theta t} - 2e^{-\theta t}\left(1 - e^{-\theta t}\right)\right)\right), \tag{2}$$

where $\lambda \in [-1, 1]$ and $\theta > 0$. Plots of probability density function are as follows.

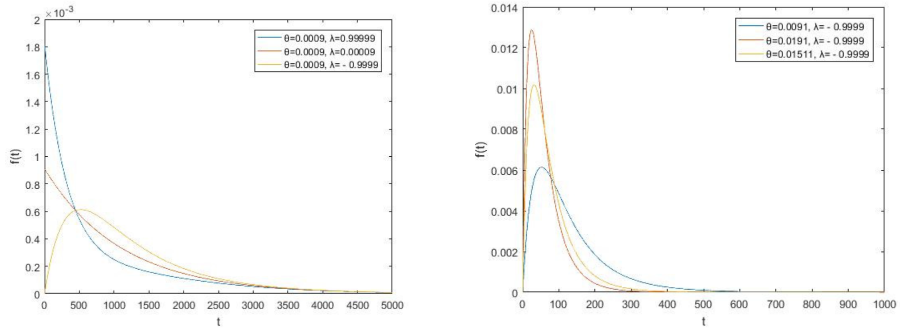

FIGURE 1. The pdf graphs for some parameters

According to plots in Figure 1, it was easily seen that parameter λ is the shape parameter and parameter θ is the location parameter. With the value of the parameter λ the shape of the probability density function changes significantly and this specialty gives us hope for this distribution to use in different kinds of data sets at the same time.

Survival and hazard rate functions of new distribution are as follows;

$$\bar{F}(t) = e^{-\theta t} - \lambda e^{-2\theta t} + \lambda e^{-3\theta t} = e^{-\theta t}\left(1 - \lambda e^{-\theta t}\left(1 - e^{-\theta t}\right)\right)$$

and

$$r(t) = \frac{f(t)}{\bar{F}(t)} = \theta\left[2 - \frac{1 - \lambda e^{-2\theta t}}{1 - \lambda e^{-\theta t}\left(1 - e^{-\theta t}\right)}\right].$$

If we want to calculate the risk in the starting point, we reach this value as below.

$$\lim_{t \to 0}\left(\theta\left[2 - \frac{1 - \lambda e^{-2\theta t}}{1 - \lambda e^{-\theta t}\left(1 - e^{-\theta t}\right)}\right]\right) = (1 + \lambda)\theta.$$

If we want to calculate long term risk, we reach this value as below.

$$\lim_{t \to \infty}\left(\theta\left[2 - \frac{1 - \lambda e^{-2\theta t}}{1 - \lambda e^{-\theta t}\left(1 - e^{-\theta t}\right)}\right]\right) = \theta.$$

In Figures 1 and 2, it can be seen easily that parameter λ changes both the shapes of probability density function and hazard rate function. Therefore, we consider that this new distribution may be successful in analyzing different data sets which may have opposite kinds of risk in the same time.

When parameter λ is between $(0, 1]$, the shape of the hazard rate function becomes bathtub. With this there are decreasing starting deaths, and in the beginning some components rapidly break down. After that there is nearly a constant hazard rate for a while. At last in the final part, the components which complete life time, break down in increasing rate and the process completes.

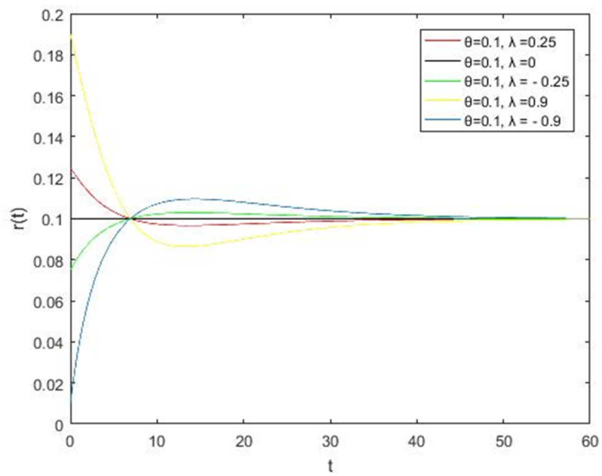

Figure 2. The plots of hazard rate function

When parameter λ is between $[-1, 0)$, the shape of the hazard rate function becomes the inverse position of the bathtub shape. This curve is symmetric to value of parameter θ which is the hazard rate of the exponential distribution. With this, there are increasing starting deaths, and at the beginning some components break down rapidly. After that there is a balance and nearly constant hazard rate. At last, the components which complete life time, break down in decreasing rate and the process completes. This shape calls upside-down bathtub or inverse bathtub.

3. Characteristics of Distribution

3.1. **Moment Generating Function (mgf).**

$$
\begin{aligned}
M_T(v) &= E\left(e^{vT}\right) \\
&= \int_0^\infty e^{vt}\left(\theta e^{-\theta t}\right)\left(1+\lambda\left(e^{-2\theta t}-2e^{-\theta t}\left(1-e^{-\theta t}\right)\right)\right)dt \\
&= \int_0^\infty \left(\theta e^{-t(\theta-v)} - 2\lambda\theta e^{-t(2\theta-v)} + 3\lambda\theta e^{-t(3\theta-v)}\right)dt \\
&= \int_0^\infty \theta e^{-t(\theta-v)}dt - 2\lambda\int_0^\infty \theta e^{-t(2\theta-v)}dt + 3\lambda\int_0^\infty \theta e^{-t(3\theta-v)}dt \\
&= \frac{\theta}{\theta-v} - \frac{2\lambda\theta}{2\theta-v} + \frac{3\lambda\theta}{3\theta-v},
\end{aligned}
$$

where $\theta > v$. This is a linear combination of mgf's of exponential distributions with three different means $\frac{1}{\theta}$, $\frac{1}{2\theta}$ and $\frac{1}{3\theta}$. In other words, for $Y_j \sim Exponential\left(\frac{1}{j\theta}\right)$, $j = 1, 2, 3$ this mgf can be represented as a mgf's of Y_j which are $M_{Y_j}(v) = \frac{j\theta}{j\theta - v}$.

$$M_T(v) = M_{Y_1}(v) - \lambda M_{Y_2}(v) + \lambda M_{Y_3}(v), \quad \theta > v. \tag{3}$$

3.2. **k. th Raw Moment.** We can provide raw moment easily by using (3) as follows:

$$E\left(T^k\right) = \frac{\Gamma(k+1)}{\theta^k} - \lambda\frac{\Gamma(k+1)}{2^k\theta^k} + \lambda\frac{\Gamma(k+1)}{3^k\theta^k} = \frac{k!}{\theta^k}\left[1 - \lambda\frac{1}{2^k} + \lambda\frac{1}{3^k}\right]$$

3.3. **Expected Value and Second Order Raw Moment.**

$$E(T) = \frac{1}{\theta} - \frac{\lambda}{2\theta} + \frac{\lambda}{3\theta} = \frac{6-\lambda}{6\theta},$$

$$E\left(T^2\right) = \frac{2}{\theta^2} - \frac{\lambda}{2\theta^2} + \frac{2\lambda}{9\theta^2} = \frac{36 - 5\lambda}{18\theta^2}.$$

3.4. **Variance.**

$$Var(T) = E\left(T^2\right) - E(T)^2 = \frac{36-5\lambda}{18\theta^2} - \left(\frac{6-\lambda}{6\theta}\right)^2 = \frac{36 + 2\lambda - \lambda^2}{36\theta^2}.$$

3.5. **Maximum Likelihood Estimation.** The log-likelihood function for a random sample $T_1, T_2, \cdots, T_n$ from (1) is:

$$\ell(\theta, \lambda\ ; \underline{t}) = \log(L(\theta, \lambda; \underline{t})) = n\log\theta - \theta\sum_{i=1}^{n} t_i + \sum_{i=1}^{n}\log\left(1 + \lambda\left(3e^{-2\theta t_i} - 2e^{-\theta t_i}\right)\right).$$

Now, by using Log-likelihood function, we get partial derivatives with respect to λ and θ as follows:

$$\frac{\partial}{\partial\lambda}\ell(\theta, \lambda\ ; \underline{t}) = \sum_{i=1}^{n}\frac{\left(3e^{-2\theta t_i} - 2e^{-\theta t_i}\right)}{1 + \lambda\left(3e^{-2\theta t_i} - 2e^{-\theta t_i}\right)} = 0, \tag{4}$$

$$\frac{\partial}{\partial\theta}\ell(\theta, \lambda\ ; \underline{t}) = \frac{n}{\theta} - \sum_{i=1}^{n} t_i + \sum_{i=1}^{n}\frac{2\lambda t e^{-\theta t_i} - 6\lambda t e^{-2\theta t_i}}{1 + \lambda\left(3e^{-2\theta t_i} - 2e^{-\theta t_i}\right)} = 0. \tag{5}$$

Equating these two expressions (4) and (5) to zero and solving them simultaneously yields the ML estimates of the θ and λ.

4. Results and Discussions

Now, we will compare our new distribution with most known lifetime distributions by some different kinds of data sets. While comparing distributions, we will use Kolmogorov-Smirnov test statistics. In using Kolmogorov-Smirnov statistics, least statistic value is appraised as best modeling. $p$value of Kolmogorov-Smirnov statistics informs us about plausibility of the conformity.

Data 1: This data sets represent waiting times of bank customers (see Table 1). Data set was first used by [6] and later it was evaluated by [1], [14]. We compare new distribution with Lindley and CFGMWEM, because these distributions were used in modeling before.

Table 1. Customer waiting times

0,1	0,2	0,3	0,7	0,9	1,1	1,2	1,8	1,9	2
2,2	2,3	2,3	2,3	2,5	2,6	2,7	2,7	2,9	3,1
3,1	3,2	3,4	3,4	3,5	3,9	4	4,2	4,5	4,7
5,3	5,6	5,6	6,2	6,3	6,6	6,8	7,3	7,5	7,7
7,7	8	8	8,5	8,5	8,7	9,5	10,7	10,9	11
12,1	12,3	12,8	12,9	13,2	13,7	14,5	16	16,5	28

Table 2. Customer waiting times test results

Model	K-S	p
Lindley	0,08	0,84
CFGMWEM	0,0618	0,9651
New Distribution	0,061	0,9689

Once examining Table 2, it is clear that this new distribution is capable in modeling waiting times and offer a strong model. According to Kolmogorov-Smirnov test statistics the most appropriate model is the new generated distribution.

Data 2: Second data set represent broken times of ventilation in airplanes (see Table 3). It was used by [7] and later [12] used for comparing distributions.

Table 3. Broken times of ventilation in airplanes

23	261	87	7	120	14	62	47	225	71
246	21	42	20	5	12	120	11	3	14
71	11	14	11	16	90	1	16	52	95

TABLE 4. Test results of broken times of ventilation in airplanes

Model	K-S	p
Exponential Poisson-Lindley	0,129	0,6531
Weibull	0,1531	0,4394
CFGMWEM	0,1528	0,4414
New Distribution	0,1157	0,7745

When Table 4 is examined it is clear that this new distribution is capable in modeling broken times and offer a strong model. According to Kolmogorov-Smirnov test statistics the most appropriate model is the new generated distribution.

Data 3: We evaluate the time intervals for earthquakes in Iran (see Table 5). These data were analyzed by [3]. This data set was also studied in Alpha-Power Transformed Lindley Distribution by [5].

TABLE 5. Time intervals of earthquakes in Iran

136	1187	117	944	24	70	716	1126	378	166
152	264	275							

TABLE 6. Test results of time intervals of earthquakes in Iran

Model	K-S	p
Exponential Lindley	0,1307	0,9585
Weibull	0,1527	0,8783
New Distribution	0,1241	0,9735

In Table 6, it is clear that this new distribution is capable in modeling time intervals and offer a strong model. According to Kolmogorov-Smirnov test statistics the most appropriate model is the new generated distribution.

5. CONCLUSION

Although there are many different and capable statistical distributions in use today, many new distributions may be needed with different data sets and better modeling opportunities. The new distribution which introduced in this study is capable in modeling time data sets. There are many lifetime distributions but this distribution may be very helpful in analyzing times more appropriately.

But why our new distribution is capable in modeling different kinds of data sets? In part two we showed that the value of parameter λ could change the structure of our new distribution. So, we consider that the values of this parameter in modeling may be important. In Table 7 there are maximum likelihood estimations of the parameters in modeling data1 to data 3.

TABLE 7. Values of Parameters in Models

Data	θ	λ
Customer waiting times	0,1715	-0,622
Broken times of ventilation	0,0141	1
Time intervals of earthquakes	0,0022	0,4041

We see that the new distribution fits the datasets better than the other distributions. According to test results in Table 2 to Table 6 we suggest that the new distribution can be used in many kinds of time data sets.

Authors Contribution Statement The authors contributed equally and significantly in this manuscript, and they read and approved the final manuscript.

Declaration of Competing Interest The authors declare that they have no known competing financial interests or personal relationships that could have appeared to influence the work reported in this paper.

Acknowledgement We thank the two anonymous reviewers whose comments/ suggestions helped improve and clarify this manuscript.

REFERENCES

[1] Al-Mutairi, D. K., Ghitany, M. E., Kundu, D., Inferences on stress-strength reliability from Lindley distributions, *Communications in Statistics, Theory and Methods,* 42(8) (2013), 1443–1463, https://dx.doi.org/10.1080/03610926.2011.563011.

[2] Alghamedi, A., Dey, S., Kumar, D., Dobbah, S. A., A new extension of extended exponential distribution with applications, *Annals of Data Science,* 7(1) (2020), 139–162, https://dx.doi.org/10.1007/s40745-020-00240-w.

[3] Barreto-Souza, W., Bakouch, H. S., A new lifetime model with decreasing failure rate, *Statistics,* 47(2) (2013), 465–476, https://dx.doi.org/10.1080/02331888.2011.595489.

[4] Devore, J. L., Probability and Statistics for Engineering and the Sciences, 8. ed., Internat. Student ed., Brooks/Cole, Cengage Learning, [Belmont, Calif. [u.a.]], 2012.

[5] Dey, S., Ghosh, I., Kumar, D., Alpha-power transformed lindley distribution: Properties and associated inference with application to earthquake data, *Sankhya,* 73 (2011), 623–650, https://dx.doi.org/10.1007/s40745-018-0163-2.

[6] Ghitany, M. E., Atieh, B., Nadarajah, S., Lindley distribution and its application, *Mathematics and computers in simulation,* 78(4) (2008), 493–506.

[7] Linhart, H., Zucchini, W., Model Selection, John Wiley, 1986.

[8] Nadarajah, S., Haghighi, F., An extension of the exponential distribution, *Statistics,* 45(6) (2011), 543–558, https://dx.doi.org/10.1080/02331881003678678.

[9] Nelsen, R. B., An Introduction to Copulas, Second Edition, @Springer Series in Statistics, Springer Science+Business Media, Inc, New York, NY, 2006.

[10] Rather, N. A., Rather, T. A., New generalizations of exponential distribution with applications, *Journal of Probability and Statistics,* 2017(2017), 1–9.

[11] Ross, S. M., Introduction to Probability Models, Elsevier, 2010.

[12] Shanker, R., Fesshaye, H., Selvaraj, S., On modeling of lifetimes data using exponential and lindley distributions, *Biometrics* & *Biostatistics International Journal,* 2(5) (2015), 1–9, https://dx.doi.org/10.15406/bbij.2015.02.00042.

[13] Sklar, A., Fonctions de repartition an dimensionset leurs marges, *Publ. Inst. Statis. Univ* (1959), 229–231.

[14] Ünözkan, H., Yilmaz, M., A new method for generating distributions: An application to flow data, *International Journal of Statistics and Applications,* 9(3) (2019), 92–99, https://dx.doi.org/10.5923/j.statistics.20190903.04.

http://communications.science.ankara.edu.tr

Commun.Fac.Sci.Univ.Ank.Ser. A1 Math. Stat.
Volume 72, Number 2, Pages 407–416 (2023)
DOI:10.31801/cfsuasmas.1138441
ISSN 1303-5991 E-ISSN 2618-6470

Research Article; Received: June 30, 2022; Accepted: January 1, 2023

ON A NEW FAMILY OF THE GENERALIZED GAUSSIAN K-PELL-LUCAS NUMBERS AND THEIR POLYNOMIALS

Hayrullah ÖZİMAMOĞLU[1] and Ahmet KAYA[2]

[1,2]Department of Mathematics, Nevşehir Hacı Bektaş Veli University, Nevşehir, TÜRKİYE

Abstract. In this paper, we generalize the known Gaussian Pell-Lucas numbers, and call such numbers as the generalized Gaussian k-Pell-Lucas numbers. We obtain relations between the family of the generalized Gaussian k-Pell-Lucas numbers and the known Gaussian Pell-Lucas numbers. We generalize the known Gaussian Pell-Lucas polynomials, and call such polynomials as the generalized Gaussian k-Pell-Lucas polynomials. We obtain relations between the family of the generalized Gaussian k-Pell-Lucas polynomials and the known Gaussian Pell-Lucas polynomials. In addition, we present the new generalizations of these numbers and polynomials in matrix form. Then, we get Cassini's identities for these numbers and polynomials.

1. Introduction

Fibonacci and Lucas numbers have gained popularity in recent years, and they are now used in a variety of branches of mathematics, including linear algebra, applied mathematics, and calculus. In 1832, Gauss discovered Gaussian numbers, which are complex numbers $z = x+yi, x, y \in \mathbb{Z}$. These numbers were used to generalize special sequences by numerous researchers. Therefore, the study of Gaussian numbers is a very interesting academic area and several studies have been done on it. Horadam [7] introduced the complex Fibonacci numbers that is Gaussian Fibonacci numbers in 1963. Then Jordan [8] investigated Gaussian Fibonacci numbers and Lucas numbers. These numbers are defined by $GF_{n+1} = GF_n + GF_{n-1}$, where $GF_0 = i, GF_1 = 1$ and $GL_{n+1} = GL_n + GL_{n-1}$, where $GL_0 = 2 - i, GL_1 = 1 + 2i$, respectively. Also, many authors [1–3,5,6,12,15] have studied Gaussian Fibonacci, Gaussian Lucas, Gaussian Jacobsthal, Gaussian Jacobsthal-Lucas, Gaussian Pell,

2020 *Mathematics Subject Classification.* 11B37, 11B39, 11B83.
Keywords. Gaussian Pell-Lucas numbers, Gaussian Pell-Lucas polynomials, Cassini's identity.
[1] h.ozimamoglu@nevsehir.edu.tr-Corresponding author; 0000-0001-7844-1840
[2] ahmetkaya@nevsehir.edu.tr; 0000-0001-5109-8130 .

Gaussian Pell-Lucas etc. numbers and their polynomials. A new family of k-Gaussian Fibonacci numbers is given by Taş [13] and a new family of Gaussian k-Fibonacci polynomials are defined by Taştan and Özkan [14]. Moreover they [10,11] presented a new families of Gaussian k-Jacobsthal numbers, Gaussian k-Jacobsthal-Lucas numbers and their polynomials and a new family of Gaussian k-Lucas numbers and their polynomials. In [9], Kaya and Özimamoğlu generalized the Gaussian Pell numbers and Gauss Pell polynomials, and defined generalized Gauss k-Pell numbers and generalized Gaussian k-Pell polynomials. They obtained Cassini's identities for these numbers and polynomials.

Next, we give the structure of the paper. In Section 2, we demonstrate several well-known definitions and characteristics. In Section 3.1, we define a new family of the generalized Gaussian k-Pell-Lucas numbers. These numbers are a generalization of the Gaussian Pell-Lucas numbers in [6]. We give relations between the generalized Gaussian k-Pell-Lucas numbers and the Gaussian Pell-Lucas numbers. Also, we determine the new generalization of these numbers in matrix form. Then we demonstrate Cassini's identity for these numbers.

In Section 3.2, we define a new family of the generalized Gaussian k-Pell-Lucas polynomials. These polynomials are a generalization of the Gaussian Pell-Lucas polynomials in [15]. We give relations between the generalized Gaussian k-Pell-Lucas polynomials and the Gaussian Pell-Lucas polynomials. Moreover, we determine the new generalization of these polynomials in matrix form. Then we demonstrate Cassini's identity for these polynomials. In Section 4, we conclude the paper.

2. Material and Methods

We provide the Gaussian Pell-Lucas numbers GQ_n, the Gaussian Pell-Lucas polynomials $GQ_n(x)$, and the Gaussian Pell-Lucas polynomial matrix $gq_n(x)$ in this section.

Definition 1. *The Gaussian Pell-Lucas numbers* $\{GQ_n\}_{n=0}^{\infty}$ *are defined by the following recurrence relation:*

$$GQ_{n+1} = 2GQ_n + GQ_{n-1}, n \geq 1 \tag{1}$$

with initial conditions $GQ_0 = 2 - 2i$ *and* $GQ_1 = 2 + 2i$ *[6].*

The Binet formulas for GQ_n are given as follows:

$$GQ_n = (\alpha^n + \beta^n) - i\left(\alpha\beta^n + \beta\alpha^n\right), \tag{2}$$

where $\alpha = 1 + \sqrt{2}$ and $\beta = 1 - \sqrt{2}$ [6].

The Cassini's identity [6] for the Gaussian Pell-Lucas numbers are given as follows:

$$GQ_{n+1}GQ_{n-1} - GQ_n^2 = (-1)^{n+1}\, 16\,(1 - i)\,,\ n \geq 1. \tag{3}$$

Definition 2. *The Gaussian Pell-Lucas polynomials* $\{GQ_n(x)\}_{n=0}^{\infty}$ *are defined by the recurrence relation shown below:*

$$GQ_{n+1}(x) = 2xGQ_n(x) + GQ_{n-1}(x), n \geq 1 \tag{4}$$

with initial conditions $GQ_0(x) = 2 - 2xi$ *and* $GQ_1 = 2x + 2i$ *[15].*

The following are the Binet formulas for $GQ_n(x)$:

$$GQ_n(x) = (\alpha^n(x) + \beta^n(x)) - i(\alpha(x)\beta^n(x) + \beta(x)\alpha^n(x)), \tag{5}$$

where $\alpha(x) = x + \sqrt{1+x^2}$ and $\beta(x) = x - \sqrt{1+x^2}$ [15].

The Cassini's identity [15] for the Gaussian Pell-Lucas polynomials are given as follows:

$$GQ_{n+1}(x)GQ_{n-1}(x) - GQ_n^2(x) = 8(-1)^{n-1}\left(1+x^2\right)(1-xi), \ n \geq 1. \tag{6}$$

In [15], The Gaussian Pell-Lucas polynomial matrix $gq_n(x)$ is defined by

$$gq_n(x) = \begin{bmatrix} GQ_{n+2}(x) & GQ_{n+1}(x) \\ GQ_{n+1}(x) & GQ_n(x) \end{bmatrix}, n \geq 1.$$

3. Main Results

3.1. The generalized Gaussian k-Pell-Lucas numbers.

Definition 3. *There are unique numbers* m *and* r *such that* $n = mk + r$ *and* $0 \leq r < k$*, for* $n, k \in \mathbb{N}(k \neq 0)$*. Then we define the generalized Gaussian* k*-Pell-Lucas numbers* $GQ_n^{(k)}$ *by*

$$\begin{aligned} GQ_n^{(k)} &:= [(\alpha^m + \beta^m) - i(\alpha\beta^m + \beta\alpha^m)]^{k-r} \\ &\quad \times \left[\left(\alpha^{m+1} + \beta^{m+1}\right) - i\left(\alpha\beta^{m+1} + \beta\alpha^{m+1}\right)\right]^r, \end{aligned}$$

where $\alpha = 1 + \sqrt{2}$ *and* $\beta = 1 - \sqrt{2}$.

Furthermore, using the matrix methods, we can derive the generalized Gaussian k-Pell-Lucas number. Clearly, it can be said that

$$GQ_n^{k-1}gq_n = \begin{bmatrix} GQ_{kn+1}^{(k)} & GQ_{kn}^{(k)} \\ GQ_{kn}^{(k)} & GQ_{kn-1}^{(k)} \end{bmatrix},$$

where $n > 0$ and

$$gq_n = \begin{bmatrix} GQ_{n+1} & GQ_n \\ GQ_n & GQ_{n-1} \end{bmatrix}.$$

Various values for the generalized Gaussian k-Pell-Lucas numbers are given in Table 1. From (2) and Definition 3, we get the following relationship between the generalized Gaussian k-Pell-Lucas numbers and the Gaussian Pell-Lucas numbers.

$$GQ_n^{(k)} := (GQ_m)^{k-r}(GQ_{m+1})^r, \ n = mk + r. \tag{7}$$

If we take $k = 1$ in (7), then we have that $m = n$ and $r = 0$ so $GQ_n^{(1)} = GQ_n$. Throughout this article, let $k, m \in \{1, 2, 3, \ldots\}$.

TABLE 1. The generalized Gaussian k-Pell-Lucas numbers $GQ_n^{(k)}$ for some k and n.

$GQ_n^{(k)}$	$k=1$	$k=2$	$k=3$	$k=4$	$k=5$	$k=6$
$GQ_0^{(k)}$	$2-2i$	$-8i$	$-16-16i$	-64	$-128+128i$	$512i$
$GQ_1^{(k)}$	$2+2i$	8	$16-16i$	$-64i$	$-128-128i$	-512
$GQ_2^{(k)}$	$6+2i$	$8i$	$16+16i$	64	$128-128i$	$-512i$
$GQ_3^{(k)}$	$14+6i$	$8+16i$	$-16+16i$	$64i$	$128+128i$	512
$GQ_4^{(k)}$	$34+14i$	$32+24i$	$-16+48i$	-64	$-128+128i$	$512i$
$GQ_5^{(k)}$	$82+34i$	$72+64i$	$16+112i$	$-128+64i$	$-128-128i$	-512
$GQ_6^{(k)}$	$198+82i$	$160+168i$	$144+208i$	$-192+256i$	$-384-128i$	$-512i$
$GQ_7^{(k)}$	$478+198i$	$392+400i$	$304+528i$	$-128+704i$	$-896+128i$	$-512-1024i$
$GQ_8^{(k)}$	$1154+478i$	$960+952i$	$624+1328i$	$448+1536i$	$-1664+1152i$	$-2048-1536i$
$GQ_9^{(k)}$	$2786+1154i$	$2312+2304i$	$1232+3312i$	$768+3776i$	$-2176+3968i$	$-5632-1024i$
$GQ_{10}^{(k)}$	$6726+2786i$	$5568+5576i$	$3088+7952i$	$1088+9216i$	$-384+10112i$	$-12288+3584i$

For $k=2,3,4$ and n, we get the following relations between the generalized Gaussian k-Pell-Lucas numbers and the Gaussian Pell-Lucas numbers by (1) and (7):

(1) $GQ_{2n}^{(2)} = GQ_n^2$,
(2) $GQ_{2n+1}^{(2)} = GQ_n GQ_{n+1}$
(3) $GQ_{2n+1}^{(2)} = 2GQ_{2n}^{(2)} + GQ_{2n-1}^{(2)}$,
(4) $GQ_{3n}^{(2)} = GQ_n^3$,
(5) $GQ_{3n+1}^{(3)} = GQ_n^2 GQ_{n+1}$,
(6) $GQ_{3n+1}^{(3)} = 2GQ_{3n}^{(3)} + GQ_{3n-1}^{(3)}$,
(7) $GQ_{3n+2}^{(3)} = GQ_n GQ_{n+1}^2$,
(8) $GQ_{4n}^{(4)} = GQ_n^4$,
(9) $GQ_{4n+1}^{(4)} = GQ_n^3 GQ_{n+1}$,
(10) $GQ_{4n+1}^{(4)} = 2GQ_{4n}^{(4)} + GQ_{4n-1}^{(4)}$,
(11) $GQ_{4n+2}^{(4)} = GQ_n^2 GQ_{n+1}^2$,
(12) $GQ_{4n+3}^{(4)} = GQ_n GQ_{n+1}^3$.

Proposition 1. *For k and n, we have $GQ_{kn}^{(k)} = GQ_n^k$.*

Proof. By (7), we get $GQ_{kn}^{(k)} = GQ_n^k GQ_{n+1}^0 = GQ_n^k$. □

Theorem 1. *For n and s such that $n+s \geq 2$, we have*

$$GQ_{n+s}GQ_{n+s-2} - GQ_{2(n+s-1)}^{(2)} = (-1)^{n+s}\, 16\,(1-i)\,.$$

Proof. By Proposition 1 and (3), we get

$$\begin{aligned} GQ_{n+s}GQ_{n+s-2} - GQ_{2(n+s-1)}^{(2)} &= GQ_{n+s}GQ_{n+s-2} - GQ_{n+s-1}^2 \\ &= (-1)^{n+s}\, 16\,(1-i)\,. \end{aligned}$$

□

Theorem 2. *For k and s, we have*

$$GQ^k_{s+1} - GQ^k_s = GQ^{(k)}_{(s+1)k} - GQ^{(k)}_{sk}. \tag{8}$$

Proof. By (7) and Proposition 1, we get

$$\begin{aligned} GQ^{(k)}_{(s+1)k} - GQ^{(k)}_{sk} &= GQ^{k-k}_s GQ^k_{s+1} - GQ^k_s \\ &= GQ^k_{s+1} - GQ^k_s. \end{aligned}$$

□

Theorem 3. *For k and n, we have the relation*

$$GQ^{(k)}_{kn+1} = 2GQ^{(k)}_{kn} + GQ^{(k)}_{kn-1}.$$

Proof. By (1), (7) and Proposition 1, we obtain

$$\begin{aligned} 2GQ^{(k)}_{kn} + GQ^{(k)}_{kn-1} &= 2GQ^k_n + GQ_{n-1}GQ^{k-1}_n \\ &= GQ^{k-1}_n \left(2GQ_n + GQ_{n-1}\right) \\ &= GQ^{k-1}_n GQ_{n+1} \\ &= GQ^{(k)}_{kn+1}. \end{aligned}$$

□

Theorem 4. ***(Cassini's Identity)*** *Let $GQ^{(k)}_n$ be the generalized Gaussian k-Pell-Lucas numbers. For $n, k \geq 2$, the following gives the Cassini's identity for $GQ^{(k)}_n$:*

$$GQ^{(k)}_{kn+t} GQ^{(k)}_{kn+t-2} - \left(GQ^{(k)}_{kn+t-1}\right)^2 = \begin{cases} GQ^{2k-2}_n \left(-1\right)^{n+1} 16\left(1-i\right), & t = 1, \\ 0, & t \neq 1. \end{cases}$$

Proof. If $t = 1$, by (3), (7) and Proposition 1, then we have

$$\begin{aligned} GQ^{(k)}_{kn+1} GQ^{(k)}_{kn-1} - \left(GQ^{(k)}_{kn}\right)^2 &= \left(GQ^{k-1}_n GQ_{n+1}\right)\left(GQ_{n-1}GQ^{k-1}_n\right) - \left(GQ^k_n\right)^2 \\ &= GQ^{2k-2}_n \left(GQ_{n+1}GQ_{n-1} - GQ^2_n\right) \\ &= GQ^{2k-2}_n \left(-1\right)^{n+1} 16\left(1-i\right), \end{aligned}$$

and if $t \neq 1$, by (7), then we have

$$\begin{aligned} GQ^{(k)}_{kn+t} GQ^{(k)}_{kn+t-2} - \left(GQ^{(k)}_{kn+t-1}\right)^2 &= \left(GQ^{k-t}_n GQ^t_{n+1}\right)\left(GQ^{k-t+2}_n GQ^{t-2}_{n+1}\right) \\ &\quad - \left(GQ^{k-t+1}_n GQ^{t-1}_{n+1}\right)^2 \\ &= GQ^{2k-2t+2}_n \left(GQ^{2t-2}_{n+1} - GQ^{2t-2}_{n+1}\right) \\ &= 0. \end{aligned}$$

□

For $t = 0, 1, 2, \ldots, k-1$, we have the following relations:

$$GQ_{kn+t}^{(k)} = GQ_n^{k-t} GQ_{n+1}^t.$$

3.2. The generalized Gaussian k-Pell-Lucas polynomials.

Definition 4. *There are unique numbers m and r such that $n = mk + r$ and $0 \leq r < k$, for $n, k \in \mathbb{N}\,(k \neq 0)$. Then we define the generalized Gaussian k-Pell-Lucas numbers $GQ_n^{(k)}(x)$ by*

$$\begin{aligned} GQ_n^{(k)}(x) \quad := \quad & [(\alpha^m(x) + \beta^m(x)) - i(\alpha(x)\beta^m(x) + \beta(x)\alpha^m(x))]^{k-r} \\ & \times \left[\left(\alpha^{m+1}(x) + \beta^{m+1}(x)\right) - i\left(\alpha(x)\beta^{m+1}(x) + \beta(x)\alpha^{m+1}(x)\right)\right]^r, \end{aligned}$$

where $\alpha(x) = x + \sqrt{1+x^2}$ and $\beta(x) = x - \sqrt{1+x^2}$.

In addition, using the matrix methods, we can derive the generalized Gaussian k-Pell-Lucas polynomials. Indeed, it is obvious that

$$GQ_n^{k-1}(x)\, gq_n(x) = \begin{bmatrix} GQ_{kn+1}^{(k)}(x) & GQ_{kn}^{(k)}(x) \\ GQ_{kn}^{(k)}(x) & GQ_{kn-1}^{(k)}(x) \end{bmatrix},$$

where $n > 0$ and

$$gq_n(x) = \begin{bmatrix} GQ_{n+1}(x) & GQ_n(x) \\ GQ_n(x) & GQ_{n-1}(x) \end{bmatrix}.$$

Various values for the generalized Gaussian k-Pell-Lucas polynomials are given in Table 2. From (5) and Definition 4, we have the following relationship between the generalized Gaussian k-Pell-Lucas polynomials and the Gaussian Pell-Lucas polynomials.

$$GQ_n^{(k)}(x) := (GQ_m(x))^{k-r}(GQ_{m+1}(x))^r, \; n = mk + r \tag{9}$$

If we take $k = 1$ in (9), then we have that $m = n$ and $r = 0$ so $GQ_n^{(1)}(x) = GQ_n(x)$.

For $k = 2, 3, 4$ and n, we have the following relations between the generalized Gaussian k-Pell-Lucas polynomials and the Gaussian Pell-Lucas polynomials by (4) and (9):

(1) $GQ_{2n}^{(2)}(x) = GQ_n^2(x)$,
(2) $GQ_{2n+1}^{(2)}(x) = GQ_n(x)\, GQ_{n+1}(x)$,
(3) $GQ_{2n+1}^{(2)}(x) = 2xGQ_{2n}^{(2)}(x) + GQ_{2n-1}^{(2)}(x)$,
(4) $GQ_{3n}^{(2)}(x) = GQ_n^3(x)$,
(5) $GQ_{3n+1}^{(3)}(x) = GQ_n^2(x)\, GQ_{n+1}(x)$,
(6) $GQ_{3n+1}^{(3)}(x) = 2xGQ_{3n}^{(3)}(x) + GQ_{3n-1}^{(3)}(x)$,
(7) $GQ_{3n+2}^{(3)}(x) = GQ_n(x)\, GQ_{n+1}^2(x)$,
(8) $GQ_{4n}^{(4)}(x) = GQ_n^4(x)$,
(9) $GQ_{4n+1}^{(4)}(x) = GQ_n^3(x)\, GQ_{n+1}(x)$,

TABLE 2. The generalized Gaussian k-Pell-Lucas polynomials $GQ_n^{(k)}(x)$ for some k and n.

$GQ_n^{(k)}(x)$	$k=1$	$k=2$	$k=3$	$k=4$
$GQ_0^{(k)}(x)$	$2-2xi$	$-4x^2+4-8xi$	$-24x^2+8$ $+\left(8x^3-24x\right)i$	$16x^4-96x^2+16$ $+\left(64x^3-64x\right)i$
$GQ_1^{(k)}(x)$	$2x+2i$	$8x+\left(-4x^2+4\right)i$	$-8x^3+24x$ $+\left(-24x^2+8\right)i$	$-64x^3+64x$ $+\left(16x^4-96x^2+16\right)i$
$GQ_2^{(k)}(x)$	$4x^2+2+2xi$	$4x^2-4+8xi$	$24x^2-8$ $+\left(-8x^3+24x\right)i$	$-16x^4+96x^2-16$ $+\left(-64x^3+64x\right)i$
$GQ_3^{(k)}(x)$	$8x^3+6x$ $+\left(4x^2+2\right)i$	$8x^3+\left(12x^2+4\right)i$	$8x^3-24x$ $+\left(24x^2-8\right)i$	$64x^3-64x$ $+\left(-16x^4+96x^2-16\right)i$
$GQ_4^{(k)}(x)$	$16x^4+16x^2+2$ $+\left(8x^3+6x\right)i$	$16x^4+12x^2+4$ $+\left(16x^3+8x\right)i$	$16x^4-24x^2-8$ $+\left(40x^3+8x\right)i$	$16x^4-96x^2+16$ $+\left(64x^3-64x\right)i$
$GQ_5^{(k)}(x)$	$32x^5+40x^3+10x$ $+\left(16x^4+16x^2+2\right)i$	$32x^5+32x^3+8x$ $+\left(32x^4+28x^2+4\right)i$	$32x^5-8x^3-8x$ $+\left(64x^4+40x^2+8\right)i$	$32x^5-128x^3-32x$ $+\left(112x^4-32x^2-16\right)i$
$GQ_6^{(k)}(x)$	$64x^6+96x^4+36x^2$ $+2+(32x^5+40x^3$ $+10x)i$	$64x^6+80x^4+20x^2$ $-4+(64x^5+80x^3$ $+24x)i$	$64x^6+48x^4+24x^2$ $+8+(96x^5+88x^3$ $+24x)i$	$64x^6-144x^4-96x^2$ $-16+\left(192x^5+64x^3\right)i$
$GQ_7^{(k)}(x)$	$128x^7+224x^5$ $+112x^3+14x+(64x^6$ $+96x^4+36x^2+2)i$	$128x^7+192x^5$ $+72x^3+(128x^6$ $+192x^4+76x^2+4)i$	$128x^7+128x^5$ $+40x^3+8x+(192x^6$ $+240x^4+88x^2+8)i$	$128x^7-96x^5$ $-128x^3-32x+(320x^6)$ $+270x^4+96x^2+16)i$

(10) $GQ_{4n+1}^{(4)}(x) = 2xGQ_{4n}^{(4)}(x) + GQ_{4n-1}^{(4)}(x)$,
(11) $GQ_{4n+2}^{(4)}(x) = GQ_n^2(x)\,GQ_{n+1}^2(x)$,
(12) $GQ_{4n+3}^{(4)}(x) = GQ_n(x)\,GQ_{n+1}^3(x)$.

Proposition 2. *For k and n, we have $GQ_{kn}^{(k)}(x) = GQ_n^k(x)$.*

Proof. By (9), we get $GQ_{kn}^{(k)}(x) = GQ_n^k(x)\,GQ_{n+1}^0(x) = GQ_n^k(x)$. □

Theorem 5. *For n and s such that $n+s \geq 2$, we have*

$$GQ_{n+s}(x)\,GQ_{n+s-2}(x) - GQ_{2(n+s-1)}^{(2)}(x) = 8(-1)^{n+s}\left(1+x^2\right)(1-xi).$$

Proof. By Proposition 2 and (6), we get

$$\begin{aligned} GQ_{n+s}(x)\,GQ_{n+s-2}(x) - GQ_{2(n+s-1)}^{(2)}(x) &= GQ_{n+s}(x)\,GQ_{n+s-2}(x) - GQ_{n+s-1}^2(x) \\ &= 8(-1)^{n+s}\left(1+x^2\right)(1-xi). \end{aligned}$$

□

Theorem 6. *For k and s, we have*

$$GQ_{s+1}^k(x) - GQ_s^k(x) = GQ_{(s+1)k}^{(k)}(x) - GQ_{sk}^{(k)}(x). \tag{10}$$

Proof. By (9) and Proposition 2, we get

$$\begin{aligned} GQ_{(s+1)k}^{(k)}(x) - GQ_{sk}^{(k)}(x) &= GQ_s^{k-k}(x)\,GQ_{s+1}^k(x) - GQ_s^k(x) \\ &= GQ_{s+1}^k(x) - GQ_s^k(x). \end{aligned}$$

□

Theorem 7. *For k and n, we have the relation*

$$GQ_{kn+1}^{(k)}(x) = 2xGQ_{kn}^{(k)}(x) + GQ_{kn-1}^{(k)}(x).$$

Proof. By (4), (9) and Proposition 2, we obtain

$$\begin{aligned} 2xGQ_{kn}^{(k)}(x) + GQ_{kn-1}^{(k)}(x) &= 2xGQ_n^k(x) + GQ_{n-1}(x)\,GQ_n^{k-1}(x) \\ &= GQ_n^{k-1}(x)\left(2xGQ_n(x) + GQ_{n-1}(x)\right) \\ &= GQ_n^{k-1}(x)\,GQ_{n+1}(x) \\ &= GQ_{kn+1}^{(k)}(x). \end{aligned}$$

□

Theorem 8. ***(Cassini's Identity)*** *Let $GQ_n^{(k)}(x)$ be the generalized Gaussian k-Pell-Lucas polynomials. For $n, k \geq 2$, the following gives the Cassini's identity for $GQ_n^{(k)}(x)$:*

$$\begin{aligned} & GQ_{kn+t}^{(k)}(x)\,GQ_{kn+t-2}^{(k)}(x) - \left(GQ_{kn+t-1}^{(k)}(x)\right)^2 \\ = & \begin{cases} GQ_n^{2k-2}(x)\,8\,(-1)^{n-1}\left(1+x^2\right)(1-xi)\,, & t=1, \\ 0, & t \neq 1. \end{cases} \end{aligned}$$

Proof. If $t=1$, by (6), (9) and Proosition 2, then we have

$$\begin{aligned} & GQ_{kn+1}^{(k)}(x)\,GQ_{kn-1}^{(k)}(x) - \left(GQ_{kn}^{(k)}(x)\right)^2 \\ = & \left(GQ_n^{k-1}(x)\,GQ_{n+1}(x)\right)\left(GQ_{n-1}(x)\,GQ_n^{k-1}(x)\right) - \left(GQ_n^k(x)\right)^2 \\ = & GQ_n^{2k-2}(x)\left(GQ_{n+1}(x)\,GQ_{n-1}(x) - GQ_n^2(x)\right) \\ = & GQ_n^{2k-2}(x)\,8\,(-1)^{n-1}\left(1+x^2\right)(1-xi)\,, \end{aligned}$$

and if $t \neq 1$, by (9), then we have

$$\begin{aligned} & GQ_{kn+t}^{(k)}(x)\,GQ_{kn+t-2}^{(k)}(x) - \left(GQ_{kn+t-1}^{(k)}\right)^2(x) \\ = & \left(GQ_n^{k-t}(x)\,GQ_{n+1}^t(x)\right)\left(GQ_n^{k-t+2}(x)\,GQ_{n+1}^{t-2}(x)\right) \\ & - \left(GQ_n^{k-t+1}(x)\,GQ_{n+1}^{t-1}(x)\right)^2 \\ = & GQ_n^{2k-2t+2}(x)\left(GQ_{n+1}^{2t-2}(x) - GQ_{n+1}^{2t-2}(x)\right) \\ = & 0. \end{aligned}$$

□

For $t = 0, 1, 2, \ldots, k-1$, we have the following relations:

$$GQ_{kn+t}^{(k)}(x) = GQ_n^{k-t}(x)\,GQ_{n+1}^t(x).$$

4. Conclusions

Halıcı and Öz defined Gaussian Pell-Lucas numbers in [6]. We introduced a generalization of these numbers as the generalized Gaussian k-Pell-Lucas numbers. Also, Yağmur defined Gaussian Pell-Lucas polynomials in [15]. We introduced a generalization of these polynomials as the generalized Gaussian k-Pell-Lucas polynomials. Some relations between the family of the generalized Gaussian k-Pell-Lucas numbers and the known Gaussian Pell-Lucas numbers are presented. Some relations between the family of the generalized Gaussian k-Pell-Lucas polynomials and the known Gaussian Pell-Lucas polynomials are presented. Then identities for these numbers and polynomials are proved.

Author Contribution Statements The authors jointly worked on the results and they read and approved the final manuscript.

Declaration of Competing Interests The authors declare that they have no competing interest.

References

[1] Aşcı, M., Gürel, E., Gaussian Jacobsthal and Gaussian Jacobsthal Lucas numbers, *Ars Combinatoria*, 111 (2013), 53–63.

[2] Aşcı, M., Gürel, E., Gaussian Jacobsthal and Gaussian Jacobsthal Lucas polynomials, *Notes on Number Theory and Discrete Mathematics*, 19(1) (2013), 25–36.

[3] Berzsenyi, G., Gaussian Fibonacci numbers, *Fibonacci Quarterly*, 15(3) (1997), 233–236.

[4] El-Mikkawy, M., Sogabe, T., A new family of k-Fibonacci numbers, *Applied Mathematics and Computation*, 215(12) (2010), 4456–4461. https://doi.org/10.1016/j.amc.2009.12.069

[5] Halıcı, S., Öz, S., On Gaussian Pell polynomials and their some properties, *Palestine Journal of Mathematics*, 7(1) (2018), 251–256.

[6] Halıcı, S., Öz, S., On some Gaussian Pell and Pell-Lucas numbers, *Ordu University Journal of Science and Technology*, 6(1) (2016), 8–18.

[7] Horadam, A. F., Complex Fibonacci numbers and Fibonacci quaternions, *The American Mathematical Monthly*, 70(3) (1963), 289–291. https://doi.org/10.2307/2313129

[8] Jordan, J. H., Gaussian Fibonacci and Lucas numbers, *Fibonacci Quarterly*, 3(4) (1965), 315–318.

[9] Kaya, A., Özimamoğlu, H., On a new class of the generalized Gauss k-Pell numbers and their polynomials, *Notes on Number Theory and Discrete Mathematics*, 28(4) (2022), 593–602. https://doi.org/10.7546/nntdm.2022.28.4.593-602

[10] Özkan, E., Taştan, M., A new families of Gauss k-Jacobsthal numbers and Gauss k-Jacobsthal-Lucas numbers and their polynomials, *Journal of Science and Arts.*, 4(53) (2020), 893–908. https://doi.org/10.46939/j.sci.arts-20.4-a10

[11] Özkan, E., Taştan, M., On a new family of Gauss k-Lucas numbers and their polynomials, *Asian-European Journal of Mathematics*, 14(06) (2021), 2150101. https://doi.org/10.1142/S1793557121501011

[12] Özkan, E., Taştan, M., On Gauss Fibonacci polynomials, on Gauss Lucas polynomials and their applications, *Communications in Algebra*, 48(3) (2020), 952–960. https://doi.org/10.1080/00927872.2019.1670193

[13] Taş, S., A new family of k-Gaussian Fibonacci numbers, *Journal of Balıkesır University Institute of Science and Technology*, 21(1) (2019), 184–189. https://doi.org/10.25092/baunfbed.542440

[14] Taştan, M., Özkan, E., On the Gauss k-Fibonacci polynomials, *Electronic Journal of Mathematical Analysis and Applications*, 9(1) (2021), 124–130.

[15] Yağmur, T., Gaussian Pell-Lucas polynomials, *Communications in Mathematics and Applications*, 10(4) (2019), 673–679. https://doi.org/10.26713/cma.v10i4.804

http://communications.science.ankara.edu.tr

Commun.Fac.Sci.Univ.Ank.Ser. A1 Math. Stat.
Volume 72, Number 2, Pages 417–428 (2023)
DOI:10.31801/cfsuasmas.1165123
ISSN 1303-5991 E-ISSN 2618-6470

COMMUNICATIONS SERIES A1

Research Article; Received: August 22, 2022; Accepted: December 30, 2022

THE FLOW-CURVATURE OF PLANE PARAMETRIZED CURVES

Mircea CRASMAREANU

Faculty of Mathematics, University Al. I. Cuza, Iasi, 700506, ROMANIA

Abstract. We introduce and study a new frame and a new curvature function for a fixed parametrization of a plane curve. This new frame is called *flow* since it involves the time-dependent rotation of the usual Frenet flow; the angle of rotation is exactly the current parameter. The flow-curvature is calculated for several examples obtaining the logarithmic spirals (and the circle as limit case) and the Grim Reaper as flat-flow curves. A main result is that the scaling with $\frac{1}{\sqrt{2}}$ of both Frenet and flow-frame belong to the same fiber of the Hopf bundle. Moreover, the flow-Fermi-Walker derivative is defined and studied.

1. Introduction

The theory of geometric flows is a new and fascinating field of research in geometric analysis. The most simple of them is *the curve shortening flow* and already the excellent survey [3] is twenty years old. Recall that the main geometric tool in this last flow is the well-known curvature of plane curves. Hence, to give a re-start to this problem seams to search for variants of the curvature, or in terms of [9], *deformations* of the usual curvature. The goal of this short note is to propose such a deformation which in turn defines a Fermi-Walker type derivative.

Fix an open interval $I \subseteq \mathbb{R}$ and consider $C \subset \mathbb{R}^2$ a regular parametrized curve of equation:

$$C : r(t) = (x(t), y(t)) = x(t)\bar{i} + y(t)\bar{j}, \quad \|r'(t)\| > 0, \quad t \in I.'$$

The ambient setting $\mathbb{R}^2$ is an Euclidean vector space with respect to the canonical inner product:

$$\langle u, v\rangle = x^1y^1 + x^2y^2, u = (x^1, x^2) \in \mathbb{R}^2, v = (y^1, y^2) \in \mathbb{R}^2, \quad 0 \leq \|u\|^2 = \langle u, u\rangle.$$

2020 *Mathematics Subject Classification.* 53A04, 53A45, 53A55.
Keywords. Plane parametrized curve, angular vector field, flow-frame, flow-curvature.
mcrasm@uaic.ro; 0000-0002-5230-2751.

The infinitesimal generator of the rotations in $\mathbb{R}^2 = \mathbb{C}$ is the linear vector field, called *angular*:

$$\xi(u) := -x^2\frac{\partial}{\partial x^1} + x^1\frac{\partial}{\partial x^2}, \quad \xi(u) = i\cdot u = i\cdot(x^1 + ix^2), \quad i = \sqrt{-1}.$$

It is a complete vector field with integral curves the circles $\mathcal{C}(O, r)$:

$$\begin{cases} \gamma^{\xi}_{u_0}(t) = (u^1_0\cos t - u^2_0\sin t, u^1_0\sin t + u^2_0\cos t) = R(t)\cdot\begin{pmatrix} u^1_0 \\ u^2_0 \end{pmatrix}, \quad t\in\mathbb{R}, \\ r = \|u_0\| = \|(u^1_0, u^2_0)\|, \quad R(t) := \begin{pmatrix} \cos t & -\sin t \\ \sin t & \cos t \end{pmatrix} \in SO(2) = S^1 \end{cases}$$

and since the rotations $R(t)$ are isometries of the Riemannian metric $g_{can} = dx^2 + dy^2 = |dz|^2$ it follows that ξ is a Killing vector field of the Riemannian manifold $(\mathbb{R}^2, g_{can})$. The first integrals of ξ are the Gaussian functions i.e. multiples of the square norm: $f_\alpha(x, y) = \alpha(x^2 + y^2)$, $\alpha\in\mathbb{R}$. For an arbitrary vector field $X = A(x, y)\frac{\partial}{\partial x} + B(x, y)\frac{\partial}{\partial y}$ its Lie bracket with ξ is:

$$[X, \xi] = (yA_x - xA_y - B)\frac{\partial}{\partial x} + (A + yB_x - xB_y)\frac{\partial}{\partial y},$$

where the subscript denotes the variable corresponding to the partial derivative. For example, ξ commutes with *the radial* (or Euler) vector field $E(x, y) = x\frac{\partial}{\partial x} + y\frac{\partial}{\partial y}$, which is also a complete vector field having as integral curves the homotheties $\gamma^E_{u_0}(t) = e^t u_0$ for all $t\in\mathbb{R}$.

The Frenet apparatus of the curve C is provided by:

$$\begin{cases} T(t) = \frac{r'(t)}{\|r'(t)\|}, \quad N(t) = i\cdot T(t) = \frac{1}{\|r'(t)\|}(-y'(t), x'(t)), \\ k(t) = \frac{1}{\|r'(t)\|}\langle T'(t), N(t)\rangle = \frac{1}{\|r'(t)\|^3}\langle r''(t), ir'(t)\rangle = \frac{1}{\|r'(t)\|^3}[x'(t)y''(t) - y'(t)x''(t)]. \end{cases}$$

Hence, if C is naturally parametrized (or parametrized by arc-length) i.e. $\|r'(s)\| = 1$ for all $s\in I$ then $r''(s) = k(s)ir'(s)$. In a complex approach based on $z(t) = x(t) + iy(t)\in\mathbb{C} = \mathbb{R}^2$ we have:

$$\begin{cases} k(t) = \frac{1}{|z'(t)|^3}Im(\bar{z}'(t)\cdot z''(t)) = \frac{1}{|z'(t)|}Im\left(\frac{z''(t)}{z'(t)}\right) = \frac{1}{|z'(t)|}Im\left[\frac{d}{dt}\left(\ln z'(t)\right)\right]\in\mathbb{R}, \\ Re(\bar{z}'(t)\cdot z''(t)) = \frac{1}{2}\frac{d}{dt}\|r'(t)\|^2, \quad f_\alpha(z) = \alpha|z|^2. \end{cases}$$

The multiplication with the complex unit i corresponds to the rotation $R\left(\frac{\pi}{2}\right)$; we have also:

$$\frac{d}{dt}R(t) = R\left(t + \frac{\pi}{2}\right) = R(t)R\left(\frac{\pi}{2}\right) = R\left(\frac{\pi}{2}\right)R(t),$$

and the Frenet equations can be unified by means of the column matrix $\mathcal{F}(t) = \begin{pmatrix} T \\ N \end{pmatrix}(t)$ as:

$$\frac{d}{dt}\mathcal{F}(t) = \|r'(t)\|k(t)R\left(-\frac{\pi}{2}\right)\mathcal{F}(t).$$

It is an amazing fact that if the general rotation $R(t)$ belongs to the Lie group $SO(2) = S^1$ its particular values $R\left(\pm\frac{\pi}{2}\right)$ are elements of its Lie algebra $so(2)$ of skew-symmetric 2×2 matrices. In fact, $\{R\left(\frac{\pi}{2}\right)\}$ is exactly the basis of $so(2)$.

2. Main Results

This short note defines a new frame and correspondingly a new curvature function for C:

Definition 1. *The flow-frame of C consists in the pair of unit vectors $(E_1^f(t), E_2^f(t)) \in T^2 := S^1 \times S^1$ given by:*

$$\mathcal{E}(t) := \begin{pmatrix} E_1^f \\ E_2^f \end{pmatrix}(t) = R(t)\mathcal{F}(t) = \begin{pmatrix} \cos tT(t) - \sin tN(t) \\ \sin tT(t) + \cos tN(t) \end{pmatrix} \tag{1}$$

the letter f being the initial of the word "flow". The flow-curvature of C is the smooth function $k_f : I \to \mathbb{R}$ given by the flow-equations:

$$\frac{d}{dt}\mathcal{E}(t) = \|r'(t)\| k_f(t) R\left(-\frac{\pi}{2}\right)\mathcal{E}(t). \tag{2}$$

Before starting its study we point out that this work is dedicated the memory of Academician Radu Miron (1927-2022). He was always interested in the geometry of curves and besides his theory of *Myller configurations* ([11]) he generalized also a type of curvature for space curves in [10]. We remark also that this note follows the idea of Bishop in his delightful note [2] and that the flow-curvature of spacelike parametrized curves in the Lorentz plane was introduced by the author in [4]. The hyperbolic curves are studied also by the author in [5].

Returning to our subject we note as a first main result:

Proposition 1. *The expression of the flow-curvature is:*

$$k_f(t) = k(t) - \frac{1}{\|r'(t)\|} < k(t). \tag{3}$$

As a consequence, the curve C and its trigonometrical rotation iC share the same flow-curvature.

Proof We have directly in the flow-frame:

$$\|r'(t)\| k_f(t) R\left(-\frac{\pi}{2}\right) = R\left(t + \frac{\pi}{2}\right) R(-t) + \|r'(t)\| k(t) R(t) R\left(-\frac{\pi}{2}\right) R(-t) \tag{4}$$

and the conclusion follows. Concerning the consequence it is obvious that C and $iC : t \to (-y(t), x(t))$ share the same curvature k and the same second term from (3). $\square$

Example 1. *i) If C is the line $r_0 + tu, t \in \mathbb{R}$ with the vector $u \neq \bar{0} = (0,0)$ then k_f is constant:*

$$k_f(t) = -\frac{1}{\|u\|} = constant < 0. \tag{5}$$

In particular, if u is an unit vector then $k_f(t) = -1$.
ii) The circle $\mathcal{C}(O,R)$ with the usual parametrization $r(t) = Re^{it}$ is a flat-flow curve i.e. $k_f = 0$. Indeed, the flow-frame is constant and universal for the families of concentric circles i.e. it does not depend on the radius R (exactly as the Frenet frame):

$$E_1^f = (0,1) = \bar{j}, \quad E_2^f = (-1,0) = -\bar{i}. \tag{6}$$

More generally, if C is expressed in polar coordinates as $C : \rho = \rho(t)$ for $t \in I$ then C is a flat-flow curve if and only if C is a logarithmic spiral $\rho_{R,\alpha}(t) = Re^{\alpha t}$, $R, \alpha > 0$ and $t \in \mathbb{R}$. The limit case $\alpha \to 0$ gives the circle $\mathcal{C}(O,R)$ and the flow-frame of the logarithmic spiral is: $E_1^f = \frac{1}{\sqrt{\alpha^2+1}}(\alpha,1)$, $E_2^f = \frac{1}{\sqrt{\alpha^2+1}}(-1,\alpha)$; if $\alpha = \cot\varphi$ then $E_1^f = e^{\varphi i}$, $E_2^f = e^{i\left(\frac{\pi}{2}+\varphi\right)}$.
iii) Fix $R \in (0,+\infty)$ and the plane curve $C : w = F(Re^{it})$ with t as an increasing parameter and $F = F(z)$ a holomorphic function. Then the curvatures are:

$$k(t) = \frac{1}{|zF'(z)|} Re\left(1 + \frac{zF''(z)}{F'(z)}\right), \quad k_f(t) = \frac{1}{|zF'(z)|} Re\left(\frac{zF''(z)}{F'(z)}\right). \tag{7}$$

For the circle example of $F(z) = z^2$ it results $k = \frac{1}{R^2} = constant$ and $k_f = \frac{1}{2R^2} = constant$ which proves the proper dependence of k_f on the parametrizations of C.
□

Remark 1. *i) Suppose that I is symmetric with respect to $0 \in \mathbb{R}$ and that C is positively oriented in the terms of Definition 1.14 from [14, p. 17]. Suppose also the C is convex; then applying the Theorem 1.18 of page 19 from the same book it results for the usual curvature the inequality $k \geq 0$. Hence the opposite curve $C^- : t \in I \to r(-t)$ has the flow-curvature $k_f < 0$.*
ii) An important tool in dynamics is the Fermi-Walker derivative. Let $\mathcal{X}_C$ be the set of vector fields along the curve C. Then the Fermi-Walker derivative is the map ([6]) $\nabla_C^{FW} : \mathcal{X}_C \to \mathcal{X}_C$:

$$\nabla_C^{FW}(X) := \frac{d}{dt}X + \|r'(\cdot)\|k[\langle X,N\rangle T - \langle X,T\rangle N] = \frac{d}{dt}X + \|r'(\cdot)\|k[X^\flat(N)T - X^\flat(T)N] \tag{8}$$

with $X^\flat$ the differential 1-form dual to X with respect to the Euclidean metric. In a matrix form we can express this as follows:

$$\nabla_C^{FW} = \frac{d}{dt} - \|r'\|k \begin{vmatrix} (\cdot)^\flat(T) & (\cdot)^\flat(N) \\ T & N \end{vmatrix} = \frac{d}{dt} + \|r'\|k \begin{vmatrix} T & (\cdot)^\flat(T) \\ N & (\cdot)^\flat(N) \end{vmatrix}. \tag{9}$$

It is natural to make here a remark concerning rotation-minimizing fields $X \in \mathcal{X}_C$ i.e. fields satisfying:

$$\frac{d}{dt}X(t) = \lambda(t)T(t), \quad \langle X(t), T(t)\rangle = 0$$

for a smooth function $\lambda = \lambda(t)$. Then the Fermi-Walker derivative of such X is also parallel with the tangent T:

$$\nabla^{FW}_C X(t) = [\lambda(t) + \|r'(t)\| k(t)\langle X(t), N(t)\rangle]T(t).$$

Calculating the Fermi-Walker derivative on our frames we get:

$$\nabla^{FW}_C(T) = \nabla^{FW}_C(N) = 0, \quad \nabla^{FW}_C(E^f_1) = -E^f_2, \quad \nabla^{FW}_C(E^f_2) = E^f_1. \tag{10}$$

With the matrix notation we can express these relations as:

$$\nabla^{FW}_C(\mathcal{F}) = \begin{pmatrix} 0 \\ 0 \end{pmatrix}, \quad \nabla^{FW}_C(\mathcal{E}) = R\left(\frac{\pi}{2}\right)\mathcal{E} \tag{11}$$

and the Fermi-Walker derivative can be expressed in terms of k_f as:

$$\nabla^{FW}_C(X) = \frac{d}{dt}X + (1 + \|r'\| k_f)[X^\flat(N)T - X^\flat(T)N]. \tag{12}$$

Also, we can define the flow-Fermi-Walker derivative as:

$$\nabla^{fFW}_C(X) := \frac{d}{dt}X + \|r'(\cdot)\| k_f[X^\flat(N)T - X^\flat(T)N] = \nabla^{FW}_C(X) + T \wedge N(X) \tag{13}$$

with the skew-symmetric endomorphism $\wedge \in so(2)$ defined by:

$$X \wedge Y := \langle X, \cdot\rangle Y - \langle Y, \cdot\rangle X = (X^1Y^2 - X^2Y^1)R\left(\frac{\pi}{2}\right), X = (X^1, X^2), Y = (Y^1, Y^2).$$

Then:

$$\nabla^{fFW}_C(\mathcal{F}) = R\left(-\frac{\pi}{2}\right)\mathcal{F}, \quad \nabla^{fFW}_C(\mathcal{E}) = \begin{pmatrix} 0 \\ 0 \end{pmatrix}. \tag{14}$$

As in the usual case, if $V, W \in \mathcal{X}_C$ are flow-Fermi-Walker fields i.e. with zero flow-Fermi-Walker derivative then the value $< V, W > \in \mathbb{R}$ is constant along C.
iii) Remark that the 4-dimensional vectors $\frac{1}{\sqrt{2}}\mathcal{F}$ and $\frac{1}{\sqrt{2}}\mathcal{E}$ belong to the Clifford torus $\frac{1}{\sqrt{2}}T^2 \subset S^3$. A remarkable Riemannian submersion is the Hopf map $H : S^3 \subset \mathbb{C}^2 \to S^2(\frac{1}{2}) \subset \mathbb{R} \times \mathbb{C}$:

$$H(z, w) = \left(\frac{1}{2}(|z|^2 - |w|^2), z\bar{w}\right). \tag{15}$$

It follows:

$$H\left(\frac{1}{\sqrt{2}}\mathcal{F}(t)\right) = \left(0, \frac{1}{2}T(t)\bar{N}(t)\right) = \left(0, -\frac{i}{2}\right) = H\left(\frac{1}{\sqrt{2}}\mathcal{E}(t)\right). \tag{16}$$

Hence, considering H as a projection map of the S^1-principal bundle $S^3 \to S^2(\frac{1}{2})$ we have that $\frac{1}{\sqrt{2}}\mathcal{F}$ and $\frac{1}{\sqrt{2}}\mathcal{E}$ belong to the same fiber, namely that over the South *pole of the sphere* $S^2(\frac{1}{2})$.

iv) Suppose now that our curve C *belongs to the plane* xOz *of the physical space* $\mathbb{R}^3$ *as* $C : r(t) = (f(t), 0, F(t))$ *with* $f > 0$ *on* I *and consider the rotational surface generated by* C *as:*

$$\Sigma : \bar{r}(t, \varphi) := (f(t)\cos\varphi, f(t)\sin\varphi, F(t)), \quad \varphi \in S^1.$$

Its principal curvatures depend only on t, *[8, p. 85]:*

$$k_1 = k, \quad k_2 = \frac{F'}{\|r'\| f} \tag{17}$$

and then for $F' = f$ *we have that* k_f *of* C *is exactly the difference* $k_1 - k_2$ *of the principal curvatures of* Σ*; consequently the umbilic circles of* Σ *are provided by the zeros of* k_f *and are parametrized by* $\varphi \in S^1$.

For $F' = f$ *the curvatures of* C *are expressed only through the function* F *as:*

$$k(t) = \frac{[F''(t)]^2 - F'(t)F'''(t)}{[F'(t)^2 + F''(t)^2]^{\frac{3}{2}}}, \quad k_f(t) = \frac{-F'(t)F'''(t) - [F'(t)]^2}{[F'(t)^2 + F''(t)^2]^{\frac{3}{2}}} \tag{18}$$

and due to the presence of the third derivative of F *we recall its Schwarzian derivative:*

$$S_F = \frac{F'''}{F'} - \frac{3}{2}\left(\frac{F''}{F'}\right)^2 \tag{19}$$

which implies the new formulae:

$$k = \frac{(F'')^2 - 2(F')^2 S_F}{2[(F')^2 + (F'')^2]^{\frac{3}{2}}}, \quad k_f = \frac{-3(F'')^2 - 2(F')^2 S_F - 2(F')^2}{2[(F')^2 + (F'')^2]^{\frac{3}{2}}}. \tag{20}$$

In conclusion, a smooth F *with negative Schwarzian derivative will give a positive curvature* k *for* C *while a positive Schwarzian derivative* S_F *produces a negative flow-curvature* k_f.

v) The nature and the relationship between our frames can be put in the framework of moving frames of [8, p. 32]. Recall that the set of all orientation-preserving Euclidean isometries forms a Lie group, $E(2) := \mathbb{R}^2 \times SO(2)$, *with the standard projection* π_1 *on the first factor making* $E(2) \to \mathbb{R}^2$ *an* S^1*-principal bundle. A moving frame along* C *is a map* $F : I \to E(2)$ *such that* $\pi_1 \circ F = r$. *But* C *defines also a* 1*-parameter family of bijections of* $SO(2)$*:*

$L^C : I \to Bijections(SO(2)), t \to L^C(t) : SO(2) \to SO(2), A \to R(t)A, (L^C(t))^{-1} = L^C(-t)$.

Then our frames are $\mathcal{F} : I \to E(2)$ *as* $\mathcal{F}(t) = (r(t), T(t), N(t))$ *and* $\mathcal{E} : I \to E(2)$ *as* $\mathcal{E}(t) = (r(t), (L^C(t) \circ \pi_2 \circ \mathcal{F})(t))$.

vi) Suppose now that the curve C *is in the space* $\mathbb{R}^3$ *and is bi-regular; hence it has the Frenet frame* (T, N, B) *and the pair (curvature, torsion)=*(k, τ). *We define its flow-frame as:*

$$\begin{pmatrix} T \\ E_2^f \\ E_3^f \end{pmatrix}(t) := \begin{pmatrix} 1 & 0_2(h) \\ 0_2(v) & R(t) \end{pmatrix} \begin{pmatrix} T \\ N \\ B \end{pmatrix}, \quad 0_2(h) := (0, 0), \quad 0_2(v) := \begin{pmatrix} 0 \\ 0 \end{pmatrix}$$

and then, its matrix moving equation is:

$$\frac{d}{dt}\begin{pmatrix} T \\ E_2^f \\ E_3^f \end{pmatrix}(t) = \|r'(t)\| \begin{pmatrix} 0 & k_f^2(t) & k_f^3(t) \\ -k_f^2(t) & 0 & \tau_f(t) \\ -k_f^3(t) & -\tau_f(t) & 0 \end{pmatrix} \begin{pmatrix} T \\ E_2^f \\ E_3^f \end{pmatrix}(t).$$

A similar computation yields:

$$k_f^2(t) = k(t)\cos t, \quad k_f^3(t) = k(t)\sin t, \quad \tau_f(t) = \tau(t) - \frac{1}{\|r'(t)\|} < \tau(t).$$

We point out the formal similarity with the Darboux equations of a curve on a given surface and then a curve C with vanishing τ_f will be called flow-geodesic in $\mathbb{R}^3$. Hence, if C is naturally parametrized then C is a flow-geodesic if and only if its torsion has the constant value 1; for this class of space curves and examples see [1]. In order to express the above moving equation in the compact form as in the theory of space curves:

$$\omega_f(t) \times T(t) = T'(t), \quad \omega_f(t) \times E_2^f(t) = (E_2^f)'(t), \quad \omega_f(t) \times E_3^f(t) = (E_3^f)'(t)$$

we associate a vector field along C, called flow-Darboux:

$$\omega_f(t) := \|\gamma'(t)\|[\tau_f(t)T(t) - k_f^3(t)E_f^2(t) + k_f^2(t)E_3^f(t)].$$

Something similar but with the rotation with respect to an angle $\theta = \theta(s)$ appears in [13] under the name of quasi frame for C. Our choice corresponds to the angle $\theta(s) = -s$.
vii) Suppose that the curvature function $t \to k(t)$ is always strictly positive (or strictly negative). Then the evolute of C is the curve:

$$C_e : r_e(t) := r(t) + \frac{1}{k(t)}N(t).$$

With this model in mind, for a non-flat-flow curve we associate its flow-evolute as being the curve:

$$C_{fe} : r_{fe}(t) := r(t) + \frac{1}{k_f(t)}E_2^f(t).$$

We will obtain this curve for some examples below. So, the line C discussed in the example 1i has the flow-evolute

$$C_{fe} : r_{fe}(t) = r_0 + (t - \sin t)u - \cos t(iu)$$

and for $r_0 = (0, 1) = iu$ this last curve is exactly the cycloid of radius $R = 1$ according to the example 3 below. □

Returning to the plane curves let $J \subseteq \mathbb{R}$ be another open interval and fix the diffeomorphism $\varphi : s \in J \to t \in I$ with the smooth inverse $\varphi^{-1} : t \in I \to s \in J$. Since

$r'(s) = \varphi'(s)r'(t(s))$ we restrict our study to the class $Diff_+(J, I)$ of orientation-preserving diffeomorphisms: $\varphi'(s) > 0$, for all $s \in J$. The transformation of the flow-curvature under the action of φ is:

$$k_f(s) = k(t) - \frac{1}{\varphi'(s)\|r'(t)\|} \tag{21}$$

and then:

$$k_f(s) - k_f(t) = \frac{1}{\|r'(t)\|}\left[1 - \frac{1}{\varphi'(s)}\right]. \tag{22}$$

Proposition 2. *(the rigidity of the flow-curvature) The only orientation-preserving diffeomorphism φ which preserves also the flow-curvature of C is an interval shift on the real line $\varphi(s) = s + s_0, \quad s_0 \in (0, +\infty)$.*

A natural important problem is the class of curves with prescribed flow-curvature. For example, if we ask the vanishing of the flow-curvature for a graphic curve $C_F : r(t) = (t, F(t))$ then it follows the differential equation:

$$\frac{F''(t)}{[1 + (F'(t))^2]^{\frac{3}{2}}} = \frac{1}{[1 + (F'(t))^2]^{\frac{1}{2}}}. \tag{23}$$

Since this equation reads:

$$\frac{F''(t)}{1 + (F'(t))^2} = 1 \tag{24}$$

we have exactly the Grim Reaper solution, [3, p. 28], a famous solution of the curve shortening flow:

$$F_u(t) = u - \ln(\cos t), \quad t \in \left(-\frac{\pi}{2}, \frac{\pi}{2}\right), \quad u \in \mathbb{R} \tag{25}$$

with the usual curvature $k(t) = \cos t$ and the frames:

$$\mathcal{F}(t) = \begin{pmatrix} e^{it} \\ e^{i\left(t + \frac{\pi}{2}\right)} \end{pmatrix}, \quad \mathcal{E} = \begin{pmatrix} (1,0) = \bar{i} \\ (0,1) = \bar{j} \end{pmatrix} = constant. \tag{26}$$

Another formalism is that of [15, p. 2] if $r : S^1 \simeq [0, 2\pi) \to \mathbb{R}^2$ is naturally parametrized then there exists the smooth function $\theta : S^1 \to \mathbb{R}$, called *normal angle*, such that:

$$N(s) = e^{i\theta(s)} = (\cos\theta(s), \sin\theta(s)), \quad T(s) = -iN(s) = -ie^{i\theta(s)} = e^{i\left(\theta(s) - \frac{\pi}{2}\right)} \tag{27}$$

and then the Frenet equations yield:

$$\frac{d\theta}{ds}(s) = k(s). \tag{28}$$

In conclusion, the constant value $\beta \in \mathbb{R}$ of the flow-curvature of a closed convex curve means $\theta(s) = (\beta+1)s + \alpha$ for all $s \in S^1$ with $\alpha \in \mathbb{R}$ an arbitrary constant. The flow-frame corresponding to the equations (27) is:

$$E_1^f(s) = (\sin(\theta(s)-t(s)), -\cos(\theta(s)-t(s))), E_2^f(s) = (\cos(\theta(s)-t(s)), \sin(\theta(s)-t(s))) \tag{29}$$

which, in turn, is the Frenet frame of a new curve with the same natural parameter s but having the normal angle $\tilde{\theta}(s) := \theta(s) - t(s)$.

The formula (28) can be replaced with $\frac{d(\theta-\pi/2)}{ds}(s) = k(s)$ which expresses the curvature k as the derivative of the angle between $T \in \mathcal{X}_C$ and the unit vector $\bar{i}$. Following this approach the paper [7] generalizes k to a curvature-type function k_V defined with respect to an arbitrary $V \in \mathcal{X}_C$. A main result of the cited work is that $k_V = k_W$ if and only if the angle between V and W is constant along C. Hence, we can apply the last statement of the Remark ii) and then two flow-Fermi-Walker unit vectors $V, W \in \mathcal{X}_C$ yield the same curvature-type function.

In the following we present a couple of examples in order to remark the computational aspects of our approach.

Example 2. *The involute of the unit circle S^1 is:*

$$C : r(t) = (\cos t + t\sin t, \sin t - t\cos t) = (1-it)e^{it}, \quad t \in (0, +\infty). \tag{30}$$

A direct computation gives:

$$r'(t) = (t\cos t, t\sin t) = te^{it}, \quad \|r'(t)\| = t, \quad k(t) = \frac{1}{t} > 0, \tag{31}$$

and then this curve is also a flat-flow one and having the same flow-frame as the Grim Reaper. This example can be treated also with respect to a natural parameter $s \in (0, +\infty)$ which is provided by $t := \sqrt{2s}$. For example, the normal angle function is $\theta(s) = \frac{\pi}{2} + \sqrt{2s}$ since then $r'(s) = e^{i\sqrt{2s}}$. Comparing with the approach above it results the constants $\alpha = \frac{\pi}{2}$ and $\beta = \sqrt{2} - 1$. $\square$

Example 3. *Recall that for $R > 0$ the cycloid of radius R has the equation:*

$$C : r(t) = R(t - \sin t, 1 - \cos t) = R[(t, 1) - e^{i(\frac{\pi}{2} - t)}], \quad t \in \mathbb{R}. \tag{32}$$

Remark that here we have a twisted situation of the Remark iv) namely the derivative of the first component of the vector $r(t)$ is exactly the second component. The Schwarzian derivative is:

$$S_{t-\sin t}(t) = \frac{\cos t}{\sin t} - \frac{3}{2}\left(\frac{\cos \frac{t}{2}}{\sin \frac{t}{2}}\right)^2, \quad t \in \mathbb{R} \setminus \mathbb{Z}\pi. \tag{33}$$

We have immediately:

$$r'(t) = R(1-\cos t, \sin t) = R[(1,0)-e^{it}], \|r'(t)\| = 2R|\sin\frac{t}{2}|, k(t) = -\frac{1}{4R|\sin\frac{t}{2}|}, \tag{34}$$

and then we restrict our definition domain to $(0,\pi)$. *It follows:*

$$\begin{cases} k_f(t) = -\frac{3}{4R\sin\frac{t}{2}} < 0, \\ E_1^f(t) = (\sin\frac{3t}{2}, \cos\frac{3t}{2}) = e^{i\left(\frac{\pi}{2}-\frac{3t}{2}\right)}, E_2^f(t) = (-\cos\frac{3t}{2}, \sin\frac{3t}{2}) = e^{i\left(\pi-\frac{3t}{2}\right)}. \end{cases} \tag{35}$$

Again a natural parameter s *is provided by:* $t = 2\arccos\left(1-\frac{s}{4R}\right)$ *and the flow-evolute of* C *is the curve:*

$$C_{fe} : r_{fe}(t) = R(t-\sin t, 1-\cos t) + \frac{4}{3}R\sin\frac{t}{2}(\cos t, -\sin t), \quad t \in (0,\pi).$$

□

Example 4. *The derivative curve* r' *from* (31) *is an Archimedes' spiral. This spiral is given in polar coordinates as:*

$$A(spiral) : \rho(t) = Rt, \quad R > 0 \tag{36}$$

and hence:

$$k_f(t) = \frac{1}{R(t^2+1)^{\frac{3}{2}}} > 0 \tag{37}$$

while its flow-evolute is the curve:

$$C_{fe} : r_{fe}(t) = R(t\cos t, t\sin t) + R(1+t^2)(-\sin t - t\cos t, \cos t - t\sin t).$$

□

Example 5. *Fix* $\alpha \in \mathbb{R}^*$ *and the naturally parametrized curve* C. *Then the* α*-parallel curve of* C *is the new curve:*

$$C_\alpha : \tilde{r}(t) := r(t) + \alpha N(t), \quad t \in I \tag{38}$$

with:

$$\tilde{T}(t) = \frac{1-\alpha k(t)}{|1-\alpha k(t)|}T(t), \quad \tilde{N}(t) = \frac{1-\alpha k(t)}{|1-\alpha k(t)|}N(t), \quad \tilde{k}(t) = k(t). \tag{39}$$

Hence, we consider that α *does not belongs to the range of the function* $\frac{1}{k}$ *and the new flow-curvature is:*

$$\tilde{k}_f(t) = k(t) - \frac{1}{|1-\alpha k(t)|}. \tag{40}$$

□

We finish this note with the problem raised in the beginning, namely the possible variants of the curve shortening flow. Recall that the setting of this question consists in a 1-parameter family of plane curves $C_u : r = r_u(t) = r(t,u)$ satisfying:

$$\frac{\partial r(t,u)}{\partial u} = k(t,u)N(t,u). \tag{41}$$

It follows immediately an expression in terms of flow-apparatus:

$$\frac{\partial r(t,u)}{\partial u} = \left(k_f(t,u) + \frac{1}{\|r'(t,u)\|}\right)[-\sin t E_1^f(t,u) + \cos t E_2^f(t,u)]. \tag{42}$$

The first variant which we propose as an open problem is to study the flow-variant of (41):

$$\frac{\partial r(t,u)}{\partial u} = k_f(t,u)E_2^f(t,u). \tag{43}$$

The second variant is to generalize all this study through a general smooth function $\Omega \in C^\infty(\mathbb{R})$. More precisely, we use the equation (1) with R replaced by $R \circ \Omega$ to define the notion of Ω-frame for the plane curve C; we note that for a particular choice of Ω the 3-dimensional variant of the remark vi) is called *positional adapted frame* in [12]. Then the Ω-curvature of the plane curve C is:

$$k_\Omega(t) = k(t) - \frac{\Omega'(t)}{\|r'(t)\|} \tag{44}$$

and the curves in polar coordinates with vanishing Ω-curvature are provided by:

$$\rho(t) = Re^{\int_{t_0}^{t} \cot[\Omega(u)-u+C]du}, \quad R > 0, \quad C \in \mathbb{R}. \tag{45}$$

The flow-curvature corresponds to the identity map $\Omega = 1_{\mathbb{R}}$. Moreover, if C is naturally parametrized then $k_\Omega = (\theta - \Omega)'$ which means that the case $\Omega = \theta + constant$ provides a zero Ω-curvature.

Declaration of Competing Interests The author declare that there is no conflict of interest regarding the publication of this article

Acknowledgements I am grateful to Professor Dr. Vladimir Balan for several corrections to an initial version of this work. Also, I am extremely indebted to two anonymous referees for their remarks concerning my paper.

References

[1] Bates, L. M., Melko, O. M., On curves of constant torsion I, *J. Geom.*, 104 (2) (2013), 213–227. https://doi.org/10.1007/s00022-013-0166-2

[2] Bishop, R. L., There is more than one way to frame a curve, *Am. Math. Mon.*, 82 (1975), 246–251. https://doi.org/10.2307/2319846

[3] Chou, K.-S., Zhu, X.-P., The Curve Shortening Problem, Boca Raton, FL: Chapman & Hall/CRC, 2001. Zbl 1061.53045

[4] Crasmareanu, M., The flow-curvature of spacelike parametrized curves in the Lorentz plane, *Proceedings of the International Geometry Center*, 15 (2) (2022), 100–108. https://doi.org/10.15673/tmgc.v15i2.2281

[5] Crasmareanu, M., The flow-geodesic curvature and the flow-evolute of hyperbolic plane curves, *Int. Electron. J. Geom.*, 16 (2023), no. 1, 225—231. https://doi.org/10.36890/iejg.1229215

[6] Crasmareanu, M., Frigioiu, C. Unitary vector fields are Fermi-Walker transported along Rytov-Legendre curves, *Int. J. Geom. Methods Mod. Phys.*, 12 (10) (2015), , Article ID 1550111. https://doi.org/10.1142/S021988781550111X

[7] Góźdź, S., Curvature type functions for plane curves, *An. Ştiinţ. Univ. Al. I. Cuza Iaşi Mat.*, 39 (3) (1993), 295–303. Zbl 0851.53001

[8] Jensen, G. R., Musso, E., Nicolodi, L., Surfaces in Classical Geometries. A Treatment by Moving Frames, Universitext, Springer, 2016. Zbl 1347.53001

[9] Mazur, B., Perturbations, deformations, and variations (and "near-misses") in geometry, physics, and number theory, *Bull. Am. Math. Soc.*, 41 (3) (2004), 307–336. https://doi.org/10.1090/S0273-0979-04-01024-9

[10] Miron, R., Une généralisation de la notion de courbure de parallélisme, *Gaz. Mat. Fiz., Bucureşti, Ser. A* 10 (63) (1958), 705–708. Zbl 0087.36101

[11] Miron, R., The geometry of Myller configurations. Applications to theory of surfaces and nonholonomic manifolds, Bucharest: Editura Academiei Române, 2010. Zbl 1206.53003

[12] Özen, K. E., Tosun, M., A new moving frame for trajectories with non-vanishing angular momentum, *J. of Mathematical Sciences and Modelling*, 4 (1) (2021), 7–18. https://doi.org/10.33187/jmsm.869698

[13] Soliman, M. A., Nassar, H.A.-A., Hussien, R. A., Youssef, T., Evolutions of the ruled surfaces via the evolution of their directrix using quasi frame along a space curve, *J. of Applied Mathematics and Physics*, 6 (2018), 1748–1756. https://doi.org/10.4236/jamp.2018.68149

[14] Younes, L., Shapes and Diffeomorphisms, 2nd Updated Edition, Applied Mathematical Sciences 171, Berlin, Springer, 2019. Zbl 1423.53002

[15] Zhu, X.-P., Lectures on Mean Curvature Flows, AMS/IP Studies in Advanced Mathematics vol. 32, Providence, RI: American Mathematical Society, 2002. Zbl 1197.53087

http://communications.science.ankara.edu.tr

Commun.Fac.Sci.Univ.Ank.Ser. A1 Math. Stat.
Volume 72, Number 2, Pages 429–437 (2023)
DOI:10.31801/cfsuasmas.1171026
ISSN 1303-5991 E-ISSN 2618-6470

Research Article; Received: September 6, 2022; Accepted: December 9, 2022

ON SOME DIFFERENTIAL PROPERTIES OF FUNCTIONS IN GENERALIZED GRAND SOBOLEV-MORREY SPACES

Alik M. NAJAFOV[1,2], Ahmet EROGLU[3] and Firide MUSTAFAYEVA[4]

[1]Azerbaijan University of Architecture and Construction, Baku, AZERBAIJAN
[2]Institute of Mathematics and Mechanics of NAS of Azerbaijan, Baku, AZERBAIJAN
[3]Department of Mathematics, Nigde Omer Halisdemir University, Niğde, TÜRKİYE
[4]Shamakhi Branch of Azerbaijan State Pedagogical University, Shamakhi, AZERBAIJAN

Abstract. In this paper we introduce a generalized grand Sobolev-Morrey spaces. Some differential and differential-difference properties of functions from this spaces are proved by means of the integral representation.

1. Introduction and Preliminary Notes

Note that the grand Lebesgue spaces $L_{p)}(G)$ $(|G| < \infty)$ introduced in [4] by T. Iwaniec and C. Sbordone. After a vast amount of research about grand Lebesgue, small Lebesgue, grand Lebesgue-Morrey, grand grand Lebesgue-Morrey, grand grand Sobolev-Morrey, small small Sobolev-Morrey, grand grand Nikolskii Morrey and generalized grand Lebesgue-Morrey spaces has been introduced and studied by many mathematicians (see, e.g. [2,3], [5]- [14]) etc.

In this paper we construct a generalized grand Sobolev-Morrey spaces $W^{l}_{p),\phi}(G)$ and we study some differential properties with help of the method of integral representation of functions in view of embedding theory. Let $G \subset \mathbb{R}^n$ and $B \subset G$ be any Lebesgue measurable set, $l \in \mathbb{N}^n$, $p \in [1,\infty)$, and let $\phi(\cdot, |B|)$ be a function on $[0, p-1)$ which is a positive bounded and satisfies $\phi(0, |B|) = \phi(|B|)$. And also $\phi(\varepsilon, \cdot)$ is a positive bounded function defined on $(0, h_0]$ and h_0 is a fixed positive number.

2020 *Mathematics Subject Classification.* 46E35, 35A31.
Keywords. Generalized grand Sobolev-Morrey spaces, integral representation, flexible-horn condition, Hölder condition.

[1,2] aliknajafov@gmail.com-Corresponding author; 0000-0002-4289-9056
[3] aeroglu@ohu.edu.tr; 0000-0002-2642-3154
[4] mustafayevafiride@gmail.com; 0000-0002-0738-4911.

Definition 1. *Denote by $W^{l}_{p),\phi}(G)$ a space of locally summable functions f on G having the generalized derivatives $D_i^{l_i}f$ ($l_i > 0$ are integers $i = 1, 2, \ldots, n$) with the finite norm*

$$\|f\|_{W^{l}_{p),\phi}(G)} = \|f\|_{p),\phi,G} + \sum_{i=1}^{n} \left\|D_i^{l_i} f\right\|_{p),\phi,G}, \tag{1}$$

where

$$\|f\|_{p),\phi;G} = \|f\|_{L_{p),\phi}(G)} = \sup_{\substack{0 \le \varepsilon < p-1,\\ B \subset G}} \phi(\varepsilon, |B|) \left(\int_B |f(x)|^{p-\varepsilon} dx\right)^{\frac{1}{p-\varepsilon}}. \tag{2}$$

Here $|B|$ is the Lebesgue measure of B.

Note that

(1) If $\phi(\varepsilon, |B|) = \left(\frac{\varepsilon^{\theta}}{|B|^{\lambda+n}}\right)^{\frac{1}{p-\varepsilon}}, \theta > 0$, then $L_{p),\phi}(G) \equiv L^{\theta}_{p),\lambda}(G)$; in case $\theta = 1$, then $L_{p),\phi}(G) \equiv L_{p),\lambda}(G)$;

(2) If $\phi(\varepsilon, |B|) = \left(\frac{\varepsilon^{\theta}}{|B|^{n}}\right)^{\frac{1}{p-\varepsilon}}, \theta > 0$, then $L_{p),\phi}(G) \equiv L^{\theta}_{p)}(G)$; in case $\theta = 1, L_{p),\phi}(G) \equiv L_{p)}(G)$; $(B \equiv B(x, r))$;

(3) If $\phi(\varepsilon, |B|) = \left(\frac{\varepsilon^{\theta}}{r^{|\chi|a+|\chi|}}\right)^{\frac{1}{p-\varepsilon}}, \theta > 0$, then $L_{p),\phi}(G) \equiv L^{\theta}_{p),\chi,a}(G)$; in case $\theta = 1$, then $L_{p),\phi}(G) \equiv L_{p),\chi,a}(G)$;

(4) If $\phi(\varepsilon, |B|) = \left(\frac{1}{|B|^{\lambda}}\right)^{\frac{1}{p}}$, then $L_{p),\phi}(G) \equiv L_{1,\lambda}(G)$;

Observe some properties of $L_{p),\phi}(G)$ and $W^{l}_{p),\phi}(G)$.

(1) The following embedding hold:

$$L_{p),\phi}(G) \to L_{p)}(G), W^{l}_{p),\phi}(G) \to W^{l}_{p)}(G),$$

i.e.,
$\|f\|_{p);G} \le \|f\|_{p);\phi;G}$ and $\|f\|_{W^{l}_{p)}(G)} \le \|f\|_{W^{l}_{p),\phi}(G)}$
where

$$\|f\|_{W^{l}_{p)}G} \le \|f\|_{p),G} + \sum_{i=1}^{n} \left\|D_i^{l_i} f\right\|_{p),G}$$

$$\|f\|_{p),G} = \|f\|_{L_{p)}(G)} = \sup_{0 \le \varepsilon < p-1,} \phi(\varepsilon, |G|) \left(\int_G |f(x)|^{p-\varepsilon} dx\right)^{\frac{1}{p-\varepsilon}}.$$

Indeed,

$$\|f\|_{p),\phi,G} = \sup_{\substack{0 \le \varepsilon < p-1\\ B \subset G}} \phi(\varepsilon, |B|) \left(\int_G |f(x)|^{p-\varepsilon} dx\right)^{\frac{1}{p-\varepsilon}}$$

$$\geq \sup_{0\leq\varepsilon<p-1} \phi(\varepsilon,|G|)\left(\int_G |f(x)|^{p-\varepsilon}dx\right)^{\frac{1}{p-\varepsilon}} = \|f\|_{p),G}\,.$$

(1) $L_{p),\phi}(G)$ and $W^l_{p),\phi}(G)$ are complete.

The proof of completeness properties of these spaces is similar to [10].

It can be shown that, for $f\in W^l_{p-\varepsilon}(G)$ has the integral representation $(x\in U\subset G)$

$$D^\nu f(x) = f_h^{(\nu)}(x) + \sum_{i=1}^n \int_0^h \int_{R^n} L_i^{(\nu)}\left(\frac{y}{\psi(v)}\right) D_i^{l_i} f(x+y) \times$$

$$\times \prod_{j=1}^n \left(\psi_j(v)\right)^{-1-\nu_j} \left(\psi_i(v)\right)^{-1+l_i} \psi_i'(v)\,dydv, \tag{3}$$

$$f_h^{(\nu)}(x) = \prod_{j=1}^n \left(\psi_j(v)\right)^{-1-\nu_j} \int_{R^n} f(x+y)\,\Omega^{(\nu)}\left(\frac{y}{\psi(h)}\right)dy, \tag{4}$$

where $\frac{y}{\psi(v)} = \left(\frac{y_1}{\psi_1(v)}, \frac{y_2}{\psi_2(v)}, \ldots, \frac{y_n}{\psi_n(v)}\right)$, $\psi_i(v) =\ \ i = 1,2,\ldots,n$ is arbitrary differentiable non-decreasing functions defined for $0<v\leq h\leq h_0$, $\lim\limits_{v\to+0}\psi_i(v)=0$, $L_i(\cdot)\,,\,\Omega(\cdot)\in C_0^\infty(R^n)\,S(M) =\ \operatorname{supp} M\subset I_{\psi(h_0)} = \left\{y : |y_j| < \psi_j(h_0)\,, j=1,2,\ldots,n\right\}$ and the ψ horn $x+V = x+\bigcup_{0<h\leq h_0}\left\{y : \frac{y}{\psi(h)}\in S(\Omega)\right\}$ is the support of the representation (3), (4) and $\nu = (\nu_1,\ldots,\nu_n)\,,\ \nu_j\geq 0$ are integers $(j=1,2,\ldots,n)\,.$

Lemma 1. *Let $1<p<q\leq r\leq\infty$, $0<\eta,v\leq h\leq h_0$, $\nu=(\nu_1,\ldots,\nu_n)\,,\ \nu_j\geq 0$ be integers $(j=1,2,\ldots,n)\,,\quad \varphi\in L_{p),\phi}(G)$ and*

$$R^i_\eta = \int_0^\eta \prod_{j=1}^n \left(\psi_j(v)\right)^{-\nu_j-\frac{1}{p-\varepsilon}+\frac{1}{q-\varepsilon}} \left(\psi_i(v)\right)^{-1+l_i}\psi_i'(v)\,dv, \tag{5}$$

$$A^i_\eta(x) = \int_0^\eta \prod_{j=1}^n \left(\psi_j(v)\right)^{-1-\nu_j}\left(\psi_i(v)\right)^{-1+l_i}\psi_i^1(v)\int_{R^n}\varphi(x+y)\,K\left(\frac{y}{\psi(v)}\right)dydv, \tag{6}$$

$$A^i_{\eta,h}(x) = \int_\eta^h \prod_{j=1}^n \left(\psi_j(v)\right)^{-1-\nu_j}\left(\psi_i(v)\right)^{-1+l_i}\psi_i'(v)\int_{R^n}\varphi(x+y)\,K\left(\frac{y}{\psi(v)}\right)dydv. \tag{7}$$

Then

$$\left\|A^i_\eta\right\|_{q-\varepsilon,U} \leq c_1\|\varphi\|_{p),\phi,G}\left(\phi(\varepsilon,|U|)\right)^{-\frac{p-\varepsilon}{q-\varepsilon}}\left(\phi(\varepsilon,|B|)\right)^{-1+\frac{p-\varepsilon}{q-\varepsilon}}\left|R^i_\eta\right|\ \ \left(R^i_\eta<\infty\right) \tag{8}$$

$$\left\|A^i_{\eta\,h}\right\|_{q-\varepsilon,U} \leq c_2\|\varphi\|_{p),\phi,G}\left(\phi(\varepsilon,|U|)\right)^{-\frac{p-\varepsilon}{q-\varepsilon}}\left(\phi(\varepsilon,|B|)\right)^{-1+\frac{p-\varepsilon}{q-\varepsilon}}\left|R^i_{\eta,h}\right|, \tag{9}$$

where $R^i_{\eta,h} = \int_\eta^h\prod_{j=1}^n\left(\psi_j(v)\right)^{-\nu_j-\frac{1}{p-\varepsilon}+\frac{1}{q-\varepsilon}}\left(\psi_i(v)\right)^{-1+l_i}\psi_i'(v)\,dv$, and U is an open set containing in the domain G.

Proof. Applying the generalized Minkowski inequality, we deduce

$$\left\|A_\eta^i\right\|_{q-\varepsilon,U} \le \int_0^\eta \prod_{j=1}^n \left(\psi_j(\upsilon)\right)^{-1-\nu_j} \left(\psi_i(\upsilon)\right)^{-1+l_i} \psi_i'(\upsilon) \left\|F(\cdot,\upsilon)\right\|_{q-\varepsilon,U} d\upsilon, \quad (10)$$

for every

$$F(x,\upsilon) = \int_{R^n} \varphi(x+y) K\left(\frac{y}{\psi(\upsilon)}\right) dy. \quad (11)$$

Estimate of the norm $\|F(\cdot,\upsilon)\|_{q-\varepsilon,U}$. From Hölders inequality $(q \le r)$ we obtain

$$\|F(\cdot,\upsilon)\|_{q-\varepsilon,U} \le \|F(\cdot,\upsilon)\|_{r-\varepsilon,U} |U|^{\frac{1}{q-\varepsilon}-\frac{1}{r-\varepsilon}}. \quad (12)$$

Let X be the characteristic function of $S(K)$. It is obvious that

$$\|\varphi K\| = \left(|\varphi|^{p-\varepsilon}|K|^s\right)^{\frac{1}{r-\varepsilon}} \left(|\varphi|^{p-\varepsilon} X\right)^{\frac{1}{p-\varepsilon}-\frac{1}{r-\varepsilon}} \left(|K|^s\right)^{\frac{1}{s}-\frac{1}{r-\varepsilon}},$$

where $\frac{1}{s} = 1 - \frac{1}{p-\varepsilon} + \frac{1}{r-\varepsilon}$.

And applying again Hölders inequality $\left(\frac{1}{r-\varepsilon} + \left(\frac{1}{p-\varepsilon} - \frac{1}{r-\varepsilon}\right) + \left(\frac{1}{s} - \frac{1}{r-\varepsilon}\right) = 1\right)$ we have

$$\|F(\cdot,\upsilon)\|_{r-\varepsilon,U} \le \sup_{x\in U}\left(\int_{R^n} |\varphi(x+y)|^{p-\varepsilon} X\left(\frac{y}{\psi}\right) dy\right)^{\frac{1}{p-\varepsilon}-\frac{1}{r-\varepsilon}}$$

$$\times \sup_{y\in\upsilon}\left(\int_U |\varphi(x+y)|^{p-\varepsilon} dx\right)^{\frac{1}{r-\varepsilon}} \left(\int_{R^n}\left|K\left(\frac{y}{\psi}\right)\right|^s dy\right)^{\frac{1}{s}}. \quad (13)$$

For every $x \in U$ we have

$$\int_{R^n} |\varphi(x+y)|^{p-\varepsilon} X\left(\frac{y}{\psi}\right) dy \le \int_{I_{\psi(\upsilon)}} |\varphi(x+y)|^{p-\varepsilon} dy \le \|\varphi\|^{p-\varepsilon}_{p-\varepsilon, I_{\psi(\upsilon)}}$$

$$\le \|\varphi\|^{p-\varepsilon}_{p),\phi,G} \left(\phi\left(\varepsilon, \left|I_{\psi(\upsilon)}\right|\right)\right|^{-(p-\varepsilon)}. \quad (14)$$

For

$$\int_U |\varphi(x+y)|^{p-\varepsilon} dx \le \|\varphi\|^{p-\varepsilon}_{p-\varepsilon,U} \le \|\varphi\|^{p-\varepsilon}_{p),\phi,U} |\phi(\varepsilon,|U|)|^{-(p-\varepsilon)}$$

$$\le \|\varphi\|^{p-\varepsilon}_{p),\phi,G} \left(\phi(\varepsilon,|U|)\right)^{-(p-\varepsilon)}, \quad (15)$$

$$\int_{R^n}\left|K\left(\frac{y}{\psi}\right)\right|^s dy = \prod_{j=1}^n \psi_j(\upsilon) \|K\|_s^s. \quad (16)$$

It follows from (12)-(16) for $r = q$ that

$$\|F(\cdot,\upsilon)\|_{q-\varepsilon,U} \le \|\varphi\|_{p),\phi,G} \left|\phi\left(\varepsilon, \left|I_{\psi(\upsilon)}\right|\right)\right|^{-1+\frac{p-\varepsilon}{q-\varepsilon}} \phi(\varepsilon,|U|)^{-\frac{p-\varepsilon}{q-\varepsilon}} \|K\|_s |\psi(\upsilon)|^{\frac{1}{s}}. \quad (17)$$

Unseating this inequality in (10) we have

$$\left\|A_\eta^i\right\|_{q-\varepsilon,U} \le c\|\varphi\|_{p),\phi,G} \left(\phi(\varepsilon,|U|)\right)^{-\frac{p-\varepsilon}{q-\varepsilon}} \left(\phi(\varepsilon,|B|)\right)^{-1+\frac{p-\varepsilon}{q-\varepsilon}} \left|R_\eta^i\right| \left(R_\eta^i < \infty\right) \quad (18)$$

□

2. Main Results

Now we will prove two theorems on the properties of the functions from spaces $W^l_{p),\phi}(G)$.

Theorem 1. *Let $G \subset R^n$ be an open set such that it satisfies the horn condition, $1 \le p < \infty$, $\nu = (\nu_1, \nu_2, \dots, \nu_n)$, $\nu_j \ge 0$ be integers $(j = 1, 2, \dots, n)$, $R^i_h < \infty$ $(i = 1, 2, \dots, n)$ and $f \in W^l_{p),\phi}(G)$.*

Then $D^\nu : W^l_{p),\phi}(G) \to L_{q-\varepsilon}(G)$ holds for any $\varepsilon\,(0 \le \varepsilon < p - 1)$.

Moreover, the following inequality is valid

$$\|D^\nu f\|_{q-\varepsilon,G} \le c(\varepsilon)\left(\|f\|_{p),\phi;G} + \sum_{i=1}^{n}\left|R^i_h\right|\left\|D_i^{l_i} f\right\|_{p),\phi;G}\right). \tag{19}$$

In particular, if

$$R^{i,0}_h = \int_0^h \prod_{j=1}^{n}\left(\psi_j(v)\right)^{-\nu_j - \frac{1}{p-\varepsilon}}\left(\psi_i(v)\right)^{-1+l_i}\psi_i'(v)\,dv < \infty,$$

$i = 1, 2, \dots, n$, then $D^\nu f(x)$ is continuous on G and

$$\sup_{x\in G}\|D^\nu f(x)\| \le c(\varepsilon)\left(\|f\|_{p),\phi;G} + \sum_{i=1}^{n}\left|R^{i,0}_h\right|\left\|D_i^{l_i} f\right\|_{p),\phi;G}\right), \tag{20}$$

where $0 < h \le h_0$, h_0 is fixed positive number, $c(\varepsilon) = C \cdot (\phi(\varepsilon, |B|))^{-1+\frac{p-\varepsilon}{q-\varepsilon}}$ and C is a constant independent of f, h and ε.

Proof. Under the conditions of our theorem, the weak derivatives $D^\nu f$ exists. Since $p < q$ and $W^l_{p),\phi}(G) \to W^l_{p)}(G) \to W^l_{p-\varepsilon}(G)$ $(p - \varepsilon > 1)$. Then $D^\nu f$ exists on G (for all $B \subseteq I_{\psi(h_0)} \subset G$) has the integral representation

$$\begin{gathered} D^\nu f(x) = f_h^{(\nu)}(x) + \sum_{i=1}^{n}\int_0^h\int_{R^n} L_i^{(\nu)}\left(\tfrac{y}{B}\right)\times \\ \times D_i^{l_i} f(x+y)\prod_{j=1}^{n}\left(\psi_j(v)\right)^{-1-\nu_j}\left(\psi_i(v)\right)^{-1-\nu_i}\psi_i'(v)\,dvdy, \end{gathered} \tag{21}$$

where

$$f_h^{(\nu)}(x) = \prod_{j=1}^{n}\left(\psi_j(h)\right)^{-1-\nu_j}\int_{R^n} f(x+y)\,\Omega^{(\nu)}\left(\frac{y}{B}\right)dy, \tag{22}$$

$0 < h \le h_0$, L_i and $\Omega \in C_0^\infty(R^n)$, $i = 1, 2, \dots, n$, and $\frac{y}{B} = \left(\frac{y_1}{\left|B^{(1)}\right|}, \frac{y_2}{\left|B^{(2)}\right|}, \dots, \frac{y_n}{\left|B^{(n)}\right|}\right)$, $B^{(i)} = \left\{x : x = \left(x_1^0, x_2^0, \dots, x_i^0, x_i, x_{i+1}^0, \dots x_n^0\right)\right\}$ i.e., $B^{(i)} = proj_{x_i} B$. The representation (21), (22) carrier is contained in the set $x + V \subset G$. Hence, using Minkowski's inequality we arrive

$$\|D^\nu f\|_{q-\varepsilon,G} \le \left\|f_h^{(\nu)}\right\|_{q-\varepsilon,G} + \sum_{i=1}^n \left\|F_h^l\right\|_{q-\varepsilon,G}. \tag{23}$$

By (17) for $U = G,\ \varphi = f,\ K = \Omega^{(v)}, I_{\psi(h)} = B$, we have

$$\left\|f_h^{(\nu)}\right\|_{q-\varepsilon,G} \le c\,\|f\|_{p),\phi,G}\,|\phi(\varepsilon,|B|)|^{-1+\frac{p-\varepsilon}{q-\varepsilon}}\,|\phi(\varepsilon,|U|)|^{-\frac{p-\varepsilon}{q-\varepsilon}} \le c_1(\varepsilon)\,\|f\|_{p),\phi,G}$$

By (8) for $U = G,\ \varphi = D_i^{l_i} f,\ K = L_i^{(\nu)}, I_{\psi(v)} = B,\ \eta = h$ we have

$$\left\|F_h^i\right\|_{q-\varepsilon,G} \le c(\varepsilon)\left\|D_i^{l_i} f\right\|_{p),\phi,G}\left|R_h^i\right|.$$

Consequently,

$$\|D^\nu f\|_{q-\varepsilon,G} \le C(\varepsilon)\left(\|f\|_{p),\phi;G} + \sum_{i=1}^n \left|R_h^i\right|\left\|D_i^{l_i} f\right\|_{p),\phi;G}\right). \tag{24}$$

Now let

$$R_{h,0}^i = \int_0^h \prod_{j=1}^n \left(\psi_j(v)\right)^{-\nu_j-\frac{1}{p-\varepsilon}}\left(\psi_i(v)\right)^{-1+l_i}\psi_i'(v)\,dv < \infty\ (i = 1,2,\ldots,n).$$

We show that $D^v f$ is continuous on G. By (23) and (24) for $q = \infty$ we obtain:

$$\left\|D^\nu f - f_h^{(\nu)}\right\|_{\infty,G} \le C(\varepsilon)\sum_{i=1}^n \left|R_h^i\right|\left\|D_i^{l_i} f\right\|_{p),\phi;G}.$$

It follows that the left-hand part of the last inequality tends to zero as $h \to 0$. Since $f_h^{(\nu)}$ is continuous on G, in our case the convergence in $L_\infty(G)$ coincides with uniform convergence; consequently, $D^\nu f$ is continuous on G.

Thus the theorem is proved. □

Let γ be an n dimensional vector.

Theorem 2. *Suppose that the domain G the parameters p, q and vector v satisfy the condition of Theorem 1. If $R_h^i < \infty$ $(i = 1,2,\ldots,n)$, then $D^v f$ satisfies the Hölder condition on G in the metric of $L_{q-\varepsilon}$, more exactly*

$$\|\Delta(\gamma,G)\,D^\nu f\|_{q-\varepsilon,G} \le c(\varepsilon)\,\|f\|_{W^l_{p),\phi}(G)}\left|R_{h,\gamma}^1\right|. \tag{25}$$

If $R_h^i < \infty$ $(i = 1,2,\ldots,n)$, then

$$\sup_{x\in G}\|\Delta(\gamma,G)\,D^\nu f(x)\| \le c(\varepsilon)\,\|f\|_{W^l_{p),\phi}(G)}\left|R_{h,\gamma}^{1,0}\right|, \tag{26}$$

where

$$R_{h,\gamma}^1 = \max_i\left\{|\gamma|,\ |\gamma|\,|R_h^i|,\ |\gamma|\,|R_{h,\gamma}^i|\right\}$$

and

$$R^{1,0}_{h,\gamma} = \max_i \left\{ |\gamma| \,, \ |\gamma| \, |R^{i,0}_h|, \ |\gamma| \, |R^{i,0}_{h,\gamma}| \right\}.$$

Proof. By Lemma 8.6 of [1], there is a domain $G_\sigma \subset G$ $(G = \xi\rho(x)\,,\ \xi > 0,\ \rho(x) = = dist\,(x, \partial G)\,, x \in G)$ and $|\gamma| < \sigma$. Then, for every $x \in G_\sigma$ then the line segment joining the points x and $x + \gamma$ is contained in G. Identities (21), (22) are valid for all points of the segment with some kernels. After simple transformations, we have

$$|\Delta(\gamma, G)\, D^\nu f(x)| \leq \prod_{j=1}^n \left(\psi_j(h)\right)^{-1-\nu_j} \int_{R^n} |f(x+y)| \left| \Omega^{(\nu)}\left(\frac{y-\gamma}{B}\right) - \Omega^{(\nu)}\left(\frac{y}{B}\right) \right| dy$$

$$+ \sum_{i=1}^n \left\{ \int_0^{|\gamma|} \prod_{j=1}^n \left(\psi_j(\upsilon)\right)^{-1-\nu_j} \left(\psi_j(\upsilon)\right)^{-1+l_i} \int_{R^n} \left(\left| D_i^{l_i} f(x+\gamma+y) \right| + \left| D_i^{l_i} f(x+y) \right| \right) \right.$$

$$\times \left| L_i^{(\nu)}\left(\frac{y}{B}\right) \right| \psi_i'(\upsilon) d\upsilon dy + \int_{|\gamma|}^h \prod_{j=1}^n \left(\psi_j(\upsilon)\right)^{-1-\nu_j} \left(\psi_i(\upsilon)\right)^{-1+l_i}$$

$$\times \int_{R^n} \left| D_i^{l_i} f(x+y) \right| \left| L_i^{(\nu)}\left(\frac{y-\gamma}{B}\right) - L_i^{(\nu)}\left(\frac{y}{B}\right) \right| \psi_i'(\upsilon) d\upsilon dy$$

$$= A(x,\gamma) + \sum_{i=1}^n \left(A_1(x,\gamma) + A_2(x,\gamma)\right), \tag{27}$$

where $0 < h \leq h_0$. We also assume that $|\gamma| < h$ consequently $|\gamma| \leq \min(\sigma, h)$. If $x \in G \backslash G_\sigma$, then by definition $\Delta(\gamma, G)\, D^\nu f(x) = 0$. By (27)

$$\|\Delta(\gamma, G)\, D^\nu f\|_{q-\varepsilon, G} = \|\Delta(\gamma, G)\, D^\nu f\|_{q-\varepsilon, G_\sigma} \leq \|A(\cdot,\gamma)\|_{q-\varepsilon, G_\sigma}$$

$$+ \sum_{i=1}^n \left(\|A_1(\cdot,\gamma)\|_{q-\varepsilon, G_\sigma} + \|A_2(\cdot,\gamma)\|_{q-\varepsilon, G_\sigma} \right).$$

Note that

$$\left| \Omega^{(\nu)}\left(\frac{y-\gamma}{B}\right) - \Omega^{(\nu)}\left(\frac{y}{B}\right) \right| \leq \left| \int_0^{|\gamma|} \frac{d}{d\xi} \Omega^{(\nu)}\left(\left(y - \xi \frac{\gamma}{|\gamma|} \right) : B \right) d\xi \right|$$

$$\leq \sum_{j=1}^n \left| B^{(j)} \right|^{-1} \int_0^{|\gamma|} \left| D_j \Omega^{(\nu)}\left((y - \xi e_\gamma) : B\right) \right| d\xi,\ \ e_\gamma = \frac{\gamma}{|\gamma|}.$$

Therefore,

$$A(x,\gamma) \leq \prod_{j=1}^n \left(\psi_j(\upsilon)\right)^{-1-\nu_j} \sum_{j=1}^n \left| B^{(j)} \right|^{-1} \times$$

$$\times \int_0^{|\gamma|} d\xi \int_{R^n} |f(x + \xi e_j + y)| \left| D_j \Omega^{(\nu)}\left(\frac{y}{B}\right) \right| dy. \tag{28}$$

Similarly,

$$A_2(x,\gamma) \leq \sum_{j=1}^{n} \left| B^{(j)} \right|^{-1} \int_0^{|\gamma|} d\xi \int_{|\gamma|}^{h} \prod_{j=1}^{n} \left(\psi_j(\upsilon)\right)^{-1-\nu_j} \left(\psi_i(\upsilon)\right)^{-1+l_i} \left(\psi_i'(\upsilon)\right) d\upsilon$$

$$\times \int_{R^n} \left| D_i^{l_i} f(x+\xi e_j + y) \right| \left| D_j L_i^{(\nu)} \left(\frac{y}{B}\right) \right| dy, \tag{29}$$

Using (17) for $U = G,\ \varphi = f,\ \eta = |\gamma|,\ K = \Omega^{(\nu)}$, we obtain

$$\|A(\cdot,\gamma)\|_{q-\varepsilon,G} \leq c_1(\varepsilon)\,|\gamma|\,\|f\|_{p),\phi;G}, \tag{30}$$

with the help of (8) for $U = G,\ \varphi = D_i^{l_i} f,\ \eta = |\gamma|,\ K = L_i^{(\nu)}$ we obtain

$$\|A_1(\cdot,\gamma)\|_{q-\varepsilon,G} \leq c_2(\varepsilon)\,|\gamma| \left\| D_i^{l_i} f \right\|_{p),\phi;G} \left| R_h^i \right|, \tag{31}$$

and from (9) for $U = G,\ \varphi = D_i^{l_i} f,\ \eta = |\gamma|,\ K = L_i^{(\nu)}$ we obtain

$$\|A_2(\cdot,\gamma)\|_{q-\varepsilon,G} \leq c_3(\varepsilon)\, R_{h,\gamma}^i \left\| D_i^{l_i} f \right\|_{p),\phi;G}. \tag{32}$$

It follows from (27), (30)-(32) that

$$\|\Delta(\gamma,G)\,D^\nu f\|_{q-\varepsilon,G} \leq c(\varepsilon)\,\|f\|_{W^l_{p),\phi;G}(G)} \left| R_{h,\gamma}^1 \right|,$$

where

$$R_{h,\gamma}^1 = \max_i \left\{ |\gamma|,\ |\gamma|\,|R_h^i|,\ \ |\gamma|\,|R_{h,\gamma}^i| \right\}.$$

Suppose now that $|\gamma| \geq \min(\sigma,T)$. Then

$$\|\Delta(\gamma,G)\,D^\nu f\|_{q-\varepsilon,G} \leq 2\,\|D^\nu f\|_{q-\varepsilon,G} \leq c(\sigma,h)\,\|D^\nu f\|_{q-\varepsilon,G}\,|R_{h,\gamma}|.$$

Estimating $\|D^\nu f\|_{q-\varepsilon,G}$ by means of (21) we obtain the sought inequality in this case as well. Thus the theorem is proved . □

Author Contribution Statements The authors contributed equally to this work. All authors read and approved the final copy of this paper.

Declaration of Competing Interest The authors declare that they have no competing interest.

References

[1] Besov, O. V., Ilyin, V. P., Nikolskii, S. M., Integralnye Predstavleniya Funktsi i Teoremy Vlozheniya (Russian) (Integral Representations of Functions and Embedding Theorems), Fizmatlit "Nauka", Moscow, 1996.

[2] Fiorenza, A., Formica, M., Gogatishvili, A., On grand and small Lebesgue equations and applications, *Differ. Equ. Appl.,* 10(1) (2018), 21-46. dx.doi.org/10.7153/dea-2018-10-03

[3] He, S., Tao, Sh., Boundedness of some operators on grand generalized Morrey spaces over non-homogeneous spaces, *AIMS Mathematics,* 7(1) (2022), 1000-1014. doi:10.39341 math.2022060

[4] Iwaniec, T., Sbordone, C., On the integrability of the Jacobian under minimal hypoteses, *Arch. Rational Mech. Anal.,* 119(2) (1992), 129-143. https://doi.org/10.1007/BF00375119

[5] Kokilashvili, V. M., Meskhi, A., Rafeiro, H., Riesz type potential operators in generalized grand Morrey spaces, *Georgian Math. J.,* 20(1) (2013), 43-64. https://doi.org/10.1515/gmj-2013-0009

[6] Liu, Y., Yuan, W., Interpolation and duality of generalized grand Morrey spaces on quasi-metric measure spaces, *Czechoslovak Math. J.,* 67(3) (2017), 715-732. DOI: 10.21136/CMJ.2017.0081-16

[7] Meskhi, A., Maximal functions potentials and singular integrals in grand Morrey spaces, *Comp. Var. Ellip. Equations,* 56(10-11) (2011), 1003-1019. https://doi.org/10.1080/17476933.2010.534793

[8] Mizuta, Y., Ohno, T., Trudingers exponential integrability for Riesz potentials of function in generalized grand Morrey spaces, *J. Math. Anal. Appl.,* 420(1) (2014). https://doi.org/10.1016/j.jmaa.2014.05.082

[9] Najafov, A. M., Alekberli, S. T., On properties of functions from grand Sobolev-Morrey spaces, *J. Baku Engineering Univ.,* 2(1) (2018), 27-36.

[10] Najafov, A. M., Rustamova, N. R., Some differential properties of anisotropic grand Sobolev Morrey spaces, *Trans. A. Razmadze Math. Inst.,* 172(1) (2018), 82-89. https://doi.org/10.1016/j.trmi.2017.10.001

[11] Najafov, A. M., Gasimova, A. M., On embedding theorems in grand grand Nikolski-Morrey spaces, *Eur. J. Pure Appl. Math.,* 12(4) (2019), 1602-1611. https://doi.org/10.29020/nybg.ejpam.v12i4.3567

[12] Najafov, A. M., On some properties differential properties of small small Sobolev-Morrey spaces, *Eurasian Math. J.,* 12(1) (2021), 57-67. https://doi.org/10.32523/2077-9879-2021-12-1-57-67

[13] Rafeiro, H., A note on boundedness of operators in grand grand Morrey spaces, *Operator Theory: Advances and Applications*, 229 (2013) 349–356. DOI:10.1007/978-3-0348-0516-2_19

[14] Umarkhadzhiev, S., The boundedness of the Riesz potential operator from generalized grand Lebesgue spaces to generalized grand Morrey spaces, Operator Theory, Operator Algebras and Applications, 363-373, Oper. Theory Adv. Appl., 242, Birkhäuser, Springer, Basel, 2014. DOI:10.1007/978-3-0348-0816-3_22

http://communications.science.ankara.edu.tr

Commun.Fac.Sci.Univ.Ank.Ser. A1 Math. Stat.
Volume 72, Number 2, Pages 438–448 (2023)
DOI:10.31801/cfsuasmas.1124351
ISSN 1303-5991 E-ISSN 2618-6470

Research Article; Received: June 1, 2022; Accepted: November 22, 2022

ON STATISTICAL LIMIT POINTS WITH RESPECT TO POWER SERIES METHODS AND MODULUS FUNCTIONS

Canan SÜMBÜL[1], Cemal BELEN[2] and Mustafa YILDIRIM[1,3]

[1]Cumhuriyet University, Faculty of Arts and Sciences, Department of Mathematics, 58140 Sivas, TÜRKİYE

[2]Department of Mathematics Education, Ordu University, 52200, Ordu, TÜRKİYE

Abstract. In this study, we define a new type of statistical limit point using the notions of statistical convergence with respect to the J_p power series method and then we present some examples to show the relations between these points and ordinary limit points. After that we also study statistical limit points of a sequence with the help of a modulus function in the sense of the J_p power series method. Namely, we define f-J_p- statistical limit and cluster points of the real sequences and compare the set of these limit points with the set of ordinary points.

1. Introduction

The concept of statistical convergence was initially introduced by Fast [9]. The important properties of statistical convergence were established by Salat [15] and Fridy [11]. Fridy [12] introduced the concepts of statistical limit points and statistical cluster points of real sequences and compared them with ordinary limit points.

By using the modulus functions, Aizpuru et al. [1] introduced the concept of f -statistical convergence which depends on the other new concept of f-density of subsets of natural numbers (where f is a modulus function). Listán-García [13] gave the definition of f-statistical limit points and cluster points with respect to a modulus function f and proved some relations including the properties of the sets of f-statistical limit points and f-cluster points.

Ünver and Orhan [18] discussed the idea of statistical convergence via power series methods and they defined a new concept so-called P-statistical convergence.

2020 *Mathematics Subject Classification.* 40G15, 40F05, 40C15, 40G10.

Keywords. J_p-statistical limit points, J_p-statistical cluster points, f-J_p- statistical limit points.

[1] cnnhhs@gmail.com-Corresponding author; 0000-0002-8905-1247

[2] cbelen52@gmail.com; 0000-0002-8832-1524

[3] yildirim@cumhuriyet.edu.tr; 00000-0002-8880-5457.

Many authors used P-statistical convergence to obtain new results. In [3], Bayram gave some criteria for statistical convergence according to the power series methods. In [4], Bayram and Yıldız gave various Korovkin-type approximation theorems for linear operators defined on derivatives of functions, using statistical convergence according to power series methods. The recent results including P-statistical convergence can be seen in [2], [5], [8], [16], [17], [19].

In [6], the authors of this work developed the idea of statistical convergence by using J_p power series summability methods and a modulus function.

In this study, we introduce and study on the concepts of statistical limit points and statistical cluster points determined by the power series methods. Later on these notions are strenghtened via an unbounded modulus function. Some detailed examples are also presented to obtain strict inclusion relations.

Now recall some basic notions used in this paper.

Let $\mathbb{N}_0$ be the set of nonnegative integers, $E \subset \mathbb{N}_0$ and $E(n) = \{k \leq n : k \in E\}$. By $|E(n)|$, denote the cardinality of the set of $E(n)$. If limit

$$\lim_{n\to\infty} \frac{|E(n)|}{n+1}$$

exists, then E is said to have natural density and it is denoted by $\delta(E)$ [10]. Any number sequence $x = (x_k)$ is statistical convergent to L if for every $\varepsilon > 0$, $\delta(E_\varepsilon) = 0$, where $E_\varepsilon = \{k \in \mathbb{N}_0 : |x_k - L| \geq \varepsilon\}$. In this case we write $st\text{-}\lim x = L$.

Let $\left(x_{k(j)}\right)$ be any subsequence of $x = (x_k)$ and $K = \{k(j) : j \in \mathbb{N}_0\}$, then $\left(x_{k(j)}\right)$ is denoted by $\{x\}_K$. $\{x\}_K$ is called a thin subsequence of x if $\delta(K) = 0$. If $\delta(K) \neq 0$, $\{x\}_K$ is called a nonthin subsequence of x [12]. We know that L is ordinary limit point of x if there exists a subsequence of x that converges to L. The definition of statistical limit point is given below. Following Fridy [12], we say that the number λ is a statistical limit point of the sequence x if there exists a nonthin subsequence of x that converges to λ. For any real sequence x, Λ_x denotes the set of statistical limit points of x, and L_x denotes the set of ordinary limit points of x. Also if $\delta(\{k \in \mathbb{N} : |x - \gamma| < \varepsilon\}) \neq 0$ for every $\varepsilon > 0$, the number γ is called a statistical cluster point of the number sequence x [12]. Γ_x denotes the set of all statistical cluster points of x. For every sequence x, we have $\Lambda_x \subset \Gamma_x \subset L_x$.

2. J_p-Statistical Limit Points

Let $(p_k)_{k\in\mathbb{N}_0}$ be a sequence of nonnegative integers with $p_0 > 0$,

$$P_n = \sum_{k=0}^{n} p_k \to \infty \quad (n \to \infty)$$

and

$$p(t) = \sum_{k=0}^{\infty} p_k t^k < \infty$$

for $0<t<1$. For any real sequence $x=(x_k)$, assume that

$$p_x(t)=\sum_{k=0}^{\infty}p_k t^k x_k \text{ convergent for } 0<t<1.$$

Then we say that (x_k) is J_p-convergent to L or J_p-summable to L if

$$\lim_{t\to 1^-}\frac{p_x(t)}{p(t)}=L.$$

In this case we write $x_k\to L\ (J_p)$. The condition $p(t)\to\infty\ (t\to 1^-)$ assures that J_p-method is regular (see, [7]). So we only consider regular J_p methods.

The ideas of natural density and statistical convergence are extended to power series methods by Unver and Orhan [18].

Let $E\subset\mathbb{N}_0$ be any set. If the limit

$$\delta_{J_p}(E)=\lim_{t\to 1^-}\frac{1}{p(t)}\sum_{k\in E}p_k t^k$$

exits, then $\delta_{J_p}(E)$ is called J_p-density of E. From the definition it is clear that if $\delta_{J_p}(E)$ exists, then $0\le\delta_{J_p}(E)\le 1$ and $\delta_{J_p}(E)=1-\delta_{J_p}(\mathbb{N}_0\backslash E)$. If E is finite, then $\delta_{J_p}(E)=0$. Note that J_p-density and natural density of any $E\subset\mathbb{N}_0$ need not to be equal to each other. For instance, let $(p_k)=(1,0,1,0,...)$. Then $p(t)=\sum_{k=0}^{\infty}t^{2k}=1/\left(1-t^2\right)$ for $0<t<1$. Now if $E=\{2k+1:k\in\mathbb{N}_0\}$, then $\delta_{J_p}(E)=0$ but $\delta(E)=1/2$ (see [18]).

A real sequence $x=(x_k)$ is called J_p-statistically convergent to L if for every $\varepsilon>0$

$$\lim_{t\to 1^-}\frac{1}{p(t)}\sum_{k\in E_\varepsilon}p_k t^k=0.$$

where, $E_\varepsilon=\{k\in\mathbb{N}_0:|x_k-L|\ge\varepsilon\}$.That is, for every $\varepsilon>0$, $\delta_{J_p}(E_\varepsilon)=0$. In this case, we write $st_{J_p}\text{-}\lim x=L$. The set of all J_p-statistically convergent sequences is denoted by st_{J_p}.

The following example shows that a sequence x can be J_p statistical convergent even if x is not convergent or statistical convergent.

Example 1. *Let $(p_k)=(1,0,1,0,...)$ and $(x_k)=(0,1,0,1,...)$. Observe that (x_k) is neither convergent nor statistically convergent. But, since*

$$\delta_{J_p}(\{k\in\mathbb{N}_0:|x_k|\ge\varepsilon\})=\delta_{J_p}(\{2k+1:k\in\mathbb{N}_0\})=0$$

for each $\varepsilon>0$, we have $st_{J_p}\text{-}\lim x=0$.

Definition 1. *If $\delta_{J_p}(K)=0$, $\{x\}_K$ is called J_p-thin subsequence and if $\delta_{J_p}(K)\neq 0$, $\{x\}_K$ is called a J_p-nonthin subsequence of x. If there exists a J_p-nonthin subsequence of the real sequence x that converges to λ, then the number λ is said to be a J_p-statistical limit point of x.*

For any sequence x , $\Lambda_x^{J_p}$ denote the set of J_p-statistical limit points of x. It is clear that $\Lambda_x^{J_p} \subset L_x$ for any sequence x. The following example shows that the inclusion is strict.

Example 2. *Let (p_k) and (x_k) be in 1 and*

$$E_1 = \{k : k = 2n+1,\ n \in \mathbb{N}_0\ \} \text{ and } E_2 = \{k : k = 2n,\ n \in \mathbb{N}_0\}.$$

In this case we have

$$\begin{aligned} p(t) &= \sum_{k=0}^{\infty} p_k t^k = \sum_{k=0}^{\infty} p_{2k+1} t^{2k+1} + \sum_{k=0}^{\infty} p_{2k} t^{2k} \\ &= \sum_{k=0}^{\infty} 0.t^{2k} + \sum_{k=0}^{\infty} 1.t^{2k+1} \\ &= \frac{t}{1-t^2},\ |t| < 1, \end{aligned}$$

$$\begin{aligned} \delta_{J_p}(E_1) &= \lim_{t\to 1^-} \frac{1}{p(t)} \sum_{k\in E_1} p_k t^k = \lim_{t\to 1^-} \frac{1}{p(t)} \sum_{k=0}^{\infty} 1.t^{2k+1} = 1, \\ \delta_{J_p}(E_2) &= \lim_{t\to 1^-} \frac{1}{p(t)} \sum_{k\in E_2} p_k t^k = \lim_{t\to 1^-} \frac{1}{p(t)} \sum_{k=0}^{\infty} 0.t^{2k} = 0. \end{aligned}$$

Since $\{x\}_{E_1} \to 1$ and $\delta_{J_p}(E_1) \neq 0$, we obtain that $\Lambda_x^{J_p} = \{1\}$. But, it is clear that $L_x = \{0, 1\}$.

We write an example that shows Λ_x and $\Lambda_x^{J_p}$ are not same.

Remark 1. *The notions of statistical limit point and J_p-statistical limit point are not comparable. For instance, let J_p-method be determined by the sequence*

$$p_k = \begin{cases} 1 & \text{, if } k \text{ is square} \\ 0 & \text{, if } k \text{ is nonsquare} \end{cases}$$

and consider the sequence $x = (x_k)$ defined by

$$x_k = \begin{cases} 2 & \text{, if } k \text{ is square} \\ 1, & \text{, if } k \text{ is an odd nonsquare} \\ 0 & \text{, if } k \text{ is an even nonsquare} \end{cases}$$

Then we easily see that $\Lambda_x = \{0, 1\}$ and $\Lambda_x^{J_p} = \{2\}$.

We give an example below to show that $\Lambda_x^{J_p}$ and L_x can be very different.

Example 3. *Let $\{r_k\}_{k=1}^{\infty}$ be a sequence whose range is the set of all rational numbers and define*

$$x_k := \begin{cases} r_k & \text{, if } k = 2n \\ k & \text{, if } k = 2n+1 \end{cases} , n \in \mathbb{N}_0$$

$$p_k := \begin{cases} 1 & \text{, if } k = 2n+1 \\ 0 & \text{,if } k = 2n \end{cases} , n \in \mathbb{N}_0$$

Also let $E_1 = \{k : k = 2n+1,\ n \in \mathbb{N}_0\ \}$ *and* $E_2 = \{k : k = 2n,\ n \in \mathbb{N}_0\}$. *Since*

$$\delta_{J_p}(E_2) \quad = \lim_{t\to 1^-} \frac{1}{p(t)} \sum_{k\in E_2} p_k t^k = \lim_{t\to 1^-} \frac{1}{p(t)} \sum_{k=0}^{\infty} 0.t^{2k} = 0,$$

we have $\Lambda_x^{J_p} = \emptyset$. *But* $L_x = \mathbb{R}$, *since* $\{r_k : k \in \mathbb{N}_0\}$ *is dense in* $\mathbb{R}$.

Definition 2. *If* $\delta_{J_p}(\{k \in \mathbb{N} : |x_k - \gamma| < \varepsilon\}) \neq 0$ *for every* $\varepsilon > 0$, *then* γ *is called* J_p-*statistical cluster point of the sequence* $x = (x_k)$.

We show the set of all J_p-statistical cluster points of x with $\Gamma_x^{J_p}$.

Theorem 1. *For every sequence* x, $\Gamma_x^{J_p} \subset L_x$.

Proof. Assume that $\gamma \in \Gamma_x^{J_p}$. For every $\varepsilon > 0$, $\delta_{J_p}(\{k \in \mathbb{N} : |x_k - \gamma| < \varepsilon\}) \neq 0$. So the set $A := \{k \in \mathbb{N} : |x_k - \gamma| < \varepsilon\}$ is infinite. That means that there are infinitely many $x_k \in (\gamma - \varepsilon, \gamma + \varepsilon)$. From this we get $\gamma \in L_x$. □

Theorem 2. *For any number sequence* x, $\Lambda_x^{J_p} \subset \Gamma_x^{J_p}$.

Proof. Assume that $\lambda \in \Lambda_x^{J_p}$. Then there exists $K = \{k(j) : j \in \mathbb{N}_0\}$ such that $\{x\}_K$ is a J_p-nonthin subsequence of x. Thus for every $\varepsilon > 0$ there exists $n_0 \in \mathbb{N}$ such that for all $k(j) > n_0$, $\left|x_{k(j)} - \lambda\right| < \varepsilon$ and $\delta_{J_p}(K) \neq 0$. Also it is clear that

$$\left\{k(j) \in K : \left|x_{k(j)} - \lambda\right| < \varepsilon\right\} \subset \{k \in \mathbb{N}_0 : |x_k - \lambda| < \varepsilon\}.$$

From this we have

$$0 \neq \delta_{J_p}\left\{k(j) \in K : \left|x_{k(j)} - \lambda\right| < \varepsilon\right\} \subset \delta_{J_p}\{k \in \mathbb{N} : |x_k - \lambda| < \varepsilon\}.$$

Thus $\lambda \in \Gamma_x^{J_p}$ and so $\Lambda_x^{J_p} \subset \Gamma_x^{J_p}$. □

The following example shows that the inclusion $\Lambda_x^{J_p} \subset \Gamma_x^{J_p}$ is strict.

Example 4. *Define the sequence* x *by*

$$x_k = \begin{cases} 0, & \text{if } k = 0 \\ \frac{1}{r} & \text{if } k = 2^{r-1}(2q+1). \end{cases}$$

Also let $(p_k) = (1, 1, 1, ...)$. *Then* $p(t) = 1/(1-t)$ *for* $|t| < 1$, *and*

$$\delta_{J_p}(\{k : x_k = 1\}) = \delta_{J_p}(\{k = 2n+1 : n \in \mathbb{N}_0)\}) = \lim_{t\to 1^-} (1-t) \sum_{k=0}^{\infty} t^{2k+1} = 2^{-1},$$

$$\delta_{J_p}(\{k : x_k = 1/2\}) = \delta_{J_p}(\{k = 4n+2 : n \in \mathbb{N}_0)\}) = \lim_{t\to 1^-} (1-t) \sum_{k=0}^{\infty} t^{4k+2} = 2^{-2},$$

$$\delta_{J_p}(\{k : x_k = 1/2\}) = \delta_{J_p}(\{k = 8n+4 : n \in \mathbb{N}_0)\}) = \lim_{t\to 1^-} (1-t) \sum_{k=0}^{\infty} t^{8k+4} = 2^{-3},$$

$$\vdots$$

Thus we have for each r that $\delta_{J_p}(\{k : x_k = 1/r\}) = 2^{-r} > 0$, whence $\frac{1}{r} \in \Lambda_x^{J_p}$. It can be seen by a similar method that

$$\delta_{J_p}\left(\left\{k : |x_k| < \frac{1}{r}\right\}\right) = \delta_{J_p}\left(\left\{k : 0 < x_k < \frac{1}{r}\right\}\right) = 2^{-r}.$$

Hence we get $0 \in \Gamma_x^{J_p}$ and so $\Gamma_x^{J_p} = \{0\} \cup \left\{\frac{1}{r}\right\}_{r=1}^{\infty}$. Now we claim that $0 \notin \Lambda_x^{J_p}$. For this, if the limit of the subsequence $\{x\}_K$ is zero then we show that $\delta_{J_p}(K) = 0$. For each r we have

$$\begin{aligned} \delta_{J_p}(K) &= \lim_{t\to 1^-} \frac{1}{p(t)} \sum_{k\in K,\ x_k<1/r} p_k t^k + \lim_{t\to 1^-} \frac{1}{p(t)} \sum_{k\in K,\ x_k\geq 1/r} t^k \\ &\leq 2^{-r} + O(1). \end{aligned}$$

Since $r > 0$ is arbitrary, we conclude that $\delta_{J_p}(K) = 0$.

Theorem 3. *For any sequence x, the set $\Gamma_x^{J_p}$ is a closed point set.*

Proof. Assume that α is an accumulation point of $\Gamma_x^{J_p}$. Then for all $\varepsilon > 0$, $\Gamma_x^{J_p}$ contains some points

$$\gamma \in (\alpha - \varepsilon, \alpha + \varepsilon).$$

Choose ε' so that

$$(\alpha - \varepsilon', \alpha + \varepsilon') \subset (\alpha - \varepsilon, \alpha + \varepsilon).$$

Since $\gamma \in \Gamma_x^{J_p}$

$$\delta_{J_p}(\{k : x_k \in (\gamma - \varepsilon', \gamma + \varepsilon')\}) \neq 0.$$

From this

$$\delta_{J_p}(\{k : x_k \in (\alpha - \varepsilon, \alpha + \varepsilon)\}) \neq 0.$$

So we get $\alpha \in \Gamma_x^{J_p}$. □

If x and y are sequences such that $\delta_{J_p}(\{k : x_k \neq y_k\}) = 0$ then we say that $x_k = y_k$ for almost all k.

Theorem 4. *If x and y are sequences such that $x_k = y_k$ for almost all k, then $\Lambda_x^{J_p} = \Lambda_y^{J_p}$ and $\Gamma_x^{J_p} = \Gamma_y^{J_p}$.*

Proof. Let $\delta_{J_p}(\{k : x_k \neq y_k\}) = 0$ and $\lambda \in \Lambda_x^{J_p}$. Then there exists a J_p-nonthin subsequence $\{x\}_K$ of x which is convergent to λ. Since $\delta_{J_p}(\{k \in K : x_k \neq y_k\}) = 0$, $\delta_{J_p}(\{k : k \in K \text{ and } x_k = y_k\}) \neq 0$. From this if we take $K' = \{k \in \mathbb{N} : x_k = y_k\}$, then $\{y\}_{K'}$is a J_p-nonthin subsequence of $\{y\}_K$ which is convergent to λ. Thus $\lambda \in \Lambda_y^{J_p}$and so we get $\Lambda_x^{J_p} \subset \Lambda_y^{J_p}$. Likewise, it can be shown that $\Lambda_y^{J_p} \subset \Lambda_x^{J_p}$. Hence we get $\Lambda_x^{J_p} = \Lambda_y^{J_p}$. Now let $\gamma \in \Gamma_x^{J_p}$ and show that $\Gamma_x^{J_p} = \Gamma_y^{J_p}$. For every $\varepsilon > 0$, $\delta_{J_p}(\{k \in \mathbb{N} : |x_k - \gamma| < \varepsilon\}) \neq 0$. Define the sets $E' := \{k \in \mathbb{N} : |x_k - \gamma| < \varepsilon\}$, $E'' := \{k \in \mathbb{N} : x_k \neq y_k \text{ and } |x_k - \gamma| < \varepsilon\}$, $E''' := \{k \in \mathbb{N} : x_k = y_k \text{ and } |x_k - \gamma| < \varepsilon\}$. Since

$$\frac{1}{p(t)} \sum_{k\in E'} p_k t^k = \frac{1}{p(t)} \sum_{k\in E''} p_k t^k + \frac{1}{p(t)} \sum_{k\in E'''} p_k t^k$$

we get

$$0 \neq \lim_{t \to 1^-} \frac{1}{p(t)} \sum_{k \in E'} p_k t^k = \frac{1}{p(t)} \sum_{k \in E'''} p_k t^k$$

i.e., for every $\varepsilon > 0$, $\delta_{J_p}(\{k \in \mathbb{N} : |y_k - \gamma| < \varepsilon\}) \neq 0$. Hence $\gamma \in \Gamma_y^{J_p}$. The inclusion $\Gamma_y^{J_p} \subset \Gamma_x^{J_p}$ can be shown similarly. □

The following result can be obtained by a similar way to the Theorem 2 of [12].

Theorem 5. *If x is a number sequence then there exists a sequence y such that $L_y = \Gamma_x^{J_p}$ and $y_k = x_k$ for almost all k ; moreover, the range of y is a subset of the range of x.*

Note that L_x is always closed set while $\Lambda_x^{J_p}$ is not (see Example 4). Hence the conclusion of Theorem 4 is not valid if we replace $\Gamma_x^{J_p}$ with $\Lambda_x^{J_p}$.

Following the line of Fridy (see [12], Section 3), we can prove the J_p-statistical analogues of some of the well-known completeness theorems of real numbers theorems.

Theorem 6. *Let x be a real sequence and $M = \{k : x_k \leq x_{k+1}\}$. If $\delta_{J_p}(M) = 1$ and x is bounded on M then x is J_p-statistically convergent.*

Theorem 7. *If x contains a bounded J_p-nonthin subsequence then x has a J_p-statistical cluster point.*

This theorem leads naturally to the following corollary.

Corollary 1. *If x is a bounded sequence then x has a J_p-statistical cluster point.*

Theorem 8. *If x is a bounded sequence, then x has a J_p-nonthin subsequence $\{x\}_K$ such that $\{x_k : k \in \mathbb{N} \backslash K\} \cup \Gamma_x^{J_p}$ is compact set.*

3. f-J_p-Statistical Limit Points

In this section, we aim to examine the f-J_p-statistical version of cluster points and limit points and relate them to classical limit points.

Any function $f : \mathbb{R}^+ \to \mathbb{R}^+$ with the following properties is called a modulus function;

1. $f(x) = 0$ if and only if $x = 0$,
2. $f(x + y) \leq f(x) + f(y)$ for all $x, y \in \mathbb{R}^+$,
3. f is increasing,
4. f, is continuous from the right at zero [14].

$f(x) = \frac{x}{1+x}$ and $f(x) = x^p$ for $0 < p \leq 1$ are examples of modulus functions. A modulus function can be bounded or unbounded.

Definition 3. *Let f be an unbounded modulus function and $E \subset \mathbb{N}_0$. If the limit*

$$\delta_{J_p}^{f}(E) := \lim_{t \to 1^-} \frac{1}{f(p(t))} f\left(\sum_{k \in E} p_k t^k\right)$$

exists, then $\delta_{J_p}^{f}(E)$ is called f-J_p-density of E [6].

Definition 4. *Let $x = (x_n)$ be a real sequence and f be a unbounded modulus function. If a set $K \subset \mathbb{N}_0$ has the propert $\delta_{J_p}^{f}(K) = 0$, then $\{x\}_K$ is called f-J_p-thin subsequence of x. If $\delta_{J_p}^{f}(K) \neq 0$, then $\{x\}_K$ is called f-J_p-nonthin subsequence of x.*

Definition 5. *Let $x = (x_n)$ be a real sequence. If x has a f-J_p-nonthin subsequence that converges to ℓ, then ℓ is called f-J_p-statistical limit point of x. The set of all f-J_p-statistical limit point of x is denoted by $\Lambda_x^{f-J_p}$.*

Definition 6. *Let $x = (x_n)$ be a real sequence. If $\delta_{J_p}^{f}(\{n \in \mathbb{N} : |x_n - \gamma| < \varepsilon\}) \neq 0$ for each $\varepsilon > 0$, then γ is called an f-J_p-statistical cluster point of x. The set of all f-J_p-statistical cluster point of x is denoted by $\Gamma_x^{f-J_p}$.*

It is known that $\delta_{J_p}^{f}(A) = 0$ means $\delta_{J_p}(A) = 0$ for any unbounded modulus function f and for any $A \subseteq \mathbb{N}$ [6].

Theorem 9. *x is a sequence in $\mathbb{R}$, then the followings hold:*
i) $\Lambda_x^{J_p} \subset \Lambda_x^{f-J_p}$
ii) $\Gamma_x^{J_p} \subset \Gamma_x^{f-J_p}$
iii) $\Lambda_x^{f-J_p} \subset \Gamma_x^{f-J_p}$
iv) $\Gamma_x^{f-J_p} \subset L_x$.

Proof. (i) - (ii) Since f-J_p-density zero sets are J_p-density zero, it is clear that $\Lambda_x^{J_p} \subset \Lambda_x^{f-J_p}$ and $\Gamma_x^{J_p} \subset \Gamma_x^{f-J_p}$.
(iii) To show $\Lambda_x^{f-J_p} \subset \Gamma_x^{f-J_p}$ assume that $\gamma \in \Lambda_x^{f-J_p}$. In this case there exists $K \subseteq \mathbb{N}$ such that $\delta_{J_p}^{f}(K) \neq 0$ and $\lim_{k \in K} x_k = \gamma$. For every $\varepsilon > 0$, $A = \{n \in K \ : |x_n - \gamma| \geq \varepsilon\}$ is finite which implies $\delta_{J_p}^{f}(K \backslash A) \geq \delta_{J_p}^{f}(K) - \delta_{J_p}^{f}(A) = \delta_{J_p}^{f}(K) \neq 0$. Since f is increasing and $K \backslash A \subseteq \{n \in \mathbb{N} : |x_n - \gamma| < \varepsilon\}$,

$$\delta_{J_p}^{f}(\{n \in \mathbb{N} : |x_n - \gamma| < \varepsilon\}) \geq \delta_{J_p}^{f}(K \backslash A) \neq 0$$

hence $\gamma \in \Gamma_x^{f-J_p}$.
(iv) We show that $\Gamma_x^{f-J_p} \subseteq L_x$. Assume that $\gamma \in \Gamma_x^{f-J_p}$. For each $j \in \mathbb{N}$, we have

$$\delta_{J_p}^{f}\left(\left\{n \in \mathbb{N} : |x_n - \gamma| < \frac{1}{j}\right\}\right) \neq 0.$$

Thus if we say $A_j = \left\{n \in \mathbb{N} : |x_n - \gamma| < \frac{1}{j}\right\}$, then $A_j \subset \mathbb{N}$ and for each $j \in \mathbb{N}$, $A_{j+1} \subset A_j$. We can now take an increasing sequence of indices $n_1 < n_2 < \cdots$ with each $n_j \in A_j$. If $k \geq j$, $j \in \mathbb{N}$, then $|x_{n_k} - \gamma| < \frac{1}{k} \leq \frac{1}{j}$. So (x_{n_k}) is a subsequence of x that converges to γ, therefore $x \in L_x$. □

Note that all inclusions in Theorem 9 are strict. For instance for (i), we present the following example.

Example 5. *Let (x_k) and (p_k) are defined as*

$$x_k := \begin{cases} 1 & , k = 2j \\ 2 & , k = 2j+1 \end{cases} \quad , j = 0, 1, 2, ...$$

$$p_k = \begin{cases} \dfrac{1}{k} & , k = 2j+1 \\ 1 & , k = 2j \end{cases} \quad , j = 0, 1, 2, ...$$

In this case,

$$p(t) = \sum_{k=0}^{\infty} p_k t^k = \frac{1}{2} \ln \left(\frac{1+t}{1-t}\right) + \frac{1}{1-t^2}$$

for $0 < t < 1$ and then we get $\delta_{J_p}(E_1) = 1$ and $\delta_{J_p}(E_2) = 0$ for the sets $E_1 := \{2j : j \in \mathbb{N}_0\}$ and $E_2 := \{2j+1 : j \in \mathbb{N}_0\}$. Hence $\Lambda_x^{J_p} = \{2\}$. Indeed $\{x\}_{\mathbb{N}/E_1}$ is the subsequence of x which converges to 2 and $\delta_{J_p}(\mathbb{N} \backslash E_1) \neq 0$. For the modulus function $f(x) = \log(x+1)$, observe that

$$\delta_{J_p}^f(E_1) = \lim_{t \to 1^-} \frac{1}{f(p(t))} f\left(\sum_{k \in E_1} p_k t^k\right) = 1.$$

So we obtain that $\Lambda_x^{f-J_p} = \{1, 2\}$. Thus we see that the inclusion $\Lambda_x^{J_p} \subset \Lambda_x^{f-J_p}$ is strict.

Definition 7. *If there exists a bounded set B such that $\delta_{J_p}^f(\{n \in \mathbb{N} : x_n \notin B\}) = 0$, then $x = (x_n)$ is called f-J_p-statistical bounded sequence.*

Theorem 10. *If $x = (x_n)$ and $y = (y_n)$ are sequences in $\mathbb{R}$ such that $\delta_{J_p}^f(\{n \in \mathbb{N} : x_n \neq y_n\}) = 0$, then $\Lambda_x^{f-J_p} = \Lambda_y^{f-J_p}$ and $\Gamma_x^{f-J_p} = \Gamma_y^{f-J_p}$.*

Proof. Let $\alpha \in \Lambda_x^{f-J_p}$. In this case there exists a set $B \subset \mathbb{N}$ such that

$$\lim_{n \in B} x_n = \alpha$$

where $\delta_{J_p}^f(B) \neq 0$ and $|B|$ is infinite. We get the set $A = \{n \in \mathbb{N} : x_n \neq y_n\}$ for which $\delta_{J_p}^f(A) = 0$. Now take the sequence $(y_n)_{n \in B \backslash A}$, that convergence to α and $(y_n)_{n \in B \backslash A}$ is f-J_p-nonthin subsequence of y. Indeed, if $\delta_{J_p}^f(B \backslash A) = 0$, then

$$\delta_{J_p}^f(A \cup B) = \delta_{J_p}^f(A \cup (B \backslash A)) \leq \delta_{J_p}^f(A) + \delta_{J_p}^f(B \backslash A) = 0,$$

but $B \subset A \cup B$ and B doesn't have null f-J_p-density. Thus we get $\alpha \in \Lambda_y^{f-J_p}$. The other side of the equation can be shown in a similar way. Now take $\gamma \in \Gamma_x^{f-J_p}$. For $\varepsilon > 0$, $\delta_{J_p}^f(\{n \in \mathbb{N} : |x_n - \gamma| < \varepsilon\}) \neq 0$. Consider the sets

$$B_\varepsilon = \{n \in \mathbb{N} : |x_n - \gamma| < \varepsilon\} \text{ and } C_\varepsilon = \{n \in \mathbb{N} : |y_n - \gamma| < \varepsilon\}$$

for given $\varepsilon > 0$. We get $B_\varepsilon \backslash A \subseteq C_\varepsilon$ and so

$$\delta_{J_p}^f(C_\varepsilon) \geq \delta_{J_p}^f(B_\varepsilon \backslash A) \geq \delta_{J_p}^f(B_\varepsilon) - \delta_{J_p}^f(A) = \delta_{J_p}^f(B_\varepsilon) \neq 0.$$

Thus we get $\gamma \in \Gamma_y^{f-J_p}$. The other side of the equation can be shown similarly. □

From this theorem, the following result is obtained.

Corollary 2. *Let $x = (x_n)$ be a f-J_p-statistical bounded real sequence. Then $\Gamma_x^{f-J_p}$ is bounded.*

Author Contribution Statements The authors contributed equally to this work. All authors read and approved the final copy of this paper.

Declaration of Competing Interests The authors declare that they have no known competing financial interest or personal relationships that could have appeared to influence the work reported in this paper.

Acknowledgement The authors are thankful to the referees for making valuable suggestions leading to the better presentations of this paper.

References

[1] Aizpuru, A., Listán-García, M. C., Rambla-Barreno F., Density by moduli and statistical convergence, *Quaestiones Mathematicae*, 37 (2014), 525-530. https://doi.org/10.2989/16073606.2014.981683

[2] Arif, A., Yurdakadim, T., Approximation results on nonlinear operators by P_p-statistical convergence, *Advanced Studies: Euro-Tbilisi Mathematical Journal,* 15(3) (2022), 1-10. DOI: 10.32513/asetmj/19322008220

[3] Bayram, N. Ş., Criteria for statistical convergence with respect to power series methods, *Positivity.* 25, (2021), 1097-1105. https://doi.org/10.1007/s11117-020-00801-6

[4] Bayram, N. Ş., Yıldız, S., Approximation by statistical convergence with respect to power series methods, *Hacet. J. Math. Stat.,* 51(4) (2022), 1108-1120. DOI: 10.15672/hujms.1022072

[5] Bayram, N. Ş., P-strong convergence with respect to an Orlicz function, *Turk J Math.,* 46 (2022), 832-838. https://doi.org/10.55730/1300-0098.3126

[6] Belen, C., Yıldırım, M., Sümbül, C., On statistical and strong convergence with respect to a modulus function and a power series method, *Filomat*, 34(12) (2020), 3981-3993. https://doi.org/10.2298/FIL2012981B

[7] Boos, J., Classical and modern methods in summability, Oxford University Press, Oxford, 2000.

[8] Demirci, K., Dirik, F., Yıldız, S., Approximation via equi-statistical convergence in the sense of power series method, *RACSAM Rev. R. Acad. Cienc. Exactas Fis. Nat. Ser. A Mat.*, 116(65) (2022). https://doi.org/10.1007/s13398-021-01191-4
[9] Fast, H., Sur la convergence statistique, *Colloq. Math.,* 2 (1951), 241-244.
[10] Freedman, A. R., Sember, J. J., Densities and summability, *Pacific J. Math.,* 95(2) (1981), 293-305.
[11] Fridy, J. A., On statistical convergence, *Analysis* 5 (1985), 301-313.
[12] Fridy, J.A., Statistical limit points, *Proc. Amer. Math. Soc.*, 118(8) (1993), 1187-1193.
[13] Listán-García, M. C., f-statistical convergence, completeness and f-cluster points, *Bull. Belg. Math. Soc. Simon Stevin,* 23(2) (2016), 235-245.
[14] Nakano, H., Concave modulars, *J. Math. Soc. Japan*, 5 (1953), 29-49.
[15] Šalát, T., On statistically convergent sequences of real numbers, *Math. Slovaca*, 30(2) (1980), 139-150.
[16] Söylemez, D., A Korovkin type approximation theorem for Balázs Type Bleimann, Butzer and Hahn Operators via power series statistical convergence, *Math. Slovaca*, 72(1) (2022), 153-164. https://doi.org/10.1515/ms-2022-0011
[17] Sümbül, C., Belen, C., Yıldırım, M., Properties of J_p-statistical convergence, *Cumhuriyet Sci. J.*, 43(2) (2022), 294-298. https://doi.org/10.17776/csj.1064559
[18] Ünver, M., Orhan, C., Statistical convergence with respect to power series methods and applications to approximation theory, *Numer. Func. Anal Opt.,* 40(5) (2019), 535-547. https://doi.org/10.1080/01630563.2018.1561467
[19] Ünver, M., Bayram, N. Ş., On statistical convergence with respect to power series methods, *Positivity* (2022), 26-55. https://doi.org/10.1007/s11117-022-00921-1

http://communications.science.ankara.edu.tr

Commun.Fac.Sci.Univ.Ank.Ser. A1 Math. Stat.
Volume 72, Number 2, Pages 449–461 (2023)
DOI:10.31801/cfsuasmas.1114983
ISSN 1303-5991 E-ISSN 2618-6470

COMMUNICATIONS SERIES A1

Research Article; Received: May 10, 2022; Accepted: August 11, 2022

NEW SUMMABILITY METHODS VIA $\widetilde{\phi}$ FUNCTIONS

Rabia SAVAŞ

Department of Mathematics and Science Education, Istanbul Medeniyet University, Istanbul, TÜRKİYE

Abstract. In 1971, the definition of Orlicz $\widetilde{\phi}$ functions was introduced by Lindenstrauss and Tzafriri and moreover in 2006, the notion of double lacunary sequences was presented by Savaş and Patterson. The primary focus of this article is to introduce the double statistically $\widetilde{\phi}$-convergence and double lacunary statistically $\widetilde{\phi}$-convergence which are generalizations of the double statistically convergence [19] and double lacunary statistically convergence [24]. Additionally, some essential inclusion theorems are examined.

1. Introduction and Background

In 1951, Fast [6] and Steinhaus [26] independently put forward the idea of statistical convergence. Some fundamental characteristics of statistical convergence were established by Schoenberg [25] in 1959, and by Fridy [7] and in 1985 in the case of single sequences, and by Mursaleen and Edely [18] in 2003 in the case of multiple sequences. Ever since, numerous studies of single sequences have been devoted to this subject, such as ([4], [5], [16], [27]).

We recall that the concept of convergence for double sequences was presented by Pringsheim [20] as follows:

Definition 1. *[20] A double sequence $y = (y_{r,s})$ has Pringsheim limit ϖ (denoted by $P - \lim y = \varpi$) if for every $\varepsilon > 0$ there exists $\overline{N}_\varepsilon \in \mathbb{N}$ such that $|y_{r,s} - \varpi| < \varepsilon$, whenever $r, s > \overline{N}_\varepsilon$.*

In the recent past, the concept of statistical convergence for double sequences was studied by Mursaleen and Edely [18] as follows: A double sequence $y = (y_{r,s})$

2020 *Mathematics Subject Classification.* 40A05, 40C05, 40D25.
Keywords. Double sequences, Orlicz function, lacunary double sequence, double statistical convergence, $\widetilde{\phi}-$convergence.
rabiasavass@hotmail.com; 0000-0002-4911-9067
.

of real numbers is double statistically convergent to ϖ if for each $\varepsilon > 0$,

$$P-\lim_{z,w\to\infty}\frac{1}{zw}\left|\{(r,s)\in\mathbb{N}\times\mathbb{N}: r\leq z,\ s\leq w: |y_{r,s}-\varpi|\geq\varepsilon\}\right|=0.$$

In such a case, we can symbolize with $st_2-\lim y=\varpi$, and S_2 will represent the class of all statistically convergent double sequences. There are several papers dealing with double statistical convergence (see [2], [12], [19], [22], [23]). Also, in [24] the concept of lacunary statistically convergence for double sequence was introduced as follows:

Definition 2. *The double sequence $\Phi_{\xi,\eta}=\{(r_\xi,s_\eta)\}$ is named double lacunary if there exist two increasing sequences of integers such that*

$$r_0=0,\quad \gamma_\xi=r_\xi-r_{\xi-1}\to\infty\quad as\quad \xi\to\infty,$$

and

$$s_0=0,\quad \overline{\gamma}_\eta=s_\eta-s_{\eta-1}\to\infty\quad as\quad \eta\to\infty.$$

Also, $r_{\xi,\eta}=r_\xi s_\eta$, $\gamma_{\xi,\eta}=\gamma_\xi\overline{\gamma}_\eta$, $\zeta_\xi=\frac{r_\xi}{r_{\xi-1}}$, $\overline{\zeta}_\eta=\frac{s_\eta}{s_{\eta-1}}$, $\zeta_{\xi,\eta}=\zeta_\xi\overline{\zeta}_\eta$, and $\Phi_{\xi,\eta}$ is determined by

$$J_{\xi,\eta}=\{(r,s): r_{\xi-1}<r\leq r_\xi\ and\ s_{\eta-1}<s\leq s_\eta\}.$$

We now consider the concept of double lacunary statistically convergence as follows:

Definition 3. *[24] Let $\Phi_{\xi,\eta}$ be a double lacunary sequence. The double sequence y is $S_{\theta_{\xi,\eta}}-P-$convergent to ϖ if for every $\varepsilon>0$,*

$$P-\lim_{\xi,\eta}\frac{1}{\gamma_{\xi,\eta}}\left|\{(r,s)\in J_{\xi,\eta}: |y_{r,s}-\varpi|\geq\varepsilon\}\right|=0,$$

where the vertical bars denote the cardinality of the enclosed set.

Additionally, Lindenstrauss and Tzafriri [15] presented the following definitions.

Definition 4. *[15] A function $\widetilde{\phi}(\tau):[0,\infty)\to[0,\infty)$ is called an Orlicz function if $\widetilde{\phi}(\tau)$ is continuous, non-decreasing and convex with $\widetilde{\phi}(0)=0$, $\widetilde{\phi}(\tau)>0$ for $\tau>0$, and $\widetilde{\phi}(\tau)\to\infty$ as $\tau\to\infty$.*

Definition 5. *[15] An Orlicz function $\widetilde{\phi}(\tau)$ is said to satisfy the $\triangle_2$ condition for all values of τ, if there exists a constant $\overline{M}>0$ such that*

$$\widetilde{\phi}(2\tau)\leq\overline{M}\,.\widetilde{\phi}(\tau),\qquad(\tau\geq 0).$$

Krasnoselskii and Rutitsky [14] also showed that $\triangle_2$ condition is equivalent to the condition

$$\widetilde{\phi}\,(l\tau))\leq\overline{M}\,(l)\ .\widetilde{\phi}(\tau),\qquad(\tau\geq 0),$$

for all values of $l,\tau>1$. Recently, some papers have been dealing with Orlicz function (see [1], [3], [8], [9], [10], [11], [13], [17], [21]).

The main goal of this paper is to extend some sequence spaces defined by Orlicz functions from ordinary (i.e., single) sequences to double sequences. To accomplish this goal we present a new notion of double lacunary statistically $\widetilde{\phi}-$convergence, as more generalizations of the double statistically convergence [18] and double lacunary statistically convergence [24]. Also, we examine some inclusions relations.

2. Main Result

We now present some definitions, which will be needed in the further section.

Definition 6. *Let $\widetilde{\phi}$ be an Orlicz function. A sequence $y = (y_{r,s})$ is said to be $\widetilde{\phi}-$double convergent to ϖ if $P - \lim_{r,s} \widetilde{\phi}(y_{r,s} - \varpi) = 0$. In such a situation, ϖ is called the $\widetilde{\phi}-$limit of $(y_{r,s})$ and symbolized by $\widetilde{\phi} - lim\, y = \varpi$.*

Note 1. *If $\widetilde{\phi}(y) = |y|$, then $\widetilde{\phi}-$double convergent notions coincide with usual double convergence. Also, it is simple to control, if $y = (y_{r,s})$ is $\widetilde{\phi}-$double convergent to ϖ, then any of its subsequence is $\widetilde{\phi}-$double convergent to ϖ.*

Definition 7. *Let $\widetilde{\phi}$ be an Orlicz function. A sequence $y = (y_{r,s})$ is said to be double statistically $\widetilde{\phi}-$convergent to ϖ if for each $\varepsilon > 0$,*

$$P - \lim_{z,w} \frac{1}{zw} \left| \left\{ r \leq z, s \leq w : \widetilde{\phi}(y_{r,s} - \varpi) \geq \varepsilon \right\} \right| = 0.$$

ϖ is called the double statistical $\widetilde{\phi}-$ limit of the sequence $(y_{r,s})$ and we symbolize $S_2 - \widetilde{\phi}\ lim\, y = \varpi$ or $y_{r,s} \overset{P}{\to} \varpi(S_2 - \widetilde{\phi})$. We will denote the class of all double statistically $\widetilde{\phi}-$convergent sequences by $S_2 - \widetilde{\phi}$.

Note 2. *If $\widetilde{\phi}(y) = |y|$, then $S_2 - \widetilde{\phi}$ convergence coincides with double statistically convergence.*

Definition 8. *Let $\widetilde{\phi}$ be an Orlicz function. Let us define new sequence spaces $|\sigma_{1,1}|_{\widetilde{\phi}}$ and $N_{\Phi_{\xi,\eta}} - \widetilde{\phi}$ as follows:*

$$|\sigma_{1,1}|_{\widetilde{\phi}} = \left\{ y = (y_{r,s}) : for\ some\ \varpi,\ P - \lim_{z,w} \left(\frac{1}{zw} \sum_{r,s=1,1}^{z,w} \widetilde{\phi}(y_{r,s} - \varpi) \right) = 0 \right\}$$

and

$$N_{\Phi_{\xi,\eta}} - \widetilde{\phi} = \left\{ y = (y_{r,s}) : for\ some\ \varpi,\ P - \lim_{\xi,\eta} \left(\frac{1}{\gamma_{\xi,\eta}} \sum_{(r,s) \in J_{\xi,\eta}} \widetilde{\phi}(y_{r,s} - \varpi) \right) = 0 \right\}.$$

Note 3. *If $\widetilde{\phi}(y) = |y|$, then the spaces $|\sigma_{1,1}|_{\widetilde{\phi}}$ and $N_{\Phi_{\xi,\eta}} - \widetilde{\phi}$ coincide with $|\sigma_{1,1}|$ and $N_{\Phi_{\xi,\eta}}$, respectively, which were considered in [24].*

Definition 9. *Let $\widetilde{\phi}$ be an Orlicz function, and $\Phi_{\xi,\eta}$ be a double lacunary sequence. A sequence $y = (y_{r,s})$ is said to be double lacunary statistically $\widetilde{\phi}-$convergent to ϖ if for each $\varepsilon > 0$,*

$$P - \lim_{\xi,\eta} \frac{1}{\gamma_{\xi,\eta}} \left| \left\{ (r,s) \in J_{\xi,\eta} : \widetilde{\phi}(y_{r,s} - \varpi) \geq \varepsilon \right\} \right| = 0.$$

In this case, we write $S_{\Phi_{\xi,\eta}} - \widetilde{\phi}\, lim\, y = \varpi$ or $y_{r,s} \xrightarrow{P} \varpi(S_{\Phi_{\xi,\eta}} - \widetilde{\phi})$. We will denote the class of all double lacunary statistically $\widetilde{\phi}-$convergent sequences by $S_{\Phi_{\xi,\eta}} - \widetilde{\phi}$.

Note 4. *If $\widetilde{\phi}(y) = |y|$, then $S_{\Phi_{\xi,\eta}} - \widetilde{\phi}$ convergence coincides with $S_{\Phi_{\xi,\eta}}-$ convergence, which was studied by Savas and Patterson [24].*

Example 1. *Let $\widetilde{\phi}(y) = y^2$ and $\Phi_{\xi,\eta} = (2^\xi, 3^\eta)$. It is quite clear that $\widetilde{\phi}$ satisfies the $\triangle_2$ condition. Let us define the sequence $(y_{r,s})$ as follows:*

$$y_{r,s} = \begin{cases} \sqrt{rs}, & r = z^2 \text{ and } s = w^2, (z,w) \in \mathbb{N} \times \mathbb{N}; \\ \frac{1}{\sqrt{rs}}, & otherwise, \end{cases}$$

then the sequence $(y_{r,s})$ is $S_{\Phi_{\xi,\eta}} - \widetilde{\phi}$ convergent to 0 despite the fact that $(y_{r,s})$ is not convergent. To confirm, we obtain the following

$$\begin{aligned} & P - \lim_{\xi,\eta} \frac{1}{\gamma_{\xi,\eta}} \left| \left\{ (r,s) \in J_{\xi,\eta} : \widetilde{\phi}(y_{r,s} - \varpi) \geq \varepsilon \right\} \right| \\ = \;& P - \lim_{\xi,\eta} \frac{1}{2^{\xi-1}3^{\eta-1}} \left| \left\{ (r,s) \in (2^{\xi-1}, 3^{\xi}] \times (3^{\eta-1}, 3^\eta] : \widetilde{\phi}(y_{r,s} - 0) \geq \varepsilon \right\} \right| \\ = \;& P - \lim_{\xi,\eta} \frac{6}{2^{\xi-1}3^{\eta-1}} \left| \left\{ (r,s) \in (2^{\xi-1}, 2^{\xi}] \times (3^{\eta-1}, 3^\eta] :\, y_{r,s}^2 \geq \varepsilon \right\} \right| \\ \leq \;& P - \lim_{\xi,\eta} \frac{6}{2^{\xi-1}3^{\eta-1}} \left| \left\{ r \leq 2^\xi, s \leq 3^\eta : y_{r,s}^2 \geq \varepsilon \right\} \right| \\ = \;& P - \lim_{\xi,\eta} \frac{6}{zw} \left| \left\{ r \leq z, s \leq w :\, y_{r,s}^2 \geq \varepsilon \right\} \right| = 0. \end{aligned}$$

This demonstrates that the double sequence $(y_{r,s})$ is $S_{\Phi_{\xi,\eta}} - \widetilde{\phi}$ convergent to 0 even $(y_{r,s})$ is not convergent.

Example 2. *Let $\widetilde{\phi}$ be an Orlicz function with $\widetilde{\phi}(y) = |y|$, $\Phi_{\xi,\eta}$ be any double lacunary sequence, then the sequence $(y_{r,s})$ defined by $y_{r,s} = r^2 s^2$, for every $(r,s) \in \mathbb{N} \times \mathbb{N}$ is not $S_{\Phi_{\xi,\eta}} - \widetilde{\phi}$ convergent. To verify this let us hold any $\varpi \in \mathbb{R}$. Then $\varpi \leq 0$ or $\varpi > 0$. If $\varpi \leq 0$, choose $\varepsilon = \frac{1}{2}$, then for every $(r,s) \in \mathbb{N} \times \mathbb{N}$,*

$$R\left(\varepsilon\right) = \left\{ (r,s) \in J_{\xi,\eta} : |y_{r,s} - \varpi| \geq \varepsilon \right\} = J_{\xi,\eta}.$$

Hence, for $\varpi \leq 0$,

$$P-\lim_{\xi,\eta} \frac{1}{\gamma_{\xi,\eta}} \left|\left\{(r,s) \in J_{\xi,\eta} : |y_{r,s}-\varpi| \geq \varepsilon\right\}\right| = \lim_{\xi,\eta} \frac{1}{\gamma_{\xi,\eta}} |J_{\xi,\eta}| = 1.$$

If $\varpi > 0$, *then there exists* $(r_0, s_0) \in \mathbb{N} \times \mathbb{N}$ *in such a manner* $y_{r_0-1,s_0-1} \leq \varpi \leq y_{r_0,s_0}$. *In this circumstances, if* $\varpi < 1$, *by taking* $\varepsilon = \frac{1}{2} \min\{\varpi, 1-\varpi\}$, *we obtain*

$$R(\varepsilon) = \left\{(r,s) \in J_{\xi,\eta} : |y_{r,s}-\varpi| \geq \varepsilon\right\} = J_{\xi,\eta}.$$

Also, if $\varpi \geq 1$, *by taking* $\varepsilon = \frac{1}{2} \min\{\varpi - y_{r_0-1,s_0-1}, y_{r_0,s_0}-\varpi\}$, *we get*

$$R(\varepsilon) = \left\{(r,s) \in J_{\xi,\eta} : |y_{r,s}-\varpi| \geq \varepsilon\right\} = J_{\xi,\eta}.$$

Thus, for $\varpi > 0$,

$$\begin{aligned} & P-\lim_{\xi,\eta} \frac{1}{\gamma_{\xi,\eta}} \left|\left\{(r,s) \in J_{\xi,\eta} : |y_{r,s}-\varpi| \geq \varepsilon\right\}\right| \\ = \; & P-\lim_{\xi,\eta} \frac{1}{\gamma_{\xi,\eta}} |J_{\xi,\eta}| = 1. \end{aligned}$$

Definition 10. *A double sequence* $y = (y_{r,s})$ *is said to be double* $\widetilde{\phi}-$ *bounded with regard to the Orlicz function* $\widetilde{\phi}$, *if there exists* $\overline{M} > 0$ *such that* $\widetilde{\phi}(y_{r,s}) \leq \overline{M}$, *for every* $(r,s) \in \mathbb{N} \times \mathbb{N}$.

In subsequent theorem, we present the relationship between the spaces $N_{\Phi_{\xi,\eta}} - \widetilde{\phi}$ and $S_{\Phi_{\xi,\eta}} - \widetilde{\phi}$ and demonstrate that these two concepts are equivalent for double $\widetilde{\phi}-$ bounded spaces.

Theorem 1. *Let* $\Phi_{\xi,\eta} = (r_\xi, s_\eta)$ *be a double lacunary sequence, then*

(1) $y_{r,s} \xrightarrow{P} \varpi(N_{\Phi_{\xi,\eta}} - \widetilde{\phi})$ *implies* $y_{r,s} \xrightarrow{P} \varpi(S_{\Phi_{\xi,\eta}} - \widetilde{\phi})$, *and converse is not true.*

(2) *If* y *is double* $\widetilde{\phi}-$ *bounded and* $y_{r,s} \xrightarrow{P} \varpi(S_{\Phi_{\xi,\eta}} - \widetilde{\phi})$ *then* $y_{r,s} \xrightarrow{P} \varpi(N_{\Phi_{\xi,\eta}} - \widetilde{\phi})$.

Proof. (1) Provided that $\varepsilon > 0$ and $y_{r,s} \xrightarrow{P} \varpi(N_{\Phi_{\xi,\eta}} - \widetilde{\phi})$, then

$$\begin{aligned} \sum_{(r,s)\in J_{\xi,\eta}} \widetilde{\phi}(y_{r,s}-\varpi) \quad & \geq \sum_{\substack{(r,s)\in J_{\xi,\eta} \\ \widetilde{\phi}(y_{r,s}-\varpi)\geq\varepsilon}} \widetilde{\phi}(y_{r,s}-\varpi) \\ & \geq \varepsilon \left|\left\{(r,s) \in J_{\xi,\eta} : \widetilde{\phi}(y_{r,s}-\varpi) \geq \varepsilon\right\}\right| \end{aligned}$$

where the first result follows. In order to demonstrate the converse part, we will consider a double sequence which is in $S_{\Phi_{\xi,\eta}} - \widetilde{\phi}$ but not in $N_{\Phi_{\xi,\eta}} - \widetilde{\phi}$. For this, let $\widetilde{\phi}(y) = |y|$, proceeding as in Savas and Patterson [24], $\Phi_{\xi,\eta}$ be given and the sequence $(y_{r,s})$ is defined by

$$y_{r,s} = \begin{pmatrix} 1 & 2 & 3 & \cdots & \sqrt{\gamma_{\xi,\eta}} & 0 & \cdots \\ 2 & 2 & 3 & \cdots & \sqrt{\gamma_{\xi,\eta}} & 0 & \cdots \\ \vdots & \vdots & \vdots & \vdots & \vdots & \vdots & \vdots \\ \sqrt{\gamma_{\xi,\eta}} & \sqrt{\gamma_{\xi,\eta}} & \cdots & \cdots & \sqrt{\gamma_{\xi,\eta}} & 0 & \cdots \\ 0 & 0 & 0 & 0 & 0 & 0 & \vdots \end{pmatrix}.$$

Note that $y_{r,s}$ is not double bounded. It was displayed in Savas and Patterson [24] that $y_{r,s} \overset{P}{\to} 0(S_{\Phi_{\xi,\eta}})$. However, $y_{r,s}$ is not convergent to 0 $(N_{\Phi_{\xi,\eta}})$. From Note 2.3 and 2.4 we conclude that $y_{r,s} \overset{P}{\to} 0(S_{\Phi_{\xi,\eta}} - \widetilde{\phi})$, yet $y_{r,s}$ is not convergent to 0 $(N_{\Phi_{\xi,\eta}} - \widetilde{\phi})$. Therefore, $(N_{\Phi_{\xi,\eta}} - \widetilde{\phi}) \subseteq (S_{\Phi_{\xi,\eta}} - \widetilde{\phi})$.

(2) Let $y_{r,s} \overset{P}{\to} \varpi(S_{\Phi_{\xi,\eta}} - \widetilde{\phi})$ and y is double $\widetilde{\phi}-$ bounded, in other way $\widetilde{\phi}(y_{r,s}) \leq \overline{M}$ for every $(r,s) \in \mathbb{N} \times \mathbb{N}$. For $\varepsilon > 0$, we obtain

$$\begin{aligned} \frac{1}{\gamma_{\xi,\eta}} \sum_{(r,s)\in J_{\xi,\eta}} \widetilde{\phi}(y_{r,s} - \varpi) &= \frac{1}{\gamma_{\xi,\eta}} \sum_{\substack{(r,s)\in J_{\xi,\eta} \\ \widetilde{\phi}(y_{r,s}-\varpi)\geq\varepsilon}} \widetilde{\phi}(y_{r,s} - \varpi) + \frac{1}{\gamma_{\xi,\eta}} \sum_{\substack{(r,s)\in J_{\xi,\eta} \\ \widetilde{\phi}(y_{r,s}-\varpi)<\varepsilon}} \widetilde{\phi}(y_{r,s} - \varpi) \\ &\leq \frac{\overline{M} + \widetilde{\phi}(\varpi)}{\gamma_{\xi,\eta}} \left| \left\{ (r,s) \in J_{\xi,\eta} : \widetilde{\phi}(y_{r,s} - \varpi) \geq \varepsilon \right\} \right| + \varepsilon \end{aligned}$$

which gives us the result.

□

Note 5. *From (1) and (2) of the above theorem, we conclude that if y is double $\widetilde{\phi}-$ bounded, then $S_{\Phi_{\xi,\eta}} - \widetilde{\phi} = N_{\Phi_{\xi,\eta}} - \widetilde{\phi}$.*

In the following theorems we examine the relationship between $S_{\Phi_{\xi,\eta}} - \widetilde{\phi}$ and $S_2 - \widetilde{\phi}$ under certain restrictions on $\Phi_{\xi,\eta} = (r_\xi, s_\eta)$.

Theorem 2. *For any double lacunary sequence $\Phi_{\xi,\eta}$ and any Orlicz function $\widetilde{\phi}$, $S_2 - \widetilde{\phi}\ lim\, y = \varpi$ implies $S_{\Phi_{\xi,\eta}} - \widetilde{\phi}\ lim\, y = \varpi$ if and only if $\liminf_{\xi} \zeta_\xi > 1$ and $\liminf_{\eta} \overline{\zeta}_\eta > 1$. Provided that $\liminf_{\xi} \zeta_\xi = 1$ and $\liminf_{\eta} \overline{\zeta}_\eta = 1$, then there exists a double bounded $S_2 - \widetilde{\phi}$ double sequence that is not $S_{\Phi_{\xi,\eta}} - \widetilde{\phi}$.*

Proof. (Sufficiency) Suppose that $\liminf_{\xi} \zeta_\xi > 1$ and $\liminf_{\eta} \overline{\zeta}_\eta > 1$, then there exists a $\overline{\delta} > 0$ such that $\zeta_\xi > 1 + \overline{\delta}$ and $\overline{\zeta}_\eta > 1 + \overline{\delta}$ for sufficiently large ξ and η, which implies that $\frac{\gamma_{\xi,\eta}}{r_{\xi,\eta}} > \frac{\overline{\delta}}{1+\overline{\delta}}$. If $y_{r,s} \overset{P}{\to} \varpi(S_2 - \widetilde{\phi})$, then for every $\varepsilon > 0$ and for sufficiently large ξ and η, we are granted the following

$$\begin{aligned}\frac{1}{\gamma_{\xi,\eta}}\left|\left\{(r,s)\in J_{\xi,\eta}:\widetilde{\phi}(y_{r,s}-\varpi)\geq\varepsilon\right\}\right| &= \frac{r_{\xi,\eta}}{\gamma_{\xi,\eta}}\frac{1}{r_{\xi,\eta}}\left|\left\{(r,s)\in J_{\xi,\eta}:\widetilde{\phi}(y_{r,s}-\varpi)\geq\varepsilon\right\}\right| \\ &\leq \frac{1+\overline{\delta}}{\overline{\delta}}\frac{1}{r_{\xi,\eta}}\left|\left\{r\leq r_{\xi},s\leq s_{\eta}:\widetilde{\phi}(y_{r,s}-\varpi)\geq\varepsilon\right\}\right|.\end{aligned}$$

Thus, $y_{r,s}\overset{P}{\to}\varpi(S_{\Phi_{\xi,\eta}}-\widetilde{\phi})$.

(Necessity) Assume that $\underset{\xi}{lim\,inf}\,\zeta_{\xi}=1$ or $\underset{\eta}{lim\,inf}\,\overline{\zeta}_{\eta}=1$ and consider a sequence which is $S_2-\widetilde{\phi}$ convergent, but not $S_{\Phi_{\xi,\eta}}-\widetilde{\phi}$ convergent. For this, let $\widetilde{\phi}(y)=|y|$ and let us select a double subsequence $(r_{\xi_{\overline{i}},\eta_{\overline{j}}}=r_{\xi_{\overline{i}}}s_{\eta_{\overline{j}}})$ of the double lacunary sequence $\Phi_{\xi,\eta}$ such that $\frac{r_{\xi_{\overline{i}}}}{r_{\xi_{\overline{i}-1}}}<1+\frac{1}{\overline{i}}$, $\frac{s_{\eta_{\overline{j}}}}{s_{\eta_{\overline{j}-1}}}<1+\frac{1}{\overline{j}}$, $\frac{r_{\xi_{\overline{i}}-1}}{r_{\xi_{\overline{i}-1}}}>\overline{i}$, and $\frac{s_{\eta_{\overline{j}}-1}}{s_{\eta_{\overline{j}-1}}}>\overline{j}$ where $\xi_{\overline{i}}\geq\xi_{\overline{i}-1}+2$ and $\eta_{\overline{j}}\geq\eta_{\overline{j}-1}+2$. Also, let us define $y=(y_{\overline{i},\overline{j}})$ by

$$y_{\overline{i},\overline{j}}=\begin{cases}1, & \text{if } (r,s)\in J_{\xi_{\overline{i}},\eta_{\overline{j}}},\ \overline{i},\overline{j}=1,2,3...\\ 0, & \text{otherwise.}\end{cases}$$

Then for any real ϖ, we are granted the following

$$\frac{1}{\gamma_{\xi_{\overline{i}},\eta_{\overline{j}}}}\sum_{J_{\xi_{\overline{i}},\eta_{\overline{j}}}}\left|y_{\overline{i},\overline{j}}-\varpi\right|=|1-\varpi|\ \text{ for } \overline{i},\overline{j}=1,2,3,...,$$

and

$$\frac{1}{\gamma_{\xi_{\overline{i}},\eta_{\overline{j}}}}\sum_{J_{\xi,\eta}}\left|y_{\overline{i},\overline{j}}-\varpi\right|=|\varpi|\,,\text{for } \xi\neq\xi_{\overline{i}} \text{ and } \eta\neq\eta_{\overline{j}}.$$

That means

$$P-\underset{\xi,\eta}{lim}\frac{1}{\gamma_{\xi,\eta}}\left|\left\{(r,s)\in J_{\xi,\eta}:\widetilde{\phi}(y_{r,s}-\varpi)\geq\varepsilon\right\}\right|\neq 0.$$

Therefore, y is not $S_{\Phi_{\xi,\eta}}-\widetilde{\phi}$ convergent to ϖ. However, y is $S_2-\widetilde{\phi}-$convergent, since if $\overline{t}$ and $\overline{v}$ are any quite enough large integers we can identify the unique $\overline{i}$ and $\overline{j}$ for which $r_{\xi_{\overline{i}}-1}<\overline{t}\leq r_{\xi_{\overline{i}+1}-1}$ and $s_{\eta_{\overline{j}}-1}<\overline{v}\leq s_{\eta_{\overline{j}+1}-1}$, and we write the following

$$\begin{aligned}\frac{1}{\overline{t}\overline{v}}\sum_{\overline{i},\overline{j}=1,1}^{\overline{t}\overline{v}}\widetilde{\phi}\left(y_{\overline{i},\overline{j}}\right) &= \frac{1}{\overline{t}\overline{v}}\sum_{\overline{i},\overline{j}=1,1}^{\overline{t}\overline{v}}\left|y_{\overline{i},\overline{j}}\right| \\ &\leq \left(\frac{r_{\xi_{\overline{i}}-1}+\gamma_{\xi_{\overline{i}}}}{r_{\xi_{\overline{i}}-1}}\right)\cdot\left(\frac{s_{\eta_{\overline{j}}-1}+\overline{\gamma}_{\eta_{\overline{j}}}}{s_{\eta_{\overline{j}}-1}}\right)\end{aligned}$$

$$\begin{aligned}
&\leq \frac{r_{\xi_{\bar{i}}-1,\eta_{\bar{j}}-1}}{r_{\xi_{\bar{i}}-1,\eta_{\bar{j}}-1}} + \frac{r_{\xi_{\bar{i}}-1}\overline{\gamma}_{s_{\bar{j}}}}{r_{\xi_{\bar{i}}-1,\eta_{\bar{j}}-1}} + \frac{\gamma_{\xi_{\bar{i}}} s_{\eta_{\bar{j}}-1}}{r_{\xi_{\bar{i}}-1,\eta_{\bar{j}}-1}} + \frac{\gamma_{\xi_{\bar{i}}}\overline{\gamma}_{\eta_{\bar{j}}}}{r_{\xi_{\bar{i}}-1,\eta_{\bar{j}}-1}} \\
&\leq 1 + \frac{\overline{\gamma}_{\eta_{\bar{j}}}}{s_{\eta_{\bar{j}}-1}} + \frac{\gamma_{\xi_{\bar{i}}}}{r_{\xi_{\bar{i}}-1}} + \frac{\gamma_{\xi_{\bar{i}}}\overline{\gamma}_{\eta_{\bar{j}}}}{r_{\xi_{\bar{i}}-1,\eta_{\bar{j}}-1}} \\
&\leq 1 + \frac{\left(s_{\eta_{\bar{j}}} - s_{\eta_{\bar{j}}-1}\right)}{s_{\eta_{\bar{j}}-1}} + \frac{\left(r_{\xi_{\bar{i}}} - r_{\xi_{\bar{i}}-1}\right)}{r_{\xi_{\bar{i}}-1}} + \left(\frac{r_{\xi_{\bar{i}}} - r_{\xi_{\bar{i}}-1}}{r_{\xi_{\bar{i}}-1}}\right)\left(\frac{s_{\eta_{\bar{j}}} - s_{\eta_{\bar{j}}-1}}{s_{\eta_{\bar{j}}-1}}\right) \\
&\leq 1 + \frac{s_{\eta_{\bar{j}}}}{s_{\eta_{\bar{j}}-1}} - 1 + \frac{r_{\xi_{\bar{i}}}}{r_{\xi_{\bar{i}}-1}} - 1 + \left(\frac{r_{\xi_{\bar{i}}}}{r_{\xi_{\bar{i}}-1}} - 1\right)\left(\frac{s_{\eta_{\bar{j}}}}{s_{\eta_{\bar{j}}-1}} - 1\right) \\
&\leq \left(1 + \frac{1}{\bar{i}}\right) + \left(1 + \frac{1}{\bar{j}}\right) + \frac{1}{\bar{i}}\frac{1}{\bar{j}} - 1 \\
&\leq 1 + \frac{1}{\bar{\bar{i}}} + \frac{1}{\bar{\bar{j}}} + \frac{1}{\bar{\bar{i}}}\frac{1}{\bar{\bar{j}}}
\end{aligned}$$

as $\bar{t} \to \infty$ and $\overline{v} \to \infty$, it follows that $\bar{i}, \bar{j} \to \infty$. Thus, from Note 2, y is $S_2 - \widetilde{\phi}$ convergent. □

The following example demonstrates that there exists a $S_{\Phi_{\xi,\eta}} - \widetilde{\phi}$ convergent sequence which has a double subsequence that is not $S_{\Phi_{\xi,\eta}} - \widetilde{\phi}$–convergent.

Example 3. *Let $\Phi_{\xi,\eta} = (2^{\xi}, 3^{\eta})$ be the double lacunary sequence, $\widetilde{\phi}(y) = |y|$ be an Orlicz function and $(y_{r,s})$ is defined by*

$$y_{r,s} = \begin{cases} rs, & r = z^2 \text{ and } s = w^2, (z,w) \in \mathbb{N} \times \mathbb{N} \\ \frac{1}{rs}, & \text{otherwise} \end{cases}$$

then the sequence $(y_{r,s})$ is $S_{\Phi_{\xi,\eta}} - \widetilde{\phi}$ convergent to 0. However, $(y_{r,s})$ has a double subsequence, which is not $S_{\Phi_{\xi,\eta}} - \widetilde{\phi}$ convergent.

Theorem 3. *For any lacunary sequence $\Phi_{\xi,\eta}$ and any Orlicz function $\widetilde{\phi}$, $S_{\Phi_{\xi,\eta}} - \widetilde{\phi}$ $\lim y = \varpi$ implies $S_2 - \widetilde{\phi}$ $\lim y = \varpi$ if and only if $\limsup_{\xi} \zeta_{\xi} < \infty$ and $\limsup_{\eta} \overline{\zeta}_{\eta} < \infty$. If $\limsup_{\xi} \zeta_{\xi} = \infty$ and $\limsup_{\eta} \overline{\zeta}_{\eta} = \infty$ then there exists a double bounded $S_{\Phi_{\xi,\eta}} - \widetilde{\phi}$ summable sequence that is not $S_2 - \widetilde{\phi}$.*

Proof. If $\limsup_{\xi} \zeta_{\xi} < \infty$ and $\limsup_{\eta} \overline{\zeta}_{\eta} < \infty$, then there is an $\widehat{H} > 0$ such that $\zeta_{\xi} < \widehat{H}$ and $\overline{\zeta}_{\eta} < \widehat{H}$ for all ξ and η. It is assumed that $y_{r,s} \xrightarrow{P} \varpi(S_{\Phi_{\xi,\eta}} - \widetilde{\phi})$, and let

$$N_{\xi,\eta} = \left|\left\{(r,s) \in J_{\xi,\eta} : \widetilde{\phi}(y_{r,s} - \varpi) \geq \varepsilon\right\}\right|.$$

By the definition of $S_{\Phi_{\xi,\eta}} - \widetilde{\phi}$ convergent and given any $\varepsilon' > 0$, there is an $\xi_0, \eta_0 \in \mathbb{N}$ such that $\frac{N_{\xi,\eta}}{\gamma_{\xi,\eta}} < \varepsilon'$ for all $\xi > \xi_0$ and $\eta > \eta_0$. Now let

$$M = max\{N_{\xi,\eta} : 1 \le \xi \le \xi_0 \ \& \ 1 \le \eta \le \eta_0\}$$

and let z and w be any integers satisfying $r_{\xi-1} < z \le r_\xi$ and $s_{\eta-1} < w \le s_\eta$; then we can write

$$\begin{aligned}
& \frac{1}{zw}\left|\left\{r \le z,\ s \le w : \widetilde{\phi}(y_{r,s} - \varpi) \ge \varepsilon\right\}\right| \\
\le\ & \frac{1}{r_{\xi-1}s_{\eta-1}}\left|\left\{r \le r_\xi, s \le s_\eta : \widetilde{\phi}(y_{r,s} - \varpi) \ge \varepsilon\right\}\right| \\
=\ & \frac{1}{r_{\xi-1}s_{\eta-1}}\left\{N_{1,1} + N_{2,2} + \cdots + N_{\xi_0+1,\eta_0+1} + \cdots + N_{\xi,\eta}\right\} \\
\le\ & \frac{M^2}{r_{\xi-1}s_{\eta-1}}\xi_0\eta_0 \\
& + \frac{1}{r_{\xi-1}s_{\eta-1}}\left\{\gamma_{\xi_0+1,\eta_0+1}\frac{N_{\xi_0+1,\eta_0+1}}{\gamma_{\xi_0+1,\eta_0+1}} + \cdots + \gamma_{\xi,\eta}\frac{N_{\xi,\eta}}{\gamma_{\xi,\eta}}\right\} \\
\le\ & \frac{\xi_0\eta_0M^2}{r_{\xi-1}s_{\eta-1}} + \\
& \frac{1}{r_{\xi-1}s_{\eta-1}}\Big(\sup_{\xi>\xi_0 \& \ \eta>\eta_0}\frac{N_{\xi,\eta}}{\gamma_{\xi,\eta}}\Big)\{\gamma_{\xi_0+1,\eta_0+1} + \cdots\cdots + \gamma_{\xi,\eta}\} \\
\le\ & \frac{\xi_0 M}{r_{\xi-1}}\frac{\eta_0 M}{s_{\eta-1}} + \varepsilon'\frac{r_\xi - r_{\xi_0}}{r_{\xi-1}}\frac{s_\eta - s_{\eta_0}}{s_{\eta-1}} \\
\le\ & \frac{\xi_0 M}{r_{\xi-1}}\frac{\eta_0 M}{s_{\eta-1}} + \varepsilon'\zeta_\xi\overline{\zeta}_\eta \le \frac{\xi_0 M}{r_{\xi-1}}\frac{\eta_0 M}{s_{\eta-1}} + \varepsilon'\widehat{H}^2.
\end{aligned}$$

For converse, suppose that $\lim\sup_\xi \zeta_\xi = \infty$ and $\lim\sup_\eta \overline{\zeta}_\eta = \infty$ and consider a sequence which is $S_{\Phi_{\xi,\eta}} - \widetilde{\phi}$ convergent, but not $S_2 - \widetilde{\phi}$ convergent. For this, let $\widetilde{\phi}(y) = |y|$ and select a double subsequence $(r_{\xi_{\overline{i}},\eta_{\overline{j}}})$ of the double lacunary sequence $\Phi_{\xi,\eta} = (r_\xi, s_\eta)$ such that $\zeta_{\xi_{\overline{i}}} > \overline{i}$ and $\overline{\zeta}_{\eta_{\overline{j}}} > \overline{j}$ define a double bounded sequence $y = (y_{z,w})$ by

$$y_{z,w} = \begin{cases} 1, & r_{\xi_{\overline{i}}-1} < z \le 2r_{\xi_{\overline{i}}-1} \ \& \ s_{\eta_{\overline{j}}-1} < w \le 2s_{\eta_{\overline{j}}-1} \text{ for } \overline{i},\ \overline{j} = 1,2,3... \\ 0, & otherwise. \end{cases}$$

Hence, $y \in N_{\Phi_{\xi,\eta}}$ but $y \notin |\sigma_{1,1}|$. From [24], y is $S_{\Phi_{\xi,\eta}}$-convergent. The above Note 2.4 implies that y is $S_{\Phi_{\xi,\eta}} - \widetilde{\phi}$ convergent, but y is not S_2-convergent. Consequently, by above Note 2 implies y is not $S_2 - \widetilde{\phi}$ convergent.

□

By combining the above two theorems let us present following theorem.

Theorem 4. *Let $\Phi_{\xi,\eta}$ be any double lacunary sequence; then $S_2-\widetilde{\phi} = S_{\Phi_{\xi,\eta}}-\widetilde{\phi}$ if and only if*

$$1 < \liminf_{\xi} \zeta_\xi \le \limsup_{\xi} \zeta_\xi < \infty$$

and

$$1 < \liminf_{\eta} \overline{\zeta}_\eta \le \limsup_{\eta} \overline{\zeta}_\eta < \infty.$$

Theorem 5. *Let $\Phi_{\xi,\eta}$ be any double lacunary sequence and $\widetilde{\phi}$ be an Orlicz function. If the sequence $(y_{r,s})$ is $S_{\Phi_{\xi,\eta}}-\widetilde{\phi}$ convergent, then $S_{\Phi_{\xi,\eta}}-\widetilde{\phi}$ limit of $(y_{r,s})$ is unique.*

Proof. Let $S_{\Phi_{\xi,\eta}}-\widetilde{\phi}\, lim\, y_{r,s} = \varpi_0$ and $S_{\Phi_{\xi,\eta}}-\widetilde{\phi}\ lim\, y_{r,s} = \kappa_0$. Then

$$P-\lim_{\xi,\eta} \frac{1}{\gamma_{\xi,\eta}} \left|\left\{(r,s)\in J_{\xi,\eta} : \widetilde{\phi}(y_{r,s}-\varpi_0) \ge \varepsilon\right\}\right| = 0$$

and

$$P-\lim_{\xi,\eta} \frac{1}{\gamma_{\xi,\eta}} \left|\left\{(r,s)\in J_{\xi,\eta} : \widetilde{\phi}(y_{r,s}-\kappa_0) \ge \varepsilon\right\}\right| = 0$$

i.e.

$$\begin{aligned} & P-\lim_{\xi,\eta} \frac{1}{\gamma_{\xi,\eta}} \left|\left\{(r,s)\in J_{\xi,\eta} : \widetilde{\phi}(y_{r,s}-\varpi_0) < \varepsilon\right\}\right| \\ = \quad & 1 = P-\lim_{\xi,\eta} \frac{1}{\gamma_{\xi,\eta}} \left|\left\{(r,s)\in J_{\xi,\eta} : \widetilde{\phi}(y_{r,s}-\kappa_0) < \varepsilon\right\}\right|. \end{aligned}$$

Let us consider such $(r,s)\in J_{\xi,\eta}$ for which both of $\widetilde{\phi}(y_{r,s}-\varpi_0) < \varepsilon$ and $\widetilde{\phi}(y_{r,s}-\kappa_0) < \varepsilon$ are true. For such $(r,s)\in J_{\xi,\eta}$ we have

$$\begin{aligned} \widetilde{\phi}\left(\frac{1}{2}(\varpi_0-\kappa_0)\right) &= \widetilde{\phi}\left(\frac{1}{2}(\varpi_0 - y_{r,s} + y_{r,s} - \kappa_0)\right) \\ &\le \frac{1}{2}\widetilde{\phi}(y_{r,s}-\varpi_0) + \frac{1}{2}\widetilde{\phi}(y_{r,s}-\kappa_0) = \varepsilon. \end{aligned}$$

□

For the consequence we presume the Orlicz function which fulfils $\triangle_2$ condition, unless otherwise claimed.

Theorem 6. *If $(y_{r,s})$ and $(z_{r,s})$ are $S_{\Phi_{\xi,\eta}}-\widetilde{\phi}$ convergent and α is any real constant, then*

(1) $(y_{r,s}+z_{r,s})$ is $S_{\Phi_{\xi,\eta}}-\widetilde{\phi}$ convergent and $S_{\Phi_{\xi,\eta}}-\widetilde{\phi}\ lim\,(y_{r,s}+z_{r,s}) = S_{\Phi_{\xi,\eta}}-\widetilde{\phi}\ lim\, y_{r,s} + S_{\Phi_{\xi,\eta}}-\widetilde{\phi}\, lim\, z_{r,s}$,

(2) $(\alpha y_{r,s})$ is $S_{\Phi_{\xi,\eta}}-\widetilde{\phi}$ convergent and $S_{\Phi_{\xi,\eta}}-\widetilde{\phi}\ lim\,(\alpha y_{r,s}) = \alpha.\, S_{\theta_{\xi,\eta}}-\widetilde{\phi}\ lim\, y_{r,s}$.

Proof. Since $\widetilde{\phi}$ fullfils the $\triangle_2-$ condition, then there exists $\overline{M} > 0$ such that $\widetilde{\phi}(2y) \leq \overline{M}.\widetilde{\phi}(y)$, for every $y \in \mathbb{R}$.

(1) Let $S_{\Phi_{\xi,\eta}} - \widetilde{\phi}\, lim\, y_{r,s} = L$ and $S_{\Phi_{\xi,\eta}} - \widetilde{\phi}\ lim\, z_{r,s} = \varpi$

i.e.

$$\begin{aligned} & P - \lim_{\xi,\eta} \frac{1}{\gamma_{\xi,\eta}} \left| \left\{ (r,s) \in J_{\xi,\eta} : \widetilde{\phi}(y_{r,s} - \varpi) \geq \varepsilon \right\} \right| \\ = \quad & 0 = P - \lim_{\xi,\eta} \frac{1}{\gamma_{\xi,\eta}} \left| \left\{ (r,s) \in J_{\xi,\eta} : \widetilde{\phi}(z_{r,s} - \kappa) \geq \varepsilon \right\} \right| \end{aligned}$$

i.e.

$$\begin{aligned} & P - \lim_{\xi,\eta} \frac{1}{\gamma_{\xi,\eta}} \left| \left\{ (r,s) \in J_{\xi,\eta} : \widetilde{\phi}(y_{r,s} - \varpi) < \varepsilon \right\} \right| \\ = \quad & 1 = P - \lim_{\xi,\eta} \frac{1}{\gamma_{\xi,\eta}} \left| \left\{ (r,s) \in J_{\xi,\eta} : \widetilde{\phi}(z_{r,s} - \kappa) < \varepsilon \right\} \right|. \end{aligned}$$

Let us consider such $(r,s) \in J_{\xi,\eta}$ for which both of $\widetilde{\phi}(y_{r,s} - \varpi) < \frac{\varepsilon}{2\overline{M}}$ and $\widetilde{\phi}(z_{r,s} - \kappa) < \frac{\varepsilon}{2\overline{M}}$ are true. Then for such $(r,s) \in J_{\xi,\eta}$, we are granted the following

$$\begin{aligned} \widetilde{\phi}((y_{r,s} + z_{r,s}) - (\varpi + \kappa)) &= \widetilde{\phi}((y_{r,s} - \varpi) + (z_{r,s} - \kappa)) \leq \widetilde{\phi}(2(y_{r,s} - \varpi) + 2(z_{r,s} - \kappa)) \\ &\leq \overline{M}(\widetilde{\phi}(y_{r,s} - \varpi) + \widetilde{\phi}(z_{r,s} - \kappa)) = \overline{M}.\left(\frac{\varepsilon}{2\overline{M}} + \frac{\varepsilon}{2\overline{M}} \right) = \varepsilon. \end{aligned}$$

Therefore,

$$P - \lim_{\xi,\eta} \frac{1}{\gamma_{\xi,\eta}} \left| \left\{ (r,s) \in J_{\xi,\eta} : \widetilde{\phi}(y_{r,s} + z_{r,s} - \varpi - \kappa) < \varepsilon \right\} \right| = 1$$

i.e.

$$P - \lim_{\xi,\eta} \frac{1}{\gamma_{\xi,\eta}} \left| \left\{ (r,s) \in J_{\xi,\eta} : \widetilde{\phi}(y_{r,s} + z_{r,s} - \varpi - \kappa) \geq \varepsilon \right\} \right| = 0$$

that means

$S_{\Phi_{\xi,\eta}} - \widetilde{\phi}\ lim\,(y_{r,s} + z_{r,s}) = \varpi + \kappa = S_{\Phi_{\xi,\eta}} - \widetilde{\phi}\ \ lim\, y_{r,s} + S_{\Phi_{\xi,\eta}} - \widetilde{\phi}\ \ lim\, z_{r,s}$.

(2) Let $p \in \mathbb{N}$ such that $|\alpha| \leq 2^p$ and $S_{\Phi_{\xi,\eta}} - \widetilde{\phi}\ lim\, y_{r,s} = \varpi$, then

$$P - \lim_{\xi,\eta} \frac{1}{\gamma_{\xi,\eta}} \left| \left\{ (r,s) \in J_{\xi,\eta} : \widetilde{\phi}(y_{r,s} - \varpi) < \varepsilon \right\} \right| = 1.$$

Let us consider such $(r,s) \in J_{\xi,\eta}$ for which $\widetilde{\phi}(y_{r,s} - \varpi) < \frac{\varepsilon}{2^p}$, then

$$\begin{aligned} \widetilde{\phi}(\alpha(y_{r,s} - \varpi)) &= \widetilde{\phi}(|\alpha|\,(y_{r,s} - \varpi)) \leq \widetilde{\phi}(2^p(y_{r,s} - \varpi)) \\ &\leq 2^p\widetilde{\phi}(y_{r,s} - \varpi) \leq 2^p.\frac{\varepsilon}{2^p} = \varepsilon. \end{aligned}$$

Hence,

$$P - \lim_{\xi,\eta} \frac{1}{\gamma_{\xi,\eta}} \left| \left\{ (r,s) \in J_{\xi,\eta} : \widetilde{\phi}(\alpha(y_{r,s} - \varpi)) < \varepsilon \right\} \right| = 1,$$

i.e.

$$P - \lim_{\xi,\eta} \frac{1}{\gamma_{\xi,\eta}} \left| \left\{ (r,s) \in J_{\xi,\eta} : \widetilde{\phi}(\alpha(y_{r,s} - \varpi)) \geq \varepsilon \right\} \right| = 0.$$

Thus, $S_{\Phi_{\xi,\eta}} - \widetilde{\phi}\ lim\,(\alpha y_{r,s}) = \alpha.y = \alpha.\, S_{\Phi_{\xi,\eta}} - \widetilde{\phi}\ lim\, y_{r,s}$. This concludes the proof of the theorem. □

Acknowledgement The author is sincerely grateful to the referees for their useful remarks.

Declaration of Competing Interests The author declares that she has no conflict of interest and this article does not contain any studies with human participants performed by the author.

References

[1] Alotaibi, A., Mursaleen, M., Raj, K., Double sequence spaces by means of Orlicz functions, *Abstr. Appl. Anal.*, Article ID 260326 (2014). https://doi.org/ 10.1155/2014/260326

[2] Çolak, R., Altin, Y., Statistical convergence of double sequences of order α, *J. Funct. Spaces Appl.*, Article ID 682823 (2013). https://doi.org/10.1155/2013/682823

[3] Demirci, I. A., Gürdal, M., Lacunary statistical convergence for sets of triple sequences via Orlicz function, *Theory. App. Math. & Computer Sci.*, 11(1) (2021), 1-13.

[4] Demirci, I. A., Gürdal, M., On lacunary statistically $\phi-$convergence for triple sequences of sets via ideals, *J. Appl. Math. and Inf.*, 40(3-4) (2022), 433-444. https://doi.org/10.14317/jami.2022.433

[5] Et, M., Nuray, F., m-statistical convergence, *Indian J. Pure Appl. Math*,, 32(6) (2001), 961-969.

[6] Fast, H., Sur la convergence statistique, *Colloq. Math.*, 2 (1951), 241-244.

[7] Fridy, J.A., On statistical convergence, *Analysis*, 5 (1985), 301-313.

[8] Huban, M. B., Gürdal, M., Wijsman lacunary invariant statistical convergence for triple sequences via Orlicz function, *J. Class. Anal.*, 17(2) (2021), 119-128. https://doi.org/10.7153/jca-2021-17-08

[9] Huban, M. B., Gürdal, M., Deferred invariant statistical convergent triple sequences via Orlicz function, *Bull. Math. Sci. Appl.*, 13(3) (2021), 25-38.

[10] Huban, M. B., Gürdal, M., On asymptotically lacunary statistical equivalent triple sequences via ideals and Orlicz function, *Honam Math. J.*, 43(2) (2021), 343-357.

[11] Huban, M. B., Gürdal, M., On asymptotically invariant $\lambda-$statistical $\phi-$equivalent triple sequences, *Electron. J. Math. Anal. Appl.*, 10(1) (2022), 175-183.

[12] Kişi, Ö., Güler, E., Deferred statistical convergence of double sequences in intuitionistic fuzzy normed linear spaces, *Turk. J. Math. and Comp. Sci.*, 11 (2019), 95-104.

[13] Khan, V., Khan, N., Esi, A., Tabassum, S., I-pre-Cauchy double sequences and Orlicz functions, *Engineering*, 5(5A) (2013), 52-356. https:// 10.4236/eng.2013.55A008

[14] Krasnoselski, M. A., Rutitsky, Y. B., Convex Functions and Orlicz Spaces, Groningen, Netherlands, 1961.

[15] Lindenstrauss, J., Tzafriri, L., On Orlicz sequence spaces, *Isr. J. Math.*, 10(3) (1971), 379-390.

[16] Miller, H. I., A measure theoretical subsequence characterization of statistical convergence, *Trans. Amer. Math. Soc.*, 347 (1995), 1811-1819.

[17] Mohiuddine, S. A., Raj, K., Alotaibi, A., Generalized spaces of double sequences for Orlicz functions and bounded-regular matrices over n-Normed spaces, *J. Inequal. Appl.*, 332 (2014). https://doi.org/10.1186/1029-242X-2014-332

[18] Mursaleen, M., Edely, O. H., Statistical convergence of double sequences, *J. Math. Anal. Appl.*, 288 (2003), 223-231.

[19] Mursaleen, M., Cakan, C., Mohiuddine, S. A., Savas, E., Generalized statistical convergence and statistical core of double sequences, *Acta Math. Sin. Engl. Ser.*, 26(11) (2010), 2131-2144.

[20] Pringsheim, A., Zur theorie der zweifach unendlichen zahlen folgen, *Math. Ann.*, 53 (1900), 289-321.

[21] Savas, E., Patterson, R. F., Some $\sigma-$double sequence spaces defined by Orlicz function, *J. Math. Anal. Appl.*, 324 (2006), 525-531.

[22] Savas, E., Lacunary statistical convergence of double sequences in topological groups, *J. Inequal. Appl.*, 480 (2014). https://doi.org/10.1186/1029-242X-2014-480

[23] Savas, E., $I_\lambda-$double statistical convergence of order α in topological groups, *Ukrainian Math. J.*, 68 (2016), 1251-1258.

[24] Savas, E., Patterson, R. F., Lacunary statistical convergence of multiple sequences, *Appl. Math. Lett.*, 19 (2006), 527-534. https://doi.org/10.1016/j.aml.2005.06.018

[25] Schoenberg, I. J., The integrability of certain functions and related summability methods, *Amer. Math. Monthly.*, 66 (1959), 361-375.

[26] Steinhaus, H., Sur la convergence ordinaire et la convergence asymptotique, *Colloq. Math.*, 2 (1951), 73-74.

[27] Zygmund, A., Trigonometric Series, Cambridge University Press, New York, NY, USA, 1st edition, 1959.

http://communications.science.ankara.edu.tr

Commun.Fac.Sci.Univ.Ank.Ser. A1 Math. Stat.
Volume 72, Number 2, Pages 462–481 (2023)
DOI:10.31801/cfsuasmas.1163955
ISSN 1303-5991 E-ISSN 2618-6470

COMMUNICATIONS SERIES A1

Research Article; Received:August 18, 2022; Accepted: October 26, 2022

ON SOLUTIONS OF THREE-DIMENSIONAL SYSTEM OF DIFFERENCE EQUATIONS WITH CONSTANT COEFFICIENTS*

Merve KARA[1] and Ömer AKTAŞ[2]
[1]Department of Mathematics, Kamil Ozdag Science Faculty Karamanoglu Mehmetbey University, Karaman, TÜRKİYE
[2]Department of Mathematics, Kamil Ozdag Science Faculty Karamanoglu Mehmetbey University, Karaman, TÜRKİYE

Abstract. In this study, we show that the system of difference equations

$$x_n = \frac{x_{n-2}y_{n-3}}{y_{n-1}\left(a + bx_{n-2}y_{n-3}\right)},$$
$$y_n = \frac{y_{n-2}z_{n-3}}{z_{n-1}\left(c + dy_{n-2}z_{n-3}\right)}, n \in \mathbb{N}_0,$$
$$z_n = \frac{z_{n-2}x_{n-3}}{x_{n-1}\left(e + fz_{n-2}x_{n-3}\right)},$$

where the initial values x_{-i}, y_{-i}, z_{-i}, $i = \overline{1,3}$ and the parameters a, b, c, d, e, f are non-zero real numbers, can be solved in closed form. Moreover, we obtain the solutions of above system in explicit form according to the parameters a, c and e are equal 1 or not equal 1. In addition, we get periodic solutions of aforementioned system. Finally, we define the forbidden set of the initial conditions by using the acquired formulas.

1. Introduction

In recent years, many authors have been interested in non-linear difference equations and non-linear systems of difference equations [1–3, 5, 6, 8–10, 12–14, 20–23, 25–41]. One of the important topics in this field is the solvability of non-linear difference equations or non-linear difference equations systems. There are different methods for obtaining solutions of non-linear difference equations and non-linear systems of difference equations (two-dimensional or three-dimensional). One of the

2020 *Mathematics Subject Classification.* 39A10, 39A20, 39A23.
Keywords. Explicit form, forbidden set, periodicity.
[1] mervekara@kmu.edu.tr-Corresponding author; 0000-0001-8081-0254
[2] aktas.omer10@gmail.com; 0000-0002-5763-0308

*This study is a part of the second author's Master Thesis.

methods for solving non-linear difference equations and non-linear difference equations systems is to use the change of variables. Then, aforementioned difference equations or their systems can be reduced to a linear difference equation with constant or variable coefficients. The other method is to use induction method. For instance, El-Metwally et al. solved the following non-linear difference equations

$$x_{n+1} = \frac{x_{n-1}x_{n-2}}{x_n\left(\pm 1 \pm x_{n-1}x_{n-2}\right)},\ n \in \mathbb{N}_0, \tag{1}$$

by using induction method in [7]. In addition, they investigated the behavior of the solutions of difference equations in (1).

In addition, Ibrahim et al. in [15] obtained the solutions of the following difference equation

$$x_{n+1} = \frac{x_{n-1}x_{n-2}}{x_n\left(a_n + b_n x_{n-1}x_{n-2}\right)},\ n \in \mathbb{N}_0, \tag{2}$$

where initial conditions x_{-2}, x_{-1}, x_0 are non-zero real numbers and $(a_n)_{n\in\mathbb{N}_0}$, $(b_n)_{n\in\mathbb{N}_0}$ are real two-periodic sequences. They used induction method to acquire the solutions of equation (2).

Ahmed et al. in [4], investigated the periodic character and the form of the solutions of the following two-dimensional difference equations systems

$$x_{n+1} = \frac{x_{n-1}y_{n-2}}{y_n\left(-1 \pm x_{n-1}y_{n-2}\right)},\ y_{n+1} = \frac{y_{n-1}x_{n-2}}{x_n\left(\pm 1 \pm y_{n-1}x_{n-2}\right)},\ n \in \mathbb{N}_0, \tag{3}$$

by induction with $x_{-j},\ y_{-j}\ , j = \overline{0,2}$ are nonzero real numbers.

A few years ago, in [16], Kara and Yazlik showed that the following two-dimensional difference equations system

$$x_n = \frac{x_{n-2}y_{n-3}}{y_{n-1}\left(a_n + b_n x_{n-2}y_{n-3}\right)},\ y_n = \frac{y_{n-2}x_{n-3}}{x_{n-1}\left(\alpha_n + \beta_n y_{n-2}x_{n-3}\right)},\ n \in \mathbb{N}_0, \tag{4}$$

where the initial conditions $x_{-j}, y_{-j}, j \in \{1,2,3\}$ and the sequences $(a_n)_{n\in\mathbb{N}_0}$, $(b_n)_{n\in\mathbb{N}_0}$, $(\alpha_n)_{n\in\mathbb{N}_0}$, $(\beta_n)_{n\in\mathbb{N}_0}$ are non-zero real numbers can be solved in closed-form. In addition, they acquired the forbidden set of the initial values x_{-j}, y_{-j}, $j = \overline{1,3}$ for system (4) and gave a study of the long-term behavior of its solutions when for every $n \in \mathbb{N}_0$, all the sequences $(a_n), (b_n), (\alpha_n), (\beta_n)$ are constant. They used the change of variables to acquire the solutions of system (4).

Recently, the authors of [11], obtained exact formulas for the solutions of the two-dimensional system of difference equations

$$x_{n+1} = \frac{x_{n-k+1}y_{n-k}}{y_n\left(a_n + b_n x_{n-k+1}y_{n-k}\right)},\ y_{n+1} = \frac{x_{n-k}y_{n-k+1}}{x_n\left(c_n + d_n y_{n-k}y_{n-k+1}\right)},\ n \in \mathbb{N}_0, \tag{5}$$

where $(a_n)_{n\in\mathbb{N}_0}, (b_n)_{n\in\mathbb{N}_0}, (c_n)_{n\in\mathbb{N}_0}$ and $(d_n)_{n\in\mathbb{N}_0}$ are non-zero real sequences. Note that, system (4) can be obtained by taking $k = 2$ in system (5).

In addition, Kara and Yazlik showed that the following two-dimensional system of non-linear difference equations

$$x_n = \frac{x_{n-k}y_{n-k-l}}{y_{n-l}\left(a_n + b_n x_{n-k}y_{n-k-l}\right)}, \; y_n = \frac{y_{n-k}x_{n-k-l}}{x_{n-l}\left(\alpha_n + \beta_n y_{n-k}x_{n-k-l}\right)}, \; n \in \mathbb{N}_0, \quad (6)$$

where $k, l \in \mathbb{N}$, $(a_n)_{n\in\mathbb{N}_0}, (b_n)_{n\in\mathbb{N}_0}, (\alpha_n)_{n\in\mathbb{N}_0}$, $(\beta_n)_{n\in\mathbb{N}_0}$ and the initial values x_{-i}, y_{-i}, $i = \overline{1, k+l}$, are real numbers can be solved in [17]. Also, by using these obtained formulas, they investigated the asymptotic behavior of well-defined solutions of system (6) for the case $k = 2$, $l = k$. They used the change of variables to obtain the solutions of system (6).

Quite recently, authors of [18] showed that three-dimensional system of difference equations

$$\begin{aligned} x_n &= \frac{x_{n-2}z_{n-3}}{z_{n-1}\left(a_n + b_n x_{n-2}z_{n-3}\right)}, \\ y_n &= \frac{y_{n-2}x_{n-3}}{x_{n-1}\left(\alpha_n + \beta_n y_{n-2}x_{n-3}\right)}, \; n \in \mathbb{N}_0, \\ z_n &= \frac{z_{n-2}y_{n-3}}{y_{n-1}\left(A_n + B_n z_{n-2}y_{n-3}\right)}, \end{aligned} \quad (7)$$

where the initial values x_{-j}, y_{-j}, z_{-j}, $j \in \{1, 2, 3\}$ and the sequences $(a_n)_{n\in\mathbb{N}_0}$, $(b_n)_{n\in\mathbb{N}_0}$, $(\alpha_n)_{n\in\mathbb{N}_0}$, $(\beta_n)_{n\in\mathbb{N}_0}$, $(A_n)_{n\in\mathbb{N}_0}$, $(B_n)_{n\in\mathbb{N}_0}$ are non-zero real numbers, can be solved in closed form. They used the change of variables to acquire the solutions of system (7).

Finally, in [19], Kara et al. obtained explicit formulas for the well defined solutions of the following system of difference equations

$$\begin{aligned} x_{n+1} &= \frac{\prod_{j=0}^{k} z_{n-3j}}{\prod_{j=1}^{k} x_{n-(3j-1)}\left(a_n + b_n \prod_{j=0}^{k} z_{n-3j}\right)}, \\ y_{n+1} &= \frac{\prod_{j=0}^{k} x_{n-3j}}{\prod_{j=1}^{k} y_{n-(3j-1)}\left(c_n + d_n \prod_{j=0}^{k} x_{n-3j}\right)}, \; n \in \mathbb{N}_0, \\ z_{n+1} &= \frac{\prod_{j=0}^{k} y_{n-3j}}{\prod_{j=1}^{k} z_{n-(3j-1)}\left(e_n + f_n \prod_{j=0}^{k} y_{n-3j}\right)}, \end{aligned} \quad (8)$$

where $k \in \mathbb{N}_0$, the initial conditions x_{-i}, y_{-i}, z_{-i}, $i = \overline{0, 3k}$ and the sequences $(a_n)_{n\in\mathbb{N}_0}$, $(b_n)_{n\in\mathbb{N}_0}$, $(c_n)_{n\in\mathbb{N}_0}$, $(d_n)_{n\in\mathbb{N}_0}$, $(e_n)_{n\in\mathbb{N}_0}$, $(f_n)_{n\in\mathbb{N}_0}$ are real numbers. They used change of variables to obtain the solutions of system (8).

In this paper, we study the following three-dimensional system of difference equations

$$\begin{aligned} x_n =& \frac{x_{n-2}y_{n-3}}{y_{n-1}\left(a+bx_{n-2}y_{n-3}\right)},\\ y_n =& \frac{y_{n-2}z_{n-3}}{z_{n-1}\left(c+dy_{n-2}z_{n-3}\right)}, n\in\mathbb{N}_0,\\ z_n =& \frac{z_{n-2}x_{n-3}}{x_{n-1}\left(e+fz_{n-2}x_{n-3}\right)}, \end{aligned} \tag{9}$$

where the initial values x_{-i}, y_{-i}, z_{-i}, $i=\overline{1,3}$ and the parameters a, b, c, d, e, f are non-zero real numbers. We solve system (9) in closed form by using convenient transformation. We obtain the solutions of system (9) in explicit form according to the parameters a, c and e are equal 1 or not equal 1. In addition, we get periodic solutions of system (9). Finally, we define the forbidden set of the initial conditions by using the obtained formulas. Note that system (9) is three-dimensional form of equation (2) and system (4).

Definition 1. (**Periodicity**) Let $(x_n, y_n, z_n)_{n\geq -3}$ be solution to difference equations system (9). The solution $(x_n, y_n, z_n)_{n\geq -3}$ is said to be eventually periodic p if $x_{n+p}=x_n$, $y_{n+p}=y_n$, $z_{n+p}=z_n$ for all $n\geq n_0$ where $n_0\in\mathbb{Z}$, $p\in\mathbb{Z}^+$. If $n_0=-3$ is said that the solution is periodic with period p.

Lemma 1. [24] Let $(\alpha_n)_{n\in\mathbb{N}_0}$ and $(\beta_n)_{n\in\mathbb{N}_0}$ be two sequences of real numbers and the sequences x_{2m+i}, $i\in\{0,1\}$, be solutions of the equations

$$x_{2m+i}=\alpha_{2m+i}x_{2(m-1)+i}+\beta_{2m+i},\ m\in\mathbb{N}_0. \tag{10}$$

Then, for each fixed $i\in\{0,1\}$ and $m\geq -1$, equation (10) has the general solution

$$x_{2m+i}=x_{i-2}\prod_{j=0}^{m}\alpha_{2j+i}+\sum_{l=0}^{m}\beta_{2l+i}\prod_{j=l+1}^{m}\alpha_{2j+i}.$$

Further, if $(\alpha_n)_{n\in\mathbb{N}_0}$ and $(\beta_n)_{n\in\mathbb{N}_0}$ are constant and $i\in\{0,1\}$, then

$$x_{2m+i}=\begin{cases}\alpha^{m+1}x_{i-2}+\beta\frac{1-\alpha^{m+1}}{1-\alpha}, & \text{if } \alpha\neq 1,\\ x_{i-2}+\beta\left(m+1\right), & \text{if } \alpha=1.\end{cases}$$

2. The Solutions of System (9) in Closed Form

Let $\{(x_n, y_n, z_n)\}_{n\geq -3}$ be a solution of system (9). If at least one of the initial conditions x_{-j}, y_{-j}, z_{-j}, $j=\overline{1,3}$, is equal to zero, then the solution of system (9) is not defined. For example, if $x_{-3}=0$, then $z_0=0$ and so y_1 is not defined. Similarly, if $y_{-3}=0$ (or $z_{-3}=0$), then $x_0=0$ (or $y_0=0$) and so z_1 (or x_1) is not defined. For $j=1,2$, the other cases are similar. On the other hand, if

$x_{n_0} = 0$ ($n_0 \in \mathbb{N}_0$), $x_n \neq 0$, for $-3 \leq n \leq n_0 - 1$, and x_k, y_k and z_k are defined for $-3 \leq k \leq n_0 - 1$, then according to the first equation in (9) we get that $y_{n_0-3} = 0$. If $n_0 - 3 \leq -1$, then $y_{-j_0} = 0$, for $j_0 \in \{1, 2, 3\}$. If $3 \leq n_0 \leq 5$ then from this and the second equation in (9) we have that $y_{n_0-5} = 0$ or $z_{n_0-6} = 0$. If $n_0 - 5 \leq 0$, then $z_{-j_0} = 0$, for $j_0 \in \{1, 2, 3\}$ and $y_{-j_1} = 0$, for $j_1 \in \{1, 2\}$. If $n_0 > 5$ from this and first equation in (9) we have that $y_{n_0-5} = 0$ or $z_{n_0-6} = 0$. If $n_0 > 5$ and $z_{n_0-6} = 0$ from this and third, second, first equations in (9) we have that $x_{n_0-2} = 0$, which is a contradiction. The other cases ($y_{n_1} = 0$ and $z_{n_2} = 0$) can be similarly proved. Thus, for every well-defined solution of system (9) we have that $x_n y_n z_n \neq 0$, $n \geq -3$, if and only if $x_{-i} y_{-i} z_{-i} \neq 0$, for $i = \overline{1, 3}$. Note that the system (9) can be written in the form

$$\begin{aligned} \frac{1}{x_n y_{n-1}} &= \frac{a + b x_{n-2} y_{n-3}}{x_{n-2} y_{n-3}}, \\ \frac{1}{y_n z_{n-1}} &= \frac{c + d y_{n-2} z_{n-3}}{y_{n-2} z_{n-3}}, \ n \in \mathbb{N}_0, \\ \frac{1}{z_n x_{n-1}} &= \frac{e + f z_{n-2} x_{n-3}}{z_{n-2} x_{n-3}}. \end{aligned} \tag{11}$$

Using the following variables

$$u_n = \frac{1}{x_n y_{n-1}}, \ v_n = \frac{1}{y_n z_{n-1}}, \ w_n = \frac{1}{z_n x_{n-1}}, \ n \geq -2, \tag{12}$$

then system (11) transforms to the following linear difference equations

$$u_n = a u_{n-2} + b, \ v_n = c v_{n-2} + d, \ w_n = e w_{n-2} + f, \ n \in \mathbb{N}_0, \tag{13}$$

From Lemma 1, the solutions of equations in (13) are

$$\begin{aligned} u_{2m+i} &= \begin{cases} a^{m+1} u_{i-2} + \frac{1-a^{m+1}}{1-a} b, & \text{if } a \neq 1, \\ u_{i-2} + (m+1) b & \text{if } a = 1, \end{cases} \\ v_{2m+i} &= \begin{cases} c^{m+1} v_{i-2} + \frac{1-c^{m+1}}{1-c} d, & \text{if } c \neq 1, \\ v_{i-2} + (m+1) d, & \text{if } c = 1, \end{cases} \quad m \in \mathbb{N}_0, \\ w_{2m+i} &= \begin{cases} e^{m+1} w_{i-2} + \frac{1-e^{m+1}}{1-e} f, & \text{if } e \neq 1, \\ w_{i-2} + (m+1) f, & \text{if } e = 1, \end{cases} \end{aligned} \tag{14}$$

for $i \in \{0, 1\}$. From equations in (12) we get

$$\begin{aligned} x_{2m+i} &= \frac{v_{2m+i-1}}{u_{2m+i}} \frac{u_{2m+i-3}}{w_{2m+i-2}} \frac{w_{2m+i-5}}{v_{2m+i-4}} x_{2(m-3)+i}, \\ y_{2m+i} &= \frac{w_{2m+i-1}}{v_{2m+i}} \frac{v_{2m+i-3}}{u_{2m+i-2}} \frac{u_{2m+i-5}}{w_{2m+i-4}} y_{2(m-3)+i}, \ m \in \mathbb{N}, \\ z_{2m+i} &= \frac{u_{2m+i-1}}{w_{2m+i}} \frac{w_{2m+i-3}}{v_{2m+i-2}} \frac{v_{2m+i-5}}{u_{2m+i-4}} z_{2(m-3)+i}, \end{aligned}$$

where $i \in \{1,2\}$, and consequently

$$\begin{aligned} x_{6m+l} &= \frac{v_{6m+l-1}}{u_{6m+l}}\frac{u_{6m+l-3}}{w_{6m+l-2}}\frac{w_{6m+l-5}}{v_{6m+l-4}}x_{6(m-1)+l}, \ m \in \mathbb{N}_0,\\ y_{6m+l} &= \frac{w_{6m+l-1}}{v_{6m+l}}\frac{v_{6m+l-3}}{u_{6m+l-2}}\frac{u_{6m+l-5}}{w_{6m+l-4}}y_{6(m-1)+l}, \ m \in \mathbb{N}_0,\\ z_{6m+l} &= \frac{u_{6m+l-1}}{w_{6m+l}}\frac{w_{6m+l-3}}{v_{6m+l-2}}\frac{v_{6m+l-5}}{u_{6m+l-4}}z_{6(m-1)+l}, \ m \in \mathbb{N}_0, \end{aligned} \tag{15}$$

where $l = \overline{3,8}$, as far as $6m+l \geq 3$. From (15), we have that

$$\begin{aligned} x_{6m+l} &= x_{l-6}\prod_{s=0}^{m}\frac{v_{6s+l-1}}{u_{6s+l}}\frac{u_{6s+l-3}}{w_{6s+l-2}}\frac{w_{6s+l-5}}{v_{6s+l-4}},\\ y_{6m+l} &= y_{l-6}\prod_{s=0}^{m}\frac{w_{6s+l-1}}{v_{6s+l}}\frac{v_{6s+l-3}}{u_{6s+l-2}}\frac{u_{6s+l-5}}{w_{6s+l-4}},\\ z_{6m+l} &= z_{l-6}\prod_{s=0}^{m}\frac{u_{6s+l-1}}{w_{6s+l}}\frac{w_{6s+l-3}}{v_{6s+l-2}}\frac{v_{6s+l-5}}{u_{6s+l-4}}, \end{aligned} \tag{16}$$

where $m \geq -1$ and $l = \overline{3,8}$. From (16), we get

$$\begin{aligned} x_{6m+2t+k} &= x_{2t+k-6}\prod_{s=0}^{m}\frac{v_{6s+2t+k-1}}{u_{6s+2t+k}}\frac{u_{6s+2t+k-3}}{w_{6s+2t+k-2}}\frac{w_{6s+2t+k-5}}{v_{6s+2t+k-4}},\\ y_{6m+2t+k} &= y_{2t+k-6}\prod_{s=0}^{m}\frac{w_{6s+2t+k-1}}{v_{6s+2t+k}}\frac{v_{6s+2t+k-3}}{u_{6s+2t+k-2}}\frac{u_{6s+2t+k-5}}{w_{6s+2t+k-4}},\\ z_{6m+2t+k} &= z_{2t+k-6}\prod_{s=0}^{m}\frac{u_{6s+2t+k-1}}{w_{6s+2t+k}}\frac{w_{6s+2t+k-3}}{v_{6s+2t+k-2}}\frac{v_{6s+2t+k-5}}{u_{6s+2t+k-4}}, \end{aligned} \tag{17}$$

for $t \in \{1,2,3\}$ and $k \in \{1,2\}$. Employing (14) in (17), we get solutions of system (9).

3. Particular Cases of System (9)

Now, we will examine the solutions in 8 different cases depending on whether the parameters a, c and e are equal 1 or not equal 1.

3.1. Case $a \neq 1$, $c \neq 1$, $e \neq 1$

In this case, the solutions of system (9) can be written in the following form

$$\begin{aligned} x_{6m+2t+1} = x_{2t-5}\prod_{s=0}^{m}&\frac{x_{-1}y_{-1}z_{-1}}{x_{-3}y_{-3}z_{-3}}\frac{c^{3s+t+1}\left((1-c)-y_{-2}z_{-3}d\right)+y_{-2}z_{-3}d}{a^{3s+t+1}\left((1-a)-x_{-1}y_{-2}b\right)+x_{-1}y_{-2}b}\\ &\times\frac{a^{3s+t}\left((1-a)-x_{-2}y_{-3}b\right)+x_{-2}y_{-3}b}{e^{3s+t}\left((1-e)-x_{-2}z_{-1}f\right)+x_{-2}z_{-1}f}\\ &\times\frac{e^{3s+t-1}\left((1-e)-x_{-3}z_{-2}f\right)+x_{-3}z_{-2}f}{c^{3s+t-1}\left((1-c)-y_{-1}z_{-2}d\right)+y_{-1}z_{-2}d}, \end{aligned}$$

$$
\begin{aligned}
x_{6m+2t+2} = x_{2t-4} \prod_{s=0}^{m} & \frac{x_{-3}y_{-3}z_{-3}}{x_{-1}y_{-1}z_{-1}} \frac{c^{3s+t+1}\left((1-c)-y_{-1}z_{-2}d\right)+y_{-1}z_{-2}d}{a^{3s+t+2}\left((1-a)-x_{-2}y_{-3}b\right)+x_{-2}y_{-3}b} \\
& \times \frac{a^{3s+t}\left((1-a)-x_{-1}y_{-2}b\right)+x_{-1}y_{-2}b}{e^{3s+t+1}\left((1-e)-x_{-3}z_{-2}f\right)+x_{-3}z_{-2}f} \\
& \times \frac{e^{3s+t-1}\left((1-e)-x_{-2}z_{-1}f\right)+x_{-2}z_{-1}f}{c^{3s+t}\left((1-c)-y_{-2}z_{-3}d\right)+y_{-2}z_{-3}d},
\end{aligned}
$$

$$
\begin{aligned}
y_{6m+2t+1} = y_{2t-5} \prod_{s=0}^{m} & \frac{x_{-1}y_{-1}z_{-1}}{x_{-3}y_{-3}z_{-3}} \frac{e^{3s+t+1}\left((1-e)-x_{-3}z_{-2}f\right)+x_{-3}z_{-2}f}{c^{3s+t+1}\left((1-c)-y_{-1}z_{-2}d\right)+y_{-1}z_{-2}d} \\
& \times \frac{c^{3s+t}\left((1-c)-y_{-2}z_{-3}d\right)+y_{-2}z_{-3}d}{a^{3s+t}\left((1-a)-x_{-1}y_{-2}b\right)+x_{-1}y_{-2}b} \\
& \times \frac{a^{3s+t-1}\left((1-a)-x_{-2}y_{-3}b\right)+x_{-2}y_{-3}b}{e^{3s+t-1}\left((1-e)-x_{-2}z_{-1}f\right)+x_{-2}z_{-1}f},
\end{aligned}
$$

$$
\begin{aligned}
y_{6m+2t+2} = y_{2t-4} \prod_{s=0}^{m} & \frac{x_{-3}y_{-3}z_{-3}}{x_{-1}y_{-1}z_{-1}} \frac{e^{3s+t+1}\left((1-e)-x_{-2}z_{-1}f\right)+x_{-2}z_{-1}f}{c^{3s+t+2}\left((1-c)-y_{-2}z_{-3}d\right)+y_{-2}z_{-3}d} \\
& \times \frac{c^{3s+t}\left((1-c)-y_{-1}z_{-2}d\right)+y_{-1}z_{-2}d}{a^{3s+t+1}\left((1-a)-x_{-2}y_{-3}b\right)+x_{-2}y_{-3}b} \\
& \times \frac{a^{3s+t-1}\left((1-a)-x_{-1}y_{-2}b\right)+x_{-1}y_{-2}b}{e^{3s+t}\left((1-e)-x_{-3}z_{-2}f\right)+x_{-3}z_{-2}f},
\end{aligned}
$$

$$
\begin{aligned}
z_{6m+2t+1} = z_{2t-5} \prod_{s=0}^{m} & \frac{x_{-1}y_{-1}z_{-1}}{x_{-3}y_{-3}z_{-3}} \frac{a^{3s+t+1}\left((1-a)-x_{-2}y_{-3}b\right)+x_{-2}y_{-3}b}{e^{3s+t+1}\left((1-e)-z_{-1}x_{-2}f\right)+z_{-1}x_{-2}f} \\
& \times \frac{e^{3s+t}\left((1-e)-z_{-2}x_{-3}f\right)+z_{-2}x_{-3}f}{c^{3s+t}\left((1-c)-y_{-1}z_{-2}d\right)+y_{-1}z_{-2}d} \\
& \times \frac{c^{3s+t-1}\left((1-c)-y_{-2}z_{-3}d\right)+y_{-2}z_{-3}d}{a^{3s+t-1}\left((1-a)-y_{-2}x_{-1}b\right)+y_{-2}x_{-1}b},
\end{aligned}
$$

$$
\begin{aligned}
z_{6m+2t+2} = z_{2t-4} \prod_{s=0}^{m} & \frac{x_{-3}y_{-3}z_{-3}}{x_{-1}y_{-1}z_{-1}} \frac{a^{3s+t+1}\left((1-a)-y_{-2}x_{-1}b\right)+y_{-2}x_{-1}b}{e^{3s+t+2}\left((1-e)-z_{-2}x_{-3}f\right)+z_{-2}x_{-3}f} \\
& \times \frac{e^{3s+t}\left((1-e)-z_{-1}x_{-2}f\right)+z_{-1}x_{-2}f}{c^{3s+t+1}\left((1-c)-y_{-2}z_{-3}d\right)+y_{-2}z_{-3}d} \\
& \times \frac{c^{3s+t-1}\left((1-c)-y_{-1}z_{-2}d\right)+y_{-1}z_{-2}d}{a^{3s+t}\left((1-a)-y_{-3}x_{-2}b\right)+y_{-3}x_{-2}b},
\end{aligned}
$$

for $m \geq -1$ and $t \in \{1, 2, 3\}$.

3.2. Case $a = 1$, $c \neq 1$, $e \neq 1$

In this case, solutions of system (9) are as follows

$$x_{6m+2t+1} = x_{2t-5} \prod_{s=0}^{m} \frac{x_{-1}y_{-1}z_{-1}}{x_{-3}y_{-3}z_{-3}} \frac{c^{3s+t+1}\left((1-c) - y_{-2}z_{-3}d\right) + y_{-2}z_{-3}d}{1 + x_{-1}y_{-2}(3s+t+1)b}$$
$$\times \frac{1 + x_{-2}y_{-3}(3s+t)b}{e^{3s+t}\left((1-e) - x_{-2}z_{-1}f\right) + x_{-2}z_{-1}f}$$
$$\times \frac{e^{3s+t-1}\left((1-e) - x_{-3}z_{-2}f\right) + x_{-3}z_{-2}f}{c^{3s+t-1}\left((1-c) - y_{-1}z_{-2}d\right) + y_{-1}z_{-2}d},$$

$$x_{6m+2t+2} = x_{2t-4} \prod_{s=0}^{m} \frac{x_{-3}y_{-3}z_{-3}}{x_{-1}y_{-1}z_{-1}} \frac{c^{3s+t+1}\left((1-c) - y_{-1}z_{-2}d\right) + y_{-1}z_{-2}d}{1 + x_{-2}y_{-3}(3s+t+2)b}$$
$$\times \frac{1 + x_{-1}y_{-2}(3s+t)b}{e^{3s+t+1}\left((1-e) - x_{-3}z_{-2}f\right) + x_{-3}z_{-2}f}$$
$$\times \frac{e^{3s+t-1}\left((1-e) - x_{-2}z_{-1}f\right) + x_{-2}z_{-1}f}{c^{3s+t}\left((1-c) - y_{-2}z_{-3}d\right) + y_{-2}z_{-3}d},$$

$$y_{6m+2t+1} = y_{2t-5} \prod_{s=0}^{m} \frac{x_{-1}y_{-1}z_{-1}}{x_{-3}y_{-3}z_{-3}} \frac{e^{3s+t+1}\left((1-e) - x_{-3}z_{-2}f\right) + x_{-3}z_{-2}f}{c^{3s+t+1}\left((1-c) - y_{-1}z_{-2}d\right) + y_{-1}z_{-2}d}$$
$$\times \frac{c^{3s+t}\left((1-c) - y_{-2}z_{-3}d\right) + y_{-2}z_{-3}d}{1 + x_{-1}y_{-2}(3s+t)b}$$
$$\times \frac{1 + x_{-2}y_{-3}(3s+t-1)b}{e^{3s+t-1}\left((1-e) - x_{-2}z_{-1}f\right) + x_{-2}z_{-1}f},$$

$$y_{6m+2t+2} = y_{2t-4} \prod_{s=0}^{m} \frac{x_{-3}y_{-3}z_{-3}}{x_{-1}y_{-1}z_{-1}} \frac{e^{3s+t+1}\left((1-e) - x_{-2}z_{-1}f\right) + x_{-2}z_{-1}f}{c^{3s+t+2}\left((1-c) - y_{-2}z_{-3}d\right) + y_{-2}z_{-3}d}$$
$$\times \frac{c^{3s+t}\left((1-c) - y_{-1}z_{-2}d\right) + y_{-1}z_{-2}d}{1 + x_{-2}y_{-3}(3s+t+1)b}$$
$$\times \frac{1 + x_{-1}y_{-2}(3s+t-1)b}{e^{3s+t}\left((1-e) - x_{-3}z_{-2}f\right) + x_{-3}z_{-2}f},$$

$$z_{6m+2t+1} = z_{2t-5} \prod_{s=0}^{m} \frac{x_{-1}y_{-1}z_{-1}}{x_{-3}y_{-3}z_{-3}} \frac{1 + x_{-2}y_{-3}(3s+t+1)b}{e^{3s+t+1}\left((1-e) - x_{-2}z_{-1}f\right) + x_{-2}z_{-1}f}$$
$$\times \frac{e^{3s+t}\left((1-e) - x_{-3}z_{-2}f\right) + x_{-3}z_{-2}f}{c^{3s+t}\left((1-c) - y_{-1}z_{-2}d\right) + y_{-1}z_{-2}d}$$
$$\times \frac{c^{3s+t-1}\left((1-c) - y_{-2}z_{-3}d\right) + y_{-2}z_{-3}d}{1 + x_{-1}y_{-2}(3s+t-1)b},$$

$$z_{6m+2t+2} = z_{2t-4} \prod_{s=0}^{m} \frac{x_{-3}y_{-3}z_{-3}}{x_{-1}y_{-1}z_{-1}} \frac{1 + x_{-1}y_{-2}(3s+t+1)b}{e^{3s+t+2}\left((1-e) - x_{-3}z_{-2}f\right) + x_{-3}z_{-2}f}$$
$$\times \frac{e^{3s+t}\left((1-e) - x_{-2}z_{-1}f\right) + x_{-2}z_{-1}f}{c^{3s+t+1}\left((1-c) - y_{-2}z_{-3}d\right) + y_{-2}z_{-3}d}$$
$$\times \frac{c^{3s+t-1}\left((1-c) - y_{-1}z_{-2}d\right) + y_{-1}z_{-2}d}{1 + x_{-2}y_{-3}(3s+t)b},$$

for $m \geq -1$ and $t \in \{1, 2, 3\}$.

3.3. Case $a \neq 1$, $c = 1$, $e \neq 1$

In this case, the solutions of system (9) can be written in the following form

$$x_{6m+2t+1} = x_{2t-5} \prod_{s=0}^{m} \frac{x_{-1}y_{-1}z_{-1}}{x_{-3}y_{-3}z_{-3}} \frac{1 + y_{-2}z_{-3}(3s+t+1)d}{a^{3s+t+1}\left((1-a) - x_{-1}y_{-2}b\right) + x_{-1}y_{-2}b}$$
$$\times \frac{a^{3s+t}\left((1-a) - x_{-2}y_{-3}b\right) + x_{-2}y_{-3}b}{e^{3s+t}\left((1-e) - x_{-2}z_{-1}f\right) + x_{-2}z_{-1}f}$$
$$\times \frac{e^{3s+t-1}\left((1-e) - x_{-3}z_{-2}f\right) + x_{-3}z_{-2}f}{1 + y_{-1}z_{-2}(3s+t-1)d},$$

$$x_{6m+2t+2} = x_{2t-4} \prod_{s=0}^{m} \frac{x_{-3}y_{-3}z_{-3}}{x_{-1}y_{-1}z_{-1}} \frac{1 + y_{-1}z_{-2}(3s+t+1)d}{a^{3s+t+2}\left((1-a) - x_{-2}y_{-3}b\right) + x_{-2}y_{-3}b}$$
$$\times \frac{a^{3s+t}\left((1-a) - x_{-1}y_{-2}b\right) + x_{-1}y_{-2}b}{e^{3s+t+1}\left((1-e) - x_{-3}z_{-2}f\right) + x_{-3}z_{-2}f}$$
$$\times \frac{e^{3s+t-1}\left((1-e) - x_{-2}z_{-1}f\right) + x_{-2}z_{-1}f}{1 + y_{-2}z_{-3}(3s+t)d},$$

$$y_{6m+2t+1} = y_{2t-5} \prod_{s=0}^{m} \frac{x_{-1}y_{-1}z_{-1}}{x_{-3}y_{-3}z_{-3}} \frac{e^{3s+t+1}\left((1-e) - x_{-3}z_{-2}f\right) + x_{-3}z_{-2}f}{1 + y_{-1}z_{-2}(3s+t+1)d}$$
$$\times \frac{1 + y_{-2}z_{-3}(3s+t)d}{a^{3s+t}\left((1-a) - x_{-1}y_{-2}b\right) + x_{-1}y_{-2}b}$$
$$\times \frac{a^{3s+t-1}\left((1-a) - x_{-2}y_{-3}b\right) + x_{-2}y_{-3}b}{e^{3s+t-1}\left((1-e) - x_{-2}z_{-1}f\right) + x_{-2}z_{-1}f},$$

$$y_{6m+2t+2} = y_{2t-4} \prod_{s=0}^{m} \frac{x_{-3}y_{-3}z_{-3}}{x_{-1}y_{-1}z_{-1}} \frac{e^{3s+t+1}\left((1-e) - x_{-2}z_{-1}f\right) + x_{-2}z_{-1}f}{1 + y_{-2}z_{-3}(3s+t+2)d}$$
$$\times \frac{1 + y_{-1}z_{-2}(3s+t)d}{a^{3s+t+1}\left((1-a) - x_{-2}y_{-3}b\right) + x_{-2}y_{-3}b}$$

$$\times \frac{a^{3s+t-1}\left((1-a)-x_{-1}y_{-2}b\right)+x_{-1}y_{-2}b}{e^{3s+t}\left((1-e)-x_{-3}z_{-2}f\right)+x_{-3}z_{-2}f},$$

$$z_{6m+2t+1} = z_{2t-5}\prod_{s=0}^{m}\frac{x_{-1}y_{-1}z_{-1}}{x_{-3}y_{-3}z_{-3}}\frac{a^{3s+t+1}\left((1-a)-x_{-2}y_{-3}b\right)+x_{-2}y_{-3}b}{e^{3s+t+1}\left((1-e)-x_{-2}z_{-1}f\right)+x_{-2}z_{-1}f}$$
$$\times \frac{e^{3s+t}\left((1-e)-x_{-3}z_{-2}f\right)+x_{-3}z_{-2}f}{1+y_{-1}z_{-2}(3s+t)d}$$
$$\times \frac{1+y_{-2}z_{-3}(3s+t-1)d}{a^{3s+t-1}\left((1-a)-x_{-1}y_{-2}b\right)+x_{-1}y_{-2}b},$$

$$z_{6m+2t+2} = z_{2t-4}\prod_{s=0}^{m}\frac{x_{-3}y_{-3}z_{-3}}{x_{-1}y_{-1}z_{-1}}\frac{a^{3s+t+1}\left((1-a)-x_{-1}y_{-2}b\right)+x_{-1}y_{-2}b}{e^{3s+t+2}\left((1-e)-x_{-3}z_{-2}f\right)+x_{-3}z_{-2}f}$$
$$\times \frac{e^{3s+t}\left((1-e)-x_{-2}z_{-1}f\right)+x_{-2}z_{-1}f}{1+y_{-2}z_{-3}(3s+t+1)d}$$
$$\times \frac{1+y_{-1}z_{-2}(3s+t-1)d}{a^{3s+t}\left((1-a)-x_{-2}y_{-3}b\right)+x_{-2}y_{-3}b},$$

for $m \geq -1$ and $t \in \{1,2,3\}$.

3.4. Case $a \neq 1$, $c \neq 1$, $e = 1$

In this case, solutions of system (9) are as follows

$$x_{6m+2t+1} = x_{2t-5}\prod_{s=0}^{m}\frac{x_{-1}y_{-1}z_{-1}}{x_{-3}y_{-3}z_{-3}}\frac{c^{3s+t+1}\left((1-c)-y_{-2}z_{-3}d\right)+y_{-2}z_{-3}d}{a^{3s+t+1}\left((1-a)-x_{-1}y_{-2}b\right)+x_{-1}y_{-2}b}$$
$$\times \frac{a^{3s+t}\left((1-a)-x_{-2}y_{-3}b\right)+x_{-2}y_{-3}b}{1+x_{-2}z_{-1}(3s+t)f}$$
$$\times \frac{1+x_{-3}z_{-2}(3s+t-1)f}{c^{3s+t-1}\left((1-c)-y_{-1}z_{-2}d\right)+y_{-1}z_{-2}d},$$

$$x_{6m+2t+2} = x_{2t-4}\prod_{s=0}^{m}\frac{x_{-3}y_{-3}z_{-3}}{x_{-1}y_{-1}z_{-1}}\frac{c^{3s+t+1}\left((1-c)-y_{-1}z_{-2}d\right)+y_{-1}z_{-2}d}{a^{3s+t+2}\left((1-a)-x_{-2}y_{-3}b\right)+x_{-2}y_{-3}b}$$
$$\times \frac{a^{3s+t}\left((1-a)-x_{-1}y_{-2}b\right)+x_{-1}y_{-2}b}{1+x_{-3}z_{-2}(3s+t+1)f}$$
$$\times \frac{1+x_{-2}z_{-1}(3s+t-1)f}{c^{3s+t}\left((1-c)-y_{-2}z_{-3}d\right)+y_{-2}z_{-3}d},$$

$$y_{6m+2t+1} = y_{2t-5}\prod_{s=0}^{m}\frac{x_{-1}y_{-1}z_{-1}}{x_{-3}y_{-3}z_{-3}}\frac{1+x_{-3}z_{-2}(3s+t+1)f}{c^{3s+t+1}\left((1-c)-y_{-1}z_{-2}d\right)+y_{-1}z_{-2}d}$$

$$\times \frac{c^{3s+t}\left((1-c)-y_{-2}z_{-3}d\right)+y_{-2}z_{-3}d}{a^{3s+t}\left((1-a)-x_{-1}y_{-2}b\right)+x_{-1}y_{-2}b}$$
$$\times \frac{a^{3s+t-1}\left((1-a)-x_{-2}y_{-3}b\right)+x_{-2}y_{-3}b}{1+x_{-2}z_{-1}(3s+t-1)f},$$

$$y_{6m+2t+2} = y_{2t-4}\prod_{s=0}^{m}\frac{x_{-3}y_{-3}z_{-3}}{x_{-1}y_{-1}z_{-1}}\frac{1+x_{-2}z_{-1}(3s+t+1)f}{c^{3s+t+2}\left((1-c)-y_{-2}z_{-3}d\right)+y_{-2}z_{-3}d}$$
$$\times \frac{c^{3s+t}\left((1-c)-y_{-1}z_{-2}d\right)+y_{-1}z_{-2}d}{a^{3s+t+1}\left((1-a)-x_{-2}y_{-3}b\right)+x_{-2}y_{-3}b}$$
$$\times \frac{a^{3s+t-1}\left((1-a)-x_{-1}y_{-2}b\right)+x_{-1}y_{-2}b}{1+x_{-3}z_{-2}(3s+t)f},$$

$$z_{6m+2t+1} = z_{2t-5}\prod_{s=0}^{m}\frac{x_{-1}y_{-1}z_{-1}}{x_{-3}y_{-3}z_{-3}}\frac{a^{3s+t+1}\left((1-a)-x_{-2}y_{-3}b\right)+x_{-2}y_{-3}b}{1+x_{-2}z_{-1}(3s+t+1)f}$$
$$\times \frac{1+x_{-3}z_{-2}(3s+t)f}{c^{3s+t}\left((1-c)-y_{-1}z_{-2}d\right)+y_{-1}z_{-2}d}$$
$$\times \frac{c^{3s+t-1}\left((1-c)-y_{-2}z_{-3}d\right)+y_{-2}z_{-3}d}{a^{3s+t-1}\left((1-a)-x_{-1}y_{-2}b\right)+x_{-1}y_{-2}b},$$

$$z_{6m+2t+2} = z_{2t-4}\prod_{s=0}^{m}\frac{x_{-3}y_{-3}z_{-3}}{x_{-1}y_{-1}z_{-1}}\frac{a^{3s+t+1}\left((1-a)-x_{-1}y_{-2}b\right)+x_{-1}y_{-2}b}{1+x_{-3}z_{-2}(3s+t+2)f}$$
$$\times \frac{1+x_{-2}z_{-1}(3s+t)f}{c^{3s+t+1}\left((1-c)-y_{-2}z_{-3}d\right)+y_{-2}z_{-3}d}$$
$$\times \frac{c^{3s+t-1}\left((1-c)-y_{-1}z_{-2}d\right)+y_{-1}z_{-2}d}{a^{3s+t}\left((1-a)-x_{-2}y_{-3}b\right)+x_{-2}y_{-3}b},$$

for $m \geq -1$ and $t \in \{1,2,3\}$.

3.5. Case $a = 1$, $c = 1$, $e \neq 1$

In this case, the solution of system (9) can be written in the following form

$$x_{6m+2t+1} = x_{2t-5}\prod_{s=0}^{m}\frac{x_{-1}y_{-1}z_{-1}}{x_{-3}y_{-3}z_{-3}}\frac{1+y_{-2}z_{-3}(3s+t+1)d}{1+x_{-1}y_{-2}(3s+t+1)b}$$
$$\times \frac{1+x_{-2}y_{-3}(3s+t)b}{e^{3s+t}\left((1-e)-x_{-2}z_{-1}f\right)+x_{-2}z_{-1}f}$$
$$\times \frac{e^{3s+t-1}\left((1-e)-x_{-3}z_{-2}f\right)+x_{-3}z_{-2}f}{1+y_{-1}z_{-2}(3s+t-1)d},$$

$$x_{6m+2t+2} = x_{2t-4} \prod_{s=0}^{m} \frac{x_{-3}y_{-3}z_{-3}}{x_{-1}y_{-1}z_{-1}} \frac{1 + y_{-1}z_{-2}(3s+t+1)d}{1 + x_{-2}y_{-3}(3s+t+2)b} \times \frac{1 + x_{-1}y_{-2}(3s+t)b}{e^{3s+t+1}\left((1-e) - x_{-3}z_{-2}f\right) + x_{-3}z_{-2}f} \times \frac{e^{3s+t-1}\left((1-e) - x_{-2}z_{-1}f\right) + x_{-2}z_{-1}f}{1 + y_{-2}z_{-3}(3s+t)d},$$

$$y_{6m+2t+1} = y_{2t-5} \prod_{s=0}^{m} \frac{x_{-1}y_{-1}z_{-1}}{x_{-3}y_{-3}z_{-3}} \frac{e^{3s+t+1}\left((1-e) - x_{-3}z_{-2}f\right) + x_{-3}z_{-2}f}{1 + y_{-1}z_{-2}(3s+t+1)d} \times \frac{1 + y_{-2}z_{-3}(3s+t)d}{1 + x_{-1}y_{-2}(3s+t)b} \frac{1 + x_{-2}y_{-3}(3s+t-1)b}{e^{3s+t-1}\left((1-e) - x_{-2}z_{-1}f\right) + x_{-2}z_{-1}f},$$

$$y_{6m+2t+2} = y_{2t-4} \prod_{s=0}^{m} \frac{x_{-3}y_{-3}z_{-3}}{x_{-1}y_{-1}z_{-1}} \frac{e^{3s+t+1}\left((1-e) - x_{-2}z_{-1}f\right) + x_{-2}z_{-1}f}{1 + y_{-2}z_{-3}(3s+t+2)d} \times \frac{1 + y_{-1}z_{-2}(3s+t)d}{1 + x_{-2}y_{-3}(3s+t+1)b} \frac{1 + x_{-1}y_{-2}(3s+t-1)b}{e^{3s+t}\left((1-e) - x_{-3}z_{-2}f\right) + x_{-3}z_{-2}f},$$

$$z_{6m+2t+1} = z_{2t-5} \prod_{s=0}^{m} \frac{x_{-1}y_{-1}z_{-1}}{x_{-3}y_{-3}z_{-3}} \frac{1 + x_{-2}y_{-3}(3s+t+1)b}{e^{3s+t+1}\left((1-e) - x_{-2}z_{-1}f\right) + x_{-2}z_{-1}f} \times \frac{e^{3s+t}\left((1-e) - x_{-3}z_{-2}f\right) + x_{-3}z_{-2}f}{1 + y_{-1}z_{-2}(3s+t)d} \frac{1 + y_{-2}z_{-3}(3s+t-1)d}{1 + x_{-1}y_{-2}(3s+t-1)b},$$

$$z_{6m+2t+2} = z_{2t-4} \prod_{s=0}^{m} \frac{x_{-3}y_{-3}z_{-3}}{x_{-1}y_{-1}z_{-1}} \frac{1 + x_{-1}y_{-2}(3s+t+1)b}{e^{3s+t+2}\left((1-e) - x_{-3}z_{-2}f\right) + x_{-3}z_{-2}f} \times \frac{e^{3s+t}\left((1-e) - x_{-2}z_{-1}f\right) + x_{-2}z_{-1}f}{1 + y_{-2}z_{-3}(3s+t+1)d} \frac{1 + y_{-1}z_{-2}(3s+t-1)d}{1 + x_{-2}y_{-3}(3s+t)b},$$

for $m \geq -1$ and $t \in \{1, 2, 3\}$.

3.6. Case $a = 1$, $c \neq 1$, $e = 1$

In this case, solutions of system (9) are as follows

$$x_{6m+2t+1} = x_{2t-5} \prod_{s=0}^{m} \frac{x_{-1}y_{-1}z_{-1}}{x_{-3}y_{-3}z_{-3}} \frac{c^{3s+t+1}\left((1-c) - y_{-2}z_{-3}d\right) + y_{-2}z_{-3}d}{1 + x_{-1}y_{-2}(3s+t+1)b} \times \frac{1 + x_{-2}y_{-3}(3s+t)b}{1 + x_{-2}z_{-1}(3s+t)f} \frac{1 + x_{-3}z_{-2}(3s+t-1)f}{c^{3s+t-1}\left((1-c) - y_{-1}z_{-2}d\right) + y_{-1}z_{-2}d},$$

$$x_{6m+2t+2} = x_{2t-4}\prod_{s=0}^{m}\frac{x_{-3}y_{-3}z_{-3}}{x_{-1}y_{-1}z_{-1}}\frac{c^{3s+t+1}\left((1-c)-y_{-1}z_{-2}d\right)+y_{-1}z_{-2}d}{1+x_{-2}y_{-3}(3s+t+2)b}$$
$$\times\frac{1+x_{-1}y_{-2}(3s+t)b}{1+x_{-3}z_{-2}(3s+t+1)f}\frac{1+x_{-2}z_{-1}(3s+t-1)f}{c^{3s+t}\left((1-c)-y_{-2}z_{-3}d\right)+y_{-2}z_{-3}d},$$

$$y_{6m+2t+1} = y_{2t-5}\prod_{s=0}^{m}\frac{x_{-1}y_{-1}z_{-1}}{x_{-3}y_{-3}z_{-3}}\frac{1+x_{-3}z_{-2}(3s+t+1)f}{c^{3s+t+1}\left((1-c)-y_{-1}z_{-2}d\right)+y_{-1}z_{-2}d}$$
$$\times\frac{c^{3s+t}\left((1-c)-y_{-2}z_{-3}d\right)+y_{-2}z_{-3}d}{1+x_{-1}y_{-2}(3s+t)b}\frac{1+x_{-2}y_{-3}(3s+t-1)b}{1+x_{-2}z_{-1}(3s+t-1)f},$$

$$y_{6m+2t+2} = y_{2t-4}\prod_{s=0}^{m}\frac{x_{-3}y_{-3}z_{-3}}{x_{-1}y_{-1}z_{-1}}\frac{1+x_{-2}z_{-1}(3s+t+1)f}{c^{3s+t+2}\left((1-c)-y_{-2}z_{-3}d\right)+y_{-2}z_{-3}d}$$
$$\times\frac{c^{3s+t}\left((1-c)-y_{-1}z_{-2}d\right)+y_{-1}z_{-2}d}{1+x_{-2}y_{-3}(3s+t+1)b}\frac{1+x_{-1}y_{-2}(3s+t-1)b}{1+x_{-3}z_{-2}(3s+t)f},$$

$$z_{6m+2t+1} = z_{2t-5}\prod_{s=0}^{m}\frac{x_{-1}y_{-1}z_{-1}}{x_{-3}y_{-3}z_{-3}}\frac{1+x_{-2}y_{-3}(3s+t+1)b}{1+x_{-2}z_{-1}(3s+t+1)f}$$
$$\times\frac{1+x_{-3}z_{-2}(3s+t)f}{c^{3s+t}\left((1-c)-y_{-1}z_{-2}d\right)+y_{-1}z_{-2}d}$$
$$\times\frac{c^{3s+t-1}\left((1-c)-y_{-2}z_{-3}d\right)+y_{-2}z_{-3}d}{1+x_{-1}y_{-2}(3s+t-1)b},$$

$$z_{6m+2t+2} = z_{2t-4}\prod_{s=0}^{m}\frac{x_{-3}y_{-3}z_{-3}}{x_{-1}y_{-1}z_{-1}}\frac{1+x_{-1}y_{-2}(3s+t+1)b}{1+x_{-3}z_{-2}(3s+t+2)f}$$
$$\times\frac{1+x_{-2}z_{-1}(3s+t)f}{c^{3s+t+1}\left((1-c)-y_{-2}z_{-3}d\right)+y_{-2}z_{-3}d}$$
$$\times\frac{c^{3s+t-1}\left((1-c)-y_{-1}z_{-2}d\right)+y_{-1}z_{-2}d}{1+x_{-2}y_{-3}(3s+t)b},$$

for $m \geq -1$ and $t \in \{1,2,3\}$.

3.7. Case $a \neq 1$, $c = 1$, $e = 1$

In this case, the solution of system (9) can be written in the following form

$$x_{6m+2t+1} = x_{2t-5}\prod_{s=0}^{m}\frac{x_{-1}y_{-1}z_{-1}}{x_{-3}y_{-3}z_{-3}}\frac{1+y_{-2}z_{-3}(3s+t+1)d}{a^{3s+t+1}\left((1-a)-x_{-1}y_{-2}b\right)+x_{-1}y_{-2}b}$$

$$\times \frac{a^{3s+t}\left((1-a)-x_{-2}y_{-3}b\right)+x_{-2}y_{-3}b}{1+x_{-2}z_{-1}(3s+t)f}\frac{1+x_{-3}z_{-2}(3s+t-1)f}{1+y_{-1}z_{-2}(3s+t-1)d},$$

$$x_{6m+2t+2}=x_{2t-4}\prod_{s=0}^{m}\frac{x_{-3}y_{-3}z_{-3}}{x_{-1}y_{-1}z_{-1}}\frac{1+y_{-1}z_{-2}(3s+t+1)d}{a^{3s+t+2}\left((1-a)-x_{-2}y_{-3}b\right)+x_{-2}y_{-3}b}$$
$$\times \frac{a^{3s+t}\left((1-a)-x_{-1}y_{-2}b\right)+x_{-1}y_{-2}b}{1+x_{-3}z_{-2}(3s+t+1)f}\frac{1+x_{-2}z_{-1}(3s+t-1)f}{1+y_{-2}z_{-3}(3s+t)d},$$

$$y_{6m+2t+1}=y_{2t-5}\prod_{s=0}^{m}\frac{x_{-1}y_{-1}z_{-1}}{x_{-3}y_{-3}z_{-3}}\frac{1+x_{-3}z_{-2}(3s+t+1)f}{1+y_{-1}z_{-2}(3s+t+1)d}$$
$$\times \frac{1+y_{-2}z_{-3}(3s+t)d}{a^{3s+t}\left((1-a)-x_{-1}y_{-2}b\right)+x_{-1}y_{-2}b}$$
$$\times \frac{a^{3s+t-1}\left((1-a)-x_{-2}y_{-3}b\right)+x_{-2}y_{-3}b}{1+x_{-2}z_{-1}(3s+t-1)f},$$

$$y_{6m+2t+2}=y_{2t-4}\prod_{s=0}^{m}\frac{x_{-3}y_{-3}z_{-3}}{x_{-1}y_{-1}z_{-1}}\frac{1+x_{-2}z_{-1}(3s+t+1)f}{1+y_{-2}z_{-3}(3s+t+2)d}$$
$$\times \frac{1+y_{-1}z_{-2}(3s+t)d}{a^{3s+t+1}\left((1-a)-x_{-2}y_{-3}b\right)+x_{-2}y_{-3}b}$$
$$\times \frac{a^{3s+t-1}\left((1-a)-x_{-1}y_{-2}b\right)+x_{-1}y_{-2}b}{1+x_{-3}z_{-2}(3s+t)f},$$

$$z_{6m+2t+1}=z_{2t-5}\prod_{s=0}^{m}\frac{x_{-1}y_{-1}z_{-1}}{x_{-3}y_{-3}z_{-3}}\frac{a^{3s+t+1}\left((1-a)-x_{-2}y_{-3}b\right)+x_{-2}y_{-3}b}{1+x_{-2}z_{-1}(3s+t+1)f}$$
$$\times \frac{1+x_{-3}z_{-2}(3s+t)f}{1+y_{-1}z_{-2}(3s+t)d}\frac{1+y_{-2}z_{-3}(3s+t-1)d}{a^{3s+t-1}\left((1-a)-x_{-1}y_{-2}b\right)+x_{-1}y_{-2}b},$$

$$z_{6m+2t+2}=z_{2t-4}\prod_{s=0}^{m}\frac{x_{-3}y_{-3}z_{-3}}{x_{-1}y_{-1}z_{-1}}\frac{a^{3s+t+1}\left((1-a)-x_{-1}y_{-2}b\right)+x_{-1}y_{-2}b}{1+x_{-3}z_{-2}(3s+t+2)f}$$
$$\times \frac{1+x_{-2}z_{-1}(3s+t)f}{1+y_{-2}z_{-3}(3s+t+1)d}\frac{1+y_{-1}z_{-2}(3s+t-1)d}{a^{3s+t}\left((1-a)-x_{-2}y_{-3}b\right)+x_{-2}y_{-3}b},$$

for $m\geq -1$ and $t\in\{1,2,3\}$.

3.8. Case $a=1$, $c=1$, $e=1$

In this case, solutions of system (9) are as follows

$$x_{6m+2t+1}=x_{2t-5}\prod_{s=0}^{m}\frac{x_{-1}y_{-1}z_{-1}}{x_{-3}y_{-3}z_{-3}}\frac{1+y_{-2}z_{-3}(3s+t+1)d}{1+x_{-1}y_{-2}(3s+t+1)b}\times\frac{1+x_{-2}y_{-3}(3s+t)b}{1+x_{-2}z_{-1}(3s+t)f}\frac{1+x_{-3}z_{-2}(3s+t-1)f}{1+y_{-1}z_{-2}(3s+t-1)d},$$

$$x_{6m+2t+2}=x_{2t-4}\prod_{s=0}^{m}\frac{x_{-3}y_{-3}z_{-3}}{x_{-1}y_{-1}z_{-1}}\frac{1+y_{-1}z_{-2}(3s+t+1)d}{1+x_{-2}y_{-3}(3s+t+2)b}\times\frac{1+x_{-1}y_{-2}(3s+t)b}{1+x_{-3}z_{-2}(3s+t+1)f}\frac{1+x_{-2}z_{-1}(3s+t-1)f}{1+y_{-2}z_{-3}(3s+t)d},$$

$$y_{6m+2t+1}=y_{2t-5}\prod_{s=0}^{m}\frac{x_{-1}y_{-1}z_{-1}}{x_{-3}y_{-3}z_{-3}}\frac{1+x_{-3}z_{-2}(3s+t+1)f}{1+y_{-1}z_{-2}(3s+t+1)d}\times\frac{1+y_{-2}z_{-3}(3s+t)d}{1+x_{-1}y_{-2}(3s+t)b}\frac{1+x_{-2}y_{-3}(3s+t-1)b}{1+x_{-2}z_{-1}(3s+t-1)f},$$

$$y_{6m+2t+2}=y_{2t-4}\prod_{s=0}^{m}\frac{x_{-3}y_{-3}z_{-3}}{x_{-1}y_{-1}z_{-1}}\frac{1+x_{-2}z_{-1}(3s+t+1)f}{1+y_{-2}z_{-3}(3s+t+2)d}\times\frac{1+y_{-1}z_{-2}(3s+t)d}{1+x_{-2}y_{-3}(3s+t+1)b}\frac{1+x_{-1}y_{-2}(3s+t-1)b}{1+x_{-3}z_{-2}(3s+t)f}$$

$$z_{6m+2t+1}=z_{2t-5}\prod_{s=0}^{m}\frac{x_{-1}y_{-1}z_{-1}}{x_{-3}y_{-3}z_{-3}}\frac{1+x_{-2}y_{-3}(3s+t+1)b}{1+x_{-2}z_{-1}(3s+t+1)f}\times\frac{1+x_{-3}z_{-2}(3s+t)f}{1+y_{-1}z_{-2}(3s+t)d}\frac{1+y_{-2}z_{-3}(3s+t-1)d}{1+x_{-1}y_{-2}(3s+t-1)b},$$

$$z_{6m+2t+2}=z_{2t-4}\prod_{s=0}^{m}\frac{x_{-3}y_{-3}z_{-3}}{x_{-1}y_{-1}z_{-1}}\frac{1+x_{-1}y_{-2}(3s+t+1)b}{1+x_{-3}z_{-2}(3s+t+2)f}\times\frac{1+x_{-2}z_{-1}(3s+t)f}{1+y_{-2}z_{-3}(3s+t+1)d}\frac{1+y_{-1}z_{-2}(3s+t-1)d}{1+x_{-2}y_{-3}(3s+t)b},$$

for $m\geq -1$ and $t\in\{1,2,3\}$.

Lemma 2. *If $a\neq 1$, $c\neq 1$, $e\neq 1$, $b\neq 0$, $d\neq 0$ and $f\neq 0$, then the system (9) has $6-$periodic solutions.*

Proof. Let

$$\alpha_n = x_{n-2}y_{n-3}, \quad \beta_n = y_{n-2}z_{n-3} \quad \text{and} \quad \gamma_n = z_{n-2}x_{n-3}, \; n \in \mathbb{N}_0.$$

Then from (9) we get

$$\alpha_{n+2} = \frac{\alpha_n}{a + b\alpha_n}, \quad \beta_{n+2} = \frac{\beta_n}{c + d\beta_n} \quad \text{and} \quad \gamma_{n+2} = \frac{\gamma_n}{e + f\gamma_n}, \; n \in \mathbb{N}_0. \tag{18}$$

If $b \neq 0$, $d \neq 0$ and $f \neq 0$, then system (18) has a unique equilibrium solution which $(\overline{\alpha}, \overline{\beta}, \overline{\gamma})$ is different from $(0,0,0)$, that is,

$$\alpha_n = \overline{\alpha} = \frac{1-a}{b} \neq 0, \quad \beta_n = \overline{\beta} = \frac{1-c}{d} \neq 0, \quad \gamma_n = \overline{\gamma} = \frac{1-e}{f} \neq 0, \quad n \in \mathbb{N}_0.$$

If $\overline{\alpha} = 0$ or $\overline{\beta} = 0$ or $\overline{\gamma} = 0$, then system (9) has not well-defined solutions. From (18), we have

$$\begin{aligned} x_{n-2} &= \frac{1-a}{by_{n-3}} = \frac{(1-a)d}{b(1-c)} z_{n-4} = \frac{(1-a)d(1-e)}{b(1-c)fx_{n-5}}, \\ &= \frac{d(1-e)}{(1-c)f} y_{n-6} = \frac{1-e}{fz_{n-7}} = x_{n-8}, \; n \geq 5, \\ y_{n-2} &= \frac{1-c}{dz_{n-3}} = \frac{(1-c)f}{d(1-e)} x_{n-4} = \frac{(1-c)f(1-a)}{d(1-e)by_{n-5}} \\ &= \frac{f(1-a)}{(1-e)b} z_{n-6} = \frac{1-a}{bx_{n-7}} = y_{n-8}, \; n \geq 5, \\ z_{n-2} &= \frac{1-e}{fx_{n-3}} = \frac{(1-e)b}{f(1-a)} y_{n-4} = \frac{(1-e)b(1-c)}{f(1-a)dz_{n-5}} \\ &= \frac{b(1-c)}{(1-a)d} x_{n-6} = \frac{1-c}{dy_{n-7}} = z_{n-8}, \; n \geq 5, \end{aligned}$$

from which along with the assumptions in Lemma 2, the results can be easily seen. □

The following theorem give the forbidden set of the initial conditions for system (9).

Theorem 1. *Assume that $a \neq 0$, $b \neq 0$, $c \neq 0$, $d \neq 0$, $e \neq 0$, $f \neq 0$. The forbidden set of the initial values for system (9) is given by the set*

$$\begin{aligned} \mathbb{F} = \bigcup_{m \in \mathbb{N}_0} \bigcup_{i=0}^{1} \Big\{ &\frac{1}{x_{i-2}y_{i-3}} = \widehat{f}^{-m-1}\left(-\frac{b}{a}\right), \quad \frac{1}{y_{i-2}z_{i-3}} = g^{-m-1}\left(-\frac{d}{c}\right), \\ &\frac{1}{z_{i-2}x_{i-3}} = h^{-m-1}\left(-\frac{f}{e}\right) \Big\} \bigcup \bigcup_{j=1}^{3} \Big\{ \left(\vec{x}_{-(3,1)}, \vec{y}_{-(3,1)}, \vec{z}_{-(3,1)}\right) \in \mathbb{R}^9 : \\ &x_{-j} = 0 \text{ or } y_{-j} = 0 \text{ or } z_{-j} = 0 \Big\}, \end{aligned} \tag{19}$$

where $\vec{x}_{-(3,1)} = (x_{-3}, x_{-2}, x_{-1})$, $\vec{y}_{-(3,1)} = (y_{-3}, y_{-2}, y_{-1})$, $\vec{z}_{-(3,1)} = (z_{-3}, z_{-2}, z_{-1})$.

Proof. We have obtained that the set

$$\bigcup_{j=1}^{3} \left\{ \left(\vec{x}_{-(3,1)}, \vec{y}_{-(3,1)}, \vec{z}_{-(3,1)}\right) \in \mathbb{R}^9 : \ x_{-j} = 0 \text{ or } y_{-j} = 0 \text{ or } z_{-j} = 0 \right\},$$

where $\vec{x}_{-(3,1)} = (x_{-3}, x_{-2}, x_{-1})$, $\vec{y}_{-(3,1)} = (y_{-3}, y_{-2}, y_{-1})$, $\vec{z}_{-(3,1)} = (z_{-3}, z_{-2}, z_{-1})$, belongs to the forbidden set of the initial values for system (9) at the beginning of Section 2. If $x_{-j} \neq 0$, $y_{-j} \neq 0$ and $z_{-j} \neq 0$, $j \in \{1, 2, 3\}$, then system (9) is undefined if and only if

$$a + bx_{n-2}y_{n-3} = 0, \ c + dy_{n-2}z_{n-3} = 0, \ e + fz_{n-2}x_{n-3} = 0, \ n \in \mathbb{N}_0.$$

By taking into account the change of variables (12), we can write the corresponding conditions

$$u_{n-2} = -\frac{b}{a}, \ v_{n-2} = -\frac{d}{c} \text{ and } \ w_{n-2} = -\frac{f}{e}, \ n \in \mathbb{N}_0. \tag{20}$$

Therefore, we can determine the forbidden set of the initial values for system (9) by using system (13). We know that the statements

$$u_{2m+i} = \widehat{f}^{m+1}\left(u_{i-2}\right), \tag{21}$$

$$v_{2m+i} = g^{m+1}\left(v_{i-2}\right), \tag{22}$$

$$w_{2m+i} = h^{m+1}\left(w_{i-2}\right), \tag{23}$$

where $m \in \mathbb{N}_0$, $i \in \{0, 1\}$, $\widehat{f}(x) = ax + b$, $g(x) = cx + d$ and $h(x) = ex + f$, characterize the solutions of system (9). By using the conditions (20) and the statements (21)-(23), we have

$$u_{i-2} = \widehat{f}^{-m-1}\left(-\frac{b}{a}\right), \tag{24}$$

$$v_{i-2} = g^{-m-1}\left(-\frac{d}{c}\right), \tag{25}$$

$$w_{i-2} = h^{-m-1}\left(-\frac{f}{e}\right), \tag{26}$$

where $m \in \mathbb{N}_0$, $i \in \{0, 1\}$ and $abcdef \neq 0$. This means that if one of the conditions in (24)-(26) holds, then $m-$th iteration or $(m+1)-$th iteration in system (9) can not be calculated. Consequently, we obtain the result in (19). □

4. Conclusion

In this paper, we have solved the following three-dimensional system of difference equations

$$x_n = \frac{x_{n-2}y_{n-3}}{y_{n-1}\left(a + bx_{n-2}y_{n-3}\right)},$$

$$y_n = \frac{y_{n-2}z_{n-3}}{z_{n-1}\left(c+dy_{n-2}z_{n-3}\right)}, n \in \mathbb{N}_0,$$
$$z_n = \frac{z_{n-2}x_{n-3}}{x_{n-1}\left(e+fz_{n-2}x_{n-3}\right)},$$

where the initial values x_{-i}, y_{-i}, z_{-i}, $i=\overline{1,3}$ and the parameters a, b, c, d, e, f are non-zero real numbers. In addition, we have obtained the solutions of above system in explicit form according to the parameters a, c and e are equal 1 or not equal 1. Moreover, we have got periodic solutions of aforementioned system. Finally, we have identified the forbidden set of the initial conditions by using the acquired formulas.

Author Contribution Statements All authors contributed equally and significantly to this manuscript and they read and approved the final manuscript.

Declaration of Competing Interests The authors declare that they have no competing interest.

Acknowledgements This paper was presented in 4th International Conference on Pure and Applied Mathematics (ICPAM - VAN 2022), Van-Turkey, June 22-23, 2022. This work is supported by the Scientific Research Project Fund of Karamanoglu Mehmetbey University under the project number 13-YL-22.

References

[1] Abo-Zeid, R., Kamal, H., Global behavior of two rational third order difference equations, *Univers. J. Math. Appl.*, 2(4) (2019), 212-217. https://doi.org/10.32323/ujma.626465.

[2] Abo-Zeid, R., Behavior of solutions of a second order rational difference equation, *Math. Morav.*, 23(1) (2019), 11-25. https://doi.org/10.5937/MatMor1901011A.

[3] Abo-Zeid, R., Global behavior and oscillation of a third order difference equation, *Quaest. Math.*, 44(9) (2021), 1261-1280. https://doi.org/10.2989/16073606.2020.1787537.

[4] Ahmed, A. M., Elsayed, E. M., The expressions of solutions and the periodicity of some rational difference equations systems, *J. Appl. Math. Inform.*, 34(1-2) (2016), 35-48. https://doi.org/10.14317/jami.2016.035.

[5] Cinar, C., Toufik, M., Yalcinkaya, I., On the difference equation of higher order, *Util. Math.*, 92 (2013), 161–166.

[6] Cinar, C., On the positive solutions of the difference equation $x_{n+1} = \frac{x_{n-1}}{1+x_n x_{n-1}}$, *Appl. Math. Comput.*, 150(1) (2004), 21-24. https://doi.org/10.1016/S0096-3003(03)00194-2.

[7] El-Metwally, H., Elsayed, E. M., Solution and behavior of a third rational difference equation, *Util. Math.*, 88 (2012), 27-42.

[8] Elsayed, E. M., Ahmed, A. M., Dynamics of a three dimensional system of rational difference equations, *Math. Methods Appl. Sci.*, 39(5) (2016), 1026–1038. https://doi.org/10.1002/mma.3540.

[9] Elsayed, E. M., Alotaibi, A., Almaylabi, H. A., On a solutions of fourth order rational systems of difference equations, *J. Comput. Anal. Appl.*, 22(7) (2017), 1298-1308.

[10] Elsayed, E. M., On the solutions and periodic nature of some systems of difference equations, *Int. J. Biomath.*, 7(6) (2014), 1-26. https://doi.org/10.1142/S1793524514500673.

[11] Folly-Gbetoula, M., Nyirenda, D., A generalized two-dimensional system of higher order recursive sequences, *J. Difference Equ. Appl.*, 26(2) (2020), 244-260. https://doi.org/10.1080/10236198.2020.1718667.

[12] Gelisken, A., Kara, M., Some general systems of rational difference equations, *J. Difference Equ.*, 396757 (2015), 1-7. http://dx.doi.org/10.1155/2015/396757.

[13] Halim, Y., Touafek, N., Yazlik, Y., Dynamic behavior of a second-order nonlinear rational difference equation, *Turk. J. Math.*, 39(6) (2015), 1004-1018. https://doi.org/10.3906/mat-1503-80.

[14] Halim, Y., Rabago, J. F. T., On the solutions of a second-order difference equation in terms of generalized Padovan sequences, *Math. Slovaca.*, 68(3) (2018), 625–638. https://doi.org/10.1515/ms-2017-0130.

[15] Ibrahim, T. F., Touafek, N., On a third order rational difference equation with variable coefficients, *Dyn. Contin. Discrete Impuls. Syst. Ser. B Appl. Algorithms.*, 20 (2013), 251-264.

[16] Kara, M., Yazlik, Y., On the system of difference equations $x_n = \frac{x_{n-2}y_{n-3}}{y_{n-1}(a_n+b_nx_{n-2}y_{n-3})}$, $y_n = \frac{y_{n-2}x_{n-3}}{x_{n-1}(\alpha_n+\beta_ny_{n-2}x_{n-3})}$, *J. Math. Extension.*, 14(1) (2020), 41-59.

[17] Kara, M., Yazlik, Y., Solvability of a system of nonlinear difference equations of higher order, *Turk. J. Math.*, 43(3) (2019), 1533-1565. https://doi.org/10.3906/mat-1902-24.

[18] Kara, M., Yazlik, Y., On a solvable system of non-linear difference equations with variable coefficients, *J. Sci. Arts.*, 1(54) (2021), 145-162. https://doi.org/10.46939/J.Sci.Arts-21.1-a13.

[19] Kara, M., Yazlik, Y., Touafek, N., Akrour, Y., On a three-dimensional system of difference equations with variable coefficients, *J. Appl. Math. Inform.*, 39(3-4) (2021), 381-403. https://doi.org/10.14317/jami.2021.381.

[20] Kara, M., Yazlik, Y., On the solutions of three-dimensional system of difference equations via recursive relations of order two and applications, *J. Appl. Anal. Comput.*, 12(2) (2022), 736-753. https://doi.org/10.11948/20210305.

[21] Kara, M., Yazlik, Y., On a solvable system of rational difference equations of higher order, *Turk. J. Math.*, 46 (2022), 587-611. https://doi.org/10.3906/mat-2106-1.

[22] Kara, M., Solvability of a three-dimensional system of non-liner difference equations, *Math. Sci. Appl. E-Notes.*, 10(1) (2022), 1-15. https://doi.org/10.36753/mathenot.992987.

[23] Kara, M., Yazlik, Y., Solutions formulas for three-dimensional difference equations system with constant coefficients, *Turk. J. Math. Comput. Sci.*, 14(1) (2022), 107-116. https://doi.org/10.47000/tjmcs.1060075.

[24] Elaydi, S., An Introduction to Difference Equations, Springer, New York, 1996.

[25] Taskara, N., Uslu, K., Tollu, D. T., The periodicity and solutions of the rational difference equation with periodic coefficients, *Comput. Math. Appl.*, 62(4) (2011), 1807-1813. https://doi.org/10.1016/j.camwa.2011.06.024.

[26] Taskara, N., Tollu, D. T., Yazlik, Y., Solutions of rational difference system of order three in terms of Padovan numbers, *J. Adv. Res. Appl. Math.*, 7(3) (2015), 18–29. https://doi.org/10.5373/jaram.2223.120914.

[27] Taskara, N., Tollu, D. T., Touafek, N., Yazlik, Y., A solvable system of difference equations, *Comm. Korean Math. Soc.*, 35(1) (2020), 301-319. https://doi.org/10.4134/CKMS.c180472.

[28] Tollu, D. T., Yazlik, Y., Taskara, N., On fourteen solvable systems of difference equations, *Appl. Math. Comput.*, 233 (2014), 310-319. https://doi.org/10.1016/j.amc.2014.02.001.

[29] Tollu, D. T., Yazlik, Y., Taskara, N., Behavior of positive solutions of a difference equation, *J. Appl. Math. Inform.*, 35(3-4) (2017), 217–230. https://doi.org/10.14317/jami.2017.217.

[30] Tollu, D. T., Yazlik, Y., Taskara, N., On the solutions of two special types of Riccati difference equation via Fibonacci numbers, *Adv. Difference Equ.*, 174 (2013), 1-7. https://doi.org/10.1186/1687-1847-2013-174.

[31] Tollu, D. T., Yazlik, Y., Taskara, N., On a solvable nonlinear difference equation of higher-order, *Turk. J. Math.*, 42(4) (2018), 1765-1778. https://doi.org/10.3906/mat-1705-33.

[32] Tollu, D. T., Yalcinkaya, I., Global behavior of a three-dimensional system of difference equations of order three, *Commun. Fac. Sci. Univ. Ank. Ser. A1 Math. Stat.*, 68(1) (2019), 1-16. https://doi.org/10.31801/cfsuasmas.443530.

[33] Touafek, N., On a second order rational difference equation, *Hacet. J. Math. Stat.*, 41 (2012), 867-874.

[34] Touafek, N., Elsayed, E. M., On a second order rational systems of difference equations, *Hokkaido Math. J.*, 44(1) (2015), 29-45.

[35] Yalcinkaya, I., Cinar, C., Global asymptotic stability of a system of two nonlinear difference equations, *Fasc. Math.*, 43 (2010), 171-180.

[36] Yalcinkaya, I., Hamza, A. E., Cinar, C., Global behavior of a recursive sequence, *Selçuk J. Appl. Math.*, 14(1) (2013), 3-10.

[37] Yalcinkaya, I., Tollu, D. T., Global behavior of a second order system of difference equations, *Adv. Stud. Contemp. Math.*, 26(4) (2016), 653-667.

[38] Yazlik, Y., Tollu, D. T., Taskara, N., Behaviour of solutions for a system of two higher-order difference equations, *J. Sci. Arts.*, 4(45) (2018), 813-826.

[39] Yazlik, Y., Kara, M., On a solvable system of difference equations of fifth-order, *Eskisehir Tech. Univ. J. Sci. Tech. B-Theoret. Sci.*, 7(1) (2019), 29-45. https://doi.org/10.20290/aubtdb.422910.

[40] Yazlik, Y., Gungor, M., On the solvable of nonlinear difference equation of sixth-order, *J. Sci. Arts.*, 2(47) (2019), 399-414.

[41] Yazlik, Y., Kara, M., On a solvable system of difference equations of higher-order with period two coefficients, *Commun. Fac. Sci. Univ. Ank. Ser. A1 Math. Stat.*, 68(2) (2019), 1675-1693. https://doi.org/10.31801/cfsuasmas.548262.

http://communications.science.ankara.edu.tr

Commun.Fac.Sci.Univ.Ank.Ser. A1 Math. Stat.
Volume 72, Number 2, Pages 482–499 (2023)
DOI:10.31801/cfsuasmas.1202806
ISSN 1303-5991 E-ISSN 2618-6470

Research Article; Received: November 11, 2022; Accepted: December 27, 2022

DETECTION OF MONKEYPOX DISEASE FROM SKIN LESION IMAGES USING MOBILENETV2 ARCHITECTURE

Oznur OZALTIN[1] and Ozgur YENIAY[2]

[1,2]Department of Statistics, Hacettepe University, Beytepe Campus, 06800 Ankara, TÜRKİYE

Abstract. Monkeypox has recently become an endemic disease that threatens the whole world. The most distinctive feature of this disease is occurring skin lesions. However, in other types of diseases such as chickenpox, measles, and smallpox skin lesions can also be seen. The main aim of this study was to quickly detect monkeypox disease from others through deep learning approaches based on skin images. In this study, MobileNetv2 was used to determine in images whether it was monkeypox or non-monkeypox. To find splitting methods and optimization methods, a comprehensive analysis was performed. The splitting methods included training and testing (70:30 and 80:20) and 10 fold cross validation. The optimization methods as adaptive moment estimation (adam), root mean square propagation (rmsprop), and stochastic gradient descent momentum (sgdm) were used. Then, MobileNetv2 was tasked as a deep feature extractor and features were obtained from the global pooling layer. The Chi-Square feature selection method was used to reduce feature dimensions. Finally, selected features were classified using the Support Vector Machine (SVM) with different kernel functions. In this study, 10 fold cross validation and adam were seen as the best splitting and optimization methods, respectively, with an accuracy of 98.59%. Then, significant features were selected via the Chi-Square method and while classifying 500 features with SVM, an accuracy of 99.69% was observed.

1. Introduction

Monkeypox virus, a zoonotic orthopox DNA virus related to the virus that reasons smallpox, was first observed in humans in 1970 in the Democratic Republic of Congo (namely Zaire) [1,2]. Sporadic outbreaks of infection have been declared in Africa, typically resulting from contact with wildlife reservoirs (especially rodents) [2,3]. Such epidemics and travel-related events outside Africa have had

2020 *Mathematics Subject Classification.* 68T07, 68U10.
Keywords. Chi-Square method, deep learning, feature selection, monkeypox, optimization.
oznurozaltin@hacettepe.edu.tr-Corresponding author; 0000-0001-9841-1702
yeniay@hacettepe.edu.tr; 0000-0002-0287-4524.

restricted secondary spread, and thus human-to-human infection has been assumed ineffective [2,4–7]. Although the monkeypox virus has been prevalent for years in zones where it was conventionally an endemic disease, the search for monkeypox has been disregarded and non-financed [2]. As of early May 2022, more than 3000 monkeypox virus infections have been noticed in more than 50 countries through five zones, canalizing the World Health Organization to declare monkeypox a developing medium public health fear threat on June 23, 2022 [2,8]. Anxieties about the appearance of various infections in the coronavirus pandemic have been rising daily. The monkeypox disease was also feared by the people. To diagnose monkeypox early and take the necessary precautions, deep learning algorithms could be preferred by speeding up the process. For this purpose, one of the deep learning algorithms was used to detect monkeypox disease. Nowadays, deep learning algorithms have been widely used, particularly in image classification [9–15]. When images were classified, generally convolutional neural network (CNN) was utilized as a classifier. However, it has been considered that creating a novel CNN was difficult. Therefore, pre-trained architectures were determined as facilitators of this problem. In this study, MobileNetv2 which was a pre-trained architecture was preferred because of faster and more effective to recognize monkeypox disease. For determining the disease, the dataset was utilized from the publicly available website. This dataset contained monkeypox skin images and non-monkeypox skin images. Not only MobileNetv2 was used as a classifier but also performed as a deep feature extractor from these images. First, it was utilized as a classifier in different ways and then, it was performed as a feature extractor and merged with the Chi-Square feature selection method and Support Vector Machine (SVM) algorithm to provide confidence in the structure. Therefore, created this structure was called the hybrid algorithm. The pipeline of this study was displayed in Figure 1. The main contributions of this study are as follows:

- Used MobileNetv2 to detect monkeypox disease from skin images.
- Different splitting methods as training and testing (70:30 and 80:20) and 10 fold cross validation were carried out.
- Diverse optimization methods: adam, rmsprop and sgdm were also investigated in terms of classification success.
- Found the best splitting method as 10 fold cross validation and the best optimization method as adam based on performance metrics: accuracy, specificity, sensitivity, precision, G-Mean, F1-score, and AUC (Area Under Curve).
- Extracted 1280 features for each image from global average pooling of MobileNetv2 to improve monkeypox detection.
- Reduced these features to 250, 500, and 1000 by using the Chi-Square method and decisioned to the number of the minimum features was 500 according to results.

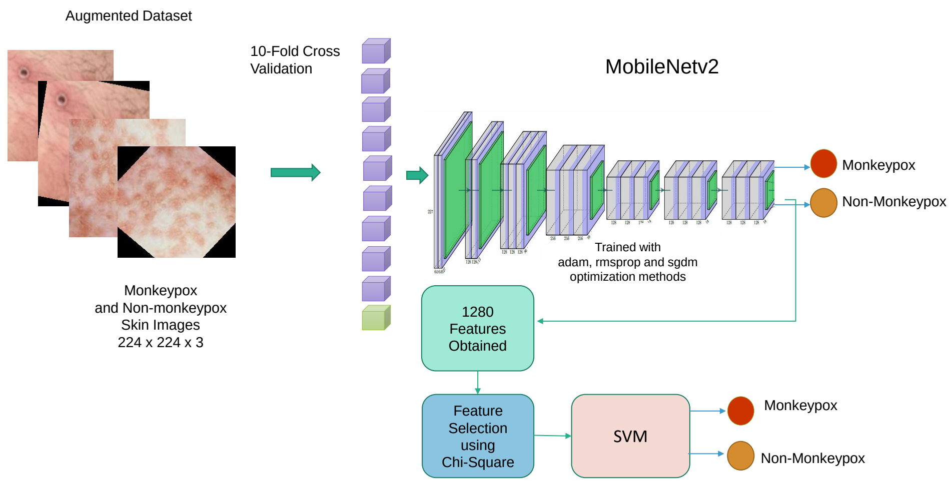

FIGURE 1. The pipeline of the study.

- Classified the reduced features based on SVM with linear, gaussian, and polynomial kernel functions to detect as monkeypox or non-monkeypox in the final of the study.
- Obtained the top results with the hybrid algorithm.

The rest of the study is organized as follows: In Section 1, the literature review was expressed. Then, utilized methods were stated in Section 2. In Section 3; the dataset, performance metrics, Receiver operating characteristic (ROC) curve, cross validation, hyperparameter selection, and experimental results were clarified. Then, the advantages and disadvantages of this study were discussed in Section 4. Finally, the study has been finalized the study in Section 5.

1.1. **Literature Review.** In this study, when the monkeypox image classification studies were searched, not much more studies were seen. Though monkeypox disease emerged in 1970 [16], deep learning based studies have been newly raised. Sahin et al. [16] used a monkeypox image dataset to detect monkeypox via mobile device. They performed some pre-trained architectures: ResNet18, GoogleNet, Efficientb0, NasnetMobile, ShuffleNet, MobileNetv2. At the end of their study, the best performance was obtained based on MobileNetv2 with an accuracy of 91.11%. Ali et al. [17] utilized a monkeypox image dataset for binary classification using pre-trained architectures: VGG-16, ResNet50, and InceptionV3 with 3 fold cross validation. Final of the study, ResNet50 obtained the highest accuracy at 82.96%. Ahsan et al. [18] created two studies for recognizing monkeypox virus from images.

First one was which detecting monkeypox from original collected images, another was which detecting monkeypox from augmented images. Both studies were analyzed through deep learning based algorithms. They also benefited from one of the pre-trained architectures, VGG-16. Eventually, they obtained an accuracy of 97% and 88% for original images and augmented images to classify, respectively. Alakus and Baykara [19] researched to find monkeypox disease from DNA sequences via a deep learning approach. This is because monkeypox disease has different DNA sequences from warts and sometimes warts and monkeypox are not differentiable from each other. Therefore, they obtained DNA sequences of both warts and monkeypox and mapped them. Then, the mapped sequences were classified to detect monkeypox via bidirectional long/short term memory (BiLSTM) algorithm. In final, their study acquired an average accuracy of 96.08%. Sitaula and Shahi [20] used monkeypox image dataset to determine the disease via deep learning algorithm. Firstly, they performed two different visualization methods: Gradient weighted Class Activation Mapping (Grand-CAM) and Local Interpretable Model-Agnostic Explanations (LIME). Next, Xception architecture was used for classifying monkeypox dataset and it obtained an accuracy of 86.51%. Akin et al. [21] employed 12 different pre-trained architectures to classify the monkeypox image dataset into normal and monkeypox classes. At the end of the comparison, MobileNetv2 hit to top with an accuracy of 98.25%. Abdelhamid et al. [22] classified monkeypox image dataset based on transfer learning method with created hybrid deep learning algorithm. The algorithm first realized deep feature extraction via GoogleNet and then, it selected significant features through the Al-Biruni earth radius optimization algorithm. Finally, their proposed hybrid algorithm reached an accuracy of 98.8%.

2. Methods

2.1. **Convolutional Neural Network.** Convolutional Neural Network (CNN) has been one of the deep learning algorithms to analyze data generally used for images [23]. This name has come from the mathematical linear operation between matrices called convolution [24].It has been inspired by the structure of the animal visual cortex [23, 25, 26] and also created to automatically learn spatial hierarchies of features, from low to high level forms. CNN has had a complex mathematical structure because of including black-box [27]. The CNN processes an image in different layers and separates all its properties. The most generally applied layers have been: convolution layer, activation layer, pooling layer (maximum, average, or global), flattening layer, fully connected layer expressed as [28–30].

2.2. **MobileNetv2: Classification architecture and Deep Feature Extractor.** MobileNetv2 [31, 32] has used lightweight depth wise convolutions to filter features. It has two main blocks and contained the initial fully convolutional layer with 32 filters. Then, 19 residual bottleneck layers have been traced. In fact, it was put forward for mobile devices. MobileNetv2 is known as pre-trained architecture. In general, a CNN is created very hard and consumed time. Therefore, this situation was considered and this architecture was effectively used as a classifier and deep feature extractor. MobileNetv2 utilized in this study possesses some advantages: speedy performance, few parameters, needs little memory, etc. In addition, it can be employed in mobile applications, as well [12]. When a pre-trained architecture or other CNN architectures were applied, Stochastic gradient descent momentum (sgdm) [33] had been preferred as an optimization method [10,12,34]. However, the presented study, not only used sgdm but also employed Adaptive moment estimation (adam) [35] and Root Mean Square Propagation (rmsprop) [36]. In this study, 1280 features of each monkeypox image were obtained from the global average pooling layer called global-average while it was applied as a deep feature extractor. Next, obtained features were selected via Chi-Square (χ^2) method.

2.3. **Feature Selection through Chi-Square(χ^2)Method.** The Chi-Square has been a preferable statistical method to generate a rank about the effectively of a cell in a knowledge table. Sometimes, it has been expressed as the Pearson Chi-Square test or the Chi-Square test [12]. The rank is determined by using the difference between the expected value and the actual value of a cell in a Chi-Square test [12,37,38]. The Chi-Square value is computed as follows in Equation(1) [37,38]:

$$\chi^2 = \sum_{i=1}^{R} \sum_{j=1}^{C} \frac{(f_{ij} - e_{ij})^2}{e_{ij}} \tag{1}$$

where f_{ij} : actual value, e_{ij} : expected value, R : row, C : column, $i = 1, 2, ..., R$, $j = 1, 2, ..., C$, and χ^2: calculated Chi-Square value are represented. In first, the expected value is calculated for each cell. Then, it is calculated squared of the actual value and the expected value difference and divided by the expected value for each cell. After that, calculated these values are summed up. To obtain p-value, this sum is utilized in the probability density function(pdf) [12]. Before this stage is initiated, the degree of freedom should be found as follows in Equation (2):

$$\nu = (R - 1)(C - 1) \tag{2}$$

The pdf is calculated as follows in Equation (3) [39]:

$$f\left(x, \nu\right) = \frac{1}{2^{\frac{\nu}{2}} \Gamma\left(\frac{\nu}{2}\right)} x^{\frac{\nu}{2}-1} e^{-\frac{\nu}{2}}, x > 0 \tag{3}$$

The p-value is also seen as follows in Equation (4) [12]:

$$p - value = \int_{\chi^2}^{\infty} f\left(x, \nu\right) dx \tag{4}$$

p-value is widely found through Chi-Square tables instead of calculating in many implementations since integrating this equation is not an easy way [12]. When applied to feature selection, the table for which the Chi-Square value should be computed is composed of set feature records against classes [12]. Therefore, this value was computed and features were sorted via their relation with class. Then, the highest related 250, 500, and 1000 features were investigated. At the end of the part, the dimension of the features was effectively reduced through Chi-Square method.

2.4. **Support Vector Machine (SVM).** In general, a classical learning approach is constructed to minimize errors in the training dataset based on empirical theory [40]. However, a Support Vector Machine (SVM) is built for the minimization of structural risk based on the statistical learning theory. Additionally, it can be explained with mathematical equations [41]. For this reason, it can be preferred in healthcare analysis. SVM possesses the potential to tackle very large feature spaces. This is because the training of SVM is realized so that the dimension of classified vectors does not have as different an effect on the performance of SVM as it possesses on the performance of the conventional classifier [40]. Therefore, it is observed to be mainly effective in big classification problems [40]. In this study, SVM was efficiently employed as a classifier after selecting features from monkeypox images with Gaussian, Linear, and Polynomial kernel functions.

3. Results

3.1. **Monkeypox Dataset.** In this study, Monkeypox skin image dataset was used for binary classification (monkeypox and non-monkeypox) and obtained from Kaggle website [42]. The non-monkeypox images consisted of both chickenpox and others, and it could be expressed that non-monkeypox images were similar to monkeypox. In fact, the dataset included original images: 102 monkeypox, and 126 non-monkeypox. However, if the original dataset was used for classification, it would be overfitting because of including fewer images. Therefore, the augmented dataset was performed to overcome overfitting. The augmented dataset contained 1428 monkeypox and 1764 non-monkeypox images. In total, 3192 images were employed to detect monkeypox disease. Besides, each image dimension was 224 x 224 and in RGB (Red, Green, Blue) format, and thus the dimension was 224 x 224 x 3. Two different splitting methods were applied in this study: training testing and cross validation. The ratio: 70:30, 80:20 training and testing were performed. In addition, a 10 fold cross validation was carried out.

3.2. **Performance metrics.** In this study, classifier performance was evaluated with accuracy, sensitivity, specificity, precision, F1-Score, and Geometric mean (G-Mean) and detailed in Table 1 [43–45].
where TP :True Positive, FP : False Positive, TN : True Negative, and FN : False Negative were shown.

TABLE 1. Formulas of performance metrics.

Performance Metric	Formulas
Accuracy	$\frac{TP+TN}{TP+TN+FP+FN}$
F1-Score	$\frac{2\times TP}{2\times TP+FP+FN}$
G-Mean	$\sqrt{Sensitivity \times Specificity}$
Precision	$\frac{TP}{TP+FP}$
Sensitivity	$\frac{TP}{TP+FN}$
Specificity	$\frac{TN}{TN+FP}$

3.3. **Receiver operating characteristic (ROC) curve.** While any classifier performance was calculated, the receiver operating characteristic (ROC) curve was widely carried out in a classification issue. Here, the false positive rate and true positive rate are respectively displayed as the ROC curve's x-axis and y-axis. Generally, the area under the curve (AUC) is also computed to identify whether a particular condition exists considering test data. When found the AUC value is approximately 1, the classifier has perfect performance [44, 46]. In this study, the AUC value was calculated to evaluate classification performance, and also ROC curve was demonstrated.

3.4. **Cross Validation.** To obtain trusted results from processes that contain black boxes like deep learning, cross validation has been widely preferred as a splitting method to avoid overfitting [47–49]. This method randomly splits the dataset with specified fold number (k) and thinks that one of the subconvolutions has been trained as a test set and leftovers [9, 50]. This operation is repeated up to k folds and tested in the pipeline [51]. In this study, k was determined as 10 for confident classification results.

3.5. **Hyper-parameters Selection.** In this study, hyperparameters were used to achieve better performance in classifying monkeypox images. Parameters identified were that adam, sgdm, rmsprop were performed as optimization methods, the learning rate was 0.0001 as a constant, the maximum epoch was 5, and the minibatch size was 8. All hyperparameters were determined by trial and error.

3.6. **Experimental Results.** In this study, the classification of the monkeypox skin image dataset effectively benefitted from a deep learning algorithm. This deep learning algorithm was MobileNetv2 pre-trained architecture which accepted images with 224x224 dimensions. The architecture was adapted with a transfer learning method to detect monkeypox disease from images both classifier and deep feature extractor. This is because deep learning algorithms can be carried out feature extraction from images without expert opinion, efficiently. First, the monkeypox image dataset was classified using different splitting (70:30, 80:20 training-testing, 10 fold cross validation) and optimization methods (adam, sgdm, rmsprop) where the best splitting and optimization method was found. Although the results obtained in this section were very good, the goal was to achieve excellent results in the detection of monkeypox disease. Thereafter, one of the feature selection methods: Chi-Square was used to reduce the dimension of features obtained from the MobileNetv2 global average pooling layer. More related 250,500, and 1000 features were chosen via Chi-Square method. Eventually, selected features were classified with SVM. Therefore, novel hybrid algorithm was designed via MobileNetv2, Chi-Square, and SVM. The results were acquired in MATLAB 2021b through intel core i7 7500U CPU, NVIDIA GeForce GTX 950M,16 GB RAM, and 64-bit operating system. All performance results are seen in Table 2 and Table 3.

TABLE 2. Mobilenetv2 performance metrics to classify Monkeypox images by different optimization methods and splitting methods.

Splitting Method	Optimization Method	Sensitivity	Specificity	Precision	F1-Score	G-Mean	Accuracy	AUC
70:30 Train-test	adam	0.9252	0.9887	0.9851	0.9542	0.9564	0.9603	0.9933
	rmsprop	0.9369	0.9773	0.9709	0.9536	0.9569	0.9592	0.9900
	sgdm	0.8341	0.9679	0.9545	0.8903	0.8985	0.9080	0.9780
80:20 Train-test	adam	0.9371	0.9433	0.9306	0.9338	0.9402	0.9405	0.9866
	rmsprop	0.9161	0.9802	0.9740	0.9441	0.9476	0.9515	0.9930
	sgdm	0.8986	0.9292	0.9113	0.9049	0.9138	0.9155	0.9806
10 Fold Cross Validation	adam	**0.9811**	**0.9898**	**0.9873**	**0.9842**	**0.9854**	**0.9859**	**0.9985**
	rmsprop	0.9692	0.9881	0.9851	0.9771	0.9786	0.9796	0.9979
	sgdm	0.8704	0.9654	0.9532	0.9100	0.9167	0.9229	0.9747

*Bold values were shown as the highest metrics in this part.

According to Table 2, in the examined 70:30 splitting method, the best ones had an accuracy of 96.03%, an AUC of 0.9933, an F1 score of 0.9542, a precision of 98.51% and a specificity of 98.87% obtained "adam" optimization method. A sensitivity of 92.52% and G-Mean of 95.64% were achieved to classify the monkeypox image dataset in this experiment.

Furthermore, Table 2 showed that the highest had an accuracy of 95.15%, an AUC of 0.9930, a G-Mean of 94.76%, an F1 score of 0.9476, a precision of 97.4%, and a specificity of 98.02% by using 80:20 splitting method and "rmsprop" optimization method. In this experiment, a sensitivity of 93.71% was achieved to classify monkeypox image datasets. When training and test splitting methods were interpreted, it was found that the 70:30 was more successful than another.

When Table 2 was investigated in regards 10 fold cross validation, the top had an accuracy of 98.59%, an AUC of 0.9985, a G-Mean of 98.54%, an F1-Score of

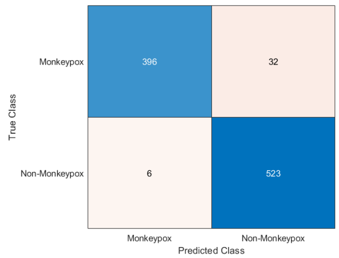

(A) 70:20

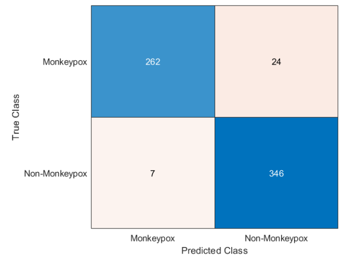

(B) 80:20

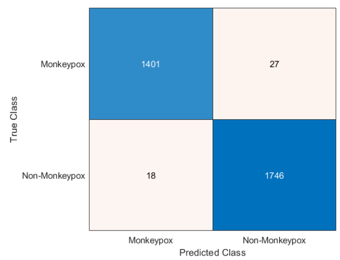

(C) 10 fold cross validation

Figure 2. Confusion matrices of MobileNetv2 by using diverse splitting methods.

0.9842, a precision of 98.73%, a specificity of 98.98% and a sensitivity of 98.11%. This experiment demonstrated that all performance metrics hit to top based on 10 fold cross validation and "adam" optimization method and hence, it could be expressed that cross validation was the best splitting method and adam was the best optimization method to classify the monkeypox image dataset. The confusion matrix and ROC Curve belonging to the 10 fold cross validation and "adam" optimization method were shown in Figure 2(C) and Figure 3. In addition, Figure 2(A) and (B) displayed confusion matrices of other splitting methods.

Although the results of this experiment were remarkably good, the aim was to further enhance these results in the recognition of monkeypox disease. Then, MobileNetv2 was used as a feature extractor from images and 1280 features for each image were obtained from its global average pooling layer. Then, these features were diminished to association 250, 500, and 1000 features using Chi-Square feature selection method. The rank of the 1280 features based on Chi-Square was demonstrated in Figure 4. After all, SVM was utilized to classify these features with different kernel functions in this part. Therefore, MobileNetv2- Chi Square-

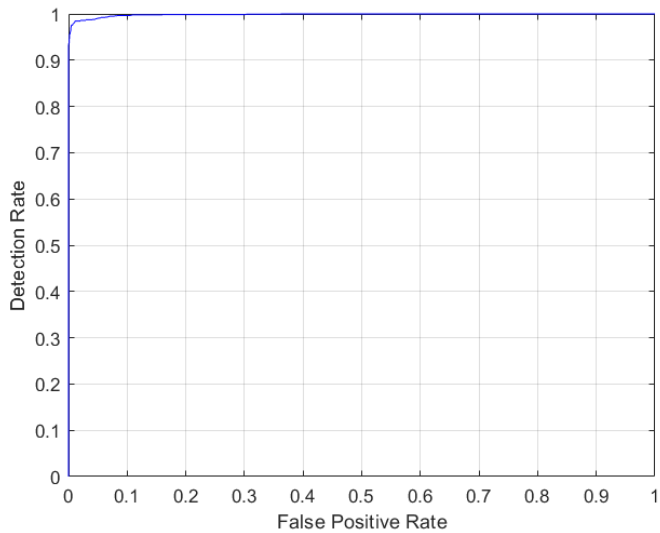

Figure 3. ROC curve of MobileNetv2.

SVM structure was named as Hybrid Algorithm. Experimental results were displayed in Table 3.

When Table 3 was examined in terms of both the number of features and different kernel functions, it was seen that the highest success was obtained with the number of 500 features and the polynomial kernel function. The performance metrics were as follows: an accuracy of 99.69%, an AUC of 0.9999, a G-Mean of 99.69%, an F1-Score of 0.9965, a precision of 100%, a specificity of 100% and a sensitivity of 99.30%.

Other interesting results shown in Table 3 for the number of 250 and 1000 features as follows: The first, linear and gaussian kernel functions gave the same performance metrics for both features. The second, although the polynomial kernel function displayed the maximum level for the number of 500 features, it was the opposite in others. This situation may be due to random selection.

Moreover, the results in Table 3 were increased in all experiments. For selected 250 features, when linear and gaussian kernel functions were used, the results had an accuracy of 98.96%, an AUC of 0.9986, a G-Mean of 98.9%, an F1-Score of 0.9883, a precision of 99.29%, a specificity of 99.43% and a sensitivity of 98.36%. While the polynomial kernel function was performed, the results had an accuracy of 98.33%, an AUC of 0.9984, a G-Mean of 98.33%, an F1-Score of 0.9814, a precision of 97.91%, a specificity of 98.30% and a sensitivity of 98.36%.

For selected 500 features, when linear and gaussian kernel functions were applied,

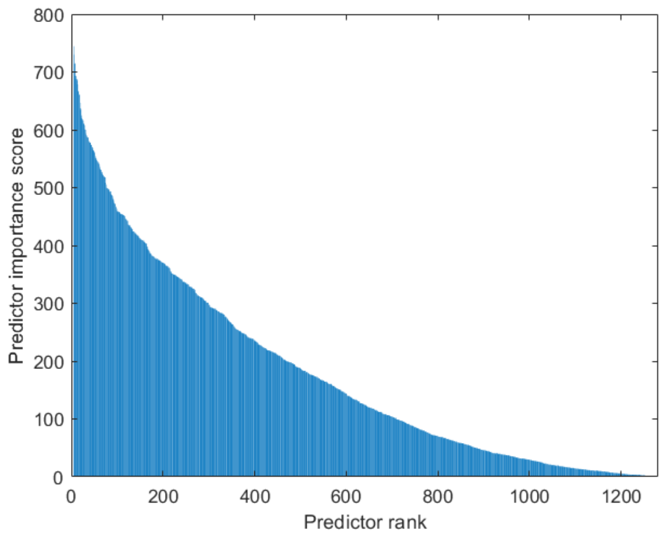

FIGURE 4. The ranks of features by importance rating using the Chi-Square method.

TABLE 3. Performance of the Hybrid Algorithm using the Chi-Square Feature Selection Method.

Number of Features	Kernel Function	Sensitivity	Specificity	Precision	F1-Score	G-Mean	Accuracy	AUC
250	gaussian	0.9836	0.9943	0.9929	0.9883	0.9890	0.9896	0.9986
	linear	0.9836	0.9943	0.9929	0.9883	0.9890	0.9896	0.9986
	polynomial	0.9836	0.9830	0.9791	0.9814	0.9833	0.9833	0.9984
500	gaussian	0.9860	1.0000	1.0000	0.9929	0.9930	0.9937	1.0000
	linear	0.9860	1.0000	1.0000	0.9929	0.9930	0.9937	1.0000
	polynomial	0.9930	1.0000	1.0000	0.9965	0.9969	0.9969	0.9999
1000	gaussian	0.9930	0.9943	0.9930	0.9930	0.9937	0.9937	0.9989
	linear	0.9930	0.9943	0.9930	0.9930	0.9937	0.9937	0.9989
	polynomial	0.9907	0.9735	0.9680	0.9792	0.9821	0.9812	0.9967

the results had an accuracy of 99.37%, an AUC of 1.000, a G-Mean of 99.30%, an F1-Score of 0.9929, a precision of 100%, a specificity of 100% and a sensitivity of 98.60%. When 1000 features were specified, the results had an accuracy of 99.37%, an AUC of 0.9989, a G-Mean of 99.37%, an F1-Score of 0.9930, a precision of 99.30%, a specificity of 99.43% and a sensitivity of 99.30% by using linear and gaussian kernel functions. While the polynomial kernel function was performed, the results had an accuracy of 98.12%, an AUC of 0.9967, a G-Mean of 98.21%, an F1-Score of 0.9792, a precision of 96.80%, a specificity of 97.35% and a sensitivity of

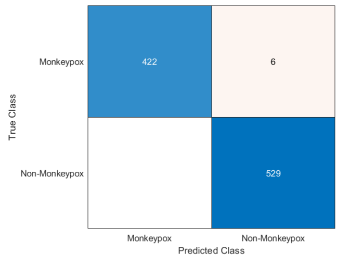

(A) Gaussian

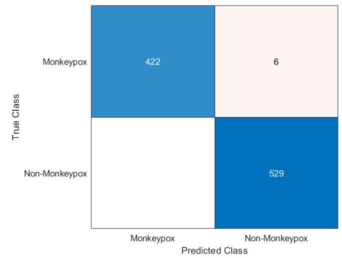

(B) Linear

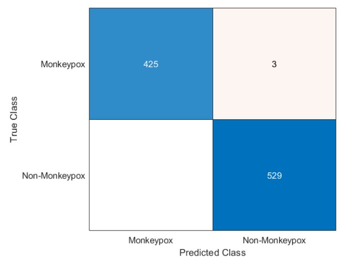

(C) Polynomial

FIGURE 5. Confusion matrices of hybrid algorithms using different kernel functions.

99.07%. Therefore, it could be stated that minimum 500 features should be selected to detect monkeypox disease via this hybrid algorithm. The confusion matrices for different kernel functions were exhibited in Figure 5. ROC Curve of the hybrid algorithm was shown in Figure 6 by utilizing 500 features and polynomial kernel function.

4. Discussion

In this part of the study, some advantages and disadvantages were submitted. As a first step, the advantages of the study were presented as follows: (i) To detect monkeypox disease from skin images, MobileNetv2 was employed with different perspectives. (ii) The comprehensive comparisons were done in regard to splitting methods and optimization methods. Two training-testing set splitting ratios were investigated 70:30 and 80:20. Besides, cross validation was also examined and the k value was taken as 10 in this study. In addition to adam, rmsprop and sgdm were also evaluated as optimization methods and their effectiveness in the classification was shown. (iii) The best splitting method as 10 fold cross validation and the best

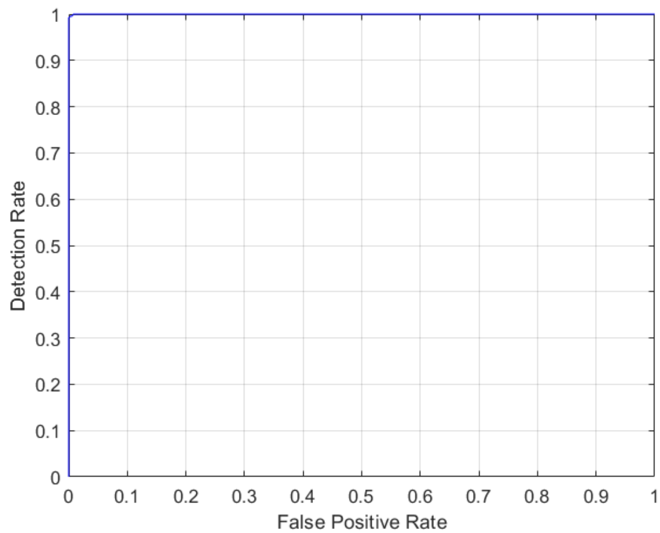

FIGURE 6. ROC Curve of hybrid algorithm.

optimization method as adam were determined with accuracy, specificity, sensitivity, precision, G-Mean, F1-score, and AUC. So far, Mobilenetv2 was assigned as the classifier. (iv) To improve monkeypox detection, MobileNetv2 was used to automatically extract features from the global pooling layer. (v) The Chi-Square method was carried out as feature selection and so, the dimension of the features was reduced using it. (vi) Finally, SVM was utilized with diverse kernel functions to classify as monkeypox or non-monkeypox based on these reduced features. Next, the disadvantage of the study was mentioned in that limited classes were investigated, which could be seen effectiveness of the study.

5. Conclusion

Concerns about the emergence of various diseases related to the coronavirus pandemic have been increasing day by day. Monkeypox was one of them. By diagnosing monkeypox early and taking the necessary precautions, it could be prevented from becoming a pandemic. To accelerate solving of this issue, the deep learning algorithm would be a savior. Through this impulse, monkeypox disease was aimed at detection using a deep learning algorithm: MobileNetv2 pre-trained architecture with transfer learning method. This architecture was used both a classifier and a deep feature extractor. First, it was performed as a classifier and investigated with comprehensive perspectives in terms of splitting (70:30 and 80:20 training-testing, and 10 fold cross validation) and optimization methods (Adam, rmsprop, and sgdm).

When viewing 70:30 splitting method, the best accuracy of 96.03%, an AUC of 0.9933 were achieved using adam optimization method to classify monkeypox image dataset in this experiment. When examining the 80:20 splitting method, the highest accuracy of 95.15%, and an AUC of 0.9930 were obtained by utilizing rmsprop optimization method to detect the monkeypox image dataset in this experiment. Note that, when using adam optimization method, the results were close to the highest one. At the end of this splitting method, it might be seen that 70:30 was better than another. When investigating 10 fold cross validation, it was hit to the top accuracy of 98.59%, and an AUC of 0.9985 using "adam" optimization method. As a result, cross validation and adam were the best splitting method and optimization method, respectively to determine monkeypox disease from image dataset. Next, it was performed a deep feature extractor from images and 1280 features were obtained from the global average pooling layer of MobileNetv2. To select significant features, Chi-Square method was utilized and 250, 500, and 1000 features were chosen by using it. Finally, selected features were classified via SVM classifier by using diverse kernel functions.

While selecting 250 features and using the SVM, results of linear and gaussian kernel functions were obtained the same: an accuracy of 98.96% and an AUC of 0.9986. However, polynomial kernel function result was lower than the others. While identifying 500 features, it was seen an accuracy of 99.37%, and an AUC of 1 for linear and gaussian kernel functions. An interesting result was shown with polynomial kernel function in this experiment. It was observed an accuracy of 99.69% and an AUC of 0.9999. Finally, the results of linear and gaussian kernel functions while choosing 1000 features, it was achieved an accuracy of 99.37% and an AUC of 0.9989. As well as polynomial kernel function result was the lowest. Therefore, it could be remarked that a minimum of 500 features should be chosen in order to diagnose monkeypox disease using this hybrid algorithm.

As a result, the performance was significantly increased and confidence in the study was enhanced by the hybrid algorithm created. In this study, the highest performance was obtained to diagnose monkeypox from skin images with an accuracy of 99.69% by MobileNetv2- Chi Square-SVM. Finally, it could be said that our designed pipeline had a perfect performance. In future works, it has been aimed to determine monkeypox disease better with new structures to be created.

Author Contribution Statements Ozaltin O. analyzed the dataset and wrote this study. Yeniay O. supervised and approved final manuscript.

Declaration of Competing Interests The authors declared that they have no competing interests.

References

[1] Ladnyj, I., Ziegler, P., Kima, E., A human infection caused by monkeypox virus in Basankusu Territory, Democratic Republic of the Congo, *Bulletin of the World Health Organization*, 46(5) (1972), 593.

[2] Thornhill, J. P., Barkati, S., Walmsley, S., Rockstroh, J., Antinori, A., Harrison, L. B., Palich, R., Nori, A., Reeves, I., Habibi, M. S., Apea, V., Boesecke, C., Vandekerckhove, L., Yakubovsky, M., Sendagorta, E., Blanco, J. L., Florence, E., Moschese, D., Maltez, F. M., Goorhuis, A., Pourcher, V., Migaud, P., Noe, S., Pintado, C., Maggi, F., Hansen, A. E., Hoffmann, C., Lezama, J. I., Mussini, C., Cattelan, A., Makofane, K., Tan, D., Nozza, S., Nemeth, J., Klein, M. B., Orkin, C. M., SHARE-net Clinical Group, Monkeypox virus infection in humans across 16 countries-April–June 2022, *New England Journal of Medicine*, 387(8) (2022), 679-691.doi:10.1056/NEJMoa2207323

[3] Aplogan, A., Szczeniowski, M., Human monkeypox–Kasai Oriental, Democratic Republic of Congo, *MMWR: Morbidity & Mortality Weekly Report,* 46(49) (1997), 1168-1171.

[4] Durski, K. N., McCollum, A. M., Nakazawa, Y., Petersen B. W., Reynolds, M. G., Briand, S., Djingarey, M. H., Olson, V., Damon, I. K., Khalakdina, A., Emergence of monkeypox-west and central Africa, 1970-2017, *Morbidity and Mortality Weekly Report*, 67(10) (2018), 306-310.doi:10.15585/mmwr.mm6710a5

[5] Vaughan, A., Aarons, E., Astbury, J., Balasegaram, S., Beadsworth, M., Beck, C. R., Chand, M., O'Connor, C., Dunning, J., Ghebrehewet, S., Harper, N., Howlett-Shipley, R., Ihekweazu, C., Jacobs, M., Kaindama, L., Katwa, P., Khoo, S., Lamb, L., Mawdsley, S., Morgan, D., Palmer, R., Phin, N., Russell, K., Said, B., Simpson, A., Vivancos, R., Wade, M., Walsh, A., Wilburn, J., Two cases of monkeypox imported to the United Kingdom, September 2018, *Eurosurveillance,* 23(38) (2018), 1800509. https://doi.org/10.2807/1560-7917.ES.2018.23.38.1800509

[6] Erez, N., Achdout, H., Milrot, E., Schwartz, Y., Wiener-Well, Y., Paran, N., Politi, B., Tamir, H., Israely, T., Weiss, S., Beth-Din, A., Shifman, O., Israeli, O., Yitzhaki, S., Shapira, S. C., Melamed, S., Schwartz, E., Diagnosis of imported monkeypox, Israel, 2018, *Emerging Infectious Diseases*, 25(5) (2019), 980-983.doi:10.3201/eid2505.190076

[7] Bunge, E. M., Hoet, B., Chen, L., Lienert, F., Weidenthaler, H., Baer, L. R., Steffen, R., The changing epidemiology of human monkeypox-A potential threat? A systematic review, *PLoS Neglected Tropical Diseases*, 16(2) (2022), e0010141.https://doi.org/10.1371/journal.pntd.0010141

[8] Organization WH. Multi-country monkeypox outbreak, situation update, (2022).

[9] Özaltın, Ö., Köklü, M., Yonar, A., Yeniay, Ö., Automatically image classification based on a new CNN architecture, *III International Applied Statistics Conference (UYIK - 2022),* Skopje, N Macedonia, 22-24 June 2022, (2022), 21-32.

[10] Ozaltin, O., Coskun, O., Yeniay, O., Subasi, A., Classification of brain hemorrhage computed tomography images using OzNet hybrid algorithm, *International Journal of Imaging Systems and Technology*, (2022),1-23.https://doi.org/10.1002/ima.22806

[11] Özaltın, Ö., Yeniay, Ö., Ecg classification performing feature extraction automatically using a hybrid cnn-svm algorithm, *IEEE, 2021 3rd International Congress on Human-Computer Interaction, Optimization and Robotic Applications (HORA)*, (2021), 1-5.doi:10.1109/HORA52670.2021.9461295

[12] Koklu, M., Unlersen, M. F., Ozkan, I. A., Aslan, M. F., Sabanci, K., A CNN-SVM study based on selected deep features for grapevine leaves classification, *Measurement*, 188 (2022), 110425.https://doi.org/10.1016/j.measurement.2021.110425

[13] Tuncer, T., Ozyurt, F., Dogan, S., Subasi, A., A novel Covid-19 and pneumonia classification method based on F-transform, *Chemometrics and Intelligent Laboratory Systems*, 210 (2021), 104256.https://doi.org/10.1016/j.chemolab.2021.104256

[14] Ozaltin, O., Coskun, O., Yeniay, O., Subasi, A., A deep learning approach for detecting stroke from brain CT images using OzNet, *Bioengineering*, 9(12) (2022), 783.https://doi.org/10.3390/bioengineering9120783

[15] Ozaltin, O., Yeniay, O., A novel proposed CNN-SVM architecture for ECG scalograms classification, *Soft Computing*, (2022).https://doi.org/10.1007/s00500-022-07729-x

[16] Sahin, V. H., Oztel, I., Yolcu Oztel, G., Human monkeypox classification from skin lesion images with deep pre-trained network using mobile application, *Journal of Medical Systems*, 46(11) (2022), 1-10.https://doi.org/10.1007/s10916-022-01863-7

[17] Ali, S. N., Ahmed, M., Paul, J., Jahan, T., Sani, S., Noor, N., Hasan, T., Monkeypox skin lesion detection using deep learning models: A feasibility study, arXiv preprint arXiv:220703342, (2022).https://doi.org/10.48550/arXiv.2207.03342

[18] Ahsan, M. M., Uddin, M. R., Farjana, M., Sakib, A. N., Momin, K. A., Luna, S. A., Image data collection and implementation of deep learning-based model in detecting monkeypox disease using modified VGG16, arXiv preprint arXiv:220601862, (2022). https://doi.org/10.48550/arXiv.2206.01862

[19] Alakus, T. B., Baykara, M., Comparison of monkeypox and wart DNA sequences with deep learning model, *Applied Sciences*, 12(20) (2022),10216.https://doi.org/10.3390/app122010216

[20] Sitaula, C., Shahi, T. B., Monkeypox virus detection using pre-trained deep learning-based approaches, *Journal of Medical Systems*, 46(11) (2022), 1-9.https://doi.org/10.1007/s10916-022-01868-2

[21] Akin, K. D., Gurkan, C., Budak, A., Karatas, H., Classification of monkeypox skin lesion using the explainable artificial intelligence assisted convolutional neural networks, *Avrupa Bilim ve Teknoloji Dergisi,* 40 (2022), 106-10.https://doi.org/10.31590/ejosat.1171816

[22] Abdelhamid, A. A., El-Kenawy, E-SM., Khodadadi, N., Mirjalili, S., Khafaga, D. S., Alharbi, A. H., Ibrahim, A., Eid, M. M., Saber, M., Classification of monkeypox images based on transfer learning and the Al-Biruni earth radius optimization algorithm, *Mathematics*, 10(19) (2022), 3614. https://doi.org/10.3390/math10193614

[23] Yamashita, R., Nishio, M., Do, R. K. G., Togashi, K., Convolutional neural networks: an overview and application in radiology, *Insights Into Imaging*, 9(4) (2018), 611-29.

[24] Albawi, S., Mohammed, T. A., Al-Zawi, S., Understanding of a convolutional neural network, *2017 International Conference on Engineering and Technology (ICET), IEEE*, (2017).doi:10.1109/ICEngTechnol.2017.8308186

[25] Hubel, D. H., Wiesel, T. N., Receptive fields and functional architecture of monkey striate cortex, *The Journal of Physiology*, 195(1) (1968), 215-43.https://doi.org/10.1113/jphysiol.1968.sp008455

[26] Fukushima, K., Neocognitron: A self-organizing neural network model for a mechanism of pattern recognition unaffected by shift in position, *Biological Cybernetics*, 36 (1980), 193-202.

[27] Bilbrey, J. A., Heindel, J. P., Schram, M., Bandyopadhyay, P., Xantheas, S. S., Choudhury, S., A look inside the black box: Using graph-theoretical descriptors to interpret a Continuous-Filter Convolutional Neural Network (CF-CNN) trained on the global and local minimum energy structures of neutral water clusters, *The Journal of Chemical Physics*, 153(2) (2020), 024302.https://doi.org/10.1063/5.0009933

[28] Baloglu, U. B., Talo, M., Yildirim, O., San Tan, R., Acharya, U. R., Classification of myocardial infarction with multi-lead ECG signals and deep CNN, *Pattern Recognition Letters*, 122 (2019), 23-30. https://doi.org/10.1016/j.patrec.2019.02.016

[29] Acharya, U. R., Fujita, H., Oh SL., Hagiwara, Y., Tan, J. H., Adam, M., Application of deep convolutional neural network for automated detection of myocardial infarction using ECG signals, *Information Sciences*, 415 (2017), 190-8.https://doi.org/10.1016/j.ins.2017.06.027

[30] Lee, H. K., Choi, Y. S., Application of continuous wavelet transform and convolutional neural network in decoding motor imagery brain-computer interface, *Entropy*, 21(12) (2019), 1199. https://doi.org/10.3390/e21121199

[31] Howard, A. G., Zhu, M., Chen, B., Kalenichenko, D., Wang, W., Weyand, T., Andreetto, M., Adam, H., Mobilenets: Efficient convolutional neural networks for mobile vision applications, arXiv preprint arXiv:170404861, (2017). https://doi.org/10.48550/arXiv.1704.04861

[32] Sandler, M., Howard, A., Zhu, M., Zhmoginov, A., Chen, L. C., Mobilenetv2: Inverted residuals and linear bottlenecks, *Proceedings of the IEEE Conference on Computer Vision and Pattern Recognition*, (2018).

[33] Sutskever, I., Martens, J., Dahl, G., Hinton, G., On the importance of initialization and momentum in deep learning, *International Conference on Machine Learning*, (2013) PMLR. https://proceedings.mlr.press/v28/sutskever13.html

[34] Yang, J., Yang, G., Modified convolutional neural network based on dropout and the stochastic gradient descent optimizer, *Algorithms*, 11(3) (2018), 28. https://doi.org/10.3390/a11030028

[35] Kingma, D. P., Ba, J., Adam: A method for stochastic optimization, arXiv preprint arXiv:14126980, (2014). https://doi.org/10.48550/arXiv.1412.6980

[36] Tieleman, T., Hinton, G., Lecture 6.5-rmsprop: Divide the gradient by a running average of its recent magnitude, Coursera: Neural networks for machine learning, 4(2) (2012), 26-31.

[37] McHugh, M. L., The chi-square test of independence, *Biochemia Medica*, 23(2) (2013), 143-9.https://doi.org/10.11613/BM.2013.018

[38] Sharpe, D., Chi-square test is statistically significant: Now what?, *Practical Assessment, Research, and Evaluation*, 20(1) (2015), 8. https://doi.org/10.7275/tbfa-x148

[39] Sankaran, M., Approximations to the non-central chi-square distribution, *Biometrika*, 50(1/2) (1963), 199-204.

[40] Widodo, A., Yang, B-S., Support vector machine in machine condition monitoring and fault diagnosis, *Mechanical Systems and Signal Processing*, 21(6) (2007), 2560-74.https://doi.org/10.1016/j.ymssp.2006.12.007

[41] Das, A., Rad, P., Opportunities and challenges in explainable artificial intelligence (xai): A survey, arXiv preprint arXiv:200611371, (2020). https://doi.org/10.48550/arXiv.2006.11371

[42] Kaggle, Monkeypox Skin Dataset 2022 [Available from: https://www.kaggle.com/datasets/nafin59/monkeypox-skin-lesion-dataset].

[43] Sharifrazi, D., Alizadehsani, R., Roshanzamir, M., Joloudari, J. H., Shoeibi, A., Jafari, M., Hussain, S., Sani, Z. A., Hasanzadeh, F., Khozeimeh, F., Khosravi, A., Nahavandi, S., Panahiazar, M., Zare, A., Islam, S. M. S., Acharya, U. R., Fusion of convolution neural network, support vector machine and Sobel filter for accurate detection of COVID-19 patients using X-ray images, *Biomedical Signal Processing and Control*, 68 (2021), 102622.https://doi.org/10.1016/j.bspc.2021.102622

[44] Singh, D., Taspinar, Y. S., Kursun, R., Cinar, I., Koklu, M., Ozkan, I. A., Lee, H. N., Classification and analysis of Pistachio species with pre-trained deep learning models, *Electronics*, 11(7) (2022), 981.https://doi.org/10.3390/electronics11070981

[45] Rajinikanth, V., Joseph Raj, A. N., Thanaraj, K. P., Naik, G. R., A customized VGG19 network with concatenation of deep and handcrafted features for brain tumor detection, *Applied Sciences*, 10(10) (2020), 3429.https://doi.org/10.3390/app10103429

[46] Taspinar, Y. S., Cinar, I., Koklu, M., Classification by a stacking model using CNN features for COVID-19 infection diagnosis, *Journal of X-ray Science and Technology*, (2021), 1-16. doi:10.3233/XST-211031

[47] Subasi, A., Medical decision support system for diagnosis of neuromuscular disorders using DWT and fuzzy support vector machines, *Computers in Biology and Medicine*, 42(8) (2012), 806-15.https://doi.org/10.1016/j.compbiomed.2012.06.004

[48] Lopez-del Rio, A., Nonell-Canals, A., Vidal, D., Perera-Lluna, A., Evaluation of cross validation strategies in sequence-based binding prediction using deep learning, *Journal of Chemical Information and Modeling*, 59(4) (2019), 1645-57. doi:10.1021/acs.jcim.8b00663

[49] Saber, A., Sakr, M., Abo-Seida, O. M., Keshk, A., Chen, H., A novel deep-learning model for automatic detection and classification of breast cancer using the transfer-learning technique, *IEEE Access*, 9 (2021), 71194-71209. doi:10.1109/ACCESS.2021.3079204

[50] Koklu, M., Ozkan, I. A., Multiclass classification of dry beans using computer vision and machine learning techniques, *Computers and Electronics in Agriculture*, 174 (2020), 105507.https://doi.org/10.1016/j.compag.2020.105507

[51] Arlot, S., Celisse, A., A survey of cross-validation procedures for model selection, *Statistics Surveys*, 4 (2010), 40-79.doi:10.1214/09-SS054

http://communications.science.ankara.edu.tr

Commun.Fac.Sci.Univ.Ank.Ser. A1 Math. Stat.
Volume 72, Number 2, Pages 500–511 (2023)
DOI:10.31801/cfsuasmas.1127250
ISSN 1303-5991 E-ISSN 2618-6470

COMMUNICATIONS SERIES A1

Research Article; Received:June 07, 2022; Accepted: October 31, 2022

IDENTIFICATION OF THE TIME-DEPENDENT LOWEST TERM IN A FOURTH ORDER IN TIME PARTIAL DIFFERENTIAL EQUATION

Ibrahim TEKIN
Department of Fundamental Sciences, Rafet Kayis Faculty of Engineering,
Alanya Alaaddin Keykubat University, Antalya, TÜRKİYE

Abstract. In this article, identification of the time-dependent lowest term in a fourth order in time partial differential equation (PDE) from knowledge of a boundary measurement is studied by means of contraction mapping.

1. Introduction

Fourth order derivative in time arises in various fields. For instance, in the Taylor series expansion of the Hubble law [22], in the study of chaotic hyper jerk systems [2] and in the kinematic performance of long-dwell mechanisms of linkage type [8]. The fourth order in time equation, that is our motivation point, was introduced and investigated by Dell'Oro and Pata [5] for the first time

$$\partial_{\tau\tau\tau\tau}y(x,\tau)+\alpha\partial_{\tau\tau\tau}y(x,\tau)+\beta\partial_{\tau\tau}y(x,\tau)-\gamma\partial_{xx\tau\tau}y(x,\tau)-\delta\partial_{xx\tau}y(x,\tau)-\rho\partial_{xx}y(x,\tau)=0$$

where $\alpha,\beta,\gamma,\delta,\rho$ are real numbers. This model is obtained from the third-order Moore–Gibson–Thompson equation with memory, which has been extensively studied in the literature, [7,13,14]. More recently, this model has attracted the attention of many authors, see [3,15,16,18,19].

Consider the third order in time nonlinear partial differential equation model in abstract form

$$\partial_{\tau\tau\tau}y(x,\tau)+\alpha\partial_{\tau\tau}y(x,\tau)-c^2\partial_{xx}y(x,\tau)-b\partial_{xx\tau}y(x,\tau)=G(x,\tau,y,y_\tau,y_{\tau\tau}) \tag{1}$$

where $G(x,t,y,y_\tau,y_{\tau\tau})$ is a non-linear or linear function and $\alpha,c,b>0$ are given parameters. This type of model is often called Moore-Gibson-Thompson equation and appeared in many scientific fields such as nonlinear acoustics, medical ultrasound, viscoelasticity and thermoelasticity, [4,6,10–12,20].

2020 *Mathematics Subject Classification.* 35R30, 35G05, 45D05.
Keywords. Inverse problems for PDEs, fourth order in time PDE, existence and uniqueness.
ibrahim.tekin@alanya.edu.tr 0000-0001-6725-5663
.

Taking the subtraction

$$\partial_\tau(1) - \alpha(1),$$

we obtain

$$\partial_{\tau\tau\tau\tau}y(x,\tau) - \alpha^2\partial_{\tau\tau}y(x,\tau) - b\partial_{xx\tau\tau}y(x,\tau) \\ + \alpha c^2\partial_{xx}y(x,\tau) + (\alpha b - c^2)\partial_{xx\tau}y(x,\tau) = \partial_\tau G - \alpha G. \quad (2)$$

Taking into account that the critical parameter ($C.P. \equiv \alpha - \frac{c^2}{b}$) of the third order in time equation (1) is zero. i.e. the energy is conservative and no decay of the energy occurs. Then $\alpha b - c^2 = 0$. In this case, the fourth order in time equation (2) reads

$$\partial_{\tau\tau\tau\tau}y(x,\tau) + \beta\partial_{\tau\tau}y(x,\tau) - \gamma\partial_{xx\tau\tau}y(x,\tau) - \rho\partial_{xx}y(x,\tau) = F(x,\tau,y,y_\tau,y_{\tau\tau}), \quad (3)$$

where $F(x,\tau,y,y_\tau,y_{\tau\tau}) = \partial_\tau G - \alpha G$, $\beta = -\alpha^2$, $\gamma = b$ and $\rho = -\alpha c^2$.

In this paper, we choose the right hand side of the fourth order in time PDE (3) as a linear function such that $F(x,\tau,y,y_\tau,y_{\tau\tau}) = a(\tau)y(x,\tau) + f(x,\tau)$. Our aim is to investigate the solvability of the inverse problem of simultaneous identification of the solely time-dependent lowest term ($a(\tau)$) and displacement function ($y(x,\tau)$) in the fourth order in time PDE

$$\partial_{\tau\tau\tau\tau}y(x,\tau) + \beta\partial_{\tau\tau}y(x,\tau) - \gamma\partial_{xx\tau\tau}y(x,\tau) - \rho\partial_{xx}y(x,\tau) = a(\tau)y(x,\tau) + f(x,\tau), \quad (4)$$

for $(x,\tau) \in D_T$ subject to the initial conditions

$$y(x,0) = \xi_0(x),\ y_\tau(x,0) = \xi_1(x), y_{\tau\tau}(x,0) = \xi_2(x), y_{\tau\tau\tau}(x,0) = \xi_3(x),\ x \in [0,1], \quad (5)$$

and the boundary conditions

$$y(0,\tau) = y_x(1,\tau) = 0,\ \tau \in [0,T], \quad (6)$$

and the additional condition

$$y(1,\tau) = h(\tau),\ \tau \in [0,T], \quad (7)$$

where $D_T = \{(x,\tau) : 0 \le x \le 1,\ 0 \le \tau \le T\}$ for some fixed $T > 0$, $\beta,\gamma,\rho > 0$ are given constants, $f(x,\tau)$ is the force function, $\xi_0(x)$, $\xi_1(x)$, $\xi_2(x)$, $\xi_3(x)$ are initial displacements, and $h(\tau)$ is the extra measurement to obtain the solution of the inverse problem.

The inverse problems of determining time or space dependent coefficients for the higher order in time (more than 2) PDEs attract many scientists. The inverse problem of recovering the solely space dependent and solely time dependent coefficients for the third order in time PDEs are studied by [1] and [21], respectively. More recently, in [9] authors studied the inverse problem of determining time dependent potential and time dependent force terms from the third order in time partial differential equation by considering the critical parameter equal to zero.

Main purpose of this paper is the simultaneous identification of the time-dependent lowest coefficient $a(\tau)$, and $y(x,\tau)$, for the first time, from the equation (4), initial conditions (5), homogeneous boundary conditions (6) and additional condition (7) under the assumption on the parameters.

The article is organized as following: In Section 2, we first present the eigenvalues and eigenfunctions of the corresponding Sturm-Liouville spectral problem for equation (4). Then two Banach spaces are introduced and roots of the fourth order polynomial (quartic) are investigated. In Section 3, we transform the inverse problem into the system of integral equations which are Volterra type by using the eigenfunction expansion method. Then, the theorem of the existence and uniqueness of the solution of the inverse problem is proved via Banach fixed point theorem for sufficiently small times under some conformity and consistency conditions on the initial and boundary data.

2. Auxiliary Spectral Problem and Preliminaries

The corresponding spectral problem of the inverse problem (4)-(7) is

$$\begin{cases} W''(x) + \lambda W(x) = 0, \quad 0 \le x \le 1, \\ \\ W(0) = W'(1) = 0. \end{cases} \tag{8}$$

The eigenvalues and corresponding eigenfunctions of these eigenvalues of the spectral problem (8) are $\lambda_n = \left(\frac{2n+1}{2}\pi\right)^2$ and $W_n(x) = \sqrt{2}\sin(\sqrt{\lambda_n}x)$, $n = 0, 1, 2, ...$, respectively. The system of eigenfunctions $W_n(x)$ are biorthonormal on $[0, 1]$, i.e.:

$$\int_0^1 W_n(x)W_m(x)dx = \begin{cases} 1 & , m = n \\ 0 & , m \neq n \end{cases} .$$

Also the system $W_n(x) = \sqrt{2}\sin(\sqrt{\lambda_n}x)$, $n = 0, 1, 2, ...$ forms a Riesz basis in $L_2[0, 1]$.

Now, let us introduce two Banach spaces that are connected with the eigenvalues and eigenfunctions of the auxiliary spectral problem (8):

i:

$$B_T = \Big\{ y(x,\tau) = \sum_{n=0}^{\infty} y_n(\tau)W_n(x) : \ y_n(\tau) \in C[0,T],$$
$$J_T(y) = \left(\sum_{n=0}^{\infty} (\lambda_n^{5/2} \|y_n(\tau)\|_{C[0,T]})^2 \right)^{1/2} < +\infty \Big\}, \tag{9}$$

where $J_T(y) := \|y(x,\tau)\|_{B_T}$ is the norm of the function $y(x,\tau)$.

ii: $E_T = B_T \times C[0,T]$ is a Banach space with the norm

$$\|\nu(x,\tau)\|_{E_T} = \|y(x,\tau)\|_{B_T} + \|a(\tau)\|_{C[0,T]} ,$$

where $\nu(x,\tau) = \{y(x,\tau), a(\tau)\}$ is a vector function.

These spaces are suitable to investigate the solution of the inverse problem (4)-(7).

Consider the quartic polynomial $P(k)$

$$P(k) = k^4 + (\beta + \gamma\lambda_n)k^2 + \rho\lambda_n.$$

Let us denote $\Delta_n = (\beta + \gamma\lambda_n)^2 - 4\rho\lambda_n$, and consider $\Delta_n > 0$. Therefore, the roots of the quartic polynomial $P(k)$ are

$$k_{1,2} = \pm\sqrt{-s_n},$$
$$k_{3,4} = \pm\sqrt{-\overline{s}_n},$$

where $s_n = \frac{\beta+\gamma\lambda_n-\sqrt{\Delta_n}}{2}$, and $\overline{s}_n = \frac{\beta+\gamma\lambda_n+\sqrt{\Delta_n}}{2}$. Since β, γ, ρ, and λ_n are strictly positive, s_n, and $\overline{s}_n$ are also positive. Thus we have four complex conjugate roots

$$k_{1,2} = \pm ip_n,$$
$$k_{3,4} = \pm ir_n,$$

where $p_n = \sqrt{\frac{\beta+\gamma\lambda_n-\sqrt{\Delta_n}}{2}}$, $r_n = \sqrt{\frac{\beta+\gamma\lambda_n+\sqrt{\Delta_n}}{2}}$ and $s_n = p_n^2$, $\overline{s}_n = r_n^2$.

3. Existence and Uniqueness

In this section, our aim is to set and prove the main theorem that is about the unique solvability of the inverse problem for the fourth order in time PDE. Before giving these let us define the classical solution of the inverse problem.

Let the pair of functions $\{y(x,\tau), a(\tau)\}$ be from the class $C^{2,4}(D_T) \times C[0,T]$ and satisfies the equation (4) and conditions (5)-(7). Then we call that the pair $\{y(x,\tau), a(\tau)\}$ is the classical solution of the inverse problem (4)-(7).

The existence and uniqueness theorem of the solution of the inverse problem is as follows:

Theorem 1. *Let the assumptions*

A_1: $\xi_0(x) \in C^4[0,1]$, $\xi_0^{(5)}(x) \in L_2[0,1]$,
$\xi_0(0) = \xi_0'(1) = \xi_0''(0) = \xi_0'''(1) = \xi_0^{(4)}(0) = 0$,
A_2: $\xi_1(x) \in C^3[0,1]$, $\xi_1^{(4)}(x) \in L_2[0,1]$,
$\xi_1(0) = \xi_1'(1) = \xi_1''(0) = \xi_1'''(1) = 0$,
A_3: $\xi_2(x) \in C^2[0,1]$, $\xi_2'''(x) \in L_2[0,1]$,
$\xi_2(0) = \xi_2'(1) = \xi_2''(0) = 0$,
A_4: $\xi_3(x) \in C^1[0,1]$, $\xi_3''(x) \in L_2[0,1]$,
$\xi_3(0) = \xi_3'(1) = 0$,
A_5: $h(\tau) \in C^4[0,T]$, $h(\tau) \neq 0$, $\forall\tau \in [0,T]$,
$h(0) = \xi_0(1)$, $h'(0) = \xi_1(1), h''(0) = \xi_2(1), h'''(0) = \xi_3(1)$,
A_6: $f(x,\tau) \in C(\overline{D}_T)$, $f_x, f_{xx}, f_{xxx} \in C[0,1]$, $\forall\tau \in [0,T]$,
$f(0,\tau) = f_x(1,\tau) = f_{xx}(0,\tau) = 0$,

be satisfied, $\beta, \gamma, \rho > 0$, and $\Delta_n = (\beta + \gamma\lambda_n)^2 - 4\rho\lambda_n > 0$. Then, the inverse problem (4)-(7) has a unique solution for small T.

Proof. Let $a(\tau) \in C[0,T]$ be an arbitrary function. Thus,we will use the Fourier (Eigenfunction expansion) method to construct the formal solution of the inverse problem (4)-(7). In keeping with this aim, let us consider

$$y(x,\tau)=\sum_{n=0}^{\infty} y_n(\tau)W_n(x), \tag{10}$$

is a formal solution of the inverse problem (4)-(7).

Since $y(x,\tau)$ is the formal solution of the inverse problem (4)-(7), we get the following Cauchy problems with respect to $y_n(\tau)$ from the equation (4) and initial conditions (5);

$$\begin{cases} y_n^{(4)}(\tau)+(\beta+\gamma\lambda_n)y_n''(\tau)+\rho\lambda_n y_n(\tau)=F_n(\tau;a,y), \\ y_n(0)=\xi_{0n},\ y_n'(0)=\xi_{1n},\ y_n''(0)=\xi_{2n}, y_n'''(0)=\xi_{3n},\ n=0,1,2,.... \end{cases} \tag{11}$$

Here

$$F_n(\tau;a,y)=a(\tau)y_n(\tau)+f_n(\tau),$$
$$y_n(\tau)=\sqrt{2}\int_0^1 y(x,\tau)\sin(\sqrt{\lambda_n}x)dx,$$
$$f_n(\tau)=\sqrt{2}\int_0^1 f(x,\tau)\sin(\sqrt{\lambda_n}x)dx,$$

and

$$\xi_{in}=\sqrt{2}\int_0^1 \xi_i(x)\sin(\sqrt{\lambda_n}x)dx,\ i=0,1,2,3,\ n=0,1,2,....$$

These Cauchy problems have the quartic characteristic polynomial

$$P(k)=k^4+(\beta+\gamma\lambda_n)k^2+\rho\lambda_n.$$

Since $\Delta_n=(\beta+\gamma\lambda_n)^2-4\rho\lambda_n>0$, solving (11) by using the roots of this characteristic polynomial that are investigated in previous section, we obtain

$$\begin{aligned} y_n(t)=&\frac{r_n^2\cos(p_n\tau)-p_n^2\cos(r_n\tau)}{\sqrt{\Delta_n}}\xi_{0n}+\frac{r_n^3\sin(r_n\tau)-p_n^3\sin(p_n\tau)}{p_n r_n\sqrt{\Delta_n}}\xi_{1n} \\ &+\frac{\cos(p_n\tau)-\cos(r_n\tau)}{\sqrt{\Delta_n}}\xi_{2n}+\frac{r_n\sin(r_n\tau)-p_n\sin(p_n\tau)}{p_n r_n\sqrt{\Delta_n}}\xi_{3n} \\ &+\int_0^\tau\left[\frac{p_n}{\sqrt{\Delta_n\rho\lambda_n}}\sin(r_n(\tau-\eta))-\frac{r_n}{\sqrt{\Delta_n\rho\lambda_n}}\sin(p_n(\tau-\eta))\right]F_n(\eta;a,y)d\eta. \end{aligned} \tag{12}$$

Substitute the expression (12) into (10) to determine $y(x,\tau)$. Then we get

$$y(x,\tau)=\sum_{n=0}^{\infty}\left[\frac{r_n^2\cos(p_n\tau)-p_n^2\cos(r_n\tau)}{\sqrt{\Delta_n}}\xi_{0n}+\frac{r_n^3\sin(r_n\tau)-p_n^3\sin(p_n\tau)}{p_n r_n\sqrt{\Delta_n}}\xi_{1n}\right.$$

$$+\frac{\cos(p_n\tau)-\cos(r_n\tau)}{\sqrt{\Delta_n}}\xi_{2n}+\frac{r_n\sin(r_n\tau)-p_n\sin(p_n\tau)}{p_nr_n\sqrt{\Delta_n}}\xi_{3n}$$
$$+\int_0^\tau\left[\frac{p_n}{\sqrt{\Delta_n\rho\lambda_n}}\sin(r_n(\tau-\eta))-\frac{r_n}{\sqrt{\Delta_n\rho\lambda_n}}\sin(p_n(\tau-\eta))\right]F_n(\eta;a,y)d\eta\Bigg]$$
$$\times W_n(x). \tag{13}$$

Let us derive the equation of $a(\tau)$. If we evaluate the equation (4) at $x=1$ and consider the additional condition (7), then we have:

$$a(\tau)=\frac{1}{h(\tau)}\left[h^{(4)}(\tau)+\beta h''(\tau)-f(1,\tau)+\sum_{n=0}^{\infty}(-1)^{n+1}\lambda_n\left(\gamma y_n''(\tau)+\rho y_n(\tau)\right)\right] \tag{14}$$

where $y_n(\tau)$ is defined in (12) and

$$y_n''(\tau)=\frac{p_n^2r_n^2\left(\cos(r_n\tau)-\cos(p_n\tau)\right)}{\sqrt{\Delta_n}}\xi_{0n}+\frac{r_n^5\sin(p_n\tau)-p_n^5\sin(r_n\tau)}{p_nr_n\sqrt{\Delta_n}}\xi_{1n}$$
$$+\frac{r_n^2\cos(r_n\tau)-p_n^2\cos(p_n\tau)}{\sqrt{\Delta_n}}\xi_{2n}+\frac{p_n^3\sin(p_n\tau)-r_n^3\sin(r_n\tau)}{p_nr_n\sqrt{\Delta_n}}\xi_{3n}$$
$$+\int_0^\tau\left[\frac{p_n^2r_n}{\sqrt{\Delta_n\rho\lambda_n}}\sin(p_n(\tau-\eta))-\frac{r_n^2p_n}{\sqrt{\Delta_n\rho\lambda_n}}\sin(r_n(\tau-\eta))\right]F_n(\eta;a,y)d\eta. \tag{15}$$

We convert the inverse problem (4)-(7) into the system of Volterra integral equations (13)-(14) with respect to $y(x,\tau)$ and $a(\tau)$ by considering

$$y_n(\tau)=\int_0^1 y(x,\tau)W_n(x)dx,\ \ n=0,1,2,...$$

is the solution of the system of differential equations (11). Analogously, we can prove that if $\{y(x,\tau),a(\tau)\}$ is a solution of the inverse problem (4)-(7), then $y_n(\tau),\ n=0,1,2,...$satisfy the system of differential equations (11). For proof of this assertion please see ([17]). From this assertion we can conclude that proving the uniqueness of the solution of the inverse problem (4)-(7), It is enough to prove the unique solvability of the system (13)-(14).

To prove the existence of a unique solution of the system (13) and (14) we need to rewrite this system into operator form and to show that this operator a contraction operator. Consider $\nu(x,\tau)=[y(x,\tau),a(\tau)]^T$ is a 2×1 inverse problem's solution vector function. Thus, we can rewrite the system of equations (13) and (14) into the operator equation form as

$$\nu=\underline{\mathbf{O}}(\nu) \tag{16}$$

where $\underline{\mathbf{O}}(\nu)\equiv[O_1,O_2]^T$ and ϕ_1 and ϕ_2 are

$$O_1(\nu)=\sum_{n=0}^{\infty}\Bigg[\frac{r_n^2\cos(p_n\tau)-p_n^2\cos(r_n\tau)}{\sqrt{\Delta_n}}\xi_{0n}+\frac{r_n^3\sin(r_n\tau)-p_n^3\sin(p_n\tau)}{p_nr_n\sqrt{\Delta_n}}\xi_{1n}$$

$$+\frac{\cos(p_n\tau)-\cos(r_n\tau)}{\sqrt{\Delta_n}}\xi_{2n}+\frac{r_n\sin(r_n\tau)-p_n\sin(p_n\tau)}{p_nr_n\sqrt{\Delta_n}}\xi_{3n}$$
$$+\int_0^\tau\left[\frac{p_n}{\sqrt{\Delta_n\rho\lambda_n}}\sin(r_n(\tau-\eta))-\frac{r_n}{\sqrt{\Delta_n\rho\lambda_n}}\sin(p_n(\tau-\eta))\right]F_n(\eta;a,y)d\eta\Bigg]$$
$$\times X_n(x),$$

and

$$O_2(\nu)=\frac{1}{h(\tau)}\left[h^{(4)}(\tau)+\beta h''(\tau)-f(1,\tau)+\sum_{n=0}^{\infty}(-1)^{n+1}\lambda_n\left(\gamma y_n''(\tau)+\rho y_n(\tau)\right)\right].$$

We can easily obtain following equalities

$$\xi_{0n}=\frac{1}{\lambda_n^{5/2}}\alpha_{0n},\ \xi_{1n}=\frac{1}{\lambda_n^{2}}\alpha_{1n},\ \xi_{2n}=\frac{1}{\lambda_n^{3/2}}\alpha_{2n},\ \xi_{3n}=\frac{1}{\lambda_n}\alpha_{3n},\ f_n(\tau)=\frac{1}{\lambda_n^{3/2}}\omega_n(\tau),$$

using integration by parts under consideration of the assumptions $(A_1)-(A_6)$, where

$$\begin{aligned}\omega_n(\tau)&=-\sqrt{2}\int_0^1 f_{xxx}(x,\tau)\cos(\sqrt{\lambda_n}x)dx,\\ \alpha_{0n}&=\sqrt{2}\int_0^1\xi_0^{(5)}(x)\cos(\sqrt{\lambda_n}x)dx,\\ \alpha_{1n}&=\sqrt{2}\int_0^1\xi_1^{(4)}(x)\sin(\sqrt{\lambda_n}x)dx,\\ \alpha_{2n}&=-\sqrt{2}\int_0^1\xi_2'''(x)\cos(\sqrt{\lambda_n}x)dx,\end{aligned}$$

and

$$\alpha_{3n}=-\sqrt{2}\int_0^1\xi_3''(x)\sin(\sqrt{\lambda_n}x)dx.$$

Since $\sqrt{2}\sin(\sqrt{\lambda_n}x)$ (or $\sqrt{2}\cos(\sqrt{\lambda_n}x)$) forms a biorthonormal system of functions on $[0,1]$, by using Bessel's inequality we get the estimates

$$\sum_{n=0}^{\infty}|\alpha_{0n}|^2\le\left\|\xi_0^{(5)}\right\|_{L_2[0,1]}^2,\ \sum_{n=0}^{\infty}|\alpha_{1n}|^2\le\left\|\xi_1^{(4)}\right\|_{L_2[0,1]}^2,$$

$$\sum_{n=0}^{\infty}|\alpha_{2n}|^2\le\left\|\xi_2'''\right\|_{L_2[0,1]}^2,\ \sum_{n=0}^{\infty}|\alpha_{3n}|^2\le\left\|\xi_3''\right\|_{L_2[0,1]}^2,$$

$$\sum_{n=0}^{\infty}|\omega_n(\tau)|^2\le\|f_{xxx}(\cdot,\tau)\|_{L_2[0,1]}^2. \tag{17}$$

Also we can easily obtain the following estimates of the coefficients which arise in the operator equations $O_1(\nu)$ and $O_2(\nu)$:

$$|\chi_1(\tau)| \le d_1,\ |\chi_2(\tau)| \le \frac{d_2}{\sqrt{\lambda_n}},\ |\chi_3(\tau)| \le \frac{d_3}{\lambda_n},\ |\chi_4(\tau)| \le \frac{d_4}{\lambda_n^{3/2}},\ |\chi_5(\tau)| \le \frac{d_5}{\lambda_n},$$

$$|\Gamma_1(\tau)| \le \lambda_n D_1,\ |\Gamma_2(\tau)| \le \sqrt{\lambda_n} D_2,\ |\Gamma_3(\tau)| \le D_3,\ |\Gamma_4(\tau)| \le \frac{D_4}{\sqrt{\lambda_n}},\ |\Gamma_5(\tau)| \le D_5, \tag{18}$$

where

$$\chi_1(\tau) = \frac{r_n^2\cos(p_n\tau) - p_n^2\cos(r_n\tau)}{\sqrt{\Delta_n}},\ \chi_2(\tau) = \frac{r_n^3\sin(r_n\tau) - p_n^3\sin(p_n\tau)}{p_n r_n\sqrt{\Delta_n}},$$
$$\chi_3(\tau) = \frac{\cos(p_n\tau) - \cos(r_n\tau)}{\sqrt{\Delta_n}},\ \chi_4(\tau) = \frac{r_n\sin(r_n\tau) - p_n\sin(p_n\tau)}{p_n r_n\sqrt{\Delta_n}},$$
$$\chi_5(t) = \frac{p_n}{\sqrt{\Delta_n\rho\lambda_n}}\sin(r_n(\tau-\eta)) - \frac{r_n}{\sqrt{\Delta_n\rho\lambda_n}}\sin(p_n(\tau-\eta)),$$

$\Gamma_i(\tau) = \chi_i''(\tau)$, $i = \overline{1,5}$, d_i and D_i, $i = \overline{1,5}$ are positive real constants. (These boundaries can be obtained by taking λ_n common multiplier)

Now we can show in two steps that $\underline{\mathbf{O}}$ is a contraction operator by considering the assumptions and estimates are given above.

I) First let us verify that $\underline{\mathbf{O}}$ is a continuous map which maps the space E_T onto itself continuously. That is to say, our aim is to show $O_1(\nu) \in B_T$ and $O_2(\nu) \in C[0,T]$ for arbitrary $\nu(x,\tau) = [y(x,\tau), a(\tau)]^T$ such that $y(x,\tau) \in B_T$, $a(\tau) \in C[0,T]$.

Let us start with $O_1(\nu) \in B_T$, i.e. we need to verify

$$J_T(O_1) = \left(\sum_{n=0}^{\infty}(\lambda_n^{5/2}\left\|O_{1,n}(\tau)\right\|_{C[0,T]})^2\right)^{1/2} < +\infty,$$

where

$$\begin{aligned} O_{1,n}(\tau) =& \frac{r_n^2\cos(p_n\tau) - p_n^2\cos(r_n\tau)}{\sqrt{\Delta_n}}\xi_{0n} + \frac{r_n^3\sin(r_n\tau) - p_n^3\sin(p_n\tau)}{p_n r_n\sqrt{\Delta_n}}\xi_{1n} \\ &+ \frac{\cos(p_n\tau) - \cos(r_n\tau)}{\sqrt{\Delta_n}}\xi_{2n} + \frac{r_n\sin(r_n\tau) - p_n\sin(p_n\tau)}{p_n r_n\sqrt{\Delta_n}}\xi_{3n} \\ &+ \int_0^{\tau}\left[\frac{p_n}{\sqrt{\Delta_n\rho\lambda_n}}\sin(r_n(\tau-\eta)) - \frac{r_n}{\sqrt{\Delta_n\rho\lambda_n}}\sin(p_n(\tau-\eta))\right]F_n(\eta;a,y)d\eta. \end{aligned}$$

After some manipulations under the assumptions $(A_1)-(A_6)$, using the estimates (18) we obtain

$$
\begin{aligned}
(J_T(O_1))^2 = &\sum_{n=0}^{\infty}(\lambda_n^{5/2}\left\|O_{1,n}(\tau)\right\|_{C[0,T]})^2 \\
\le &6d_1^2\sum_{n=0}^{\infty}|\alpha_{0n}|^2 + 6d_2^2\sum_{n=0}^{\infty}|\alpha_{1n}|^2 + 6d_3^2\sum_{n=0}^{\infty}|\alpha_{2n}|^2 + 6d_4^2\sum_{n=0}^{\infty}|\alpha_{3n}|^2 \\
&+ 6d_5^2T^2\sum_{n=0}^{\infty}\left(\max_{0\le\tau\le T}|\omega_n(\tau)|\right)^2 \\
&+ 6d_5^2T^2\left(\max_{0\le\tau\le T}|a(\tau)|\right)^2\sum_{n=0}^{\infty}\left(\lambda_n^{5/2}\left\|y_n(\tau)\right\|_{C[0,T]}\right)^2.
\end{aligned}
$$

Since $y(x,\tau)$, $a(\tau)$ belong to the spaces B_T, and $C[0,T]$, respectively, the series at the right hand side of $(J_T(\phi_1))^2$ are convergent from the Bessel's inequality (considering the estimates (17)). $J_T(O_1)$ is convergent (i.e. $J_T(O_1) < +\infty$) because $(J_T(O_1))^2$ is bounded above. Thus we can conclude that $O_1(\nu)$ belongs to the space B_T.

Now let us prove that $O_2(\nu) \in C[0,T]$. By using the equation of $a(\tau)$ (14), we can write

$$
\begin{aligned}
|O_2(\nu)| \le &\frac{1}{\min_{0\le\tau\le T}|h(\tau)|}\left[\left|h^{(4)}(\tau)\right| + \beta\left|h''(\tau)\right| + |f(1,\tau)|\right. \\
&\left. + \sum_{n=0}^{\infty}\lambda_n\left(\gamma\left|y_n''(\tau)\right| + \rho\left|y_n(\tau)\right|\right)\right].
\end{aligned}
$$

Taking into account the estimates (17) and (18) and using the Cauchy-Schwartz inequality, from the inequality for $|\phi_2(\nu)|$ we get

$$
\begin{aligned}
\max_{0\le\tau\le T}|O_2(\nu)| \le &\frac{1}{\min_{0\le\tau\le T}|h(\tau)|}\left[\left|h^{(4)}(\tau)\right| + \beta\left|h''(\tau)\right| + |f(1,\tau)|\right. \\
&+ m_1\sum_{n=0}^{\infty}|\alpha_{0n}|^2 + m_2\sum_{n=0}^{\infty}|\alpha_{1n}|^2 + m_3\sum_{n=0}^{\infty}|\alpha_{2n}|^2 + m_4\sum_{n=0}^{\infty}|\alpha_{3n}|^2 \\
&+ m_5T\left(\max_{0\le\tau\le T}|a(\tau)|\right)^2\sum_{n=0}^{\infty}\left(\lambda_n^{5/2}\left\|y_n(\tau)\right\|_{C[0,T]}\right)^2 \\
&\left.+ m_6T\sum_{n=0}^{\infty}\left(\max_{0\le\tau\le T}|\omega_n(\tau)|\right)\right],
\end{aligned}
\tag{19}
$$

where $m_i = \gamma D_i \left(\sum_{n=0}^{\infty} \frac{1}{\lambda_n}\right)^{1/2} + \rho d_i \left(\sum_{n=0}^{\infty} \frac{1}{\lambda_n^3}\right)^{1/2},\ i = \overline{1,5}$ and
$m_6 = \gamma D_5 \left(\sum_{n=0}^{\infty} \frac{1}{\lambda_n^3}\right)^{1/2} + \rho d_5 \left(\sum_{n=0}^{\infty} \frac{1}{\lambda_n^5}\right)^{1/2}$. Considering the estimates (17) and $\sum_{n=0}^{\infty} \frac{1}{\lambda_n}$, $\sum_{n=0}^{\infty} \frac{1}{\lambda_n^3}$ and $\sum_{n=0}^{\infty} \frac{1}{\lambda_n^5}$ are convergent, the majorizing series (19) are convergent. According to Weierstrass M-test $O_2(\nu)$ is absolutely continuous. Thus, $O_2(\nu)$ belongs to the space $C[0,T]$.

Thereby, we have shown that $\underline{\mathbf{O}}$ is a continuous and onto map on E_T.

II) Since $\underline{\mathbf{O}}$ in a continuous map onto E_T, let us prove that the operator $\underline{\mathbf{O}}$ is contraction mapping operator. Assume that let ν_1 and ν_2 be any two elements of E_T such that $\nu_i = \left[y^{(i)}(x,\tau), a^{(i)}(\tau)\right]^T$, $i = 1,2$. From the definition of the space E_T, we have $\|\underline{\mathbf{O}}(\nu_1) - \underline{\mathbf{O}}(\nu_2)\|_{E_T} = \|O_1(\nu_1) - O_1(\nu_2)\|_{B_T} + \|O_2(\nu_1) - O_2(\nu_2)\|_{C[0,T]}$. For the convenience of this norm, let us consider the following differences

$$O_1(\nu_1) - O_1(\nu_2) = \sum_{n=0}^{\infty} \left[\int_0^{\tau} \left(\frac{p_n}{\sqrt{\Delta_n \rho \lambda_n}} \sin(r_n(\tau-\eta)) - \frac{r_n}{\sqrt{\Delta_n \rho \lambda_n}} \sin(p_n(\tau-\eta))\right) \times \left(F_n(\eta; a^1, y^1) - F_n(\eta; a^2, y^2)\right) d\eta\right] W_n(x),$$

$$O_2(\nu_1) - O_2(\nu_2) = \frac{1}{h(\tau)} \left[\sum_{n=0}^{\infty} \lambda_n \left\{\gamma \int_0^{\tau} \left[\frac{p_n^2 r_n}{\sqrt{\Delta_n \rho \lambda_n}} \sin(p_n(\tau-\eta)) - \frac{r_n^2 p_n}{\sqrt{\Delta_n \rho \lambda_n}} \sin(r_n(\tau-\eta))\right] \times \left(F_n(\eta; a^1, y^1) - F_n(\eta; a^2, y^2)\right) d\eta + \rho \int_0^{\tau} \left[\frac{p_n}{\sqrt{\Delta_n \rho \lambda_n}} \sin(r_n(\tau-\eta)) - \frac{r_n}{\sqrt{\Delta_n \rho \lambda_n}} \sin(p_n(\tau-\eta))\right] \times \left(F_n(\eta; a^1, y^1) - F_n(\eta; a^2, y^2)\right) d\eta\right\}\right].$$

After some manipulations in last equations under the assumptions (A_1)-(A_6) and using the estimates (17)-(18) , we obtain

$$\|O_1(\nu_1) - O_1(\nu_2)\|_{B_T} \le T\left[C_1 \left\|y^{(1)} - y^{(2)}\right\|_{B_T} + C_2 \left\|a^{(1)} - a^{(2)}\right\|_{C[0,T]}\right],$$
$$\|O_2(\nu_1) - O_2(\nu_2)\|_{C[0,T]} \le \frac{T}{\min\limits_{0\le\tau\le T} |h(\tau)|}\left[C_3 \left\|y^{(1)} - y^{(2)}\right\|_{B_T} + C_4 \left\|a^{(1)} - a^{(2)}\right\|_{C[0,T]}\right],$$

where C_k, $k = \overline{1,4}$ are the constants depend on the norms $\|a^{(1)}\|_{C[0,T]}$, $\|y^{(2)}\|_{B_T}$, m_5, and m_6 . From the last inequalities it follows that

$$\|\underline{\mathbf{O}}(\nu_1) - \underline{\mathbf{O}}(\nu_2)\|_{E_T} \le A(T) C(a^{(1)}, y^{(2)}, m_5, m_6) \|\nu_1 - \nu_2\|_{E_T}$$

where $A(T) = T\left(1 + \frac{1}{\min_{0\le\tau\le T}|h(\tau)|}\right)$ and $C(a^{(1)}, y^{(2)}, m_5, m_6) = \max\{C_1, C_2, C_3, C_4\}$ is the constant depends on the norms $\|a^{(1)}\|_{C[0,T]}$, $\|y^{(2)}\|_{B_T}$, m_5, and m_6.

Since $h(\tau) \in C^4[0,T]$, $h(\tau) \neq 0$, $\forall \tau \in [0,T]$, $a^{(1)}(\tau) \in C[0,T]$, $y^{(2)}(x,\tau) \in B_T$ and m_5, m_6 are finite constants, $\frac{1}{\min\limits_{0\leq\tau\leq T}|h(\tau)|}$ and $C(a^{(1)}, y^{(2)}, m_5, m_6)$ are bounded above. Thus $A(T)C(a^{(1)}, y^{(2)}, m_5, m_6)$ tends to zero as $T \to 0$. In other words, for sufficiently small T we have $0 < A(T)C(a^{(1)}, y^{(2)}, m_5, m_6) < 1$. This means that the operator $\underline{\mathbf{O}}$ is a contraction mapping operator.

From the first and second steps, the operator $\underline{\mathbf{O}}$ is contraction mapping operator that is a continuous and onto map on E_T. Then according to Banach fixed point theorem the solution of the operator equation (16) exists and it is unique. □

4. Conclusion

The paper studies the inverse initial-boundary value problem of determining the time dependent lowest term together with the displacement function in a fourth order in time PDE from an additional observation. The unique solvability of the solution of the inverse problem on a sufficiently small time interval has been proved by using of the contraction principle. The proposed work is novel and has never been solved theoretically nor numerically before. Our results shed light on the methodology for the existence and uniqueness of the inverse problem for the fourth order in time PDEs in two dimensions.

Declaration of Competing Interests This work does not have any conflicts of interest.

References

[1] Arancibia, R., Lecaros, R., Mercado, A., Zamorano, S., An inverse problem for Moore-Gibson-Thompson equation arising in high intensity ultrasound, *Journal of Inverse and Ill-posed Problems*, 30(5) 82022, 659-675. https://doi.org/10.1515/jiip-2020-0090

[2] Chlouverakis, K. E., Sprott, J. C., Chaotic hyperjerk systems, *Chaos, Solitons & Fractals*, 28(3) (2006),739-746. https://doi.org/10.1016/j.chaos.2005.08.019

[3] Choucha, A., Boulaaras, S., Ouchenane, D., Abdalla, M., Mekawy, I., Benbella, A., Existence and uniqueness for Moore-Gibson-Thompson equation with, source terms, viscoelastic memory and integral condition, *AIMS Mathematics*, 6(7) (2021), 7585-7624.

[4] Conti, M., Pata, V., Quintanilla, R., Thermoelasticity of Moore-Gibson-Thompson type with history dependence in the temperature, *Asymptotic Analysis,* 120(1-2) (2020), 1-21. https://doi.org/10.3233/ASY-191576

[5] Dell'Oro, F., Pata, V., On a fourth-order equation of Moore-Gibson-Thompson type, *Milan J. Math.*, 85 (2017), 215-234.

[6] Dell'Oro, F., Pata, V., On the Moore-Gibson-Thompson equation and its relation to linear viscoelasticity, *Applied Mathematics & Optimization*, 7683 (2017), 641-655. https://doi.org/10.1007/s00245-016-9365-1

[7] Dell' Oro, F., Lasiecka, I., Pata, V., The Moore-Gibson-Thompson equation with memory in the critical case, *J Differ Equ.*, 261 (2016), 4188-4222. https://doi.org/10.1016/j.jde.2016.06.025

[8] Figliolini, G., Lanni, C., Jerk and jounce relevance for the kinematic performance of long-dwell mechanisms, *Mechanisms and Machine Science*, 73 (2019), 219-228. https://doi.org/10.1007/978-3-030-20131-9_22

[9] Huntul, M. J., Tekin, I., On an inverse problem for a nonlinear third order in time partial differential equation, *Results in Applied Mathematics*, 15 (2022), 100314. https://doi.org/10.1016/j.rinam.2022.100314

[10] Kaltenbacher, B., Lasiecka, I., Pospieszalska, M. K., Well-posedness and exponential decay of the energy in the nonlinear Jordan-Moore-Gibson-Thompson equation arising in high intensity ultrasound, *Mathematical Models and Methods in Applied Sciences*, 22(11) (2012), 1250035. https://doi.org/10.1142/S0218202512500352

[11] Kaltenbacher, B., Nikolić, V., The Jordan-Moore-Gibson-Thompson equation: well-posedness with quadratic gradient nonlinearity and singular limit for vanishing relaxation time, *Mathematical Models and Methods in Applied Sciences*, 29(13) (2019), 2523-2556. https://doi.org/10.1142/S0218202519500532

[12] Kaltenbacher, B., Mathematics of nonlinear acoustics, *Evolution Equations & Control Theory,* 4(4) (2015), 447-491.

[13] Lasiecka, I., Wang, X., Moore-Gibson-Thompson equation with memory, part I: exponential decay of energy, *Zeitschrift für angewandte Mathematik und Physik,* 67(2) (2016), 1-23. https://doi.org/10.1007/s00033-015-0597-8

[14] Lasiecka, I., Wang, X., Moore-Gibson-Thompson equation with memory, part II: general decay of energy, *Journal of Differential Equations*, 259(12) (2015), 7610-7635. https://doi.org/10.1016/j.jde.2015.08.052

[15] Liu, W., Chen, Z., Tu, Z., New general decay result for a fourth-order Moore-Gibson-Thompson equation with memory, *Electronic Research Archive*, 28(1) (2020), 433. https://doi.org/10.3934/era.2020025

[16] Lizama, C., Murillo-Arcila, M., well-posedness for a fourth-order equation of Moore-Gibson-Thompson type, *Electronic Journal of Qualitative Theory of Differential Equations*, 81 (2021), 1-18. https://doi.org/10.14232/ejqtde.2021.1.81

[17] Mehraliyev, Y. T., On solvability of an inverse boundary value problem for a second order elliptic equation, *Bulletin of Tver State University, Series: Applied mathematics*, 23 (2011), 25-38.(in Russian)

[18] Mesloub, A., Zara, A., Mesloub, F., Cherif, B. B., Abdalla, M., The Galerkin method for fourth-Order equation of the Moore-Gibson-Thompson type with integral condition, *Advances in Mathematical Physics*, (2021), 2021. https://doi.org/10.1155/2021/5532691

[19] Murillo-Arcila, M., Well-posedness for the fourth-order Moore-Gibson-Thompson equation in the class of Banach-space-valued Hölder-continuous functions, *Mathematical Methods in the Applied Sciences*, (2022), 1-10. doi:10.1002/mma.8618

[20] Pellicer Sabadí, M., Said-Houari,B., Well posedness and decay rates for the Cauchy problem of the Moore-Gibson-Thompson equation arising in high intensity ultrasound, *Applied Mathematics and Optimization*, 80(2) 82019), 447-478. https://doi.org/10.1007/s00245-017-9471-8

[21] Tekin, I., Inverse problem for a nonlinear third order in time partial differential equation, *Mathematical Methods in the Applied Sciences*, 44(11) (2021), 9571-9581. https://doi.org/10.1002/mma.7380

[22] Visser, M., Jerk, snap and the cosmological equation of state, *Classical and Quantum Gravity*, 21(11) (2004), 2603. https://doi.org/10.1088/0264-9381/21/11/006

http://communications.science.ankara.edu.tr

Commun.Fac.Sci.Univ.Ank.Ser. A1 Math. Stat.
Volume 72, Number 2, Pages 512–529 (2023)
DOI:10.31801/cfsuasmas.1144644
ISSN 1303-5991 E-ISSN 2618-6470

Research Article; Received: July 17, 2022; Accepted: November 7, 2022

M-LAURICELLA HYPERGEOMETRIC FUNCTIONS: INTEGRAL REPRESENTATIONS AND SOLUTION OF FRACTIONAL DIFFERENTIAL EQUATIONS

Enes ATA
Department of Mathematics, Kırşehir Ahi Evran University, Kırşehir, TÜRKİYE

Abstract. In this paper, using the modified beta function involving the generalized M-series in its kernel, we describe new extensions for the Lauricella hypergeometric functions $F_A^{(r)}$, $F_B^{(r)}$, $F_C^{(r)}$ and $F_D^{(r)}$. Furthermore, we find various integral representations for the newly defined extended Lauricella hypergeometric functions. Then, we obtain solution of fractional differential equations involving new extensions of Lauricella hypergeometric functions, as examples.

1. Introduction and Preliminaries

Scientists have conducted a lot of research in recent years on various generalizations of special functions (see for example [1, 5–13, 15, 19–22, 24, 26, 27, 29, 33]). Particularly, the modified gamma and beta functions for $\Re(\alpha) > 0$, $\Re(\rho) > 0$, $\Re(x) > 0$, $\Re(y) > 0$ and $\xi_1, \ldots, \xi_p, \eta_1, \ldots, \eta_q \neq 0, -1, -2, \ldots$ was introduced by Ata in [8], respectively, as follows:

$$\begin{aligned} {}^M\Gamma_{p,q}^{(\alpha,\beta)}(x;\rho) &= {}^M\Gamma_{p,q}^{(\alpha,\beta)}(\xi_1,\ldots,\xi_p;\eta_1,\ldots,\eta_q;x;\rho) \\ &= \int_0^1 \Delta^{x-1}\ {}_p^{\alpha}M_q^{\beta}\left(\xi_1,\ldots,\xi_p;\eta_1,\ldots,\eta_q;-\Delta-\frac{\rho}{\Delta}\right)d\Delta, \end{aligned}$$

and

$$\begin{aligned} {}^MB_{p,q}^{(\alpha,\beta)}(x,y;\rho) &= {}^MB_{p,q}^{(\alpha,\beta)}(\xi_1,\ldots,\xi_p;\eta_1,\ldots,\eta_q;x,y;\rho) \\ &= \int_0^1 \Delta^{x-1}(1-\Delta)^{y-1}\ {}_p^{\alpha}M_q^{\beta}\left(\xi_1,\ldots,\xi_p;\eta_1,\ldots,\eta_q;\frac{-\rho}{\Delta(1-\Delta)}\right)d\Delta. \end{aligned} \quad (1)$$

2020 *Mathematics Subject Classification.* 26A33, 33B15, 33C15, 33C65, 34A08, 44A10.
Keywords. Fractional derivatives and integrals, beta function, confluent hypergeometric function, Lauricella functions, fractional differential equations, Laplace transform.

enesata.tr@gmail.com 0000-0001-6893-8693.

If we take $\Delta = (\sin\phi)^2$ in Eq. (1), then

$$
\begin{aligned}
{}^{M}B_{p,q}^{(\alpha,\beta)}(x,y;\rho) = 2\int_0^{\frac{\pi}{2}} & (\sin\phi)^{2x-1}(\cos\phi)^{2y-1} \\
& \times {}_{p}^{\alpha}M_{q}^{\beta}\left(\xi_1,\ldots,\xi_p;\eta_1,\ldots,\eta_q;-\rho(\sec\phi)^2(\csc\phi)^2\right)d\phi. \qquad (2)
\end{aligned}
$$

If we take $\Delta = \frac{u}{1+u}$ in Eq. (1), then

$$
\begin{aligned}
{}^{M}B_{p,q}^{(\alpha,\beta)}(x,y;\rho) = \int_0^{\infty} & \frac{u^{x-1}}{(1+u)^{x+y}} \\
& \times {}_{p}^{\alpha}M_{q}^{\beta}\left(\xi_1,\ldots,\xi_p;\eta_1,\ldots,\eta_q;-2\rho-\rho\left(u+\frac{1}{u}\right)\right)du. \qquad (3)
\end{aligned}
$$

If we take $\Delta = \frac{u-a}{b-a}$ in Eq. (1), then

$$
\begin{aligned}
{}^{M}B_{p,q}^{(\alpha,\beta)}(x,y;\rho) = (b-a)^{1-x-y}\int_a^{b} & (u-a)^{x-1}(b-u)^{y-1} \\
& \times {}_{p}^{\alpha}M_{q}^{\beta}\left(\xi_1,\ldots,\xi_p;\eta_1,\ldots,\eta_q;\frac{-\rho(b-a)^2}{(u-a)(b-u)}\right)du. \qquad (4)
\end{aligned}
$$

Then, the modified confluent hypergeometric function for $\Re(\alpha) > 0$, $\Re(\rho) > 0$, $\Re(\chi_3) > \Re(\chi_2) > 0$ and $\xi_1,\ldots,\xi_p,\eta_1,\ldots,\eta_q \neq 0,-1,-2,\ldots$ was introduced by Ata in [8], as follows:

$$
\begin{aligned}
{}^{M}\Phi_{p,q}^{(\alpha,\beta)}(\chi_2;\chi_3;z;\rho) &= {}^{M}\Phi_{p,q}^{(\alpha,\beta)}(\xi_1,\ldots,\xi_p;\eta_1,\ldots,\eta_q;\chi_2;\chi_3;z;\rho) \\
&= \sum_{n=0}^{\infty}\frac{{}^{M}B_{p,q}^{(\alpha,\beta)}(\chi_2+n,\chi_3-\chi_2;\rho)}{B(\chi_2,\chi_3-\chi_2)}\frac{z^n}{n!}. \qquad (5)
\end{aligned}
$$

Also, the following formula holds true [8]:

$$
{}^{M}\Phi_{p,q}^{(\alpha,\beta)}(\chi_2;\chi_3;z;\rho) = \exp(z)\ {}^{M}\Phi_{p,q}^{(\alpha,\beta)}(\chi_3-\chi_2;\chi_3;-z;\rho). \qquad (6)
$$

Respectively, Ata called them as M-gamma, M-beta and M-confluent hypergeometric functions. If we put $\rho = 0$ and $p = q = \xi_1 = \eta_1 = \alpha = \beta = 1$ to the M-gamma, M-beta and M-confluent hypergeometric functions, we get the following classical special functions [3,4], respectively:

- The gamma function for $\Re(x) > 0$

$$
\Gamma(x) = \int_0^{\infty}\Delta^{x-1}\exp(-\Delta)d\Delta.
$$

- The beta function for $\Re(x) > 0$ and $\Re(y) > 0$

$$
B(x,y) = \int_0^{1}\Delta^{x-1}(1-\Delta)^{y-1}d\Delta.
$$

- The confluent hypergeometric function for $\Re(\chi_3) > \Re(\chi_2) > 0$

$$\Phi(\chi_2;\chi_3;z) = \sum_{n=0}^{\infty} \frac{B(\chi_2+n,\chi_3-\chi_2)}{B(\chi_2,\chi_3-\chi_2)} \frac{z^n}{n!}.$$

The function ${}_{p}^{\alpha}M_q^{\beta}$ used above is known as the generalized M-series [28] for $\Re(\alpha) > 0$ and $\xi_1,\ldots,\xi_p,\eta_1,\ldots,\eta_q \neq 0,-1,-2,\ldots$ which defined as:

$${}_{p}^{\alpha}M_q^{\beta}(z) = {}_{p}^{\alpha}M_q^{\beta}(\xi_1,\ldots,\xi_p;\eta_1,\ldots,\eta_q;z) = \sum_{n=0}^{\infty} \frac{(\xi_1)_n\ldots(\xi_p)_n}{(\eta_1)_n\ldots(\eta_q)_n} \frac{z^n}{\Gamma(\alpha n+\beta)}.$$

$(\cdot)_n$ used above denotes the Pochhammer symbol [4] is defined by

$$(\zeta)_n = \frac{\Gamma(\zeta+n)}{\Gamma(\zeta)} = \begin{cases} \zeta(\zeta+1)\ldots(\zeta+n-1), & n=1,2,\ldots, \\ 1, & n=0. \end{cases} \tag{7}$$

The binomial theorem [4] is as follows:

$$(1-\Delta)^{-\zeta} = \sum_{n=0}^{\infty} (\zeta)_n \frac{\Delta^n}{n!}, \quad (|\Delta|<1). \tag{8}$$

The Caputo fractional derivative [18] for $m-1 < \Re(\epsilon) < m$, $m \in \mathbb{N}$ is given by

$${}^{c}D_{\rho}^{\epsilon}\{f(\rho)\} = \frac{1}{\Gamma(m-\epsilon)} \int_0^{\rho} (\rho-\omega)^{m-\epsilon-1} f^{(m)}(\omega)d\omega, \quad (\Re(\epsilon)>0;\rho>0).$$

The Laplace and inverse Laplace transforms [14] are defined by

$$\mathfrak{L}\{f(\rho);s\} = F(s) = \int_0^{\infty} \exp(-s\rho)f(\rho)d\rho, \quad (\Re(s)>0),$$

and

$$\mathfrak{L}^{-1}\{F(s)\} = f(\rho) = \frac{1}{2\pi i} \int_{c-i\infty}^{c+i\infty} \exp(s\rho)F(s)ds, \quad (c>0).$$

Also, the Laplace transform of the Caputo fractional derivative is as follows [25]:

$$\mathfrak{L}\left\{{}^{c}D_{\rho}^{\epsilon}\{f(\rho)\};s\right\} = s^{\epsilon}F(s) - \sum_{k=0}^{m-1} s^{\epsilon-k-1}f^{(k)}(0), \quad (m-1<\Re(\epsilon)\leq m). \tag{9}$$

Respectively, the Lauricella hypergeometric functions $F_A^{(r)}$, $F_B^{(r)}$, $F_C^{(r)}$ and $F_D^{(r)}$ [30,31] are as follows:

$$\begin{aligned} &F_A^{(r)}(\kappa,\mu_1,\ldots,\mu_r;\nu_1,\ldots,\nu_r;x_1,\ldots,x_r) \\ &= \sum_{n_1,\ldots,n_r=0}^{\infty} \frac{(\kappa)_{n_1+\ldots+n_r}(\mu_1)_{n_1}\ldots(\mu_r)_{n_r}}{(\nu_1)_{n_1}\ldots(\nu_r)_{n_r}} \frac{x_1^{n_1}}{n_1!}\ldots\frac{x_r^{n_r}}{n_r!}, \\ &(|x_1|+\ldots+|x_r|<1), \end{aligned} \tag{10}$$

$$F_B^{(r)}(\kappa_1,\ldots,\kappa_r,\mu_1,\ldots,\mu_r;\nu;x_1,\ldots,x_r)$$

$$= \sum_{n_1,\ldots,n_r=0}^{\infty} \frac{(\kappa_1)_{n_1}\ldots(\kappa_r)_{n_r}(\mu_1)_{n_1}\ldots(\mu_r)_{n_r}}{(\nu)_{n_1+\ldots+n_r}} \frac{x_1^{n_1}}{n_1!}\cdots\frac{x_r^{n_r}}{n_r!}, \tag{11}$$

$$(\max\{|x_1|,\ldots,|x_r|\}<1),$$

$$F_C^{(r)}(\kappa,\mu;\nu_1,\ldots,\nu_r;x_1,\ldots,x_r)$$
$$= \sum_{n_1,\ldots,n_r=0}^{\infty} \frac{(\kappa)_{n_1+\ldots+n_r}(\mu)_{n_1+\ldots+n_r}}{(\nu_1)_{n_1}\ldots(\nu_r)_{n_r}} \frac{x_1^{n_1}}{n_1!}\cdots\frac{x_r^{n_r}}{n_r!}, \tag{12}$$

$$(\sqrt{x_1}+\ldots+\sqrt{x_r}<1),$$

$$F_D^{(r)}(\kappa,\mu_1,\ldots,\mu_r;\nu;x_1,\ldots,x_r)$$
$$= \sum_{n_1,\ldots,n_r=0}^{\infty} \frac{(\kappa)_{n_1+\ldots+n_r}(\mu_1)_{n_1}\ldots(\mu_r)_{n_r}}{(\nu)_{n_1+\ldots+n_r}} \frac{x_1^{n_1}}{n_1!}\cdots\frac{x_r^{n_r}}{n_r!}, \tag{13}$$

$$(\max\{|x_1|,\ldots,|x_r|\}<1).$$

2. New Extended Lauricella Hypergeometric Functions

Scientists have studied on various extended of Lauricella hypergeometric functions (see for example [2,16,17,23,32]). Motivated by these studies, we introduce the newly extended Lauricella hypergeometric functions $F_A^{(r)}$, $F_B^{(r)}$, $F_C^{(r)}$ and $F_D^{(r)}$ using the modified beta function involving the generalized M-series in its kernel, in this section.

Definition 1. *Let $\Re(\alpha)>0$, $\Re(\rho)>0$, $\Re(\nu_i)>\Re(\mu_i)>0$ for $i=1,\ldots,r$ and $|x_1|+\ldots+|x_r|<1$. Then, new extended Lauricella hypergeometric function $F_A^{(r)}$ is defined as:*

$$\begin{aligned}
&{}^{M}F_{A,p,q}^{(\alpha,\beta;r)}(\kappa,\mu_1,\ldots,\mu_r;\nu_1,\ldots,\nu_r;x_1,\ldots,x_r;\rho)\\
&= {}^{M}F_{A,p,q}^{(\alpha,\beta;r)}(\xi_1,\ldots,\xi_p;\eta_1,\ldots,\eta_q;\kappa,\mu_1,\ldots,\mu_r;\nu_1,\ldots,\nu_r;x_1,\ldots,x_r;\rho)\\
&:= \sum_{n_1,\ldots,n_r=0}^{\infty}(\kappa)_{n_1+\ldots+n_r}\frac{{}^{M}B_{p,q}^{(\alpha,\beta)}(\mu_1+n_1,\nu_1-\mu_1;\rho)}{B(\mu_1,\nu_1-\mu_1)}\cdots\\
&\quad\times\frac{{}^{M}B_{p,q}^{(\alpha,\beta)}(\mu_r+n_r,\nu_r-\mu_r;\rho)}{B(\mu_r,\nu_r-\mu_r)}\frac{x_1^{n_1}}{n_1!}\cdots\frac{x_r^{n_r}}{n_r!}.
\end{aligned}$$

Definition 2. *Let $\Re(\alpha)>0$, $\Re(\rho)>0$, $\Re(\lambda)>\Re(\mu_1)>0$ and $\max\{|x_1|,\ldots,|x_r|\}<1$. Then, new extended Lauricella hypergeometric function $F_B^{(r)}$ is defined as:*

$$\begin{aligned}
&{}^{M}F_{B,p,q}^{(\alpha,\beta;r)}(\kappa_1,\ldots,\kappa_r,\mu_1,\ldots,\mu_r;\nu;x_1,\ldots,x_r;\rho;\lambda)\\
&= {}^{M}F_{B,p,q}^{(\alpha,\beta;r)}(\xi_1,\ldots,\xi_p;\eta_1,\ldots,\eta_q;\kappa_1,\ldots,\kappa_r,\mu_1,\ldots,\mu_r;\nu;x_1,\ldots,x_r;\rho;\lambda)
\end{aligned}$$

$$:= \sum_{n_1,\ldots,n_r=0}^{\infty} \frac{(\kappa_1)_{n_1}\ldots(\kappa_r)_{n_r}(\lambda)_{n_1}(\mu_2)_{n_2}\ldots(\mu_r)_{n_r}}{(\nu)_{n_1+\ldots+n_r}}$$
$$\times \frac{{}^{M}B_{p,q}^{(\alpha,\beta)}(\mu_1+n_1,\lambda-\mu_1;\rho)}{B(\mu_1,\lambda-\mu_1)} \frac{x_1^{n_1}}{n_1!}\cdots\frac{x_r^{n_r}}{n_r!}.$$

Definition 3. *Let* $\Re(\alpha)>0, \Re(\rho)>0, \Re(\nu_1)>\Re(\lambda)>0$ *and* $\sqrt{|x_1|}+\ldots+\sqrt{|x_r|}<1$. *Then, new extended Lauricella hypergeometric function* $F_C^{(r)}$ *is defined as:*

$$\begin{aligned}
&{}^{M}F_{C,p,q}^{(\alpha,\beta;r)}(\kappa,\mu;\nu_1,\ldots,\nu_r;x_1,\ldots,x_r;\rho;\lambda)\\
&= {}^{M}F_{C,p,q}^{(\alpha,\beta;r)}(\xi_1,\ldots,\xi_p;\eta_1,\ldots,\eta_q;\kappa,\mu;\nu_1,\ldots,\nu_r;x_1,\ldots,x_r;\rho;\lambda)\\
&:= \sum_{n_1,\ldots,n_r=0}^{\infty} \frac{(\kappa)_{n_1+\ldots+n_r}(\mu)_{n_1+\ldots+n_r}}{(\lambda)_{n_1}(\nu_2)_{n_2}\ldots(\nu_r)_{n_r}} \frac{{}^{M}B_{p,q}^{(\alpha,\beta)}(\lambda+n_1,\nu_1-\lambda;\rho)}{B(\lambda,\nu_1-\lambda)} \frac{x_1^{n_1}}{n_1!}\cdots\frac{x_r^{n_r}}{n_r!}.
\end{aligned}$$

Definition 4. *Let* $\Re(\alpha)>0, \Re(\rho)>0, \Re(\nu)>\Re(\kappa)>0$ *and* $\max\{|x_1|,\ldots,|x_r|\}<1$. *Then, new extended Lauricella hypergeometric function* $F_D^{(r)}$ *is defined as:*

$$\begin{aligned}
&{}^{M}F_{D,p,q}^{(\alpha,\beta;r)}(\kappa,\mu_1,\ldots,\mu_r;\nu;x_1,\ldots,x_r;\rho)\\
&= {}^{M}F_{D,p,q}^{(\alpha,\beta;r)}(\xi_1,\ldots,\xi_p;\eta_1,\ldots,\eta_q;\kappa,\mu_1,\ldots,\mu_r;\nu;x_1,\ldots,x_r;\rho)\\
&:= \sum_{n_1,\ldots,n_r=0}^{\infty} (\mu_1)_{n_1}\ldots(\mu_r)_{n_r} \frac{{}^{M}B_{p,q}^{(\alpha,\beta)}(\kappa+n_1+\ldots+n_r,\nu-\kappa;\rho)}{B(\kappa,\nu-\kappa)} \frac{x_1^{n_1}}{n_1!}\cdots\frac{x_r^{n_r}}{n_r!}.
\end{aligned}$$

Respectively, we call them as M-Lauricella hypergeometric function $F_A^{(r)}$, M-Lauricella hypergeometric function $F_B^{(r)}$, M-Lauricella hypergeometric function $F_C^{(r)}$ and M-Lauricella hypergeometric function $F_D^{(r)}$.

Remark 1. *If we take* $\rho=0$ *and* $p=q=\xi_1=\eta_1=\alpha=\beta=1$ *in these functions, we get Eqs.* (10), (11), (12) *and* (13).

3. Integral Representations for M-Lauricella Hypergeometric Function $F_A^{(r)}$

Theorem 1. *Let* $\Re(\alpha)>0$, $\Re(\rho)>0$, $\Re(\nu_i)>\Re(\mu_i)>0$ *for* $i=1,\ldots,r$. *Then,*

$$\begin{aligned}
&{}^{M}F_{A,p,q}^{(\alpha,\beta;r)}(\kappa,\mu_1,\ldots,\mu_r;\nu_1,\ldots,\nu_r;x_1,\ldots,x_r;\rho)\\
&= \frac{1}{B(\mu_1,\nu_1-\mu_1)\ldots B(\mu_r,\nu_r-\mu_r)} \int_0^1\cdots\int_0^1 \Delta_1^{\mu_1-1}\ldots\ \Delta_r^{\mu_r-1}\\
&\times (1-\Delta_1)^{\nu_1-\mu_1-1}\ldots\ (1-\Delta_r)^{\nu_r-\mu_r-1}\\
&\times {}_{p}^{\alpha}M_q^{\beta}\left(\frac{-\rho}{\Delta_1(1-\Delta_1)}\right)\ldots\ {}_{p}^{\alpha}M_q^{\beta}\left(\frac{-\rho}{\Delta_r(1-\Delta_r)}\right)\\
&\times F_A^{(r)}(\kappa,\mu_1,\ldots,\mu_r;\mu_1,\ldots,\mu_r;\Delta_1x_1,\ldots,\Delta_rx_r)d\Delta_1\ldots d\Delta_r.
\end{aligned}$$

Proof. Using the integral representation (1) of M-beta function in the definition of M-Lauricella hypergeometric function $F_A^{(r)}$, we have

$$
\begin{aligned}
&{}^{M}F_{A,p,q}^{(\alpha,\beta;r)}(\kappa,\mu_1,\dots,\mu_r;\nu_1,\dots,\nu_r;x_1,\dots,x_r;\rho)\\
&\quad=\sum_{n_1,\dots,n_r=0}^{\infty}(\kappa)_{n_1+\dots+n_r}\frac{{}^{M}B_{p,q}^{(\alpha,\beta)}(\mu_1+n_1,\nu_1-\mu_1;\rho)}{B(\mu_1,\nu_1-\mu_1)}\dots\\
&\quad\times\frac{{}^{M}B_{p,q}^{(\alpha,\beta)}(\mu_r+n_r,\nu_r-\mu_r;\rho)}{B(\mu_r,\nu_r-\mu_r)}\frac{x_1^{n_1}}{n_1!}\dots\frac{x_r^{n_r}}{n_r!}\\
&\quad=\frac{1}{B(\mu_1,\nu_1-\mu_1)\dots B(\mu_r,\nu_r-\mu_r)}\sum_{n_1,\dots,n_r=0}^{\infty}(\kappa)_{n_1+\dots+n_r}\\
&\quad\times\int_0^1\Delta_1^{\mu_1+n_1-1}(1-\Delta_1)^{\nu_1-\mu_1-1}\,{}_{p}^{\alpha}M_q^{\beta}\left(\frac{-\rho}{\Delta_1(1-\Delta_1)}\right)\dots\\
&\quad\times\int_0^1\Delta_r^{\mu_r+n_r-1}(1-\Delta_r)^{\nu_r-\mu_r-1}\,{}_{p}^{\alpha}M_q^{\beta}\left(\frac{-\rho}{\Delta_r(1-\Delta_r)}\right)\\
&\quad\times\frac{x_1^{n_1}}{n_1!}\dots\frac{x_r^{n_r}}{n_r!}d\Delta_1\dots d\Delta_r\\
&\quad=\frac{1}{B(\mu_1,\nu_1-\mu_1)\dots B(\mu_r,\nu_r-\mu_r)}\sum_{n_1,\dots,n_r=0}^{\infty}(\kappa)_{n_1+\dots+n_r}\\
&\quad\times\int_0^1\Delta_1^{\mu_1-1}(1-\Delta_1)^{\nu_1-\mu_1-1}\,{}_{p}^{\alpha}M_q^{\beta}\left(\frac{-\rho}{\Delta_1(1-\Delta_1)}\right)\dots\\
&\quad\times\int_0^1\Delta_r^{\mu_r-1}(1-\Delta_r)^{\nu_r-\mu_r-1}\,{}_{p}^{\alpha}M_q^{\beta}\left(\frac{-\rho}{\Delta_r(1-\Delta_r)}\right)\\
&\quad\times\frac{(x_1\Delta_1)^{n_1}}{n_1!}\dots\frac{(x_r\Delta_r)^{n_r}}{n_r!}d\Delta_1\dots d\Delta_r.
\end{aligned}
$$

Multiplied by $\frac{(\mu_1)_{n_1}\cdots(\mu_r)_{n_r}}{(\mu_1)_{n_1}\cdots(\mu_r)_{n_r}}$ and considering Eq. (10), we get

$$
\begin{aligned}
&{}^{M}F_{A,p,q}^{(\alpha,\beta;r)}(\kappa,\mu_1,\dots,\mu_r;\nu_1,\dots,\nu_r;x_1,\dots,x_r;\rho)\\
&\quad=\frac{1}{B(\mu_1,\nu_1-\mu_1)\dots B(\mu_r,\nu_r-\mu_r)}\int_0^1\dots\int_0^1\Delta_1^{\mu_1-1}\dots\ \Delta_r^{\mu_r-1}\\
&\quad\times(1-\Delta_1)^{\nu_1-\mu_1-1}\dots\ (1-\Delta_r)^{\nu_r-\mu_r-1}\\
&\quad\times{}_{p}^{\alpha}M_q^{\beta}\left(\frac{-\rho}{\Delta_1(1-\Delta_1)}\right)\dots\ {}_{p}^{\alpha}M_q^{\beta}\left(\frac{-\rho}{\Delta_r(1-\Delta_r)}\right)\\
&\quad\times F_A^{(r)}(\kappa,\mu_1,\dots,\mu_r;\mu_1,\dots,\mu_r;\Delta_1x_1,\dots,\Delta_rx_r)d\Delta_1\dots d\Delta_r.\qquad\square
\end{aligned}
$$

Theorem 2. *Let $\Re(\alpha) > 0$, $\Re(\rho) > 0$, $\Re(\nu_i) > \Re(\mu_i) > 0$ for $i = 1, \ldots, r$. Then,*

$$\begin{aligned} &{}^{M}F_{A,p,q}^{(\alpha,\beta;r)}(\kappa, \mu_1, \ldots, \mu_r; \nu_1, \ldots, \nu_r; x_1, \ldots, x_r; \rho) \\ &\quad = \frac{1}{\Gamma(\kappa)} \int_0^\infty \Delta^{\kappa-1} \exp(-\Delta) \\ &\qquad \times {}^{M}\Phi_{p,q}^{(\alpha,\beta)}(\mu_1; \nu_1; \Delta x_1; \rho) \ldots {}^{M}\Phi_{p,q}^{(\alpha,\beta)}(\mu_r; \nu_r; \Delta x_r; \rho) d\Delta. \end{aligned} \tag{14}$$

Proof. Using Eq. (7) in the definition of M-Lauricella hypergeometric function $F_A^{(r)}$, we have

$$\begin{aligned} &{}^{M}F_{A,p,q}^{(\alpha,\beta;r)}(\kappa, \mu_1, \ldots, \mu_r; \nu_1, \ldots, \nu_r; x_1, \ldots, x_r; \rho) \\ &\quad = \sum_{n_1,\ldots,n_r=0}^{\infty} (\kappa)_{n_1+\ldots+n_r} \frac{{}^{M}B_{p,q}^{(\alpha,\beta)}(\mu_1 + n_1, \nu_1 - \mu_1; \rho)}{B(\mu_1, \nu_1 - \mu_1)} \ldots \\ &\qquad \times \frac{{}^{M}B_{p,q}^{(\alpha,\beta)}(\mu_r + n_r, \nu_r - \mu_r; \rho)}{B(\mu_r, \nu_r - \mu_r)} \frac{x_1^{n_1}}{n_1!} \ldots \frac{x_r^{n_r}}{n_r!} \\ &\quad = \sum_{n_1,\ldots,n_r=0}^{\infty} \frac{\Gamma(\kappa + n_1 + \ldots + n_r)}{\Gamma(\kappa)} \frac{{}^{M}B_{p,q}^{(\alpha,\beta)}(\mu_1 + n_1, \nu_1 - \mu_1; \rho)}{B(\mu_1, \nu_1 - \mu_1)} \ldots \\ &\qquad \times \frac{{}^{M}B_{p,q}^{(\alpha,\beta)}(\mu_r + n_r, \nu_r - \mu_r; \rho)}{B(\mu_r, \nu_r - \mu_r)} \frac{x_1^{n_1}}{n_1!} \ldots \frac{x_r^{n_r}}{n_r!}. \end{aligned}$$

Using the integral representation of gamma function and considering Eq. (5), we get

$$\begin{aligned} &{}^{M}F_{A,p,q}^{(\alpha,\beta;r)}(\kappa, \mu_1, \ldots, \mu_r; \nu_1, \ldots, \nu_r; x_1, \ldots, x_r; \rho) \\ &\quad = \frac{1}{\Gamma(\kappa)} \int_0^\infty \Delta^{\kappa-1} \exp(-\Delta) \\ &\qquad \times {}^{M}\Phi_{p,q}^{(\alpha,\beta)}(\mu_1; \nu_1; \Delta x_1; \rho) \ldots {}^{M}\Phi_{p,q}^{(\alpha,\beta)}(\mu_r; \nu_r; \Delta x_r; \rho) d\Delta. \end{aligned}$$ □

Theorem 3. *Let $\Re(\alpha) > 0$, $\Re(\rho) > 0$, $\Re(\nu_i) > \Re(\mu_i) > 0$ for $i = 1, \ldots, r$. Then,*

$$\begin{aligned} &{}^{M}F_{A,p,q}^{(\alpha,\beta;r)}(\kappa, \mu_1, \ldots, \mu_r; \nu_1, \ldots, \nu_r; x_1, \ldots, x_r; \rho) \\ &\quad = \frac{1}{\Gamma(\kappa)} \int_0^\infty \Delta^{\kappa-1} \exp\big(-\Delta(1 - x_1 - \ldots - x_r)\big) \\ &\qquad \times {}^{M}\Phi_{p,q}^{(\alpha,\beta)}(\nu_1 - \mu_1; \nu_1; -\Delta x_1; \rho) \ldots {}^{M}\Phi_{p,q}^{(\alpha,\beta)}(\nu_r - \mu_r; \nu_r; -\Delta x_r; \rho) d\Delta. \end{aligned}$$

Proof. Using Eq. (6) in Eq. (14), proof is complete. □

Theorem 4. *Let $\Re(\alpha) > 0$, $\Re(\rho) > 0$, $\Re(\nu_i) > \Re(\mu_i) > 0$ for $i = 1, \ldots, r$. Then,*

$$\begin{aligned} &{}^{M}F_{A,p,q}^{(\alpha,\beta;r)}(\kappa, \mu_1, \ldots, \mu_r; \nu_1, \ldots, \nu_r; x_1, \ldots, x_r; \rho) \\ &\quad = \frac{2^r}{B(\mu_1, \nu_1 - \mu_1) \ldots B(\mu_r, \nu_r - \mu_r)} \int_0^{\frac{\pi}{2}} \ldots \int_0^{\frac{\pi}{2}} \end{aligned}$$

$$\times (\sin\phi_1)^{2\mu_1-1}\dots\ (\sin\phi_r)^{2\mu_r-1}(\cos\phi_1)^{2\nu_1-2\mu_1-1}\dots\ (\cos\phi_r)^{2\nu_r-2\mu_r-1}$$
$$\times {}_p^{\alpha}M_q^{\beta}\left(-\rho(\sec\phi_1)^2(\csc\phi_1)^2\right)\dots\ {}_p^{\alpha}M_q^{\beta}\left(-\rho(\sec\phi_r)^2(\csc\phi_r)^2\right)$$
$$\times F_A^{(r)}\left(\kappa,\mu_1,\dots,\mu_r;\mu_1,\dots,\mu_r;x_1(\sin\phi_1)^2,\dots,x_r(\sin\phi_r)^2\right)d\phi_1\dots d\phi_r.$$

Proof. Using the integral representation (2) of M-beta function in the definition of M-Lauricella hypergeometric function $F_A^{(r)}$ and making similar calculations in the proof of Theorem 1, proof is complete. □

Theorem 5. *Let $\Re(\alpha)>0$, $\Re(\rho)>0$, $\Re(\nu_i)>\Re(\mu_i)>0$ for $i=1,\dots,r$. Then,*

$$\begin{aligned}&{}^{M}F_{A,p,q}^{(\alpha,\beta;r)}(\kappa,\mu_1,\dots,\mu_r;\nu_1,\dots,\nu_r;x_1,\dots,x_r;\rho)\\
&=\frac{1}{B(\mu_1,\nu_1-\mu_1)\dots B(\mu_r,\nu_r-\mu_r)}\int_0^\infty\dots\int_0^\infty\frac{u_1^{\mu_1-1}}{(1+u_1)^{\nu_1}}\dots\frac{u_r^{\mu_r-1}}{(1+u_r)^{\nu_r}}\\
&\times {}_p^{\alpha}M_q^{\beta}\left(-2\rho-\rho\left(u_1+\frac{1}{u_1}\right)\right)\dots\ {}_p^{\alpha}M_q^{\beta}\left(-2\rho-\rho\left(u_r+\frac{1}{u_r}\right)\right)\\
&\times F_A^{(r)}\left(\kappa,\mu_1,\dots,\mu_r;\mu_1,\dots,\mu_r;\frac{x_1u_1}{1+u_1},\dots,\frac{x_ru_r}{1+u_r}\right)du_1\dots du_r.\end{aligned}$$

Proof. Using the integral representation (3) of M-beta function in the definition of M-Lauricella hypergeometric function $F_A^{(r)}$ and making similar calculations in the proof of Theorem 1, proof is complete. □

Theorem 6. *Let $\Re(\alpha)>0$, $\Re(\rho)>0$, $\Re(\nu_i)>\Re(\mu_i)>0$ for $i=1,\dots,r$. Then,*

$$\begin{aligned}&{}^{M}F_{A,p,q}^{(\alpha,\beta;r)}(\kappa,\mu_1,\dots,\mu_r;\nu_1,\dots,\nu_r;x_1,\dots,x_r;\rho)\\
&=\frac{(b-a)^{r-(\nu_1+\dots+\nu_r)}}{B(\mu_1,\nu_1-\mu_1)\dots B(\mu_r,\nu_r-\mu_r)}\int_a^b\dots\int_a^b(u_1-a)^{\mu_1-1}\dots\ (u_r-a)^{\mu_r-1}\\
&\times(b-u_1)^{\nu_1-\mu_1-1}\dots\ (b-u_r)^{\nu_r-\mu_r-1}\\
&\times {}_p^{\alpha}M_q^{\beta}\left(\frac{-\rho(b-a)^2}{(u_1-a)(b-u_1)}\right)\dots\ {}_p^{\alpha}M_q^{\beta}\left(\frac{-\rho(b-a)^2}{(u_r-a)(b-u_r)}\right)\\
&\times F_A^{(r)}\left(\kappa,\mu_1,\dots,\mu_r;\mu_1,\dots,\mu_r;\frac{x_1(u_1-a)}{b-a},\dots,\frac{x_r(u_r-a)}{b-a}\right)du_1\dots du_r.\end{aligned}$$

Proof. Using the integral representation (4) of M-beta function in the definition of M-Lauricella hypergeometric function $F_A^{(r)}$ and making similar calculations in the proof of Theorem 1, proof is complete. □

4. Integral Representations for M-Lauricella Hypergeometric Function $F_B^{(r)}$

Theorem 7. *Let $\Re(\alpha)>0$, $\Re(\rho)>0$, $\Re(\lambda)>\Re(\mu_1)>0$. Then,*

$${}^{M}F_{B,p,q}^{(\alpha,\beta;r)}(\kappa_1,\dots,\kappa_r,\mu_1,\dots,\mu_r;\nu;x_1,\dots,x_r;\rho;\lambda)$$

$$= \frac{1}{B(\mu_1, \lambda-\mu_1)} \int_0^1 \Delta^{\mu_1-1}(1-\Delta)^{\lambda-\mu_1-1} \ {}_p^\alpha M_q^\beta \left(\frac{-\rho}{\Delta(1-\Delta)}\right) \times F_B^{(r)}(\kappa_1, \ldots, \kappa_r, \lambda, \mu_2, \ldots, \mu_r; \nu; \Delta x_1, x_2, \ldots, x_r) d\Delta.$$

Proof. Using the integral representation (1) of M-beta function in the definition of M-Lauricella hypergeometric function $F_B^{(r)}$, we have

$$\begin{aligned} &{}^M F_{B,p,q}^{(\alpha,\beta;r)}(\kappa_1, \ldots, \kappa_r, \mu_1, \ldots, \mu_r; \nu; x_1, \ldots, x_r; \rho; \lambda) \\ &= \sum_{n_1,\ldots,n_r=0}^{\infty} \frac{(\kappa_1)_{n_1} \ldots (\kappa_r)_{n_r} (\lambda)_{n_1} (\mu_2)_{n_2} \ldots (\mu_r)_{n_r}}{(\nu)_{n_1+\ldots+n_r}} \\ &\times \frac{{}^M B_{p,q}^{(\alpha,\beta)}(\mu_1+n_1, \lambda-\mu_1; \rho)}{B(\mu_1, \lambda-\mu_1)} \frac{x_1^{n_1}}{n_1!} \cdots \frac{x_r^{n_r}}{n_r!} \\ &= \frac{1}{B(\mu_1, \lambda-\mu_1)} \sum_{n_1,\ldots,n_r=0}^{\infty} \frac{(\kappa_1)_{n_1} \ldots (\kappa_r)_{n_r} (\lambda)_{n_1} (\mu_2)_{n_2} \ldots (\mu_r)_{n_r}}{(\nu)_{n_1+\ldots+n_r}} \\ &\times \int_0^1 \Delta^{\mu_1+n_1-1}(1-\Delta)^{\lambda-\mu_1-1} \ {}_p^\alpha M_q^\beta \left(\frac{-\rho}{\Delta(1-\Delta)}\right) \frac{x_1^{n_1}}{n_1!} \cdots \frac{x_r^{n_r}}{n_r!} d\Delta \end{aligned}$$

$$\begin{aligned} &= \frac{1}{B(\mu_1, \lambda-\mu_1)} \int_0^1 \Delta^{\mu_1-1}(1-\Delta)^{\lambda-\mu_1-1} \ {}_p^\alpha M_q^\beta \left(\frac{-\rho}{\Delta(1-\Delta)}\right) \\ &\times \sum_{n_1,\ldots,n_r=0}^{\infty} \frac{(\kappa_1)_{n_1} \ldots (\kappa_r)_{n_r} (\lambda)_{n_1} (\mu_2)_{n_2} \ldots (\mu_r)_{n_r}}{(\nu)_{n_1+\ldots+n_r}} \frac{(\Delta x_1)^{n_1}}{n_1!} \frac{x_2^{n_2}}{n_2!} \cdots \frac{x_r^{n_r}}{n_r!} d\Delta. \end{aligned}$$

Considering Eq. (11), we get

$$\begin{aligned} &{}^M F_{B,p,q}^{(\alpha,\beta;r)}(\kappa_1, \ldots, \kappa_r, \mu_1, \ldots, \mu_r; \nu; x_1, \ldots, x_r; \rho; \lambda) \\ &= \frac{1}{B(\mu_1, \lambda-\mu_1)} \int_0^1 \Delta^{\mu_1-1}(1-\Delta)^{\lambda-\mu_1-1} \ {}_p^\alpha M_q^\beta \left(\frac{-\rho}{\Delta(1-\Delta)}\right) \\ &\times F_B^{(r)}(\kappa_1, \ldots, \kappa_r, \lambda, \mu_2, \ldots, \mu_r; \nu; \Delta x_1, x_2, \ldots, x_r) d\Delta. \end{aligned}$$ □

Theorem 8. *Let* $\Re(\alpha) > 0$, $\Re(\rho) > 0$, $\Re(\lambda) > \Re(\mu_1) > 0$. *Then,*

$$\begin{aligned} &{}^M F_{B,p,q}^{(\alpha,\beta;r)}(\kappa_1, \ldots, \kappa_r, \mu_1, \ldots, \mu_r; \nu; x_1, \ldots, x_r; \rho; \lambda) \\ &= \frac{2}{B(\mu_1, \lambda-\mu_1)} \int_0^{\frac{\pi}{2}} (\sin\phi)^{2\mu_1-1}(\cos\phi)^{2\lambda-2\mu_1-1} \ {}_p^\alpha M_q^\beta \left(-\rho(\sec\phi)^2(\csc\phi)^2\right) \\ &\times F_B^{(r)}(\kappa_1, \ldots, \kappa_r, \lambda, \mu_2, \ldots, \mu_r; \nu; x_1(\sin\phi)^2, x_2, \ldots, x_r) d\phi. \end{aligned}$$

Proof. Using the integral representation (2) of M-beta function in the definition of M-Lauricella hypergeometric function $F_B^{(r)}$ and making similar calculations in the proof of Theorem 7, proof is complete. □

Theorem 9. *Let* $\Re(\alpha) > 0$, $\Re(\rho) > 0$, $\Re(\lambda) > \Re(\mu_1) > 0$. *Then,*

$$\begin{aligned}
&{}^{M}F_{B,p,q}^{(\alpha,\beta;r)}(\kappa_1,\ldots,\kappa_r,\mu_1,\ldots,\mu_r;\nu;x_1,\ldots,x_r;\rho;\lambda)\\
&= \frac{1}{B(\mu_1,\lambda-\mu_1)}\int_0^\infty \frac{u^{\mu_1-1}}{(1+u)^\lambda}\, {}_{p}^{\alpha}M_q^{\beta}\left(-2\rho-\rho\left(u+\frac{1}{u}\right)\right)\\
&\quad\times F_B^{(r)}\left(\kappa_1,\ldots,\kappa_r,\lambda,\mu_2,\ldots,\mu_r;\nu;\frac{x_1u}{1+u},x_2,\ldots,x_r\right)du.
\end{aligned}$$

Proof. Using the integral representation (3) of M-beta function in the definition of M-Lauricella hypergeometric function $F_B^{(r)}$ and making similar calculations in the proof of Theorem 7, proof is complete. □

Theorem 10. *Let* $\Re(\alpha) > 0$, $\Re(\rho) > 0$, $\Re(\lambda) > \Re(\mu_1) > 0$. *Then,*

$$\begin{aligned}
&{}^{M}F_{B,p,q}^{(\alpha,\beta;r)}(\kappa_1,\ldots,\kappa_r,\mu_1,\ldots,\mu_r;\nu;x_1,\ldots,x_r;\rho;\lambda)\\
&= \frac{(b-a)^{1-\lambda}}{B(\mu_1,\lambda-\mu_1)}\int_a^b (u-a)^{\mu_1-1}(b-u)^{\lambda-\mu_1-1}\, {}_{p}^{\alpha}M_q^{\beta}\left(\frac{-\rho(b-a)^2}{(u-a)(b-u)}\right)\\
&\quad\times F_B^{(r)}\left(\kappa_1,\ldots,\kappa_r,\lambda,\mu_2,\ldots,\mu_r;\nu;\frac{x_1(u-a)}{b-a},x_2,\ldots,x_r\right)du.
\end{aligned}$$

Proof. Using the integral representation (4) of M-beta function in the definition of M-Lauricella hypergeometric function $F_B^{(r)}$ and making similar calculations in the proof of Theorem 7, proof is complete. □

5. Integral Representations for M-Lauricella Hypergeometric Function $F_C^{(r)}$

Theorem 11. *Let* $\Re(\alpha) > 0$, $\Re(\rho) > 0$, $\Re(\nu_1) > \Re(\lambda) > 0$. *Then,*

$$\begin{aligned}
&{}^{M}F_{C,p,q}^{(\alpha,\beta;r)}(\kappa,\mu;\nu_1,\ldots,\nu_r;x_1,\ldots,x_r;\rho;\lambda)\\
&= \frac{1}{B(\lambda,\nu_1-\lambda)}\int_0^1 \Delta^{\lambda-1}(1-\Delta)^{\nu_1-\lambda-1}\, {}_{p}^{\alpha}M_q^{\beta}\left(\frac{-\rho}{\Delta(1-\Delta)}\right)\\
&\quad\times F_C^{(r)}(\kappa,\mu;\lambda,\nu_2,\ldots,\nu_r;\Delta x_1,x_2,\ldots,x_r)d\Delta.
\end{aligned}$$

Proof. Using the integral representation (1) of M-beta function in the definition of M-Lauricella hypergeometric function $F_C^{(r)}$, we have

$$\begin{aligned}
&{}^{M}F_{C,p,q}^{(\alpha,\beta;r)}(\kappa,\mu;\nu_1,\ldots,\nu_r;x_1,\ldots,x_r;\rho;\lambda)\\
&= \sum_{n_1,\ldots,n_r=0}^{\infty}\frac{(\kappa)_{n_1+\ldots+n_r}(\mu)_{n_1+\ldots+n_r}}{(\lambda)_{n_1}(\nu_2)_{n_2}\ldots(\nu_r)_{n_r}}\frac{{}^{M}B_{p,q}^{(\alpha,\beta)}(\lambda+n_1,\nu_1-\lambda;\rho)}{B(\lambda,\nu_1-\lambda)}\frac{x_1^{n_1}}{n_1!}\cdots\frac{x_r^{n_r}}{n_r!}\\
&= \frac{1}{B(\lambda,\nu_1-\lambda)}\sum_{n_1,\ldots,n_r=0}^{\infty}\frac{(\kappa)_{n_1+\ldots+n_r}(\mu)_{n_1+\ldots+n_r}}{(\lambda)_{n_1}(\nu_2)_{n_2}\ldots(\nu_r)_{n_r}}
\end{aligned}$$

$$\times \int_0^1 \Delta^{\lambda+n_1-1}(1-\Delta)^{\nu_1-\lambda-1}\ {}_p^{\alpha}M_q^{\beta}\left(\frac{-\rho}{\Delta(1-\Delta)}\right)\frac{x_1^{n_1}}{n_1!}\cdots\frac{x_r^{n_r}}{n_r!}d\Delta$$

$$= \frac{1}{B(\lambda,\nu_1-\lambda)}\int_0^1 \Delta^{\lambda-1}(1-\Delta)^{\nu_1-\lambda-1}\ {}_p^{\alpha}M_q^{\beta}\left(\frac{-\rho}{\Delta(1-\Delta)}\right)$$

$$\times \sum_{n_1,\ldots,n_r=0}^{\infty}\frac{(\kappa)_{n_1+\ldots+n_r}(\mu)_{n_1+\ldots+n_r}}{(\lambda)_{n_1}(\nu_2)_{n_2}\ldots(\nu_r)_{n_r}}\frac{(\Delta x_1)^{n_1}}{n_1!}\frac{x_2^{n_2}}{n_2!}\cdots\frac{x_r^{n_r}}{n_r!}d\Delta.$$

Considering Eq. (12), we get

$$ {}^{M}F_{C,p,q}^{(\alpha,\beta;r)}(\kappa,\mu;\nu_1,\ldots,\nu_r;x_1,\ldots,x_r;\rho;\lambda)$$

$$= \frac{1}{B(\lambda,\nu_1-\lambda)}\int_0^1 \Delta^{\lambda-1}(1-\Delta)^{\nu_1-\lambda-1}\ {}_p^{\alpha}M_q^{\beta}\left(\frac{-\rho}{\Delta(1-\Delta)}\right)$$

$$\times F_C^{(r)}(\kappa,\mu;\lambda,\nu_2,\ldots,\nu_r;\Delta x_1,x_2,\ldots,x_r)d\Delta. \qquad \square$$

Theorem 12. *Let* $\Re(\alpha)>0$, $\Re(\rho)>0$, $\Re(\nu_1)>\Re(\lambda)>0$. *Then,*

$$ {}^{M}F_{C,p,q}^{(\alpha,\beta;r)}(\kappa,\mu;\nu_1,\ldots,\nu_r;x_1,\ldots,x_r;\rho;\lambda)$$

$$= \frac{2}{B(\lambda,\nu_1-\lambda)}\int_0^{\frac{\pi}{2}} (\sin\phi)^{2\lambda-1}(\cos\phi)^{2\nu_1-2\lambda-1}\ {}_p^{\alpha}M_q^{\beta}\left(-\rho(\sec\phi)^2(\csc\phi)^2\right)$$

$$\times F_C^{(r)}(\kappa,\mu;\lambda,\nu_2,\ldots,\nu_r;x_1(\sin\phi)^2,x_2,\ldots,x_r)d\phi.$$

Proof. Using the integral representation (2) of M-beta function in the definition of M-Lauricella hypergeometric function $F_C^{(r)}$ and making similar calculations in the proof of Theorem 11, proof is complete. $\square$

Theorem 13. *Let* $\Re(\alpha)>0$, $\Re(\rho)>0$, $\Re(\nu_1)>\Re(\lambda)>0$. *Then,*

$$ {}^{M}F_{C,p,q}^{(\alpha,\beta;r)}(\kappa,\mu;\nu_1,\ldots,\nu_r;x_1,\ldots,x_r;\rho;\lambda)$$

$$= \frac{1}{B(\lambda,\nu_1-\lambda)}\int_0^{\infty} \frac{u^{\lambda-1}}{(1+u)^{\nu_1}}\ {}_p^{\alpha}M_q^{\beta}\left(-2\rho-\rho\left(u+\frac{1}{u}\right)\right)$$

$$\times F_C^{(r)}\left(\kappa,\mu;\lambda,\nu_2,\ldots,\nu_r;\frac{x_1u}{1+u},x_2,\ldots,x_r\right)du.$$

Proof. Using the integral representation (3) of M-beta function in the definition of M-Lauricella hypergeometric function $F_C^{(r)}$ and making similar calculations in the proof of Theorem 11, proof is complete. $\square$

Theorem 14. *Let* $\Re(\alpha)>0$, $\Re(\rho)>0$, $\Re(\nu_1)>\Re(\lambda)>0$. *Then,*

$$ {}^{M}F_{C,p,q}^{(\alpha,\beta;r)}(\kappa,\mu;\nu_1,\ldots,\nu_r;x_1,\ldots,x_r;\rho;\lambda)$$

$$= \frac{(b-a)^{1-\nu_1}}{B(\lambda,\nu_1-\lambda)}\int_a^b (u-a)^{\lambda-1}(b-u)^{\nu_1-\lambda-1}\ {}_p^{\alpha}M_q^{\beta}\left(\frac{-\rho(b-a)^2}{(u-a)(b-u)}\right)$$

$$\times F_C^{(r)}\left(\kappa,\mu;\lambda,\nu_2,\ldots,\nu_r;\frac{x_1(u-a)}{b-a},x_2,\ldots,x_r\right)du.$$

Proof. Using the integral representation (4) of M-beta function in the definition of M-Lauricella hypergeometric function $F_C^{(r)}$ and making similar calculations in the proof of Theorem 11, proof is complete. □

6. Integral Representations for M-Lauricella Hypergeometric Function $F_D^{(r)}$

Theorem 15. *Let $\Re(\alpha)>0$, $\Re(\rho)>0$, $\Re(\nu)>\Re(\kappa)>0$. Then,*

$$\begin{aligned}&{}^{M}F_{D,p,q}^{(\alpha,\beta;r)}(\kappa,\mu_1,\ldots,\mu_r;\nu;x_1,\ldots,x_r;\rho)\\&\quad=\frac{1}{B(\kappa,\nu-\kappa)}\int_0^1\Delta^{\kappa-1}(1-\Delta)^{\nu-\kappa-1}\;{}_p^{\alpha}M_q^{\beta}\left(\frac{-\rho}{\Delta(1-\Delta)}\right)\\&\quad\times F_D^{(r)}(\kappa,\mu_1,\ldots,\mu_r;\kappa;\Delta x_1,\ldots,\Delta x_r)d\Delta.\end{aligned}$$

Proof. Using the integral representation (1) of M-beta function in the definition of M-Lauricella hypergeometric function $F_D^{(r)}$, we have

$$\begin{aligned}&{}^{M}F_{D,p,q}^{(\alpha,\beta;r)}(\kappa,\mu_1,\ldots,\mu_r;\nu;x_1,\ldots,x_r;\rho)\\&=\sum_{n_1,\ldots,n_r=0}^{\infty}(\mu_1)_{n_1}\ldots(\mu_r)_{n_r}\frac{{}^{M}B_{p,q}^{(\alpha,\beta)}(\kappa+n_1+\ldots+n_r,\nu-\kappa;\rho)}{B(\kappa,\nu-\kappa)}\frac{x_1^{n_1}}{n_1!}\ldots\frac{x_r^{n_r}}{n_r!}\\&=\frac{1}{B(\kappa,\nu-\kappa)}\sum_{n_1,\ldots,n_r=0}^{\infty}(\mu_1)_{n_1}\ldots(\mu_r)_{n_r}\\&\quad\times\int_0^1\Delta^{\kappa+n_1+\ldots+n_r-1}(1-\Delta)^{\nu-\kappa-1}\;{}_p^{\alpha}M_q^{\beta}\left(\frac{-\rho}{\Delta(1-\Delta)}\right)\frac{x_1^{n_1}}{n_1!}\ldots\frac{x_r^{n_r}}{n_r!}d\Delta\\&=\frac{1}{B(\kappa,\nu-\kappa)}\int_0^1\Delta^{\kappa-1}(1-\Delta)^{\nu-\kappa-1}\;{}_p^{\alpha}M_q^{\beta}\left(\frac{-\rho}{\Delta(1-\Delta)}\right)\\&\quad\times\sum_{n_1,\ldots,n_r=0}^{\infty}(\mu_1)_{n_1}\ldots(\mu_r)_{n_r}\frac{(\Delta x_1)^{n_1}}{n_1!}\ldots\frac{(\Delta x_r)^{n_r}}{n_r!}d\Delta.\end{aligned}$$

Multiplied by $\frac{(\kappa)_{n_1+\ldots+n_r}}{(\kappa)_{n_1+\ldots+n_r}}$ and considering Eq. (13), we get

$$\begin{aligned}&{}^{M}F_{D,p,q}^{(\alpha,\beta;r)}(\kappa,\mu_1,\ldots,\mu_r;\nu;x_1,\ldots,x_r;\rho)\\&\quad=\frac{1}{B(\kappa,\nu-\kappa)}\int_0^1\Delta^{\kappa-1}(1-\Delta)^{\nu-\kappa-1}\;{}_p^{\alpha}M_q^{\beta}\left(\frac{-\rho}{\Delta(1-\Delta)}\right)\\&\quad\times\sum_{n_1,\ldots,n_r=0}^{\infty}\frac{(\kappa)_{n_1+\ldots+n_r}(\mu_1)_{n_1}\ldots(\mu_r)_{n_r}}{(\kappa)_{n_1+\ldots+n_r}}\frac{(\Delta x_1)^{n_1}}{n_1!}\ldots\frac{(\Delta x_r)^{n_r}}{n_r!}d\Delta\end{aligned}$$

$$= \frac{1}{B(\kappa,\nu-\kappa)} \int_0^1 \Delta^{\kappa-1}(1-\Delta)^{\nu-\kappa-1}\ {}_p^{\alpha}M_q^{\beta}\left(\frac{-\rho}{\Delta(1-\Delta)}\right) \times F_D^{(r)}(\kappa,\mu_1,\ldots,\mu_r;\kappa;\Delta x_1,\ldots,\Delta x_r)d\Delta. \qquad \square$$

Theorem 16. *Let* $\Re(\alpha) > 0$, $\Re(\rho) > 0$, $\Re(\nu) > \Re(\kappa) > 0$. *Then,*

$$ {}^{M}F_{D,p,q}^{(\alpha,\beta;r)}(\kappa,\mu_1,\ldots,\mu_r;\nu;x_1,\ldots,x_r;\rho) = \frac{1}{B(\kappa,\nu-\kappa)} \int_0^1 \Delta^{\kappa-1}(1-\Delta)^{\nu-\kappa-1}\ {}_p^{\alpha}M_q^{\beta}\left(\frac{-\rho}{\Delta(1-\Delta)}\right) \times (1-\Delta x_1)^{-\mu_1}\ldots(1-\Delta x_r)^{-\mu_r}d\Delta.$$

Proof. Using the integral representation (1) of M-beta function in the definition of M-Lauricella hypergeometric function $F_D^{(r)}$, we have

$$ {}^{M}F_{D,p,q}^{(\alpha,\beta;r)}(\kappa,\mu_1,\ldots,\mu_r;\nu;x_1,\ldots,x_r;\rho) = \sum_{n_1,\ldots,n_r=0}^{\infty} (\mu_1)_{n_1}\ldots(\mu_r)_{n_r} \frac{{}^{M}B_{p,q}^{(\alpha,\beta)}(\kappa+n_1+\ldots+n_r,\nu-\kappa;\rho)}{B(\kappa,\nu-\kappa)} \frac{x_1^{n_1}}{n_1!}\cdots\frac{x_r^{n_r}}{n_r!}$$

$$= \frac{1}{B(\kappa,\nu-\kappa)} \int_0^1 \Delta^{\kappa-1}(1-\Delta)^{\nu-\kappa-1}\ {}_p^{\alpha}M_q^{\beta}\left(\frac{-\rho}{\Delta(1-\Delta)}\right) \times \sum_{n_1=0}^{\infty}(\mu_1)_{n_1}\frac{(\Delta x_1)^{n_1}}{n_1!}\cdots\sum_{n_r=0}^{\infty}(\mu_r)_{n_r}\frac{(\Delta x_r)^{n_r}}{n_r!}d\Delta.$$

Considering Eq. (8), we get

$$ {}^{M}F_{D,p,q}^{(\alpha,\beta;r)}(\kappa,\mu_1,\ldots,\mu_r;\nu;x_1,\ldots,x_r;\rho) = \frac{1}{B(\kappa,\nu-\kappa)} \int_0^1 \Delta^{\kappa-1}(1-\Delta)^{\nu-\kappa-1}\ {}_p^{\alpha}M_q^{\beta}\left(\frac{-\rho}{\Delta(1-\Delta)}\right) \times (1-\Delta x_1)^{-\mu_1}\ldots\ (1-\Delta x_r)^{-\mu_r}d\Delta. \qquad \square$$

Theorem 17. *Let* $\Re(\alpha) > 0$, $\Re(\rho) > 0$, $\Re(\nu) > \Re(\kappa) > 0$. *Then,*

$$ {}^{M}F_{D,p,q}^{(\alpha,\beta;r)}(\kappa,\mu_1,\ldots,\mu_r;\nu;x_1,\ldots,x_r;\rho) = \frac{2}{B(\kappa,\nu-\kappa)} \int_0^{\frac{\pi}{2}} (\sin\phi)^{2\kappa-1}(\cos\phi)^{2\nu-2\kappa-1}\ {}_p^{\alpha}M_q^{\beta}\left(-\rho(\sec\phi)^2(\csc\phi)^2\right) \times F_D^{(r)}\left(\kappa,\mu_1,\ldots,\mu_r;\kappa;x_1(\sin\phi)^2,\ldots,x_r(\sin\phi)^2\right)d\phi.$$

Proof. Using the integral representation (2) of M-beta function in the definition of M-Lauricella hypergeometric function $F_D^{(r)}$ and making similar calculations in the proof of Theorem 15, proof is complete. $\square$

Theorem 18. *Let $\Re(\alpha) > 0$, $\Re(\rho) > 0$, $\Re(\nu) > \Re(\kappa) > 0$. Then,*

$$\begin{aligned}&{}^{M}F_{D,p,q}^{(\alpha,\beta;r)}(\kappa,\mu_1,\dots,\mu_r;\nu;x_1,\dots,x_r;\rho)\\ &\qquad= \frac{1}{B(\kappa,\nu-\kappa)}\int_0^\infty \frac{u^{\kappa-1}}{(1+u)^\nu}\ {}_p^{\alpha}M_q^{\beta}\left(-2\rho-\rho\left(u+\frac{1}{u}\right)\right)\\ &\qquad\quad\times F_D^{(r)}\left(\kappa,\mu_1,\dots,\mu_r;\kappa;\frac{x_1u}{1+u},\dots,\frac{x_ru}{1+u}\right)du.\end{aligned}$$

Proof. Using the integral representation (3) of M-beta function in the definition of M-Lauricella hypergeometric function $F_D^{(r)}$ and making similar calculations in the proof of Theorem 15, proof is complete. □

Theorem 19. *Let $\Re(\alpha) > 0$, $\Re(\rho) > 0$, $\Re(\nu) > \Re(\kappa) > 0$. Then,*

$$\begin{aligned}&{}^{M}F_{D,p,q}^{(\alpha,\beta;r)}(\kappa,\mu_1,\dots,\mu_r;\nu;x_1,\dots,x_r;\rho)\\ &\qquad= \frac{(b-a)^{1-\nu}}{B(\kappa,\nu-\kappa)}\int_a^b (u-a)^{\kappa-1}(b-u)^{\nu-\kappa-1}\ {}_p^{\alpha}M_q^{\beta}\left(\frac{-\rho(b-a)^2}{(u-a)(b-u)}\right)\\ &\qquad\quad\times F_D^{(r)}\left(\kappa,\mu_1,\dots,\mu_r;\kappa;\frac{x_1(u-a)}{b-a},\dots,\frac{x_r(u-a)}{b-a}\right)du.\end{aligned}$$

Proof. Using the integral representation (4) of M-beta function in the definition of M-Lauricella hypergeometric function $F_D^{(r)}$ and making similar calculations in the proof of Theorem 15, proof is complete. □

7. Applications of M-Lauricella Hypergeometric Functions

In this section, we obtain the solution of fractional differential equations involving the M-Lauricella hypergeometric functions.

Example 1. *Let $1 < \Re(\epsilon) \le 2$, $\Re(\alpha) > 0$, $\Re(\lambda) > \Re(\mu_1) > 0$. We consider the fractional differential equation*

$${}^{c}D_{\rho}^{\epsilon}\{f(\rho)\} = {}^{M}F_{B,p,q}^{(\alpha,\beta;r)}(\xi_1,\dots,\xi_p;\eta_1,\dots,\eta_q;\kappa_1,\dots,\kappa_r,\mu_1,\dots,\mu_r;\nu;x_1,\dots,x_r;\epsilon\rho;\lambda),$$

with the initial conditions

$$f(0) = f'(0) = 0.$$

Applying the Laplace transform to the fractional differential equation and using Eq. (9), we have

$$\begin{aligned}&\mathfrak{L}\left\{{}^{c}D_{\rho}^{\epsilon}\{f(\rho)\};s\right\}\\ &\quad= \mathfrak{L}\left\{{}^{M}F_{B,p,q}^{(\alpha,\beta;r)}(\xi_1,\dots,\xi_p;\eta_1,\dots,\eta_q;\kappa_1,\dots,\kappa_r,\mu_1,\dots,\mu_r;\nu;x_1,\dots,x_r;\epsilon\rho;\lambda);s\right\},\end{aligned}$$

then

$$s^{\epsilon}F(s) - s^{\epsilon-1}f(0) - s^{\epsilon-2}f'(0)$$
$$= \frac{{}^{M}F_{B,p+1,q}^{(\alpha,\beta;r)}\left(\xi_1,\ldots,\xi_p,1;\eta_1,\ldots,\eta_q;\kappa_1,\ldots,\kappa_r,\mu_1,\ldots,\mu_r;\nu;x_1,\ldots,x_r;\frac{\epsilon}{s};\lambda\right)}{s}.$$

Using the initial conditions, we get

$$F(s) = \frac{{}^{M}F_{B,p+1,q}^{(\alpha,\beta;r)}\left(\xi_1,\ldots,\xi_p,1;\eta_1,\ldots,\eta_q;\kappa_1,\ldots,\kappa_r,\mu_1,\ldots,\mu_r;\nu;x_1,\ldots,x_r;\frac{\epsilon}{s};\lambda\right)}{s^{\epsilon+1}}.$$

Applying the inverse Laplace transform, we obtain

$$f(\rho) = \frac{{}^{M}F_{B,p+1,q+1}^{(\alpha,\beta;r)}(\xi_1,\ldots,\xi_p,1;\eta_1,\ldots,\eta_q,1+\epsilon;\kappa_1,\ldots,\kappa_r,\mu_1,\ldots,\mu_r;\nu;x_1,\ldots,x_r;\epsilon\rho;\lambda)}{\Gamma(1+\epsilon)\rho^{-\epsilon}}.$$

Example 2. *Let $1 < \Re(\epsilon) \leq 2$, $\Re(\alpha) > 0$, $\Re(\nu_1) > \Re(\lambda) > 0$. We consider the fractional differential equation*

$${}^{c}D_{\rho}^{\epsilon}\{f(\rho)\} = {}^{M}F_{C,p,q}^{(\alpha,\beta;r)}(\xi_1,\ldots,\xi_p;\eta_1,\ldots,\eta_q;\kappa,\mu;\nu_1,\ldots,\nu_r;x_1,\ldots,x_r;\epsilon\rho;\lambda),$$

with the initial conditions

$$f(0) = f'(0) = 0.$$

Applying the Laplace transform to the fractional differential equation and using Eq. (9), we have

$$\mathfrak{L}\left\{{}^{c}D_{\rho}^{\epsilon}\{f(\rho)\};s\right\}$$
$$= \mathfrak{L}\left\{{}^{M}F_{C,p,q}^{(\alpha,\beta;r)}(\xi_1,\ldots,\xi_p;\eta_1,\ldots,\eta_q;\kappa,\mu;\nu_1,\ldots,\nu_r;x_1,\ldots,x_r;\epsilon\rho;\lambda);s\right\},$$

then

$$s^{\epsilon}F(s) - s^{\epsilon-1}f(0) - s^{\epsilon-2}f'(0)$$
$$= \frac{{}^{M}F_{C,p+1,q}^{(\alpha,\beta;r)}\left(\xi_1,\ldots,\xi_p,1;\eta_1,\ldots,\eta_q;\kappa,\mu;\nu_1,\ldots,\nu_r;x_1,\ldots,x_r;\frac{\epsilon}{s};\lambda\right)}{s}.$$

Using the initial conditions, we get

$$F(s) = \frac{{}^{M}F_{C,p+1,q}^{(\alpha,\beta;r)}\left(\xi_1,\ldots,\xi_p,1;\eta_1,\ldots,\eta_q;\kappa,\mu;\nu_1,\ldots,\nu_r;x_1,\ldots,x_r;\frac{\epsilon}{s};\lambda\right)}{s^{\epsilon+1}}.$$

Applying the inverse Laplace transform, we obtain

$$f(\rho) = \frac{{}^{M}F_{C,p+1,q+1}^{(\alpha,\beta;r)}(\xi_1,\ldots,\xi_p,1;\eta_1,\ldots,\eta_q,1+\epsilon;\kappa,\mu;\nu_1,\ldots,\nu_r;x_1,\ldots,x_r;\epsilon\rho;\lambda)}{\Gamma(1+\epsilon)\rho^{-\epsilon}}.$$

Example 3. *Let $1 < \Re(\epsilon) \leq 2$, $\Re(\alpha) > 0$, $\Re(\nu) > \Re(\kappa) > 0$. We consider the fractional differential equation*

$${}^{c}D_{\rho}^{\epsilon}\{f(\rho)\} = {}^{M}F_{D,p,q}^{(\alpha,\beta;r)}(\xi_1,\ldots,\xi_p;\eta_1,\ldots,\eta_q;\kappa,\mu_1,\ldots,\mu_r;\nu;x_1,\ldots,x_r;\epsilon\rho),$$

with the initial conditions

$$f(0) = f'(0) = 0.$$

Applying the Laplace transform to the fractional differential equation and using Eq. (9), we have

$$\begin{aligned}&\mathfrak{L}\left\{{}^{c}D_{\rho}^{\epsilon}\left\{f(\rho)\right\};s\right\}\\&\quad=\mathfrak{L}\left\{{}^{M}F_{D,p,q}^{(\alpha,\beta;r)}(\xi_1,\dots,\xi_p;\eta_1,\dots,\eta_q;\kappa,\mu_1,\dots,\mu_r;\nu;x_1,\dots,x_r;\epsilon\rho);s\right\},\end{aligned}$$

then

$$\begin{aligned}&s^{\epsilon}F(s)-s^{\epsilon-1}f(0)-s^{\epsilon-2}f'(0)\\&\qquad=\frac{{}^{M}F_{D,p+1,q}^{(\alpha,\beta;r)}\left(\xi_1,\dots,\xi_p,1;\eta_1,\dots,\eta_q;\kappa,\mu_1,\dots,\mu_r;\nu;x_1,\dots,x_r;\frac{\epsilon}{s}\right)}{s}.\end{aligned}$$

Using the initial conditions, we get

$$F(s)=\frac{{}^{M}F_{D,p+1,q}^{(\alpha,\beta;r)}\left(\xi_1,\dots,\xi_p,1;\eta_1,\dots,\eta_q;\kappa,\mu_1,\dots,\mu_r;\nu;x_1,\dots,x_r;\frac{\epsilon}{s}\right)}{s^{\epsilon+1}}.$$

Applying the inverse Laplace transform, we obtain

$$f(\rho)=\frac{{}^{M}F_{D,p+1,q+1}^{(\alpha,\beta;r)}(\xi_1,\dots,\xi_p,1;\eta_1,\dots,\eta_q,1+\epsilon;\kappa,\mu_1,\dots,\mu_r;\nu;x_1,\dots,x_r;\epsilon\rho)}{\Gamma(1+\epsilon)\rho^{-\epsilon}}.$$

8. Conclusion

In this paper, we introduced the M-Lauricella hypergeometric functions using the modified beta function involving the generalized M-series in its kernel. Then we presented various integral representations of M-Lauricella hypergeometric functions. As examples, we obtained the solution of fractional differential equations involving the M-Lauricella hypergeometric functions.

M-Lauricella hypergeometric functions can be used not only in various fractional differential equations, but also in various ordinary and partial differential equations. Therefore, we conclude this paper by believing that M-Lauricella hypergeometric functions can be used in various research areas of interest to many fields of science such as mathematics, statistics, physics, chemistry, biology, medicine, engineering, astronomy and space sciences and will contribute to the scientific world.

Author Contribution Statements The author read and approved the final copy of this paper.

Declaration of Competing Interests The author declares that there is no competing interest regarding the publication of this paper.

Acknowledgements This work was partly presented in the 4th International Conference on Pure and Applied Mathematics (ICPAM-2022) which organized by Van

Yüzüncü Yıl University on June 22-23, 2022 in Van-Turkey. The author is thankful to the referees for making valuable suggestions leading to the better presentations of this paper.

References

[1] Abubakar, U. M., A study of extended beta and associated functions connected to Fox-Wright function, *J. Frac. Calc. Appl.*, 12(3)(13) (2021), 1-23.

[2] Agarwal, R. P., Luo, M. J., Agarwal, P., On the extended Appell-Lauricella hypergeometric functions and their applications, *Filomat*, 31(12) (2017), 3693-3713. https://doi.org/10.2298/FIL1712693A

[3] Agarwal, P., Agarwal, R. P., Ruzhansky, M., Special Functions and Analysis of Differential Equations, Chapman and Hall/CRC, New York, 2020.

[4] Andrews, G. E., Askey, R., Roy, R., Special Functions, Cambridge Univ. Press, Cambridge, 1999. https://doi.org/10.1017/CBO9781107325937

[5] Ata, E., Kıymaz, İ. O., Generalized gamma, beta and hypergeometric functions defined by Wright function and applications to fractional differential equations, *Cumhuriyet Sci. J.*, 43(4) (2022), 684-695. https://doi.org/10.17776/csj.1005486

[6] Ata, E., Kıymaz, İ. O., A study on certain properties of generalized special functions defined by Fox-Wright function, *Appl. Math. Nonlinear Sci.*, 5(1) (2020), 147-162. https://doi.org/10.2478/amns.2020.1.00014

[7] Ata, E., Generalized beta function defined by Wright function, arXiv preprint https://arxiv.org/abs/1803.03121v3 [math.CA], (2021). https://doi.org/10.48550/arXiv.1803.03121

[8] Ata, E., Modified special functions defined by generalized M-series and their properties, arXiv preprint https://arxiv.org/abs/2201.00867v1 [math.CA], (2022). https://doi.org/10.48550/arXiv.2201.00867

[9] Chaudhry, M. A., Zubair, S. M., Generalized incomplete gamma functions with applications, *J. Comput. Appl. Math.*, 55 (1994), 99-124. https://doi.org/10.1016/0377-0427(94)90187-2

[10] Chaudhry, M. A., Qadir, A., Rafique, M., Zubair, S. M., Extension of Euler's beta function, *J. Comput. Appl. Math.*, 78 (1997), 19-32. https://doi.org/10.1016/S0377-0427(96)00102-1

[11] Chaudhry, M. A., Qadir, A., Srivastava, H. M., Paris, R. B., Extended hypergeometric and confluent hypergeometric functions, *Appl. Math. Comput.*, 159 (2004), 589-602. https://doi.org/10.1016/j.amc.2003.09.017

[12] Choi, J., Rathie, A. K., Parmar, R. K., Extension of extended beta, hypergeometric and confluent hypergeometric functions, *Honam Math. J.*, 36 (2014), 357-385. https://doi.org/10.5831/HMJ.2014.36.2.357

[13] Çetinkaya, A., Kıymaz, İ. O., Agarwal, P., Agarwal, R., A comparative study on generating function relations for generalized hypergeometric functions via generalized fractional operators, *Adv. Differ. Equ.*, 2018(1) (2018), 1-11. https://doi.org/10.1186/s13662-018-1612-0

[14] Debnath, L., Bhatta, D., Integral Transforms and Their Applications, CRC Press, 2014. https://doi.org/10.1201/b17670

[15] Goswami, A., Jain, S., Agarwal, P., Aracı, S., A note on the new extended beta and Gauss hypergeometric functions, *Appl. Math. Infor. Sci.*, 12 (2018), 139-144. https://doi.org/10.18576/amis/120113

[16] Hasanov, A., Srivastava, H. M., Some decomposition formulas associated with the Lauricella function $F_A^{(r)}$ and other multiple hypergeometric functions, *Appl. Math. Lett.*, 19(2) (2006), 113-121. https://doi.org/10.1016/j.aml.2005.03.009

[17] Jain, S., Agarwal, P., Kıymaz, İ. O., Fractional integral and beta transform formulas for the extended Appell-Lauricella hypergeometric functions, *Tamap J. Math, Stat.*, 2018 (2018), 1-5.

[18] Kilbas, A. A., Srivastava, H. M., Trujillo, J. J., Theory and Applications of Fractional Differential, North-Holland Mathematics Studies 204, 2006.

[19] Kulip, M. A. H., Mohsen, F. F., Barahmah, S. S., Further extended gamma and beta functions in term of generalized Wright function, *Elec. J. Uni. of Aden for Basic and Appl. Sci.*, 1(2) (2020), 78-83.

[20] Lee, D. M., Rathie, A. K., Parmar, R. K., Kim, Y. S., Generalization of extended beta function, hypergeometric and confluent hypergeometric functions, *Honam Math. J.*, 33 (2011), 187-206. https://doi.org/10.5831/HMJ.2011.33.2.187

[21] Mubeen, S., Rahman, G., Nisar, K. S., Choi, J., An extended beta function and its properties, *J. Math. Sci.*, 102 (2017), 1545-1557. https://doi.org/10.17654/MS102071545

[22] Özergin, E., Özarslan, M. A., Altın, A., Extension of gamma, beta and hypergeometric functions, *J. Comput. Appl. Math.*, 235 (2011), 4601-4610. https://doi.org/10.1016/j.cam.2010.04.019

[23] Padmanabham, P. A., Srivastava, H. M., Summation formulas associated with the Lauricella function $F_A^{(r)}$, *Appl. Math. Lett.*, 13(1) (2000), 65-70. https://doi.org/10.1016/S0893-9659(99)00146-9

[24] Parmar, R. K., A new generalization of gamma, beta, hypergeometric and confluent hypergeometric functions, *Le Matematiche*, 68 (2013), 33-52. https://doi.org/10.4418/2013.68.2.3

[25] Podlubny, I., Fractional Differential Equations: An Introduction to Fractional Derivatives, Fractional Differential Equations, to Methods of Their Solution and Some of Their Applications, Elsevier, 1998.

[26] Rahman, G., Mubeen, S., Nisar, K. S., A new generalization of extended beta and hypergeometric functions, *J. Frac. Calc. Appl.*, 11(2) (2020), 32-44.

[27] Shadab, M., Saime, J., Choi, J., An extended beta function and its applications, *J. Math. Sci.*, 103 (2018), 235-251. https://doi.org/10.17654/MS103010235

[28] Sharma, M., Jain, R., A note on a generalized M-series as a special function of fractional calculus, *Frac. Calc. Appl. Anal.*, 12(4) (2009), 449-452.

[29] Srivastava, H. M., Agarwal, P., Jain, S., Generating functions for the generalized Gauss hypergeometric functions, *Appl. Math. Comput.*, 247 (2014), 348-352. https://doi.org/10.1016/j.amc.2014.08.105

[30] Srivastava, H. M., Karlsson, P. W., Multiple Gaussian Hypergeometric Series, Ellis Horwood Series: Mathematics and its Applications, Ellis Horwood Ltd., Chichester, Halsted Press [John Wiley and Sons, Inc.], New York, 1985.

[31] Srivastava, H. M., Manocha, H. L., A Treatise On Generating Functions, Halsted Press Wiley, New York, 1984.

[32] Şahin R., An extension of some Lauricella hypergeometric functions, *AIP Conf. Proc.*, 1558(1) (2013), 1140-1143. https://doi.org/10.1063/1.4825709

[33] Şahin, R., Yağcı, O., Yağbasan, M. B., Kıymaz, İ. O., Çetinkaya, A., Further generalizations of gamma, beta and related functions, *J. Ineq. Spec. Func.*, 9(4) (2018), 1-7.

http://communications.science.ankara.edu.tr

Commun.Fac.Sci.Univ.Ank.Ser. A1 Math. Stat.
Volume 72, Number 2, Pages 530–550 (2023)
DOI:10.31801/cfsuasmas.1087827
ISSN 1303-5991 E-ISSN 2618-6470

COMMUNICATIONS SERIES A1

Research Article; Received: March 14, 2022; Accepted: November 22, 2022

FHD FLOW IN AN IRREGULAR CAVITY SUBJECTED TO A NON-UNIFORM MAGNETIC FIELD

Pelin ŞENEL
Department of Mathematics, Karadeniz Technical University, Trabzon, TÜRKİYE

Abstract. In this paper FHD flow in a rectangular pipe constricted by two analogous semi-cylinders attached to the left and the bottom walls is investigated. The laminar, axial flow is produced by a constant pressure gradient, and the flow is affected by a spatially varying non-uniform magnetic field caused by two electric wires. The current-carrying wires are placed along the axes of the semi-cylinders. The fully developed flow is studied on the 2D cross-section of the pipe, a cavity, where the wires act as point magnetic sources. The pressure equation is added to the mathematical model, and the velocity-pressure form governing equations are numerically solved by the dual reciprocity boundary element method (DRBEM). The Dirichlet type pressure boundary conditions are approximated through a process using the radial basis functions and a finite difference. The flow, velocity, and pressure variations are investigated for different magnetic field strengths and current ratios. The grid independence study is also carried out. The proposed iterative scheme is capable of generating numerical results by performing a non-uniform discretization for the boundary. Dense discretizations are applied at the places where the flow shows a sudden fluctuation. It is shown by the numerical results that the flow and the pressure variations are dominated by the strong magnetic source. With an increment in the magnetic number, the planar flow is accelerated, the axial flow is decelerated, and the pressure increases, especially around the strong point magnetic source.

1. Introduction

The interaction of electromagnetic fields and the fluid mechanics may be grouped into three main categories, namely electrohydrodynamics (EHD), magnetohydrodynamics (MHD), and ferrohydrodynamics (FHD) [27]. Electrohydrodynamics theory investigates the flow of electrically charged particles under the influence of electric

2020 *Mathematics Subject Classification.* 65N38, 76D05, 76W05.
Keywords. FHD flow, variable magnetic field, DRBEM, pressure computation.
psenel@ktu.edu.tr; 0000-0002-2096-7521
.

fields. In EHD, the electrostatic force term plays a crucial role in the momentum equations. EHD phenomena is used in designs of many engineering instruments such as pumps, printing systems, flow meters, etc. The motion of electrically conducting fluids in the presence of magnetic fields is the subject of magnetohydrodynamics. In MHD, the body force acting on the fluid is called Lorentz force. Lorentz force retards the core flow and accelerates the side flows, thus equalizes the total flow in pipes. Ferrohydrodynamics is an interdisciplinary subject having an inherent interest of a physical and mathematical nature with applications in printing [7], medicine [44], tribiology [14], separation science [47], cooling systems [32], microelectromechanical systems (MEMS) [48], etc. FHD investigates the motion of electrically insulated (non-conducting) fluid under the effect of magnetic polarization [27]. In FHD, there needs no presence of electric current flow in the fluid, but the flow undergoes a fluctuation due to the material magnetization. A ferrofluid is mainly composed of a carrier fluid (e.g. water) and nanoscale magnetic particles (e.g iron, nickel) coated by a surfactant. Biomagnetic fluid dynamics is also based on the FHD phenomena. Blood is the mostly known biomagnetic fluid which possesses its magnetization property by the hemoglobin molecule.

The spatially varying non-uniform magnetic field generated by the current-carrying wires applies a volumetric force to the fluid and has been used to control the flow in pipes. The volumetric force, so-called the Kelvin force density, drives the magnetic particles, and the translational and rotational motion of these particles are transferred to the ferrofluid. The resulting body forces alter the flow in pipes. Therefore in applications where the flow regulation is substantial the ferrofluid is a preferential choice [6].

Much computational research has been carried out on the FHD flows in pipes due to their vast variety of applications. The FHD flows in pipes are modeled in terms of the continuity and the Navier-Stokes equations. If there is heat transfer, then the energy equation is added to the system. The governing equations are coupled with highly nonlinear partial differential equations (PDEs) containing diffusion, convection, and force terms. Therefore, approximate solutions are required to understand the flow and the pressure behaviors. The pressure-linked pseudo transient method (PLEM), finite difference method (FDM), finite volume method (FVM), and finite element method (FEM) are mostly used numerical approaches to tackle the FHD flows.

The PLEM was used to investigate the effect of a single current-carrying wire placed below the rectangular pipe in [42]. It was reported that the solutions show an oscillatory behavior on a common-grid. A mathematical model on the same flow configuration for the electrically conducting fluid was presented in [41]. In that paper, both uniform and non-uniform magnetic field effects on the biomagnetic fluid flow were studied. It was concluded that the form of the magnetic field gradient substantially determines the flow in the pipe. Mousavi et al. [23] used a commercial software based on the finite volume methodology to investigate the biomagnetic flow in a three-dimensional pipe under the influence of a magnetic field due to a single current-carrying wire. They obtained grid-independent results by using a discretization covering the magnetic field accurately. The influence of an alternating magnetic field that is generated by line source dipoles on a forced convective ferrofluid flow was investigated by Goharkhah and Ashjaee [10] using a control volume technique. They reported the flow acceleration along the surface as the ferrofluid passes over the magnetic field section. Recently, A finite volume approach for a nanofluid flow through an annular pipe subjected to multiple magnetic sources was presented by Soltanipour [40]. A control volume-based FEM solution of a free convection ferrofluid flow in an enclosure subjected to multiple current-carrying wires was presented in [37]. Loukopoulos and Tzirtzilakis [19] presented a FDM solution of a biomagnetic fluid flow between two horizontal plates subjected to a single current-carrying wire. Some other computational studies on magnetizable fluids can be found in [1,3,15,22,25,28,29,33–36,38,39].

The boundary elements method (BEM) [4] is an alternative to domain discretization type methods such as FDM and FEM. In BEM, fundamental solutions are required to transform the partial differential equations into boundary integral equations. After the insertion of the boundary conditions, a shuffling process is applied to collect all the unknowns on one side of the equation. The resultant dense nonsymmetric linear equation is then treated by using an appropriate direct or iterative solver. The boundary-only discretization advantage of the BEM reduces computational time and memory usage. When the partial differential equation is nonlinear, containing body forces or time dependence, the corresponding BEM integral equation includes domain integrals. DRBEM has arisen to tackle this difficulty. In DRBEM [24], a simpler equation's fundamental solution is employed and the remaining terms are treated through a series expansion using radial basis functions, and then the reciprocity procedures are applied. The DRBEM has been applied to many types of physical problems from elasticity to fluid dynamics. Some recent advances in the DRBEM applications may be found in [2,11,16,21,31,45,46].

The previous studies demonstrated that no consideration has been given to pressure computations for FHD irregular cavity flows. Most of the present studies used domain-type numerical methods which are computationally expensive. The novelty of the present study is that low computational cost solutions for the velocity and the pressure of FHD flow in an irregular domain are presented. Therefore, the flow of a ferrofluid through a pipe subjected to a non-uniform magnetic field that is generated by two variable electric wires is investigated. The effects of the magnetic field strength and the current ratio variations are discussed. The pressure profiles are presented for the first time in the literature. The current-carrying wires are placed parallel to one of the horizontal and the vertical walls. The geometry of the pipe is formed in such a way that the current-carrying wires do not touch the electrically insulated walls. The fully developed flow is modeled on the two dimensional

cross-section of the pipe that is taken vertical to the axial flow. The governing equations in primitive variables (velocity-pressure form) are discretized by the DRBEM, and an iterative numerical solution procedure is suggested. It is observed that a non-uniform discretization is required to capture the flow behaviors. The flow and pressure variations are dominated by the electric wire possessing high current intensity. The proposed numerical scheme is capable of generating grid-independent solutions for the velocity and the pressure with less computational cost. This is the first DRBEM study on the FHD flow in a pipe contracted by two semi-cylinders carrying variable electric currents along their axes. The proposed numerical scheme provides the pressure variation which is very important in engineering design. This study is an extension of a presentation that is published as an abstract [30] at the International Conference on Applied Mathematics in Engineering (ICAME'21).
The rest of the paper is organized in the following fashion. In Section 2, the physics of the problem is introduced, and the construction of the mathematical model is presented. The numerical solution procedure and the pressure boundary condition approximations are explained in Section 3. In Section 4, the numerical solutions and discussions are presented. The consequences achieved from the present study are collected in Section 5.

2. Physical Problem and Mathematical Model

A laminar, steady, fully developed flow of an electrically insulated, magnetizable fluid is considered in a long rectangular pipe. Two semi-cylinders with radiuses $\bar{r}$ are located in the middle of the left and the bottom walls. Two electric wires (W_1 and W_2) are passing through the axes of the semi-cylinders. The pipe walls are electrically insulated. The 3D flow configuration is presented in Figure 1.

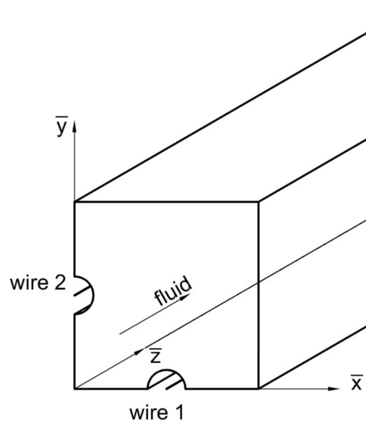

Figure 1. Fully developed flow in a pipe

The flow is driven by a constant pressure gradient in the $\bar{z}-$direction, and it is under the influence of a non-uniform magnetic field that is generated by the two wires carrying electric currents with different intensities (I_1 and I_2). The fully developed flow is modeled on the 2D cross-section of the pipe. On this cross-section (cavity), wires behave alike as point magnetic sources. Each section of the cavity boundary is smooth. Figure 2 displays the 2D problem geometry.

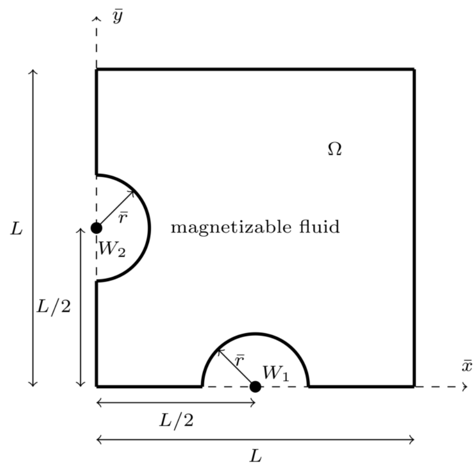

FIGURE 2. Problem geometry

The FHD flow in a cavity is defined by the continuity and Navier-Stokes equations containing the dimensional velocity $\bar{\mathbf{V}}(\bar{x},\bar{y}) = (\bar{u}(\bar{x},\bar{y}),\bar{v}(\bar{x},\bar{y}),\bar{w}(\bar{x},\bar{y}))$ and the pressure $\bar{P}(\bar{x},\bar{y},\bar{z})$ [27]. Once the flow reaches a fully developed state, the velocity and the pressure of the fluid do not vary in the pipe axis direction.

$$\frac{\partial \bar{u}}{\partial \bar{x}} + \frac{\partial \bar{v}}{\partial \bar{y}} = 0, \tag{1}$$

$$\bar{u}\frac{\partial \bar{u}}{\partial \bar{x}} + \bar{v}\frac{\partial \bar{u}}{\partial \bar{y}} = -\frac{1}{\rho}\frac{\partial \bar{P}}{\partial \bar{x}} + \nu\left(\frac{\partial^2 \bar{u}}{\partial \bar{x}^2} + \frac{\partial^2 \bar{u}}{\partial \bar{y}^2}\right) + \frac{\mu_0 \bar{M}}{\rho}\frac{\partial \bar{H}}{\partial \bar{x}}, \tag{2}$$

$$\bar{u}\frac{\partial \bar{v}}{\partial \bar{x}} + \bar{v}\frac{\partial \bar{v}}{\partial \bar{y}} = -\frac{1}{\rho}\frac{\partial \bar{P}}{\partial \bar{y}} + \nu\left(\frac{\partial^2 \bar{v}}{\partial \bar{x}^2} + \frac{\partial^2 \bar{v}}{\partial \bar{y}^2}\right) + \frac{\mu_0 \bar{M}}{\rho}\frac{\partial \bar{H}}{\partial \bar{y}}, \tag{3}$$

$$\bar{u}\frac{\partial \bar{w}}{\partial \bar{x}} + \bar{v}\frac{\partial \bar{w}}{\partial \bar{y}} = -\frac{1}{\rho}\frac{\partial \bar{P}}{\partial \bar{z}} + \nu\left(\frac{\partial^2 \bar{w}}{\partial \bar{x}^2} + \frac{\partial^2 \bar{w}}{\partial \bar{y}^2}\right), \tag{4}$$

where ρ and ν are the density and the kinematic viscosity of the fluid, μ_0 is the magnetic permeability of vacuum, and $\bar{H}$ is the magnetic field intensity. $\bar{M} = \chi\bar{H}$ is the magnetization where χ is the magnetic susceptibility of the fluid. Since the fluid is electrically insulated the force terms on the right-hand side of the momentum

equations are containing only the magnetization force in FHD. This mathematical model does not have an analytical solution.
In fully developed flows pressure $\bar{P}$ can be written as [9]

$$\bar{P}(\bar{x}, \bar{y}, \bar{z}) = \bar{P}_1(\bar{z}) + \bar{p}(\bar{x}, \bar{y}). \tag{5}$$

Since the axial flow is generated by a constant pressure gradient, one has

$$\frac{\partial \bar{P}}{\partial \bar{z}} = \frac{\partial \bar{P}_1}{\partial \bar{z}} = \bar{P}_z = \text{constant} . \tag{6}$$

The components of the magnetic field $\bar{\mathbf{H}} = (\bar{H}_x(\bar{x}, \bar{y}), \bar{H}_y(\bar{x}, \bar{y}), 0)$ generated by infinitely long, thin wires carrying steady electric currents I_1 and I_2 flowing in the same direction are given by [17, 26]

$$\bar{H}_x = -\frac{1}{2\pi} \sum_{i=1}^{2} \frac{I_i(\bar{y} - \bar{b}_i)}{(\bar{x} - \bar{a}_i)^2 + (\bar{y} - \bar{b}_i)^2}, \qquad \bar{H}_y = \frac{1}{2\pi} \sum_{i=1}^{2} \frac{I_i(\bar{x} - \bar{a}_i)}{(\bar{x} - \bar{a}_i)^2 + (\bar{y} - \bar{b}_i)^2}, \tag{7}$$

where $(\bar{a}_i, \bar{b}_i)$, $i = 1, 2$, are the locations of the point magnetic sources around the cavity. The point magnetic sources have different strengths. The intensity of the magnetic field generated by the two point magnetic sources is defined by

$$\bar{H} = \sqrt{\bar{H}_x^2 + \bar{H}_y^2} . \tag{8}$$

For the numerical simulations following non-dimensional variables are introduced

$$x = \frac{\bar{x}}{L}, \quad y = \frac{\bar{y}}{L}, \quad z = \frac{\bar{z}}{L}, \quad u = \frac{\bar{u}L}{\nu}, \quad v = \frac{\bar{v}L}{\nu}, \quad w = \frac{\bar{w}L}{\nu}, \quad P = \frac{\bar{P}L^2}{\rho\nu^2}, \quad H = \frac{\bar{H}}{H_0}. \tag{9}$$

Here, L is the height of the cavity, and $H_0 = I_1/(2\pi L)$.
The governing equations in the dimensionless form are

$$\frac{\partial u}{\partial x} + \frac{\partial v}{\partial y} = 0, \tag{10}$$

$$\frac{\partial^2 u}{\partial x^2} + \frac{\partial^2 u}{\partial y^2} = \frac{\partial p}{\partial x} + u\frac{\partial u}{\partial x} + v\frac{\partial u}{\partial y} - MnH\frac{\partial H}{\partial x}, \tag{11}$$

$$\frac{\partial^2 v}{\partial x^2} + \frac{\partial^2 v}{\partial y^2} = \frac{\partial p}{\partial y} + u\frac{\partial v}{\partial x} + v\frac{\partial v}{\partial y} - MnH\frac{\partial H}{\partial y}, \tag{12}$$

$$\frac{\partial^2 w}{\partial x^2} + \frac{\partial^2 w}{\partial y^2} = P_z + u\frac{\partial w}{\partial x} + v\frac{\partial w}{\partial y}, \tag{13}$$

where Mn is the magnetic number defined by

$$Mn = \frac{\mu_0 \chi H_0^2 L^2}{\nu^2 \rho} . \tag{14}$$

To investigate the pressure variation within the cavity, the equation of pressure is obtained. Eqs (11) and (12) are differentiated with respect to x and y, respectively. The resultant equations are added and some terms are canceled using the continuity equation. Then, the pressure equation is obtaied

$$\frac{\partial^2 p}{\partial x^2}+\frac{\partial^2 p}{\partial y^2}=Mn(\left(\frac{\partial H}{\partial x}\right)^2+\left(\frac{\partial H}{\partial y}\right)^2+H(\frac{\partial^2 H}{\partial x^2}+\frac{\partial^2 H}{\partial y^2}))-\left(\frac{\partial u}{\partial x}\right)^2-\left(\frac{\partial v}{\partial y}\right)^2-2\frac{\partial v}{\partial x}\frac{\partial u}{\partial y}\,. \tag{15}$$

The flow patterns in 2D cavities are visualized by the stream function Ψ isolines (streamlines). The stream function satisfies the continuity equation and is linked with the planar velocities in $x-$ and $y-$directions as

$$u=\frac{\partial \Psi}{\partial y}, \quad v=-\frac{\partial \Psi}{\partial x}. \tag{16}$$

From the continuity equation, the stream function equation is generated

$$\frac{\partial^2 \Psi}{\partial x^2}+\frac{\partial^2 \Psi}{\partial y^2}=\frac{\partial u}{\partial y}-\frac{\partial v}{\partial x}\,. \tag{17}$$

Non-dimensional forms of the magnetic field components are

$$H_x=-\frac{y-b_1}{(x-a_1)^2+(y-b_1)^2}-I_r\frac{y-b_2}{(x-a_2)^2+(y-b_2)^2}, \tag{18}$$

$$H_y=\frac{x-a_1}{(x-a_1)^2+(y-b_1)^2}+I_r\frac{x-a_2}{(x-a_2)^2+(y-b_2)^2}, \tag{19}$$

where $I_r=I_2/I_1$ is the current ratio, (a_1,b_1), (a_2,b_2) are the positions of magnetic sources and

$$H=\sqrt{H_x^2+H_y^2}. \tag{20}$$

No-slip boundary condition is applied on the cavity walls, thus

$$u=v=w=\Psi=0 \qquad \text{on} \quad \partial\Omega. \tag{21}$$

Here, $\partial\Omega$ stands for the boundary of the cavity Ω. Dirichlet-type pressure boundary conditions are obtained approximately by using a finite difference scheme and the radial basis functions. The details for the pressure boundary condition computations are given in the next section.

3. Application of the DRBEM

The governing partial differential equations (11)-(13), (15), and (17) are transformed into boundary integral equations by the DRBEM. The governing equations are rewritten in the Poisson type as

$$\nabla^2 R=b_R, \tag{22}$$

where R denotes u, v, w, p, or Ψ. b_R is the right-hand side of the equation for R containing convection and force terms. For the sake of practice, the construction of the DRBEM discretized system has been presented on this sample equation.

Eq. (22) is weighted by the fundamental solution of the Laplace equation ($u^* = (1/2\pi)\ln(1/r)$, [24]) and then the Green's first identity is applied to achieve

$$c_i R_i + \int_\Gamma R q^* d\Gamma - \int_\Gamma u^* \frac{\partial R}{\partial n} d\Gamma = -\int_\Omega b_R u^* d\Omega, \qquad (23)$$

with $\Gamma = \partial\Omega$ and $q^* = \partial u^*/\partial n$ notations. $c_i = \theta/2\pi$ where θ radian is the internal angle at the source point i. $c_i = 1/2$ on the smooth part of the boundary and $c_i = 1$ for the interior nodes.

b_R is approximated by using linear radial basis functions $f_j(r_i) = 1 + r_{ij}$, ($r_{ij} = \sqrt{(x_i - x_j)^2 + (y_i - y_j)^2}$) to eliminate the domain integral on the right-hand side of Eq. (23). The corresponding particular solutions $\hat{u}_j$ satisfy $\nabla^2 \hat{u}_j = f_j$. Then, by using the collocation technique one gets an approximation for b_R as

$$b_R \approx \sum_{j=1}^{N+L} (\alpha_R)_j f_j = \sum_{j=1}^{N+L} (\alpha_R)_j \nabla^2 \hat{u}_j, \qquad (24)$$

where $(\alpha_R)_j$'s are the unspecified coefficients. Here, N is the number of boundary nodes and L is the number of interior nodes.

Substituting the approximation in 24 into the integral equation 23 one has Laplace term on the right-hand side of the equation (23). Green's first identity is applied again and the irregular boundary is discretized by the constant elements. Then, the corresponding boundary integral equation is obtained

$$c_i R_i + \sum_{k=1}^{N} \int_{\Gamma_k} R q^* d\Gamma - \sum_{k=1}^{N} \int_{\Gamma_k} u^* \frac{\partial R}{\partial n} d\Gamma = \sum_{j=1}^{N+L} (\alpha_R)_j \Big(c_i \hat{u}_{ij} + \sum_{k=1}^{N} \int_{\Gamma_k} \hat{u}_j q^* d\Gamma - \sum_{k=1}^{N} \int_{\Gamma_k} u^* \frac{\partial \hat{u}_j}{\partial n} d\Gamma\Big) . \qquad (25)$$

Considering all of the nodes, Eq. (24) gives

$$\mathbf{b_R} = \mathbf{F} \boldsymbol{\alpha}_\mathbf{R}. \qquad (26)$$

Here, $\mathbf{b_R}$ and $\boldsymbol{\alpha}_\mathbf{R}$ are $(N+L) \times 1$ vectors. $(N+L) \times (N+L)$ sized DRBEM coordinate matrix $\mathbf{F}$ is constructed from the radial basis functions as $\mathbf{F}_{ij} = f_{ij}$. According to Micchelli's Theorem [20], $\mathbf{F}$ is invertible.

Thus, the vector of unspecified coefficients $\boldsymbol{\alpha}_\mathbf{R}$ is calculated from Eq. (26) as

$$\boldsymbol{\alpha}_\mathbf{R} = \mathbf{F}^{-1} \mathbf{b_R}. \qquad (27)$$

Considering all the discretization nodes and using equations (25) and (27) the system of matrix-vector equations are obtained

$$\mathbf{H}u - \mathbf{G}\frac{\partial u}{\partial n} = (\mathbf{H}\hat{\mathbf{U}} - \mathbf{G}\hat{\mathbf{Q}})\mathbf{F}^{-1}\Big(\frac{\partial p}{\partial x} + u\frac{\partial u}{\partial x} + v\frac{\partial u}{\partial y} - MnH\frac{\partial H}{\partial x}\Big), \qquad (28)$$

$$\mathbf{H}v - \mathbf{G}\frac{\partial v}{\partial n} = (\mathbf{H}\hat{\mathbf{U}} - \mathbf{G}\hat{\mathbf{Q}})\mathbf{F}^{-1}\Big(\frac{\partial p}{\partial y} + u\frac{\partial v}{\partial x} + v\frac{\partial v}{\partial y} - MnH\frac{\partial H}{\partial y}\Big), \qquad (29)$$

$$\mathbf{H}w-\mathbf{G}\frac{\partial w}{\partial n}=(\mathbf{H}\hat{\mathbf{U}}-\mathbf{G}\hat{\mathbf{Q}})\mathbf{F}^{-1}(P_z+u\frac{\partial w}{\partial x}+v\frac{\partial w}{\partial y}), \tag{30}$$

$$\begin{aligned}\mathbf{H}p-\mathbf{G}\frac{\partial p}{\partial n}=&(\mathbf{H}\hat{\mathbf{U}}-\mathbf{G}\hat{\mathbf{Q}})\mathbf{F}^{-1}(Mn(\left(\frac{\partial H}{\partial x}\right)^2+\left(\frac{\partial H}{\partial y}\right)^2+H\nabla^2 H)-\left(\frac{\partial u}{\partial x}\right)^2\\&-\left(\frac{\partial v}{\partial y}\right)^2-2\frac{\partial v}{\partial x}\frac{\partial u}{\partial y}),\end{aligned} \tag{31}$$

$$\mathbf{H}\Psi-\mathbf{G}\frac{\partial \Psi}{\partial n}=(\mathbf{H}\hat{\mathbf{U}}-\mathbf{G}\hat{\mathbf{Q}})\mathbf{F}^{-1}(\frac{\partial u}{\partial y}-\frac{\partial v}{\partial x}), \tag{32}$$

The entries of $(N+L)\times(N+L)$ sized DRBEM matrices are

$$\begin{aligned}&\mathbf{H}_{ij}=c_i\delta_{ij}+\int_{\Gamma_j}q^*d\Gamma_j,\\&\mathbf{G}_{ij}=\int_{\Gamma_j}u^*d\Gamma_j,\qquad \mathbf{G}_{ii}=\frac{l}{2\pi}(ln(\frac{2}{l})+1).\end{aligned} \tag{33}$$

Here, δ_{ij} is the Kronecker delta and l is the length of the constant element. The diagonal entries of $\mathbf{G}$ are computed analytically due to the singularities of the integrals. $\hat{\mathbf{U}}_{ij}=\hat{u}_{ij}$ and $\hat{\mathbf{Q}}_{ij}=\hat{q}_{ij}$, $\hat{q}_{ij}=\partial\hat{u}_{ij}/\partial n$.

Using the advantage of DRBEM, all the space derivatives of the unknowns in Eqs. (28)-(32) are treated by using the approximation

$$\hat{\mathbf{R}}=\mathbf{F}\xi, \tag{34}$$

where $\hat{\mathbf{R}}$ represent u, v, w, or p and ξ denotes an unspecified coefficient vector. Then one has

$$\frac{\partial\hat{\mathbf{R}}}{\partial\eta}=\frac{\partial\mathbf{F}}{\partial\eta}\mathbf{F}^{-1}\hat{\mathbf{R}}, \tag{35}$$

with η being x or y.

Once all the DRBEM constructions are completed Dirichlet type boundary conditions are inserted, and all the problem unknowns are carried to the left-hand side. This process is called shuffling. Then, one obtains a full linear system $\mathbf{Ax}=\tilde{\mathbf{b}}$. The $(N+L)\times(N+L)$ sized coefficient matrix $\mathbf{A}$ is dense having no special form. Thus, the resultant linear system is numerically solved by the LU decomposition method with less computational cost.

An iterative solution process is applied. Initially, planar velocity components are taken as zero everywhere. As can be observed from Eqs. (11) and (12) in this case, magnetization forces are balanced by the pressure gradients [27]. The iteration process is started with $\partial p/\partial x = MnH(\partial H/\partial x)+10^{-12}$ and $\partial p/\partial y = MnH(\partial H/\partial y)+10^{-12}$ initial values for the pressure gradients. Firstly, planar velocity equations (Eq. (28) and (29)) are solved. To treat the nonlinear terms, unknown velocities are taken from the previous iteration level and their space derivatives are taken from the new level. Boundary conditions for the pressure are computed repeatedly in each iteration level by using newly obtained planar velocity nodal solutions. Then, the pressure equation (Eq. (31)) is solved. Lastly, the axial velocity and the stream function equations (Eqs. (30) and (32), respectively) are solved with given boundary conditions. At each level, previously computed problem unknowns are used in the subsequent equations. Pressure is relaxed as a weighted summation of the nodal values taken from the previous and new iteration levels, $p^{(n+1)} = rp^{(n+1)} + (1-r)p^{(n)}$ where $0 < r < 1$. The stopping criterion for the iterative process is

$$\frac{||z^{(n+1)} - z^{(n)}||_\infty}{||z^{(n)}||_\infty} < 10^{-3}, \tag{36}$$

where z represents u, v, p, or Ψ and n is the number of iteration.

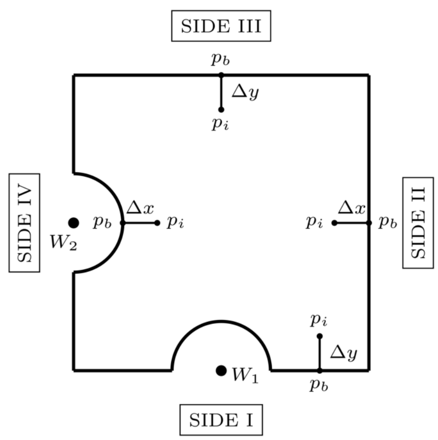

FIGURE 3. Pressure boundary condition approximation

Pressure boundary conditions are obtained by using Eqs. (11) and (12). Pressure gradients are approximated by a forward or backward difference and the terms containing the space derivatives of the planar velocities are approximated by the DRBEM coordinate matrix $\mathbf{F}$. Formulations of approximate boundary conditions for the pressure are found for each side of the cavity (Figure 3) as

$$\text{SIDE I:} \quad p_b^{(n+1)} = p_i^{(n)} - \Delta y(\mathbf{S}v^{(n+1)} + MnH\frac{\partial H}{\partial y}), \tag{37}$$

$$\text{SIDE II:} \quad p_b^{(n+1)} = p_i^{(n)} + \Delta x(\mathbf{S}u^{(n+1)} + MnH\frac{\partial H}{\partial x}), \tag{38}$$

$$\text{SIDE III:} \quad p_b^{(n+1)} = p_i^{(n)} + \Delta y(\mathbf{S}v^{(n+1)} + MnH\frac{\partial H}{\partial y}), \tag{39}$$

$$\text{SIDE IV:} \quad p_b^{(n+1)} = p_i^{(n)} - \Delta x(\mathbf{S}u^{(n+1)} + MnH\frac{\partial H}{\partial x}), \tag{40}$$

where p_i is the closest interior node to the corresponding boundary node p_b and

$$\mathbf{S} = \frac{\partial \mathbf{F}}{\partial x}F^{-1}\frac{\partial \mathbf{F}}{\partial x}F^{-1} + \frac{\partial \mathbf{F}}{\partial y}F^{-1}\frac{\partial \mathbf{F}}{\partial y}F^{-1} - \mathbf{u}^{(n+1)}\frac{\partial \mathbf{F}}{\partial x}F^{-1} - \mathbf{v}^{(n+1)}\frac{\partial \mathbf{F}}{\partial y}F^{-1}, \tag{41}$$

with $\mathbf{u}^{(n+1)}$ and $\mathbf{v}^{(n+1)}$ being the diagonal matrices constructed from $u-$ and $v-$velocity nodal solutions at the $(n+1)$st iteration, respectively.

$P_z = -8000$ is taken as in [42] and $(a_1, b_1) = (0.5, 0)$, $(a_2, b_2) = (0, 0.5)$ are the placement of point magnetic sources around the cavity. The radiuses of the semi-cylinders are $r = \bar{r}/L = 0.1$.

4. Numerical results and discussions

The influences of magnetization force and current ratio variations on the FHD cavity flow are investigated for various combinations of Mn and I_r. Numerical results are illustrated in terms of velocity, pressure, and stream function contour plots. The computer code is validated with the existing literature, a grid independence study is carried out, and an appropriate non-uniform discretization is suggested.

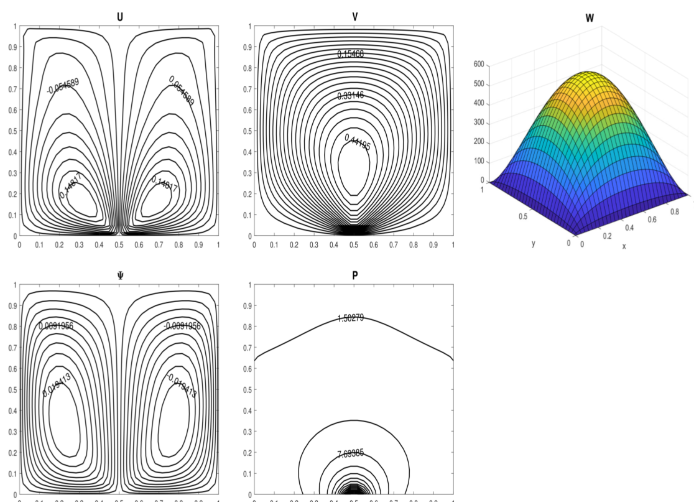

Figure 4. Square cavity flow subjected to unique point source $Mn = 90$.

The validation of the numerical procedure and the written computer code is carried out for an FHD square cavity flow subjected to a unique point source that is placed at $(0.5, -0.05)$. Figure 4 displays the flow and pressure behaviors when

$Mn = 90$. A good agreement is observed in the flow behaviors between the present study and the existing literature [42].

The magnetization force pushes the fluid towards the top wall therefore the flow on the transverse plane is separated into two symmetric vortices rotating in opposite directions. The movement of the fluid particles in front of the point magnetic source causes highly concentrated pressure at the bottom of the cavity. The $u-$velocity is divided into two vortices and the $v-$velocity is expanded through the channel section forming a boundary layer in front of the magnetic source. For small Mn values, axial velocity shows a parabolic profile.

The grid independence test is carried for $N = 192, 240, 288, 336, 384$. The numerical solutions for the pressure and the planar velocities are compared along the $x = 0.25$ line for $Mn = 10$, $I_r = 1$. Figure 5 shows that $N = 336$ gives grid-independent solutions.

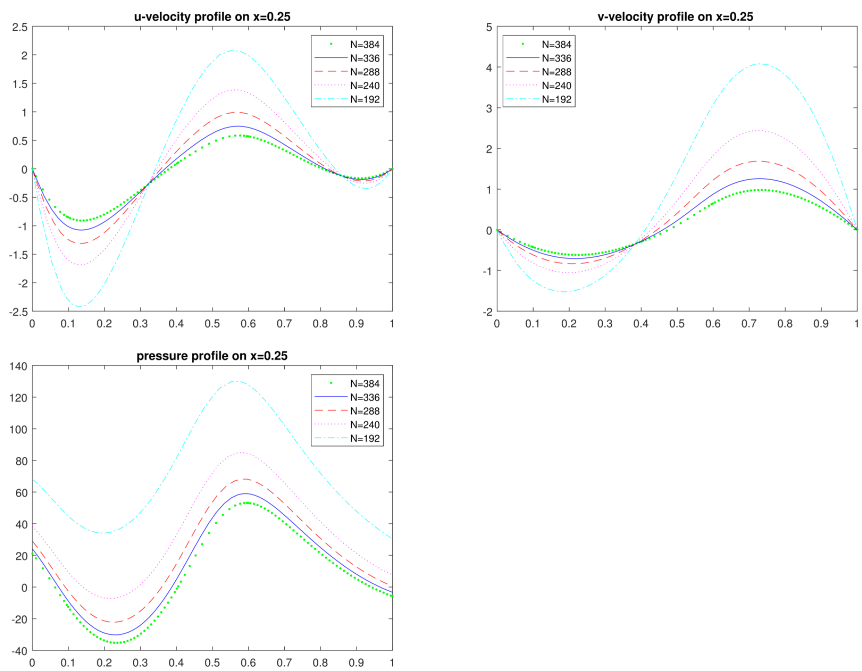

FIGURE 5. Grid independence test along the $x = 0.25$ line for $Mn = 10$, $I_r = 1$.

Table 1 displays the number of iterations needed to achieve solutions with a tolerance of 10^{-3} for $Mn = 10$, $I_r = 1$. It is observed that the number of iterations increases almost linearly as the number of boundary nodes advances. Effects of magnetic sources on the pressure and velocity behaviors are investigated for various

N=192	N=240	$N = 288$	$N = 336$	$N = 384$
573	670	812	957	1106

TABLE 1. Number of iterations for different N when $Mn = 10$, $I_r = 1$.

combinations of current ratios I_r and moderate values of magnetic numbers Mn. The boundary of the 2D computational domain is non-uniformly discretized by constant elements. In constant element discretization, the approximate solution is constant on each element and the points where the unknown values are considered (nodes) are in the middle of the element. This property enables one to deal with the corners of the irregular cavity. Each element is taken from the smooth part of the boundary section. Figure 6 shows samples for the discretization of the boundaries and the choices of the interior nodes. More interior nodes are taken at the places where the flow is expected to show a sudden fluctuation according to the strengths of the point magnetic sources and the cavity corners. In the case of the same current intensities (e.g. (a) $I_r = 1$) the discretizations are dense near the corners of the cavity. When one of the point magnetic sources is stronger than the other (e.g. (b) $I_r = 0.2$) more interior nodes are taken in front of the semi-circles.

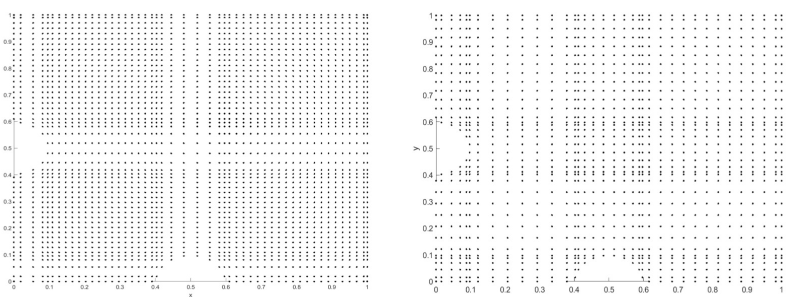

(a) (b)

FIGURE 6. Sample discretizations of the boundary and the choice of the interior nodes. (a) $I_r = 1$, (b) $I_r = 0.2$. $Mn = 10$.

The number of boundary elements is increased with Mn. At most $N = 400$ boundary and $L = 9888$ interior nodes are used for the discretization. The numerical solutions are achieved using a 64GB RAM computer.

Figure 7 shows velocity, pressure, and the stream function contour plots when both magnetic sources have the same strength ($I_r = 1$). The magnetic sources push the fluid through the opposite walls and apply the same magnetization force. This causes the division of the flow on the transverse plane into vortices that are

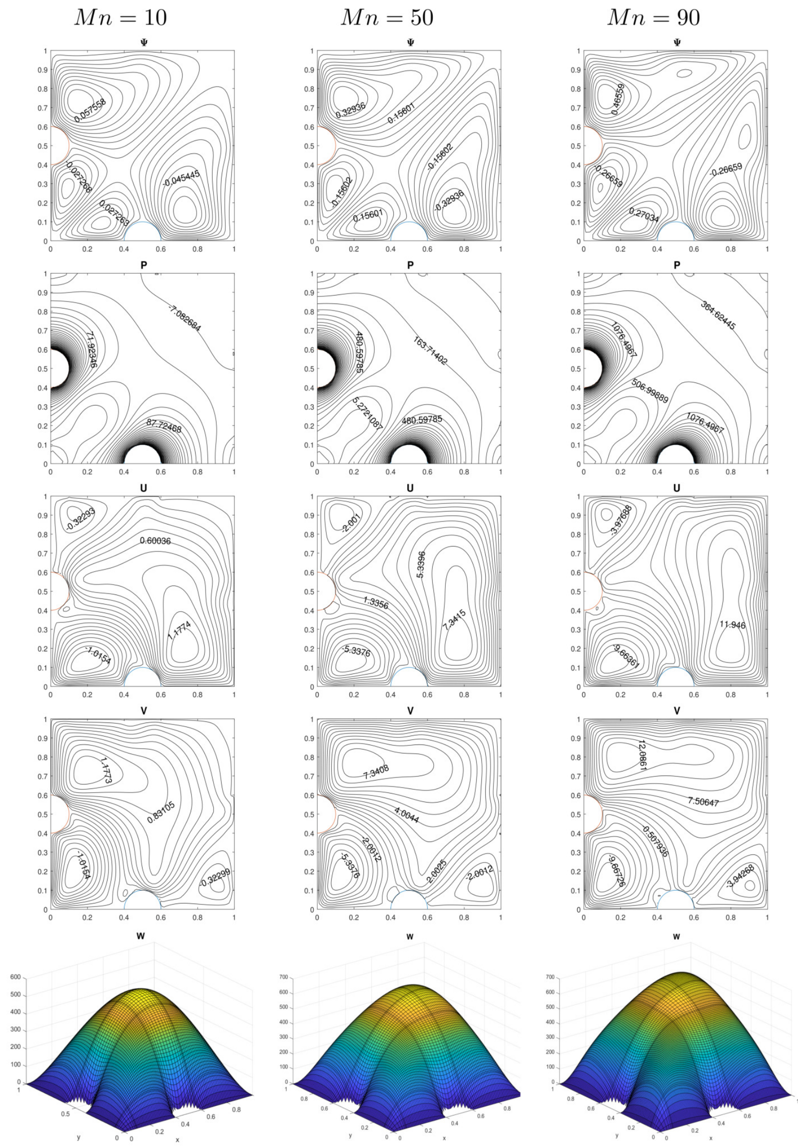

FIGURE 7. Velocity and pressure profiles for $I_r = 1$, $Mn = 10, 50, 90$.

symmetric about the $y = x$ axis, and the boundary layers are formed. Four symmetric vortices that are rotating in opposite directions are generated. Magnetic

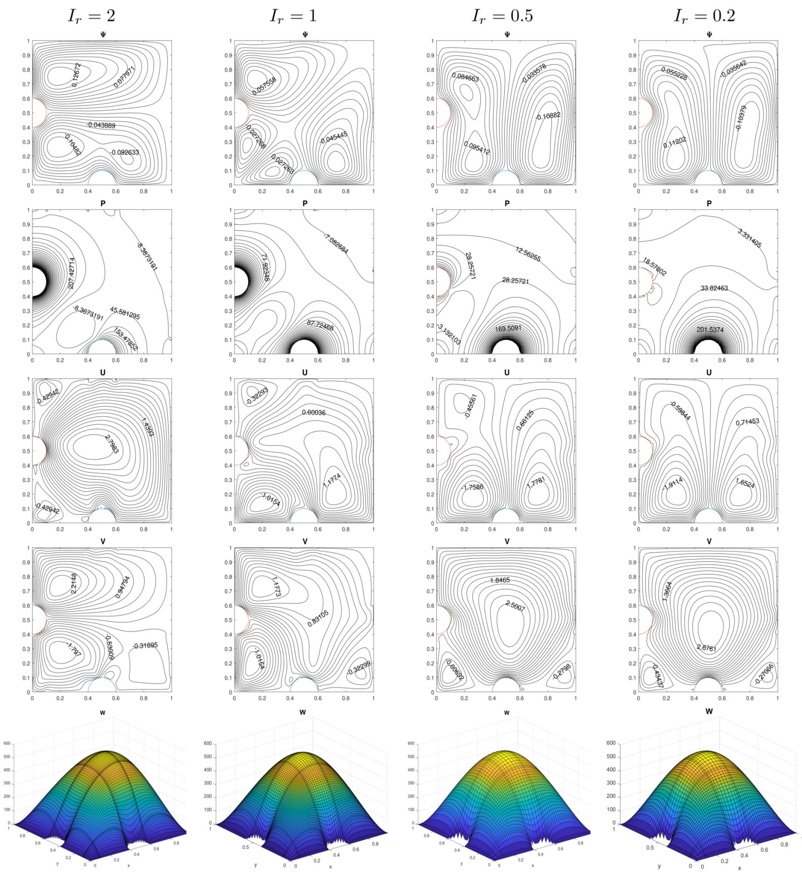

FIGURE 8. Velocity and pressure profiles for $Mn = 10$, $I_r = 0.2, 0.5, 1, 2$.

sources suppress the effects of each other, and therefore two small vortices appear at the left bottom corner of the cavity. Pressure is high around the semi-circles due to the large velocity gradients in these areas. Axial flow shows a parabolic profile obeying the shape of the cavity. $u-$ and $v-$velocity behaviors are similar due to the symmetric location of the point sources. When the ratio of the currents is kept fixed and the magnetic number increases, the magnetic field strengths of both wires increase at the same rate. Thus, an increment in Mn accelerates the planar flow (u and v velocity advance) and retards the axial flow around the semi-circles. The pressure in the cavity increases. Strong vortices are developed on the transverse plane as Mn advances. This is a well-known effect of the increment in the magnetic

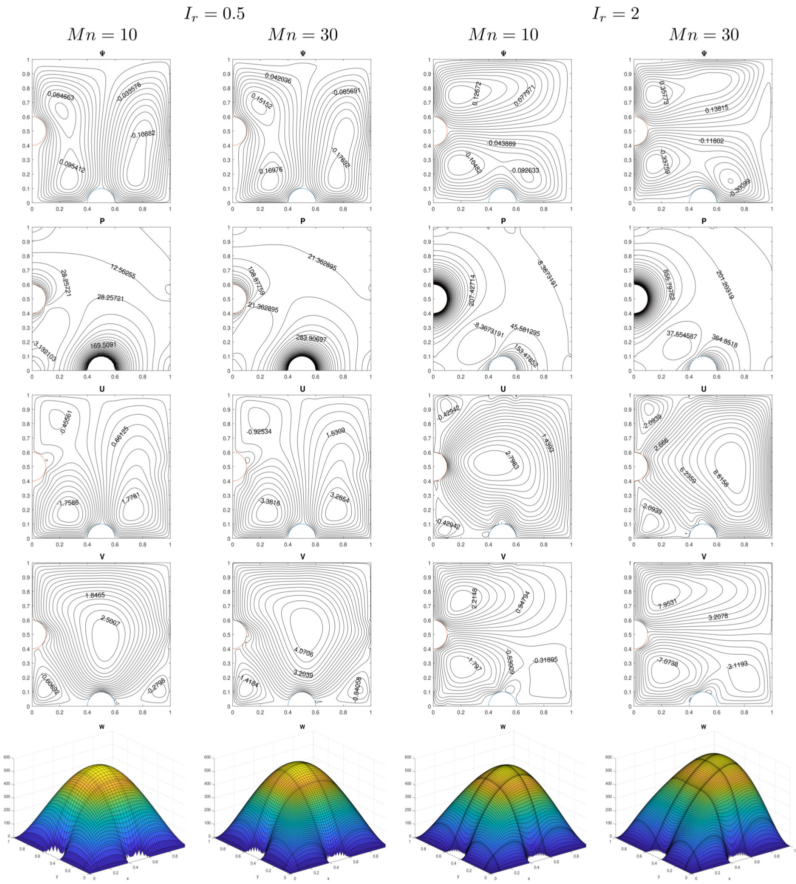

FIGURE 9. Velocity and pressure profiles for $I_r = 0.5, 2$ and $Mn = 10, 30$.

field strength.

The effect of the magnetic field generated by two wires with different current intensities is investigated for a fixed Mn. This corresponds to the case when I_1 is kept constant and I_2 changes. Figure 8 shows the flow and the pressure profiles for $I_r = I_2/I_1 = 2, 1, 0.5, 0.2$. Generally, the flow and pressure behaviors are dominated by the strong point magnetic source. When one of the point magnetic sources is two times stronger than the other one ($I_r = 0.5, 2$) two vortices develop in front of the dominant source that is analogous to the unique point source case. The weak source force the fluid to divide the vortex in front of it. Pressure concentration is high near the strong source. The flow retardation in the axial direction is mainly observed in front of the dominant point magnetic source. Planar velocity profiles are generally dominated by the strong source, except for a little deformation caused by the weak source. When the current intensity of the point source below the cavity increases (comparing $I_r = 0.5$ and $I_r = 0.2$ cases) the magnetization force applied by the strong source is increased and the flow is dominated mainly by the strong bottom point magnetic source. The flow in the cavity nearly behaves as if there was a single-point magnetic source. Pressure around the week source decreases.

In Figure 9, the effect of the magnetic number increase is investigated when one of the sources is two times stronger than the other ($I_r = 0.5$ and $I_r = 2$ cases). An increase in Mn advances the force applied to the fluid in the cavity and accelerates the planar flow. At the same time, axial velocity decreases due to the kinetic energy transfer in the axial direction into the transverse plane. The pressure in the cavity increases, and the axial flow retardation is significant, especially near the dominant magnetic source.

5. Conclusion

In this study, FHD flow in a rectangular duct constricted by two semi-cylinders under the influence of a non-uniform magnetic field is investigated. The flow is modeled in the velocity-pressure formulation and the numerical results are obtained using the DRBEM. The Dirichlet type pressure boundary conditions are computed by using a first-order finite difference scheme and the radial basis functions. The system of nonlinear PDEs is solved iteratively, and the nonlinear terms are treated by using the DRBEM coordinate matrix. The grid independence test is carried out, and it is found that $N = 336$ gives grid independent solutions for $Mn = 10$ and $I_r = 1$ case. The number of boundary nodes needs to be increased according to the magnetic number due to the alternations in the flow and pressure profiles. The influences of the magnetic field strength and the current intensity ratios are researched for moderate values of Mn. It is found that the velocity and the pressure profiles are dominated by the strong point magnetic source. An increment in the magnetic field strength results in an accelerated flow on the transverse plane, retardation in the axial flow, and an increase in the pressure, especially in front of the strong point magnetic source. When the strength of one of the sources increases further, the flow behaves as if it was under the influence of a single point magnetic source, and the pressure around the weak source decreases. The proposed numerical scheme is capable of catching flow fluctuations, and the boundary discretization nature of DRBEM provide solutions with a less computational cost. In the present study, the FHD flow is investigated in an irregular cavity with smooth boundary sections. In the subsequent works, it is worthy to research the effects of the unsmooth boundary [13, 18, 43] and analyze the hydrodynamic instability of the present FHD flow [5, 8, 12].

Declaration of Competing Interests The author declares that there is no competing interests.

Acknowledgements The author thanks to the reviewers for their valuable suggestions.

References

[1] Akter, S., Ferdows, M., Shamshuddin, M.D., Siri, Z., Similarity solution for induced magnetic field boundary layer flow of metallic nanofluids via convectively inclined stationary/moving flat plate:Spectral relaxation computation, *Journal of Applied Mathematics and Mechanics, 102* (2022), e202100179, https://dx.doi.org/10.1002/zamm.202100179.

[2] AL-Bayati, S.A., Wrobel, L.C., A novel dual reciprocity boundary element formulation for two-dimensional transient convection-diffusion-reaction problems with variable velocity, *Engineering Analysis with Boundary Elements, 94* (2018), 60–68, https://dx.doi.org/10.1016/j.enganabound.2018.06.001.

[3] Al-Kouz, W., Abderrahmane, A., Shamshuddin, M.D., Younis, O., Mohammed, S., Beg, O.A., Toghraie, D., Heat transfer and entropy generation analysis of water-Fe_3O_4/CNT hybrid magnetic nanofluid flow in a trapezoidal wavy enclosure containing porous media with Galerkin finite element method, *The European Physical Journal Plus, 136* (2021), 1184, https://dx.doi.org/10.1140/epjp/s13360-021-02192-3.

[4] Brebbia, C.A., Dominguez, J., Boundary Elements and Introductory Course, WIT Press/Computational Mechanics Publications, 1992.

[5] Curtis, R.A., Flows and wave propagation in ferrofluids, *The Physics of Fluids, 14(10)* (1971), 2096–2101, https://dx.doi.org/10.1063/1.1693299.

[6] Dalvi, S., Meer, T.H., Shahi, M., Numerical evaluation of the ferrofluid behavior under the influence of three-dimensional non-uniform magnetic field, *International Journal of Heat and Fluid Flow, 94* (2022), 108901, https://dx.doi.org/10.1016/j.ijheatfluidflow.2021.108901.

[7] Fattah, A.R.A., Ghosh, S., Puri, I.K., Printing microstructures in a polymer matrix using a ferrofluid droplet, *Journal of Magnetism and Magnetic Materials, 401* (2016), 1054–1059, https://dx.doi.org/10.1016/j.jmmm.2015.10.112.

[8] Finlayson, B.A., Convective instability of ferromagnetic fluids, *Journal of Fluid Mechanics, 40(4)* (1970), 753–767, https://dx.doi.org/10.1017/S0022112070000423.

[9] Fletcher, C.A.J., Computational Techniques for Fluid Dynamics 2, Springer, Berlin, 1991.

[10] Goharkhah, M., Ashjaee, M., Effect of an alternating nonuniform magnetic field on ferrofluid flow and heat transfer in a channel, *Journal of Magnetism and Magnetic Materials, 362* (2014), 80–89, https://dx.doi.org/10.1016/j.jmmm.2014.03.025.

[11] Han Aydin, S., Tezer-Sezgin, M., A DRBEM solution for MHD pipe flow in a conducting medium, *Journal of Computational and Applied Mathematics, 259(B)* (2014), 720–729, https://dx.doi.org/10.1016/j.cam.2013.05.010.

[12] He, J.H., Moatimid, G.M., Sayed, A., Nonlinear EHD instability of two-superposed Walters' B fluids through porous media, *Axioms, 10* (2021), 258, https://dx.doi.org/10.3390/axioms10040258.

[13] He, J.H., Qie, N., He, C.H., Solitary waves travelling along an unsmooth boundary, *Results in Physics, 24* (2021), 104104, https://dx.doi.org/10.1016/j.rinp.2021.104104.

[14] Huang, X., Zhang, X., Wang, Y., Numerical simulation of ferrofluid-lubricated rough elliptical contact with start-up motion, *Applied Mathematical Modelling, 91* (2021), 232–260, https://dx.doi.org/10.1016/j.apm.2020.09.004.

[15] Humane, P.P., Patil, V.S., Patil, A.B., Shamshuddin, M.D., Rajput, G.R., Dynamics of multiple slip boundaries effect on MHD Casson-Williamson double-diffusive nanofluid flow past an inclined magnetic stretching sheet, In *Proceedings of the Institution of Mechanical Engineers, Part E: Journal of Process Mechanical Engineering* (2022), vol. 236(5), pp. 1906–1926, https://dx.doi.org/10.1177/09544089221078153.

[16] Javaran, S.H., Khaji, N., Dynamic analysis of plane elasticity with new complex Fourier radial basis functions in the dual reciprocity boundary element method, *Applied Mathematical Modelling, 38(14)* (2014), 3641–3651, https://dx.doi.org/10.1016/j.apm.2013.12.010.

[17] Kenjeres, S., Numerical analysis of blood flow in realistic arteries subjected to strong non-uniform magnetic fields, *International Journal for Heat and Fluid Flow, 29* (2008), 752–764, https://dx.doi.org/10.1016/j.ijheatfluidflow.2008.02.014.

[18] Li, X., Wang, D., Effects of a cavity's fractal boundary on the free front interface of the polymer filling stage, *Fractals, 29(7)* (2021), 2150225, https://dx.doi.org/10.1142/S0218348X2150225X.

[19] Loukopoulos, V.C., Tzirtzilakis, E.E., Biomagnetic channel flow in spatially varying magnetic field, *International Journal of Engineering Science, 42* (2004), 571–590, https://dx.doi.org/10.1016/j.ijengsci.2003.07.007.

[20] Micchelli, C.A., Interpolation of scattered data:Distance matrices and conditionally positive definite functions, *Constructive approximation, 2* (1986), 11–22, https://dx.doi.org/10.1007/BF01893414.

[21] Mortazavinejad, S.M., Mozafarifard, M., Numerical investigation of two-dimensional heat transfer of an absorbing plate of a flat-palet solar collector using dual-reciprocity method based on boundary element, *Solar Energy, 191* (2019), 332–340, https://dx.doi.org/10.1016/j.solener.2019.08.075.

[22] Mousavi, S.M., Darzi, A.A.R., Akbari, O.A., Toghraie, D., Marzban, A., Numerical study of biomagnetic fluid flow in a duct with a constriction affected by a magnetic field, *Journal of Magnetism and Magnetic Meterials, 473* (2019), 42–50, https://dx.doi.org/10.1016/j.jmmm.2018.10.043.

[23] Mousavi, S.M., Farhadi, M., Sedighi, K., Effect of non-uniform magnetic field on biomagnetic fluid flow in a 3D channel, *Applied Mathematical Modelling, 40* (2016), 7336–7348, https://dx.doi.org/10.1016/j.apm.2016.03.012.

[24] Partridge, P.W., Brebbia, C.A., Wrobel, L.C., The Dual Reciprocity Boundary Element Method, Computational Mechanics Publications, Sauthampton, Boston, 1992.

[25] Patil, V.S., Shamshuddin, M.D., Ramesh, K., Rajput, G.R., Slipperation of thermal and flow speed impacts on natural convective two-phase nanofluid model across Riga surface: Computational scrutinization, *International Communications in Heat and Mass Transfer, 135* (2022), 106135, https://dx.doi.org/10.1016/j.icheatmasstransfer.2022.106135.

[26] Plansey, R., Collin, R.E., Principles and Applications of Electromagnetic Fields, Mc Graw-Hill, NewYork, 1961.

[27] Rosensweig, R.E., Ferrohydrodynamics, Dover Publications, Mineola, New York, 2014.

[28] Salawu, S.O., Obalalu, A.M., Shamshuddin, M.D., Nonlinear solar thermal radiation efficiency and energy optimization for magnetized hybrid Prandtl-Erying nanoliquid in aircraft, *Arabian Journal for Science and Engineering* (2022), https://dx.doi.org/10.1007/s13369-022-07080-1.

[29] Salehpour, A., Ashjaee, M., Effect of different frequency functions on ferrofluid FHD flow, *Journal of Magnetism and Magnetic Materials, 480* (2019), 112–131, https://dx.doi.org/10.1016/j.jmmm.2019.02.045.

[30] Senel, P., Flow in a cavity subjected to two variable magnetic sources, In *Abstract book of the Second International Conference on Applied Mathematics in Engineering (ICAME'21)* (Balikesir, Turkey, September 1-3, 2021), p. 73.

[31] Senel, P., Tezer-Sezgin, M., DRBEM solution to MHD flow in ducts with thin slipping side walls and separated by conducting thick Hartmann walls, *Computers and Mathematics with Applications, 78* (2019), 3165–3174, https://dx.doi.org/10.1016/j.camwa.2019.05.019.

[32] Seo, J.H., Lee, M.Y., Illuminance and heat transfer characteristics of high power LED cooling system with heat sink filled with ferrofluid, *Applied Thermal Engineering, 143* (2018), 438–449, https://dx.doi.org/10.1016/j.applthermaleng.2018.07.079.

[33] Shahzad, F., Jamshed, W., Sajid, T., Shamshuddin, M.D., Safdar, R., Salawu, S.O., Eid, M.R., Hafeez, M.B., Krawczuk, M., Electromagnetic control dynamics of generalized Burgers' nanoliquid flow containing motile microorganisms with Cattaneo-Christov relations: Galerkin finite element machanism, *Applied Sciences, 12(17)* (2022), 8636, https://dx.doi.org/10.3390/app12178636.

[34] Shamshuddin, M.D., Ghaffari, A., Usman, Radiative heat energy exploration on Casson-type nanoliquid induced by a convectively heated porous plate in conjuction with thermophoresis and Brownian movements, *International Journal of Ambient Energy, 43(1)* (2022), 6329–6340, https://dx.doi.org/10.1080/01430750.2021.2014960.

[35] Shamshuddin, M.D., Mabood, F., Rajput, G.R., Beg, O.A., Badruddin, I.A., Thermo-solutal dual stratified convective magnetized fluid flow from an exponentially stretching Riga plate sensor surface with thermophoresis, *International Communications in Heat and Mass Transfer, 134* (2022), 105997, https://dx.doi.org/10.1016/j.icheatmasstransfer.2022.105997.

[36] Sharifi, A., Motlagh, S.Y., Badfar, H., Ferro hydro dynamic analysis of heat transfer and biomagnetic fluid flow in channel under the effect of two inclined permanent magnets, *Journal of Magnetism and Magnetic Materials, 472* (2019), 115–122, https://dx.doi.org/10.1016/j.jmmm.2018.10.029.

[37] Sheikholeslami, M., Rashidi, M.M., Effect of space dependent magnetic field on free convection of Fe_3O_4 -water nanofluid, *Journal of the Taiwan Institute of Chemical Engineers, 56* (2015), 6–15, https://dx.doi.org/10.1016/j.jtice.2015.03.035.

[38] Sheikholeslami, M., Rashidi, M.M., Ferrofluid heat transfer treatment in the presence of variable magnetic field, *The European Physical Journal Plus, 130* (2015), 115–126, https://dx.doi.org/10.1140/epjp/i2015-15115-4.

[39] Siddiqa, S., Begum, N., Safdar, S., Hossain, M.A., Al-Rashed, A.A.A.A., Influence of localized magnetic field and strong viscosity on the biomagnetic fluid flow in a rectangular duct, *International Journal of Mechanical Sciences, 131-132* (2017), 451–458, https://dx.doi.org/10.1016/j.ijmecsci.2017.07.022.

[40] Soltanipour, H., Numerical analysis of two-phase ferrofluid forced convection in an annulus subjected to magnetic sources, *Applied Thermal Engineering, 196* (2021), 117278, https://dx.doi.org/10.1016/j.applthermaleng.2021.117278.

[41] Tzirtzilakis, E.E., A mathematical model for blood flow in a magnetic field, *Physics of Fluids, 17:077103* (2005), 1–15, https://dx.doi.org/10.1063/1.1978807.

[42] Tzirtzilakis, E.E., Sakalis, V.D., Kafoussias, N.G., Hatzikonstantinou PM, Biomagnetic fluid flow in a 3D rectangular duct, *International Journal for Numerical Methods in Fluids, 44* (2004), 1279–1298, https://dx.doi.org/10.1002/fld.618.

[43] Wu, P.X., Yang, Q., He, J.H., Solitary waves of the variant Boussinesq-Burgers equation in a fractal-dimensional space, *Fractals, 30(3)* (2022), 2250056, https://dx.doi.org/10.1142/S0218348X22500566.

[44] Wu, V.M., Huynh, E., Tang, S., Uskokovic, V., Brain and bone cancer targeting by a ferrofluid composed of superparamagnetic iron-oxide/silica/carbon nanoparticles (earthicles), *Acta Biomaterialia, 88* (2019), 422–447, https://dx.doi.org/10.1016/j.actbio.2019.01.064.

[45] Yu, B., Cao, G., Huo, W., Zhou, H., Atroshchenko, E., Isogeometric dual reciprocity boundary element method for solving transient heat conduction problems with heat sources, *Journal of Computational and Applied Mathematics, 385* (2021), 113197, https://dx.doi.org/10.1016/j.cam.2020.113197.

[46] Yu, B., Zhou, H.L., Chen, H.L., Tong, Y., Precise time-domain expanding dual reciprocity boundary element method for solving transient heat conduction problems, *International Journal of Heat and Mass Transfer, 91* (2015), 110–118, https://dx.doi.org/10.1016/j.ijheatmasstransfer.2015.07.109.

[47] Zeng, J., Deng, Y., Vedantam, P., Tzeng, T.R., Xuan, X., Magnetic separation of particles and cells in ferrofluid flow through a straight microchannel using two offset magnets, *Journal of Magnetism and Magnetic Materials, 346* (2013), 118–123, https://dx.doi.org/10.1016/j.jmmm.2013.07.021.

[48] Zhang, T., Wen, Z., Lei, H., Gao, Z., Chen, Y., Zhang, Y., Liu, J., Xie, Y., Sun, X., Surface-microengineering for high-performance triboelectric tactile sensor via dynamically assembled ferrofluid template, *Nano Energy, 87* (2021), 106215, https://dx.doi.org/10.1016/j.nanoen.2021.106215.

http://communications.science.ankara.edu.tr

Commun.Fac.Sci.Univ.Ank.Ser. A1 Math. Stat.
Volume 72, Number 2, Pages 551–562 (2023)
DOI:10.31801/cfsuasmas.1187009
ISSN 1303-5991 E-ISSN 2618-6470

Research Article; Received: October 10, 2022; Accepted: March 29, 2023

A STUDY ON USING ROBUST HEDONIC REGRESSION IMPLEMENTATION

Serdar Cihat GÖREN[1] and Olcay ARSLAN[2]

[1,2]Department of Statistics, Ankara University, 06100 Ankara, TÜRKİYE

ABSTRACT. This article aims to determine the features affecting the price of a product with the hedonic regression model and to estimate the contribution of each feature to the price by using robust regression estimation methods. For the analysis, the price and feature information of the laptop product group were obtained from the big data source by using the web scraping method. Four alternatives of the hedonic regression model are used to determine the features affecting the price of the laptops. The contribution of each feature to the laptop price is estimated by using the robust (Huber M-estimator) estimation method and the Ordinary Least Squares (OLS) estimation method, and the resulting estimates are compared for both methods. In the framework of the data set used in the study, it is observed that the effective model is the Logarithmic Robust Hedonic Regression Model.

1. Introduction

Statistics producers aim to provide quality and accurate statistics to their users. As in many studies, the production of statistics requires resources in terms of money, human, and time. The data collection method with a questionnaire is one of the traditional and most widely used methods. In addition, data collection methods such as administrative data and big data are also widely used. Collecting data with administrative data and big data reduces the requirements considerably. They also reduce the burden on the respondents that occurs with the survey.

The market share of laptop computers in the technology sector is quite high. There are many brands of laptop manufacturers, which creates a serious competition environment in the market. Laptop manufacturers determine customer profiles, produce computers with features suitable for these customer profiles, and offer them

2020 *Mathematics Subject Classification.* 62J05, 62J07.
Keywords. Robust regression, hedonic regression, big data.
[1] scgoren@gmail.com-Corresponding author; 0000-0002-6253-6156
[2] oarslan@ankara.edu.tr; 0000-0002-7067-4997.

for sale. On the other hand, consumers aim to buy a laptop computer that is suitable for their use and budget. Campaigns, promotions, advertisements, and more than one brand model in technology stores make consumers' decisions complicated. This competitive environment also increases the risk of consumers purchasing laptops with the wrong choice. At this point, it will be useful for consumers to research computer brands, features, and prices in detail.

When consumers want to search for laptop computer prices and models, they prefer to look at technology market websites. However, they may not always have the necessary information about which computer is suitable for their use and what the right price should be for this computer. This article aims to determine the features that affect laptop computer prices by using big data from the internet prices of technological markets.

One of the methods used to determine the value of a good by breaking it down into its components is the hedonic regression method. The word "hedonic" means pleasure, satisfaction, or benefit after the consumption of goods and services (Bulut and Zaman [4]).

According to the study by Colwell and Dilmore [5], it is stated that the first user of hedonic regression was Haas [12]. Haas [12] estimated the price of agricultural land with the hedonic regression model using the variables of distance from the city center and the size of the city center.

According to the study by Sheppard [22], it is stated that Waugh [27] was the first study to measure the effect of quality on the price of products. On the other hand, It is stated that Court [6] was the first to use the term "hedonic" to characterize heterogeneous goods and determine demands for individual preferences.

In the literature, it has been seen that price estimation with hedonic regression has a wide usage area. In recent years, the hedonic regression model was frequently used to determine the effect of housing prices and housing characteristics on the price. In addition, analyses were conducted using the hedonic regression model for different products other than housing.

Diewert et al. [8]-[9], Hülagu et al. [17], Jiang et al. [18], and Selim S. [21], used the hedonic regression model for house prices to determine the features affecting house prices. They analysed feature contributes by using the Ordinary Least Squares (OLS) method.

Fixler et al. [11] used the hedonic regression model as a quality adjustment method in the US Consumer Price Indices.

Manoel et al. [19] determined the features of laptops with the hedonic regression model, and measured the contribution of each feature to the price with the OLS method.

McCormack [20] identified the features that affect the price for new cars by using the hedonic regression model, and measured the contribution of each feature to the price with the OLS method.

In many studies conducted with hedonic regression, estimations were generally carried out by using the OLS method. However, it is known that the OLS method does not give effective results if there are outliers in the data. In this case, robust statistical methods should be preferred to estimate the parameters. Since robust statistical methods are robust against outliers.

Bourassa et al. [2] used the robust hedonic regression model for house prices to determine the features affecting house prices. The efficiency of 3 robust statistical methods and the OLS method were compared. As a result of the study, it was observed that robust methods give more effective results in the case of outliers than the OLS method.

Bulut and Zaman [4] used the robust hedonic regression model for the car of "Beetle as Turtle" models to determine the features affecting the car. The efficiency of OLS, M-estimators (Huber, Tukey, Hampel), Mutli-stage Method (MM), Least Trimmed Squares (LTS), Least Median Square (LMS), and Least Absolute Deviations (LAD) methods were compared. It was observed that the LAD method gave effective results.

In this article, four alternatives for the hedonic regression model were used to determine the features affecting the price of the laptops. The big data is obtained from technological markets for laptops by using the web scraping method. The parameters of each model were estimated by using OLS and robust methods. It was analysed how much the features contributed to the laptop prices. Robust methods and the OLS method are compared in order to find and recommend the effective method.

This article is organized as follows. In Section 2, laptop computers, big data, hedonic regression, and robust statistical methods are introduced. In Section 3, the hedonic regression model alternatives are established within the framework of the obtained data set and the estimation results are given. In the last section, the findings obtained as a result of the study are evaluated.

2. Method

2.1. **Laptop Computers.** Nowadays, laptop computers are one of the most demanded and used technological products. The most important advantage of laptop computers is portability. Like many technological products, laptops also have many technical features. They are also called hardware features in market conditions. Hardware features are processor, ram, hard disk, graphic card, screen size, etc. While some of these features directly affect the laptop price, some of them have a very limited effect on the price. Statistical methods can be used to learn this distinction and to determine how much each feature contributes to the price of the laptop. As a result of the hedonic regression analysis carried out in this article and the main features affecting the laptop computer price were highlighted.

2.2. **Big Data.** The demand and need for statistical information are increasing day by day. Data collection methods such as surveys, administrative data, and big data have been developed for the collection of data. Big data has become very popular nowadays. Because statistics producers prefer to use existing data instead of collecting data from the field to achieve their goals. Thus, statistics producers provide significant benefits in terms of human, financial, and time resources.

Although big data has many definitions, it is generally defined as data that is too large for traditional users to store and process. Examples of big data are transportation, social media, and market data. It can not be said that big data is big only because of the volume of data (Doğan and Arslantekin [10]). To define the data as big data, some requirements must be met. These requirements are defined in the literature with the 5V (Volume, Velocity, Variety, Value, Veracity) approach. Here, "volume" refers to the volume and size of the data, "velocity" refers to the speed of the data, "variety" refers to the diversity of the data, "value" refers to the value of the data, and "veracity" refers to the validity of the data.

According to an article by Aktan [1]; it was stated that the concept of big data was used for the first time in the study of Cox and Ellsworth [7]. In this study, scientific data visualization study was carried out.

2.3. **Web Scraping.** Web scraping is the set of techniques used to automatically get some information from a website instead of manually copying it. The goal of a web scraper is to look for certain kinds of information, extract, and aggregate it into new Web pages. In particular, scrapers are focused on transforming unstructured data and save them in structured databases (Vargiu and Urru [26]).

In this article, data were collected from several technology websites for a certain period by web scraping method. Since the structure of the websites was different, the Spider code was used in Python specific to each site. Selenium was used as click technology, and Scrapy libraries were used as data collection technology. Since it was only used for a certain period and in a way not to increase the data traffic of the websites, no block was encountered by the websites.

2.4. **Hedonic Regression.** Hedonic regression is a method used in order to determine the value of a good or service by breaking it down into its components. The value of each component is determined separately by regression analysis (McCormack [20]). The hedonic regression model has the completely same structure as the classical linear regression. Since the concept of hedonic is based on consumer satisfaction, it is identified with the analysis of the relationship between the prices and properties of goods.

Hedonic price functions are used for two main purposes: to create general price indices that take into account changes in the quality of manufactured goods and to analyse consumer demands for the characteristics of heterogeneous goods (Sheppard [22]). The second of these aims that Sheppard [22] has defined is one of the aims of our article. Measuring the contribution of laptop features to the price with the hedonic regression model will show us how the consumer demand for the features of this product.

By using the hedonic price model, a relationship is established between the features of a good and the price of the relevant good. In other words, the hedonic price model is a method that evaluates the price of a particular good as the sum of the values of the features it has and estimates the value of each feature using regression analysis (Shimizu et al. [23]).

$$p = h(c_i) \tag{1}$$

The hedonic price model is defined at (1). In this model, p is called the price of a good, and $h(c_i)$ is the hedonic function of the properties of that good. A hedonic function is estimated by regression analysis (McCormack [20]).

2.4.1. *Hedonic regression model alternatives.* When the hedonic regression studies in the literature are investigated, it is shown that hedonic regression model alternatives vary. The purpose of hedonic price modelling is to determine the model that will identfy the functional relationship between price and features. In the literature, we come across 4 different model structures which are Linear Model (LinLin), Logarithmic Model (LogLog), Linear Logarithmic Model (LinLog), and Logarithmic Linear Model (LogLin).

Model alternatives vary according to the structure of dependent and independent variables. The linear and logarithmic structure of the dependent and independent variables allows the hedonic regression model to be diversified and the efficiency of parameter estimations to be compared. Established hedonic regression model types show different results according to the price and features of the estimated product.

In the hedonic regression model, the dependent variable is the price of the product, while the independent variables are the features of the product. Some of the independent variables consisting of the features of the product can be quantitative and some of them can be qualitative variables. While quantitative variables can be directly included in the model, qualitative variables should be defined as dummy variables. In this case, if the qualitative variables defined as dummy variables are in the relevant product as a feature, it takes the value of 1, if not, it takes the value 0.

In this study we define the variables;

Y (dependent variable): Price of the laptop

X_1 (independent variable): Processor speed of the laptop

X_2 (independent variable): Ram size of the laptop

X_3 (independent variable): Hard disk size of the laptop

X_4 (independent variable): Processor (Intel i7) of the laptop

X_5 (independent variable): Processor (Intel i5) of the laptop

X_6 (independent variable): Processor (Intel i3) of the laptop

X_7 (independent variable): Graphic Card of the laptop

Four model structures are given at (2), (3), (4), and (5). Here, $Y_i \in R$ the price of the features is the price of the product to be estimated. In other words, it is defined as the response variable in the regression model. $\alpha \in R$ is the constant term of the model. $\beta_i \in R$ are unknown parameters. ε_i are independent and $E(\varepsilon_i) = 0$, $Var(\varepsilon_i) = \sigma^2$

- Linear Model (LinLin)

$$Y_i = \alpha + \beta_1 X_{i1} + \beta_2 X_{i2} + \beta_3 X_{i3} + \beta_4 X_{i4} + \beta_5 X_{i5} + \beta_6 X_{i6} + \beta_7 X_{i7} + \varepsilon_i \quad (2)$$

- Logarithmic Model (LogLog)

$$lnY_i = \alpha + \beta_1 lnX_{i1} + \beta_2 lnX_{i2} + \beta_3 lnX_{i3} + \beta_4 lnX_{i4} + \beta_5 lnX_{i5} + \beta_6 lnX_{i6} + \beta_7 lnX_{i7} + \varepsilon_i \quad (3)$$

- Linear Logarithmic Model (LinLog)

$$Y_i = \alpha + \beta_1 lnX_{i1} + \beta_2 lnX_{i2} + \beta_3 lnX_{i3} + \beta_4 lnX_{i4} + \beta_5 lnX_{i5} + \beta_6 lnX_{i6} + \beta_7 lnX_{i7} + \varepsilon_i \quad (4)$$

- Logarithmic Linear Model (LogLin)

$$lnY_i = \alpha + \beta_1 X_{i1} + \beta_2 X_{i2} + \beta_3 X_{i3} + \beta_4 X_{i4} + \beta_5 X_{i5} + \beta_6 X_{i6} + \beta_7 X_{i7} + \varepsilon_i \quad (5)$$

McCormack (2013) used the Logarithmic Linear (LogLin) hedonic regression model in order to determine the features that affect new car prices.

Bulut and Zaman (2018) analysed the factors affecting the price with (2), (3), (4), and (5). As a result of the study, it was stated that the most effective results were obtained with the Logarithmic Linear Model (LogLin).

Selim (2008) determined the house characteristics by using hedonic regression model. The Logarithmic Linear Model (LogLin) was used in the study and the estimations were made with the OLS method.

Jiang *et al.* (2014) analysed housing features by using the OLS method with establishing a Linear Model (LinLin) hedonic regression model.

This article aims to settle model alternatives and decide which model is effective according to the model standard error criterion. In the implementation phase of the study, the parameter estimation of the four alternative hedonic regression models was carried out by OLS and robust (Huber M-estimator) estimators. The effective model is highlighted from the estimation results obtained.

2.4.2. *Ordinary Least Square (OLS).* The Ordinary Least Square (OLS) method is widely used in regression analyses. Stigler [24] mentioned that the first users of OLS were Carl Friedrich Gauss and Adrien Marie Legendre, but which one was the first user is a matter of debate. It was stated that while Legendre had a publication on the subject in 1805, Gauss had a publication in 1809. However, it has been concluded that there is serious evidence that Gauss used the OLS method for the first time in 1795 and that the inventor of the OLS was Gauss. In addition, Stigler [24] defined the OLS method was the automobile of modern statistics, and the person who first discovered the OLS method was identified as the inventor of the automobile, Henry Ford.

The linear regression model can be written with the help of matrices at (6).

$$Y_i = X_i^T \beta + \varepsilon_i \tag{6}$$

for $\mathrm{Y}_i \in R, X_i \in R^T, \beta \in R^T, i = 1, 2..., n$.

The OLS estimators for the regression parameter vector are obtained at (7):

$$\widehat{\beta} = (XX')^{-1} X'Y \tag{7}$$

In the literature, as in linear regression, parameter estimations in the hedonic regression model are generally carried out by the OLS method. Although OLS is one of the most common statistical methods, it does not give effective results in cases there are outliers in the data. In case of outliers in the data, robust statistical methods give more effective results than the OLS method.

Conventional hedonic regression models are highly sensitive to these outliers because they are estimated by minimizing the sums of the squared residuals. This gives outliers, and particularly large outliers, disproportionately large influence. Even a small number of outliers can have a large effect. Robust methods generally down-weight observations automatically based on the size of their residuals. (Bourassa et al. [2]).

In this article, parameter estimations in the hedonic regression model were carried out with OLS and robust methods and their effectiveness was compared with each other. In the next section, robust methods are introduced.

2.4.3. *Robust Statistical Methods.* In case of outliers in the data set, it is recommended to use robust methods that are less affected by outliers compared to the OLS method when estimating parameters. As mentioned in the previous section, robust statistical methods, which reduce the effect of outliers, make the estimation more reliable.

Problematic sales prices, such as sudden discounts and foreclosure sales, seriously reduce the price. Some types of problematic transactions may be flagged in some hedonic data sets. In other cases, it may be possible to identify these transactions, but only with considerable investment of time and effort. Robust methods provide a means for responding to data problems when it is difficult or impossible to identify all of the transactions with contaminated data. (Bourassa et al. [2]).

The term robust was introduced to the statistical literature by Box [3]. The field of modern robust statistics emerged with the pioneering work of Tukey [25], Huber [15], and Hampel [13] and has been extensively developed over time (Heritier et al. [14]). In this article, parameter estimations in hedonic regression are carried out via Huber's M-estimator.

2.4.3.1. *Huber M-estimator*

The widely used M estimation method for robust regression was introduced by Huber [15]-[16]. This class of estimators has been accepted as a generalization of the maximum likelihood estimation. The M estimator method is designed to minimize an objective function that increases less rapidly than the OLS objective function.

In contrast to OLS, M-estimators minimize some function that gives decreasing weights to observations as the size of the standardized residual increases (Huber [15]).

$$\frac{1}{n}\sum_{i=1}^{n}\rho\left(Y_i - X_i^T\beta\right) \tag{8}$$

Huber M-estimation function is given at (8). Here, ρ is non-negative and non-decreasing. M estimators aim to minimize (8). If ρ is differentiable, the 1st derivative concerning β is taken and set to 0, and the following equation is obtained.

$$\frac{1}{n}\sum_{i=1}^{n}\psi\left(Y_i - X_i^T\beta\right)X_i = 0 \tag{9}$$

where psi $=\rho'$.

(9) is solved by iterative methods and $\widehat{\beta}$ is obtained.

3. Implementation

In this article, technological market data was used in order to determine the model that gives effective estimations about laptop prices. The data set was obtained by web scraping method for the period covering the last quarter of 2020. Since web scraping method was only used for a certain period and in a way not to increase the data traffic of the websites, no block was encountered by the websites. The size of data set is about 5 thousand rows.

In the data set, it was decided to use the processor, processor speed, ram, hard disk, and graphic card features that directly affect the price of a laptop computer in the hedonic regression model. In the hedonic regression models established, the dependent variable is price, and the independent variables are processor, processor speed, ram, hard disk, and graphic card. At this point, price, processor speed, ram, and hard disk variables are defined as numerical variables, while other variables are defined as categorical (no exist (1,0)) dummy variables. The definition and properties of the variables used in the study are given in the Table 1.

3.1. **Results of Analysis.**

Hedonic regression model analyses were performed in the R Package. In the regression analysis, 4 model structures were analysed, namely Linear Model (LinLin), Logarithmic Model (LogLog), Linear Logarithmic Model (LinLog), and Logarithmic Linear Model (LogLin). Coefficient estimates were carried out for each model structure with both OLS and robust M-estimators. Four different hedonic regression models were applied to the data set. They are "OLS-Logarithmic Model (O-LogLog)", "Robust (M-estimator)- Logarithmic Model (R-LogLog)", "OLS-Linear Model (O-LogLin)" and "Robust (M-estimator) - Logarithmic Linear Model (R-LogLin)". The coefficient estimates obtained for each model are given in Table 2. It is seen how much the features that affect the price of the laptop contribute to the price of the laptop. In addition, model standard errors

TABLE 1. Definitions of variables.

Variable	Name	Type	Measurement
Y	Price	Numeric	Turkish Lira
X_1	Processor speed	Numeric	Gigahertz (GHz)
X_2	Ram	Numeric	Gigabyte (Gb)
X_3	Hard disk	Numeric	Gigabyte (Gb)
X_4	Processor- Intel i7	Dummy	i7=1, other=0
X_5	Processor- Intel i5	Dummy	i5=1, other=0
X_6	Processor- Intel i3	Dummy	i3=1, other=0
X_7	Graphic card	Dummy	EXT =1, INT =0

obtained for each model are given in Table 3. According to Table 3, it is observed that the model with the lowest standard error is the "Robust Logarithmic Model (R-LogLog)".

TABLE 2. Estimations of coefficients.

Variable	O-LogLog	R-LogLog	O-LogLin	R-LogLin
μ	$6,91$	$6,90$	$8,32$	$8,33$
X_1	$0,06$	$0,05$	$0,02$	$0,03$
X_2	$0,48$	$0,45$	$0,04$	$0,04$
X_3	$0,15$	$0,16$	$0,00$	$0,00$
X_4	$0,48$	$0,46$	$0,65$	$0,62$
X_5	$0,24$	$0,23$	$0,32$	$0,30$
X_6	$0,04$	$0,00$	$-0,09$	$-0,12$
X_7	$0,01$	$0,02$	$-0,02$	$-0,02$

TABLE 3. Model standard errors.

Model	Standard errors
O-LogLog	$0,14$
R-LogLog	$0,11$
O-LogLin	$0,15$
R-LogLin	$0,15$

3.2. **Rankings of Contributions.** The coefficient estimates are obtained by using the hedonic regression models to rank the contribution of laptop features to the price for each model are shown in Table 4. When the coefficient estimates are examined, we see that the i7 processor made the biggest contribution. It is known that Intel's processors, i3, i5, and i7, are in the form of $i7 > i5 > i3$ in terms of performance.

The fact that the contribution rankings of the processors that contribute to the laptop price in all 4 models are observed as $i7 > i5 > i3$ also shows that the estimates coincide with reality.

Table 4. Rankings of contributions.

Variable	O-LogLog	R-LogLog	O-LogLin	R-LogLin	Average Rank
i7	1	1	1	1	1
Ram	2	2	3	3	2, 5
i5	3	3	2	2	2, 5
Hard disk	4	4	5	5	4, 5
Processor speed	5	5	4	4	4, 5
Graphic card	7	6	6	7	6, 5
i3	6	7	7	6	6, 5

3.3. **Case of outliers in the data.** In data sets, errors may occur due to data entry, system, and unit of measurement. These errors are sometimes difficult to detect in large data sets. In addition, there is a possibility that they may be overlooked. To address this situation, few and large amounts of incorrect data entries were added to the obtained data set. In Table 5, there are model standard errors obtained from 4 models in case of a few (Model standard error-2) or a large amount of incorrect data entry (Model standard error-3) into the data set. In addition, the model standard errors before the incorrect data entry are included in the table as “Model standard error-1” to be able to compare.

Table 5. Case of outliers in the data.

	O-LogLog	R-LogLog	O-LogLin	R-LogLin
Model standard error-1	0, 14	0, 11	0, 15	0, 14
Model standard error-2	0, 21	0, 12	0, 23	0, 15
Model standard error-3	0, 68	0, 14	0, 66	0, 18

According to the Table 5, it is seen that all model standard errors increase in case of incorrect data entries. In both cases (few and large amounts of incorrect data), R-LogLog appears to give the lowest standard error. It is observed that both models (R-LogLog and R-LogLin) obtained with a robust estimator from 4 models give lower standard errors than models estimated with OLS (E-LogLog and O-LogLin). It is seen that the model standard errors of robust estimators are considerably lower than the model standard errors of OLS, especially, in case of a large amount of incorrect data entry. In addition, the fact that the model standard errors of robust estimators do not increase much in the data set despite a few or a large amount of incorrect data entries shows that these estimators can achieve effective estimations despite incorrect entries in the data.

4. Conclusion

The article focuses on price prediction with hedonic regression models. An implementation study was carried out on the technological market data obtained for the last quarter of 2020 for laptop computers by the web scraping method. Within the scope of the implementation study, the contribution of each of the features affecting the price of the laptop to the price was predicted with four different hedonic regression models. As a result of the analysis, the efficiency of the four models was compared and it was observed that the Robust- Logarithmic Model (R-LogLog) gave the most effective estimations. According to the results obtained with this model, it has been concluded that the processor (i7, i5, i3), processor speed, ram, hard disk, and video card have an increasing effect on the price of the laptop. In addition, it was seen that the i7 processor made the most contribution to the price of the laptop.

In the outlier and residual analysis, it was determined that there was no problem in the data set. However, in case of potential errors in such data sets, which model would be more effective was also examined. It has been observed that the Robust-Logarithmic Model (R-LogLog) is the most effective estimator of the four models in case of errors in the data set by entering the data set with incorrect data.

Within the scope of the data set used in this article, the price estimation of each of the features affecting the price of the laptop and its contribution to the price was measured with the R-LogLog model. Robust methods, which are robust against outliers, are recommended to be used in such studies.

Author Contribution Statements The authors contributed equally to this paper. All authors read and approved the final copy of this paper.

Declaration of Competing Interests The authors declare that they have no competing interest.

References

[1] Aktan, E., Büyük veri: uygulama alanları, analitiği ve güvenlik boyutu, *Bilgi Yönetimi Dergisi*, (2018). https://doi.org/10.33721/by.403010

[2] Bourassa, S. C., Cantoni, E., Hoesli, M., Robust hedonic price indexes, *International Journal of Housing Markets and Analysis*, (2013), 47-65. https://doi.org/10.1108/IJHMA-11-2014-0050

[3] Box, G. E. P., Non-normality and tests on variances, *Biometrika*, 40 (1953), 318-335. https://doi.org/10.2307/2333350

[4] Bulut, H., Zaman, T., Robust hedonik modellerin karşılaştırılması: Beetle Türkiye piyasa fiyatını etkileyen faktörlerin incelenmesi, *C.Ü. İktisadi ve İdari Bilimler Dergisi*, 19 (2018), 24-43.

[5] Colwell, P. F., Dilmore, G., Who was first? An examination of an early hedonic study, *Land Economics*, 75 (1999), 620-626. https://doi.org/10.2307/3147070

[6] Court, A. T., Hedonic price indexes. The dynamics of automobile demand, *General Motors Corporation*, 1939.

[7] Cox, M., Ellsworth, D., Application-controlled demand paging for out-of-core visualization, *8th IEEE Visualization'97 Conference*, 1997. https://doi.org/10.1109/VISUAL.1997.663888
[8] Diewert, W. E., Haan, J., Hendriks, R, The decomposition of a house price index into land and structures components: A hedonic regression approach, *Economic Measurement Group Workshop*, 2010.
[9] Diewert, W. E., Haan, J., Hendriks, R., Hedonic regressions and the decomposition of a house price index into land and structure components, *Statistics Netherlands*, 2014.
[10] Doğan, K., Arslantekin, S., Big data: Its importance, structure and current status, *DTCF Journal*, 56 (2016), 15-36. https://doi.org/10.1501/Dtcfder-0000001461
[11] Fixler, D., Fortuna, C., Greenlees, J., Lane, W., The use of hedonic regressions to handle quality change: The experience in the U.S. CPI, *U.S. Bureau of Labor Statistic*, 1999.
[12] Haas, R., Transportation conditions in Europe, *The Annals of the American Academy of Political and Social Science*, 104 (1922), 157-167.
[13] Hampel, F. R., A general qualitative definition of robustness, *Ann. Math. Stat.*, 42 (1971), 1179-1186.
[14] Heritier, S., Cantoni, E., Copt, S., Victoria-Feser, M. P., Robust methods in biostatistics, *Journal of Biopharmaceutical Statistics*, 20 (2010), 482-484. https://doi.org/10.1002/bimj.201000194
[15] Huber, P. J., Robust estimation of a location parameter, *Annals of Mathematical Statistics*, 35 (1964), 73-101. https://doi.org/10.1214/aoms/1177703732
[16] Huber, P. J., Robust regression: Asymptotics, conjectures and Monte Carlo, *The Annals of Statistics*, 5 (1973), 799–821. https://doi.org/10.1214/aos/1176342503
[17] Hülagu, T., Kızılkaya, E., Gencay A., A hedonic house price index for Turkey, *Central Bank of the Republic of Turkey*, 2016.
[18] Jiang, L., Peter, C., Phillips, B., Jun, Y., A new hedonic regression for real estate prices applied to the Singapore residential market, *Cowles Foundation For Research In Economics Yale University*, 2014. https://doi.org/10.2139/ssrn.2533017
[19] Manoel, N., Felisoni, C., Roberto, M., A five-year hedonic price breakdown for desktop personal computer attributes in Brazil, *Brazilian Administration Review*, 6 (2009), 173-186. https://doi.org/10.1590/S1807-76922009000300002
[20] McCormack, K., Diagnostics for hedonic models using an example for cars, *Biometrics and Biostatistics International Journal*, 2 (2015), 23-37. https://doi.org/10.15406/bbij.2015.02.00022
[21] Selim, S., Determinants of house prices in Turkey: A hedonic regression model, *Journal of Dogus University*, 9 (2008), 65-76. https://doi.org/10.31671/dogus.2019.223
[22] Sheppard, S., Hedonic analysis of housing markets, Oberlin College, Ohio, USA, 1997.
[23] Shimizu, C., Takatsuji, H., Ono, H., Structural and temporal changes in the housing market and hedonic housing price indices: A case of the previously owned condominium market in the Tokyo metropolitan area, *International Journal of Housing Markets and Analysis*, 3 (2010), 351-368.
[24] Stigler, M. S., Gauss and the invention of least squares, *The Annals of Statistics*, 9 (1981), 465-474.
[25] Tukey, J. W., A survey of sampling from contaminated distributions. In: Oklin, I., Ed., Contributions to Probability and Statistics, Stanford University Press, 1960.
[26] Vargiu, E., Urru, M., Exploiting web scraping in a collaborative filtering based approach to web advertising, *Artificial Intelligence Research*, 2 (2013), 44-54. https://doi.org/10.5430/air.v2n1p44
[27] Waugh, F. V., Quality as a Determinant of Vegetable Prices, Columbia University Press, New York, 1929. https://doi.org/10.7312/waug92494

INSTRUCTIONS TO CONTRIBUTORS

Communications Faculty of Sciences University of Ankara Series A1 Mathematics and Statistics (Commun. Fac. Sci. Univ. Ank. Ser. A1 Math. Stat.) is a single-blind peer reviewed open access journal which has been published biannually since 1948 by Ankara University, accepts original research articles written in English in the fields of Mathematics and Statistics. It will be published four times a year from 2022. Review articles written by eminent scientists can also be invited by the Editor.

The publication costs for Communications Faculty of Sciences University of Ankara Series A1 Mathematics and Statistics are covered by the journal, so authors do not need to pay an article-processing and submission charges. The PDF copies of accepted papers are free of charges and can be downloaded from the website. Hard copies of the paper, if required, are due to be charged for the amount of which is determined by the administration each year.

All manuscripts should be submitted via our online submission system https://dergipark.org.tr/en/journal/2457/submission/step/manuscript/new. Note that only two submissions per author per year will be considered. Once a paper is submitted to our journal, all co-authors need to wait 6 months from the submission date before submitting another paper to Commun. Fac. Sci. Univ. Ank. Ser. A1 Math. Stat. Manuscripts should be submitted in the PDF form used in the peer-review process together with the COVER LETTER and the TEX file (Source File). In the cover letter the authors should suggest the most appropriate Area Editor for the manuscript and potential four reviewers with full names, universities and institutional email addresses. Proposed reviewers must be experienced researchers in your area of research and at least two of them should be from different countries. In addition, proposed reviewers must not be co-authors, advisors, students, etc. of the authors. In the cover letter, the author may enter the name of anyone who he/she would prefer not to review the manuscript, with detailed explanation of the reason. Note that the editorial office may not use these nominations, but this may help to speed up the selection of appropriate reviewers.

Manuscripts should be typeset using the LATEX typesetting system. Authors should prepare the article using the Journal's templates (commun.cls and commun.cst). Manuscripts written in AMS LaTeX format are also acceptable. A template of manuscript can be downloaded in tex form from the link https://dergipark.org.tr/en/download/journal-file/22173(or can be reviewed in pdf form). The title page should contain the title of the paper, full names of the authors, affiliations addresses and e-mail addresses of all authors. Authors are also required to submit their Open Researcher and Contributor ID (ORCID)'s which can be obtained from http://orcid.org as their URL address in the format http://orcid.org/xxxx-xxxx-xxxx-xxxx. Please indicate the corresponding author. Each manuscript should be accompanied by classification numbers from the Mathematics Subject Classification 2020 scheme. The abstract should state briefly the purpose of the research. The length of the Abstract should be between 50 to 5000 characters. At least 3 keywords are required. Formulas should be numbered consecutively in the parentheses. All tables must have numbers (TABLE 1) consecutively in accordance with their appearance in the text and a legend above the table. Please submit tables as editable text not as images. All figures must have numbers (FIGURE 1) consecutively in accordance with their appearance in the text and a caption (not on the figure itself) below the figure. Please submit figures as EPS, TIFF or JPEG format. Authors Contribution Statement, Declaration of Competing Interests and Acknowledgements should be given at the end of the article before the references. Authors are urged to use the communication.bst style in BibTeX automated bibliography. If manual entry is preferred for bibliography, then all citations must be listed in the references part and vice versa. Number of the references (numbers in squared brackets) in the list can be in alphabetical order or in the order in which they appear in the text. Use of the DOI is highly encouraged. Formal abbreviations of the journals can be used. The Editor may seek the advice of two, or three referees, depending on the response of the referees, chosen in consultation with appropriate members of the Editorial Board, from among experts in the field of specialization of the paper. The reviewing process is conducted in strict confidence and the identity of a referee is not disclosed to the authors at any point since we use a single-blind peer review process.

 It is a fundamental condition that articles submitted to COMMUNICATIONS have not been previously published and will not be simultaneously submitted or published elsewhere. After the manuscript has been accepted for publication, the author will not be permitted to make any new additions to the manuscript. Before publication the galley proof is always sent to the author for correction. Thus it is solely the author's responsibility for any typographical mistakes which occur in their article as it appears in the Journal. The contents of the manuscript published in the COMMUNICATIONS are the sole responsibility of the authors.

Declarations/Ethics:
With the submission of the manuscript authors declare that:

- All authors of the submitted research paper have directly participated in the planning, execution, or analysis of study;
- All authors of the paper have read and approved the final version submitted;
- The contents of the manuscript have not been submitted, copyrighted or published elsewhere and the visual-graphical materials such as photograph, drawing, picture, and document within the article do not have any copyright issue;
- The contents of the manuscript will not be copyrighted, submitted, or published elsewhere, while acceptance by the Journal is under consideration.
- The article is clean in terms of plagiarism, and the legal and ethical responsibility of the article belongs to the author(s). Author(s) also accept that the manuscript may go through plagiarism check using iThenticate software;
- The objectivity and transparency in research, and the principles of ethical and professional conduct have been followed. Authors have also declared that they have no potential conflict of interest (financial or non-financial), and their research does not involve any human participants and/or animals.

Research papers published in **Communications Faculty of Sciences University of Ankara** are archived in the Library of Ankara University and in Dergipark immediately following publication with no embargo.

Editor in Chief
http://communications.science.ankara.edu.tr
Ankara University, Faculty of Sciences
06100, Besevler - ANKARA TURKEY

C O M M U N I C A T I O N S

FACULTY OF SCIENCES
UNIVERSITY OF ANKARA

DE LA FACULTE DES SCIENCES
DE L'UNIVERSITE D'ANKARA

Series A1: Mathematics and Statistics

Volume: 72 **Number: 2** **Year:2023**

Research Articles